The possible effects of climate change on the spatial and temporal variation of the altitudinal temperature gradient and the consequences for growth potential in the uplands of northern England

Pepin, Nicholas Charles

THE POSSIBLE EFFECTS OF CLIMATE CHANGE ON THE SPATIAL AND TEMPORAL VARIATION OF THE ALTITUDINAL TEMPERATURE GRADIENT AND THE CONSEQUENCES FOR GROWTH POTENTIAL IN THE UPLANDS OF NORTHERN ENGLAND

Nicholas Charles Pepin

Thesis submitted for the degree of Doctor of Philosophy (PhD)
in the Department of Geography, University of Durham

Date of Submission: July 1994

Declaration: The work contained in this thesis is purely that of the author. It has not been submitted for any other degree in this or any other university.

The main body of the text (excluding preliminaries, tables, figures, plate annotations and appendices) is approximately 80,000 words in length.

Acknowledgements

It is my great pleasure to thank many people who have in different ways aided me during the production of this thesis. First and foremost I would like to thank Miss Joan Kenworthy, my principal supervisor, for her hard work, support and advice, in particular for numerous helpful suggestions concerning my approach to the subject and the expression of ideas in the thesis text. I am also extremely grateful for the help given by Dr. Nick Cox, my second supervisor, especially for his meticulous editing skills, statistical insight and computer expertise. I wish to express my thanks to other members of the geography department, in particular to Adam Swain for comments on drafts of chapters in the early stages of my research.

Among the wider academic community, I am indebted to Mr. John Sherwood at the Newcastle Weather Centre for his interest and support, Dr. J.F.R. McIlveen at the University of Lancaster, and Dr. Dave Viner at the Climatic Research Unit for the provision of GCM scenario data.

The production of a thesis requires much technical support. I would like to thank Stella Henderson for her help with photocopying, Andrew Hudspeth for printing and binding, Arthur Corner and the drawing office staff for production of Figures 4.1 and 6.1, and Patrick Crow for photographic plate 3.

The collection of meteorological data for numerous stations in Northern England would not have been possible without the kindness of the following people: Audrey Warner (Durham), Ian Findlay (Widdybank Fell), Phil Shaw (Great Dun Fell), Dennis Wheeler (Sunderland), Ken Cook (Low Etherley), Mike Cinderey (Carlton-in-Cleveland), Trevor Smith (Carlton-in-Coverdale), Ken Bond (Keswick), Robin Cutforth (Ambleside, Appleby), Geoff Thomas (High Close), Brian Kingman (Haydon Bridge), Peter Henderson (Appleby), William Clark (Aspatria), John Sherwood (Newcastle), Jess Cooper (Nenthead), S.Morgan (Whasdyke Farm) and Mick Wood at the Met Office Archives in Bracknell. Finally, I would like to thank my parents for their continued support: especially my father for photographic plates 9 and 11. I am also thankful for the numerous lifts given to me by members of my family to remote climate stations to collect data, especially to my brother Tom in this regard.

ABSTRACT

THE POSSIBLE EFFECTS OF CLIMATE CHANGE ON THE SPATIAL AND TEMPORAL VARIATION OF THE ALTITUDINAL TEMPERATURE GRADIENT AND THE CONSEQUENCES FOR GROWTH POTENTIAL IN THE UPLANDS OF NORTHERN ENGLAND

Thesis submitted for the degree of Doctor of Philosophy (PhD)
Date of Submission: July 1994

Nicholas Pepin

Department of Geography, University of Durham

This thesis studies the potential impacts of lapse rate changes on the altitudinal thermal resource gradient in Northern England and hence of climate change on upland climate.

The extreme marginality of the Pennine uplands in terms of climatic potential for plant growth is explained by reference to the maritime climate. Because the ground-based temperature lapse rate controls the altitudinal thermal resource gradient, the variation of daily temperature lapse rates by season and airflow is described, using 22 stations ranging from 8 to 847 metres above sea-level. Multiple regression models developed for each airflow in each month successfully describe surface temperature variation in most cases.

Such models are used as a basis upon which to describe altitudinal variations in growing season parameters such as accumulated temperatures and frost frequency, for the present climate. Airflow scenarios, based on the regression models, describe the effects of changes in relative frequencies of airflow patterns. The altitudinal gradient in, and absolute values of, growing season parameters depend strongly on relative frequencies of Atlantic westerlies and more blocked conditions.

Assuming the annual 1000 d°C (degree-day) isotherm to represent the altitudinal limit to agricultural cultivation, individual annual elevations between 1801 and 1990 vary by over 300 metres. Extreme sensitivity to the circulatory pattern is also illustrated. Effects of temperature variability within airflows are at least as strong as those of mean conditions in many cases.

The use of General Circulation Model output (UKHI 2 times CO_2) leads to strong changes in climatic potential. For example, few areas retain an annual temperature accumulation below 1000 d°C. Changes in frost parameters are also marked. Other climatic and non-climatic factors would have to be considered to predict land-use change. Preliminary analysis suggests that changes in other climatic elements (e.g. windiness or precipitation) will complement the effects of a temperature increase.

CONTENTS

VOLUME 1

INTRODUCTION

LITERATURE REVIEW: LAPSE RATES

AIR TEMPERATURE AND ITS PREDICTION

DATA SOURCES

VOLUME 2

THE ALTITUDINAL VARIATION OF ACCUMULATED TEMPERATURES IN THE NORTH OF ENGLAND

OTHER MEASURES OF GROWTH POTENTIAL

MEASURES OF FROST RISK

THE DEVELOPMENT OF AIRFLOW SCENARIOS TO PREDICT CHANGES IN THE TEMPERATURE REGIME AT DIFFERING ALTITUDES FROM CHANGES IN THE CIRCULATION PATTERN OVER THE BRITISH ISLES

THE GROWING SEASON IN THE DURHAM METEOROLOGICAL RECORD 1801-1990 AND IMPLIED ALTITUDINAL LIMITS TO CROP GROWTH

THE SIMULATION OF CLIMATIC VARIABILITY TO IMPROVE ESTIMATES OF ACCUMULATED TEMPERATURES

THE SIMULATION OF CLIMATIC VARIABILITY TO IMPROVE FROST ACCUMULATION ESTIMATES

THE USE OF GCM SCENARIO OUTPUT TO ILLUSTRATE EFFECTS OF FUTURE CLIMATE CHANGE ON ACCUMULATED TEMPERATURES AND FROST RISK

PREDICTED CHANGES IN CLIMATE ELEMENTS OTHER THAN TEMPERATURE FOR THE UKHI MODEL AND EFFECTS ON THE PENNINE ENVIRONMENT

SUMMARY

LIST OF FIGURES

LIST OF TABLES

LIST OF PHOTOGRAPHIC PLATES IN APPENDIX 1

Page numbers indicate where the plate is referred to in the text.

INTRODUCTION

1.1 Introduction

Over the last few decades it has become apparent that mean global temperatures have risen steadily, amounting to an increase of about 0.5°C between 1900 and 1990 (Mintzer 1992). Such fluctuation of climate can be expected as a property of any variable and chaotic system such as the atmosphere. However, scientists have suggested that this warming trend is the start of a more rapid phase of climate change caused by anthropogenic emissions of "greenhouse gases" such as carbon dioxide and methane, enhancing the natural greenhouse effect which keeps the Earth warmer than it would otherwise be. The context is complicated by the supposition that natural climate fluctuations might also be related to variations in solar output (Tavakol 1979, Hoyt 1980) and that without anthropogenic warming there may be a cooling. In any case, the detailed response of the atmosphere to forcing mechanisms is complex, involving changes in air-sea interactions. Computer models of the atmospheric system have been developed to predict the effects of increases in the carbon dioxide content of the atmosphere on global scale climate. These General Circulation Models (GCMs) are commonly constructed on a coarse spatial resolution and it is extremely difficult to predict changes in climate within an individual region (i.e. mesoscale climate variation) or at an individual location from the global scale models, an important drawback since temperature change will be temporally and spatially variable.

This thesis investigates methodologies for examining temporal and spatial climate variation on the mesoscale so that the local effects of climate change and fluctuation can be examined. Only by relating the climate of a region to the sequence of airflow patterns, can the influence of changes in the general circulation on that area be understood. Then it is sensible to speculate about detailed local effects of climate change.

A commonly neglected aspect of climate change studies is how the effect of altitude on climate elements is likely to alter. The ideas behind lapse rates are discussed

in Chapter 2 and the thesis concentrates on this aspect, investigating possible changes in the lapse rates of air temperature in Northern England should airflow patterns change.

In the maritime environment of Northern England, altitude is the major influence on surface temperature variation and, as a direct result, on variation in land use with altitude in upland areas. The region is used as an example, showing that a full understanding of the effects of climatic fluctuation and change requires detailed knowledge of the local relationships between airflow and weather on a daily basis.

Through analysis of spatial and temporal variation of the altitudinal temperature gradient, the extreme sensitivity of the area to future climatic forcing is illustrated. At present much of the upland area within Northern England is marginal in agricultural terms. If, for example, global warming were to occur, it is agreed that the greatest benefits would be realised at the northern limits of cultivation in countries such as Iceland and N. Finland (Parry 1990). Northern England has a similar climate and can also be expected to benefit. The strong altitudinal influence on temperature means that the area is especially interesting in this context, as will be explained below.

1.2 Climate Change and the Pennine Uplands of Northern England

This thesis seeks to examine the possible effects of climatic change and fluctuation with regard to possible changes in the temperature resource, i.e. changes in accumulated temperatures, the occurrence of frost and growing season indices relevant to agriculture.

The year 1990 was the warmest on record in global terms (Parker & Jones 1991), but local climate changes are much more subtle and less easy to identify. Despite the recent deluge of models simulating possible global warming (Houghton et al. 1990), the environmental consequences of these climate changes were until recently discussed only in global terms but there are now many attempts to model local response of the biosphere to global change, such as the response of specific forest types to global

warming in the Pacific region of North America (Urban et al. 1993) and the effects of climatic change on milk yields in the Great Plains (Klinedinst et al. 1993). Applications of models to mountain regions and to the Pennines in particular are few. This is partly due to the lack of a sufficiently high spatial resolution in General Circulation Model (GCM) output, critical for mountain areas (Brazel & Marcus 1991), and partly because those researchers interested in mountain climates and those interested in climatic change have only recently come together. Barry (1992a) reviews the present state of mountain climatology and asks for more research into the likely responses of mountain areas to climatic change, like his earlier work (Barry 1990). Studies comparing change in mountain areas with that in surrounding lowlands are few because of the lack of data for the uplands. In Britain the lack of observing stations above 400 m has hindered research into the climate of often remote and inaccessible uplands (Taylor 1976). Worldwide research projects include Doesken et al. (1989) comparing changes in the Rockies and Great Plains, Ilko (1991) working in the Alps, and Bücher and Dessens (1991) in the Pyrenees. Divergent trends in upland and lowland climate have been suggested for the Rockies (Doesken et al. 1989), and also for Britain, especially if the general circulation in the Atlantic were to become more progressive (Mayes 1991, Lumb 1993). Day-time lapse rates would steepen so that the beneficial effects of global warming might be less evident in the mountains where the daily temperature range would also decrease (Karl et al. 1993).

The consequences of the above climate changes in Northern England are unclear. The marginal character of much of the English uplands ensures that little activity other than sheep farming is possible in many areas at present, but this could change with a warming trend postulated by many authors (Wigley et al. 1985, Jones et al. 1986, Parker & Jones 1991). The lack of warmth is the major constraint on the distribution of many species and the cultivation of many crops. Spring and early summer are the most critical times of year. In March and April temperatures can hover for days around 6°C (the critical temperature for plant growth) and thus small spatial differences in exposure and/or elevation can lead to considerable contrasts in the progress of vegetation. Lapse rates in the prevailing polar maritime air masses are particularly steep in spring, when the air is heated from below by the rapidly warming

land surface, so that elevation can be crucially important. Taylor (1967a) and Davis (1972) illustrate the marked spatial variation in spring warmth and frost risk in Britain. Theoretically there should be a similar period at the end of the growing season (usually October and November) when differences in temperature are as critical. This is not in general the case because:

1: autumn frosts are less of a problem for vegetation than spring frosts.

2: lapse rates in October and November are generally shallower because air passing from sea to land is cooled and the sun is at a lower altitude than in March and April, encouraging greater stability. Therefore the altitudinal decrease in mean temperature is less at the end of the growing season, reducing the contrast between upland and lowland sites.

The result is that at high altitudes the shortening of the growing season in autumn is less marked than delay in its starting in spring.

The maritime environment means that small changes in mean temperature will have marked consequences for upland growing season (see section 1.3). Manley (1942) illustrated this by reference to possible changes in mean temperatures at Great Dun Fell (847 m), one of the highest summits in the Pennines. An increased frequency of calm, anticyclonic weather and drier summers is shown to be enough to account for a rise in the treeline to over 800 m, even without any general rise in lowland temperatures. On the other hand, persistent snowdrifts would be found on the Great Dun Fell summit if the mean annual temperature were to fall by 4°C. Much of this decrease could be accounted for by an increase in the frequency of polar air outbreaks alone. In cold years such as 1879 and 1888, temperatures were estimated by Manley to be 2-3°C below normal and almost cold enough to initiate permanent snowbeds.

Great environmental changes in the Pennines have occurred in the past, many connected with only slight changes in climate. There is controversial evidence of late Neolithic and early Bronze age (3000-2000 BC) occupation of the Pennine plateau up

to an elevation of 800 m (Lamb 1982), although this may have been seasonal. Climatic change is not the only documented cause of subsequent environmental deterioration. The onset of peat formation following extensive tree-clearance by hunter-gatherers encouraged further deterioration of the forest resource. Nevertheless, the climate is thought to have been warm and dry enough around the climatic optimum or Hypsithermal period (5000 BC) to support trees and cultivars to much higher altitudes than at present, possibly on all land except the highest summits of the Pennine plateau above 800 m.

Work concerned with changing altitudinal limits to cultivation in the past was carried out by Parry (1972, 1975, 1976) in the Lammermuir hills in South East Scotland, essentially a similar environment to the study area. He was concerned particularly with the response of oat cropping to climate change in a marginal area and used the 1150 d°C isotherm above a baseline of 4.4°C as the critical limit for oat cultivation. At this level the possibility of a harvest failure would be 1 in 10. Substantial changes over time in the altitude of this limit were identified. Parry cites reports from the 1280s that farmers were complaining that too little land was available for grazing, due to tillage up to high altitudes. The upper limit of cultivation is shown to have reached 425 m in the mid-13th century, though this limit fell by stages until it was 200 m lower in 1600 (Parry 1978). Moreover, Parry (1976) shows that if accumulated summer temperatures decreased linearly with altitude, the risk of harvest failure would increase quasi-exponentially. Wigley (1985) also shows that for a linear decrease in mean temperature, the change in frequency of an extreme event, such as the crossing of a climatic threshold (e.g. accumulated temperatures falling below a critical level), will change exponentially. Thus climatic "risk" is extremely sensitive to climate variation. One cold year may not lead to farm abandonment but a run of bad years would be problematic. All the great famines of history were the result of a run of bad years. The disastrous harvest of 1879 occurred after five years of below average yields and led to a peak in emigration in the 1880s as English agriculture suffered a complete collapse (Lamb 1982). In contrast, a run of warm years reflecting a change in mean climate could lead to an increase in agricultural potential, especially in cool temperate regions such as the Pennines where temperature is a limiting factor (Parry

et al. 1988). Additionally, many plant species exhibit their northern limits in the region. These can be delimited by isotherms of mean air temperature in the summer months. Iversen (1944) mapped the limits of holly, ivy and mistletoe according to the 12.5°C, 13°C and 15.8°C isotherms of July mean temperature. The limited thermal resource characteristic of Northern England (as compared with the continent) means that climatic change of any description could have far-reaching environmental consequences should the limits of many warmth-loving plants be extended to cover the region (Beerling & Woodward 1994).

The thesis shows that the Pennine area is highly sensitive to climate change. It is in maritime uplands that the first effects of climatic change are likely to be realised, through shifting vegetation patterns and changing altitudinal zonation. Sensitivity to variations in the general circulation and the air-mass types affecting the region is pronounced, as implied in Manley's (1942) comparison of the climatic potential of wet, cool and cloudy westerly summers with warmer, drier and sunnier anticyclonic ones (section 1.3). A change in airflow patterns alone is expected to have a pronounced effect on the altitudinal variation in growth potential.

1.3 The Environment of Northern England

The study area includes the whole of Northern England north of a line running approximately from Barrow-in-Furness to Bridlington. The high Pennine region, from the Tyne valley in the north to Stainmore in the south and from the Vale of Eden in the west to Durham in the east, has been described as "England's Last Wilderness" (Bellamy & Quayle 1989). This area of high, undulating, often bleak and treeless, moorland is the most extensive above 400 metres OD in England (all altitudes for British sites in this thesis are above Ordnance Datum (OD) as measured at Newlyn, Cornwall). Despite modest summit altitudes (the highest point is under 900 m at the summit of Cross Fell - Plate 1, Appendix 1) the whole area has a wilderness quality and exhibits a harsh tundra-like landscape more akin to the montane zones of the Pyrenees and Alps than to the landscape of similar medium altitude areas (<1000 m) on the near continent. The latter include the densely wooded Morvan park in Burgundy

and parts of the Massif Central. Even in Central Norway, birch scrub appears here and there above 1000 m and pine ascends to over 800 m on account of the warmer summers (Manley 1952).

At only 500 m in Upper Teesdale the treeline is reached and the tundra ecotone is apparent (Manley 1952) (Plate 2). The upland area is dominated by hardy grasses, heather and arctic and alpine plants. There are many reasons why the Pennine treeline is so low at present compared with treelines in other upland masses (see Taylor 1965, Tranquillini 1979, Leffler 1981). Not all the reasons are climatic. The low treeline and rapid decline in apparent potential for agricultural cultivation and tree growth in Northern England mean that the area exhibits a steep gradation in habitats according to altitude, equivalent to latitudinal differences over the whole of Britain. For example, many tree species are presently confined to low altitude areas but could migrate to higher altitudes, their upper limits being defined by parameters such as accumulated temperatures (Beerling 1993, Beerling & Woodward 1994). The effects of even slight climate change are likely to be evident in such a sensitive area. Great environmental changes have occurred in the past in the British uplands (Lamb 1982), as were considered in section 1.2. Anthropogenic influences on upland environments have been influential but the major reasons for the marginal nature of much of the Pennine area for agriculture and tree growth are climatic.

The high Pennines possess a sub-Arctic climate due to their position on the globe where the mid- to high-latitude westerlies are strong. The pronounced maritime climate, with cool windy summers and mild wet winters (for the latitude), is largely due to the influence of the North Atlantic which warms Britain in winter and has a cooling effect in summer. One of the major features of a maritime climate, as well as a subdued annual temperature range (Driscoll & Yee Fong 1992), is a relatively steep lapse of air temperature with altitude. The rate of decrease of temperature with altitude is commonly referred to as the **lapse rate**. Lapse rates in the unstable maritime air crossing Britain from the Atlantic are among the steepest in the world (see Table 2.1). This is especially so for air of polar origin (Harding 1978, 1979a) which is warmed from beneath as it moves south towards the British Isles.

It is the steep lapse rates in maritime air and the small seasonal swing in temperature characteristic of an oceanic location which together combine to contribute to a dramatic decrease in the length and quality of the growing season with altitude (Manley 1945a). This rapid decline is given by many authors as the explanation for the low British treeline (Bilham 1938, Pearsall 1950), although to be strictly accurate other influences of topography, drainage and lack of shelter are contributory factors.

Figure 1.1 illustrates characteristic temperature curves for maritime and continental locations (after Pearsall 1950). Both show an annual temperature trend typical of the temperate zone in the Northern hemisphere (case A), but the annual temperature range is much greater at the continental location. A decrease in mean temperature of x°C (as would be experienced by an increase in altitude) is represented by curve B and leads to a greater decrease in the area above the critical temperature threshold for growth, represented by the dotted line D, in the maritime case where the annual march of temperature is rather flat. The length of the growing season is defined as the period when mean temperatures are above the threshold (the arrows alongside the x-axis represent this period) and this also shows a greater decrease for a given drop in temperature in the maritime case. Thus given similar lapse rates, the decline in the length and strength of the growing season with altitude is more rapid at the maritime location.

The primary reason for the marginal nature of much of the Pennines is therefore the lack of real summer warmth (Parry 1976). In a more continental climate the length of the growing season and, in particular, accumulated temperatures during the growth period, are often higher despite bitterly cold winters. The very high heat resources of parts of the Chinese agricultural plain (Guoyu 1991) and the Great Plains of the USA are good examples. Screen temperatures above 20°C in the high Pennines are rare, occurring on 23 days in 1989 at Widdybank Fell (513 m) in one of the best summers on record, but on only 5 days in a cool, wet summer such as 1985. The number of "summer days", defined by Perry (1968) as days with a maximum temperature of 25°C or above, is extremely low in Northern England, even in low-lying areas. Substantial increases in the mean annual number of "summer days" may occur, however, with

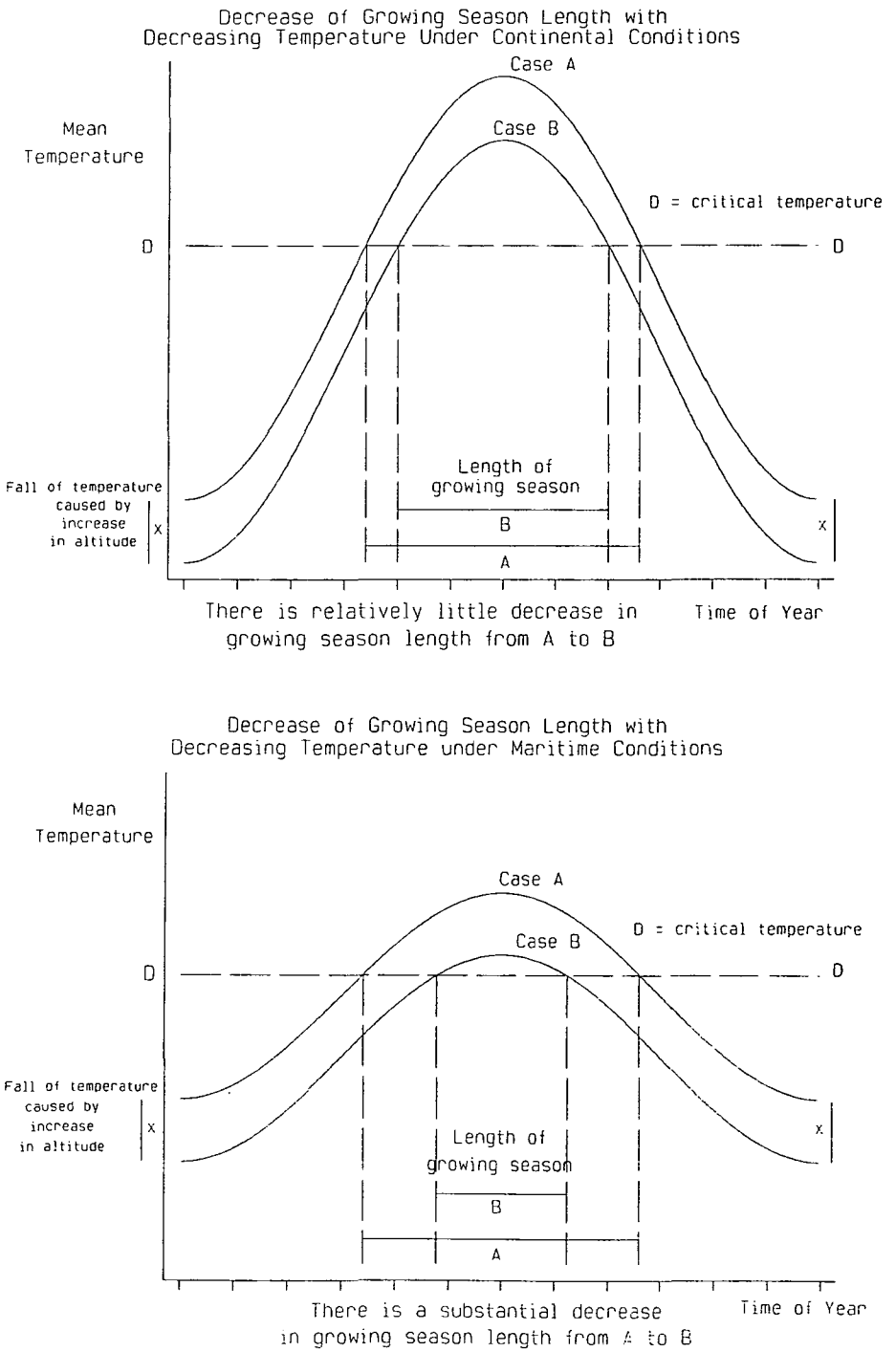

Figure 1.1 Changes in the Growing Season with Fluctuations in Mean Temperature at Maritime and Continental Locations

relatively slight global warming in such areas.

It is useful here to introduce the concept of climatic **marginality**. Near to the boundaries of successful cultivation there are areas which in a good or average year would experience enough warm weather for crop growth, but in a poor year would not. These areas are referred to as **marginal**. Areas where the climate nearly always falls short of requirements are defined as **sub-marginal**. Land may change category as the climate alters, either beneficially or detrimentally. In the Pennines a large amount of sub-marginal and marginal land occurs at relatively modest altitudes (see Chapter 18). Manley suggests that much of the uplands are climatically marginal from his work using Moor House (560 m), Great Dun Fell (847 m) and Widdybank Fell (513 m) as reference stations (1935, 1936, 1942, 1943, 1952, 1980).

In a wet and cloudy summer month, such as July 1936, the loss in a theoretical crop yield in the uplands will be far greater proportionally than at low altitudes. In such a month the aggregate deficit in mean temperature will usually be greater on high ground than at sea-level (Manley 1952). In a dry and warm anticyclonic month with little wind the temperature on high ground approaches more closely that of the lowlands (Harding 1979a, Tabony 1985). Thus two or three weeks of warm dry weather at the right time are beneficial in the lowlands but proportionately more beneficial in the uplands. The contrast between potential upland yields in different years can therefore be marked, reflecting a much greater variation in accumulated temperatures from year to year and increasing risk for the upland farmer (see Parry 1976).

Although summer temperature is the main limiting factor for widespread crop development in the Pennines, there is also a lack of insolation due to incessant cloudiness (especially in wet summers dominated by frequent depressional activity), frequent waterlogging due to high rainfall, and lack of shelter from strong winds. All these detrimental factors are exacerbated in summers dominated by a progressive westerly flow from the Atlantic. Were this maritime flow to be reduced in frequency through anticyclonic blocking, the uplands would benefit through decreased lapse rates, more solar radiation, less rainfall and less wind. The marginal nature of much of the

Pennines is therefore strongly linked with the maritime influence, the character of the seasons being greatly influenced by the airflow pattern across the British Isles. The work in this thesis examines the response of the Pennine environment to changes in general circulation patterns and warming trends simulated by GCMs. There would be a pronounced effect on the temperature resource, especially if spring and summer temperatures were to increase. It can be assumed that cooling trends would have a reverse effect.

1.4 Structure and Aims of the Thesis

The question addressed is whether there is likely to be marked change in the temperature resource and its altitudinal variation in the Pennine area, assuming certain climate changes. These changes may be in the temperatures associated with certain airflows or in the airflow patterns themselves. It is important to stress that the thesis does not attempt to predict land-use change (see Hulme et al. 1993b) in the Pennines, merely to show the sensitivity of maritime uplands to climate fluctuation and airflow changes, past, present and future.

The main aims of the thesis are:

1. to describe and model the temperature field in the Pennine region and account for its temporal and spatial variation. This involves the creation of a detailed climatic database for the North of England;

2. to analyse, in particular, the spatial and temporal variation of the altitudinal temperature gradient in the study area;

3. to use the above knowledge to relate the climate of the area to the circulation pattern occurring and provide a bridge between global scale circulation (simulated by GCMs) and local scale climate;

4. to develop parameters describing "growth potential" in the Pennines and

surrounding area and account for their changing relationship with altitude;

5. to examine evidence for past changes in "climatic potential" parameters;

6. to examine possible future changes in "climatic potential" parameters and develop scenarios for change applicable to high quality GCM data.

With these aims the thesis is divided into three main sections.

Part 1 (Chapters 1-4) contains chapters on the relevant literature concerning lapse rates of temperature, the physical background to mountain climatology and temperature prediction, a description of data sources and methods of analysis.

Part 2 (Chapters 5-9) begins by describing the temporal variation of the altitudinal lapse rate between Durham in the lee of the Pennines (102 m) and Widdybank Fell (513 m), one of the few reliable upland stations, and examining the physical factors behind this variation. Estimates of the gradient of air temperature and hence the growth potential gradient based on two stations alone can be misleading (Harrison 1974) and so, in Chapter 6, the analysis is extended spatially to include other stations. Chapter 7 is an attempt at generating a physical model to account for the spatial temperature field in the Pennines. Although the energy balance equations make intuitive sense, the wide variation in apparent solar efficiency which results suggests that a statistical approach to modelling the temperature field would be more useful.

Chapter 8 describes the development of a multiple regression model of surface maximum, minimum and mean air temperatures. The variation in coefficients between airflows and different months of the year is considerable but appears to make climatological sense, and R^2 values for the regressions are acceptable in the majority of cases. The final chapter in Part 2 uses the regression model to describe the altitudinal zonation in the Pennine area based on temperature data. The altitudes of certain strategic isotherms are defined. A comparison of the Pennines with more continental mountain ranges such as the Pyrenees (Del Barrio et al. 1990) and the Polish Tatra

(Niedzwiedz 1992) completes this description.

The remainder of the thesis (Part 3) is concerned with application of the regression models developed in Chapter 8 to description of the altitudinal variation in growth parameters and simulation of change in these parameters associated with greenhouse forcing.

Chapters 10-12 are concerned with the definition of suitable parameters. Typical rates of change of growing season length, strength (as measured by accumulated temperatures), frost occurrence, probability and length of the frost-free period with altitude are described, based on data from 26 stations for a sample six year period (1985-1990).

Chapters 13-15 introduce the importance of the general circulation in determining surface climate. Scenarios are constructed for each airflow type which is assumed in turn to dominate the circulation for a whole year. Interesting contrasts in the altitudinal variation of growth and frost parameters between these uni-directional airflow scenarios illustrate the importance of the airflow effect. Critical altitudinal thresholds are defined as theoretical upper limits to widespread cultivation. Evidence for past change in limits is evaluated on the timescale of instrumental records. The Durham temperature series (1801-present) is invaluable, allowing tentative reconstruction of altitudinal limits to growth back 190 years (Chapter 15).

Up to this point the climate scenarios are developed using expected mean conditions for each airflow. However variability is inherent in any real climate. Chapters 16-17 introduce variability in the form of a calculated standard deviation of daily temperatures, allowing a more accurate simulation of the range of variation of expected growth parameters and frost accumulation totals for each airflow component.

The GCM output from two high resolution models is used in Chapter 18 to simulate possible effects of greenhouse forcing on growth potential at all altitudes. Simulations for a world in which carbon dioxide concentrations are twice the present

value are used, derived from UKHI (United Kingdom Met. Office High Resolution Equilibrium Experiment) (Viner & Hulme 1992) and GISS (Hansen et al. 1984) models. These are compared with arbitrary temperature increases (+1°C, +2°C and +4°C), warm and cold analogues, and the control situation, in terms of the amount of marginal, sub-marginal and cultivable land and the altitudinal movement of the critical 1000 d°C isotherm. Considerable changes in the temperature resource of large areas of land, predicted to occur by 2050 for the doubled CO_2 simulations, are on a much larger scale than the changes experienced in the past. It must be stressed that the changes in climate potential predicted cannot be used to show potential land use change per se, as other factors must be taken into account (slope, edaphic, economic, etc.). Other climatic elements are discussed in Chapter 19.

In the conclusion the startling predictions in Chapters 18 and 19 are put into perspective and the methodology used evaluated. The extent of possible change and the apparently high sensitivity of the Pennine area to climate change are surprising and perhaps alarming.

There are also lessons to be learnt in the use of present day statistical models of the climate of a region as an aid to prediction of mesoscale climate change through the downscaling of coarse resolution GCM output. The methodology in this thesis can be applied to altitudinal gradients of any climate element (not just temperature) and could be applied when the differentiating factor was not altitude but say distance from the coast on a flat plain. The only assumption is that the spatial distribution of the climate element examined remains constant for an individual airflow in the future climate, i.e. local climate relationships are assumed to remain unaltered for all airflow scenarios. The methodology could be used to estimate changes in freeze-thaw cycle frequency for geomorphological applications, frost probabilities, water stress, drought severity or irrigation requirements, or to estimate changes in any climatic index which is dependent on surface weather observations.

LITERATURE REVIEW: LAPSE RATES

2.1 Introduction

The first half of the thesis describes how a statistical model was constructed to describe the spatial variation of surface temperature under contrasting airflow types. The altitudinal variation is of fundamental importance and the temporal and spatial variation in temperature lapse rates is analysed in detail over the whole region. This review concentrates therefore on studies concerned with the investigation of lapse rates throughout the world and the influence of individual factors on lapse rates measured between ground-based stations. Other literature, including that concerning temperature modelling (energy balance models and statistical approaches), climatic change, synoptic climatology, quantification and evaluation of growth potential is discussed in the relevant chapters.

2.2 Studies of Temperature Lapse Rates

Many authors have investigated variations in the lapse rate of air temperature, both in the free atmosphere and using ground-based data in mountainous regions. The rate of decrease (or occasionally increase) of temperature with altitude determines the stability of the air mass and hence associated weather creation in mountain areas, and so is very important. Detailed knowledge of lapse rates is required in many research areas, enabling investigation into the energetics of mountain areas (energy balance), the variation of climatic parameters (such as those representing agricultural potential) in mountains, temperature prediction per se, climatic reconstruction, ecological considerations and hydrological or glaciological studies in mountain areas. Lapse rates derived from numerous world-wide studies are listed in Table 2.1.

A critical lapse rate to bear in mind is the **dry adiabatic lapse rate (DALR)** (-9.8°C/km), the rate at which unsaturated air will cool if forced to ascend, without loss of heat to the immediate surroundings. Environmental lapse rates are in most cases less than this due to the effects of condensation, upland heating and sporadic

temperature inversion formation (see Chapter 3).

Table 2.1: Examples of mean lapse rates (°C km^{-1}) of mean daily temperatures calculated over hundreds of metres.

REGION	SEASON	LAPSE RATE °C km^{-1}	AUTHOR
Great Britain	Annual	8.5	Harding 1978
"	Spring	10	"
"	Winter	6-7	"
Mt.Fuji	February	6.1	Yoshino 1966
"	November	5.4	"
Austrian Alps	Winter	5.75	Hann 1906
"	Summer	7.45	"
Colorado Rockies	Winter	3.95	Doesken et al. 1989
Himalayas	September	5-6	Reiter & Heu - berger 1960
French Alps	July	6.4	De Saussure 1788
Nepal	May August December	6.55 5.4 4.7	Lambert & Chitrakar 1989
Pakistan India	July	10 (arid)	Brazel & Marcus 1991
"	"	8 (humid)	"
W.Virginia	July December	6.61 5.23	Pielke & Mehring 1977
Tatra Mts	Annual	4.8	Niedzwiedz 1992
Ahaggar Mts	January	5	Yacono 1968
"	July	8	"

Lapse rates were measured in the Alps as early as 1788 by De Saussure (Barry 1978) but one of the earliest detailed studies of lapse rates on mountain slopes was that of Hann (1906) who calculated the following mean values between Kolm Saigurn (1600 m) and Sonnblick (3106 m) in the Austrian Alps:

Winter	**-4.9°C/km (2 am)**	**-6.6°C/km (noon)**
Summer	**-6.0°C/km (2 am)**	**-8.9°C/km (noon)**

The lapse rate in this case was greatest by day and in summer, a pattern repeated in many other mountain ranges.

2.2.1 Diurnal Variation in Temperature Lapse Rates

The diurnal variation in lapse rate has been widely illustrated in Britain (Smith 1952, Harding 1978, Johnson 1985). Lapse rates of daily maximum temperature are considerably steeper than rates for daily minimum temperatures in the same area. This is because temperatures at night are less related to absolute altitude and can fall exceptionally low in valleys where cold air collects as a result of **katabatic** flow. Therefore local topography can allow temperature inversion formation at night, leaving ridge sites relatively warm (Pedgley 1979) and reducing (even inverting) the lapse rate below that recorded during the day.

In Balquhidder Glen in Scotland mean lapse rates in 1983 were -10.2°C/km for maximum temperatures but only -7.3°C/km for minimum temperatures for this reason (Johnson 1985). Similarly, in Wales a mean lapse rate of -6.7°C/km hides a strong diurnal variation (Smith 1950, 1952). Because of the relative increase in minimum temperatures on ridge sites and the increased influence of the ambient air at high altitude, diurnal temperature range usually decreases with altitude. Linacre (1982) shows a decrease in diurnal temperature range between 750 m and 3400 m from a detailed analysis of global data, supported by a simultaneous increase in windiness and cloud cover.

2.2.2 Seasonal Variation in Temperature Lapse Rates

There is also a strong seasonal variation in mean temperature lapse rates in most mountain areas (Yacono 1968, Barry 1973, Harding 1979a, Green & Harding 1980, Lambert & Chitrakar 1989, Pepin 1990, Eden 1991). In general, lapse rates in temperate latitudes are steeper in summer because of the increased solar input, longer days and a reduced tendency for temperature inversion formation. Barry (1973) found summer lapse rates to be steeper than winter ones when examining a climatic transect in the Colorado Rockies. In West Virginia the steepest mean lapse rate of -6.61°C/km was recorded in July, while the shallowest (-5.23°C/km) was recorded in December (Pielke & Mehring 1977). The example of Hann (1906) in the Alps has already been mentioned. In the Polish/Slovak Tatra Mountains intense radiation inversions reduce mean lapse rates in the winter months (Niedzwiedz 1992). The mean annual rate is reduced to only -4.8°C/km because of winter temperature inversions.

A similar seasonal fluctuation in mean lapse rate was discovered in the sub-tropical Ahaggar mountains. The mean rate reached -8°C/km in July, but was only -5°C/km in January (Yacono 1968). In the Nepalese Himalaya the seasonal fluctuation in lapse rate is strongly modified by the monsoon. Mean lapse rates peak in May at -6.55°C /km when the solar radiation input is strongest (Lambert & Chitrakar 1989). By August the mean rate has fallen to -5.4°C/km because of excessive cloud and rain, releasing latent heat in the mountains. There is evidence of a slight increase in lapse rate in September and October with the retreat of the monsoon. Reiter & Heuberger (1960) recorded mean lapse rates of nearly -6°C/km in the autumn of 1954. By December the rate has fallen to -4.7°C/km (Lambert & Chitrakar 1989), presumably due to the influence of winter temperature inversions. At this subtropical latitude the reduction in mean lapse rate in winter is less marked than further north. A mean winter lapse rate of only -3.95°C/km was recorded by Doesken et al. (1989) in the continental Rockies of North America at latitude 40°N.

In maritime areas of Northern and Western Europe the maximum lapse rate occurs in spring. Harding (1978, 1979a) showed this to be true for Britain and the

Northern Pennines in particular. The spring maximum, also found in Southern Norway (Green & Harding 1980), was shown to be related to great instability created in the prevailing polar maritime air masses as they moved south and warmed from beneath at this season. Polar maritime air is the dominant air mass influence in Northern Britain (Manley 1952). Mean lapse rates of over -10°C/km in the Pennines in spring are amongst the steepest in the world. This steep decrease in temperature in the maritime uplands is often accompanied by a deterioration in the weather, i.e. increased cloud cover, wind and precipitation (Ballantyne 1983). Lapse rates tend to be steep in unsettled weather since the air is well-stirred in its lower layers. The unsettled nature of the climate of North-West Europe is therefore also conducive to the creation of steep lapse rates.

2.2.3 Synoptic Controls on Temperature Lapse Rates

The lapse rate of air temperature on any one particular day is strongly controlled by the synoptic conditions, namely the **air mass** type present and the local **airflow direction**. The latter will interact with local topography in certain cases (see section 2 e). Weather observations on Cairn Gorm summit in the Grampians (Barton 1987) suggest the occurrence of shallow lapse rates under the influence of anticyclonic conditions in early summer. In winter, anticyclones can produce temperature inversions of up to 15°C between Cairn Gorm (1245 m) and Braemar (330 m). On the other hand, lapse rates are steep for easterly flows of polar continental air, the summit recording extremely low minima on such occasions. Omond (1910), in a similar study of Ben Nevis, reported 205 cases of lapse rates exceeding -10.5°C/km between August 1890 and July 1903, occurring predominantly on sunny afternoons with dry south-easterly airflow between April and June. In this case the lapse rate was derived by comparison with Fort William to the north-west of the summit. The lee effect of the mountain massif is partly responsible for such steep lapse rates under the influence of south-easterly flow. Nevertheless, certain airflows tend to produce higher lapse rates than others because of variations in associated stability.

In general, lapse rates are steeper for cold unstable northerly airflows than for

stable southerly flows (in the Northern hemisphere). This is because southerly flow is usually cooled from beneath as it moves north, gaining stability. Thus Yoshino (1966) showed mean lapse rates on Mt.Fuji in Japan to be related to wind direction. Mean rates were steepest (-6.1°C/km) in February due to the frequent outbreaks of polar continental air in this month, whereas they were shallowest (-5.4°C/km) in November. Lapse rates on the western side of Britain were shown to be greater than in the east due to a contrast in prevailing air-masses (Birse 1971).

In the USA, present day terrestrial lapse rates can be shown to be positively correlated with the frequency of arctic air outbreaks. Thus mean lapse rates increase from south to north (Wolfe 1990) and increase at high altitude. The problem with Wolfe's work is that lapse rates are derived with reference to places at sea-level on the Pacific coast at a similar latitude. Thus coastal/inland influences on temperature are also included in the derivation of the lapse rate, although these should largely cancel out when mean annual (not seasonal) lapse rates are examined. The values of mean annual lapse rates calculated are surprisingly low, i.e. many are between -2 and -3°C /km. This means that paleoaltitudinal estimates of fossil assemblages derived using a terrestrial lapse rate estimate of -5.5°C/km are in error (i.e. too low) (Axelrod 1966). In Britain a contrasting decrease in lapse rate from south to north (Harding 1978) was said to be related to a decrease in solar radiation, which appeared therefore to more than compensate for the increase in the frequency of polar air masses from south to north.

2.2.4 Weather Differences Affecting Lapse Rates

The mean lapse rate on Hawaii was shown to be -5.46°C/km (Blumenstock & Price 1967). However, individual monthly means ranged from -1.85°C/km to -10.93°C/km, depending on cloudiness and exposure to the trade winds. Thus lapse rates in the tropics can be extremely variable, despite subdued air-mass contrasts. Airflow direction is important in this case as it determines whether air is ascending or descending a particular slope. In general, where air is descending mean lapse rates derived from ground stations will be steeper. This produces the classic föhn effect over

a mountain range with warmer conditions on the lee side of the range. In the high country of Kashmir and Ladakh in northern India mean lapse rates in July were shown to be steeper on the arid north-facing slopes of Ladakh than on the humid south-facing slopes of Kashmir, exposed to the monsoon (Brazel & Marcus 1991). Thus the arid Ladakh region benefits from föhn effects in summer with lapse rates reaching -10°C/km (as opposed to only -8°C/km on the windward slopes).

It is difficult to reconcile this with Birse's (1971) findings for Great Britain. Since prevailing winds are westerly one would expect the mean lapse rate to be less steep on the windward westerly-facing maritime slopes than on the more continental easterly-facing lee slopes. However, mean lapse rates are steepest in the western maritime uplands. Similarly, in a study in Oregon/Washington, mean lapse rates were steeper in the marine Cascade range than in the more continental Wallowas and Steens inland (Price 1978). This is possibly due to the increased cloud and rain at high altitude in the Cascades which depresses surface temperature and the treeline to 1700 m. Therefore weather contrasts can complicate ground-based lapse rate comparisons.

2.2.5 The Influence of Topography and Relief on Lapse Rates

Extensive plateaux become warm in summer as the effect of the horizontal advection of cold air is reduced compared with an isolated summit. Intense solar heating can increase lapse rates near the ground in the free-air above the plateau in summer as the high land becomes warmer than the surrounding air (Flohn 1953, Tabony 1985). These steep free-air lapse rates go part of the way to explaining the high ground-based lapse rates recorded on arid plateaux in summer as in Tibet and Ladakh (Brazel & Marcus 1991). Steep lapse rates are also found on occasion at high elevations in arid environments because of the increased solar radiation input. A good example is the increase in mean lapse rate from -4.5°C/km at elevations below 1000 m to -7.0°C/km between 4000 and 5000 m in the Columbian Andes (Snow 1975). The lapse rate in temperature in the Northern Pennines was shown by Harding (1979a) to be positively correlated with the simultaneous gradient in sunshine hours. Solar radiation input greatly influenced the temperature lapse rate, even at relatively low altitudes

(below 1000 m).

The effects of local topography, the type of ground surface and landform on lapse rates have been illustrated by many authors (Richardson 1954, Oliver 1960, Hastenrath 1968, Ludecke & Kuhle 1991). The mean lapse rate is -7.3°C/km in South Wales (Oliver 1960) but actual values depend on the local topography. Topographical effects on temperature are also illustrated by Richardson (1954) and Reynolds (1956) in the Northern Pennines and the Wirral respectively. A lapse rate based on two ground stations alone can therefore be highly temporally variable and unrepresentative of lapse rates in a larger area (Harrison 1974) because of local exposure effects. Many of the lapse rate studies described in this review have involved unrepresentative surface stations which have led to contradictory or inconsistent results. Clearly, a mean lapse rate derived from an analysis of numerous stations is superior to a lapse rate calculated from two stations alone.

Examples of locally steep lapse rates have been illustrated over subtropical desert surfaces when solar input is strong (Hastenrath 1968), and at high altitude in the Himalayas. On the north face of K2 local lapse rates reached -13.8°C/km in one location, contrasting temperatures above a glacier and immediately below (at a névé camp). On the other hand, a rate of -4.4°C was recorded nearby on Mt.Everest over a height difference of 750 metres (Ludecke & Kuhle 1991).

A good example of extreme local differences in ground-based lapse rates is given by McCutchan et al. (1982), who investigated the influence of aspect and elevation on temperature and other meteorological variables on an isolated conical mountain in New Mexico. Because San Antonio Mountain (3325 m) is surrounded by the free-air, it is largely free from the plateau effects mentioned by Tabony (1985) and provides an excellent open-air laboratory for investigating the variation of temperature with altitude. On ten days in September and October 1981 temperatures at screen level were recorded on all sides of the mountain. Local mean lapse rates varied from a positive value (+2.51°C/km) indicating temperature inversion at 11.00 MST (Mountain Standard Time) on the upper north-west slope, to a very high -25.38°C/km on the

lower part of the same slope. Lapse rates above -10°C/km were common, especially during the day on the south-facing slopes of the mountain (exposed to the sun). The mean lapse rate reached -11.4°C/km on the north-east slope at 11.00 MST for no apparent reason.

2.2.6 Summary

The studies above illustrate the wide variation in temperature lapse rates according to the time of day, season, air-mass, airflow direction (whether up or down slope), weather differences, absolute altitude, aspect, local topography, and the type of climate (factors such as aridity and cloudiness). Tabony (1985) summarises lapse rate variation well by listing three major controls:

a. diurnal and seasonal modifications in the free-air lapse rate

b. topography (both local and large scale effects)

c. changes in climate and state of the ground surface (spatial inhomogeneity in weather).

2.3 The Importance of the Free-Air Lapse Rate

Perhaps the single most important influence on a ground-based lapse rate is the lapse rate in the free-air, which, although not the same as the former, is critically important. Free air lapse rates show great variation, partly because any mountain range will alter the energetics of the immediate surrounding atmosphere, often creating its own distinct mountain atmosphere (Ekhart 1948). The decrease of temperature with altitude is not the same as the lapse rate in the free air because the mountain itself can act as a heat source (Yeh 1982, Chen et al. 1985). Studies comparing mountain-top temperatures with those in the free air at a comparable altitude are numerous (Hann 1913, Peppler 1931, Eide 1948, Samson 1965, McCutchan et al. 1982, McCutchan 1983, Richner & Phillips 1984) and in none of these studies has the temperature

difference between the two exceeded more than 4°C at any time. Mountain tops are in general cooler than surrounding air at the same elevation, except around midday in summer when the sun heats the layer of air close to the mountain. Thus Eide (1948) found a mean difference of -2.5°C between mountain and free-air temperatures on Gaustatoppen (1792 m). The difference increased with increasing wind speed. This was supported by the work of Richner & Phillips (1984) in the Alps, who found an increase in the mountain temperature deficit below the free-air with increasing wind speed. Under calm conditions on summer afternoons the mountain top became 2°C warmer than the free air. The studies of McCutchan et al. (1982) and McCutchan (1983), in New Mexico and California respectively, also show mountain summits to be warmer than the adjacent free-air by day and colder by night.

The relative warmth of upland plateaux on calm cloud-free summer days (compared with the free-air at the same altitude) can be considerable (Flohn 1953, Tabony 1985) and leads to the concept of the **mass elevation** effect, stating that mean temperatures on the surface of a large upland massif will be higher than at the same altitude on an isolated peak which is more influenced by advection of cold free-air. This idea has been used by de Quervain (1904) to explain the elevated tree-lines and snow-lines in extensive mountain areas compared with isolated mountain ranges. In incised upland valleys extreme maximum temperatures can be very high for the altitude on calm sunny occasions. A good example is the temperature of over 30°C recorded at Braemar (in a valley) in summer at an altitude of over 300 metres above sea-level (Manley 1978). The mass elevation effect, however, is not always present and the contribution of sensible heat to the mountain atmosphere is generally only effective in summer. Thus Borisov et al. (1958) found that in the snow-covered Tien Shan mountains ground temperatures were less than free air temperatures. They describe an average ground temperature deficit of 1.8°C, even in summer, between 4700 and 7000 m on Pobeda Peak.

2.4 Lapse Rates of Weather Elements Other Than Temperature

Direct solar radiation has been shown to increase with altitude (Harding 1979b,

Lowry 1980, Olecki 1989). The increase is 5 Wm^{-2} per 100 metres increase in altitude on clear days in the Polish Tatra (Olecki 1989). Thus solar radiation intensity increases from 1000 to 1090 Wm^{-2} for an altitudinal increase of 1800 metres. Diffuse radiation decreases with altitude under clear skies (Dirmhirn 1951) but increases with overcast conditions. Altitudinal variation in both direct and diffuse radiation in the Alps depends on season and cloudiness (Sauberer & Dirmhirn 1958). Net radiation usually decreases with altitude, despite the increase in solar radiation, because of the extremely high albedo in many mountain areas (Voloshina 1966, Budyko 1974), associated with the more frequent snow cover.

Soil temperatures decrease with altitude but are less temporally variable with a subdued inter-(and intra-)diurnal variation, especially at depth. This means that the lapse rate of soil temperature is more steady than the equivalent air temperature lapse rate, with soil temperatures responding only slowly to changes in air temperature. The work of Harrison (1975), Green & Harding (1979), Nadelhöffer et al. (1991) and Morecroft et al. (1992) on altitudinal soil temperature gradients is discussed in Chapter 3.

Wind speed was found to vary with altitude in hilly terrain in a complex way in a study of the Lancashire Pennines at altitudes between 230 m and 350 m (Lawrence 1960). The sheltering effects of topography were found to be of much more importance than absolute altitude, complicating any straightforward altitudinal increase in wind strength. Nevertheless, in mid-latitudes mean wind speeds normally increase with elevation as the prevailing westerly airstream becomes stronger. This is not the pattern in the tropics because the trade winds decrease in strength at high altitude (Barry 1992b). If a temperature inversion lies just above the highest summits then a very steep increase in wind speed can be experienced towards the summits due to a vertical squeezing of the air column (Pedgley 1979).

Numerous studies of altitudinal precipitation gradients have shown an increase in totals up to and including the highest summits, at least in temperate latitudes. Osborn (1984) shows a mean increase of 0.2 mm/metre in arid Arizona, whereas Ballantyne

(1983) finds much steeper increases in the wet maritime region of North-West Scotland. In the tropics the gradient in precipitation can be reversed with a decrease above a certain altitude. Parts of the tropical high mountain belts of Africa and South America are extremely arid because they lie above most of the convectional rainfall (Lauer 1975).

Associated with the rapid decrease in temperature and increase in precipitation in the British uplands is a strong increase in both the frequency and the depth of snow cover, especially during the spring months (Manley 1939). On the highest summits snow cover occurs on average on over 100 days per annum whereas 20 days is a more typical figure in the adjacent lowlands.

2.5 Conclusions

The fact that temperature lapse rates are so spatially and temporally variable means that to reduce temperatures to sea-level using a fixed lapse rate (often assumed to be -6.5°C/km) in description of the surface temperature field of a mountainous area can be highly misleading (Pielke & Mehring 1977). Surface temperature models in mountain areas must take the temporal and spatial variation of lapse rate into account. This variation is examined in this thesis for Northern England. Additionally, the relationship between instantaneous lapse rates and synoptic conditions is of the utmost importance if one is to assess the effects of circulation changes on temperature regimes in both upland and lowland areas. Because lapse rates vary between (and indeed within) airflow types, the influence of any change in relative airflow frequencies on surface temperatures will be altitudinally selective, i.e. the pattern of temperature changes will be different at 300 m from that at sea-level. It is theoretically possible for lowland areas to experience warming while neighbouring uplands experience the opposite.

AIR TEMPERATURE AND ITS PREDICTION

3.1 Introduction

The thesis is concerned with the spatial and temporal variation of temperature in northern England and its relevance for derivation of indices describing potential for agricultural growth in the region. The dominant effect of altitude on temperature is especially important and is described through analysis of lapse rates. In order to understand lapse rate variation, the fundamental physical controls of temperature must be appreciated, especially in their relationship to the altitudinal influence. Important controls are discussed in this chapter but such physical concepts are also referred to in the construction of a physical temperature model (Chapter 7) and in the analysis of lapse rate variation (Chapters 5, 6 and 8).

3.2 What is Temperature?

The atmosphere is made up of gases and therefore must obey the gas law relating its pressure, density and temperature:

$$P/(T\times\rho) = constant \quad -----(1)$$

where P = atmospheric pressure, T = temperature & ρ = density.

At a given atmospheric pressure, cold air will be denser than warm air. Air that rises will expand and cool, while air that subsides will warm through compression. This process is **adiabatic** if there is no interchange of heat between the air concerned (usually a hypothetical parcel) and its surroundings.

The temperature of the atmosphere depends on the average kinetic energy of its molecules, which in turn depends on the speed of the molecular motion. Potential energy is available for conversion into kinetic energy through the adiabatic process and

represents the potential of air at a given level in the atmosphere to sink to the earth's surface and warm (dry adiabatically to a potential temperature at 1000 mb). As total energy must remain constant due to the first law of thermodynamics, air temperature must decrease with altitude since potential energy increases.

The Celsius scale (commonly used to represent air temperatures) is fixed according to the behaviour of water. At a temperature of absolute zero (0 K or -273°C) there is no kinetic energy present. There is no upper limit to temperature.

Heat can be defined as "energy in the process of being transferred from one object to another because of the temperature difference between them" (Ahrens 1991, p 53). Temperature change in a substance depends on the amount of heat energy absorbed. The ratio of the amount of heat energy absorbed to the corresponding temperature rise is the specific heat capacity and varies according to substance (Table 3.1).

Table 3.1: Specific heat capacities for various substances- measured in calories required to raise 1 gramme of the substance by 1°C.

SUBSTANCE	SPEC HEAT CAPACITY cal/g°C
Water	1
Mud	0.6
Ice (0°C)	0.5
Sandy Clay	0.33
Dry Air	0.24
Dry Soil	0.20
Sand	0.19

Source: Ahrens (1991).

Heat can be transferred by three mechanisms, those of convection, conduction and radiation, and so in many cases the adiabatic assumption, used when considering rising or falling air, is a gross simplification. Nevertheless, the use of this assumption

leads to interesting conclusions.

3.3 The Atmospheric Response to Heat Input and Consequences for Lapse Rates of Temperature

The heat energy responsible for changes in air temperature originally comes from the sun, 150 million km from the earth. The sun acts as an engine, powering the energy flows in the earth's atmosphere. The sun radiates heat energy outwards in all directions at a rate normally assumed to be the solar constant ($\sim 1300\ W/m^2$). Radiation from any source is proportional to the fourth power of the absolute surface temperature of that source in Kelvin (the Stefan-Boltzmann equation):

$$E=5.67\times10^{-8}\times T^4 \ldots\ldots W\,m^{-2} \text{---} (2)$$

As the sun is so much hotter than the earth it emits much more radiation. However, only one two-billionth of the total solar output is received by the earth. This radiation has little direct effect on the air (about 3% is absorbed in the stratosphere and 18% is absorbed by various gases and water droplets in the troposphere). What passes through the atmosphere, hits the ground surface and warms it. Air above the surface is heated primarily by conduction from below but air is such a poor heat conductor that this process only warms a very small layer of air near the ground. With strong solar input the temperature near the ground is much higher than that one or two metres above. The heated air near the surface therefore expands, becomes less dense and rises, transferring heat energy to the rest of the atmospheric boundary layer through convection. Thus air is heated from below, primarily through convection, and not directly from the sun. Although a mountain surface also warms the air at high altitude, especially when conditions are calm, the air temperature observed is more strongly influenced by that the advection of colder free-air at the same elevation. Temperatures are lower despite the air being 'nearer to the sun'. De Saussure (1796) was the first mountain meteorologist to explain this cause of cold at high altitude (Barry 1978).

In an adiabatic atmosphere for which the ideal gas laws are satisfied, the rate of decrease of air temperature with height, the **lapse rate**, is expected to be -9.8°C/km (McIlveen 1991). This rate, known as the dry adiabatic lapse rate (**DALR**), assumes that air would rise without condensation occurring. In reality such steep gradients are rarely obtained due to saturation. As air rises and cools, its capacity to hold moisture (its saturation vapour pressure) decreases and the air soon becomes saturated. Further ascent will bring about condensation, thus releasing latent heat. Emissions of latent heat are greater at high temperatures, so that the saturated adiabatic lapse rate (**SALR**) is lower at high temperatures. In the low troposphere it can be as low as -5°C/km. Because condensation often occurs with the ascent of air over a mountain range, lapse rates on the upwind side of a range are usually lower than on the leeward side. Relatively higher temperatures for a given altitude are produced on the leeward side.

Superadiabatic rates occur in the first few metres above a heated surface, especially when the solar input is strong and rates of -100°C/km are common. Oke (1987) describes extremely high rates recorded near Rye in Sussex, the highest rates occurring near the ground surface by day in calm weather in spring. -205°C/km was attained in the layer of air between 1 and 15 metres above the ground. The steepest gradient attained in the air layer 47-107 metres above the ground was -42°C/km, well over four times the **DALR**.

Temperature can, in certain cases, increase with height. If this occurs a **temperature inversion** has formed. The inversion layer within which temperature increases with height separates air above and below since no air can rise through the inversion. Air is trapped under the inversion until heating by the sun (or other means) allows the removal of the inversion through mixing (see Plate 3). The most common cause of a temperature inversion is excessive radiation loss on calm and cloudless nights. Temperatures in valley bottoms often fall below those on mountain slopes. Examples of severe local contrasts in resulting minima are given by Richardson (1954), Waco (1968), Bootsma (1976) and Harding (1978). Thermal belts (Chickering 1884, Dunbar 1966) occur where mean temperatures are higher on slopes than in the valleys below or on the summits above. In northern England radiation inversions are most

common in winter when nights are long enough to allow excessive cooling. Cold air can become trapped in canyons or bowl-like depressions. The latter are often referred to as frost hollows. The most famous example of a frost hollow is a dry valley in the Chilterns near Rickmansworth (Hawke 1944), but locally, the Houghall frost hollow is well-known (Manley 1952). A strong wind is required to disperse the stagnating pool of cold air and therefore inversions are most likely when conditions are calm (Austin 1957).

Because of the tendency towards topographically induced temperature inversions the mean lapse rate will be lower in a region with incised topography, where anomalously low temperatures occur in sheltered valleys at night or in winter. Manley (1978) describes data from Deeside to illustrate the severity of winter inversions. At Braemar (300 m) in an incised upland valley, night-time minima have fallen to -27°C, while minima at sites 100 metres above the valley floor were more than 10°C higher on the same occasion.

Other causes of negative lapse rates include warming of air at a high level through descent and compression. Such a high-level inversion is common in anticyclones where the air is subsiding. Summer temperature inversions are rarely low enough to affect temperatures below 800 metres. It is relatively rare for the summits of the Lake District and Pennines to poke through a high-level inversion level in an anticyclone, even in winter (Pedgley 1979) when upper-level inversions are at their lowest. If an inversion does sink low enough, rapid heating can be observed in cloud-free air immediately above, e.g. at Moor House (560 m) on 13 Jan 1940 (Manley 1947).

Finally, advective cooling over a water surface in spring can also produce an inversion (Catchpole 1966), although the local synoptic situation is often critical (Trilsbach 1988).

3.3.1 Factors Affecting Lapse Rates: A Summary

It is useful to summarise the variation in lapse rates by reference to physical factors which vary according to season. Other factors relate to the airflow type and weather experienced at the different elevations.

3.3.1 i) Solar Radiation

An increased radiation receipt in summer encourages steeper lapse rates, especially near a heated surface. This is seen clearly on a diurnal basis within the boundary layer. The vertical temperature gradient near the ground surface is positive at night but strongly negative by day (Oke 1987). In a similar way, lapse rates are often less steep in winter than in summer, because of the shorter days and lower amounts of insolation. For similar reasons lapse rates are generally steeper on sunlit slopes (Brazel & Marcus 1991) unless anabatic winds redistribute warm air upslope (Pedgley 1979).

3.3.1 ii) Wind

Increased wind speeds keep the air well stirred and, whilst distributing heat upwards from the surface layers, also increase ventilation from the free-air at higher altitudes, so that lapse rates are often steep on windy days. Under calm conditions, air may become trapped by topography and at night a temperature inversion may form. If moving air is forced downslope by topography, however, it will warm dry adiabatically. Such föhn winds create high temperatures in the lowlands to the lee of the mountains, with steep lapse rates on the lee slope.

3.3.1 iii) Cloud

Increased cloud cover per se decreases the lapse rate by day but increases it by night by preventing direct solar radiation from heating the ground and by reducing longwave radiation loss respectively. However, increased cloud in mountain areas can lower day-time maxima in comparison with those in cloud-free lowlands, increasing

the lapse rate. Such deterioration in weather in the uplands of northern England is common.

3.3.1 iv) Air-mass

Air flowing from north to south in the northern Hemisphere is inherently unstable, passing from a cold to a warm surface. It will therefore have a steeper lapse rate than air moving from south to north. Arctic air masses gain considerable heat as they move south over the north Atlantic towards Britain. In an analysis by Craddock (1951), the sensible heat gain was 36 cal $cm^{-2}hr^{-1}$ and was supplemented by latent heat gain through condensation.

Steep lapse rates occur on windy days and on days of scattered cloud cover which builds up preferentially in upland areas. Both conditions may be satisfied when polar maritime airstreams cross Northern England from the north-west or west (Manley 1952). In spring, as the air warms from below, the lapse rate can be especially steep. Alternatively, when there is an inversion aloft the increase in wind speed with altitude can be strong, air being squeezed over the mountains as over a weir (Manley 1945). This situation also favours steep lapse rates. Steep lapse rates by day also occur when the lowland station lies in a sheltered valley. The valley sides reflect back solar radiation, increasing air temperature but decreasing longwave radiation loss (Pedgley 1979).

3.4 Temporal Variation in Air Temperature

The air temperature at any location fluctuates on many timescales. Most noticeable are daily and annual cycles. The daily temperature signal can often be approximated by a sine wave with highest temperatures occurring slightly after solar noon. The exact time of the daily maximum temperature depends on whether the sky remains cloud-free all afternoon, and in mid-latitudes is later in summer than in winter. The minimum temperature usually occurs around dawn. A nomograph for predicting air temperature at any time of day, given the daily maximum and minimum and the

hours of daylight, was developed by Linacre (1992) based on the work of Walter (1967) and Evans (1980), assuming no change of cloudiness or wind direction. The minimum temperature was assumed to occur at sunrise and the maximum at 2.30 pm solar time (Linacre & Hobbs 1977). Parton and Logan (1981) developed a model predicting air or soil temperature at any time of day in the American Prairies. The diurnal temperature fluctuation was represented by a sine wave in daylight hours and an exponential decay function during the night, the lowest temperature occurring at dawn.

In northern England, the daily temperature signal is often unclear in winter due to the absence of significant solar input (noon solar elevation is only 11° at 55°N on 22 December) and temperature changes are often the result of advective influences, especially the replacement of polar by tropical maritime air. The latter air mass gains its warmth from the warm North Atlantic current. Air temperature sometimes increases during the evening and night because of its warm-air advection! For the rest of the year temperature is more strongly related to variation in insolation with the time of day.

By day, in summer, cloudiness reduces solar input and decreases air temperature. However at night, cloudiness decreases radiation loss from the earth and usually increases air temperature. The reduction in radiative loss through cloudiness is also significant by day in winter when insolation receipt is weak. Cloudy conditions usually lead to lower diurnal and annual temperature ranges.

There is a lag effect between insolation receipt and temperature response because it takes time for heat energy to be transferred to the air. The lag of surface temperature behind solar radiation over an ocean surface is about two months, while over land it is only one month (Manley 1952). Therefore in spring the sea is relatively cold and in the autumn, relatively warm. Study of the seasonal fluctuation in air temperature shows that warming is delayed in coastal regions (Prescott & Collins 1951, Trenberth 1983). In northern England this is especially true near the east coast, the North Sea remaining cold well into early summer.

On daily and weekly time scales air temperature fluctuates due to the advective

effects of moving air. In Britain northerly winds will generally be colder than southerly winds. Air from the east is warm in summer and cold in winter since it originates over the Eurasian continent. The annual temperature range is greater over cloud-free, dry areas remote from the sea. The concept of an air mass (Belasco 1952) is useful here (see Figure 4.11). Air masses develop within regions of high pressure where air stagnates, such as the polar regions, the Eurasian high pressure cell, or the Mid-Atlantic subtropical anticyclone. Surface temperatures in these air-masses are modified according to the trajectory followed. If the air is cooled from below it becomes stable, inhibiting cloud development. Air temperature often remains relatively high, however, since the air has originated from a warm region. A good example is a stable southerly flow over northern England. Air that crosses the North Sea in spring and summer will also be cooled, leading to depressed temperatures along the eastern coastal strip (Catchpole 1966). Sea-breezes develop along all coasts in summer, encouraged by local temperature contrasts (Brittain 1978).

Wind speed as well as direction can affect the temporal variation of temperature. High wind speeds prevent extreme temperatures from occurring, increasing temperatures at night and decreasing them by day. Occasionally increased wind speeds will lead to accentuated advection if there is a steep local temperature gradient. For example, temperatures could fall if a polar Arctic outbreak became stronger in winter. High wind speeds also accentuate evaporation (Penman 1948) and may increase the latent heat flux relative to the sensible heat flux, decreasing air temperature.

3.5 Spatial Variation in Air Temperature

At any one time air temperature will vary from place to place, although the variation is usually smoother than for other climatic elements (Hopkins 1977).

Latitude is fundamentally important because it relates directly to solar radiation input. Within the study area there is only a slight variation in latitude, but lowland areas in the south of the area, e.g. the Vale of York, will be slightly warmer than lowland areas in the north of the region, especially Northumberland. At a latitude of

55°N, the seasonal variation in the amount of incident solar radiation is among the largest in the world (Driscoll and Yee Fong 1992). The annual temperature range is as small as it is simply because of the advection of warm air over the North Atlantic.

Temperature may also vary with longitude. Although longitude is an indirect factor (it has no direct influence on temperature) it is often a proxy for varying continental and oceanic influences. In Europe, for example, temperatures decrease to the east in winter but increase in summer (Wallén 1970). Longitude has a dramatic influence on temperature when there is a marked discontinuity at the surface such as a land/sea boundary. Because Britain is an island, sea-surface temperatures (SSTs) are particularly important in determining a climate which is much less extreme than annual variations in solar radiation would suggest (Lumb 1961). The islands are bathed by the warm North Atlantic current in winter and cooled in summer, and have as a result one of the most benign climates for the latitude in the world. Moreover, the oceanic influence increases the role of altitude in decreasing surface temperature.

3.6 Other Site Factors which Influence Air Temperature

The aspect of a site controls the amount of incoming solar radiation received, especially in winter when solar elevation is low. South-facing slopes warm up more rapidly and can often support land-use that would normally be seen at a lower altitude, because of the high radiation receipts (Linacre 1992). In east-west orientated valleys, such as the Valais of Switzerland, the contrast between the sunny south-facing slope (adrêt) and the shady north-facing slope (ubac) can become very marked (Grunow 1952). West facing sites receive direct insolation in the afternoon and evening and maximum soil and air temperatures can be high (Oke 1987). East facing sites warm up earlier in the morning but cool earlier in the day. Maximum temperatures (and perhaps minima) will occur later on west facing slopes and are greater.

Exposure also influences air temperature. Sheltered sites receive less solar radiation due to shade from surrounding hills, but lose less longwave radiation for the same reason (Pedgley 1979). Exposure to a certain direction will influence the

temperature response to an outbreak of air from that direction. Hurry (1969) reviews local temperature differences in Glen Nevis, concluding that airflow direction is critical since it determines where föhn effects occur. In sheltered areas the lack of air movement encourages temperature extremes and the lag of temperature behind solar radiation is reduced. Exposure is quantified in Chapter 4 at all sites referred to in this study.

Topography can influence temperature indirectly through the creation of weather contrasts. One example is the influence of a ridge of high land at right-angles to the surface flow. The air will be compressed as it flows over the ridge and the wind speed will increase over the high ground, lowering air temperature, especially if there is an inversion aloft. As the air descends the ridge it will be compressed and warm. Such föhn winds are a common cause of high temperatures in winter in the lee of the Pennines, when surface flow is westerly (Manley 1952, Lockwood 1962, Webb & Meaden 1993). If precipitation occurs over the hills latent heat is released and warming may be even more rapid. The Helm wind is a similar downslope wind flowing from east to west down the steep Pennine escarpment (Manley 1945b). However, the steepness of the escarpment means that the descending air has little time to warm and the violent wind is cold.

Numerous local factors influence surface air temperature. One is soil type. Well-drained sandy soil has a low specific heat capacity and the diurnal temperature range is likely to be high, increasing the risk of ground and air frost. Chalk areas are also usually well-drained and dry valleys often act as frost hollows. Thus lapse rates of air temperature will be influenced by altitudinal changes in soil properties (Taylor 1967b). In Britain, an increase in the extent and thickness of surface peat can lower the thermal conductivity of upland soils. The altitudinal gradient of soil temperature is largest in early summer (May and June) and smallest in early winter, since the waterlogged and well-insulated upland soils take longer to respond to seasonal changes in insolation (Harrison 1975). Green & Harding (1979) found the summer gradient in soil temperature to be considerably steeper than the winter gradient from analysis in Wales (-1°C/km in winter, rising to -6°C/km in summer).

Much energy is used in the British uplands in evaporation over waterlogged peaty surfaces (Calder 1990). Indeed, air temperature can never rise far above 32°C over a waterlogged or water surface, because of the evaporative effect (Priestley & Taylor 1972). Any increase in latent heat flux will reduce air temperature since the sensible heat flux must be reduced. This effect is noticeable over an irrigated surface in desert country (Oke 1987). Night-time temperatures can, in contrast, be higher due to the large specific heat capacity of water.

Related to the amount of evaporation is the humidity of the air. Because the specific heat capacity of moist air is greater than that of dry air, temperature extremes are subdued when the air is moist. A good example is given in the comparison of mean daily maximum and minimum temperatures in the east and west of the U.S.A. In the eastern states of Alabama and Georgia, the mean daytime maximum in July is around 30°C and the minimum around 20°C, whereas in the western states of California and Arizona, at the same latitude, maxima over 40°C and minima below 10°C are common in the same month despite a similar pattern of potential insolation receipt (Ahrens 1991). Cloud cover is also greater in humid areas and direct insolation will be reduced. Convective formation of clouds can be seen as a negative feedback as it reduces incident radiation, causing cooling. Convective cloud development is common in summer and in upland areas it may be the major cloud source. The timing of the daily maximum temperature may alter, as in the high mountain country of Colorado, where summer maxima often occur before noon before cloud build-up occurs (Barry 1973).

The state of the ground surface can be important. Air temperatures will be depressed over a deep snow cover, the high albedo reducing net radiation. This is most noticeable in late winter and spring when solar elevation is fairly high and the potential for warming is likewise high. Dewey (1977) investigated the influence of snow cover on air temperatures in North America. The cooling effect was strongest in spring but negligible in winter. Snow also insulates the ground surface and soil temperatures may remain quite high, although very low night-time temperatures often occur above the fresh clean powder snow, especially when skies are clear (Pennell 1992). Temperatures below -10°C have been recorded under such circumstances in the Pennines after a

heavy snowfall.

Large urban areas also affect air temperature through alteration of the heating and cooling rates in the boundary layer (Lee 1979). The urban area acts as a great storage heater so that towns and cities usually experience higher temperatures than the countryside. This urban "heat island" effect is especially strong at night and when conditions are calm (Chandler 1965). Such heat-island effects are negligible in the upland regions of northern England.

The forecaster takes all the above factors into account when attempting to predict daily temperature maxima or minima, or the temperature at any time of day. With information gathered from previous measurements, the forecaster can usually make an intelligent guess at future air temperatures given synoptic conditions, the time of year, and an understanding of local factors.

3.7 Why is Air Temperature Important?

Air temperature controls heating and air-conditioning costs and clothing requirements. It influences leisure activities and tourism, sporting activity (especially water sports and skiing), food and drink consumption, and much economic activity including agriculture in particular through controls on plant growth. A useful index is that of accumulated temperatures, usually measured in degree days or degree hours (Shellard 1959) (Chapter 10). This index can be used or modified to represent the potential for crop and other plant growth, or any other application which relates to cumulative air temperature.

Temperature also controls respiration, photosynthesis, germination and reproduction and is therefore fundamental to plant and animal life. Plant and animal physiology is concerned with the relationship of species' functions to the external controls of temperature, moisture and sunlight. When studying the relationship with temperature, many scientists use the Q_{10} rule, stating how much faster a reaction will occur for a 10°C increase in temperature (Fitter & Hay 1981). For some plants the

increase can be as much as a factor of 5. Sutcliffe (1977) shows that most living organisms function best at an optimum temperature T_{opt}, represented in Figure 3.1. Either side of this optimum, reactions are reduced and development is slower. **Threshold** temperatures at which plant activity begins, range from 4.6°C to 6°C depending on plant type. As temperature increases the respiration rate will increase as does production of new plant matter. At high temperatures, however, certain enzymes begin to break down causing irreparable damage, so that growth rate decreases. Productivity is therefore highest over an optimum temperature range. The average earth surface temperature of 15°C lies within this optimum temperature range for many species.

In northern England the temperature during spring is important for sheep farming as well as for plant cultivation. Cold wet weather can be extremely dangerous to sheep and young lambs, causing hypothermia and even death. April is an especially critical period (Starr 1981) as lambing is taking place. Low temperatures reduce grass growth and this can cause shortages for grazing, especially early in the season.

3.8 Conclusions

The physical factors and processes influencing spatial and temporal variations in air temperature (especially those influencing lapse rates) have been described. These physical processes form the basis of the modelling in Chapter 7 which attempts to explain in more detail temperature change recorded at a particular place.

Figure 3.1 The Relationship between Plant Growth Rate and Temperature
- Source: Sutcliffe (1977)

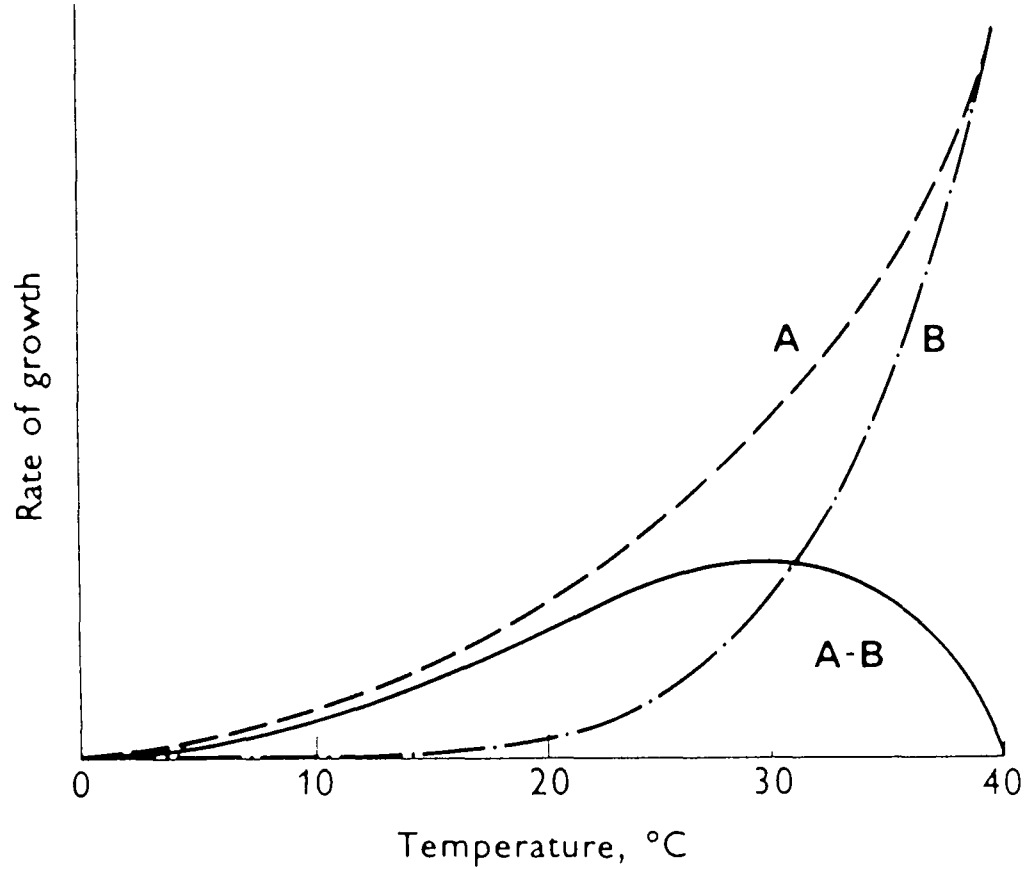

Effect of temperature on the rate of growth of a mesophilic plant. The growth curve (A–B) is the resultant of curve A which represents the increase in activation energy of chemical reactions with increasing temperature and curve B which represents the increasing inactivation of enzymes as temperature rises.

DATA SOURCES

4.1 Introduction: Data Availability

In Northern England, climatic data for recent years are recorded at over forty locations. However, the lengths of the climatic records vary, hindering spatial comparison. The time of observation at all locations must be similar to allow inter-station comparison.

The data used in this thesis consist of surface meteorological observations from 26 locations in the study area, recorded between 1 January 1985 and 31 December 1990. Additionally, the climatic record extending back to 1801 at Durham Observatory is used as well as data from two high resolution global circulation models. Available climatic data for northern England are listed in Table 4.1. Years for which data are available for temperatures, sunshine and wind direction are indicated. All records continue until the present day unless indicated otherwise.

Table 4.1: Climatic data in northern England.

LOCATION	GRID REF	ALT	TEMP	SUN	WIND
AMBLESIDE	NY 378042	90	1964-	1964-**	1964-
APPLEBY	NY 685205	150	1970-	-	1970-
ASPATRIA	NY 154423	64	1979-	1979-	1979-
CARLISLE	NY 382603	26	1961-	1963-	1962-71
CARLTON-IN CLEVELAND	NZ 509039	103	1983-	c	1983-
CARLTON-IN COVERDALE	SE 065847	270	1976-	c 1992-	1976-
DURHAM	NZ 267415	102	1847-	1882-	1847-
ESKMEALS	SD 091935	8	1956-	1979-87	1961-
GREAT DUN FELL	NY 711322	847	1964-	1965-73	1968-

Table 4.1: continued

LOCATION	GRID REF	ALT	TEMP	SUN	WIND
HARTBURN	NZ 407185	31	1958-	1958-	-
HAYDON BR	NY 839646	82	1985-	c	1985-
HIGH CLOSE	NY 338053	175	1981-	-	-
HOUGHALL	NZ 279404	37	1989-	c	1989-
KESWICK	NY 251262	100	1975-	1975-	-
KIELDER	NY 632935	201	1951-	-	-
LEEMING	SE 306890	32	1945-	1945-	-
LW ETHER	NZ 169289	162	1971-	c	1971-
NENTHEAD	NY 781441	470	1987-91	-	-
NEWCASTLE	NZ 258648	35	1967-	1967-	1967-
REDESDALE	NY 834955	235	1970-	1970-	-
SHAP	NY 556121	249	1988-	-	-
SUNDERLAND	NZ 380566	56	1974-	1974-	1980-
WARCOP	NY 734197	244	1985-	-	-
WHASDYKE	SD 434979	165	1981-	-	1981-
WIDDYBANK	NY 817295	513	1968-	1968-	1968-
WYCLIFFE	NZ 120141	120	1989-	-	-
CASTERTON	SD 6379	100?	1990-	c	1990-
HAMSTERLEY	NZ 1156	120	1993-	-	1993-
HIGH HAYRAKE	NY 834479	400	1992-	c	1992-
LEVENS	SD 8886	7	1992-	c	1992-
MOOR HOUSE	NY 758328	560	1941-70	1941-70	-
NR SAWREY	SD 3796	78	1989-	1990-	-
NEWTON RG	NY 492310	171	1960-*	1960-*	1960-*
OUSTON	NY 777259	250	1976-	-	-
PATELEY BRIDGE	SE 1467	155	1983-	1993- (c)	1993-

Table 4.1: continued

LOCATION	GRID REF	ALT	TEMP	SUN	WIND
ROWLANDS GL	NZ 164583	56	1990-	c	1992-
WESTGATE	NY 9138	335	1993-	c	1993-

* Data missing at Newton Rigg, 1983-1991.
** By rough estimation
Four figure grid references are given where the exact site is unknown. None of these stations were used in the analysis. Sites listed after Wycliffe were not used, but are listed for reference.

Daily maximum and minimum temperatures are widely recorded, and often wet and dry bulb temperatures at 0900 hrs GMT. Sunshine data are less common but cloud cover data are available as a proxy at stations marked with a "c". Wind directional data are also uncommon due to the difficulty of measurement. The period chosen for detailed analysis was 1985-1990, data being available at 22 locations for all of this period. Data at another four sites (Houghall, Nenthead, Shap and Wycliffe Hall) was available for part of the six-year period. These sites were not used in the bulk of the analysis. Climatic data for the last seventeen stations listed in Table 4.1 were unavailable between 1985 and 1990.

The 22 meteorological stations used in the description of the present baseline climate of northern England are shown on Figure 4.1. There are two contrasting types of station. The first are official climatological reporting stations, which report to the Meteorological Office, often more than once a day and always at 0900 hrs GMT. The other sites are run by enthusiastic amateurs, many of whom also send data to the Meteorological Office. The data are often more complete, although this depends on the dedication and enthusiasm of the observer. Data accuracy is likely to vary much more at such locations. Although nearly all observers use a standard observing code and practice issued by the Meteorological Office, local biases in the data are only discovered after talking with the observer concerned.

Some locations recorded data to a lower scientific accuracy than others, namely High Close and (in the earlier part of the period) Keswick. At the latter station daily

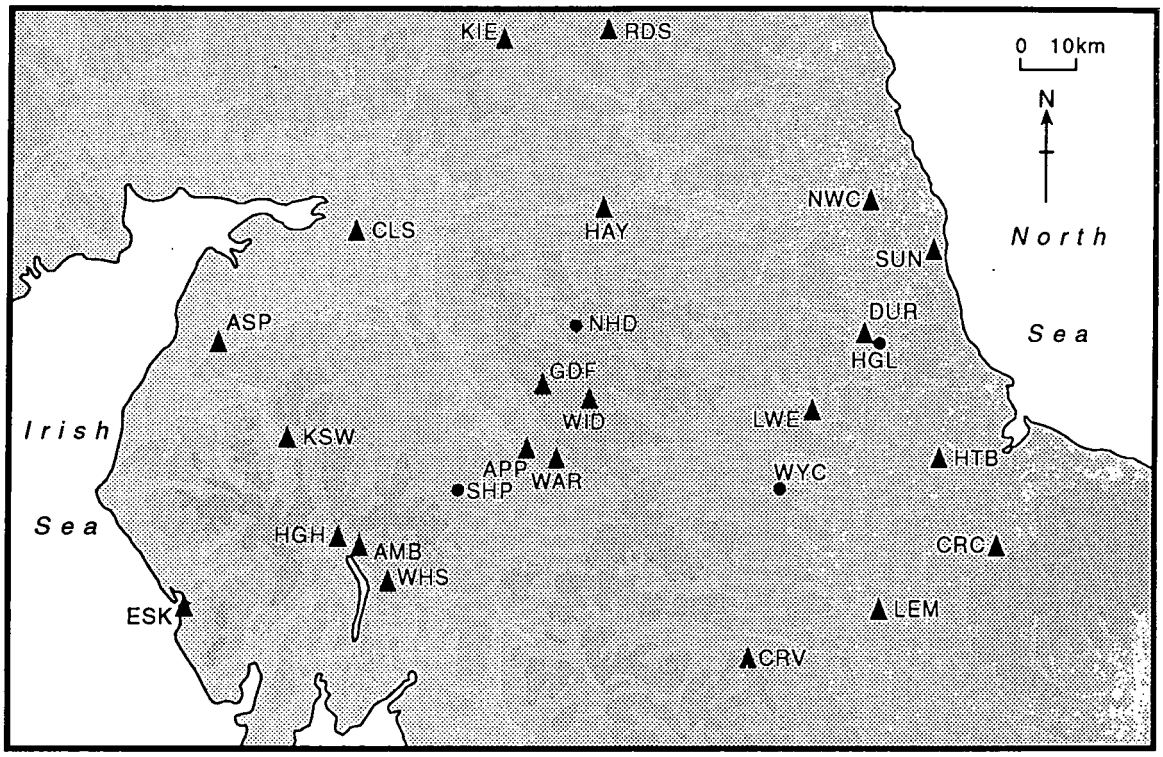

Key to Locations

AMB	Ambleside	90	HTB	Hartburn Grange	31	NWC	Newcastle	35
APP	Appleby	150	HAY	Haydon Bridge	82	RDS	Redesdale	235
ASP	Aspatria	64	HGH	High Close	175	SHP	Shap	249
CLS	Carlisle	26	HGL	Houghall	36	SUN	Sunderland	56
CRC	Carlton-in-Cleveland	103	KSW	Keswick	100	WAR	Warcop	244
CRV	Carlton-in-Coverdale	270	KIE	Kielder Castle	201	WHS	Whasdyke Farm	165
DUR	Durham	102	LEM	Leeming	32	WID	Widdybank Fell	513
ESK	Eskmeals	8	LWE	Low Etherley	162	WYC	Wycliffe Hall	120
GDF	Great Dun Fell	847	NHD	Nenthead	470			

▲ Key station - Data available for all of period (1985-90)

● Data available for part of period only

Figures represent the altitude of the Station in metres.

Land below 122m O.D. 122 - 427m Land over 427m

Fig 4.1 The Network of Climatological Stations in Northern England as used in this Study.

maximum and minimum temperatures were only recorded to the nearest degree Centigrade (not to the nearest tenth of a degree). Missing data is another problem. Many official stations do not take recordings at weekends and on bank holidays. For example, at Great Dun Fell people work only during office hours, and at Carlisle during the last two years of the period this was also the case. Fortunately, methods used in analysis do not require a continuous daily record so the consequence of sporadic missing data is not serious.

4.2 Recording Procedures

Maximum and minimum temperatures were recorded at 0900 hrs GMT. The maximum was relevant to the period running from 0900 hrs the previous day to the time of observation and would be "thrown back" to the previous day. Minima were relevant to the period from 0900 hrs the previous day to 0900 hrs on the actual day and were assumed to have occurred in the early hours of the morning.

Atmospheric temperature is measured by a mercury-in-glass thermometer in a Stevenson screen. The screen is painted white to reflect radiation and faces north, so that when the door is opened the sun does not shine onto the instruments (in the Northern Hemisphere). The screen has louvred sides to allow free air movement. The thermometer is placed to record the temperature of the ambient air in the shade at a height of 1.5 metres above the ground. Detailed reviews of instrumentation and recording procedures can be found in most text books (Linacre 1992). Stevenson Screens should stand above a grass surface although this was not always the case in practice.

A climatic record should be temporally homogeneous with few changes in observing style or at the site. Urbanisation has contributed to the recorded increase in surface temperatures over the last century at many sites (Houghton et al. 1990). Such locations are said to contain heterogeneous climatic records. The urban sites, such as Newcastle and Sunderland, are likely to have experienced the largest changes between 1985 and 1990 although in no case is this thought to be considerable. Changes of

observer or observing practice are less easy to discover although comparison of the data with a nearby location known to be homogeneous can help.

The most serious problem is the lack of meteorological stations at high or even moderate altitude (Taylor 1976). Extrapolation of upland conditions from those in the lowlands is commonly carried out because of the lack of quantitative information on the former (Harrison 1974). The mean altitude is 167.8 m. Only two locations (Widdybank Fell: 513 m and Great Dun Fell: 847 m) are above 300 m above sea-level and these are not necessarily representative of the large amount of land above this elevation. Great Dun Fell, as an exposed summit site, is hardly representative of a wide area. The lack of high altitude stations is shown in Figure 4.2. The median altitude is only 102.5 m, illustrating the positive skewness of station altitudes.

Wet and dry bulb temperatures at 0900 hrs GMT are widely available, and are used in the surface energy balance model of Chapter 7. Sunshine duration is recorded at a few locations. Summer sunshine before 0900 hrs GMT is attributed to the previous day although it would be more useful to have an estimate of sunshine from sunrise to sunset. Wind and airflow data were recorded at certain stations, allowing each day to be assigned to a particular wind direction or airflow type (see section 4.7), enabling spatial comparison of data for varying airflows or synoptic situations (Barry 1967). Wind direction was only available at four locations at 0900 hrs GMT and these values are only loosely representative of airflow over the whole region.

4.3 Choice of Data and Data Storage

Two locations were chosen as broadly representative of the lowland and upland environments in Northern England: Durham Observatory (102 m), to the east of the Pennines, and Widdybank Fell (513 m), a moorland station in Upper Teesdale. Preliminary analysis of the altitudinal temperature lapse rate concentrates on these locations, i.e. a simple comparison of lowland and upland climatic conditions (Chapter 5). The climatic record at Durham is one of the longest and most reliable in the country, running from the 1840s to the present day. Research has attempted to

Figure 4.2. The Distribution of Station Altitudes (Metres above Sea-level)

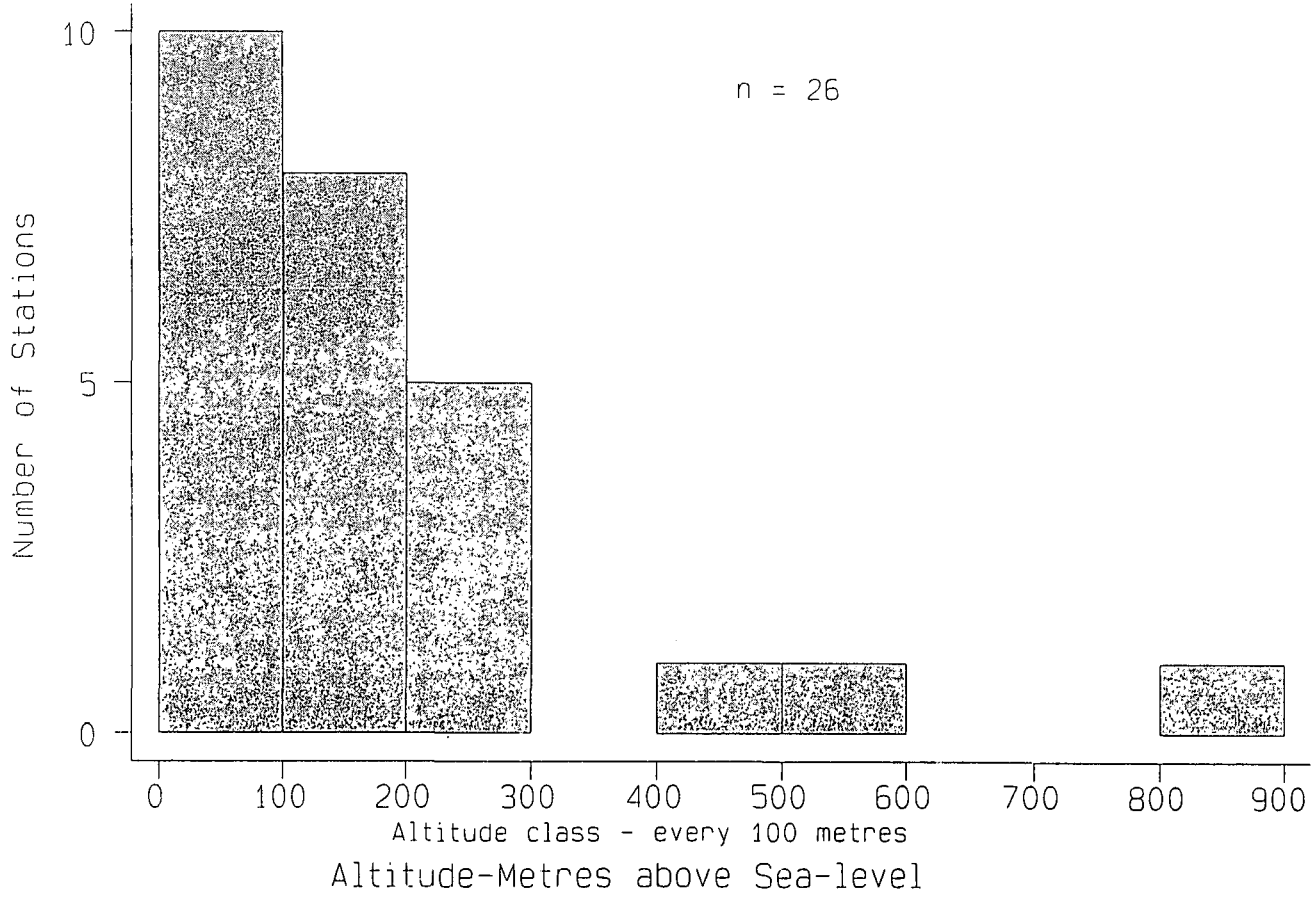

reconstruct the record back to the early 19th century (Manley 1941). The record is therefore important for studies of climatic change, especially since there has been very little urbanisation in the vicinity of the observatory during the last two centuries (Kenworthy 1985). The data have been published in daily format in annual reports back to 1962 and before that exist in manuscript form back to the turn of the century.

Widdybank Fell was chosen to represent the upland environment, it being the highest elevation station for which continuous daily data are available. The record goes back to 1968, before the Cow Green Reservoir was constructed. The climate of the high Pennines is almost completely represented by this station as observations at Moor House (560 m) used by Manley (1942, 1980) have now ceased. A detailed description of Durham and Widdybank Fell, and less detailed descriptions of the other twenty-four sites, are given in section 4.4.

When choosing a number of stations with simultaneous records for analysis, a compromise is required between choosing a few stations over a long period and many stations over a shorter period. A period of six years in length, although fairly short, did allow use of data from twenty-two stations, providing a detailed picture of climate variation throughout the north of England. A period of six years would contain days influenced by most types of synoptic situation at most seasons and a sample size of 2191 daily weather cases was assumed to be adequate to show enough of the variability of the local climate as well as of mean conditions. There is a trade-off between the amount of climate data required to be representative and that which would be practical.

Daily maximum and minimum temperatures, sunshine duration and wind direction (if available) were input to a personal computer. Wind direction was used to classify each day into an airflow category (section 4.7). The statistical program used for most of the work is STATA (Hamilton 1990, 1992).

Wind direction was classified into eight principal directions: north, north-east, east, south-east, south, south-west, west and north-west (Figure 4.3). Raw data had invariably been recorded to the nearest 10°, measured as a clockwise veer from north,

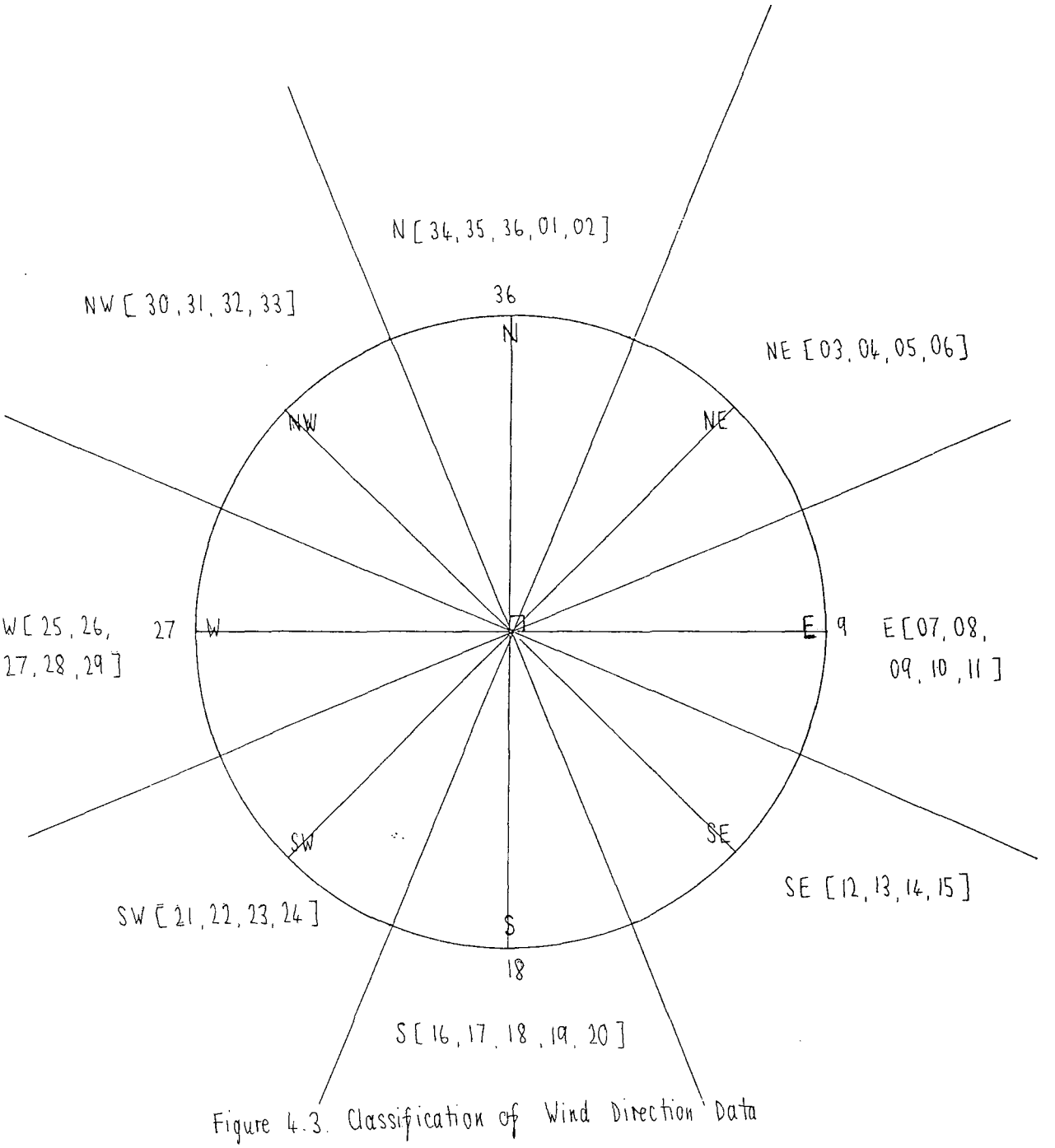

Figure 4.3. Classification of Wind Direction Data

with the final zero removed, e.g. 09 signified an easterly wind blowing from 090°, 00 represented calm, and 36 a wind from due north.

A more comprehensive data set containing variables such as wind speed, wet and dry bulb temperatures, snow cover, the state of the ground surface and cloud cover, was constructed using data from Durham and Widdybank Fell. This was used for temperature modelling in Chapter 7. Cloud cover was measured in eighths or oktas, 0 representing a totally clear sky and 8 an overcast one. The ground was recorded as snow covered if it was thought that snow was covering more than half of the ground surface at 0900 hrs GMT on the day of observation. Snow depth refers to the depth of even snow lying at the time of observation.

4.4 Descriptions of Station Sites

Site characteristics of the Durham and Widdybank Fell stations are described along with those of the other sites. Photographic plates of Durham and Widdybank are given in Appendix 1.

Durham (102 m)

The observatory is situated near the summit of a slight hill, 0.86 km to the southwest of Durham Cathedral, and south of the River Wear (Plate 4). Although the site is within the limits of Durham City, it is essentially suburban. There has been very little urbanisation in the immediate vicinity of the observatory during the last century (Manley 1941), although there has been development of housing to the north and west at Neville's Cross. Between 1985 and 1990, there was very little new construction in the area.

Although the site itself is open and well-exposed, the ridge of land on which the observatory is situated is surrounded by much higher hills. The foothills of the Pennines rise to the west within ten miles, reaching 300 m at Tow Law. The Magnesian Limestone escarpment of East Durham rises to the east between Durham and the coastal

plain. The area is in the lee of the Pennines, sheltered with respect to prevailing westerly airstreams. The observatory is approached from the south by a tarmac road running uphill between open fields. The Stevenson Screen is located on the lawn to the south of the observatory building (Plate 5). The sunshine recorder is situated on a parapet on the observatory roof at first floor level. Trees to the north-east may cut off early morning sunshine in mid-summer. Evidence of this was found in the sunshine record when compared with astronomical values of daylength (Pepin 1990), and with other locations. Wind direction is measured by a Dines Pressure Tube anemograph on the observatory roof at a height of 16 metres (Goldie 1992).

Widdybank Fell (513 m)

This upland station is situated on the gentle slopes of Cow Green Reservoir in Upper Teesdale (Plate 6). The river Tees is one of several rivers flowing east from the "High Pennine" massif. In its upper reaches it flows north-west to south-east and in 1970 was dammed to form Cow Green Reservoir. Widdybank Fell is a lip of high land separating the bowl-like depression containing Cow Green Reservoir from the lower part of Upper Teesdale. Therefore the site is similar to Durham, i.e. it is on a hill but surrounded by much higher hills. The area around the reservoir can trap cold air, escape routes being to the north-west around Tyne Head (552 m) and over Cauldron Snout to the south (Manley 1943). The presence of Cow Green reservoir to the west will moderate temperatures when the wind blows from across the water (Gregory & Smith 1967). The high Pennine escarpment rises to over 800 m to the west and north-west of Widdybank Fell, meaning that the site lies a full 300 metres below the summits of Great Dun Fell and Cross Fell and is somewhat sheltered by the escarpment. There is a complete absence of trees and substantial vegetation; the major species are heather, grasses and alpine flora. Mean wind speeds are likely to be high, there being a lack of shelter.

The aspect of Widdybank Fell is to the west. Hills to the west may reduce late evening sunshine. Despite the presence of higher land all around the location daily sunshine totals on cloudless days seem to be at least as high, if not higher, than at

Durham. In summer the advantage of Widdybank Fell's position with respect to Durham is noticeable as sunshine totals can top 15 hours on cloudless days at Widdybank but not at the lowland station (Pepin 1990).

The other twenty-four sites are described briefly below.

Ambleside (90 m)

The site is within the urban area of Ambleside and the area is very sheltered, the high fells of the Lake District rising to the west and the Kirkstone Pass rising to the east. Aspect is westerly since the site is on a steep rise to the east of the town centre.

Appleby (150 m)

Situated near the east bank of the river Eden in the suburbs of Appleby, the residential garden site is well sheltered. The house lies to the west of the Stevenson screen and at a lower level. Thus the aspect is westerly, although the house provides shelter in this direction. The Pennines rise to the east and the Lakeland Fells to the west of the Vale of Eden.

Aspatria (64 m)

Again this site is in the back garden of a private house. The house is to the south-east of the Stevenson screen and is the end of a terrace, meaning that the site is open to the north and east. The countryside around the station is essentially undulating with a slight rise towards the south and east. The foothills of the Cumbrian fells to the south-east are the only high land within 12 kilometres of the site.

Carlisle (26 m)

The site is well to the north of the city, at the headquarters of Royal Air Force (RAF) Carlisle. The site is on part of the flat estuarine plain of the River Eden near the

Solway Firth. It has a slight southerly aspect with a low ridge to the north. The site is on open grassland, the nearest buildings being over 10 m to the south. It is therefore more open than the sites at Appleby and Aspatria.

Carlton-in-Cleveland (103 m)

Another back garden site, the aspect is north-westerly with the North Yorkshire Moors escarpment rising to 400 m a few kilometres to the south-east. Land falls away gradually to the north towards the River Tees and the urban area of Middlesbrough.

Carlton-in-Coverdale (270 m)

Despite an altitude of 270 metres, the station is well sheltered, on the south-east facing side of Coverdale in the Yorkshire Dales. The dale runs from south-west to north-east so the aspect is south-easterly. Because of the shelter the possibility of a frost hollow effect at night and in winter appears to be strong. High land rising steeply to the north shelters the site from the coldest airflows and the Pennines to the west may reduce cloudiness over the station. The site is on a steep slope with the house at a lower level to the south. Land falls away steeply below the house to the river, 70 metres below.

Eskmeals (8 m)

One of the two coastal sites in the study, this is the lowest site and the only one within two kilometres of the Irish Sea. It is exposed to onshore winds from the west (Brittain 1978) while the high mountains of Cumbria rise to the east.

Great Dun Fell (847 m)

Extremely exposed at an altitude of well over 800 m, it is the only mountain summit site in the study (Plate 7). Land falls steeply away from the station in all directions but especially to the south and west, falling over 600 metres to the relative

shelter of the Eden valley. Because of the extreme exposure, there is little vegetation apart from short grasses grazed by sheep. The nearest higher land is Cross Fell, 50 metres higher and 3.1 kilometres to the north-west. The descent towards Upper Teesdale to the east is more gradual than the descent to the Eden Valley. The site is run by air traffic control personnel based at the radar station at the mountain summit, and is unattended at weekends and during holiday periods.

Hartburn Grange (31 m)

Hartburn is surrounded by fairly flat arable farmland, unusual for the North of England. The Tees Valley lies to the south and east, land falling gradually in this direction. The station is only 16 kilometres from the east coast.

Haydon Bridge (82 m)

This is another sheltered site in a school playground. The Stevenson screen is on a grass bank and is surrounded by hedges. Below the bank to the south is a tarmac play area. The aspect is southerly. High land rises immediately to the north, the site being in a valley bottom and the River Tyne passing within a kilometre of the station. Westerly winds tend to be funnelled along this west-east valley because it is the only break in the Pennine barrier at such a low altitude (Sherwood 1993 - pers comm).

High Close (175 m)

The High Close area forms a miniature col between higher land to the west and east. The terrain falls steeply south and south-westwards to Langdale and northwards to Grasmere. The site is on the south-facing side of the pass and is exposed to air movement, although higher fells surround the area. Due to the south-facing location, insolation levels are expected to be high. Temperatures are recorded by Youth Hostel wardens in the middle of an evergreen bush and are recorded to a lower scientific standard than at most of the other sites (to the nearest 1°C). The results must therefore be treated with caution.

Houghall (37 m)

The site on the flood plain of the river Wear is extremely sheltered and at an altitude of only 37 m. The screen is administered by the agricultural college and is well known for occupying a frost-hollow where low minimum temperatures and high maximum temperatures are common (Manley 1943). Data for this study were only available for 1990 and the station is only referred to for a small part of the thesis. The aspect is slightly to the east.

Keswick (100 m)

This is one of the most sheltered locations with high mountains surrounding the station on all sides. The Skiddaw range rises steeply to the north and east, sheltering the garden site from northerly airflows. This range also cuts off early morning summer sunshine. Mountains rise less suddenly across the valley to the west and south, beyond Keswick. The southerly aspect, combined with the extremely sheltered surroundings, leads to an anomalously warm site for the altitude. Maxima are often the highest in Cumbria. Surprisingly, minimum temperatures also seem to be high for such a sheltered location. The urban influence of Keswick is likely to be negligible as the well-wooded site is rural in character.

Kielder Castle (201 m)

This site is in a valley bottom in Kielder Forest to the north-west of Kielder Reservoir. The upland basin is surrounded by forested hills in all directions, especially to the north and west where the land rises to the Scottish Border. The aspect is southerly since the castle is on a spur of land about 10 metres above the valley bottom. The site is a well-known frost hollow and experiences some extraordinarily low minima.

Leeming (32 m)

The landscape around the site has virtually no local relief as Leeming is situated within the Vale of York. The station, as part of the R.A.F. complex, is one of the few locations in northern England where radiosondes are commonly used to investigate upper air patterns. Leeming is representative of the lowland plain to the north of York.

Low Etherley (162 m)

This is another garden site but is fairly open, on a ridge leading east from the Pennines. Land slopes away to the north and south. There is slight shelter to the west as land rises to about 300 m before falling towards Teesdale. The aspect of the site is northerly.

Nenthead (470 m)

The screen stands on a steep south-west facing slope of an incised valley in the Pennines. Land rises steeply in all directions but especially to the east at Killhope Cross (over 600 m) and to the north. It is a relatively sheltered location considering the high altitude. The land falls to around 430 m in the valley of the Nent so the site is not a valley bottom location. The aspect is strongly south-westerly and the farm buildings are situated to the south and east of the screen. The land on the other side of the valley rises to 600 metres.

Newcastle (35 m)

This is an urban site located on the roof of the Newcastle Weather Centre in Portman Road. The area contains many car parks and disused warehouses in various states of decay. The city centre lies less than a mile away to the south-west and the river Tyne a similar distance to the south. Land rises gradually to the north, peaking around the Town Moor (100 m). The site is unusual in that the screen is at least 10 metres above ground level.

Redesdale (235 m)

The open grassland site on the south-west side of Redesdale faces to the north and east. Hills rise to over 400 metres towards the Scottish border to the north and west, offering some shelter. The site is the furthest north in the study.

Shap (249 m)

The site is in an upland valley, with a south-easterly aspect. High land rises immediately to the west as part of the Cumbrian fells. The automatic weather station is used to give information about the state of the A6 road at Shap.

Sunderland (56 m)

An urban site near the east coast (on the roof of Sunderland University Geography Department), it is similar to that at Newcastle. The roof is at least 10 metres above the ground and conditions will be largely representative of the disturbed boundary layer. There are some higher buildings to the east in the city centre. Despite the shelter on the macroscale afforded by the Pennines, the local area is quite exposed, land falling away rapidly to the east towards Sunderland city centre and the North Sea coast, just over a kilometre away. The coastal influence is very strong and moderates temperature extremes.

Warcop (244 m)

Another automatic weather station, it is situated on the lower slopes of the Pennine escarpment rising above the Vale of Eden. The aspect is strongly south-westerly and the screen is located on part of the military firing range (moorland in character) near the village of Warcop.

Whasdyke Farm (165 m)

This is a privately run station in a field on a sheep farm. The surrounding topography is gently rolling, falling slightly to the north and rising behind the farm to the south. The area around the farm is a neck of relatively high land around 150-200 m above sea-level, separating Windermere in the west from Kendal in the east. The Cumbrian mountains rise to the north and the Coniston fells rise to the west (on the other side of Windermere). There is an open exposure to the north and east at the micro scale.

Wycliffe Hall (120 m)

The site lies on the south side of the River Tees to the west of Darlington in an area of subdued topography. The river valley runs from west to east and at this point is approximately 25 metres below the station. The aspect of the site is northerly. On the macroscale the lower Tees valley is sheltered by the Pennines to the west.

4.5 Quantification of Site Characteristics

Station location, elevation and exposure will be quantified since these site characteristics influence surface temperature. These site attributes are referred to at places in the thesis.

4.5.1. Altitude

Altitude above mean sea-level in metres is one of the most important site attributes and was calculated from the site's grid reference on a Landranger 1:50 000 Ordnance Survey map. Values ranged from 8 metres above sea-level at Eskmeals to 847 metres above sea-level at Great Dun Fell. All altitudes are measured with respect to mean sea-level Ordnance Datum (OD) at Newlyn, Cornwall.

4.5.2. Location

Longitude and latitude define station location and are easy to quantify using six figure grid references. An imaginary origin was placed at the bottom left hand corner of the grid square SD of the national grid system (Figure 4.4). The longitude of a site was measured as the number of kilometre (km) grid squares to the east of this origin and latitude as the number of kilometre grid squares to the north. For example, Durham would have a longitude of 126.7 and a latitude of 141.5 since the grid reference is NZ 267415.

4.5.3. Exposure

The exposure of a site depends on the scale of study. An example of an exposure calculation for a digital terrain model is given by Lapen & Martz (1993). The method used involved comparison of surrounding grid altitudes with the altitude of the site in question. Station exposure in this study was estimated by comparing spot heights at certain prescribed distances from the station with the station altitude itself. An exposed location would be surrounded by points of a much lower altitude whilst the opposite would be the case for a sheltered location. It is always possible that the chosen spot heights (measured with respect to the central site) will be unrepresentative, e.g. the summit of an isolated hill on an otherwise flat plain, although the sample becomes more representative when many spot heights are chosen.

Spot heights were calculated using Ordnance Survey 1:50 000 Landranger maps with a contour interval of ten metres, at distances of 0.25 km, 1 km, 5 km and 10 km from each station. This was done for transects radiating north, north-east, east, south-east, south, south-west, west and north-west. Thus thirty-two spot heights were calculated in relationship to each site. The heights were then converted to relative elevations by subtracting the height of the meteorological station. Relative heights were summed to give the exposure (Table 4.2) at each of the four distances and a total exposure value (all 32 spot heights). The total exposure '<u>extotal</u>' can be divided by

Figure 4.4 Calculation of Station Latitude and Longitude from the National Grid Reference System

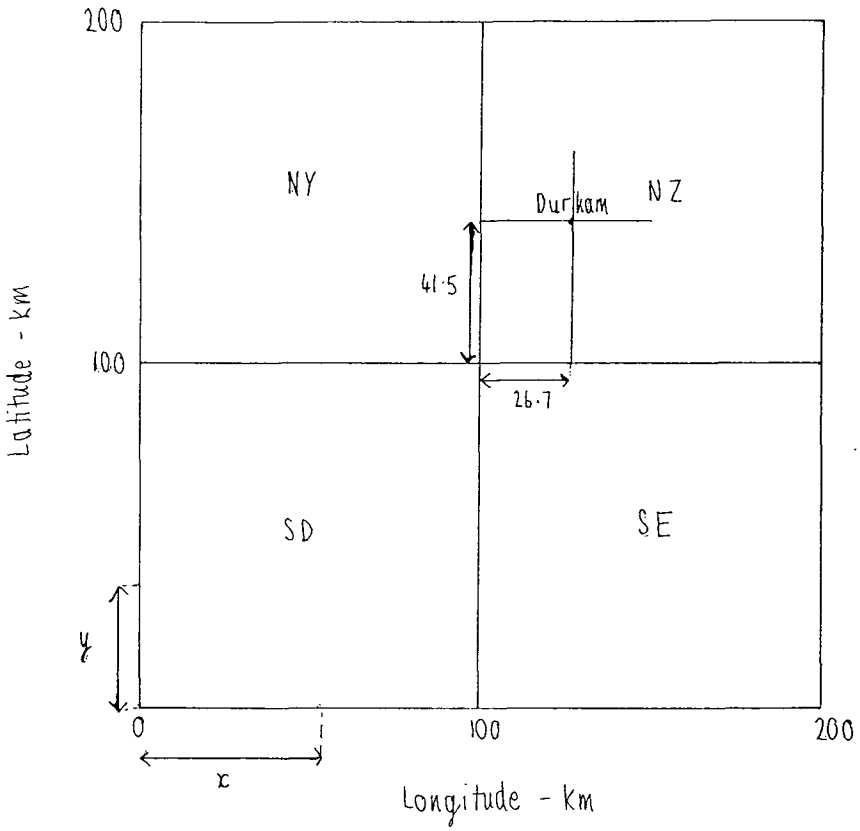

O = the imaginary origin

Longitude is taken as the distance 'x' to the east of the origin in kilomet

Latitude is taken as the distance 'y' to the north of the origin in kilomet

An example is shown for Durham - grid reference NZ 267415

Latitude = 100 + 41·5 = 141 5 Longitude = 100 + 26·7 = 126·7

Table 4.2: Exposure calculation at 0.25, 1, 5 and 10 km. A positive value shows that the site is sheltered.

STATION	ex0.25	ex1	ex5	ex10	extotal
AMBLSD	-75	415	1170	2200	3710
APPLEBY	-19	35	337	1277	1630
ASPATRIA	6	-6	109	318	427
CARLISLE	2	-44	-43	113	28
CARLTON	18	151	477	339	985
CARLTON	40	90	355	495	980
DURHAM	-101	-199	-131	269	-162
ESKMEALS	-13	7	489	656	1139
GT DN FL	-276	-1051	-2671	-3616	-7614
HARTBURN	-11	3	-9	156	139
HAYDON B	69	299	849	941	2158
HIGH CLS	-170	-397	915	2000	2348
HOUGHLL	33	169	464	699	1365
KESWICK	143	770	1463	1135	3511
KIELDER	7	447	967	1168	2563
LEEMING	5	6	71	279	361
LW ETHER	-53	-35	-149	-101	-338
NENTHEAD	-80	265	250	10	445
NEWCSTL	3	-10	272	255	520
REDESDLE	15	30	235	195	475
SHAP	45	245	580	80	950
SUNDLD	-45	-52	-130	-98	-325
WARCOP	-10	-10	590	945	1515
WHSDYKE	2	35	-30	600	607
WIDDYBNK	-38	-114	466	296	610
WYCLIFFE	-33	19	215	954	1155

thirty-two to estimate the average deviation of the spot heights from the station altitude.

Exposed sites have a negative extotal, such as Great Dun Fell (-7614). On the other hand, a sheltered site surrounded by high mountains records a high value, e.g. Keswick (3511). Most locations record a positive value for total exposure, confirming the tendency for stations to occupy valleys and lowland sites (Taylor 1976, Manley 1952). The only exposed ridge/hill-top sites appear to be Durham, Great Dun Fell, Low Etherley and Sunderland.

Exposure at the four different scales varies widely and may even change sign. The sum of the eight values calculated at a distance of 0.25 km from the station represents local exposure (ex0.25). These values remain unaffected by larger scale hill and mountain ranges. In some cases ex0.25 is very different from the overall exposure. Durham for example is a hill-top site, recording a value of -101 at the local scale (0.25 km). Because of high hills surrounding Durham the overall exposure is still only -162 which is almost negligible (an average deviation of 5.1 metres). High Close records a value of -170 for local exposure but 2348 for total exposure, largely due to the limited exposure (2000) at the 10 km scale. Exposures at different distances will be contrasting when a site is on a hill, but surrounded by higher hills, or in an upland depression. Exposure at different scales was found to be important in Chapters 16 and 17 when the variability of temperature was investigated.

Exposures to different directions will also be contrasting. A good example is given by Warcop which is very sheltered to the north and east but exposed to the south and west. When air flow is from a certain direction it is exposure to that particular direction which is often more influential than overall exposure. Table 4.3 gives total exposure values for each of the eight principal wind directions.

Table 4.3: Exposure to different compass directions. Values are calculated by summing relevant elevation anomalies at all scales for the direction concerned.

place	N	NE	E	SE	S	SW	W	NW
AMB	920	920	805	365	30	-25	390	305
APP	235	610	580	3	140	140	7	-85
ASP	-119	-63	147	457	195	-1	-91	-98
CLI	-37	37	23	26	23	36	-48	-32
CRC	-104	-7	498	298	383	109	-76	-116
CRV	60	-180	-50	140	265	360	150	235
DUR	-123	-158	-48	7	32	-53	97	84
ESK	41	204	519	438	13	-25	-27	-24
GDF	-878	-628	-698	-593	-1288	-1548	-1533	-448
HTB	48	-32	-60	10	-1	21	66	-87
HAY	437	92	-21	257	427	327	162	477
HGH	770	630	455	-325	-110	523	145	260
HGL	57	83	168	169	187	97	307	297
KSW	695	1010	505	250	-30	580	305	196
KIE	611	471	406	111	106	421	206	231
LEM	10	21	37	-9	33	92	101	76
LWE	15	-263	-113	-33	-63	50	177	-108
NHD	-265	120	320	110	235	55	20	-150
NWC	50	17	-15	-8	73	215	83	105
RDS	85	-40	-55	-50	170	170	235	-40
SHP	-25	-20	135	-20	200	245	215	220
SUN	-104	-141	-142	-126	146	54	39	-51
WAR	635	775	690	-95	-160	-85	-165	-80
WHS	697	325	-65	-95	-160	-40	100	-155
WID	153	-126	-212	33	243	-32	328	223
WYC	107	-63	-41	110	270	420	192	160

Exposure to the north will be relevant when winds are northerly. When the situation is calm the total exposure, especially at the microscale (0.25 km), is expected to be more useful.

4.6 The Creation of a Digital Terrain Model of Northern England

A digital terrain model (DTM) of Northern England was developed, showing the relief of the area in considerable detail. The relief information is used as a background upon which to plot predicted spatial distributions of climate variables such as temperatures and their changes. Such results are produced later in the thesis.

A grid spacing of 5 km was chosen. Altitudes were measured to the nearest 5 metres (unless more accuracy was required as in some very flat areas) taken from the Ordnance Survey 1:50 000 Landranger Series. Contours on these maps are shown to the nearest 10 metres and the altitude at a certain point would be interpolated between two contours by eye. Figures 4.5 a) and b) show the DTM. The map is split into an eastern and a western section to allow spot altitudes to be easily read. If the data point fell in the ocean, the altitude was assigned as missing (.). In this way the coastline can be discerned. Of 800 spot altitudes, 85 were assigned as missing. Latitude ranges from 80 to 200 (in steps of 5) and longitude from 0 to 155 (also in steps of 5).

The 5 km resolution allows identification of many of the relief features of Northern England. The graphs in Figure 4.6 highlight points above specific altitudinal thresholds, ranging from 100 to 800 m. The relief shown in a few cases is summarised below. Numbers refer to those on the graphs:

Below 100 m:	**1** Solway Firth
	2 Eastern Lowlands
	3 Vale of York
	4 Cumbrian Valleys
Below 200 m: Also	**1** Tyne Gap
	2 Vale of Eden
	3 Central Lake District Valleys
	4 Lower North Yorkshire

Figure 4.5. A Digital Terrain Model for Northern England

The Grid Resolution is 5 km by 5 km: Elevations are given in Metres

North-Western England

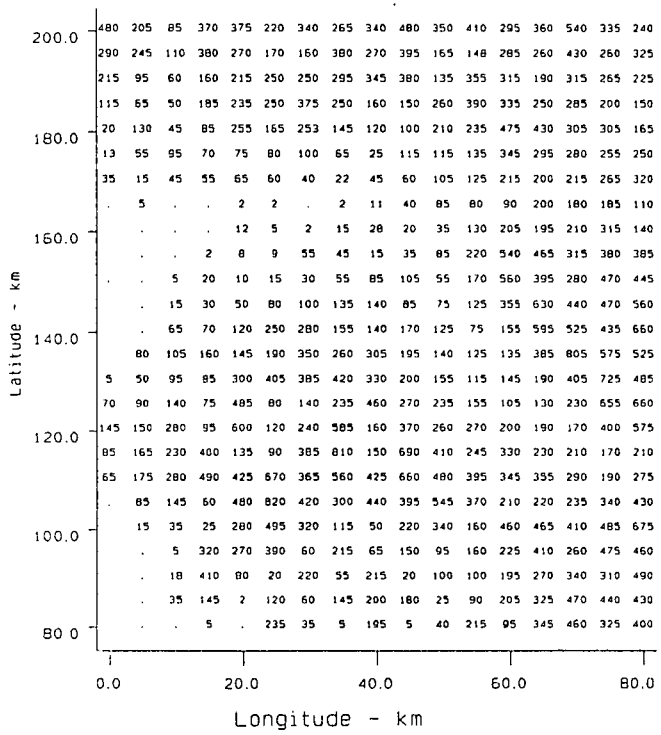

North-Eastern England

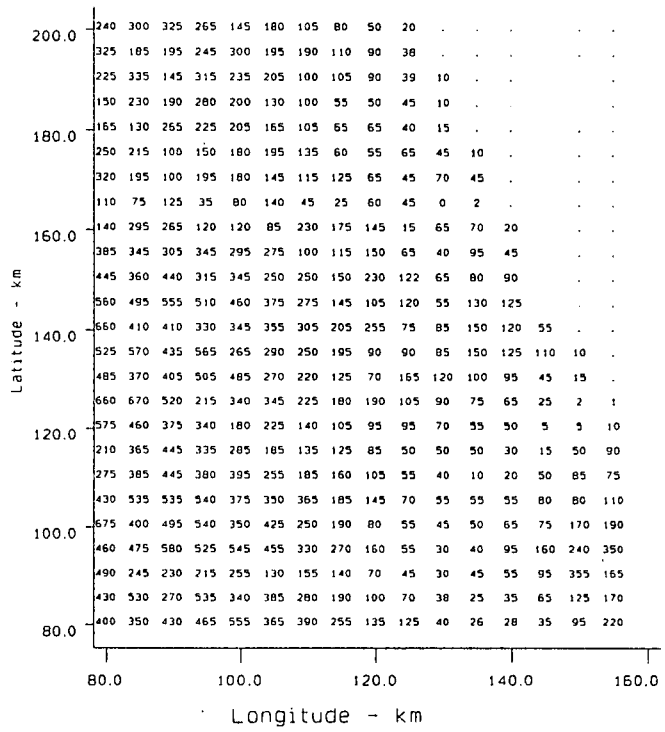

Figure 4.6. Areas above Specific Altitudinal Thresholds in the Digital Terrain Model of Northern England

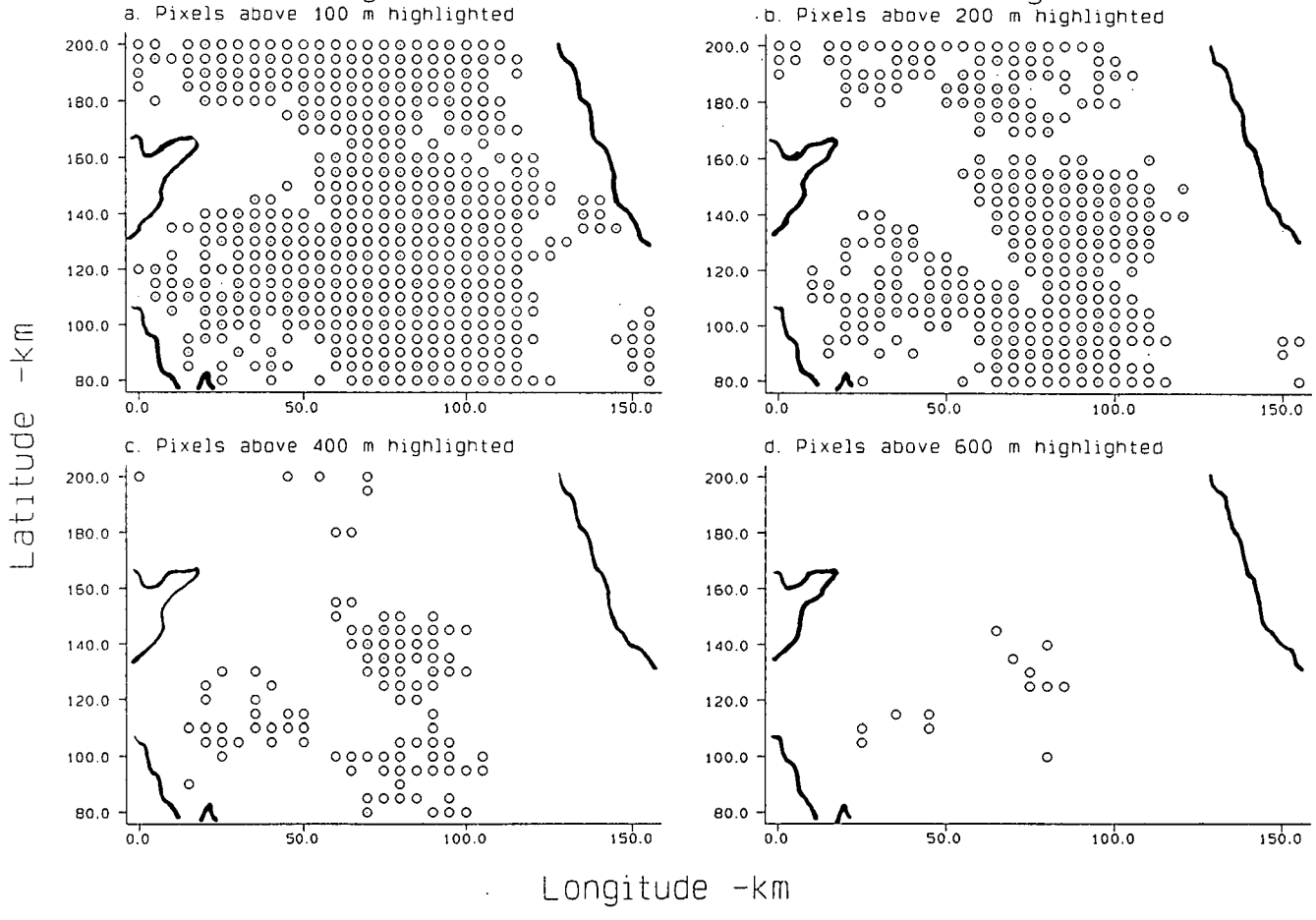

Below 300 m: Also	**1** Wensleydale
	2 Teesdale
	3 North Tynedale
Above 400 m:	**1** Stainmore
	2 Alston Block
	3 Askrigg Block
	4 Cumbrian Fells
	5 Kielder Summits
Above 700 m:	**1** Cross Fell
	2 Scafell and Helvellyn Massifs

Nearly all major relief features are shown, including the High Pennine block to the south and east of Alston. The model is better at showing the smooth relief of the Pennines and N.E England than the incised Lake District topography.

A histogram of grid altitudes (Figure 4.7) shows that the data is positively skewed with more pixels with lower altitudes, (skewness is 1). Individual altitudes range from 820 m to sea-level, and so all but the highest summits of the Lake District (over 900 m) are included in the DTM. The cumulative altitude function is graphed in Figure 4.8. 50 % of the pixels record an altitude less than 170 m. The curve is composed of a series of ascending steps since some altitude values are repeated. We can estimate from this graph the amount of land above or below a certain altitude and this is done in Chapter 10 when critical climatic limits are defined by altitude. The cumulative altitude function is fairly smooth with little evidence of extensive plateaux at any particular elevation. Below 100 m the curve becomes straighter, suggesting that there is just as much land near 100 m as at sea-level, evidence for slope convexity at low altitudes. Table 4.4 summarises the cumulative altitude function.

Figure 4.7. Frequency Histogram of Digital Terrain Model Grid Altitudes
Metres above sea-level: 800 grid points at 5 km by 5 km

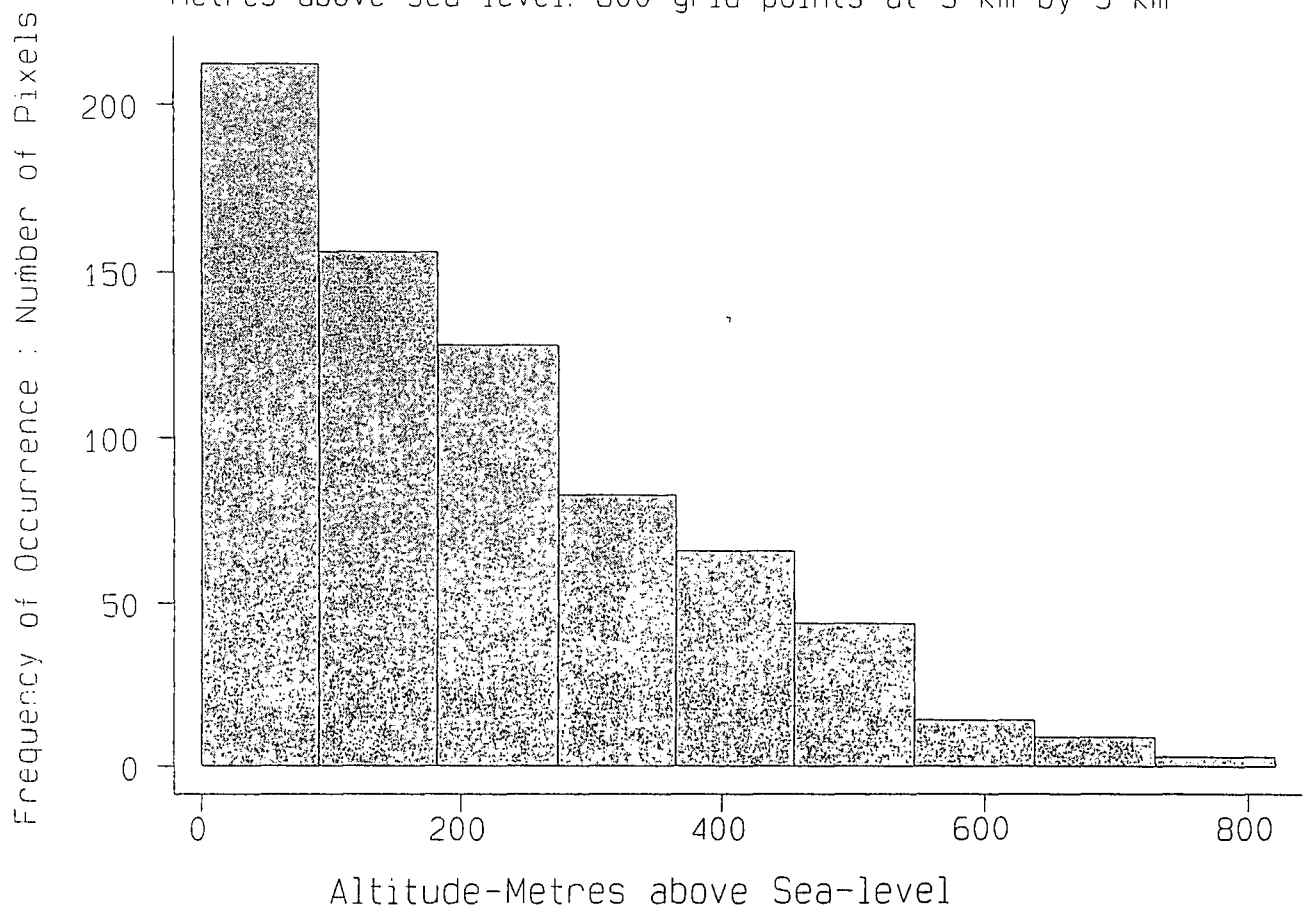

Figure 4.8. The Cumulative Altitude Function for the Digital Terrain Model Grid Altitudes (Metres above Sea-level), Representing the Proportion of Pixels at or below the Elevation Concerned

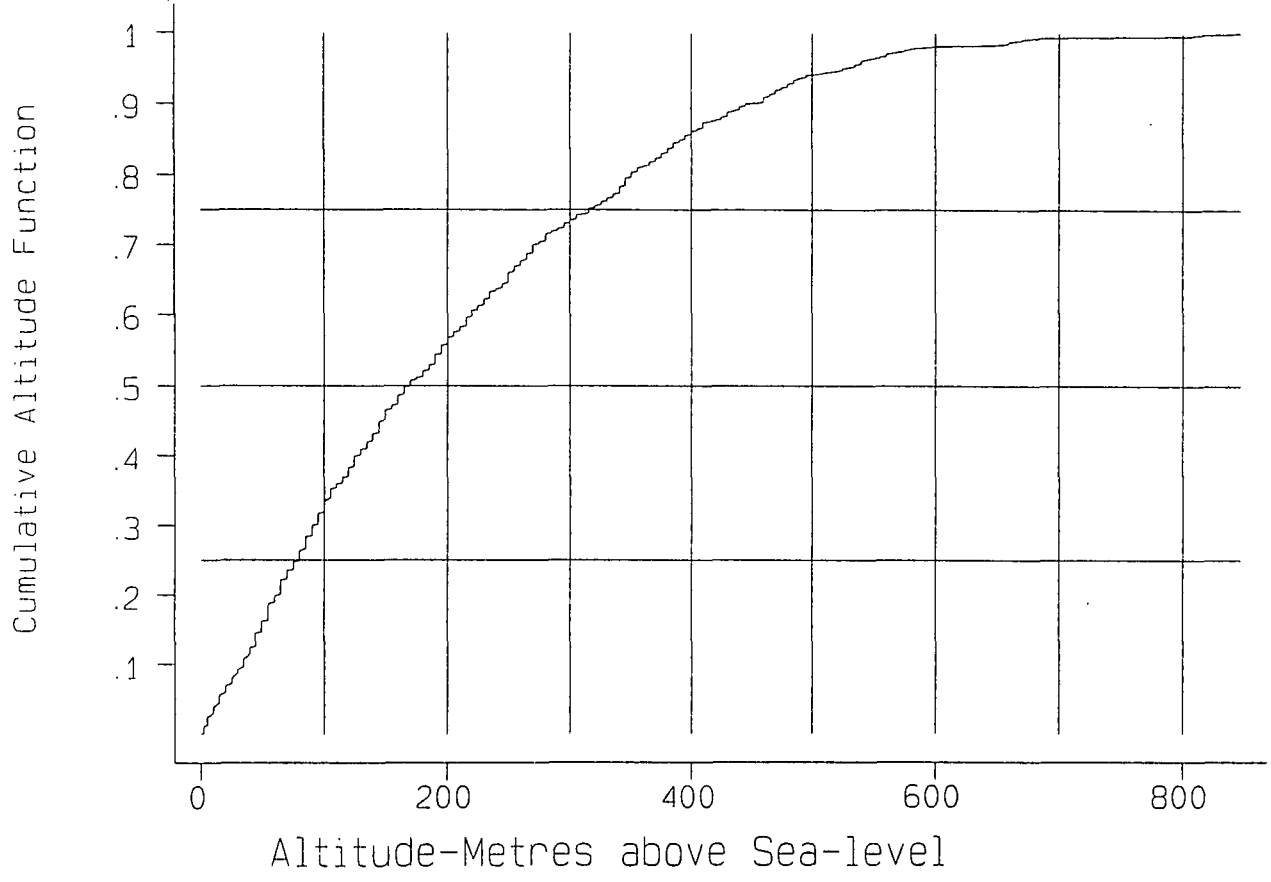

Table 4.4: The cumulative altitude function for land area in northern England.

Cumulative Function (i.e. proportion below this level)	Altitude (metres)
10 %	35
25 %	80
50 %	170
75 %	320
90 %	445
33 %	100
55 %	200
73 %	300
95 %	530

10 % of the land sampled by the DTM is below 35 m. Areas at high altitude are extremely limited. Only 10 % of land is above 445 m and only 1 % above 670 m. The marked skewness of the altitudes is also illustrated in a quantile plot (Figure 4.9 a). In Figure 4.9 b) the plot is compared with the normal distribution, using an inverse normal function. The tendency towards concavity of slope profiles with less land at high altitude is shown. This must not be confused with the concavity of the graph itself. In Figure 4.9 c) the altitude variable is transformed using square roots and the plot becomes more linear, i.e. the square root of altitude corrects most of the skewness.

4.7. Wind and Airflow Classification

In climatological analysis it is often found useful to group together days with a similar airflow or synoptic situation (Lamb 1972, O'Hare & Sweeney 1993), allowing comparison of the properties of different airflows or weather types. For example, certain airflows are expected to have stronger lapse rates than others, e.g. north-westerly polar maritime airflows in spring or cold easterly flows in winter, while temperature inversions in certain areas form only under certain synoptic situations (Trilsbach 1988). A synoptic or airflow classification allows investigation of such

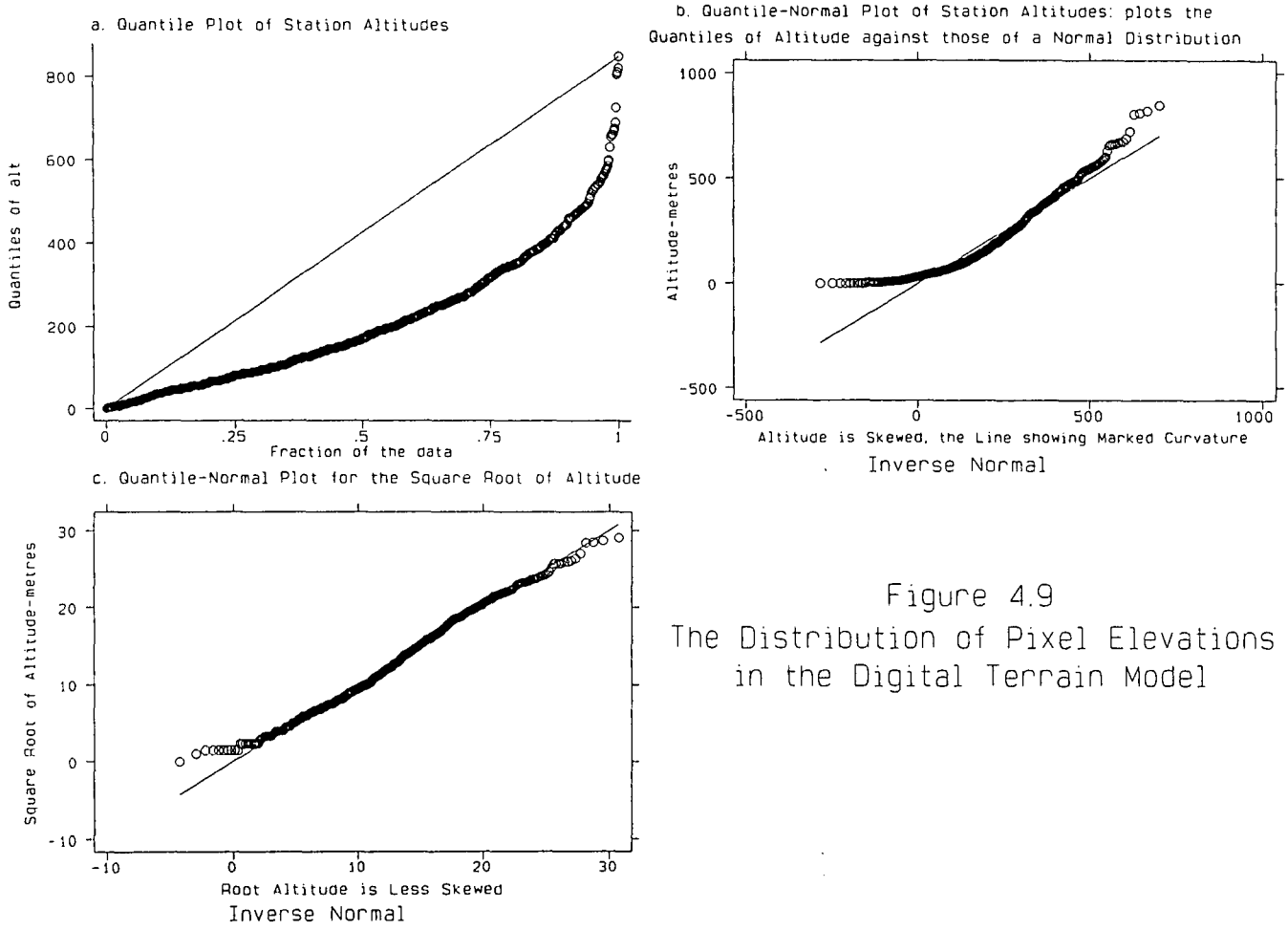

Figure 4.9
The Distribution of Pixel Elevations
in the Digital Terrain Model

trends. Attempts at synoptic and airflow classification relevant to Northern England are described below. The relationship between surface wind direction, airflow movement, synoptic situation and season is also investigated.

The simplest classification of daily circulation data, and that most frequently used in this study, is based on a two-way tabulation of month of the year and local wind direction. 108 combinations are possible since there are 9 possible wind directions (including calm) and 12 calendar months. Using the surface wind direction at Durham recorded at 0900 GMT, the number of days in each category ranges from 49 for south-westerlies in January to 1 for north-easterlies in August (Table 4.5).

Table 4.5: Surface wind direction at Durham (1985-1990).

MNTH	CLM	N	NE	E	SE	S	SW	W	NW
J	13	13	2	13	7	42	49	26	21
F	15	13	7	13	4	26	45	28	18
M	15	9	7	2	7	33	48	37	28
A	20	25	22	22	2	23	30	19	17
M	16	30	30	15	6	22	33	19	15
J	19	32	22	13	8	28	22	16	20
J	14	22	10	8	4	32	26	34	36
A	14	21	1	7	3	37	39	26	38
S	21	15	6	3	3	23	45	32	32
O	35	4	5	11	7	37	44	30	13
N	32	12	11	5	2	30	30	27	31
D	26	5	10	6	5	34	43	34	23

Use of this classification assumes that surface wind direction at Durham Observatory at 0900 hrs GMT is representative of airflow over Northern England in general. This assumption is largely (but not completely) true (see Figure 4.10 for a histogram of wind direction at Durham). When wind direction at Durham was

Figure 4.10. Wind Direction Frequencies at Durham (1985-1990)
Expressed to the Nearest 10 degrees

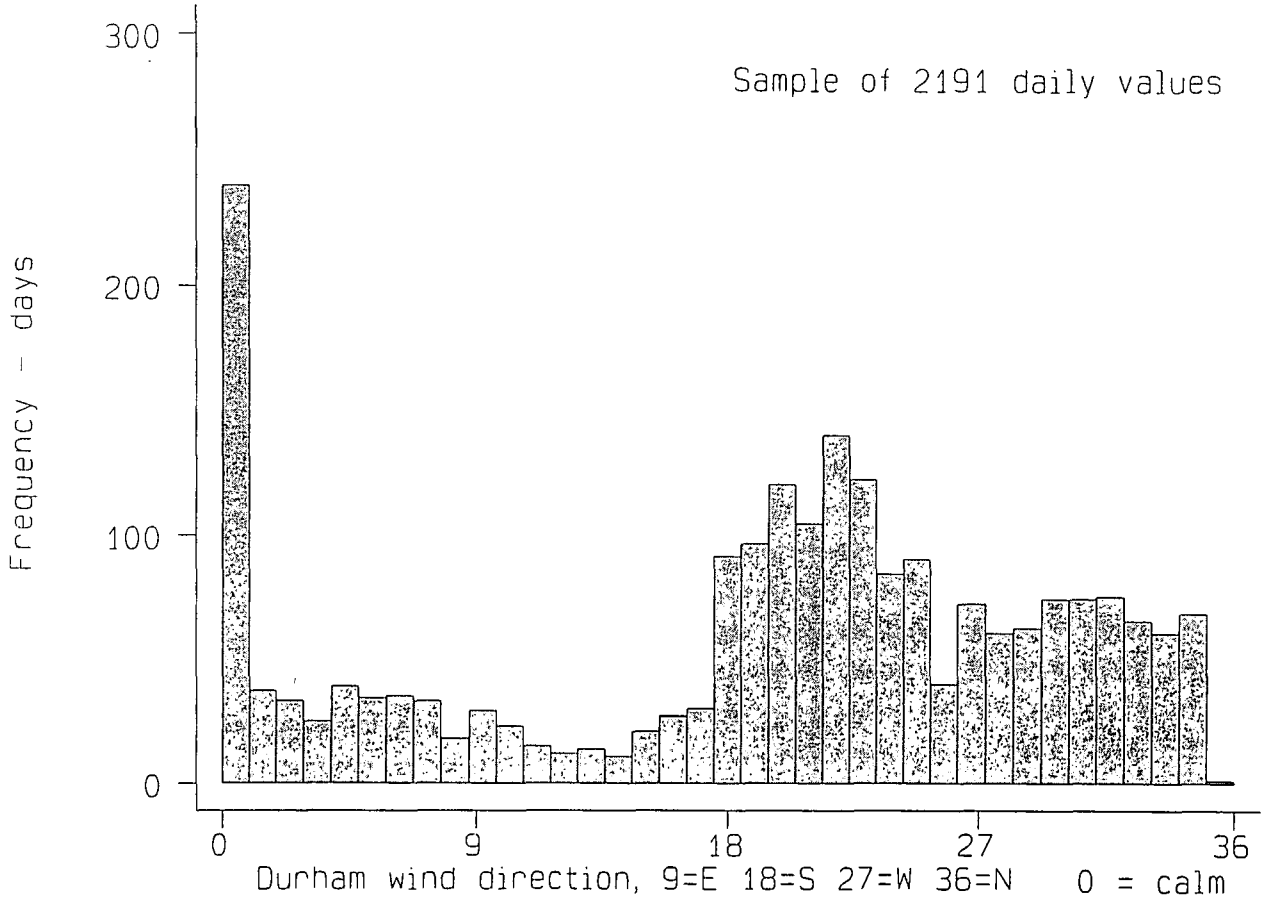

compared with that at Low Etherley (at higher altitude) and Whasdyke Farm (on the western side of the Pennines) there were sometimes contrasts in direction. One possible measure would be the average wind direction derived from the three places. This would be a vector mean since simple addition of wind direction values would be misleading.

Use of Durham surface wind directions leads to unequal sample sizes (Table 4.5). Any analysis performed separately for each wind direction/month category is more reliable for the categories with many daily cases. Confidence limits for parameters associated with north-easterly flow in August, for example, will be very wide as there is only one case. Analysis for progressive airflows (south-westerlies and westerlies) is nearly always of higher accuracy than for blocked conditions which are less common (especially easterlies and south-easterlies). From April to June, north-easterlies, easterlies and south-easterlies are more frequent than at other times of year. Also notable are the high frequency of northerlies in summer and frequent calm conditions in autumn and early winter. Lamb (1950) identified tendencies for certain airflow patterns to occur at certain times of year. Even in this six-year sample the frequencies of winds from each direction suggest trends in their variation throughout the year similar to Lamb's findings. This classification appears to have validity and is used in much of the analysis.

Limitations with the above classification are listed below:

1: The calendar month is essentially arbitrary and is of no meteorological significance. It would thus be just as appropriate to use natural seasons (Lamb 1950), i.e. periods of the year which often show similar airflow tendencies. It was found impractical to calculate natural seasons for a sample of only six years.

2: Surface wind direction is a poor indicator of airflow direction at upper levels and hence the steering of weather types. Winds back towards the ground due to friction such that there is an average deflection of 30° from the 500 mbar level to the ground surface coupled with a decrease in wind speed (Marshall 1954). This is described by the Ekman spiral (Ekman 1902). Thus when the upper airflow is westerly, surface

winds are often from the south-west or south. Deflection can be more than 30° where friction is very influential as in mountainous regions. Data on upper air winds is relatively sparse on a daily scale, apart from inference from 500 mbar pressure charts. However, the use of surface winds can be justified by noting that surface conditions are nearly always best related to surface wind direction.

3: Airflows from a given direction vary substantially in character, depending on the synoptic situation. For example, a north-westerly flow could be cyclonic, with polar maritime air flowing across the North of England associated with a cyclone to the north or north-east over the North Atlantic or the northern North Sea. However, a north-westerly flow could also be anticyclonic, flowing around a high pressure cell to the west of the British Isles. It may be necessary to differentiate between cyclonic and anticyclonic airflows and between differing air masses. Notably, a south-westerly flow could either be tropical maritime (Tm) air or returning polar maritime (Pmr) air.

Despite these limitations, the use of a classification based on local surface wind direction is extremely useful when attempting description of spatial temperature variation, as will be illustrated in forthcoming chapters. It would be possible to develop other equally suitable classifications although any classification must be applied to the local area rather than England as a whole.

Synoptic pressure charts can be used for classification. This process is subjective and leads to a multitude of classification systems. Classifications based on Northern England will be different from those using the whole British Isles. The most famous synoptic classification is that of Lamb (1972), published in Climate Monitor. The frequencies in each class are shown in Table 4.6 for 1985-1990. The classification is a combination of airflow direction and isobar curvature. Values are substantially different from the corresponding wind direction frequencies in Table 4.5.

Table 4.6: Lamb Classification (1985-1990): Aggregated by airflow direction, i.e. northerly includes CN AN and N. The heading U includes pure C, A and U.

MON	U	N	NE	E	SE	S	SW	W	NW
JAN	55	6	7	16	3	18	16	54	3
FEB	50	10	6	24	7	10	21	33	4
MAR	59	7	2	5	5	14	21	46	18
APR	80	16	9	20	5	11	4	25	2
MAY	60	19	7	24	12	11	14	14	8
JUN	79	21	9	13	2	11	6	24	6
JLY	81	4	3	-	6	5	9	54	18
AUG	64	17	1	1	2	11	19	57	7
SEP	64	10	4	2	2	10	17	51	11
OCT	71	2	1	18	13	20	14	38	6
NOV	70	15	9	6	11	12	15	30	5
DEC	65	8	2	5	9	10	31	44	5

The problem with the Lamb classification is that it may not be representative of conditions within northern England which are not necessarily the same as conditions over the whole of the British Isles. This is especially true when conditions are cyclonic. For example, a depression over Central England could result in an easterly flow over Northern England and a westerly one in the South of England leading to quite different weather conditions, especially in winter. The presence of marked air-mass transitions when fronts lie across the country can also lead to distinct temperature differences. Such subtleties are missed if the general Lamb classification is used. Lamb was more concerned with the steering of weather systems in the upper air than with surface winds. Because of this it is inappropriate to use a synoptic classification developed for the whole of the British Isles, such as Lamb (1972) or Jones et al. (1993), for a local climatic study (Shaw 1962, Smithson 1970). Any classification of airflow or synoptic situation is somewhat subjective and results will be affected slightly by the decision to use one classification instead of another.

The use of surface wind direction alone, is shown to separate contrasting fields of temperature very efficiently. However, air-mass type and synoptic situation are also influential for surface lapse rates and in creating a distinctive spatial temperature distribution. Contrasts in air-mass are part of the reason for temperature contrasts according to wind direction, as certain air-mass types are almost invariably associated with certain surface wind directions. For example, polar maritime air approaches from the north or west, while both returning polar maritime and tropical maritime approach from the south-west. Tropical continental air approaches Britain from the south or south-east. Differences between airflows are often explained by reference to air-mass contrasts although it is important to realise that air-mass type and airflow direction are not synonymous.

The concept of air-mass is subjective since there is a continuum of air mass types, as opposed to discrete categories (Belasco 1952). Air mass type can be estimated by trajectory analysis, following isobars back to a source region which is usually one of the Arctic, Eurasian continent (especially in winter), Mediterranean/N.Africa or the Atlantic (Figure 4.11). Air from the Atlantic subtropical high pressure cell is described as tropical maritime (Tm). Tropical continental (Tc) air originates from the Sahara or Mediterranean and is rare. Polar continental (Pc) air originates from the Eurasian high pressure cell and approaches Britain from the east. The use of the word 'Polar' is confusing since air from the true polar regions is called arctic Maritime (Am) or continental (Ac). The source regions are the Arctic Ocean and Greenland respectively. Polar maritime air (Pm) originates from the North Atlantic and is a less severe form of arctic maritime air. It is the most common form of air mass in the uplands of Northern England and has a characteristically steep lapse rate in its lower layers. The dividing line between arctic and polar air-masses is very subjective, the former usually referred to as a more 'severe' form of the latter, having a short sea-track south. To complicate matters further, polar maritime air that is taken far south of Britain before returning north behind the cold front of a depression is called returning polar maritime (Pmr), and acquires some of the characteristics of tropical maritime air. For a discussion of the air-mass types in more detail see Manley (1952). Distinctions between air-masses often become blurred when excessive modification has taken place. Because

Figure 4.11 *Trajectories of principal air masses affecting the British Isles* Source: Perry (1976).

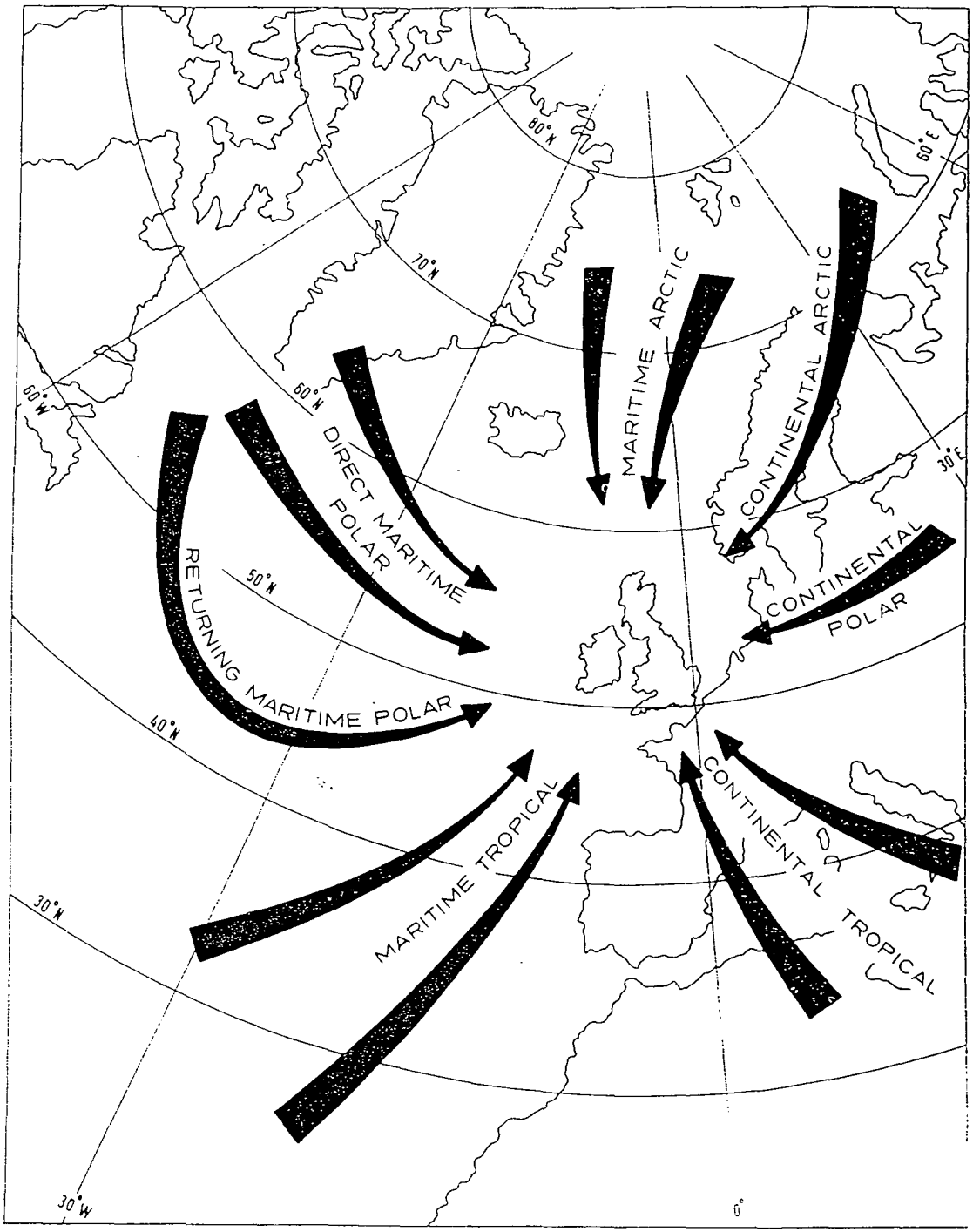

of these problems a completely successful air-mass classification was thought to be difficult to obtain and thus wind direction was more frequently used for classificatory purposes.

4.8 Summary

This chapter describes the large amount of climatic data used for this study, originating from 26 climate stations. The period of analysis is 1985-1990. Site descriptions are given for each location and the characteristics of the site (altitude, location and exposure) are quantified. A digital terrain model (DTM) of northern England is described as a backdrop before which spatial variation in climatic variables is analysed. Finally, ideas concerning classification of the data into days with similar airflow influences are discussed.

THE DURHAM-WIDDYBANK FELL TEMPERATURE GRADIENT: AN EXAMPLE OF A ALTITUDINAL TEMPERATURE LAPSE RATE

5.1 Introduction

This chapter examines the particular upland-lowland temperature contrast between two meteorological stations on the eastern slope of the Pennines, the **lapse rate** between Durham Observatory (102 m) and Widdybank Fell (513 m). These locations were chosen due to the wide availability of data and to allow expansion of previous work (Pepin 1990, 1992). Widdybank Fell is the only upland site on the Pennine plateau apart from the unrepresentative summit site of Great Dun Fell (847 m). Durham was assumed to represent the eastern lowlands. Data were analysed for 1985-1990, providing a long enough period to include most weather-types.

The lapse rate of maximum temperatures is investigated since maxima recorded at Widdybank and Durham are more representative of altitude and less dependent on **local** factors than minima. Local topography is known to be much more influential when daily minima are concerned (Harding 1978) so that prediction of frost is a more complex process (Bootsma 1976, Lengerke 1978).

5.2 Analysis and Data Handling

Daily maximum temperatures (°C), sunshine hours and wind direction (to the nearest 10°) were input to a computer file for 1985-1990 for Durham and Widdybank Fell. The 2191 daily cases were classified according to month and wind direction as described in Chapter 4. The temperature difference for each day was calculated by subtracting the maximum temperature at Widdybank from that at Durham. Differences varied from 8.7°C on 17 Oct 1989 to -5.3°C on 3 Dec 1989. The average difference over the six year period was 3.88°C, recorded over a height difference of 411 metres. This is equivalent to a mean lapse rate of -9.44°C/km, only slightly less than the DALR (Dry Adiabatic Lapse Rate), surprisingly high compared with the global average of -6.5°C/km (Barry 1992, Linacre 1992).

One slight statistical problem must be born in mind when examining lapse rate variation. When calculating a temperature difference, errors become additive (Alonso 1968). Thus the error for a calculated lapse rate is larger than the errors for the individual temperatures.

Table 5.1 shows the average difference in maximum temperature for each month and airflow direction (measured by local wind direction at Durham). Column totals indicate the overall seasonal variation and row totals variation between airflow types.

Table 5.1: Maximum temperature differences (°C) between Durham and Widdybank Fell, by month and wind direction.

°C	JAN	FEB	MAR	APR	MAY	JUN	
CALM	3.02	3.89	4.51	3.58	3.07	3.08	
N	2.98	4.13	4.69	3.74	2.90	3.06	
NE	3.95	3.96	4.41	3.18	2.02	2.56	
E	3.61	4.25	4.05	3.81	1.75	1.32	
SE	2.61	4.30	3.91	1.65	2.98	2.77	
S	3.23	3.28	4.40	3.89	3.38	3.61	
SW	3.58	3.91	4.54	4.52	4.25	4.58	
W	3.86	4.77	5.23	5.14	4.82	4.82	
NW	3.45	4.43	4.91	4.62	4.29	4.42	
TOTAL	3.42	4.06	4.70	4.02	3.28	3.44	
	JUL	AUG	SEP	OCT	NOV	DEC	TOTAL
CALM	2.59	3.72	4.05	3.19	3.14	3.02	3.37
N	3.48	3.77	4.10	3.43	3.70	3.33	3.51
NE	2.99	2.20	3.93	3.52	3.95	3.85	3.07
E	2.32	2.94	1.13	2.96	4.64	4.14	3.05
SE	4.05	5.87	3.43	3.21	2.50	3.28	3.35
S	3.73	4.42	3.90	3.49	2.62	3.33	3.60
SW	4.80	5.03	4.36	4.08	3.77	3.20	4.17
W	4.82	5.09	5.25	4.36	4.39	3.91	4.70
NW	4.65	4.50	4.92	4.12	3.97	3.26	4.36
TOTAL	4.05	4.49	4.42	3.72	3.61	3.40	3.88

A plot of the mean temperature difference for the twelve calendar months exhibits a strong seasonal variation (Figure 5.1). A six-monthly cycle with maxima in March and September and minima in June and December/January suggests a relationship of temperature difference with solar elevation. Maximum differences in temperature are recorded around the equinoxes and minimum differences around the solstices.

In summer there is a positive correlation between sunshine amount and daily maximum temperature, because of the receipt of solar radiation under clear skies. In winter this correlation is non-existent, or slightly negative (Catchpole 1966), because of the lower receipt of solar radiation under clear conditions compared with the rapid loss of heat radiated from the ground. A clear sky in winter can lead to more heat loss by outgoing longwave radiation than is gained by solar input, even in the short daytime period.

Correlations between maximum temperature and sunshine hours were examined at both Widdybank and Durham. As expected a pronounced seasonal variation was evident with high positive correlations in summer and insignificant correlations in winter (Figure 5.2). Correlations were often lower at Widdybank, especially in winter (i.e. more negative). The difference between the two correlations is shown to peak in winter and reach a minimum in summer (Figure 5.3). Taking the correlation between maximum temperature and sunshine hours as a proxy for the 'heating power of the sun', then for almost all of the year this power is less at Widdybank. In summer the sun leads to efficient heating of the mountain environment due to the increased amount of solar radiation and shorter optical air mass (Lowry 1980, Olecki 1989). This is supported by the observation that mountain temperatures are higher than those in the free air on summer afternoons while for the rest of the year the opposite is so (Peppler 1931, Richner & Philips 1984). On the contrary, in winter, spring and autumn the 'heating power of the sun' appears to be reduced at higher altitudes.

The following hypothesis was put forward to explain the seasonal cycle in lapse rate in Figure 5.1.

Figure 5.1. Mean Differences in Daily Maximum Temperature between Durham (102 m) and Widdybank Fell (513 m) by Month (1985-1990)

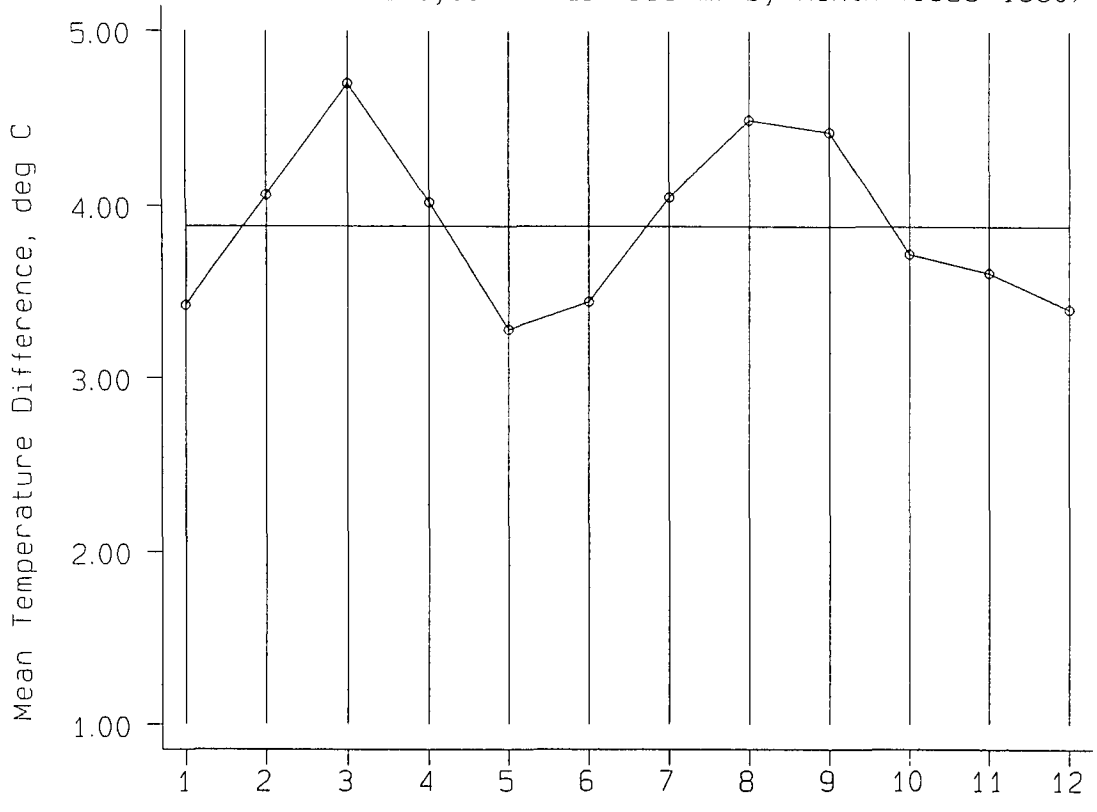

Mean Differences in Maximum Temperatures by Month

Figure 5.2. Monthly Correlations between Daily Maximum Temperatures and Sunshine Hours at Durham and Widdybank Fell

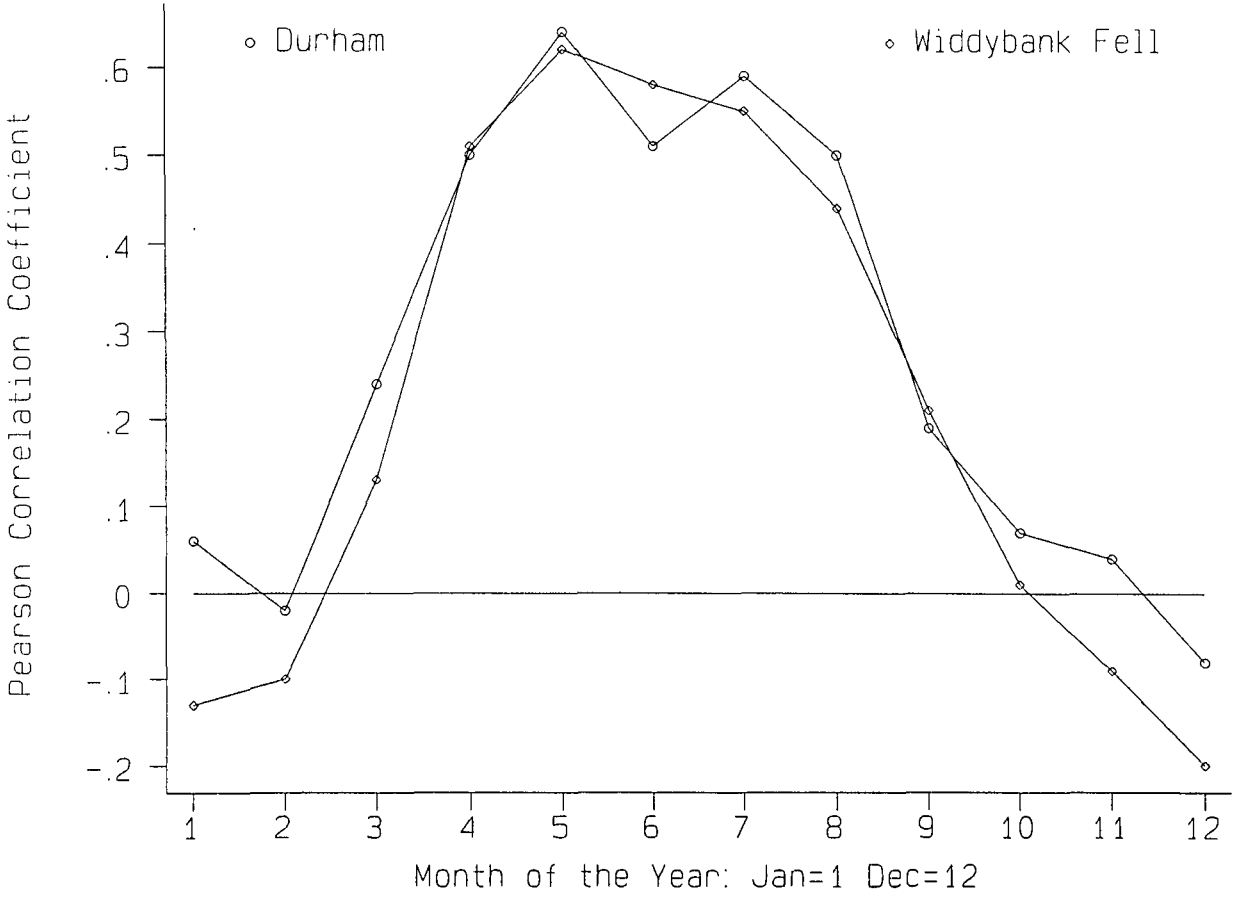

Figure 5.3. Monthly Differences in the Maximum Temperature/ Sunshine Hours Correlation between Durham and Widdybank Fell

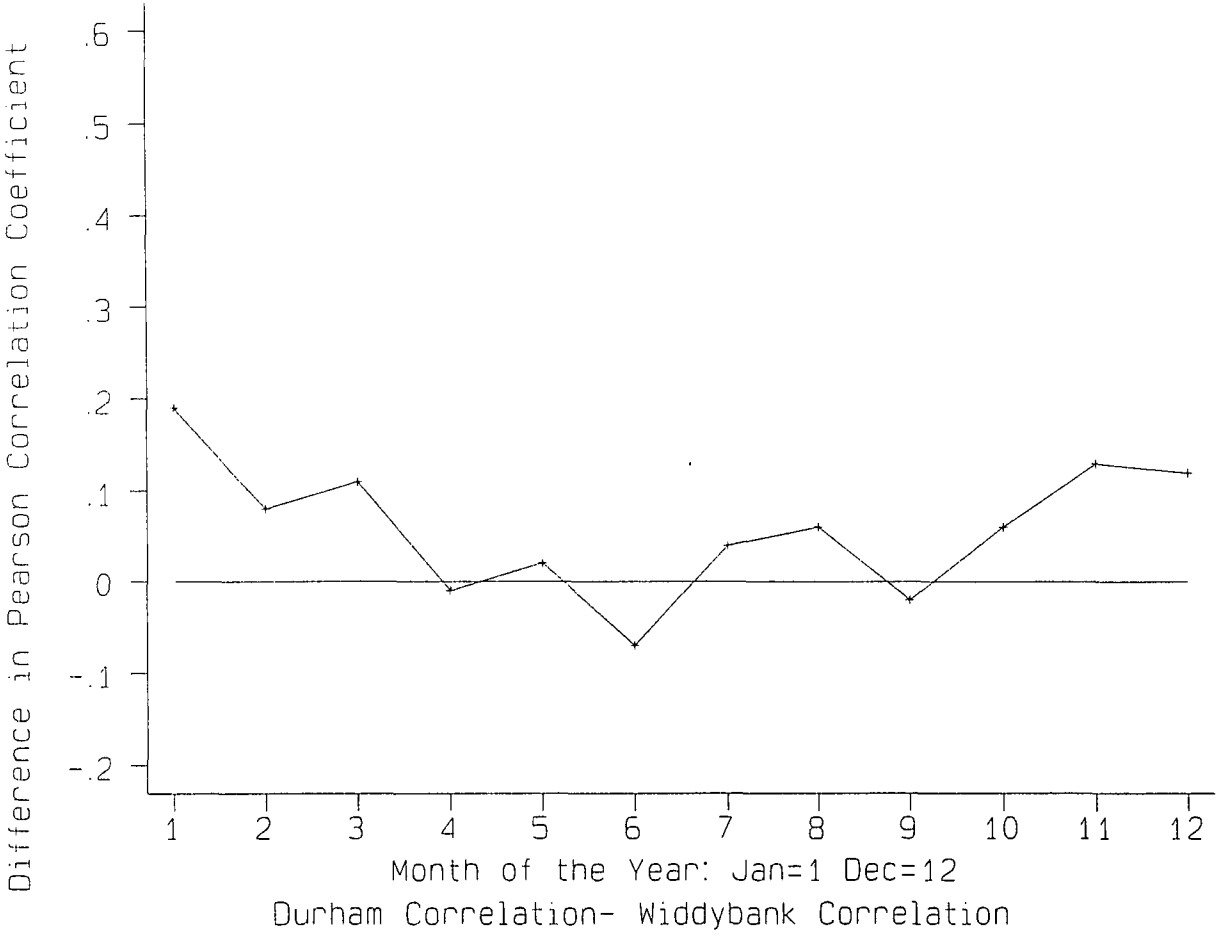

Assuming that there is a threshold angle of elevation that the sun must attain before the net effect of a clear sky induces warming at screen level, this angle must be greater in an upland area. The difference between the two correlations (Figure 5.3) is an indirect measure of the difference in the 'power' of the sun at the two altitudes. It could be envisaged that around the equinoxes the critical solar elevation is exceeded during the middle part of the day at Durham but not at Widdybank. This being the case, temperature differences would be larger in March/April and August/September, i.e. just after the vernal equinox and before the autumnal equinox (Figures 5.1 and 5.4) and the peaks in the lapse rate at these seasons would be supported. It would be expected that temperature differences in winter, when a clear sky means more longwave exitance (especially at high altitude), would be extremely large, since Widdybank Fell suffers from a relative heat deficit under clear skies. However, the nocturnal tendency for cold air to sink, creating temperature inversions, reduces the mean lapse rate dramatically (Manley 1943, Hennessy 1979).

Figures 5.5 and 5.6 show the seasonal variation of the temperature gradient for days with more than 75% of the total possible sunshine and for sunless days respectively, as measured by sunshine duration at Durham. As the above hypothesis depends on the difference in efficiency of solar input the seasonal trend in the difference should be more discernable for sunny and calm days than for sunless or windy ones. In Figure 5.5 the seasonal trend is extremely clear and the temperature difference decreases markedly near the summer solstice (especially June), suggesting that the sun is powerful enough to heat the upland atmosphere at this time. The temperature gradient is strongest near the equinoxes. In Figure 5.6 the seasonal trend is less clear, notably at mid-summer when the temperature difference remains high under cloudy conditions. The stronger seasonal signal for sunny days supports the solar hypothesis.

The assumption that the number of sunshine hours used in the correlations (**n**) represents the proportion of the time throughout the twenty-four hour day that the sky is clear is not always upheld. This is especially problematic in winter, when the amount of sunshine in the (relatively short) daylight period is not a good estimate of the

Figure 5.4. Differences in Daily Maxima between Durham and Widdybank Fell on Calm Days by Month

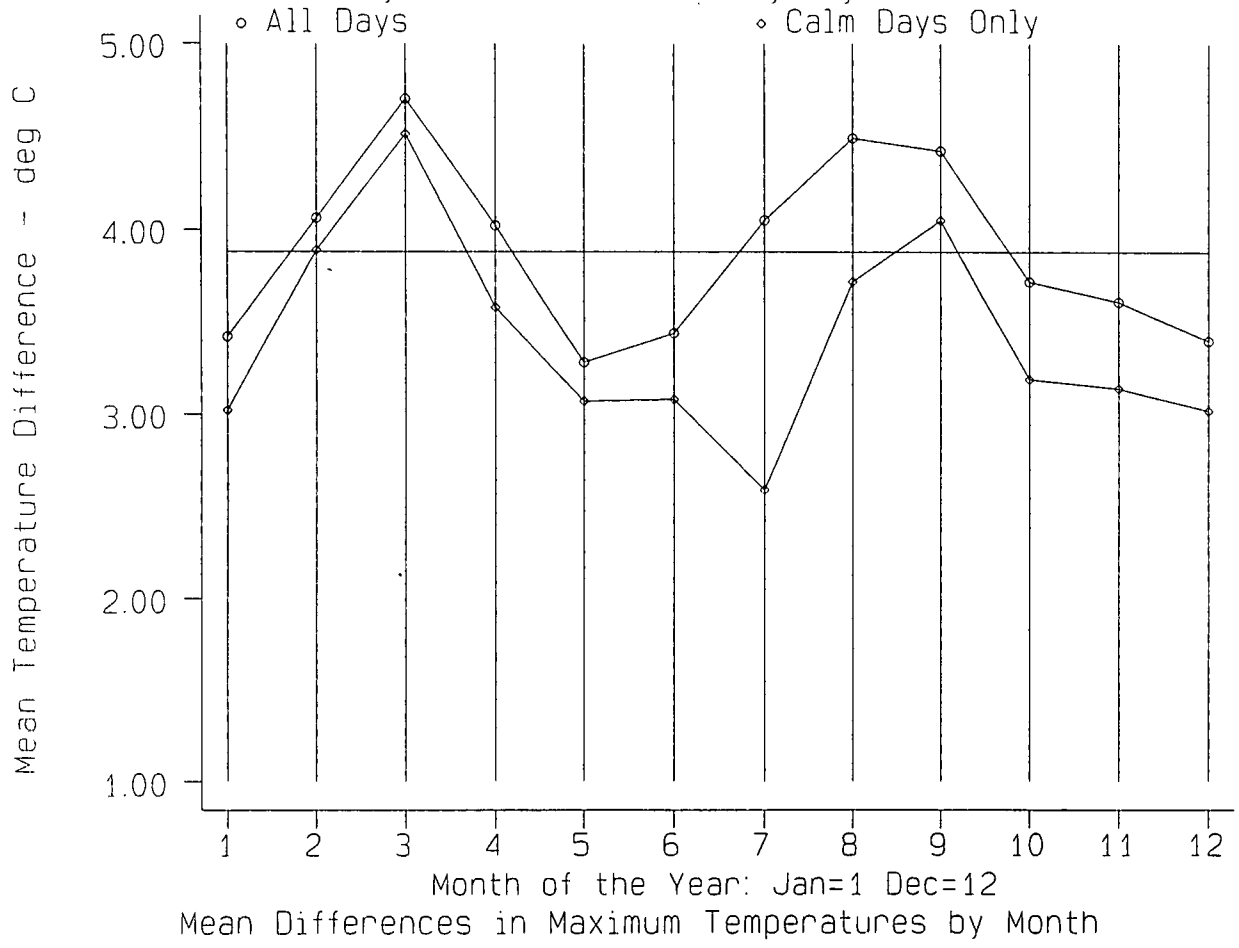

Mean Differences in Maximum Temperatures by Month

Figure 5.5. Monthly Mean Differences in Daily Maxima (between Durham and Widdybank Fell) on Days Recording more than 75% of Possible Sunshine

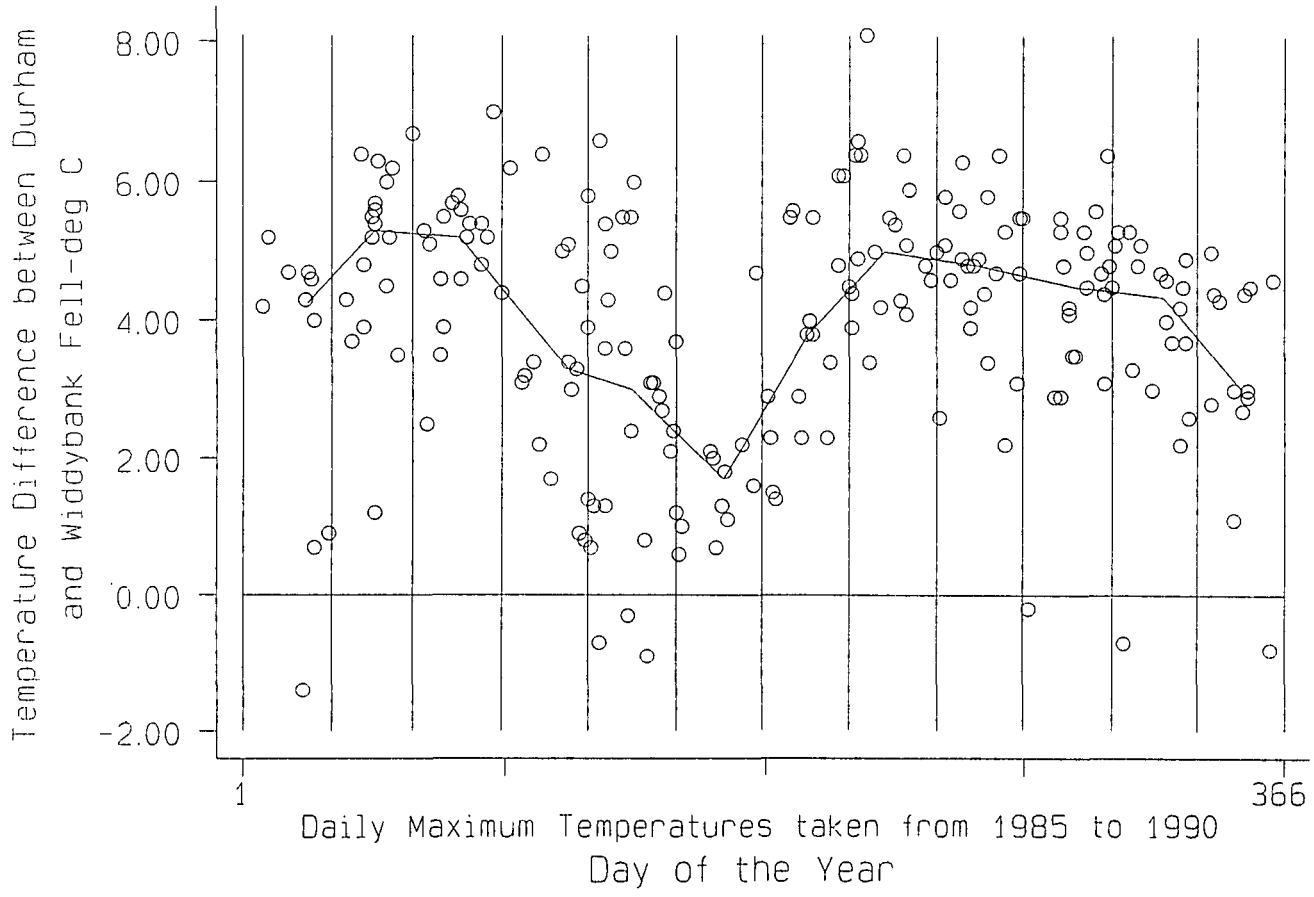

Figure 5.6. Monthly Mean Differences in Daily Maxima (between Durham and Widdybank Fell) on Sunless Days

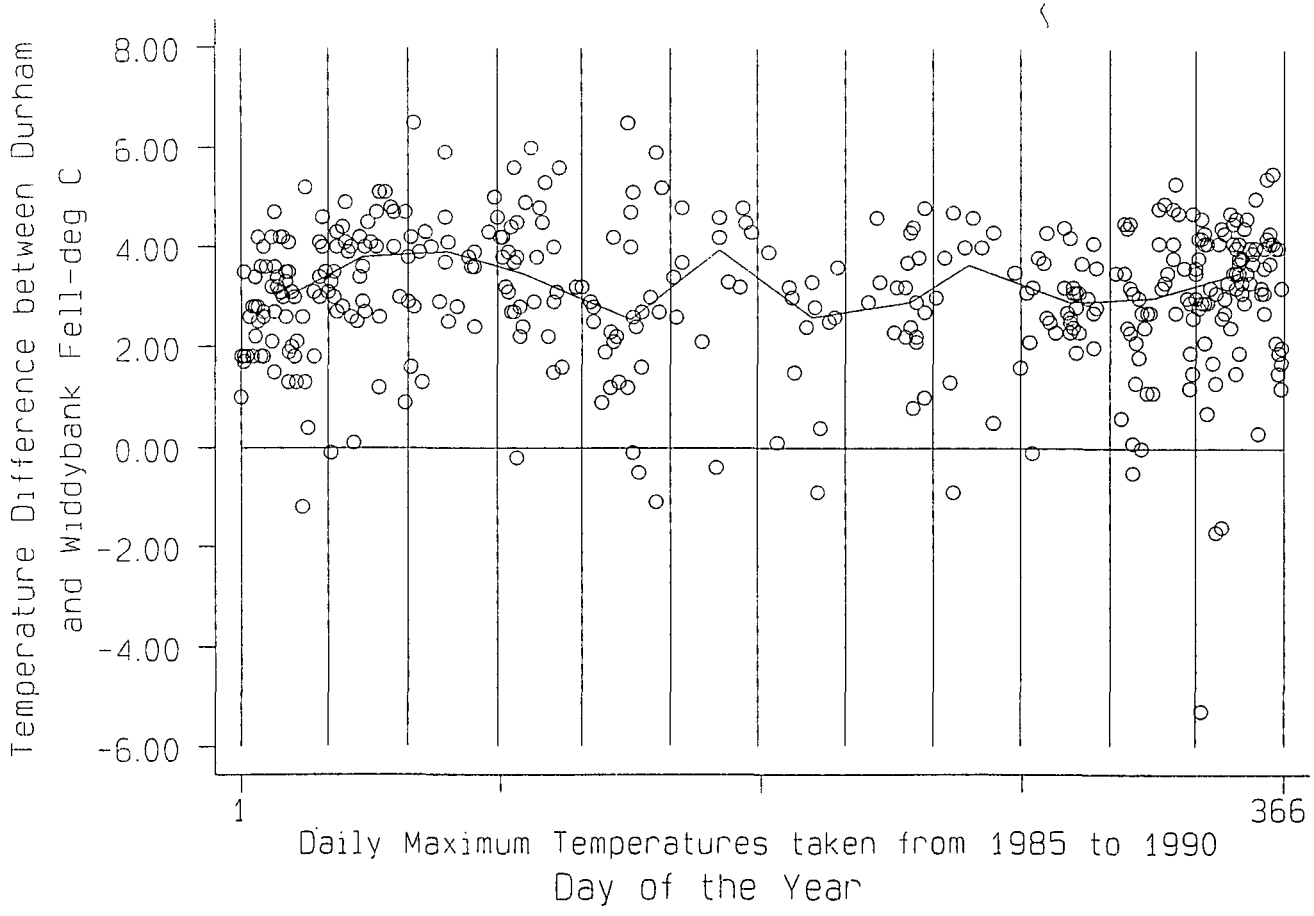

proportion of time with overcast skies. Even during daylight hours the index **sun hours/length of possible daylight** (**n/N**) is not a perfect measure of the percentage of time that the sky is clear. Whether the sun is shining indicates only whether the sky is clear at a specific point in the sky (moveable in time). If solar elevation is low then, for a given amount of cloud cover, sunshine duration will be less than if the elevation was high because solar rays, having to pass through more of the atmosphere, are more likely to meet cloud in their path (Figure 5.7). This is especially true when there are numerous cumulus clouds of convective origin. On a day typified by fair-weather cumulus, looking towards the horizon it appears that cumulus clouds cover most of the sky in its lower layers (Figure 5.8). In reality, there are no more clouds per unit area but because we are looking obliquely they appear to be on top of one another. Hence rays from a low elevation sun would very rarely reach the observer. In reality extensive cumulus clouds are uncommon when the sun is low in elevation, since such clouds are convectional in origin.

Taking sunshine hours to represent the proportion of time that the sky is clear, it must be assumed that any clouds are distributed randomly. Yet clouds often form and remain in distinct positions in the sky, especially in mountainous areas where orographic influences are strong. For example, evening sunshine at Widdybank may be reduced because of the build up of clouds over high land to the south-west. The position of the sun at different times of day relative to favoured areas of cloud development is therefore important. It has been shown by Hoyt (1977) that cloud cover estimates taken from the ground and recorded sunshine levels do not always agree. This is only partly due to projection problems experienced by observers (Malberg 1973). Since sunshine hours are only a proxy for the state of the sky, the correlations between maximum temperatures and sunshine hours only provide a general seasonal picture.

5.3 Physical Interpretation of the Annual Cycle in Lapse Rate

A possible physical explanation of the two peaks in the temperature difference around the equinoxes requires that the critical elevation of the sun above the horizon needed to create warming is lower at Durham than Widdybank, i.e. the first heating

Figure 5.7. The Relationship between Cloud Cover and Sunshine Duration: The Effect of Solar Elevation

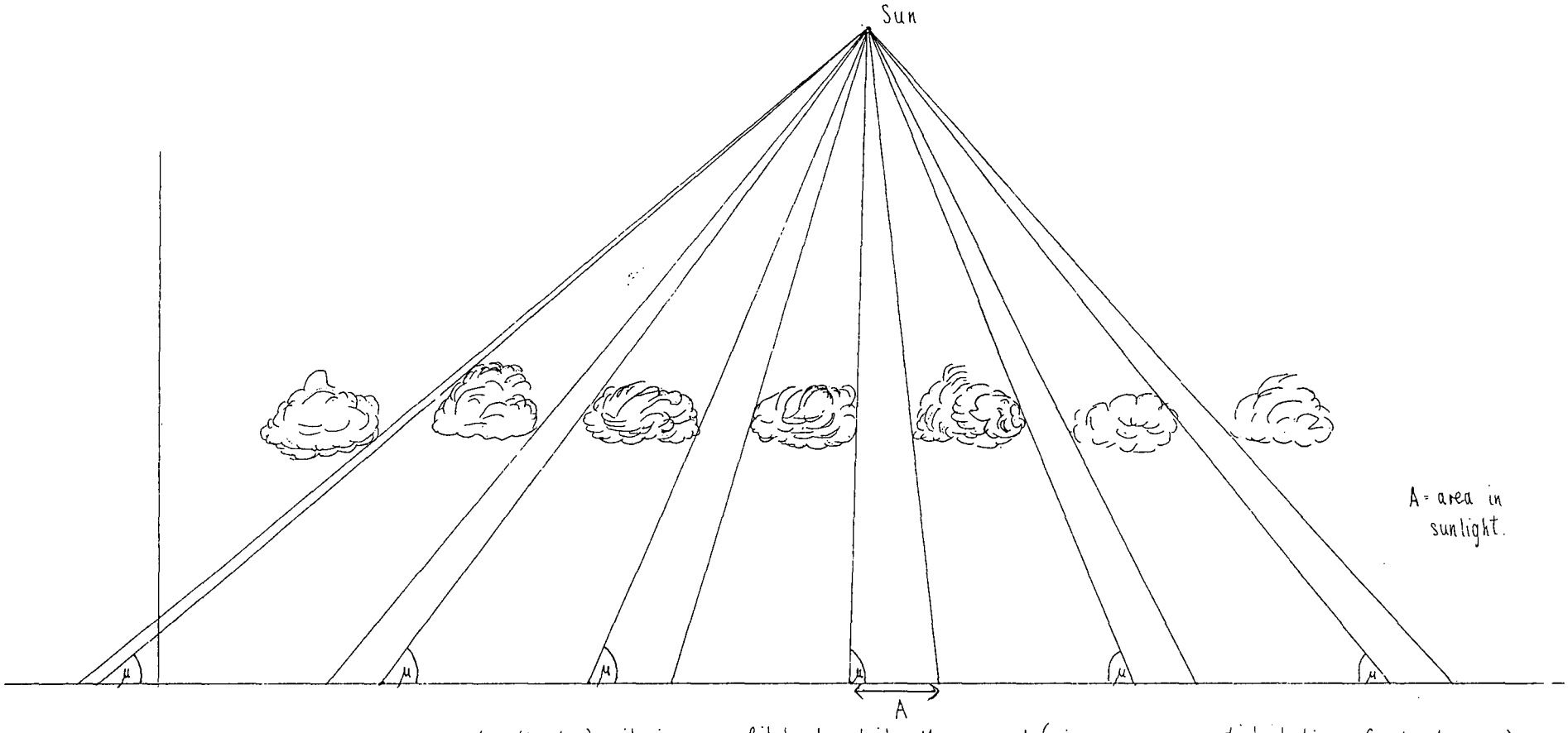

When the sun is at a high elevation (μ), it is more likely to strike the ground (given an even distribution of cloud cover), as represented in this diagram. This is because the sun's rays pass through a smaller thickness of potentially cloudy atmosphere. Another way of looking at this is that a given size of cloud will cast a larger shadow when the sun is low in the sky. Thus the relationship between cloud-cover and sunshine duration depends on solar elevation (μ). The curvature of the earth is ignored in this simplified diagram.

Figure 5.8 The Apparent Increase in Cloud-Cover Towards the Horizon on a Day with Evenly Scattered Cloud-Cover

effects of the sun in spring are experienced in lowland areas. The change in air temperature at the ground can be assumed to relate to the net irradiance at the surface $\mathbf{Q_n}$ (this is discussed in Chapter 7). Soil heat storage is ignored in the following discussion.

For albedo α , solar irradiance $\mathbf{Q_s}$, counter-radiation $\mathbf{Q_{ld}}$ and terrestrial emittance $\mathbf{Q_{lu}}$, net irradiance $\mathbf{Q_n}$ can be calculated by the formula:

$$Q_n=(1-\alpha)Q_s + Q_{ld} - Q_{lu}....W\,m^{-2} \quad ----(1)$$

(Linacre 1992)

Now:

$$Q_s=D + Q_d(\sin\mu).....W\,m^{-2} \quad ----(2)$$

where $\mathbf{D}$ = diffuse radiation, $\mathbf{Q_d}$ = direct radiation, and μ = solar elevation.

The expression $\mathbf{Q_{lu}}$ - $\mathbf{Q_{ld}}$ represents net upwards longwave exitance. As altitude increases $\mathbf{Q_{lu}}$ - $\mathbf{Q_{ld}}$ increases (Fliri 1971), α increases (especially when there is upland snow cover), and $\mathbf{Q_s}$ increases due to a small increase in $\mathbf{Q_d}$ (Harding 1979, Olecki 1989). Diffuse radiation $\mathbf{D}$ increases with elevation under cloudy conditions (Dirmhirn 1951), but decreases when the sky is clear because of the lower depth of atmosphere above. Therefore $\mathbf{Q_s}$ is more dependent on $\mathbf{Q_d}$ $\mathbf{[\sin \mu]}$ at high altitude. The temperature contrast between shady and sunny areas is greater than in the lowlands because of the dependence on direct radiation. In mid-summer there may be potential for a net warming of the upland atmosphere (Flohn 1953), but in winter there is a considerable upland heat deficit, moderated by katabatic flow and temperature inversion formation.

When net irradiance ($\mathbf{Q_n}$) is zero, there is a radiation balance. Estimating a representative value of $\mathbf{S_a}$ for such a case:

$$(1-\alpha)(D+Q_d(\sin\mu))=Q_{lu}-Q_{ld} \quad ----(3)$$

Thus:

$$\sin\mu=\frac{Q_{lu}-Q_{ld}-D(1-\alpha)}{Q_d(1-\alpha)} \quad ----(4)$$

and:

$$\mu=\arcsin\frac{Q_{lu}-Q_{ld}-D(1-\alpha)}{Q_d(1-\alpha)} \quad ----(5)$$

In an upland area $\mathbf{Q_{lu}}$-$\mathbf{Q_{ld}}$ is greater than in the lowlands and **D** is less. Hence the numerator of the right hand expression is larger. $\mathbf{Q_d}$ will increase with altitude by about 1-2%/km, due to a reduction in the path length of the solar beam but will almost certainly be offset by the decrease in 1-α. Thus the denominator of the right hand expression will be similar or smaller. Thus the critical solar elevation required for a radiation balance appears to increase in the uplands, supporting the hypothesis.

Table 5.2 presents plausible energy budget parameters for Northern England given various solar elevations. The critical elevation is always higher in the upland case. Paradoxically, critical solar elevation depends on the actual solar elevation and increases as the actual solar elevation decreases. The values in Table 5.2 are obtained with reference to a physical energy balance model developed to evaluate solar efficiency at the upland and lowland sites (Chapter 7).

All units are W/m^2 but any common unit would be acceptable as long as the units of **D**, $\mathbf{Q_d}$, $\mathbf{Q_{ld}}$ and $\mathbf{Q_{lu}}$ are identical. Given the relationship between critical solar elevation and $\mathbf{Q_d}$, $\mathbf{Q_{ld}}$, $\mathbf{Q_{lu}}$ and **D**, it would be theoretically possible to calculate the amount of time that the sun is above or below the critical elevation, i.e. the time for which actual solar elevation is larger or smaller than the critical elevation required. This would require use of complicated mathematical integration.

Table 5.2: Plausible values for energy balance components: an upland/lowland comparison.

SOLAR ELEVATION	10°	10°	20°	20°	35°	35°
PARAMETER	UPLAND	LOWLAND	UPLAND	LOWLAND	UPLAND	LOWLAND
$Q_d(W/m^2)$	50	49.5	200	198	400	395
$Q_{lu}(W/m^2)$	305.5	323.8	305.5	323.8	352.8	373.2
$Q_{ld}(W/m^2)$	208	232	208	232	268	292
ALBEDO	0.3	0.2	0.3	0.2	0.3	0.2
$D(W/m^2)$	25	29.7	50	59.4	60	79
CRITICAL ANGLE-DEG	>90°	>90°	26.5°	16.2°	8.8°	3.3°

In conclusion, the peaks in the altitudinal temperature gradient at the equinoxes may have a physical explanation. Summer differences are slightly reduced because of heating in the upland atmosphere, while winter differences are drastically reduced by temperature inversion formation. The significance of the albedo term in the calculations cannot be ignored. Snow cover is therefore likely to have a considerable influence on the upland/lowland temperature contrast.

5.4 Airflow Influences on the Altitudinal Gradient

The seasonal fluctuation in mean lapse rate is but a background upon which larger daily fluctuations of the altitudinal temperature gradient occur. Under calm conditions the seasonal pattern is fairly clear, since solar influences are strong (Figure 5.4). The seasonal variation in lapse rate is modified depending on airflow direction (measured by local surface wind direction). For some airflows a six-monthly cycle is still seen, suggesting that the **overall** seasonal variation in lapse rate is not significantly affected by changes in relative frequencies of airflow types over the course of the year (Lamb 1950). The effects of a certain airflow on temperature vary spatially. For example, the cooling effect of a north-easterly flow in spring and summer due to the North Sea is found to reduce the average temperature gradient between Durham and

Widdybank Fell by inducing an element of temperature change related to distance from the east coast. Durham experiences relative cooling and the altitudinal gradient in temperature is reduced.

The Widdybank/Durham temperature difference, like any single ground-based lapse rate, is therefore not purely controlled by altitude, being modified by advective effects expressed through longitude and latitude (i.e. position in space). Advective effects depend on airflow direction, this determining what is happening to the air between the two stations. It is important to separate the strictly altitudinal causes of temperature variation from effects such as the dynamic modification of an airflow by a mountain range. Examples of the latter include trapping of air on one side of the range, temperature inversion formation and föhn effects. All these effects are airflow-dependent. Some airflow effects are more likely to occur at certain times of year, especially those related to the land/sea temperature contrast and stability (e.g. temperature inversion formation). A division of daily data into 108 categories, each representing a particular wind direction in a particular month, is therefore useful, since airflow and seasonal effects can then be separated.

The contrast between different airflow types has already been shown in Table 5.1. A graph showing the average differences for each airflow type (Figure 5.9) exhibits a regular pattern with westerlies consistently giving steeper gradients than easterlies, and southerlies and northerlies giving intermediate values.

To understand the effects of airflows requires knowledge of the synoptic conditions likely to be associated with each airflow. Importantly, the effects of an airflow vary spatially and so position in space can be used as a proxy for the age of an airflow. In seeking to explain the magnitude of the temperature gradient, the modification of the airflow between the two stations concerned can be viewed as occurring between 'snapshots' of the airflow taken at the two stations. With northerly and southerly flows which arrive at both Durham and Widdybank Fell simultaneously, this concept is less helpful. We must look 'upstream' to assess the effects of that airflow on temperature. The distance to the sea in the direction from which the airflow

Figure 5.9. Mean Differences in Daily Maxima (between Durham and Widdybank Fell) According to Airflow Direction, as Measured by Durham Wind Direction

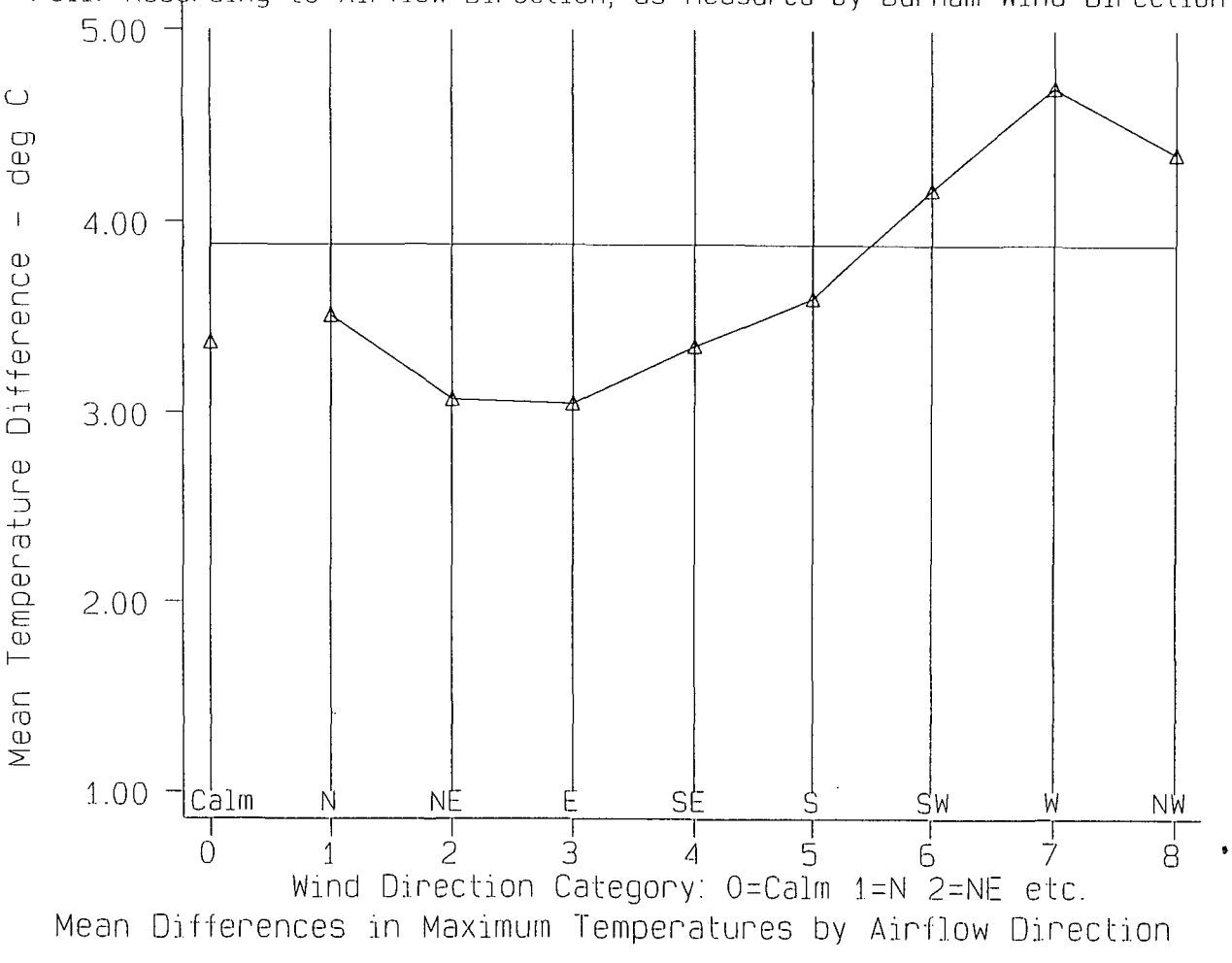

Mean Differences in Maximum Temperatures by Airflow Direction

has come is especially important (i.e. the upwind fetch).

5.5 Summary

Since both Widdybank Fell and Durham possess unusual climatic characteristics related to certain airflow directions, the recorded temperature gradient is not representative of the Pennines as a whole. Theoretically, altitudinal causes of the temperature difference (free air and solar effects) should remain **relatively** constant over space. Airflow effects (expressed spatially through latitude, longitude and distance from the sea) will cause the temperature gradient to vary depending on which stations are used. An altitudinal gradient based solely on two locations is often misleading (Harrison 1974) since only part of the gradient may be due to altitude.

The investigation is therefore extended to include other stations in the study area. Comparison of numerous ground-based lapse rates will lead to the separation of the altitude effect from secondary airflow influences on temperature which are essentially local, differentiating lee and windward slopes. Examples of altitudinal lapse rates will be calculated using stations to the north, south, east and west of the Pennine plateau, aiming to provide a more representative picture of the altitudinal influence on temperature.

SPATIAL VARIATION IN THE ALTITUDINAL LAPSE RATE OF MAXIMUM TEMPERATURE

6.1 Introduction

The temperature gradient examined in Chapter 5 is just one example of a lapse rate in the Pennines. The following discussion focuses on ten additional ground-based lapse rates in the hope that certain seasonal and spatial trends in lapse rate can be identified.

6.2 Seasonal Analysis of Ground-Based Lapse Rates

Analysis of the local Durham/Widdybank Fell temperature gradient showed that it was steepest with westerly (downslope) flow at any season and around the equinoxes. Other lapse rates were examined, using Great Dun Fell (847 m) and Widdybank Fell (513 m) as high altitude reference points. Again, daily data from 1985 to 1990 inclusive were used.

Table 6.1 lists mean lapse rates (°C/km) between Great Dun Fell, Widdybank Fell and four other stations; Durham to the east, Warcop to the south, Aspatria to the west, and Haydon Bridge to the north (Figure 6.1). A local comparison with Appleby in the Vale of Eden (Plate 8) was included as representative of the lapse rate on the Pennine escarpment (Plate 9). The elevation difference between Appleby and Great Dun Fell is nearly 700 metres although the distance between the two sites is only 12.38 km. Advective effects should be negligible for this comparison.

Rates are negative as temperatures decrease with increasing altitude. The DALR (see Chapter 3) is -9.8°C/km. Comparison of a lowland station with Widdybank Fell and then Great Dun Fell yields a slightly different picture. Figures 6.2 and 6.3 show the seasonal variation in lapse rate on all slopes using Great Dun Fell and Widdybank Fell as the upland stations respectively. The lapse rate contrast between slopes is greater when Widdybank is used.

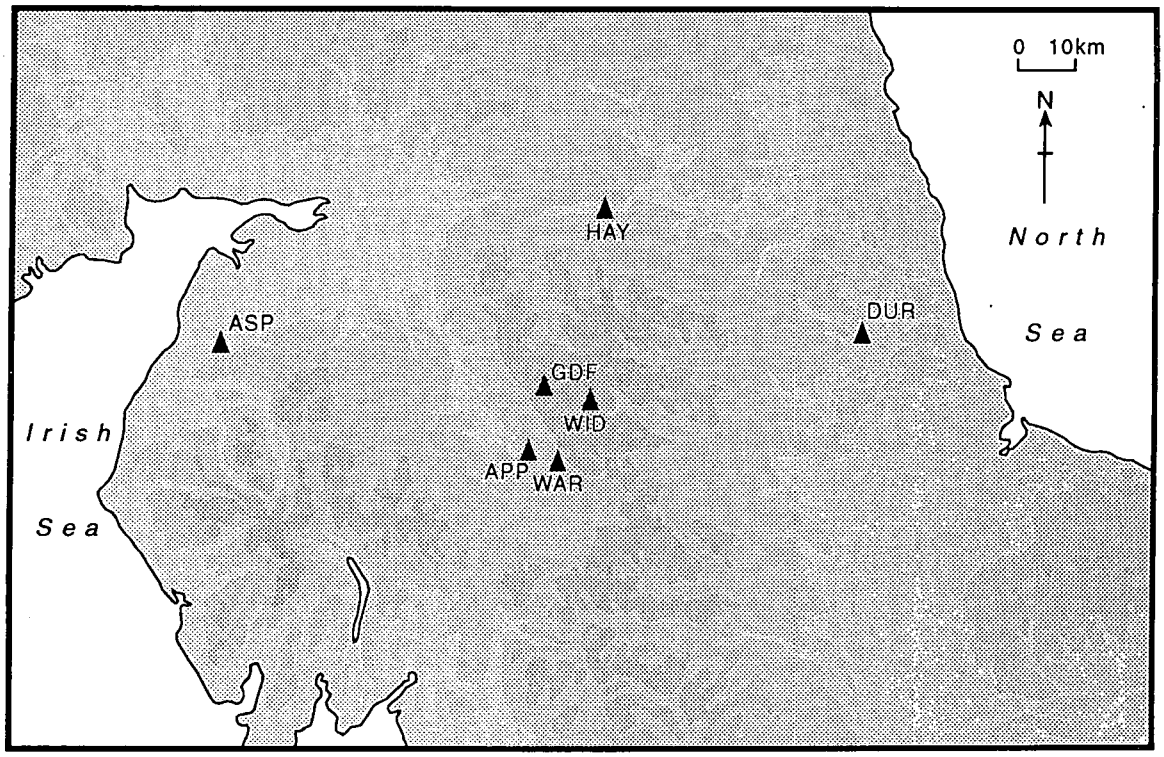

Key to Locations

APP	Appleby	150
ASP	Aspatria	64
DUR	Durham	102
GDF	Great Dun Fell	847
HAY	Haydon Bridge	82
WAR	Warcop	244
WID	Widdybank Fell	513

Figures represent the altitude of the Station in metres.

Land below 122m O.D. 122 - 427m Land over 427m

Fig 6.1 Map showing the 7 Meteorological Stations used to examine Lapse Rate Variations on different sides of the Pennines

Figure 6.2. Monthly Variation of Temperature Lapse Rates involving Great Dun Fell (847 m) as the Upland Reference Point

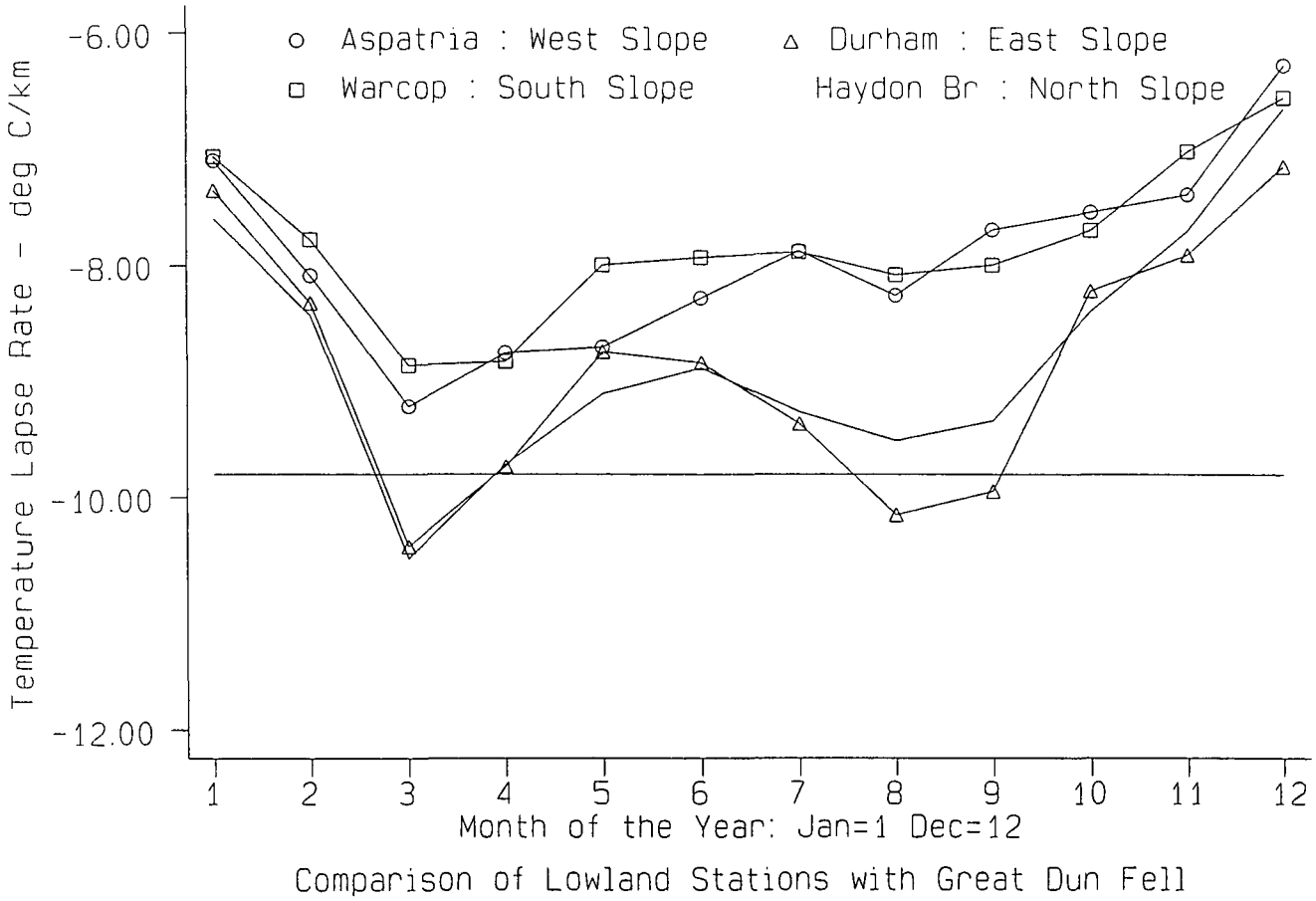

Figure 6.3. Monthly Variation of Temperature Lapse Rates involving Widdybank Fell (513 m) as the Upland Reference Point

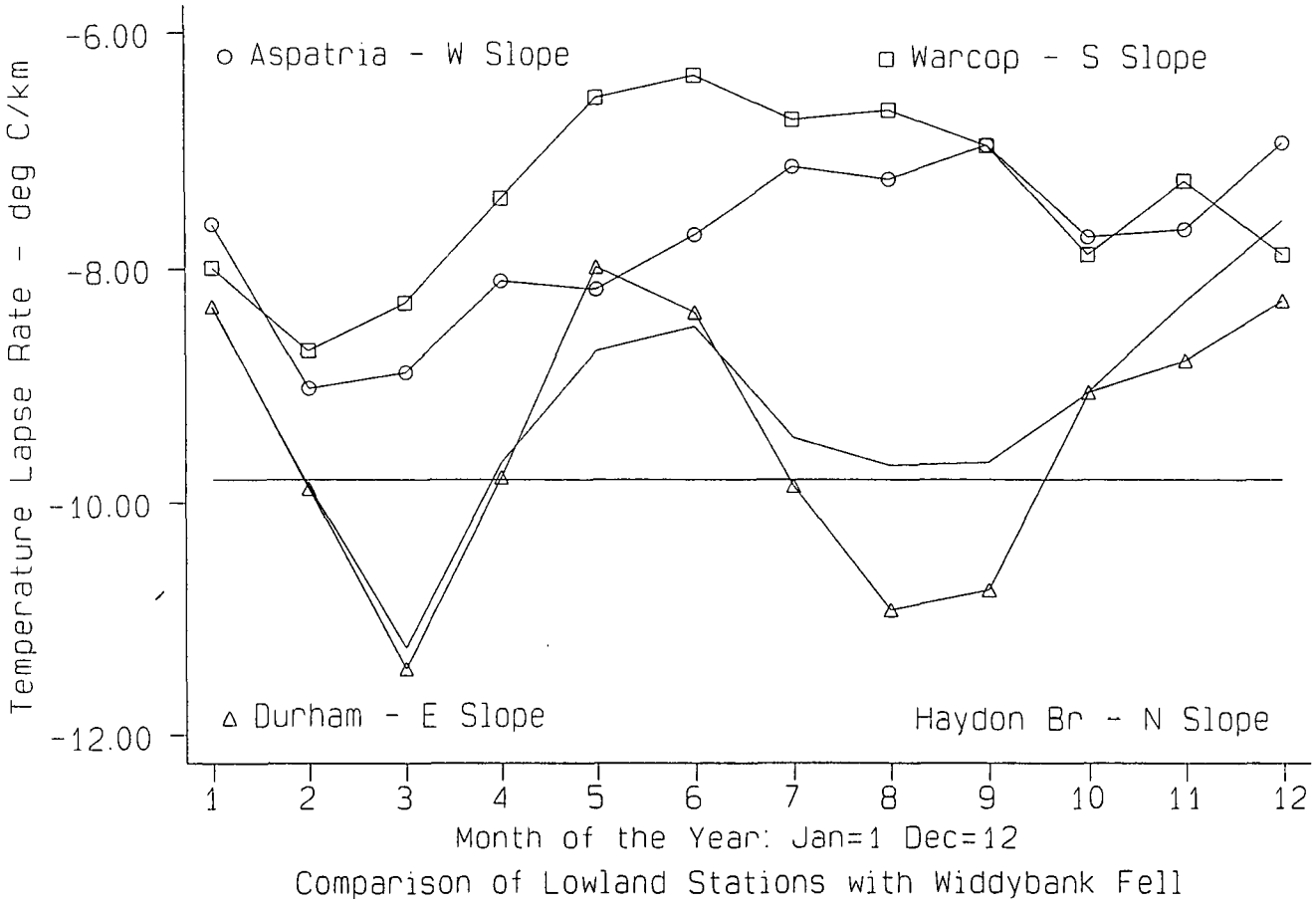

Comparison of Lowland Stations with Widdybank Fell

Table 6.1: Mean lapse Rates in 1985-1990 (°C km^{-1}). G=Great Dun Fell, W=Widdybank Fell.

STATION PAIR	JAN	FEB	MAR	APR	MAY	JUN
G-DUR	-7.36	-8.32	-10.42	-9.73	-8.74	-8.83
G-WAR	-7.06	-7.78	-8.86	-8.82	-7.99	-7.93
G-ASP	-7.10	-8.08	-9.21	-8.75	-8.70	-8.28
G-APP	-6.86	-7.95	-10.16	-9.96	-9.56	-9.70
G-HAY	-7.59	-8.43	-10.52	-9.71	-9.10	-8.88
W-DUR	-8.32	-9.88	-11.44	-9.78	-7.98	-8.37
W-WAR	-7.99	-8.70	-8.29	-7.40	-6.54	-6.36
W-ASP	-7.62	-9.02	-8.89	-8.11	-8.17	-7.71
W-APP	-7.19	-9.01	-10.28	-10.19	-10.39	-10.39
W-HAY	-8.33	-9.86	-11.25	-9.65	-8.70	-8.49
G-W	-5.96	-6.35	-9.46	-9.67	-8.92	-9.04
JUL	AUG	SEP	OCT	NOV	DEC	MEAN
-9.36	-10.15	-9.95	-8.21	-7.91	-7.14	-8.87
-7.88	-8.08	-7.99	-7.69	-7.01	-6.55	-7.79
-7.87	-8.25	-7.69	-7.54	-7.38	-6.27	-7.92
-9.45	-9.21	-9.18	-8.01	-6.59	-6.01	-8.57
-9.25	-9.50	-9.33	-8.39	-7.70	-6.64	-8.77
-9.85	-10.92	-10.75	-9.05	-8.78	-8.27	-9.44
-6.73	-6.65	-6.95	-7.88	-7.25	-7.88	-7.36
-7.13	-7.24	-6.95	-7.73	-7.66	-6.93	-7.75
-9.97	-9.17	-9.37	-8.60	-6.42	-6.34	-8.95
-9.44	-9.68	-9.65	-9.05	-8.28	-7.59	-9.16
-8.92	-9.37	-8.77	-7.49	-6.77	-5.54	-8.05

6.2.1 Eastern Slope

The temperature contrast between Widdybank Fell and Durham (to the east of the Pennines) was described in Chapter 5. Rates exceed -10°C/km in March and August/September. The mean for March reaches -11.44°C/km!

Comparison of Great Dun Fell with Durham again shows peaks in the lapse rate in spring and late summer. There are characteristic peaks near the equinoxes, in March (-10.42°C/ km) and August/ September (-10.15 and -9.95°C/km). For the average lapse rate to exceed the DALR, superadiabatic lapse rates must commonly form. Rates remain moderately high throughout summer but fall rapidly in winter. The mean rate in May is reduced to -8.74°C/km and although the reduction is not as dramatic as in the Widdybank case (-7.98°C/km), it is still noticeable and is due to a longitudinal decrease in temperature superimposed on top of the altitudinal decrease, because of the cooling North Sea influence. Air flowing from sea to land will not vary substantially in temperature from the sea-surface temperature. The difference between the two temperatures varies according to the flux of sensible heat above the ocean surface (Cayan 1980). Onshore airflows will therefore be relatively cool in summer and warm in winter. This cooling effect of the cold surface waters off the north-east coast in spring and summer produces a characteristic type of weather called the Haar (Catchpole 1966), depressing daily maximum temperatures at Durham. This is the reason for decreased lapse rates on the eastern slope in May and June. The winter trough in lapse rate can be explained by the relative warmth of Great Dun Fell in winter, temperature inversions commonly forming below summit level.

6.2.2 Western Slope

Comparison was also made between Great Dun Fell and Aspatria to the west in Cumbria. A striking similarity is seen with Warcop (described in the next section). The lapse rate peaks in March (-9.21°C/km) and then gradually decreases until December (-6.27°C /km). The simple pattern of spring maximum and winter minimum is similar to that described by Harding (1978, 1979) for Great Britain, and Green & Harding

(1980) for Southern Norway. The steeper lapse rates of late summer, present on the northern and eastern slopes, are absent. Aspatria experiences a cooling coastal influence in summer which is likely to decrease lapse rates at this season. The northern and eastern slopes show steeper lapse rates than the western slope all year, even in May and June (although the difference is least during this period). Prevailing winds being south-westerly, föhn effects on lee slopes are the most likely explanation of this. This contradicts the findings of Birse (1971), who states that the maritime western slopes of Britain have steeper mean lapse rates than the more continental eastern ones.

Comparison of Aspatria with Widdybank Fell produces yet another different seasonal lapse rate cycle. Strangely, the shallowest lapse rates to the west of the Pennines occur in September, and rates are low throughout late summer. The influence of the Irish Sea in reducing summer temperatures at Aspatria is possibly contributory to the shallow mean rates recorded during this typically progressive period of the year (Lamb 1950).

6.2.3 Southern Slope

Although Warcop is almost due south of Great Dun Fell, like Appleby it is situated in the Vale of Eden. We may expect the seasonal variation in lapse rate to be similar to the local escarpment rate (section 6.3 e). The distance between Warcop and Great Dun Fell is 12.71 km (very similar to the distance between Appleby and Great Dun Fell) and the elevation difference is just over 600 metres. On average the southern slope experiences much shallower lapse rates than the other slopes, presumably associated with more stable conditions and in contradiction to findings that mean lapse rates are steeper on sunlit slopes (McCutchan et al. 1982). Rates average -8°C/km from May to September, decreasing to less than -7°C/km in December. Southerly airflows, which affect the slope directly, are cooled from below as they move north, increasing stability. It is also possible that gusts of warm air rise up the south-facing slope by day initiated by solar heating, increasing the temperature at Great Dun Fell compared with Warcop (Pedgley 1979). There is a marked spring maximum in the lapse rate which reaches -8.86°C/km in April (this is, however, a relatively low value for April).

Superadiabatic lapse rates are absent on the southern slope. Lapse rates depend on the local climatic characteristics of both upland and lowland sites. If Appleby were to record higher maxima in summer due to increased shelter and its urban nature, this would explain the high lapse rates recorded (over -10°C/km). Warcop station is sited at 244 m on a military firing range and has a much more open exposure. This would explain the lower lapse rates.

The comparison of Warcop with Widdybank Fell yields even more unusual results (Table 6.1). The distance between the two locations is 12.84 km and the elevation gain is only 269 m. Lapse rates are low, especially in summer (-6.36°C/km in June). Unusually, the February gradient (-7.99°C/km) is the steepest! A peak in lapse rate in February (rather than March) and in early winter, and lower rates in summer (between -6 and -7°C/km from May to September), are incoherent with the other examples and may arise due to local influences. The comparison is unusual in that high land rises to about 700 m between the two sites and the overall lapse rate is thus an average of those on the south-facing and north-facing slopes. The ridge of high land acts as a climatic barrier, allowing relatively cold or warm air to become trapped on one side of the ridge leading to contrasting temperature regimes at the two locations. When Widdybank is affected by colder air the apparent "lapse rate" increases. In February, a month often characterised by calm anticyclonic weather, temperature inversions are likely in the Upper Teesdale basin (Manley 1943).

This contrast in calculated lapse rates between Great Dun Fell and Widdybank Fell when both are compared with Warcop arises because the exposed former station is unlikely to suffer from trapping of cold air whereas this often occurs at Widdybank. In the summer there is also the possibility that the area around Widdybank Fell acts as a high plateau, with increased daily maxima resulting from warming of the upland atmosphere (Flohn 1953, Tabony 1985).

6.2.4 Northern Slope

This is calculated using Haydon Bridge in the Tyne valley to the north. The

distance from Great Dun Fell is 34.74 km and the elevation difference is 765 m. The pattern of lapse rate variation is similar to that on the southern slope when Great Dun Fell is used as the upland station. The rate peaks in March (-10.52°C/km) and is lowest in December (-6.64°C/km). The northern slope rate is always steeper than the southern counterpart. There is limited evidence of a decrease in rates in May and increase in late summer, similar to the pattern on the eastern slope. Advective cooling from the east is a slight influence at Haydon Bridge, as at Durham. Comparison of Haydon Bridge with Widdybank Fell shows a similar pattern in lapse rate, with -11.25°C/km recorded in March and -7.59°C/km in December.

6.2.5 A Local Comparison: The Pennine Escarpment

Lapse rates calculated over the western Pennine escarpment (Figures 6.4 a and 6.4 b) are obtained by comparing the upland sites with Appleby. The escarpment lapse rate increases in summer, averaging nearly -10°C/km between March and September. The escarpment experiences the highest lapse rates amongst all those studied from April to July, i.e. during the period when solar radiation input is high, suggesting a steepening of the local lapse rate in response to solar heating. In March, -10.16°C/km is one of the highest mean lapse rates in the world. Steeper rates may be found over arid deserts at low levels in daytime due to the intense heating of the ground surface (Hastenrath 1968) but only in the lowest few metres. In winter the escarpment rate falls to -6.01°C/km (December), presumably due to temperature inversion formation in the Vale of Eden which is aided by drainage of cold air from the Pennine escarpment (Manley 1943).

Temperature comparison between Appleby and Widdybank Fell (Figure 6.4 b) is also representative of the local Pennine escarpment lapse rate, although Widdybank Fell lies considerably east of the Pennine watershed, complicating the comparison. The mean rate in both May and June is -10.39°C/km, falling to -9.97 °C/km in July. From November to January the rate is below those on the other four slopes, suggesting that local rate on this steep slope is strongly influenced by solar input, and less dependent on advection.

Figure 6.4. Monthly Variation of the Day-Time Lapse Rate on the Pennine Escarpment, involving Appleby as the Lowland Reference Point

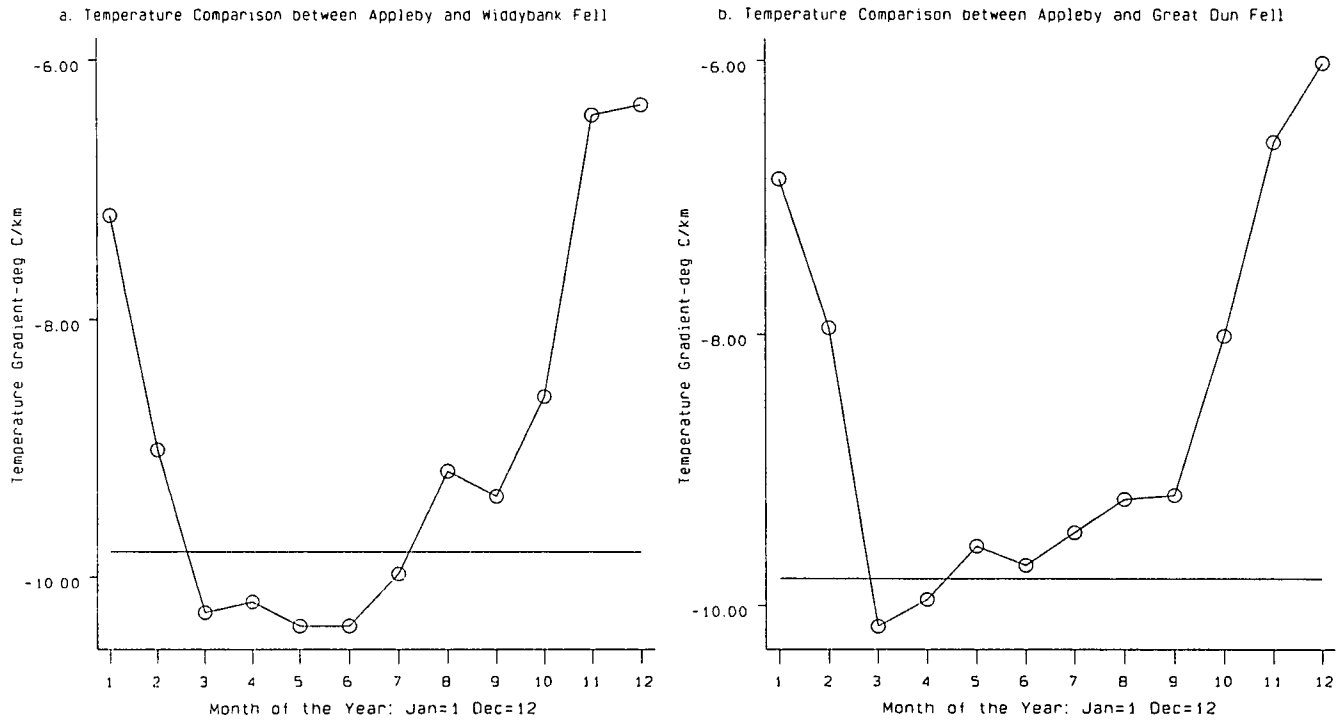

In conclusion, the steep lapse rate on the western Pennine escarpment is primarily a summer phenomenon. The lapse rate on individual days in winter may be as steep as in summer, i.e. -10°C/km or more, as mean monthly rates disguise daily variation. A few days with pronounced temperature inversions in winter would reduce the average figures dramatically.

6.2.6 The Upper Air Lapse Rate (between 513 and 847 m)

The lapse rate between the two upland locations, Great Dun Fell (847 m) and Widdybank Fell (513 m), gives an idea of air mass stability above 500 m. Although it is not equal to the lapse rate in the free air between these two altitudes, it is a good approximation. A pronounced seasonal variation in upper-air lapse rate is revealed (Figure 6.5). From November to February the shallow rates between -5 and -7°C/km are less steep than those at lower altitudes, indicating that lapse rate decreases with increasing altitude (Figure 6.6 a). This pattern suggests the presence of temperature inversions in winter in the altitudinal range of 500 to 900 m, depressing mean lapse rates at high altitude. In December a mean upper-air rate of -5.54°C/km is only just over half of the DALR and anomalously low rates remain until February.

In summer the lapse rate between Great Dun Fell and Widdybank Fell averages -8 to -9°C/km, i.e. slightly below the DALR. The highest values occur at the beginning and end of this period, i.e. in March (-9.46°C/km), April (-9.67°C/km) and September (-8.77°C/ km). The decrease of the upper air lapse rate is rapid as autumn approaches, the mean for October being only -7.49°C/km. Solar heating increases the upper-air rate in summer, and summer lapse rates increase with altitude (Figure 6.6 b). The mean lapse rate between Great Dun Fell and Widdybank Fell is fairly low (-8.05°C/km), suggesting that on an annual basis the winter trend for lapse rates to decrease with altitude is dominant. Generally, temperatures at Great Dun Fell are higher than would be expected from a linear model between temperature and altitude.

Figure 6.5. Monthly Variation of the Upper Air Lapse Rate between Widdybank Fell and Great Dun Fell

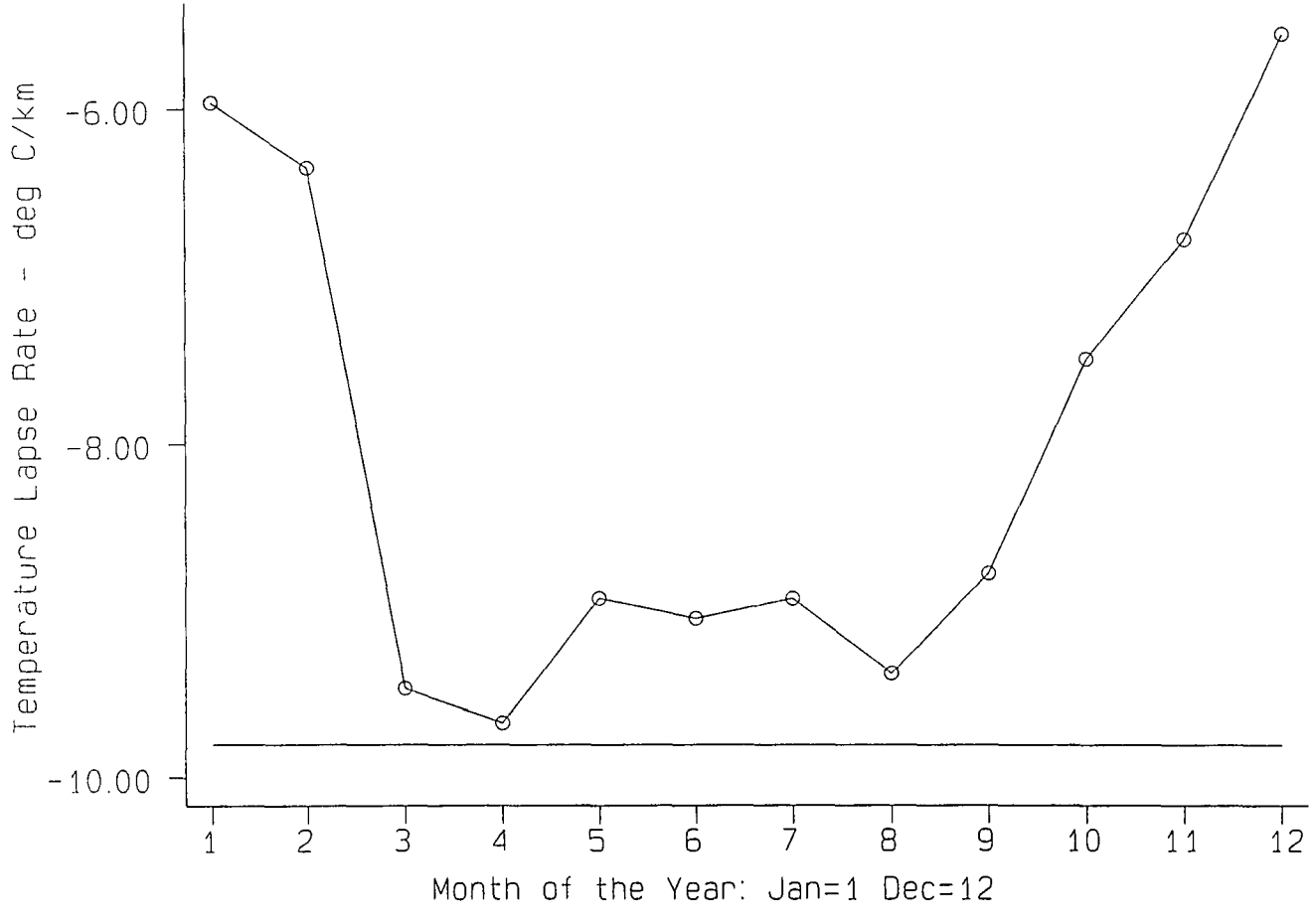

Figure 6.6. Temperature Relationships with Altitude.

a. Decrease in Lapse Rate with Altitude (Winter)

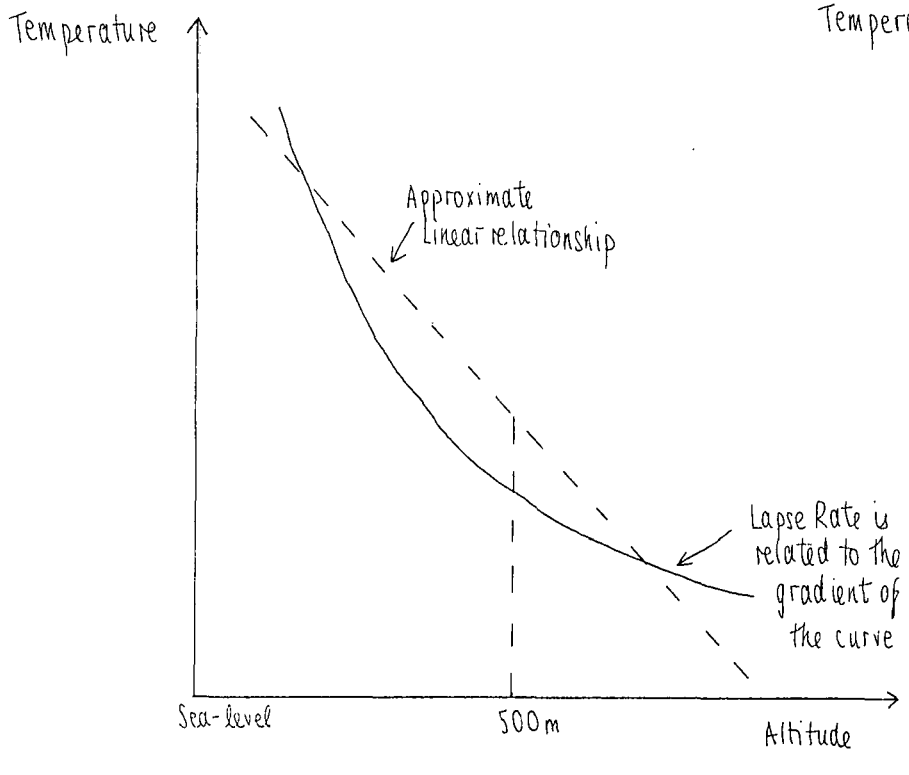

Mean Temperature at the highest elevations is higher than would be expected from a linear relationship

b). Increase in Lapse Rate with Altitude (Summer)

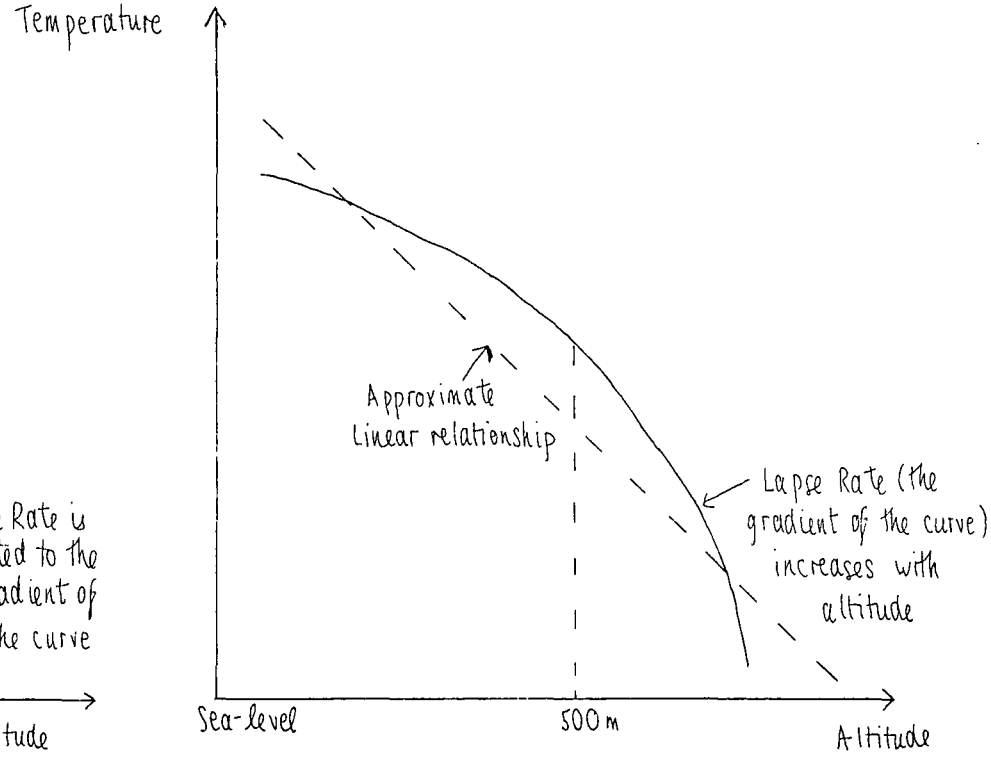

Mean Temperature at the highest elevations is lower than would be expected from a linear relationship

6.3 Summary of Seasonal Lapse Rate Variation

The above analysis shows that the lapse rate behaviour described in Chapter 5 (relating to Durham and Widdybank Fell) is not representative. The unusual nature of the original comparison is explained in part by the influence of the North Sea in depressing Durham maxima in early summer and increasing them in late summer and early autumn. Of the eleven lapse rates listed in Table 6.1, only those involving the station on the eastern side of the Pennines (i.e. Durham) show the trough of lapse rate in early summer (May and June).

In winter the southern and western slope rates are similar (Figure 6.2). In summer the southern slope has the shallowest lapse rates. Rates on the northern and eastern slopes are steeper due to lee effects all year although the difference is minimal in May and June when typically the circulation becomes less dominated by westerly flow (Lamb 1950) and the Haar cools the eastern regions. Lapse rates on all slopes peak in March due to the instability of polar maritime air (the most common air mass) at this time, and the shallowest lapse rates are experienced in winter due to temperature inversions.

Using Widdybank Fell, instead of Great Dun Fell, as the upland reference station (Figure 6.3) decreases the recorded lapse rates in summer, especially on the southern and western slopes (even to below winter rates). This is evidence of an upland heating effect in summer (Flohn 1953, Tabony 1985). This heating spreads to the east in July and August through föhn effects, increasing lapse rates on the northern and eastern slopes, but not on the southern and western slopes. All lapse rates decrease as winter approaches and temperature inversions begin to form.

The local escarpment rate remains extremely high throughout the summer (Figures 6.4 a and 6.4 b) as well as the upper air lapse rate above 500 m (Figure 6.5). The latter is reduced dramatically in winter.

It would be foolish to attempt to describe the variation in mean lapse rates using

a few stations because results are not representative. The mean lapse rate is described later using data from 22 stations. The result will be less dependent on the exposure of individual stations (Chapter 8).

6.4 Airflow Effects

The lapse rate between any two locations also varies daily. The direction of surface airflow is critical since it determines the relationship between the flow of air and the topography of the inter-station transect. Weather contrasts will be maximised when the airflow is parallel to the inter-station transect. For example, considering the eastern slope of the Pennines between Great Dun Fell and Durham, weather contrasts between the two sites are likely to be greatest for westerly and easterly airflows. In such cases the airflow reaches one station considerably before the other and can undergo modification between the two. When airflow is perpendicular to the inter-station transect differences in weather still occur because the weather experienced at each station depends on topography upwind, which will be different in each case.

Most ground-based lapse rates are expected to vary systematically according to airflow direction. This is tested for the four directional, one local and one upper air lapse rates discussed earlier. Surface wind direction is used to classify airflow direction despite discrepancies between surface and geostrophic winds (Marshall 1954). Surface winds at Durham and at Low Etherley (a location not used to generate lapse rates) are used in turn to classify wind direction. The sensitivity of results to slight changes in the airflow classification can then be assessed.

6.4.1 Durham Surface Winds

Figure 6.7 a shows the variation of the four lapse rates (using Great Dun Fell as the upland reference station) according to surface wind direction recorded at Durham. The lapse rate on the southern slope exceeds -8°C/km for westerly, northerly, north-easterly and easterly flows, whereas the rate is lowest for southerly flows. This rate is steeper for cross-slope and downslope winds than for upslope winds.

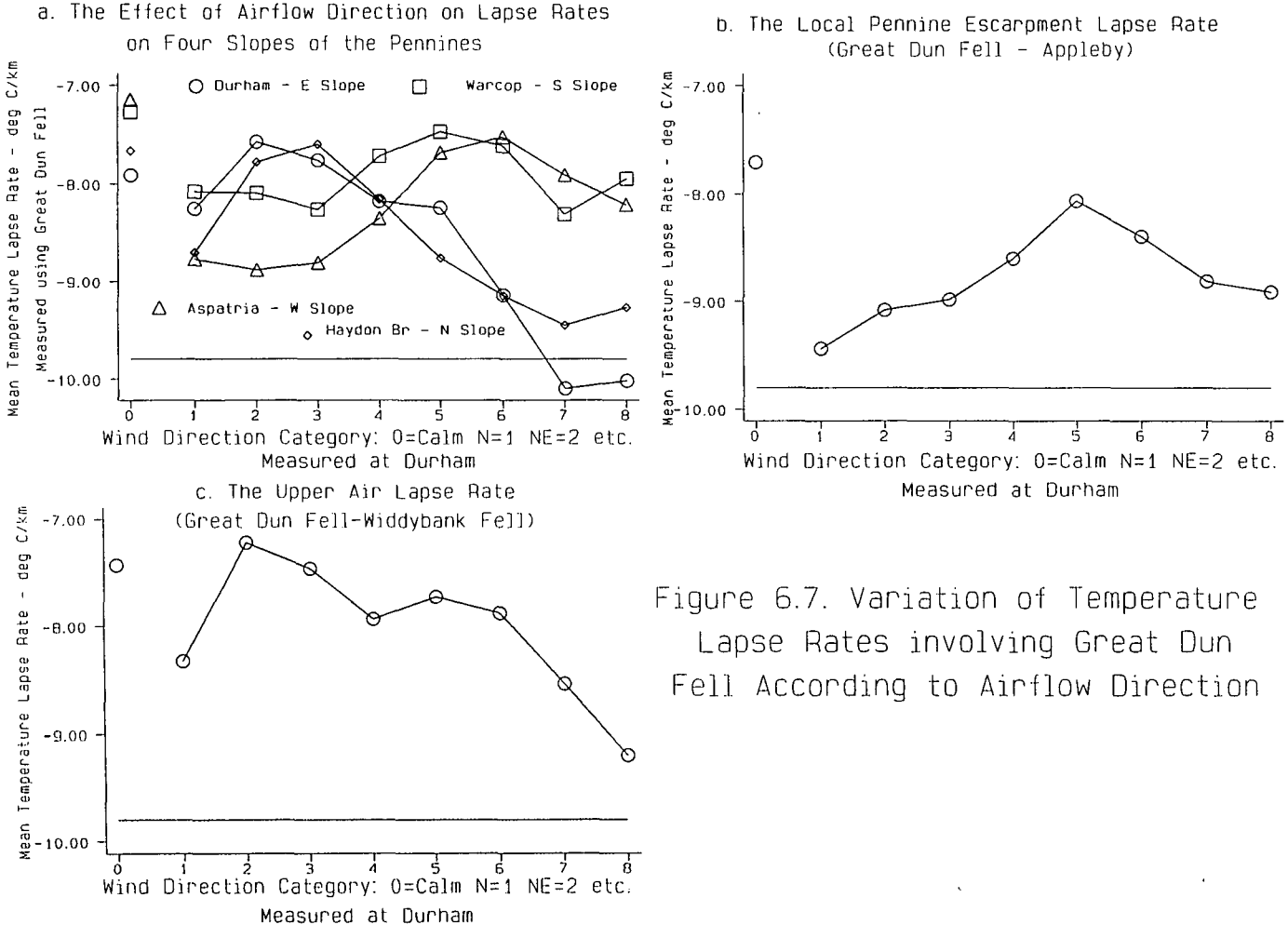

Figure 6.7. Variation of Temperature Lapse Rates involving Great Dun Fell According to Airflow Direction

The pattern is stronger on the eastern slope. Steepest lapse rates occur with downslope westerly winds (over -10°C/km) and shallowest rates for upslope north-easterly and easterly winds. The physical reasons behind this are easy to explain. As air ascends it will expand and cool and often lose excess moisture through condensation. The air therefore cools at the Saturated Adiabatic Lapse Rate (SALR) which, although dependent on temperature, is much less than the DALR. On descending a slope the air warms at the DALR. Therefore the lapse rate is steeper on the lee slope. Even if no condensation occurs, air can be forced downwards by an inversion aloft and it will still warm at the DALR (Lockwood 1962, Beran 1967). In some cases there can be a temperature inversion on the windward slope (Pedgley 1979), air trapped by topography. Superadiabatic lapse rates will then be measured on the lee slope when an improvement in weather accompanies the downward air movement. Clouds may dissipate in the lee of the hills, allowing solar heating to increase temperatures further in the lowlands. Harding (1979) showed that there was a positive correlation between the ground-based lapse rate on the eastern slope of the Pennines and the upland deficit in sunshine hours for this reason.

Lapse rates recorded on the western slope vary in reverse to those on the eastern slope, with steepest rates occurring under downslope easterly winds. For northerly, north-easterly, easterly and south-easterly flows the western slope rate is the steepest of the four, reaching -8.88°C/ km for north-easterlies. Predictably, the lowest rates are for south-westerly airflows (-7.52°C/km) and calm conditions (-7.14°C /km). The lapse rates on the northern slope are very similar to those on the eastern slope.

The local escarpment rate between Appleby and Great Dun Fell exhibits a strong relationship with wind direction, peaking for downslope northerly flow (-9.44°C/km). The rate is lowest for southerly (upslope) flow (-8.06°C/km). In between these two extremes the change of gradient with airflow direction is regular (Figure 6.7 b). The contrast between downslope northerly and upslope southerly flows is reinforced by contrasts in stability. Northerly flows are usually moving from a cold to a warmer surface. Heating from below increases the lapse rate in the free air in the lowest air layers. The opposite is true for southerly flow which is cooled from below as it moves

north.

Lapse rates on all four slopes and on the Pennine escarpment fall below -8°C/ km under calm conditions. This is a strong indication of the presence of temperature inversions below Great Dun Fell. The upper air lapse rate between Widdybank Fell and Great Dun Fell is represented in Figure 6.7 c. All rates are below the DALR. The steepest occur with north-westerly and westerly airflows, presumably in polar maritime air flowing downslope. The lowest rates occur under north-easterly airstreams (-7.22°C /km) and for calm conditions (-7.43°C/km). It is possible that north-easterly flows can sometimes allow trapping of the air by the Pennine ridge which runs from north-west to south-east. On occasions air escapes over the ridge as the violent Helm wind (Manley 1945b). Low lapse rates would be explained by the trapping of cold air in the Widdybank area.

Using Widdybank Fell instead of Great Dun Fell as the upland location produces broadly similar results (Figures 6.8 a and 6.8 b). Again, lapse rates on both northern and eastern slopes are similar, peaking for westerly airflows. The figure of -11.44°C/ km for westerly flows can only arise from a combination of descent at the DALR and a substantial warming due to a simultaneous weather improvement. In contrast, upslope north-easterly and easterly winds record rates below -8°C/km. Rates on the southern slope are almost a mirror image of those on the northern and eastern slopes. Downslope north-easterlies produce a mean rate of -9.22°C/km, possibly reinforced by a dispersion of cloud in the Eden Valley. Strangely, northerly airflows only record a mean rate of -7.51°C/km, not that different from upslope southerly winds (-6.77°C/km). The western comparison with Aspatria, however, shows a strong pattern, opposite to that on the eastern slope.

Finally, the local escarpment rate (Widdybank Fell versus Appleby) is displayed in Figure 6.8 b. A very strong pattern emerges with high rates (-10.96°C/km) for downslope north-easterlies and shallow rates for the largely upslope southerlies (-8.07°C/ km). The pattern of change between the two extremes is remarkably uniform. All four slope lapse rates and the local escarpment comparison are low under calm

Figure 6.8. Variation of Temperature Lapse Rates involving Widdybank Fell According to Airflow Direction

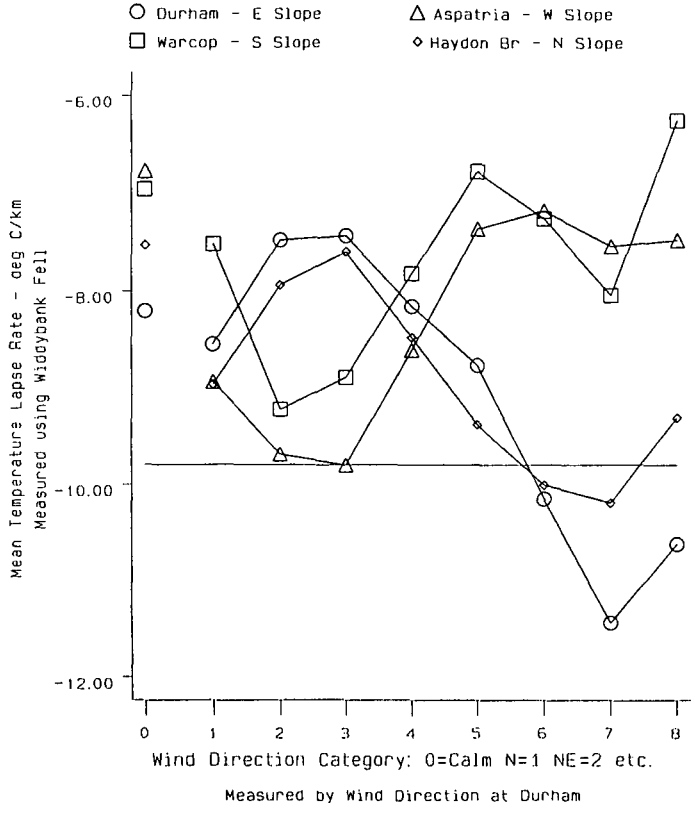

a. The Effect of Airflow Direction on Lapse Rates on Four Slopes of the Pennines

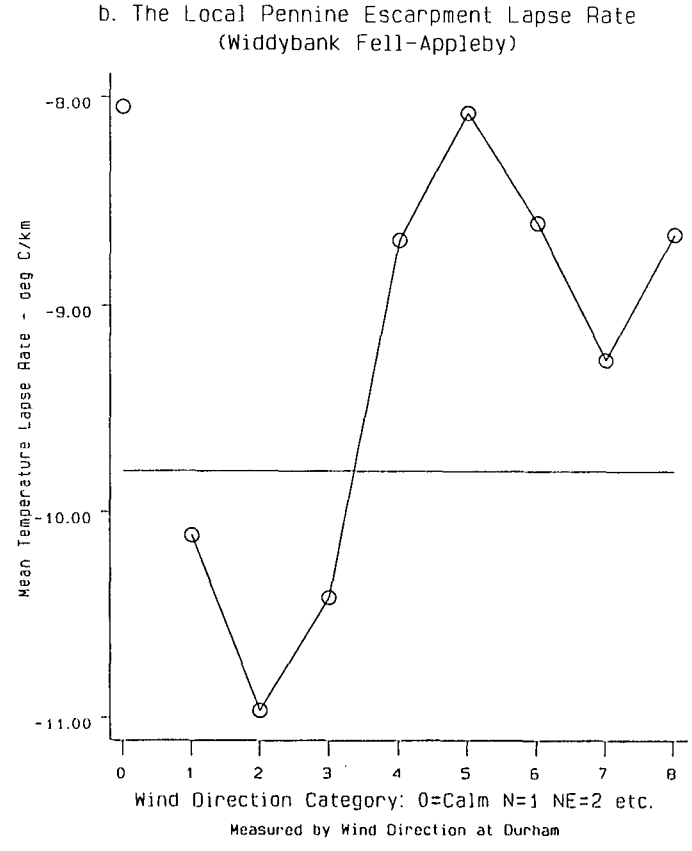

conditions, rates falling between -6 and -8°C/km.

6.4.2 Low Etherley Surface Winds

Wind direction at Low Etherley was classified into sixteen classes (as opposed to eight). The graph of the upper-air lapse rate variation according to wind direction is reproduced (Figure 6.9). Because of the greater number of airflow classes the curve is less smooth than in Figure 6.7 c. However, results are similar. Lapse rates are steeper for airflows between south and north with a westerly component, than for calm conditions and airflows between north-north-east and south-south-east. Despite a change in the airflow classification, there is little overall change in the upper-air lapse rate pattern. Similarly, the four other lapse rates are steepest when winds are downslope and shallowest for upslope winds (Figure 6.10). There is slightly more irregularity in the four graphs (Widdybank Fell is the upland station) but the main trends are the same as in Figure 6.8 a). This is reassuring, indicating that use of surface winds at either Durham or Low Etherley gives a reasonable indication of macroscale airflow direction over northern England.

6.5 Conclusions

The spatial and temporal variation of the altitudinal temperature gradient in Northern England has been investigated, using two upland and five lowland stations:

1. the four lapse rates representative of conditions to the north, east, south and west of the Pennines show different relationships with season and airflow direction;

2. seasonal and airflow contrasts are very strong for a local lapse rate measured over the steepest part of the Pennine escarpment. Airflow direction is crucial, since in nearly all cases descending air produces a steeper lapse rate than ascending air. The local escarpment rate is less affected by horizontal advection;

3. <u>local</u> climatic influences at each lowland station ensure that the lapse rate on each

Figure 6.9. The Variation of the Upper Air Lapse Rate (Great Dun Fell -Widdybank Fell) According to Airflow Direction Measured at Low Etherley

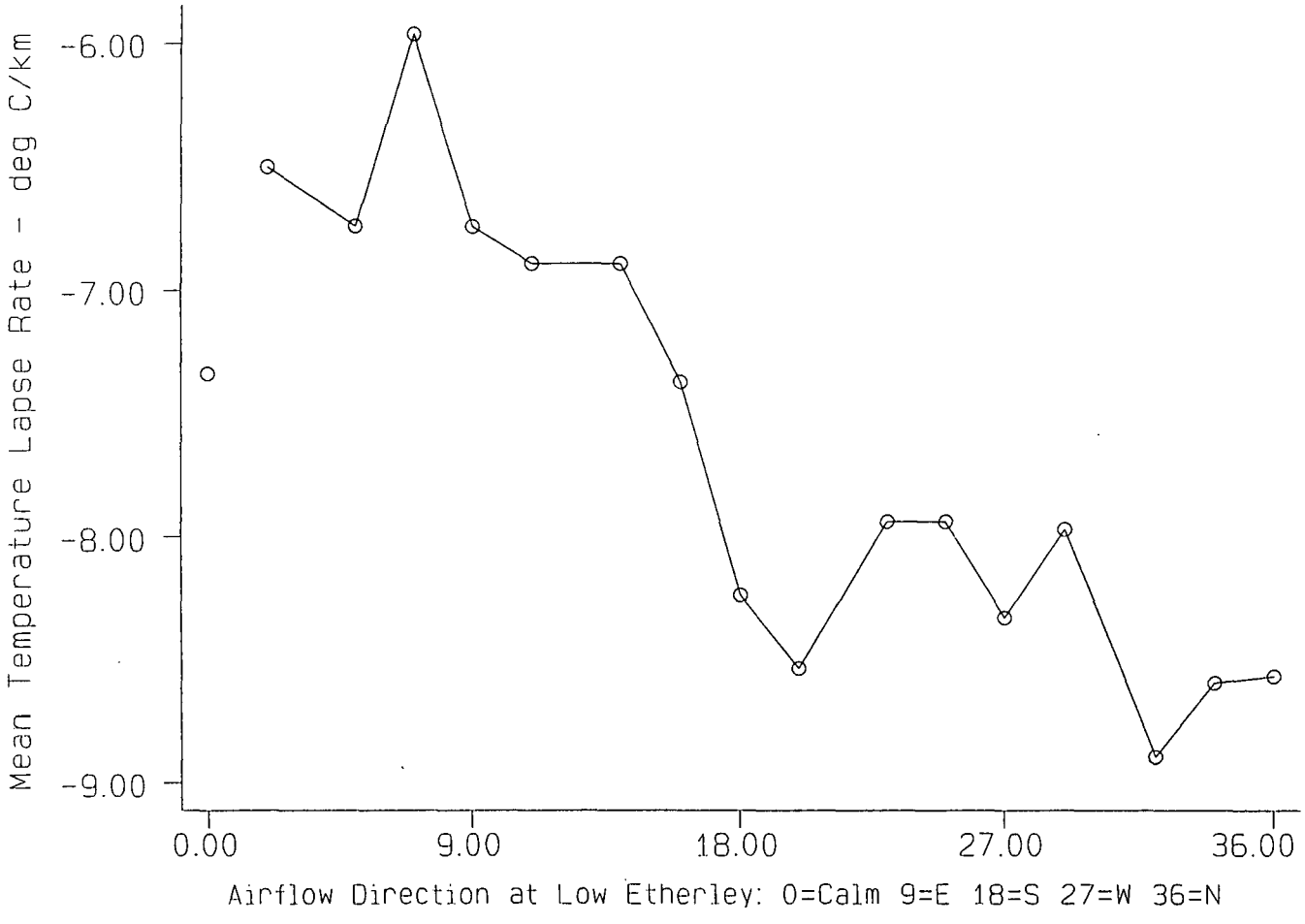

Figure 6.10. Variation of Temperature Lapse Rates on Four Slopes of the Pennines involving Widdybank Fell (513 m), According to Airflow Direction (Measured at Low Etherley)

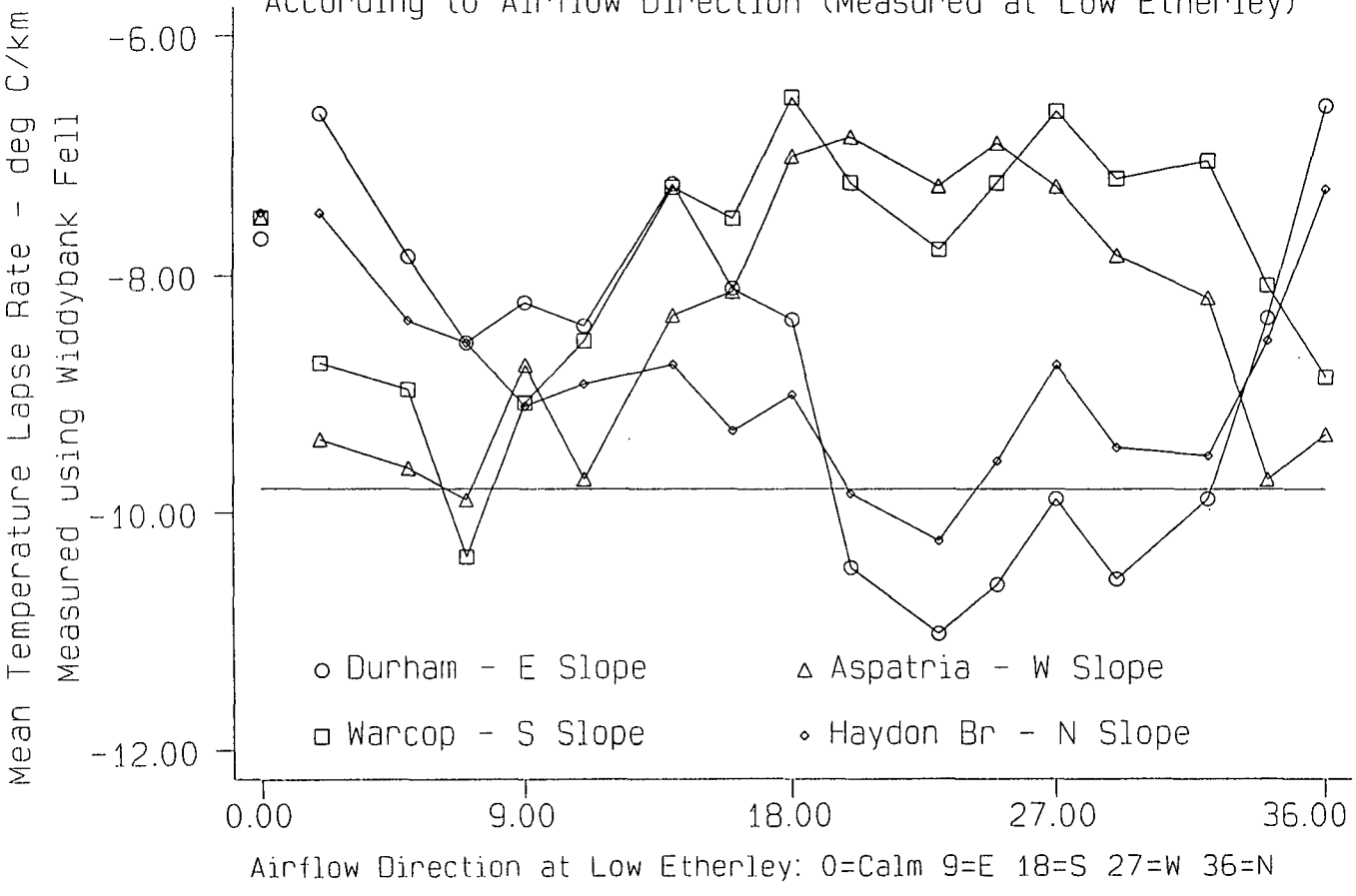

slope shows a unique seasonal fluctuation and relationship with airflow direction. It is difficult to obtain knowledge about the mean altitudinal effect on temperature in Northern England from ground-based temperature gradients alone.

Changes in the relative frequencies of airflow types would have contrasting effects on temperature in different locations. Increased westerly flow, for example, would increase mean lapse rates on the eastern slopes of the Pennines and reduce them in the west. The upper air lapse rate (between Great Dun Fell and Widdybank Fell) gives a good indication of contrasts in the free-air lapse rate between different airflows, and hence air-masses. However, there is still a topographical influence which affects any ground-measured rate.

A multiple regression analysis will be performed to extract the mean altitudinal effect on temperature using data from all stations available (Chapter 8). Once the seasonal variation and airflow contrasts in the mean altitudinal effect on temperature are known, this knowledge can be used to compare the upland/lowland temperature resource gradient under different circulation scenarios at different seasons.

Before this regression analysis is attempted the physical factors behind air temperature variation are examined. An energy balance model (EBM) is developed in the next chapter (Chapter 7) based on the response of surface temperatures recorded at Durham and Widdybank Fell to net radiation input.

THE DEVELOPMENT OF A PHYSICALLY-BASED TEMPERATURE MODEL TO INVESTIGATE DAILY RADIATION FLUXES AND THE SURFACE ENERGY BALANCE BASED ON METEOROLOGICAL DATA.

7.1 Introduction

The balance between continuous longwave radiation output and the periodic incoming shortwave input from the sun controls temperature fluctuation at the earth's surface, along with advective influences. The relationship between net irradiance (the net energy received at the earth's surface) and surface temperature fluctuation is not simple because of the variable partitioning of heat energy between the atmosphere and the ground, the variation of surface albedo and advection. Net irradiance can be calculated using astronomical parameters and sunshine data. If this could be related with surface temperature response, then a method for predicting surface temperature change has been achieved.

This chapter therefore describes a model to calculate net irradiance at the earth's surface which can then be related to surface and boundary layer temperature response. Through the development of a physical model one learns to appreciate the factors which influence air temperature at screen level. Such factors were outlined in Chapter 3 and discussed further in Chapter 5 when deriving a critical solar elevation required for net heating.

Numerous energy balance models have estimated latent and sensible heat fluxes and soil flux at many sites (Davies 1967, Linacre 1968, Polavarapu 1968, Le Drew 1975, Rayer 1987). The work in this chapter concerns the generation of a model requiring only meteorological surface data (such as that recorded at a climate station). Sloping surfaces are not considered, although the energy balance of a surface depends on aspect (Oliver 1991).

The six years of daily meteorological observations are used. This includes temperature maxima and minima, sunshine hours, wet and dry bulb temperatures (0900 GMT), wind speed and direction, snow cover, the state of the ground surface and cloud

cover. The model was developed using data from Durham Observatory (102 m) and Widdybank Fell (513 m). The model is listed, written in the STATA language, in Appendix 4.

7.2 Model Description

The basic energy balance equation is described by

$$R_n = H + S + G \quad ----(1)$$

where R_n is net radiation, H is latent heat, S is sensible heat, and G is soil flux.

There are essentially four stages to the process of calculating net radiation from meteorological data.

1. Calculation of daylength and noon solar elevation, given the day of the year. This describes the path of the sun in the sky.

2. Calculation of the transmissivity of the solar beam path, through estimation of water vapour and aerosol distribution in the air.

3. Use of **1** and **2** to derive net solar irradiance over the daylight period.

4. Calculation of net irradiance by subtraction of longwave radiation from **3**.

7.2.1 Calculation of Daylength

The declination of the sun is calculated by

$$d=23.45\times(\sin(0.986\times(day-80)\times cv)) \quad ----(2)$$

This varies from 23.45°N on June 22 to 23.45°S on December 22. A positive value represents a declination to the north of the equator. The days of the year are numbered from 1 to 365. Leap years were treated as though they had 365 days. 0.986 or (360/365) enters the equation because the number of days in a year does not equal the number of degrees in a complete rotation. The conversion factor of **2*π/360** (**cv**) converts degrees into radians.

Noon solar elevation, μ, is calculated by adding 35° to the declination. The latitude is assumed to be 55°N.

If **x = - tan A * tan d**, where **A** = latitude and **d** = declination, then the daylength (**dy**) is given by

$$dy=(\arccos(x))/7.5 \quad ----(3)$$

Linacre (1992)

tan A is equal to **(sin(55*2*π/360))/(cos(55*2*π/360))**. Equation 3 can be rewritten as

$$dy=(-\pi/2+\arctan(x/\sqrt{(1-x^2)}))/(2\times\pi\times7.5/360) \quad ----(4)$$

The model assumes that solar input during daylight varies in the form of a half sinusoidal curve with end points at sunrise and sunset, equidistant from solar noon. To calculate the instantaneous noon solar irradiance the transmissivity of the solar beam at that time must be calculated, requiring knowledge of water vapour and aerosol distribution in the air.

7.2.2 Calculation of Transmissivity of the Solar Beam

The mean of daily maximum and minimum temperatures is used to compute the mean daily air temperature:

$$T_{mean} = (T_{max} + T_{min}) / 2 \quad ----(5)$$

The altitude of a location will be defined as **alt**. Assuming that altitude (in metres) and mean daily temperature are known, one can define the Penman constants used in his equation for evaporation calculation (Penman 1948, McCulloch 1965). The Penman equation in its most general form as

$$evaporation = C1(net\ irradiance) + C2(aerodynamic\ term) \quad ---(6)$$

C1 and C2 depend on altitude and air temperature. The two constants add up to 1 and are defined by

$$C1 = \Delta / (\Delta + \gamma) : C2 = \gamma / (\Delta + \gamma) \quad ----(7)$$

where Δ = the gradient of the saturation vapour pressure curve against temperature and γ = the psychrometer constant. Both are measured in millibars/°C (Monteith & Unsworth 1990).

C1 is approximated by

$$C1 = 0.42 + (0.011 \times T_{mean}) + (3 \times 10^{5} \times alt) \quad ----(8)$$

Rouse et al. (1977)

C2 is then calculated by subtracting C1 from 1. Figures 7.1 and 7.2 show values of the two constants using daily data from Durham for 1985 (altitude = 102 m). C1, which reflects the importance of net irradiance in contributing to evaporation, varies from about 0.4 in winter to over 0.6 in summer. C2, which represents the importance of wind speed and humidity in evaporation, varies from O.6 in winter to below 0.4 in summer and is perfectly inversely related to C1. At higher altitude C1 increases and C2 decreases given a similar air temperature (Ripley 1963). Hence net irradiance is more important at high altitude in causing evaporation.

Δ can be calculated using the following equation (Monteith & Unsworth 1990):

$$\Delta = (((-12/5)\times(T_{mean})+2501)\times 18\times(6.1\times\exp[(17.27\times T_{mean})/(T_{mean}+237)]))/(8.314\times(T_{mean}+273)^2) \quad ----(9)$$

where T_{mean} is air temperature in °C (Appendix 2).

T_{mean} is used as an estimate of a representative daily temperature (not the dry bulb temperature at 0900 hrs). Δ varies from just below 0.5 when temperatures are 0°C to around 1.5 when T_{mean} is 20°C. By equation 7:

$$\gamma = (\Delta / C1) - \Delta \quad ----(10)$$

0.67 mbar°C^{-1} is given as an approximation to γ in the literature (Monteith & Unsworth 1990). When values are plotted for Durham, an increase in γ with temperature is experienced, from 0.6 in winter to 0.8 in summer. Increasing altitude would increase C1 and decrease the γ. This is consistent with reality, since:

$$\gamma = (C_p P) / (\epsilon L) \quad ----(11)$$

Figure 7.1. Constant C1 in the Penman Equation, Calculated for Durham (1985)

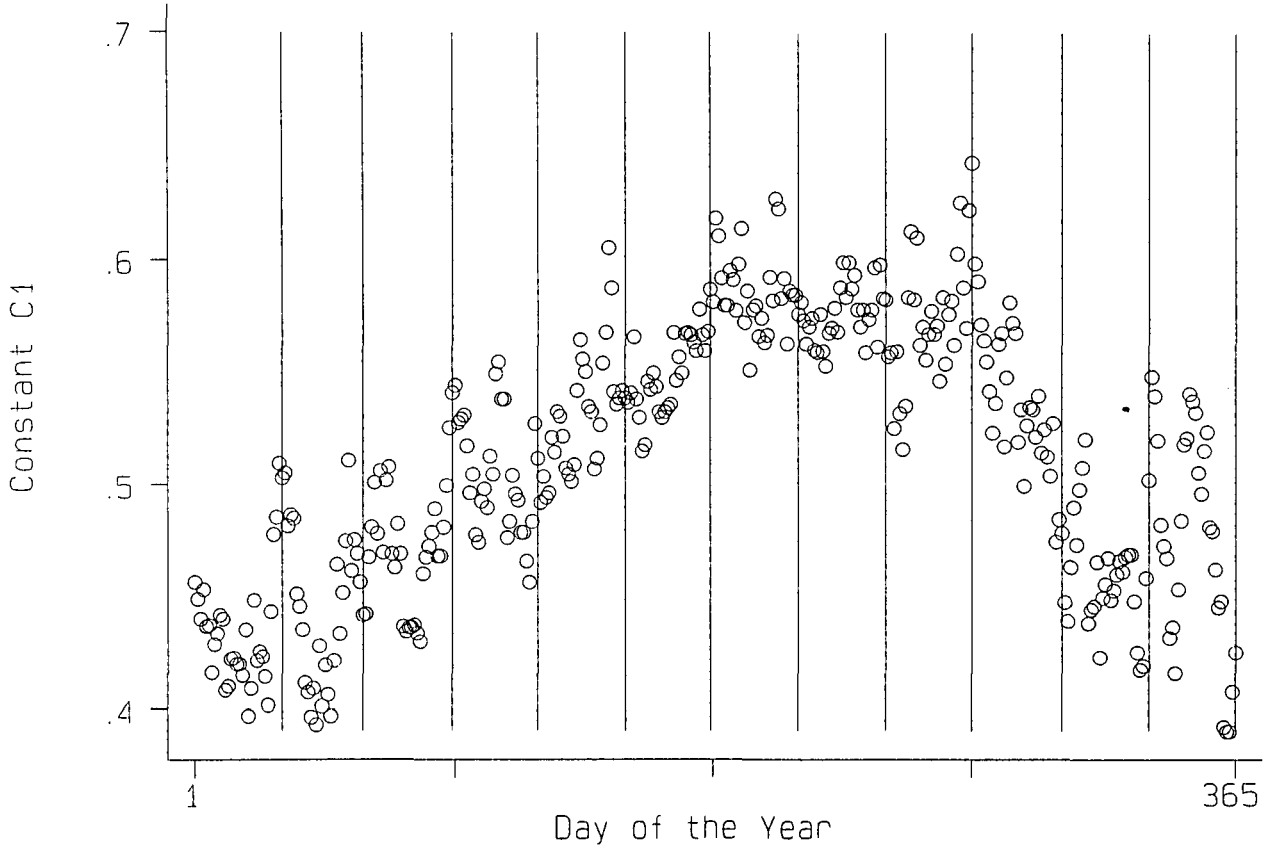

Figure 7.2. Constant C2 in the Penman Equation, Calculated for Durham (1985)

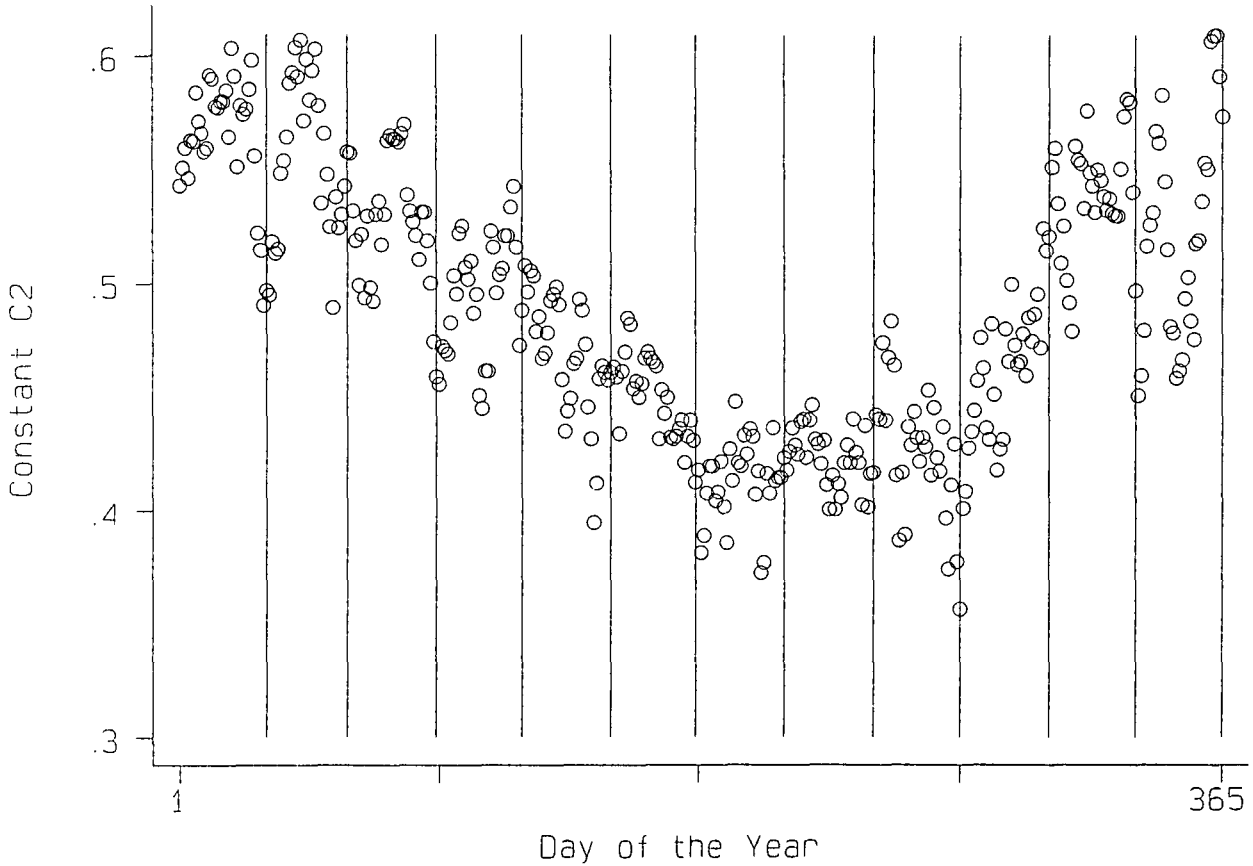

where P= atmospheric pressure, L= latent heat of vaporisation (2448.8 J g^{-1}), ϵ=density of water vapour/density of dry air, and C_p = specific heat of dry air at constant pressure (Slayter & McIlroy 1961).

Vapour pressure can be estimated from wet and dry bulb temperatures for 9 am GMT. Figure 7.3 shows the saturation vapour pressure curve plotted against air temperature. An exponential function was employed to describe this relationship:

$$satvap(e_s) = 6.1 \times (\exp((17.27 \times T)/(T+237))) \quad ----(12)$$

Saturation vapour pressures can be calculated by substituting mean daily temperature from equation 4 into equation 12. A parcel of air at point X on Figure 7.3 has dry bulb temperature T_D and wet bulb temperature T_W. The slope XY has gradient equal to $-\gamma$. Y is the saturation vapour pressure at the wet bulb temperature. The vapour pressure **e** is the vapour pressure at W, which in turn is the saturation vapour pressure $\mathbf{e_s}$ at the wet bulb temperature minus the amount represented by YW. Thus:

$$e = (6.1 \times (\exp((17.27 \times T_W)/(T_W+237)))) - (\gamma (T_D - T_W)) \quad ----(13)$$

Absolute vapour pressure can therefore be expressed in terms of γ and wet and dry bulb temperatures. Calculated pressures for Durham vary from below 4 mbar in midwinter to nearly 20 mbar (hPa) on the most humid summer days.

Relative humidity $\mathbf{H_r}$ at 9 am is calculated by dividing the vapour pressure **e** by the saturation vapour pressure at the dry bulb temperature:

$$H_r = e/(6.1 \times \exp((17.27 \times T_D)/(T_D+237))) \quad ----(14)$$

Specific humidity, representing the amount of water vapour in the air $\mathbf{H_s}$ is

Figure 7.3. Saturation Vapour Pressure Versus Temperature, Durham (1985)

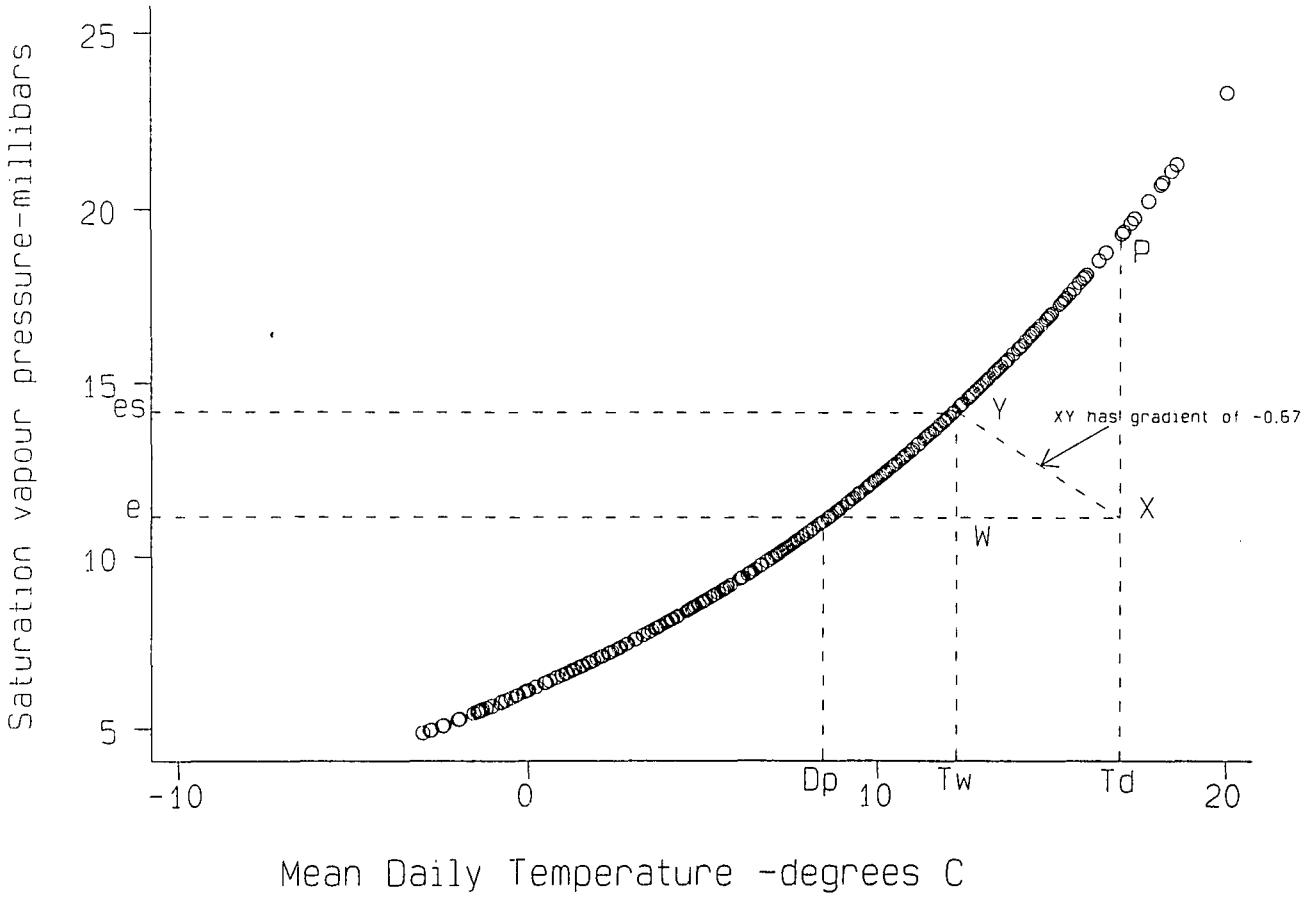

calculated by

$$H_s = (0.622e) / ((1000 - e) + (0.622e)) \quad ----(15)$$

Monteith & Unsworth (1990)

H_s is given in grammes of water vapour per gramme of air (see Appendix 3). The amount of precipitable water **w** in an air column is

$$w = (H_s \times 1000) / (500g) \quad ----(16)$$

Rayer (1987)

where **g** is the acceleration due to gravity (9.81 m s^{-2}) and 1000 represents the pressure of the air column in millibars. Units of **w** are g cm^{-2}. $\mathbf{H_s}$ must be in grammes of water vapour per kilogramme of air. **w** represents the amount of water which would be condensed from an air column, varying from 0.5 to 2.5 g cm^{-2} at Durham.

The transmissivity of the solar beam after absorption by water vapour τ_w is calculated by

$$\tau_w = 0.896 - (0.0636 \times \log[w \times \frac{1}{\sin\mu}]) \quad ----(17)$$

(Rayer 1987)

At noon transmissivity is greatest since μ reaches its maximum. At Durham noon transmissivity peaks in spring (from March to May) with high solar elevations and relatively low temperatures. Values approaching 0.9 are frequent. In December values frequently fall below 0.8 because of low solar elevations.

Transmissivity of the solar beam due to aerosols τ_a is approximated by

$$\tau_a = \exp(-0.1 \operatorname{cosec} \mu) \quad \text{----(18)}$$

Rayer (1987)

τ_a approaches 0.9 in summer but falls to 0.6 in winter.

Overall transmissivity τ of the solar beam at noon is calculated by

$$\tau = \tau_w \times \tau_a \quad \text{----(19)}$$

7.2.3 Calculation of Solar Input

Instantaneous solar irradiance at solar noon ($\mathbf{I_m}$) is given by

$$I_m = S \times \tau \times \sin\mu \ldots . W\, m^{-2} \quad \text{----(20)}$$

McIlveen (1991)

where S is the solar constant (1353 W m^{-2}).

If the daily receipt of solar radiation is assumed to follow a sinusoidal curve then the total potential irradiance during daylight ($\mathbf{I_p}$) is given by

$$I_p = (2/\pi) \times dy \times 3600 \times I_m \ldots . J\, m^{-2} \quad \text{----(21)}$$

The result is expressed in watts * seconds (or joules).

Equation 21 gives the total potential solar input on a cloudless day with a transmissivity of τ. Solar input will never reach this value due to cloudiness. Solar

irradiance consists of direct solar radiation from the sun itself and a diffuse component (modelled here as 0.36 * I_p) which comes from all sections of the sky. The latter does not depend on cloud cover.

The total shortwave radiation received ($\mathbf{I_t}$) can be expressed as:

$$I_t = I_p \times (0.36 + (0.64\beta)) \quad \text{----(22)}$$

Linacre (1992)

where β is the proportion of the time during the daylight period that the sky is clear. β is estimated by dividing recorded sunshine hours **n** by daylength **dy** (also known as **N**). This relationship was first investigated by Ångstrom (1924). It is only approximate because of the incorrect assumption that the rate at which solar insolation is received is constant throughout the day. If this was the case two hours of sunshine around noon would lead to a similar amount of solar input as two hours in late afternoon. When the day is totally overcast $\mathbf{I_t = 0.36 * I_p}$, and the total energy input is solely composed of diffuse radiation.

An alternative formula for estimating the actual total irradiance $\mathbf{I_t}$ using the daily temperature range at screen level and the value of $\mathbf{I_p}$ was developed by Cengiz in 1981 using data from Missouri.

$$I_t = (0.048 I_p) - (3.5 (T_{max} - T_{min})) + (0.029 \times I_p \times (T_{max} - T_{min})) + 24 \quad \text{----(23)}$$

This estimate, based on temperature range (a proxy for irradiance), is compared with the astronomical value of I_t (calculated from equation 22) in Figure 7.4 for the Durham data. The astronomical estimate is nearly always greater since not all solar irradiance is used to heat the air. There is, however, a strong positive correlation between the two measures, which is reassuring. The difference between the two

Figure 7.4. Two Estimates of It (Total Irradiance), Durham (1985)

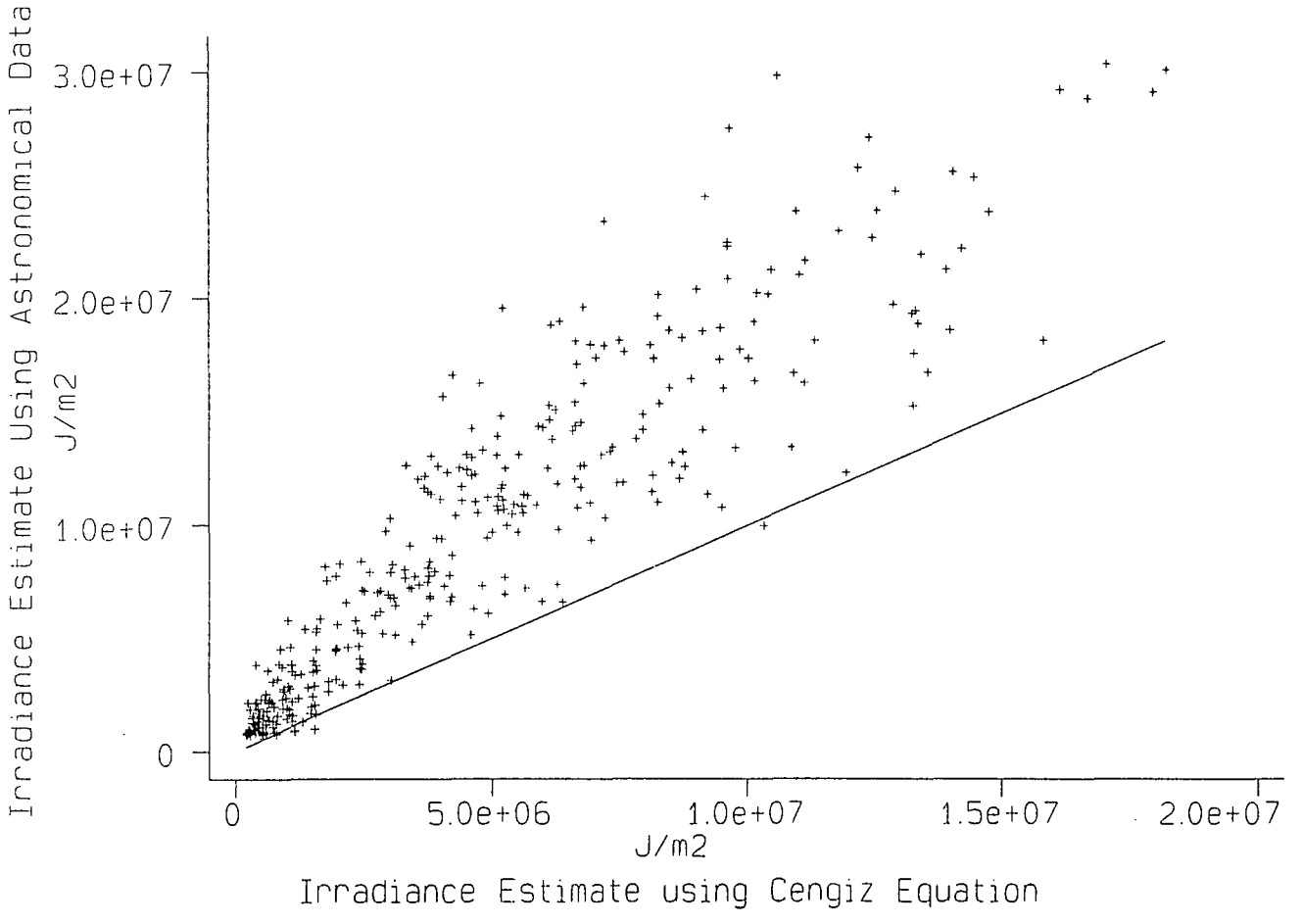

estimates relates to the efficiency of the solar radiation in producing temperature rise.

Temperature change should be related to net irradiance I_{net}, as this takes the albedo and longwave radiation loss into account:

$$I_{net} = ((1-\alpha) I_t) - E_t \quad ----(24)$$

7.2.4 Estimation of Net Irradiance

For estimation of I_b, incoming solar irradiance absorbed at the surface after reflection back to the atmosphere, the albedo (α) was assumed to be 0.2, unless there was snow cover on the ground, when it was assumed to be 0.7. Hence a simple step function was used to parameterise albedo (Linacre 1992).

$$I_b = (1-\alpha) * I_t \quad ----(25)$$

Values of I_b in J m^{-2} for each day are shown for Durham in Figure 7.5 for 1985. Values exceed 20 MJ m^{-2} in mid-summer but only just remain above zero in mid-winter. 10 MJ m^{-2} is a good estimate of I_b in spring or autumn.

To obtain the net radiation flux one must calculate longwave radiation loss.

Cloud cover **C** is calculated using

$$C = 8 (N-n) / N \quad ----(26)$$

Linacre (1992)

This varies between 0 on a cloudless day and 8 on a totally overcast one. The

Figure 7.5. Total Absorbed Solar Irradiance Ib, Durham (1985)

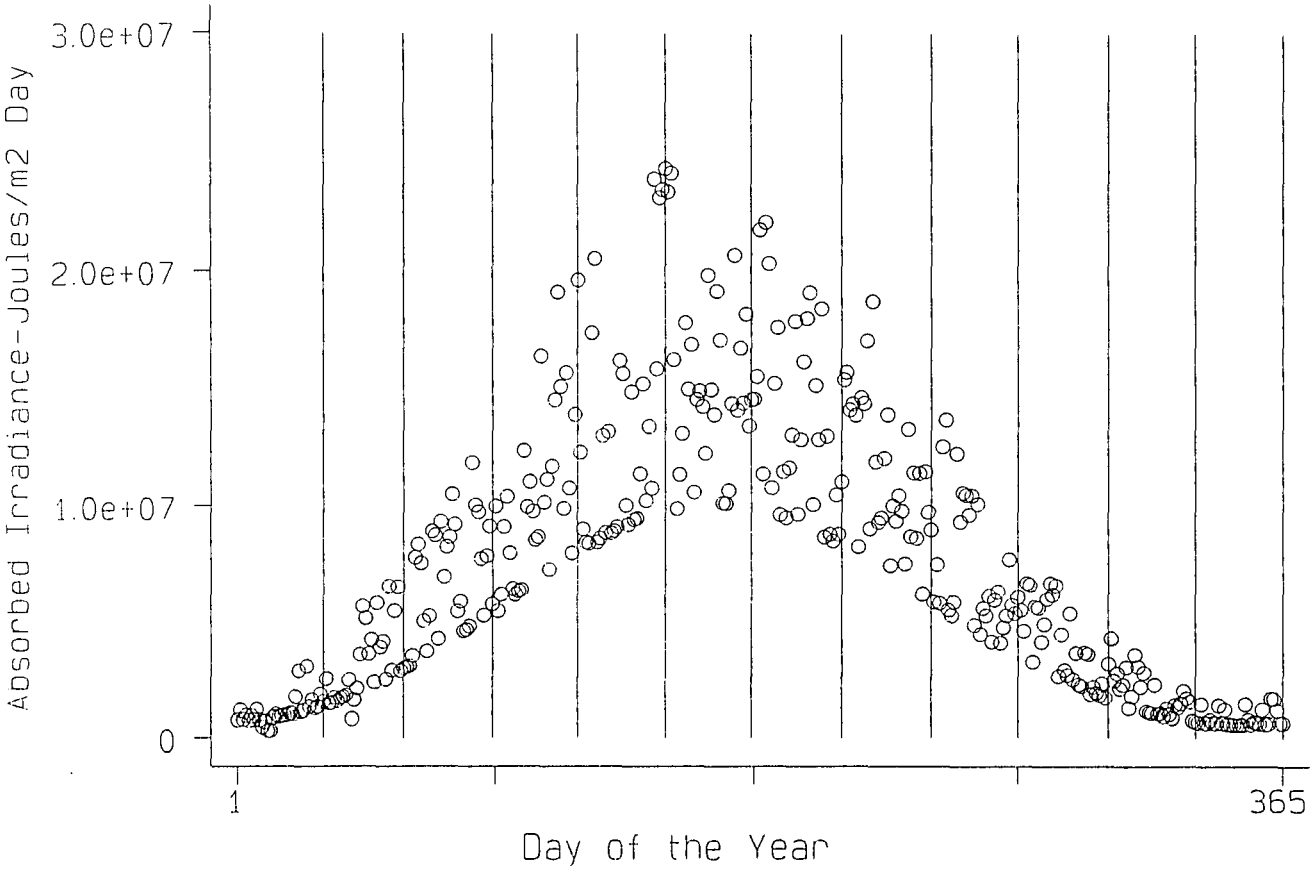

number of sunshine hours is assumed to be linearly related to cloud cover, whereas in reality this is not so (see Chapter 5 for a discussion on the relationship between cloud cover and sunshine duration (Hoyt 1977)).

Downward longwave radiation from a clear sky is estimated by

$$E_d = 208 + (6 \times T_{mean}) \quad ----(27)$$

Monteith (1973)

Cloud will increase E_d (Paltridge & Platt 1976). E_{dc} in the presence of cloud is calculated as

$$E_{dc} = E_d \times (1 + (0.0034 \times C^2)) \quad ----(28)$$

where C represents cloud cover in oktas.

The loss of longwave radiation upwards E_u is estimated by assuming that the earth radiates as a black body at its absolute temperature in Kelvin, with an emissivity of 0.97:

$$E_u = 0.97 \times ((T_{mean} + 273)^4) \times 5.67 \times (10^{-8})) \ldots . W\, m^{-2} \quad ----(29)$$

Net longwave radiation over the 24 hour period is

$$E_t = (E_u - E_{dc}) \times (24 \times 3600) \ldots . J\, m^{-2} \quad ----(30)$$

Values of E_t at Durham vary between about 8-9 MJ day^{-1} in winter to 2 MJ day^{-1} in summer, although the inter-diurnal range of variation is considerable at any season.

E_t is lower in summer because the increase in E_{dc} with temperature outweighs the increase in E_u. E_t decreases with increasing cloud cover, highlighting the insulating effect of cloud layers.

A simpler estimate of net longwave radiation E_t depends on surface temperature and cloud cover:

$$E_t = (107 - ((T_{max} + T_{min})/2) - (9C)) \times 24 \times 3600 \ldots . J\, m^{-2} \quad ----(31)$$

Linacre (1992)

The mean temperature of the day is used as the temperature input.

The two estimates of E_t are reassuringly very similar for the Durham data. Both were used in turn to give alternative estimates of net irradiance I_{net}.

$$I_{net} = I_b - E_t \quad ----(32)$$

The computer model used to calculate I_{net} is listed in the STATA language in Appendix 4.

The estimate of $\mathbf{I_{net}}$ using equation 31 is referred to as $I_{net(1)}$. Values approach 18 MJ day^{-1} in summer.

A graph of net irradiance $I_{net(2)}$ at Durham, based on the calculations of net longwave exitance in equations 27-30, is shown in Figure 7.6. Daily data were used for 1985-1990. The graph is bounded by two envelopes: one for totally overcast conditions and the other for cloudless days. In June there is a great difference between net irradiance for clear and overcast days, although values are always positive. If skies are cloudless, positive values of net irradiance are simulated from early March to mid-October. Much is the same on cloudy days although the magnitude is less. From mid-

Figure 7.6. Estimated Net Irradiance, I net[2], Durham (1985)

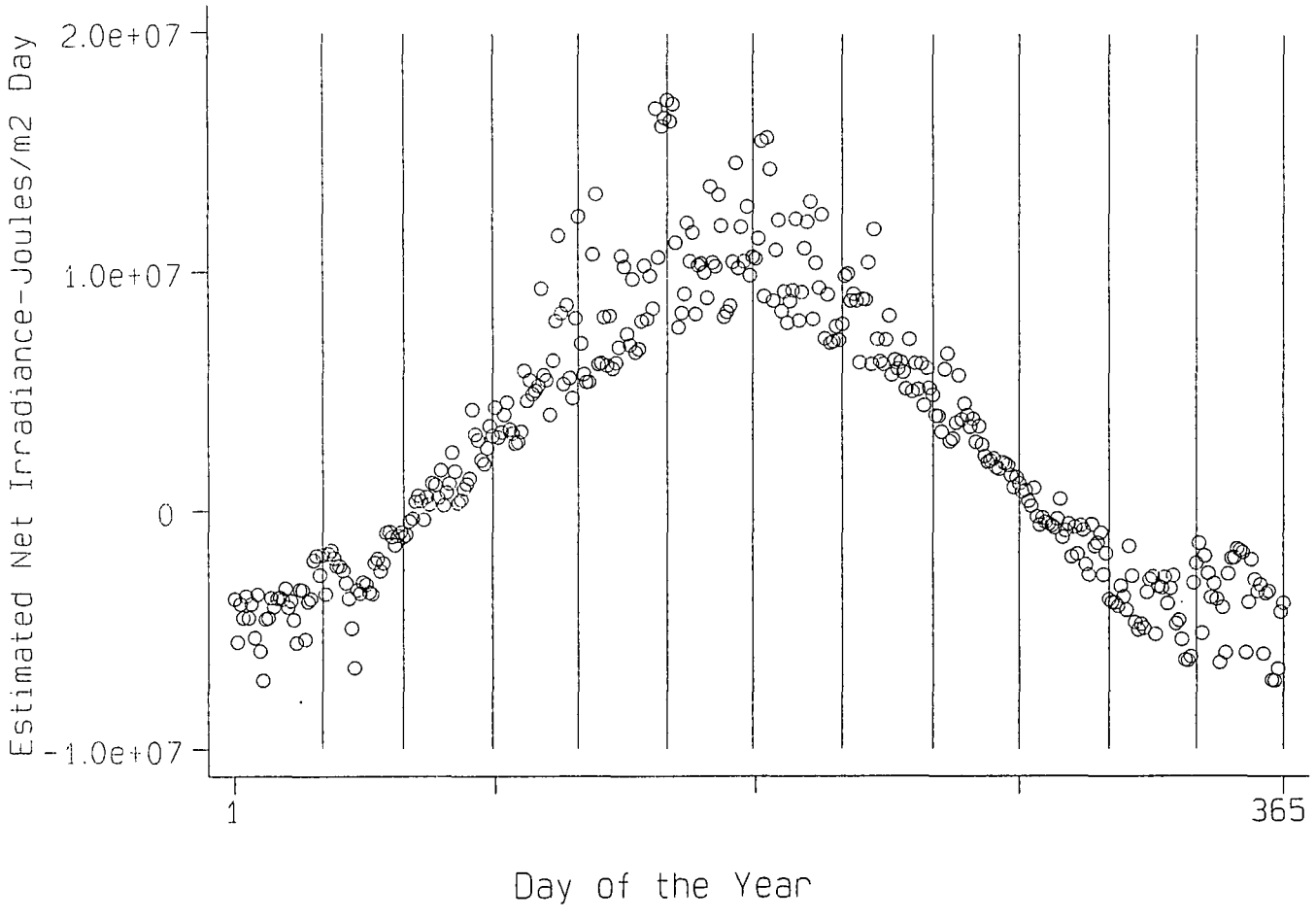

October to late February net irradiance is negative on cloudy days and is even more strongly negative on cloudless occasions. A clear sky allows more longwave radiation loss than is gained by the weak solar input. Noon solar elevation is only 11-12° at the winter solstice in Durham. A comparison of the two estimates shows that $I_{net(2)}$ is consistently smaller than $I_{net(1)}$. It appears that Linacre's equation underestimates longwave exitance, leading to a slightly larger estimate of I_{net}. This is especially true when net irradiance is negative. The difference is usually slight. In the following analysis $I_{net(2)}$ is employed as it is based on a more detailed analysis of the individual radiation components.

7.3 Comparison of the Above Model with other Energy Balance Models (EBMs)

Validation of any simple energy balance model involves comparison with others such as Davies 1967, Idso et al. 1969, Cowley 1978, Katsoulis & Leontaris 1981. Many of these models use solar radiation input I_t to estimate net radiation I_{net}. There is a strong linear relationship between the two. Figure 7.7 shows the relationship between I_t and I_{net} for the above model. Values have been converted to W m^{-2} since other models expressed the relationship in these units. The best-fit line is:

$$I_{net} = (0.74 \times I_t) - 41.5 \ldots W\,m^{-2} \quad ----(33)$$

The constants **a** and **b** in the equation $I_{net} = a(I_t) + b$ have been measured empirically in numerous studies (Table 7.1):

Figure 7.7. Inet versus It, Durham (1985)
Regression = Inet = 0.743*It - 41.5 W/m2

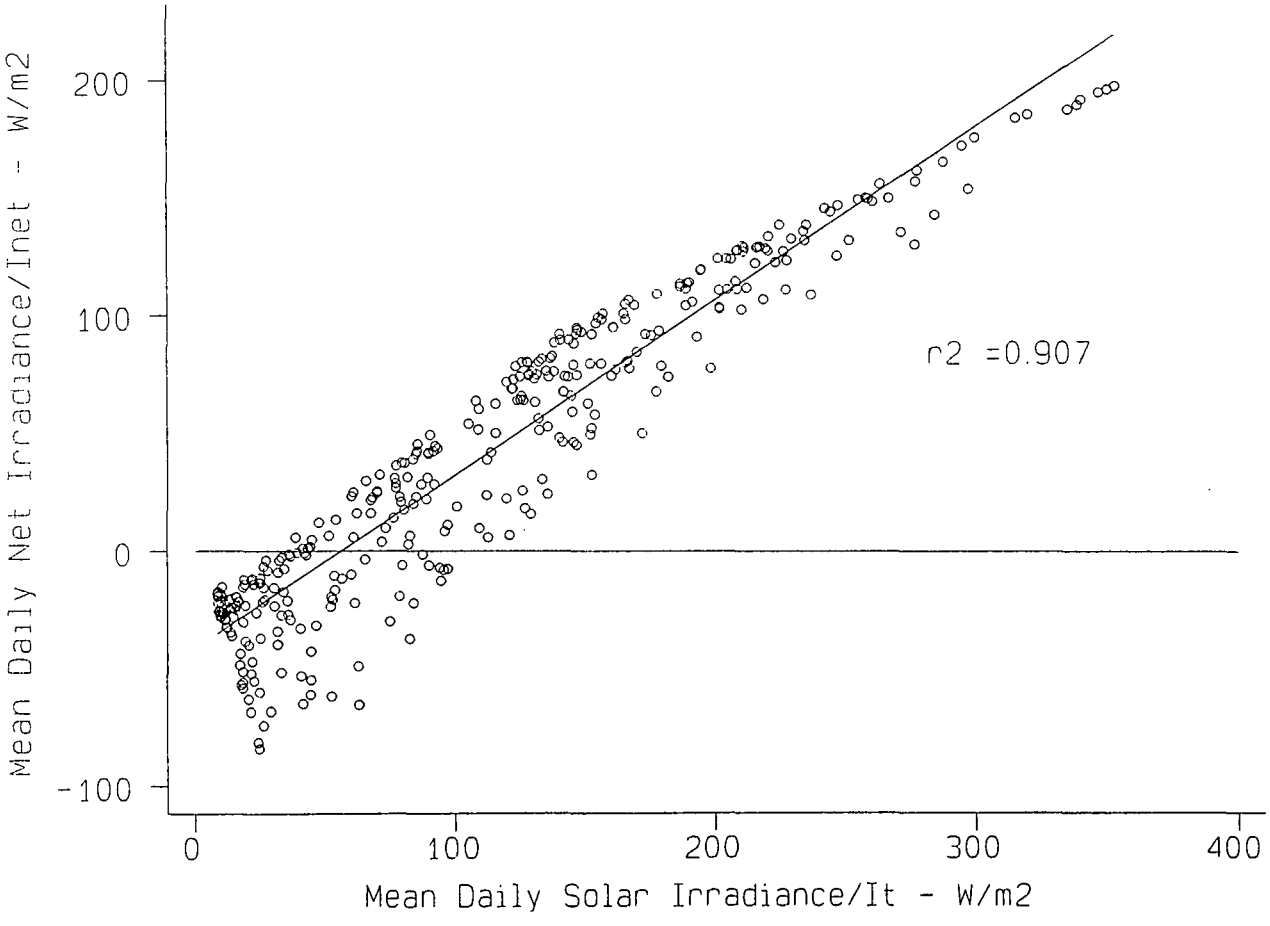

Table 7.1: Values of **a** and **b** in the equation relating solar with net irradiance.

Author	Year	a	b	Area	Crop
Davies	1967	0.612	28	W.Africa	Grass
Davies	1967	0.617	24	World	Grass
Monteith & Szeicz	1961	0.600	65	England	Grass
Fritschen	1967	0.730	83	Arizona	Various
Berland	1970	0.630	40	World	Various
Hu & Lim	1983	0.620	9	Malaysia	Grass
Pepin	1993	0.74	41.5	England	Grass

The effect of the type of surface on **a** and **b** is considerable (Monteith & Szeicz 1962). The values for the model created in this chapter are listed in the bottom line and agree fairly closely with others, although **a** is fairly high. Idso et al. (1968) related **a** to albedo

$$a=(1-\alpha)/(1+\beta) \quad ----(34)$$

α represents albedo and β a heating coefficient. Pavlov (1962) noted that

$$a=0.81-(1.39\alpha)+(0.45\alpha^2)-(0.34\alpha^3) \quad ----(35)$$

An albedo of 0.2 would give a value of 0.547 for **a**. Finally, Linacre (1968) produced the equation:

$$I_{net}=[0.93\times(1-\alpha)I_t]-0.14 \ldots cal\ cm^{-2}\ min^{-1} \quad ----(36)$$

I_{net}/I_t is the **radiation efficiency** and is generally about half, although it decreases as I_t

decreases.

Another commonly investigated relationship is that between I_t and n/N, described by Prescott (1940):

$$I_t/X_t = [\delta\,[a+b(n/N)] + (1-\delta)\,a'] \quad ----(37)$$

where $\delta = 0$ if n=0, and $\delta = 1$ if n>0 (discussed by Cowley (1978)). X_t represents the extra-terrestrial sky irradiance and is calculated from astronomical tables (Linacre & Hobbs 1977). Monthly means of X_t were obtained for 55°N and values of I_t/X_t are plotted against n/N for the Durham data (Figure 7.8).

The relationship between I_t/X_t and n/N is described by

$$I_t/X_t = [0.480\,(n/N)] + 0.24 \quad ----(38)$$

a and **b** again compare well with others in the literature (Table 7.2).

Table 7.2: Values of **a** and **b** in the equation relating $\mathbf{I_t/X_t}$ with **n/N**.

Author	**Year**	**Location**	**a**	**b**
Prescott	1940	Canberra	0.25	0.54
Penman	1948	England	0.18	0.55
Nkemdirim	1970	Scotland	0.20	0.51
Cowley	1978	England	0.24	0.55
Hanna & Siam	1981	Eskdalemuir	0.19	0.62
Katsoulis et al.	1981	Athens	0.30	0.68
Rao & Bradley	1983	Oregon	0.23	0.52
Pepin	1993	England	0.24	0.48

Figure 7.8. It/Xt versus n/N, Durham (1985)
Numbers represent month

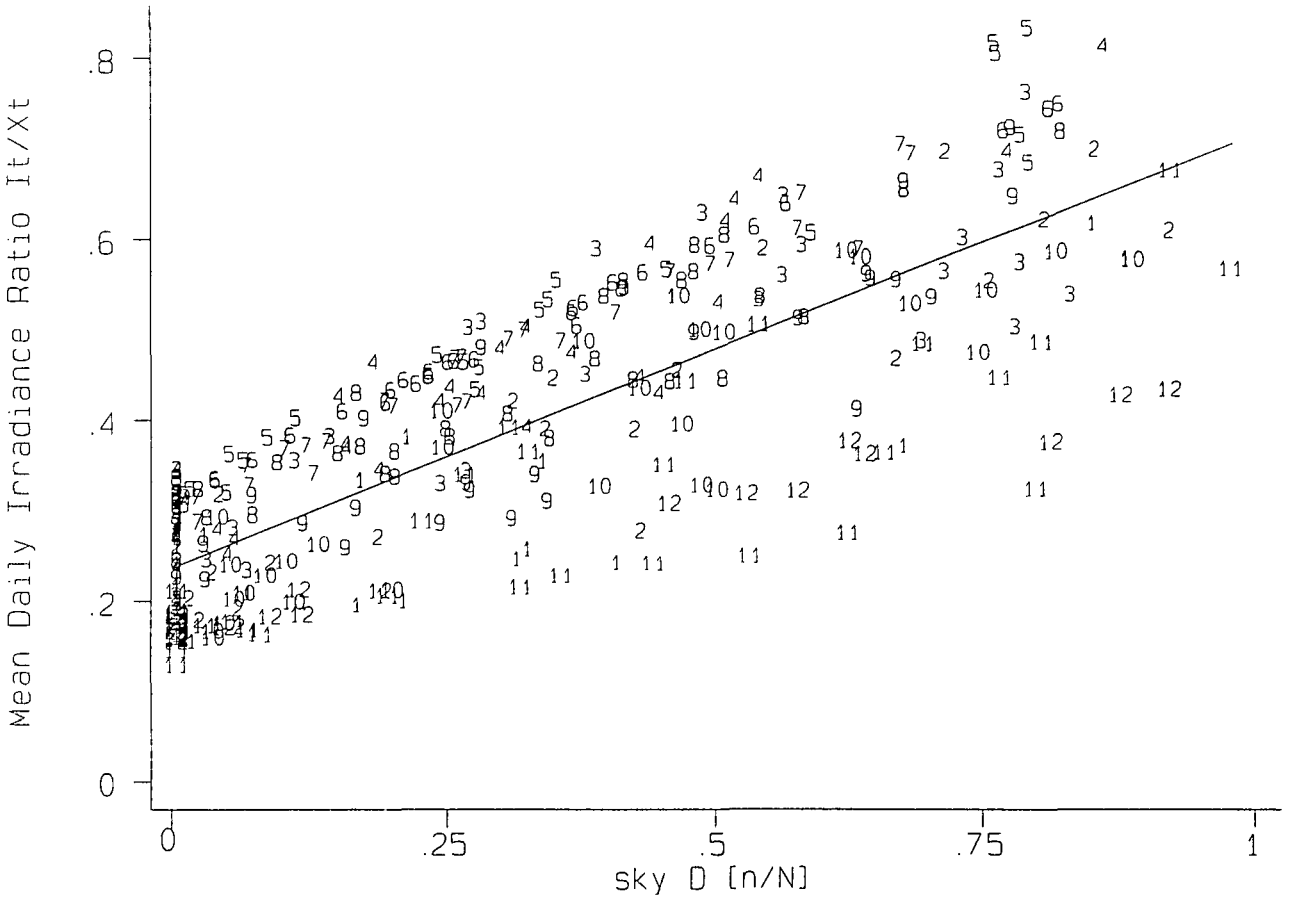

The temperature model produced in this chapter predicts relationships similar in magnitude to other models, supporting its validity.

7.4 Calculation of Apparent Heat Capacity at Durham

Relating estimated net irradiance to temperature change at Stevenson screen level allows an investigation into the efficiency of solar heating. Temperature change on any day was estimated by subtracting the daily minimum temperature from the daily maximum. The minimum was assumed to occur at dawn and the maximum to occur a few hours after solar noon, when 65.5% of the daily insolation had been received (after 60% of the daylight period). If daylength is 10 hours then the maximum temperature is assumed to occur 6 hours after dawn or one hour after solar noon. It is the case that

$$\int_0^{3\pi/5} \sin(x)\,dx \Big/ \int_0^{\pi} \sin(x)\,dx = 0.655 \quad ----(39)$$

The heat lost ($\mathbf{E_{tc}}$) between dawn and the time of the afternoon maximum is

$$E_{tc} = (0.6/24) \times dy \times E_t \ldots . J\,m^{-2} \quad ----(40)$$

Any diurnal change in the rate of longwave radiation loss (Gruber & Chen 1988) was ignored. The net heat gained during this period of temperature increase can be expressed as:

$$I_n = (0.655 I_b) - E_{tc} \ldots . J\,m^{-2} \quad ----(41)$$

I_n is over 10 MJ m^{-2} on clear summer days but is usually marginally negative between mid-November and mid-January. The apparent heat capacity of the air, ψ, is calculated by dividing the heat input I_n by the temperature range experienced. Dividing

the figure by (3600 * daylength * 0.6) the rate of heat input required in watts m^{-2} for a temperature increase of 1°C is obtained:

$$\psi = I_n / ((T_{max} - T_{min}) \times (3600 \times 0.6 \times dy)) \ldots . W\, m^{-2} \quad ----(42)$$

ψ for Durham is shown for 1985 in Figure 7.9. The reason for such variation in ψ is that variable amounts of $\mathbf{I_n}$ are lost to the ground (soil heat flux) or in convection. Convection increases the boundary layer extent which effectively increases the heat capacity, air being heated to a greater height above the ground. Advection will also subtract or add heat energy. Finally, evaporation (the latent heat flux) uses a considerable proportion of net irradiance in certain cases.

On average greater energy input is required in summer when the upward extent of the boundary layer is larger. This is a natural response to higher amounts of available solar energy. The development of summer convection redistributes heat energy from screen level to the upper air. In contrast, very low values of ψ occur in winter. Because of the virtual absence of solar radiation net irradiance is always negative, and yet temperatures do not systematically decrease throughout the winter months. Advection of heat energy is necessary to sustain temperatures, made possible by the transport of warmer air from the tropics to higher latitudes by extra-tropical depressions. The latent heat flux is also reduced. In summer, increased evaporation will increase ψ.

The scatter in ψ is considerable at any season. Many values fall near zero in winter, whereas in summer there are instances when over 50 W $m^{-2}°C^{-1}$ are required. The largest value is 73.1 W $m^{-2}°C^{-1}$. Assuming the heat capacity of dry air to be 1004 J $kg^{-1}°C^{-1}$ and the mass of air to be 360 kg m^{-3} (equal to a boundary layer height of 300 metres), the rate of heat input theoretically required for a 1°C increase in screen temperature on any day of the year is plotted in Figure 7.10. This varies from around 10 W $m^{-2}°C^{-1}$ in summer to 25 W $m^{-2}°C^{-1}$ in winter. Lower rates are required in summer as the period of potential heating is longer. ψ is nearly always higher than the

Figure 7.9. Apparent Heat Capacity, ψ, the Energy Input Required to Raise Surface Temperature by 1 deg C, Durham (1985)

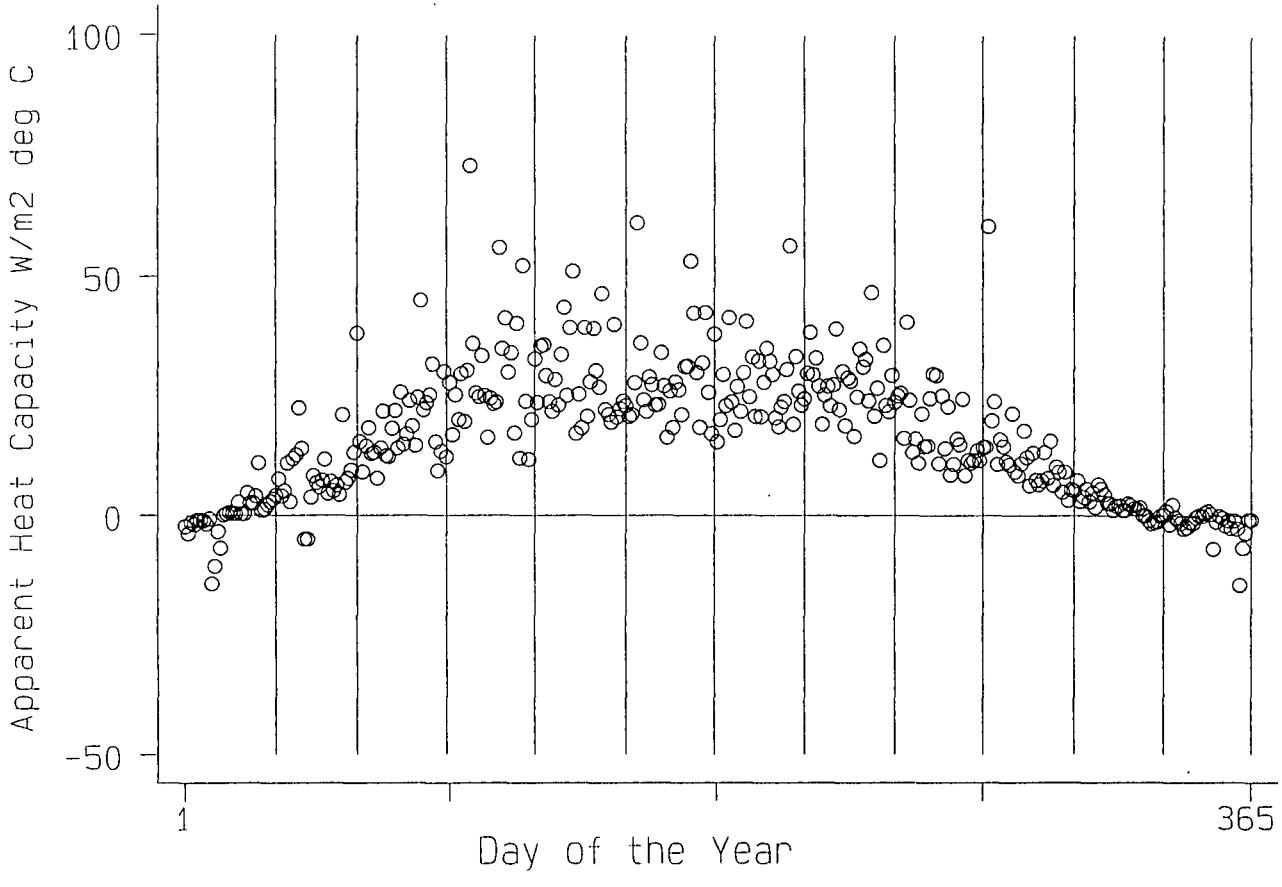

Figure 7.10. Theoretical Rate of Heat Input Required per deg C, Assuming 360 kg Air/m2 and a Heat Capacity of 1004 J/kg deg C

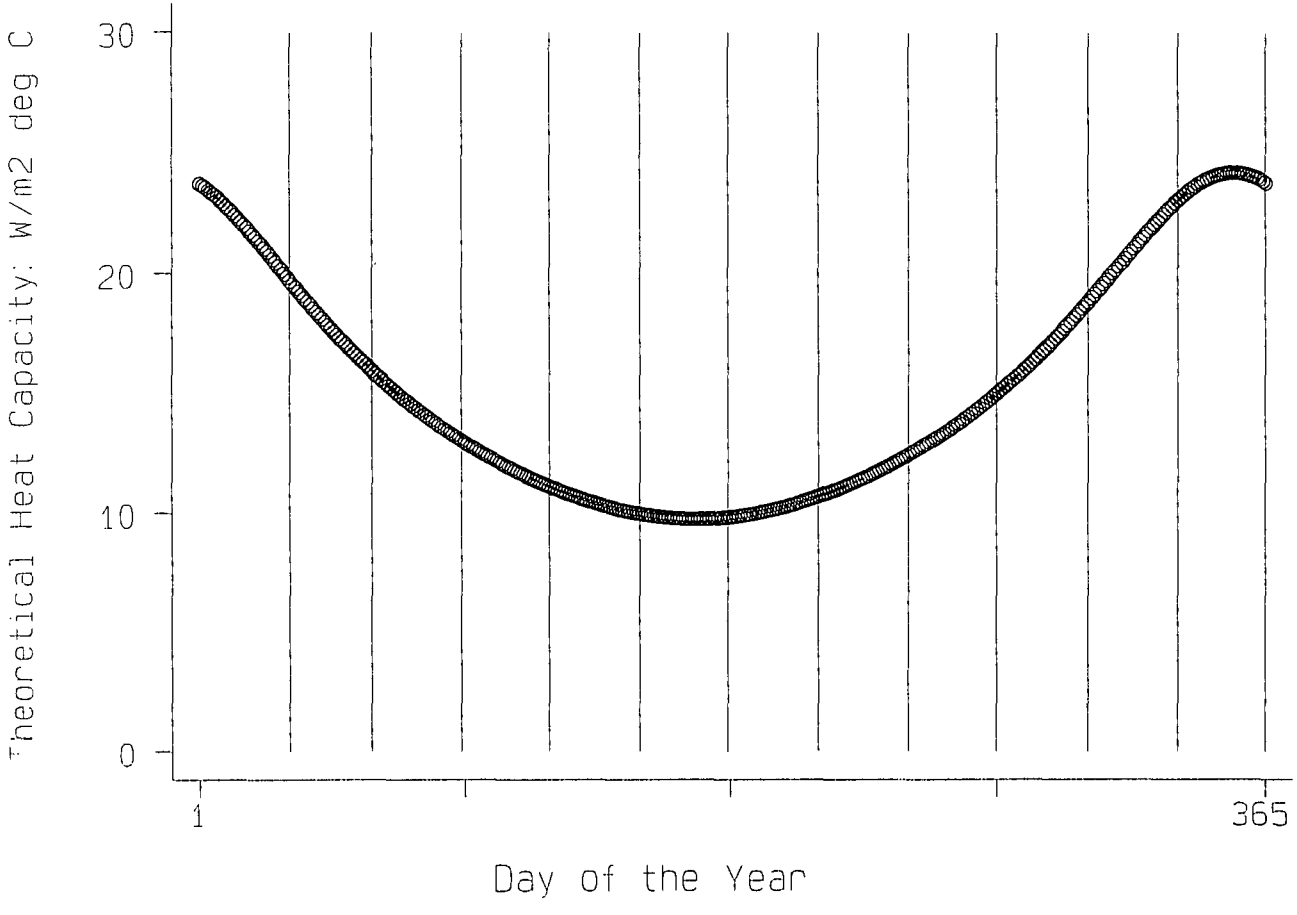

theoretical rate because not all of heat input goes into heating the air (sensible heat). The loss to the soil is only a small proportion of the total heat energy, averaging around 10% of the net radiation flux (Rider & Robinson 1951, LeDrew 1975). The mean apparent heat capacity, ψ_{mean}, is 16.84 W $m^{-2}°C^{-1}$, although the seasonal variation is much larger, mean values ranging from 29.41 W $m^{-2}°C^{-1}$ in May to -1.63 W $m^{-2}°C^{-1}$ in December.

ψ was also calculated for Widdybank Fell (513 m), but for 1990 (Figure 7.11), and was found to be consistently higher than at Durham. Exceptionally high values of ψ occur at both locations, but especially at Widdybank Fell, when the apparent rate required exceeds 100 W $m^{-2}°C^{-1}$ on a few occasions. These may be occasions with snow cover. The type of snow is important (Pennell 1992). Much radiant energy is used in melting the snow (McKay & Thurtell 1978, Ohmura 1982), depressing temperature response to irradiance (Dewey 1977). Another reason for inefficient conversion of solar energy into temperature change is strong advection of cold air associated with northerly winds.

The great variety of values of ψ in Figures 7.9 and 7.11 can be explained by reference to the following factors:

1. Albedo is parameterised very simply as a step function. In reality this is simplistic. For example, the type, age and depth of snow all affect its albedo. Changes in surface albedo will mean that actual irradiance absorbed, I_b, will not be as calculated in the model.

2. Advection is not taken into account. It would be rare for air to be still enough for a long enough period that all net radiation over the course of a day goes into heating one particular air pocket. Conditions approximate to this ideal in sheltered hollows and resulting changes in temperature can be amazingly rapid. Otherwise air movement decreases heating or cooling rates by replacing air with colder or warmer air. ψ is high on days with strong winds.

Figure 7.11. Apparent Heat Capacity, ψ, at Widdybank Fell (1990)
Altitude 513 m OD

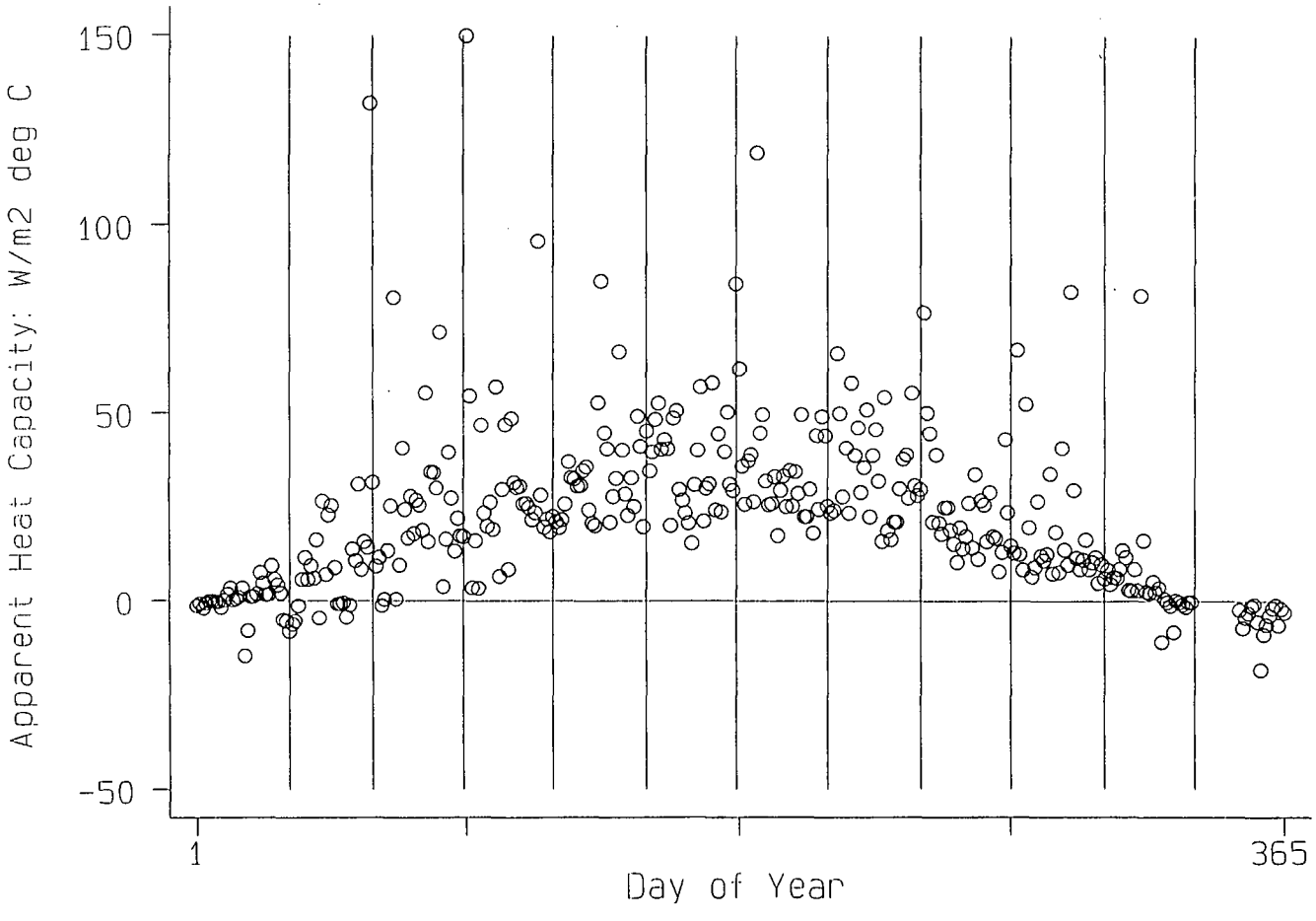

3. Convection, if it occurs, increases the apparent heat capacity by redistributing heat upwards from screen level. This explains the seasonal trend in ψ, with a peak in summer. For similar reasons ψ is expected to be high for unstable airstreams.

4. Not all net radiation is used in heating the air. Partitioning between air and soil is crucial. Melting of snow and evaporation of water from the ground surface requires heat energy. The state of the ground surface should therefore enter the model. Humidity and wind speed are required to estimate the cooling effects of evaporation.

5. The lag between radiation input and temperature response causes more variation in ψ. Analysis of annual temperature variation at Durham and Widdybank Fell shows an approximate lag of one month between maximum radiation inputs around the summer solstice and the highest temperatures in late July (Pepin 1992) (Chapter 10). There is also a lag on a shorter timescale and it is difficult to know for which period of the day net radiation input and temperature change should be compared.

6. Humidity will affect ψ since humid air has a higher heat capacity than dry air.

7. Isobaric warming and cooling is assumed (constant pressure). Pressure changes, however small, will affect ψ since the heat capacity of dry air at constant volume is not the same as the heat capacity of dry air at constant pressure.

If it were possible to take all possible factors into account, temperature changes might be estimated directly from radiation estimates derived solely from astronomical parameters and meteorological data. This is not practical and, alternatively, the apparent heat capacity must be predicted from sunshine, snow cover, cloud, humidity, air quality, state of ground, absolute temperature and wind data. The effect of altitude on ψ, is implied by comparing Durham and Widdybank Fell. Net longwave exitance usually increases with altitude (Fliri 1971) as does direct solar radiation (Harding 1979b, Lowry 1980, Olecki 1989). However net irradiance values usually decrease and the efficiency shows a similar decrease (Voloshina 1966). The precise form of this decrease is little known.

7.5 Variation in Apparent Heat Capacity (ψ) at Durham (Lowland) and Widdybank Fell (Upland)

The apparent rate of heat input required (W $m^{-2}°C^{-1}$) at Durham for each day between 1985 and 1990 (ψ) was plotted against actual temperature range achieved on the same day (Figure 7.12). The graph is bounded by two envelopes which indicate extreme temperature ranges achieved given a certain rate of heat input. For example, if the apparent heat capacity is 50 W $m^{-2}°C^{-1}$, then the daily range will fall between zero and approximately 6°C, the higher value suggesting a rate of heat input of 300 W m^{-2}. Data points in region A show evidence of advective warming as negative net radiation still leads to a temperature increase. In many cases with negative net radiation the daily minimum does not occur at dawn and the maximum does not occur just after solar noon, as assumed in the calculations. This throws doubt on the validity of these cases.

Similar data plotted for Widdybank Fell (513 m) are shown in Figure 7.13, for 1990 only, due to restricted data availability. Temperature ranges are lower and ψ is higher, especially in a few exceptional cases (one value over 150 W $m^{-2}°C^{-1}$). Greater cloudiness, higher wind speeds, higher humidity and more frequent snow cover are expected to lead to lower diurnal temperature ranges given a similar net radiation. Altitude will increase ψ on average, and this is supported by a decrease in mean daily temperature range with altitude in many areas up to 3000 m (Linacre 1982).

The next section attempts to predict ψ from given meteorological controls.

7.5.1 Wind Direction

ψ is plotted against wind direction at Durham in Figure 7.14. Wind direction is expressed as a clockwise veer from north to the nearest 10°, divided by 10. The scatter of ψ is disappointingly large within each wind direction class, showing that many variables other than wind direction are important.

Figure 7.12. Apparent Heat Capacity, ψ, versus Daily Temperature Range, Durham (1985-1990)

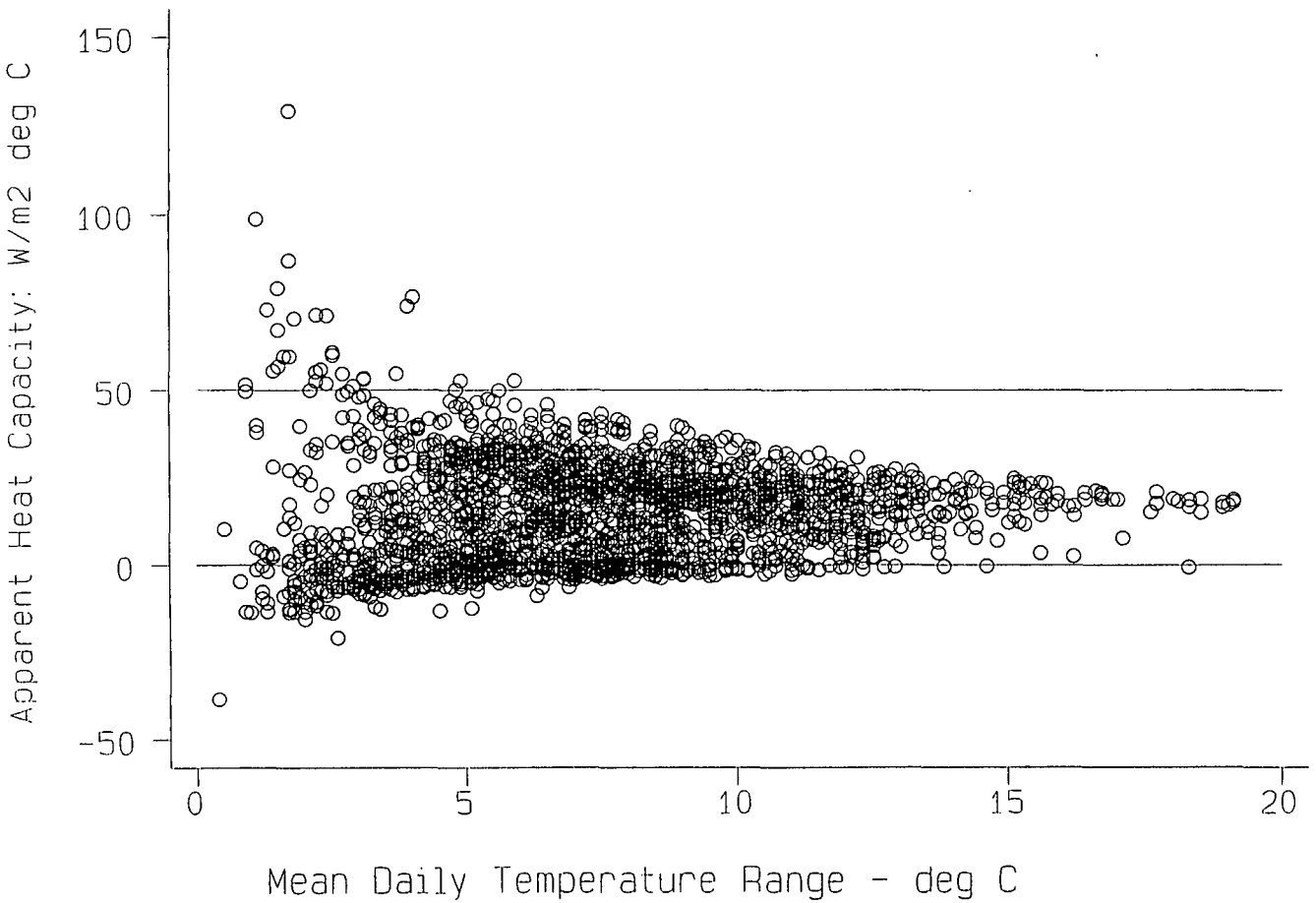

Figure 7.13. Apparent Heat Capacity, ψ, versus Daily Temperature Range
Widdybank Fell (1990)

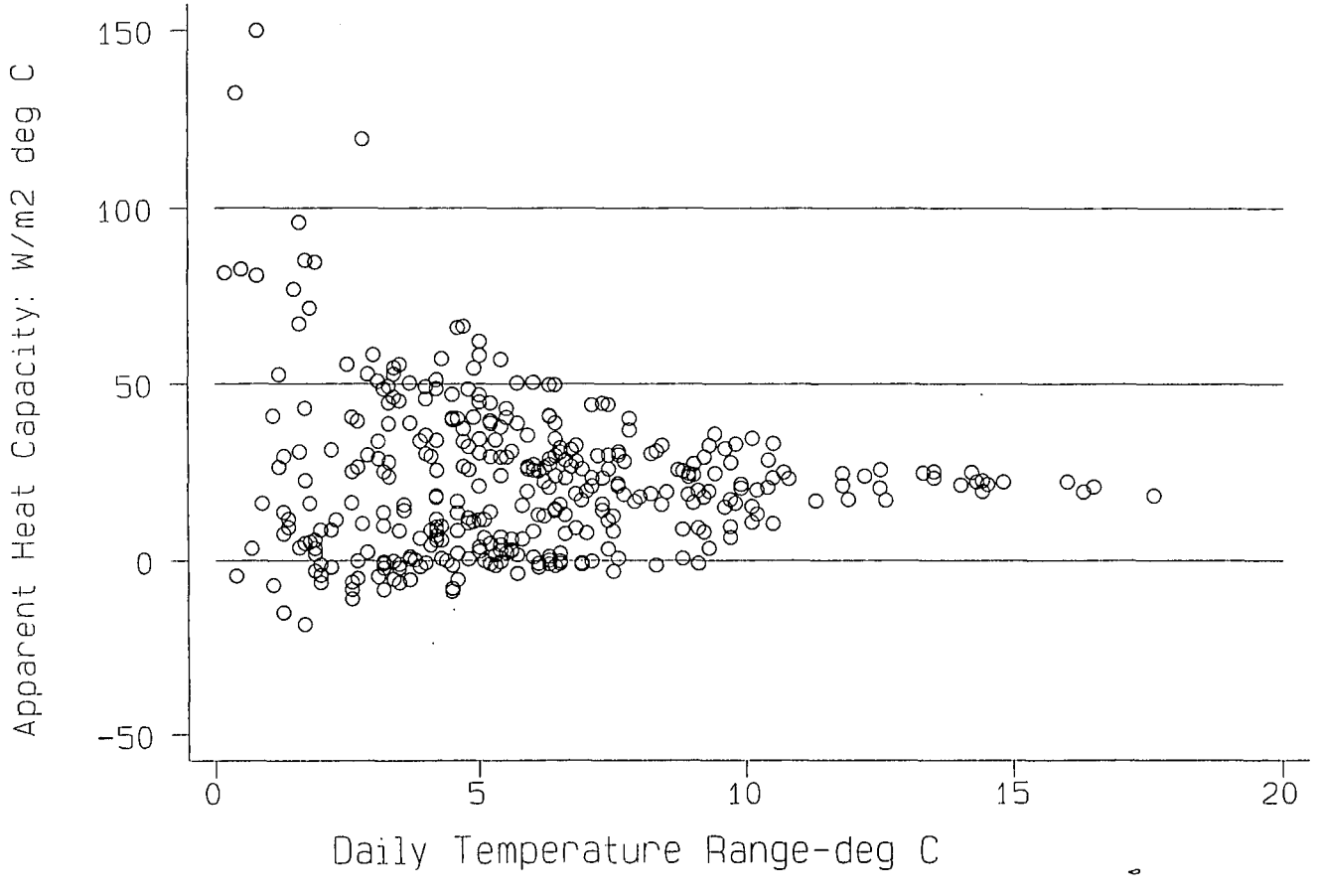

Figure 7.14. Apparent Heat Capacity, ψ, versus Wind Direction
Durham 1985-1990

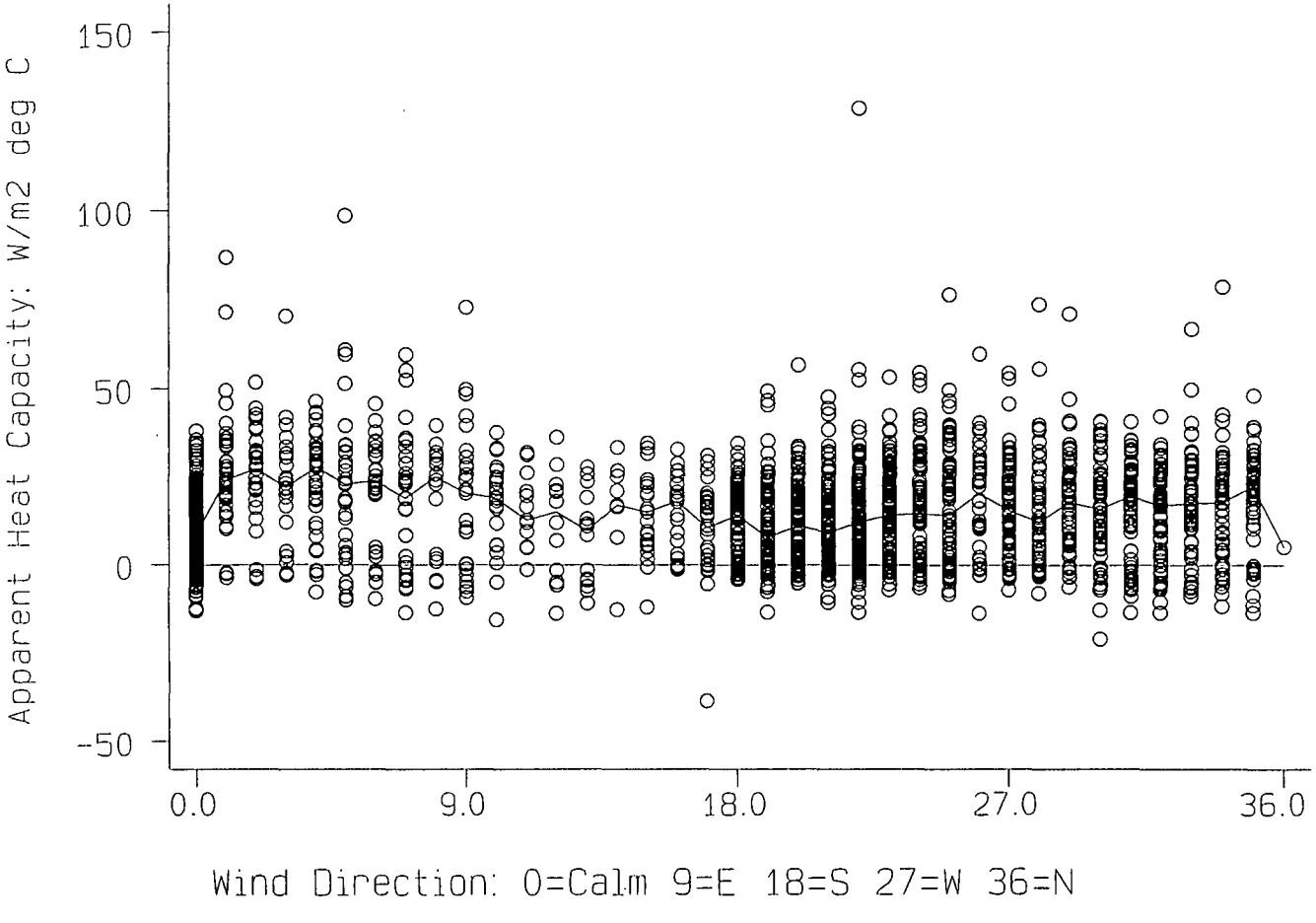

It may be expected that the more southerly the airflow the lower the mean value of ψ, since in the northern hemisphere winds from the south are usually relatively warm. In Durham ψ is often highest for north-easterly airflows, because of cold air advection from the North Sea. In Figure 7.14, the effects of wind direction were averaged over the whole year whereas advective effects of a particular airflow can vary according to season. Separate graphs are shown for mid-season months in Figure 7.15.

In January ψ clusters around zero, values being more strongly negative when winds have an easterly component. Large negative values imply negative net radiation (usual in winter) with little surface temperature response. In the other three months ψ is always positive since net radiation is positive during the day. Strong advection of cold air may account for higher values for winds between north and east in April and from a more northerly direction in July. Airflows with a southerly component show low values of ψ as do calm conditions. In summer, some westerly winds also seem to be associated with advective cooling, although the contrast between airflows is not very marked. There is little pattern in October although a few high values of ψ occur, especially for easterly flows. In the spring months the contrast in solar efficiency between southerly airflows and northerly ones is at its strongest, perhaps due to the strong meridional temperature gradient at this season (Lamb 1950, Manley 1952).

Table 7.3 summarizes ψ at Durham by wind direction and month. Some figures are less reliable, based on only 1 or 2 days' data.

The seasonal increase in ψ is dominant, summer (April to August) values approximating 25-28 W $m^{-2}°C^{-1}$. These values are slightly less than those of Bagnall (1982), who pointed out that the dividend of monthly mean I_t/T values in Australian cities is about 30 W $m^{-2}°C^{-1}$. Values fall well below this in winter because of lack of insolation and the importance of warm-air advection. Because temperature rise is calculated by subtracting the daily minimum temperature from the daily maximum, this value will be positive even if temperatures decrease throughout the day. Temperatures in winter are not strongly affected by time of day. Maximum temperatures often occur at night. Air mass is a more important predictor of surface temperature than insolation

Figure 7.15. Apparent Heat Capacity, ψ, versus Wind Direction in the Months of January, April, July and October, Durham (1985-1990)

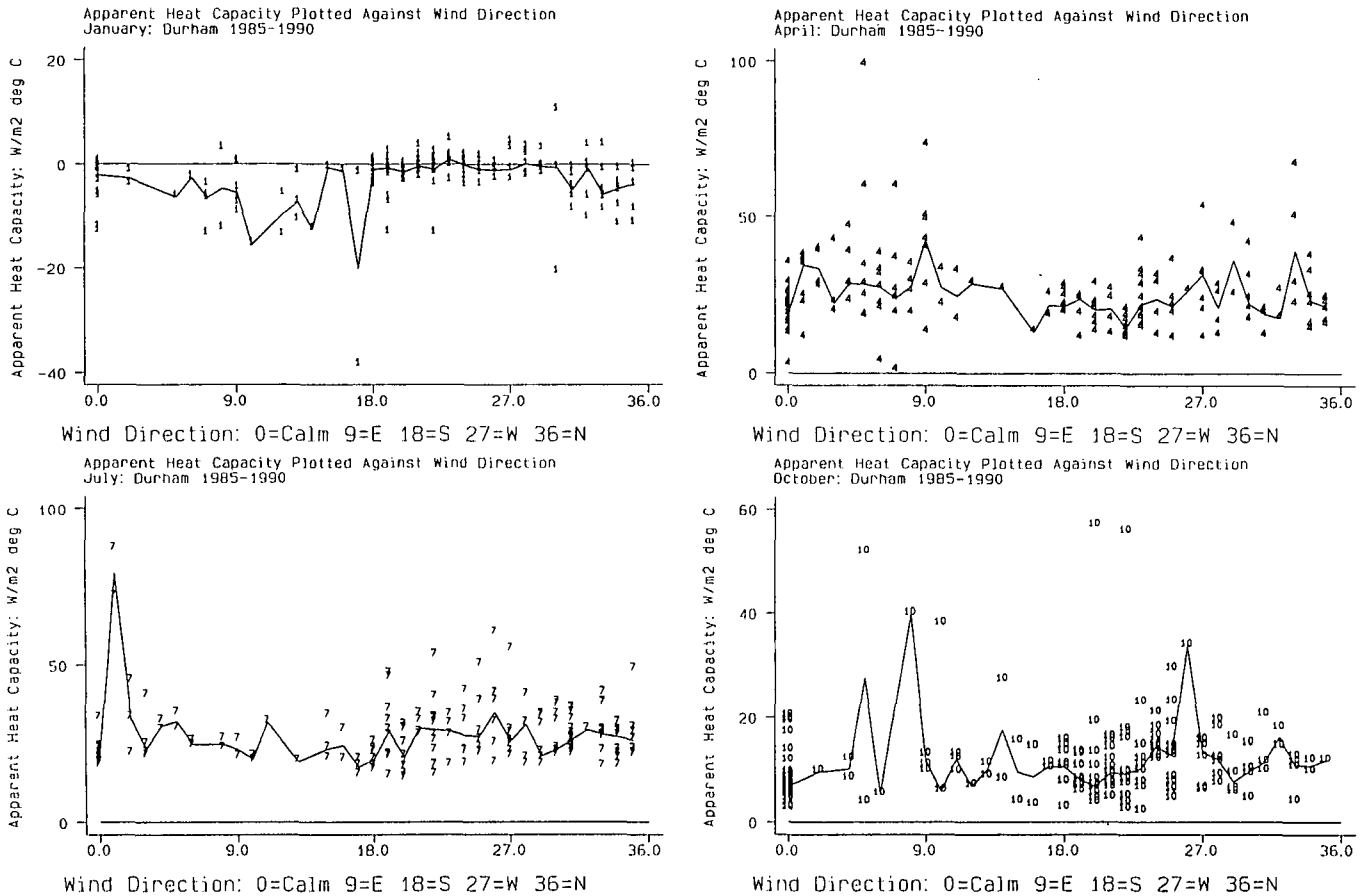

Table 7.3: Apparent Heat Capacity (ψ) at Durham (1985-1990), W $m^{-2}°C^{-1}$.

wind	JAN	FEB	MAR	APR	MAY	JUN
CALM	-3.83	3.91	12.15	19.53	21.45	22.80
N	-4.85	7.93	21.37	25.91	28.66	27.30
NE	-4.37	4.57	23.36	32.02	28.66	32.37
E	-6.29	6.58	15.10	31.67	26.89	26.50
SE	-7.43	3.22	18.82	27.78	26.32	23.62
S	-2.60	4.91	13.58	20.82	20.90	22.74
SW	-0.43	6.47	17.34	20.50	28.40	27.04
W	-0.14	9.71	20.40	26.10	36.62	32.92
NW	-3.60	9.61	16.59	26.52	25.35	26.55
MEAN	-2.50	6.84	17.20	25.20	27.40	26.90
JLY	AUG	SEPT	OCT	NOV	DEC	MEAN
21.47	20.59	13.53	8.30	1.02	-3.14	10.30
32.30	28.54	20.80	10.80	-1.57	-5.78	21.05
28.13	70.58	15.96	16.22	-0.21	-5.61	22.06
24.88	32.03	18.57	15.54	-1.03	-3.95	17.79
24.05	13.70	12.97	11.64	4.60	-4.10	12.78
23.60	22.09	14.80	10.66	2.06	-2.06	11.83
28.86	26.69	18.28	12.03	1.08	-3.11	13.86
29.59	27.99	21.15	13.03	1.36	-3.19	16.68
28.14	25.93	18.05	11.71	0.81	-5.64	15.57
27.48	25.78	17.80	11.48	0.95	-3.51	15.12

and attributing all the temperature rise to solar influences leads to low, but erroneous, values of ψ.

Advection causes ψ for some wind directions to differ markedly from the seasonal average, e.g. north-easterlies and easterlies in spring and summer. Mean

values over 30 W $m^{-2}°C^{-1}$ are recorded in April and June (for north-easterlies), indicative of cold-air advection. Occasionally, south-westerlies and westerlies show high apparent heat capacities (e.g. in May and June), the reason for which is unclear. The extreme value of 70.58 W $m^{-2}°C^{-1}$ for north-easterly flow in August is based on one day only and is unreliable. Annual mean capacities are 22.06 W $m^{-2}°C^{-1}$ for north-easterly flow, and 11.83 W $m^{-2}°C^{-1}$ for southerly flow. Values on calm days average 10.30 W $m^{-2}°C^{-1}$, highlighting the effectiveness of solar input when conditions are calm. Mean values of ψ for southerly airflows are much less than for northerly ones.

A northerly wind component (**n**) was derived to represent the "northerliness" of an airflow. This consisted of the magnitude of the meridional vector of the surface wind (i.e. in the north-south plane):

$$n=\cos[(\pi/18)\times w] \quad ----(43)$$

where **w** is the surface wind direction. **n** ranges between 1 for a northerly wind and -1 for a southerly wind. Values for easterlies and westerlies are zero. The northerly component is used in the multiple regression in section 7.6 (for predicting ψ).

ψ was also examined at Widdybank Fell (513 m) for 1990. The overall average is 22.65 W $m^{-2}°C^{-1}$ as opposed to 13.78 W $m^{-2}°C^{-1}$ for Durham (in that year), because of the windy exposed nature of Widdybank with higher humidities and wind speeds, and greater cloud cover. Values of ψ associated with calm conditions average 22.31 W m^{-2} $°C^{-1}$, higher than the mean for Durham, presumably an effect of altitude. It is surprising that efficiencies under calm conditions in 1990 do not appear to be much less than on other occasions, at least at Widdybank Fell.

7.5.2 Wind Speed

ψ is plotted against mean daily wind speed in Figure 7.16. Wind speed was measured in knots at an effective height of 16 metres (Goldie 1992). As wind speed

Figure 7.16. Apparent Heat Capacity, ψ, versus Wind Speed, Durham 1985-1990

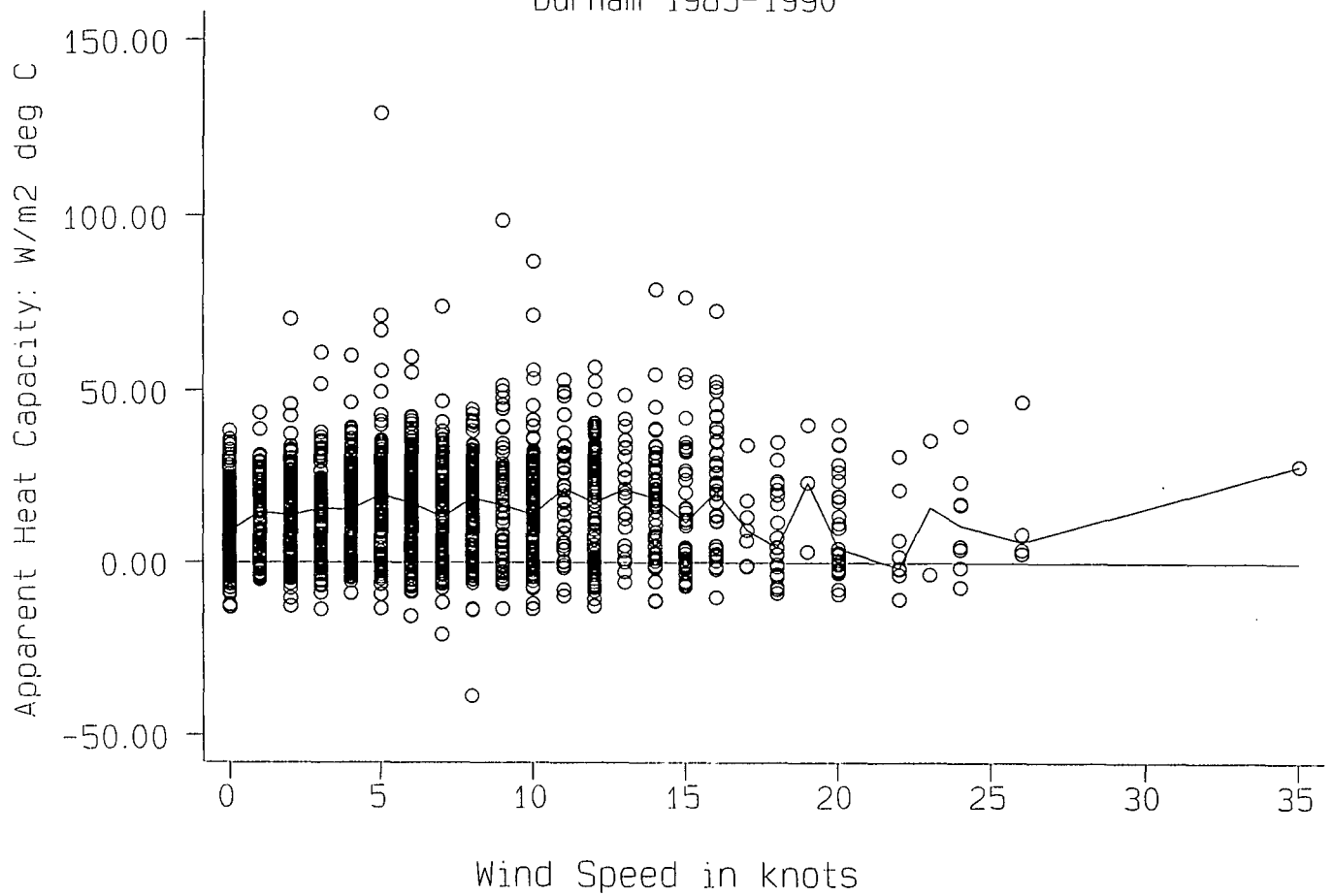

increases, solar efficiency (proportional to $1/\psi$) first decreases at low wind speeds due to the increased importance of advection and evaporation. However, at the highest wind speeds ψ appears to drop. Individual values are extremely irregular. The strongest winds occur as gales from the Atlantic and are also the strongest contributors to advection of warm air in winter. Highest wind speeds at Durham are always recorded in winter (December to February), usually from a westerly or south-westerly direction (Pepin 1993), and this would explain the tendency towards lower values of ψ at the highest wind speeds.

7.5.3 Snow Cover

The presence of snow cover should increase ψ for three reasons:

1. The high albedo will reduce the proportion of irradiance contributing to temperature rise by reflecting 70-80% of the incident solar energy back to the atmosphere (the variation in albedo is only crudely accounted for in this model);

2. Net irradiance will be used to melt snow as well as to heat the ground and air (Aguado 1985). Melting and subsequent evaporation of surface meltwater require absorption of latent heat;

3. Snow insulating the ground surface will reduce heat transfer from ground to air. Air temperatures over snow cover will be depressed (Dewey 1977).

ψ was calculated at Durham for occasions of snow cover and occasions without (Figure 7.17). Required heating rates are lower than expected when there is a snow cover (snow depth is greater than zero). This is because snow cover occurs in winter when the apparent solar efficiency is already high. Table 7.4 gives mean values of ψ for days with and without snow cover, for the whole year and in certain months (to eliminate seasonal effects).

Figure 7.17. Apparent Heat Capacity, ψ, versus Snow Depth, Durham 1985-1990

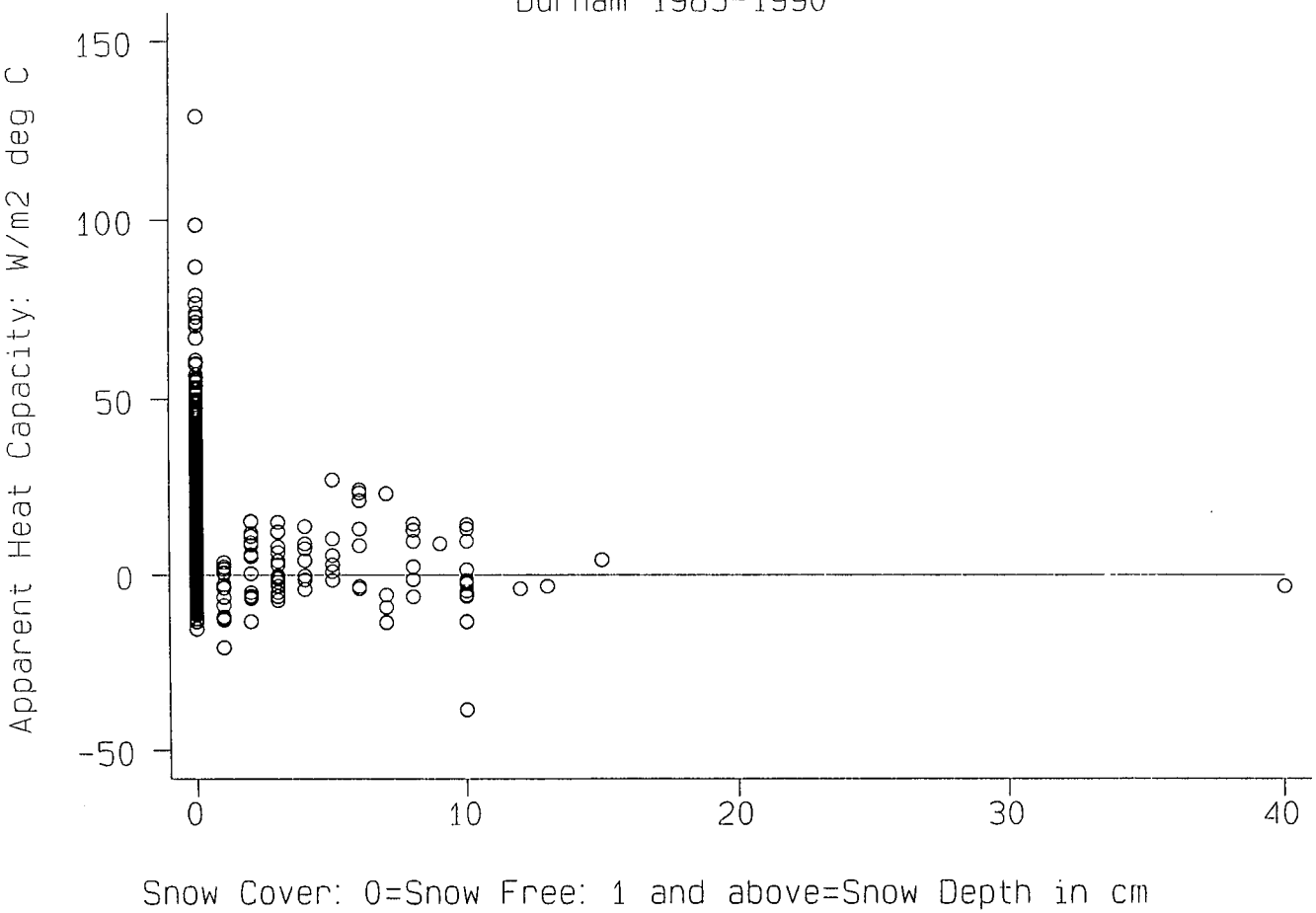

Table 7.4: Mean ($\bar{x}$) and standard Deviation (s) of ψ for days with and without snow cover (Durham), W $m^{-2}°C^{-1}$.

Period	With Snow Cover			Without Snow Cover		
	n	$\bar{x}$	s	n	$\bar{x}$	s
Annual	101	1.22	10.20	2090	15.79	14.09
Jan-Mar	88	1.82	10.69	452	8.21	11.40
January	40	-5.93	7.70	146	-1.56	3.47

Statistical significance testing of mean differences using the two-sample t-test shows that the mean efficiencies are different at the 5% level, even when January values alone are considered. The 95% confidence interval for the difference in January means is 4.37 +/- 1.65. For a discussion see Siegel (1988). Thus the presence or absence of snow cover in January accounts for a significant difference in ψ. The contrasting sizes of the two groups do not aid comparison. Part of the contrast in the means in the annual case could be due to the seasonal contrast in the two groups of days, those with snow cover only occurring in winter. The January comparison eliminates this cause and yet there is still a significant difference (at 5%).

Similar analysis was carried out for Widdybank Fell for 1990 where the number of days with snow cover was a larger proportion of the total. The two group means are significantly different at the 5% level for annual readings and for those in January-March (but only just). However, January means for days with snow cover and those without are not significantly different at the 5% level.

7.5.4 Solar Elevation (Season)

Noon solar elevation varies systematically from around 11° at the winter solstice to nearly 60° in mid-summer. Solar elevation can therefore be used as a proxy for season. It has already been remarked that the seasonal variation in ψ is strong, peaking in summer because of the convective extension of the boundary layer and increased evaporation. Figure 7.18 shows a strong positive correlation between solar elevation

Figure 7.18. Apparent Heat Capacity, ψ, versus Noon Solar Elevation
Durham (1985-1990)

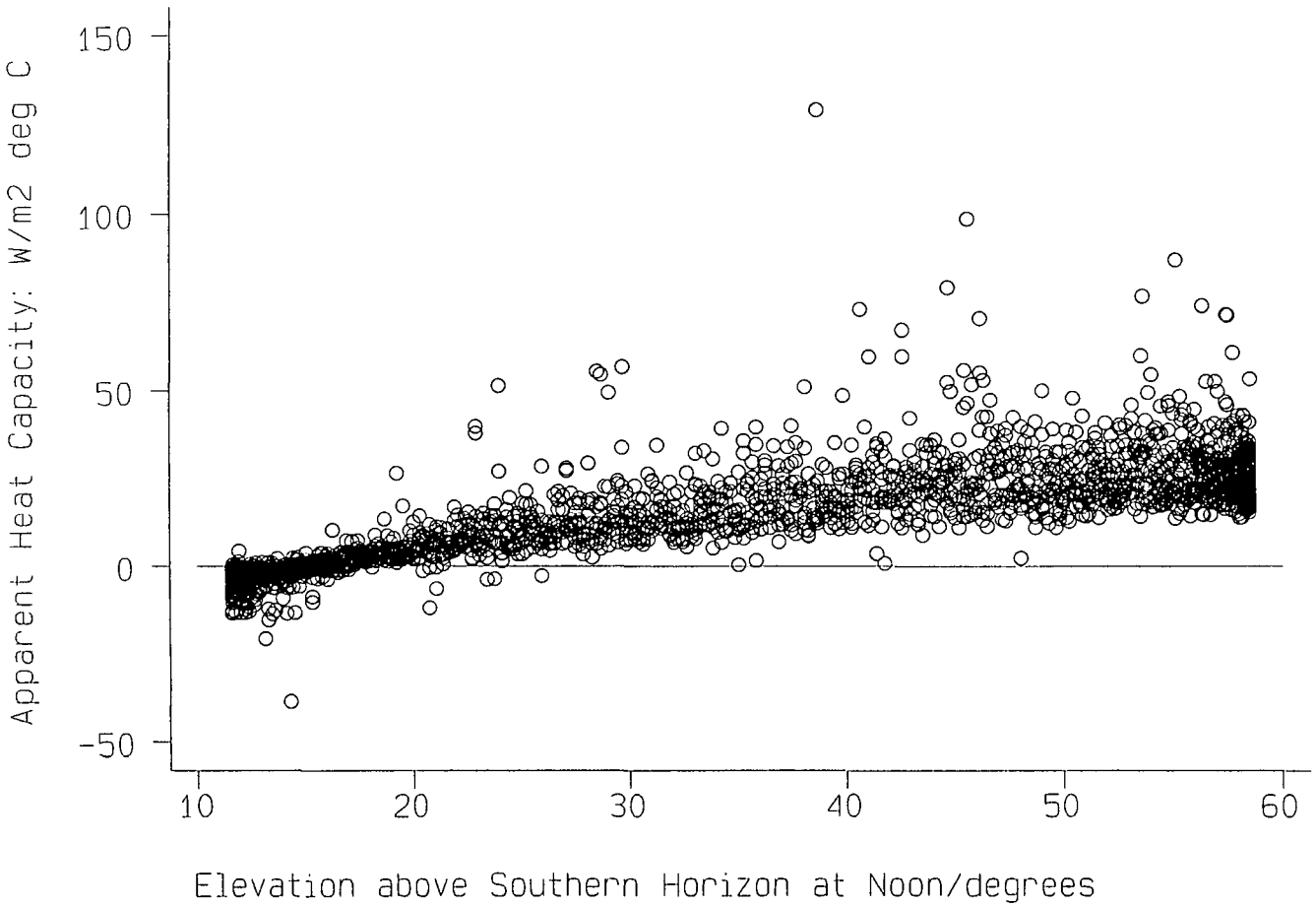

and ψ. Such seasonal variation swamps variation due to wind speed and direction.

7.5.5 Relative Humidity

A negative relationship between relative humidity and ψ is supported by Figure 7.19. When relative humidities are low the value of ψ tends towards 20 W $m^{-2}°C^{-1}$. As humidities increase, ψ decreases but there are also some extremely high values, i.e. variability increases. Nearly all negative values occur when relative humidities are above 0.7. The negative relationship is formed because of the strong inverse relationship between relative humidity and noon solar elevation. Relative humidities are consistently higher in winter when ψ happens to be low anyway. ψ may be expected to increase with increasing relative humidity because of the greater heat capacity of moist air, all other things being equal. A decrease in evaporation rate at high humidities could outweigh this. A decrease in ψ with increasing humidity occurs because the seasonal variation in ψ swamps that due to relative humidity.

7.6 Regression Analysis to Predict ψ from Meteorological Elements

A multiple regression model was developed to predict ψ from wind speed (**u**), noon solar elevation (μ, representing the time of the year), relative humidity (**rh**) and the northerly wind component (**n**). One problem is the existence of collinearity between solar elevation and relative humidity (correlation of -0.47) and between wind speed and solar elevation (less serious). This explains why the coefficients of all three factors are positive in the multiple regression equation (i.e. that of humidity has changed sign). All four factors are significant, together producing a corrected R^2 value of 0.67. The equation is as follows:

$$\psi = (0.726\mu) + (0.471u) + (10.09rh) + (1.310n) - 21.44 \quad ----(44)$$

This equation implies a decrease in apparent solar efficiency (increase in ψ) of 0.726 W $m^{-2}°C^{-1}$ for a 1° increase in noon solar elevation, a decrease of 0.471 W $m^{-2}°C^{-1}$ for

Figure 7.19. Apparent Heat Capacity, ψ, versus Relative Humidity
Durham (1985-1990)

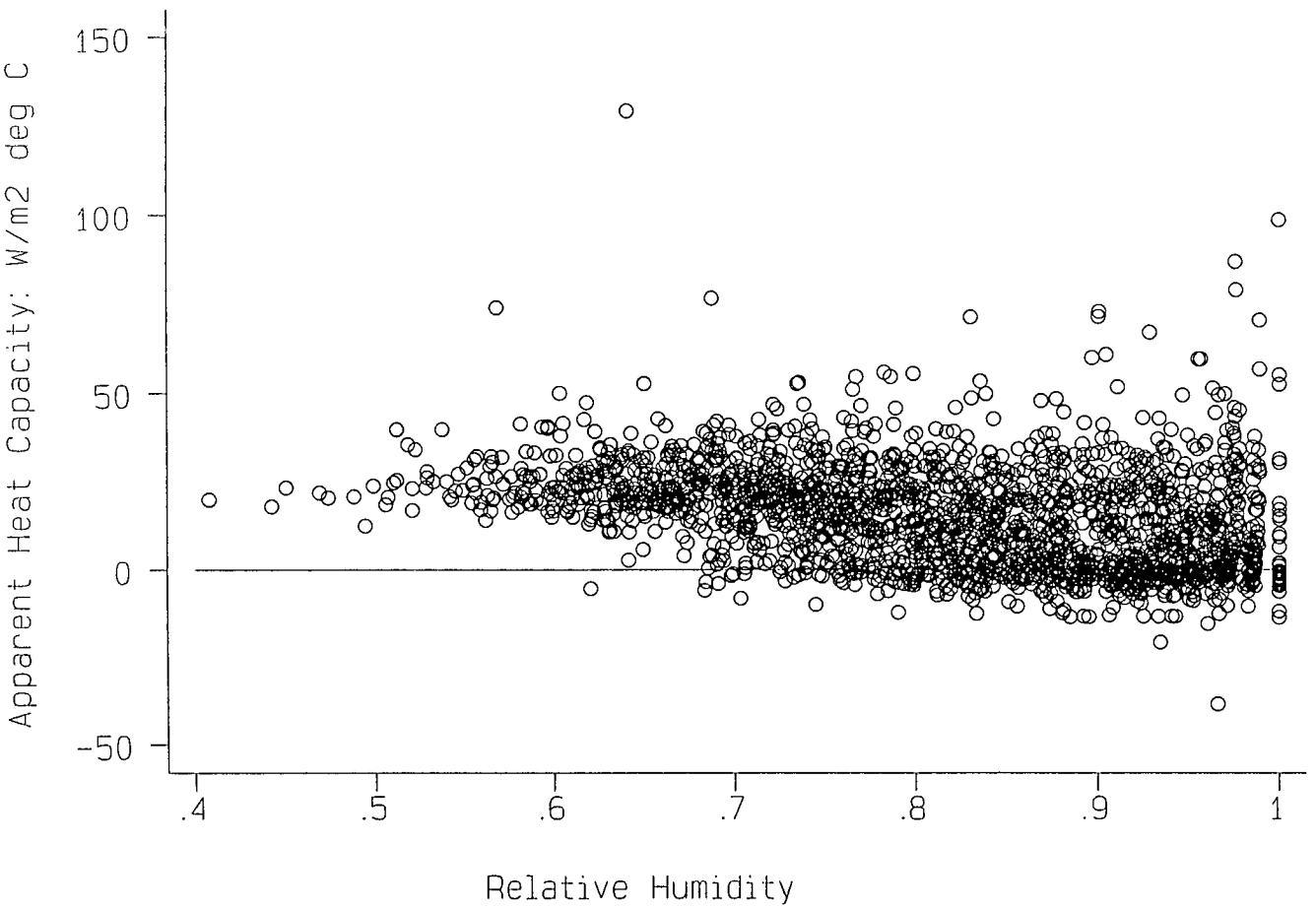

an increase in wind speed of 1 knot, a decrease in efficiency of 10.09 W $m^{-2}°C^{-1}$ for an increase in relative humidity of 1%, and a decrease in efficiency of 1.31 W $m^{-2}°C^{-1}$ for an increase in the northerly component of 1. The constant of -21.44 is physically meaningless, referring to completely dry still air with a solar elevation of zero. 67 % of the variation in solar efficiency is explained by reference to season, relative humidity, wind speed and direction.

7.7 Conclusions

In this attempt to predict the efficiency of the conversion of net irradiance into surface temperature response at Durham, 33% of the variation in ψ is left unexplained. The physical temperature model allows estimation of net radiation when a solarimeter is not available. Examination of the factors which govern the transfer of this net radiation to heating of the ambient air aids prediction of surface and ground temperature response to radiation fluxes. The mass of values of ψ in Figures 7.9 and 7.11 shows that the conversion of net radiation flux into temperature change on an individual day is not simple. However, the use of the regression equation predicting solar efficiency from meteorological factors allows conversion of net radiation estimates to temperature change. The effect of altitude in decreasing solar efficiency is as expected.

Further refinement of the physical model would require inclusion of evaporation estimates from equation 6 (Penman 1948), partitioning of the remaining sensible heat flux between the soil and the air, and a numerical estimation of advection (McIlveen 1991). This physical approach has told us much about temperature response to irradiance at a single location but little about contrasts in temperature from place to place. Additionally, it is inappropriate in mid-latitudes to relate absolute temperature, rather than daily temperature range, to net irradiance (see Walter 1969, Bagnall 1982). However, the model allows one to focus on the physical controls of air temperature and the varying response to different forcing factors at high and low altitude.

REGRESSION MODELS FOR ESTIMATING DAILY MAXIMUM AND MINIMUM TEMPERATURES IN THE NORTH OF ENGLAND

8.1 Introduction

As intimated at the end of chapter 6, the lapse rate analysis is extended here through use of multiple regression to investigate spatial patterns in surface air temperature using 22 stations. The fundamental influence of location (as measured by latitude, longitude and altitude) is stressed. Regression analysis is based on correlation between variables. If coefficients in the regression equations are to have physical meaning, the correlations must make physical sense and care must be taken to avoid collinearity (strong correlations between controlling variables).

Temperatures nearly always decrease with altitude in the free air because of increasing distance from the effective heat source (De Saussure 1796, Barry 1978). Temperature decrease with altitude at ground level is strongly influenced by the temperature of the free air at similar levels and also decreases (McCutchan 1983, Richner & Phillips 1984). Temperature also decreases with increasing latitude because of the decrease in incoming solar radiation. Temperatures may decrease or increase with increasing longitude, depending on the effects of the local land-sea configuration and continentality effects. The regression analysis is based on these relationships and attempts to separate the effects of each in accounting for the spatial variation of surface temperature.

8.2 Multiple Regression Analysis

Multiple regressions of daily maximum and minimum temperatures on altitude, latitude and longitude were calculated for each calendar month using data from 1985 to 1990 inclusive:

$$Max(X) \text{ or } Min(N) = (a \times alt) + (b \times lat) + (c \times lng) + constant \quad ----(1)$$

Data from the 22 climate stations listed in Chapter 4 were used. Altitude ranges from 8 m (Eskmeals) to 847 m (Great Dun Fell). The altitude of Great Dun Fell is an outlier, the next highest value being 513 m (Widdybank Fell). Longitude and latitude were derived from six-figure grid references (Chapter 4). Latitude ranges from 84.7 (Carlton-in-Coverdale) to 195.5 (Redesdale) and longitude from 9.1 (Eskmeals) to 150.9 (Carlton-in-Cleveland). The number of days used in each regression is variable (Table 4.5), individual totals ranging from 1 for north-easterly flow in August to 49 for south-westerly flow in January. In general the regressions for progressive airflows (westerly and south-westerly directions) are expected to be much more stable than those for flows with an easterly component because of the greater frequency of observations in the former case.

8.3 Results: Maximum Temperatures

8.3.1 Seasonal Effects

Table 8.1 gives regression coefficients in each month, along with the constant term and R^2, which describes the goodness of fit of the regression. Values of the altitudinal coefficient (**a**) are in °C/km while values of the latitudinal (**b**) and longitudinal (**c**) coefficients have been multiplied by 1000 and are in °C/1000 km.

The altitudinal coefficient (representing the mean lapse rate) is plotted against month in Figure 8.1. Values range from **-9.48°C/km** in March to **-6.85°C/km** in December. The peak in altitudinal temperature gradient in spring is supported by Manley (1942, 1943), Harding (1979a) and Green & Harding (1980), and is usually attributed to the high frequency of unstable polar maritime air at this season.

Figure 8.1. The Monthly Variation of the Altitudinal Coefficient (Representative of Lapse Rate) in the Multiple Regression Equations of Daily Maxima

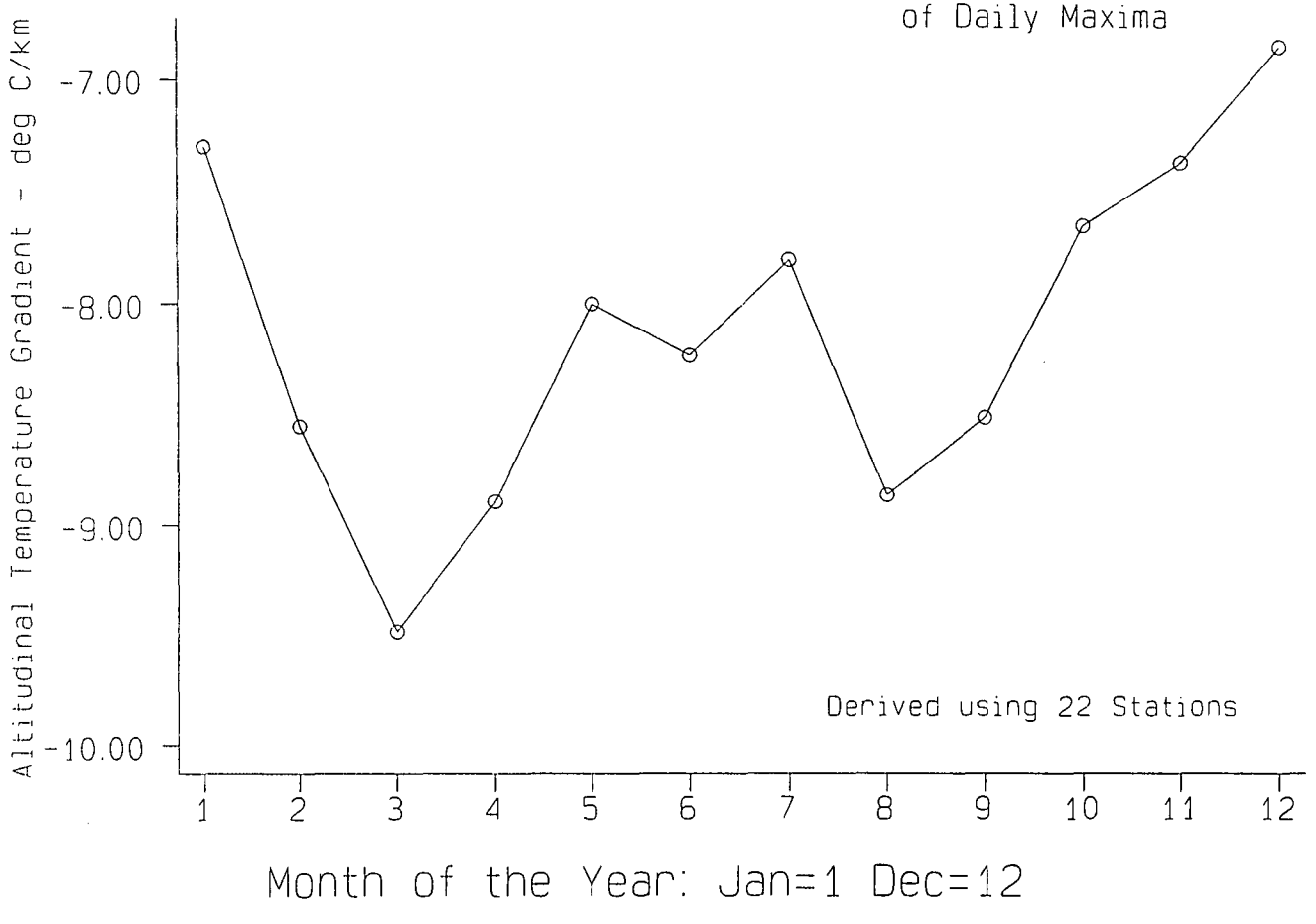

Table 8.1: Altitudinal, latitudinal and longitudinal coefficients in the monthly regressions of daily maximum temperatures.

	a	b	c	const	R^2
J	-7.30	-0.21	2.13	6.43	0.935
F	-8.55	0.23	0.85	7.00	0.942
M	-9.48	0.13	4.46	9.12	0.932
A	-8.89	-2.97	-1.57	12.22	0.899
M	-8.00	-6.86	-7.37	17.17	0.805
J	-8.23	-7.41	-2.46	19.07	0.782
J	-7.80	-6.35	7.46	20.12	0.813
A	-8.86	-2.36	11.72	18.30	0.910
S	-8.51	-4.10	10.13	16.61	0.928
O	-7.65	-2.97	4.28	13.90	0.936
N	-7.37	-0.74	0.83	9.14	0.920
D	-6.85	-0.94	2.69	8.15	0.927
YEAR					

a is only **-6.85°C/km** in December and **-7.30°C/km** in January. The altitudinal decrease in temperature is shallower in winter because of the influence of temperature inversions. Valley bottoms are often colder than slopes at higher elevations. The variation of temperature with altitude can on occasions become curvilinear, with a turning point at the inversion (Figure 8.2). Under such conditions cloud can be trapped by the inversion, with cloud-free conditions above (Manley 1947). In areas where inversions form regularly, the altitudinal band which benefits from relatively high temperatures is known as a "thermal zone" (Chickering 1884, Dunbar 1966) and can be of great importance for fruit growers.

The mean altitudinal effect on temperature is also reduced between May and July when solar input is strong. Heating of upland plateaux in high summer has been documented for high altitude areas such as the Himalayas (Yeh 1982, Chen et al.

Figure 8.2 Temperature Profile in the Presence of an Inversion.

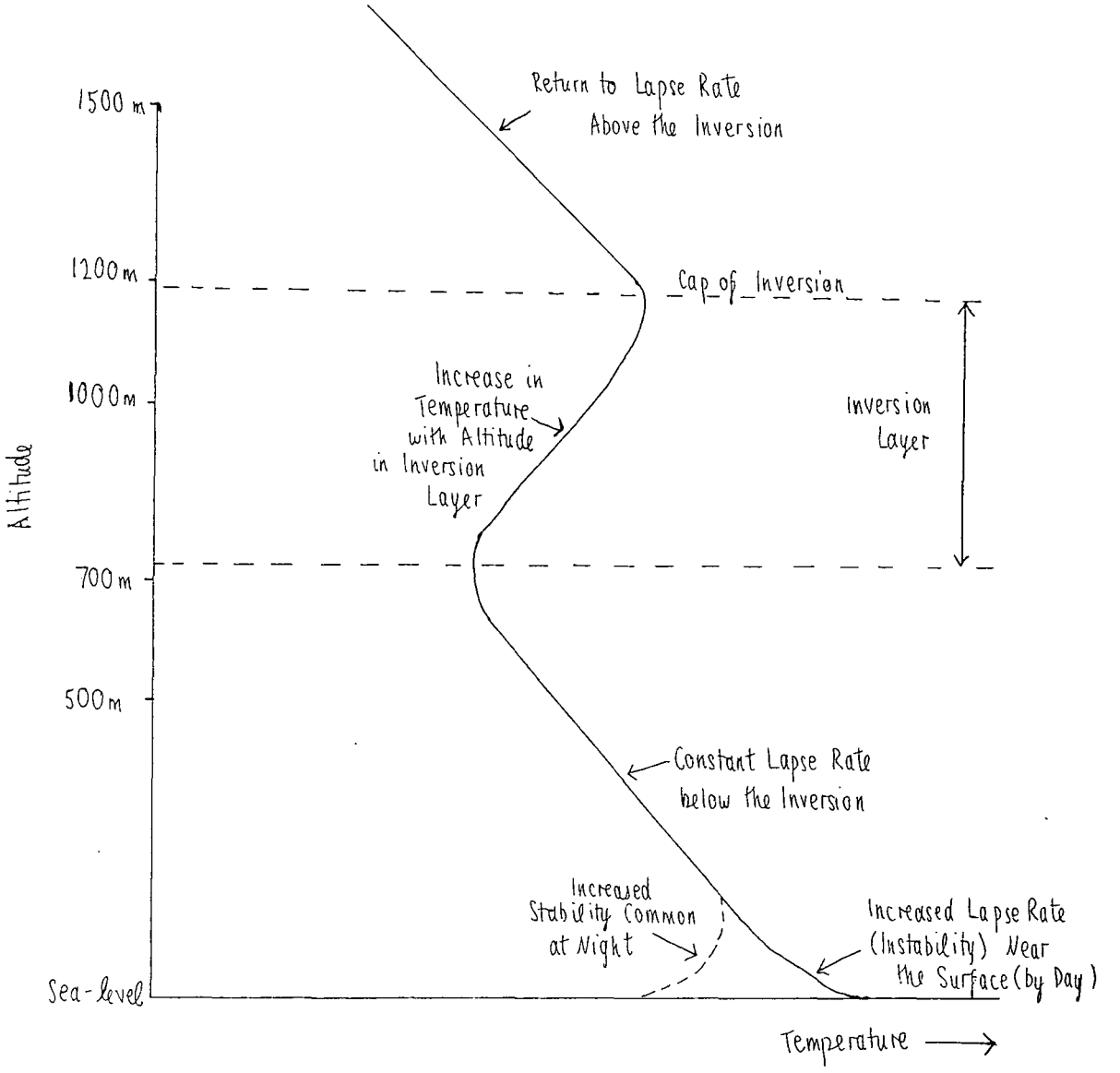

This diagram shows a hypothetical temperature inversion of about 500 metres in thickness, well above the ground surface. Inversions lower than this may form in the winter or at night as the surface is chilled by radiation loss. The inversion acts as a lid on any air trapped beneath and reduces <u>mean</u> lapse rates in the regression equations of this chapter.

1985), Rockies (Barry 1973, Tabony 1985) and the Altiplano of South America (Flohn 1953). The heating of the upland atmosphere is noticeable under calm and cloud-free conditions. Higher levels of solar radiation received at high altitude (Lowry 1980) can lead to surprisingly high summer temperatures, especially at the ground surface (Turner 1958). The importance of calm sunny weather in upland areas must not be underestimated in terms of the potential for agricultural cultivation at high altitude, especially in maritime areas such as Britain (Manley 1942).

Figure 8.3 plots **a**, **b** and **c** against month. **b** is nearly always negative, indicative of an increase in temperature from north to south. Values range from **+0.13°C/1000 km** in March to **-7.41°C/1000 km** in June. The meridional temperature gradient is therefore strongest in summer and weakest in late winter (February-March), when the altitudinal effect is strongest. The meridional gradient in solar radiation is greatest in winter so it is unexpected that isotherms run more nearly east-west in summer. Winter temperatures in northern England bear little relationship to solar input because of widespread advection of warm air from the Atlantic. Latitude therefore becomes unimportant.

c fluctuates widely throughout the year. A negative value implies a decrease in temperature from west to east. Throughout winter (from October to March) **c** is weakly positive, averaging around **+2°C/1000 km**, there being a slight increase in temperature of about 0.5°C between the west and east coasts. The width of northern England is assumed to be 250 km. From April to June **c** turns negative, falling to **-7.37°C/1000 km** in May. Sea surface temperatures are relatively cold in early summer, especially so off the east coast. Additionally, easterly winds are common at this season. Under such circumstances cold air advection from the east causes a strong reduction of temperatures in the east of the region. From July to September **c** becomes positive, reaching **+11.72°C/1000 km** in August. Associated with this increase is a warmer sea surface off the east coast coupled with a reestablishment of a more westerly circulation in many years.

Figure 8.3. Monthly Variation in Altitudinal, Latitudinal and Longitudinal Coefficients: Daily Maxima Regressions

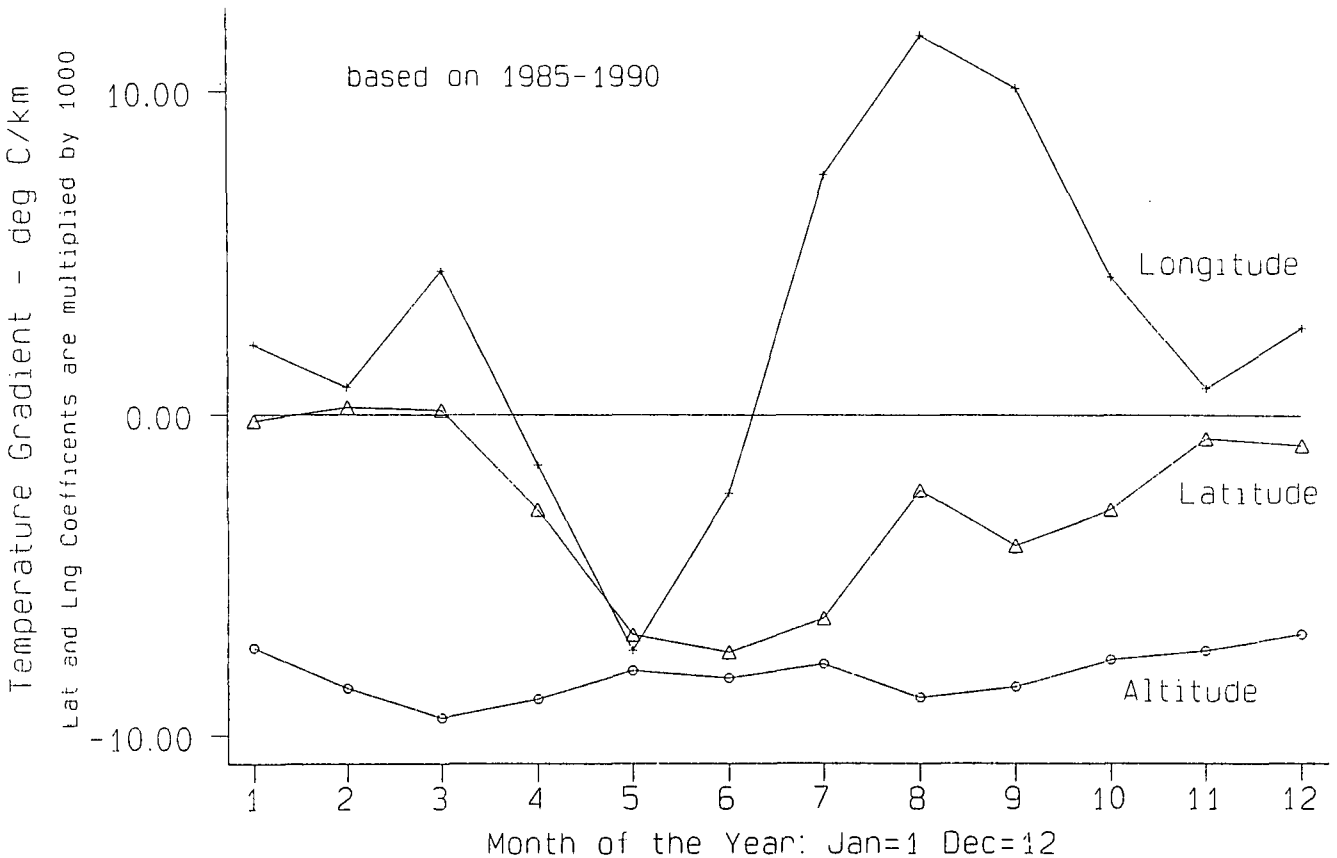

8.3.2 Airflow Effects

Airflow direction is extremely important in explaining spatial temperature distribution on any one occasion. The three coefficients are plotted against wind direction (Figure 8.4) for nine further regressions. Values of **a** are shown in Figure 8.5, varying from **-6.89°C/km** for south-easterly flow to **-8.73°C/km** for both westerly and easterly flows. Mean lapse rates are steeper when flow is from the west or east, i.e. across the Pennine range. Airflows perpendicular to the relief trend therefore undergo more temperature modification than airflows parallel to a mountain range. Föhn effects are more likely to develop in the former case, distinguishing windward and lee slopes.

Meridional airflows are associated with a shallower altitudinal gradient in maxima, especially those from the south and south-east. Warm air moving north will often be cooled from below, creating a weak lapse rate in its lower layers. Southerly flows consistently show a lower altitudinal coefficient than northerly flows. Additionally, southerly and south-easterly flows are often associated with stable anticyclonic conditions.

a is also low when conditions are calm, showing that upland areas benefit in such conditions. On windy days wind speeds can increase dramatically with altitude, reducing maxima further at high elevations. Under calm conditions this is not so and in winter, temperature inversion formation below the highest mountain summits is possible (Pedgley 1979).

b is always negative but is weakest for southerly and south-westerly flows. It appears that advection of warm air in winter prevents a strong meridional temperature gradient from developing. **b** is highest under easterly flows. Calm conditions also allow the development of a considerable gradient (**+4.33°C/ 1000 km**).

The longitudinal coefficient **c** (Figure 8.4) varies from nearly **-20°C/1000 km** to over **+10°C /1000 km**. Temperature increases with longitude for winds between south and north-west. These airflows are often associated with progressive cyclonic

Figure 8.4. Variation of the Altitudinal, Latitudinal and Longitudinal Coefficients in the Daily Maxima Regressions According to Airflow

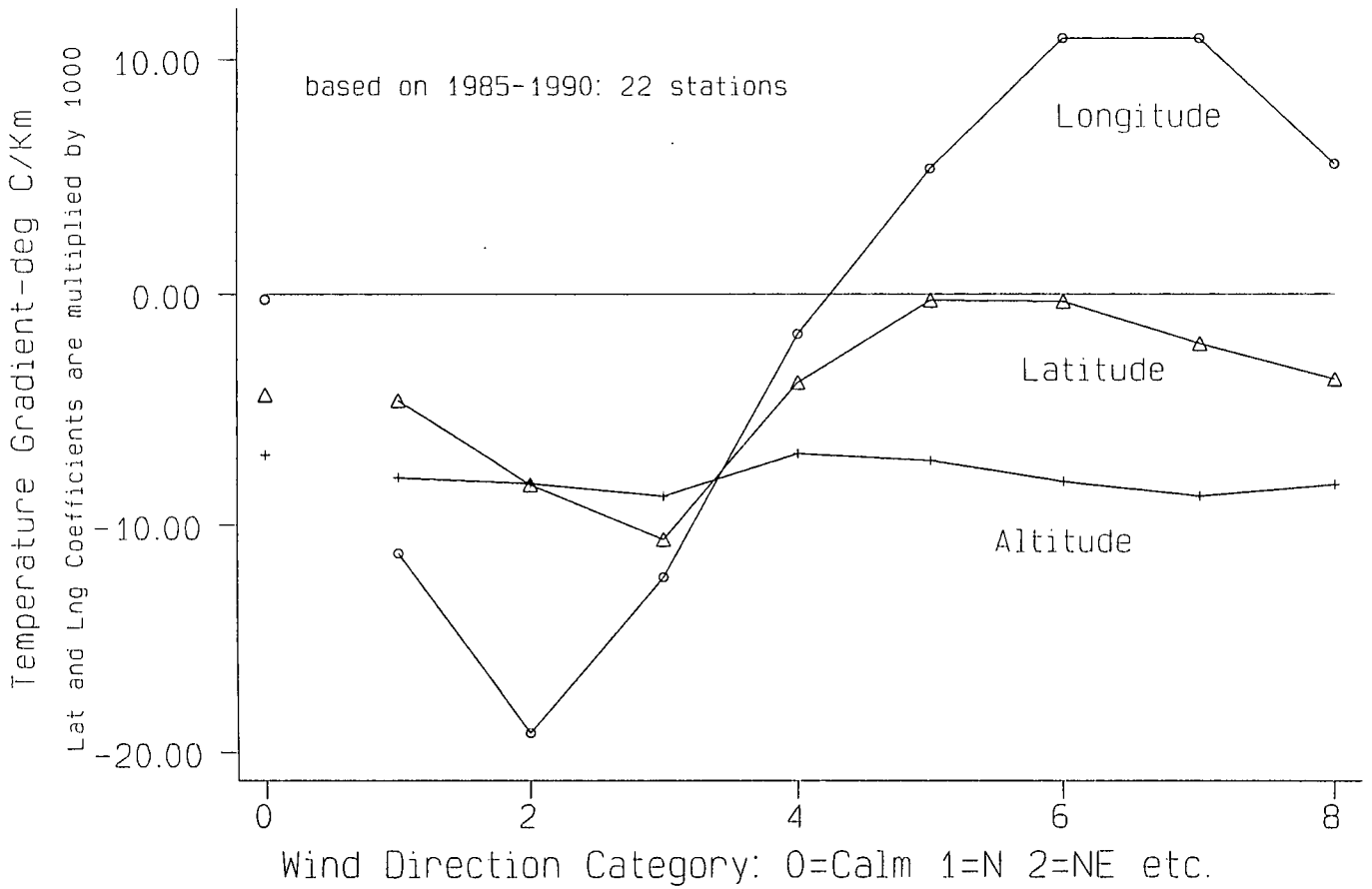

Figure 8.5. Variation of the Altitudinal Coefficient in the Daily Maxima Regressions According to Airflow Direction

flow, depressions passing from west to east over Britain. A decrease of temperature with longitude is experienced under northerly and easterly flows, common under blocked regimes. The cold advection of air from over the North Sea by north-easterly flow encourages a decrease of 5 °C between the west and east coasts. Even steeper gradients are probable between April and June when the sea is cool relative to the land.

8.3.3 Combined Seasonal and Airflow Effects

Seasonal changes in **a**, **b** and **c** are different for differing airflows. 108 multiple regressions were calculated, one each for the nine wind classes in each month. Three regressions were considered less reliable as there was no data for Great Dun Fell. The effects of leaving a data point out of a regression are investigated in section 8.6.

Table 8.2 gives the altitudinal coefficient, **a**, in each regression. Underlined values were derived from 21 stations only. Altitudinal (**a**), latitudinal (**b**) and longitudinal (**c**) coefficients are given in Appendix 5.

Table 8.2: The altitudinal coefficient, **a**, (°C km^{-1}) for each airflow in each month.

a	C	N	NE	E	SE
J	-5.78	-8.43	-10.48	-6.87	-6.87
F	-7.76	-10.17	-9.12	-9.09	-10.20
M	-10.27	-9.15	-8.03	-7.81	-8.88
A	-7.01	-9.30	-8.74	-10.25	-9.73
M	-7.09	-7.69	-7.61	-7.35	-3.59
J	-7.00	-7.39	-7.92	-11.25	-7.01
J	-4.81	-7.87	-7.47	-6.57	-4.15
A	-9.44	-7.95	-6.56	-8.20	-8.72
S	-8.28	-8.38	-7.68	-7.01	-7.20
O	-6.26	-7.32	-9.04	-8.48	-8.51
N	-7.51	-8.12	-8.84	-9.07	-8.37
D	-6.00	-9.23	-8.42	-10.46	-6.87

Table 8.2: continued

a	S	SW	W	NW	MEAN
J	-7.03	-7.76	-7.72	-7.63	-7.30
F	-7.44	-8.29	-8.86	-8.77	-8.55
M	-9.33	-9.18	-9.80	-9.99	-9.48
A	-7.52	-8.87	-9.80	-9.45	-8.89
M	-7.74	-9.37	-8.74	-8.74	-8.00
J	-8.48	-8.62	-9.07	-9.21	-8.23
J	-7.89	-9.18	-8.41	-8.30	-7.80
A	-8.62	-9.38	-9.46	-8.54	-8.86
S	-8.41	-8.28	-9.46	-9.21	-8.51
O	-7.45	-7.86	-8.57	-7.97	-7.65
N	-6.41	-6.89	-7.42	-8.13	-7.37
D	-6.17	-6.42	-7.99	-5.67	-6.85

8.3.3 i) Altitudinal Coefficient

The seasonal variation in altitudinal coefficient varies according to airflow. **a** is plotted against month in Figure 8.6 using the wind direction class as the symbol. The solid line represents the mean altitudinal gradient in each month with equal weighting for each wind direction (different from the values shown in Figure 8.1). Lapse rates over **-10°C/km** are shown for some easterly and northerly flows in winter. Such superadiabatic lapse rates may be related to instability developed over the North Sea in cold polar continental air. Values for south-easterly flow (4) are extremely irregular. In May, **-3.59°C/km** is exceptionally low and the value in July is only **-4.15 °C/km**. These rates are based on very few observations.

Easterly flows (3) show steep lapse rates in spring and early summer, with **-11.25°C/km** in June and **-10.25°C/km** in April. From July to November mean lapse rates are below **-9°C/km**. North-easterly flow (2) behaves unusually, in that a

Figure 8.6. Variation of the Altitudinal Coefficient in the Daily Maxima Regressions According to Month and Airflow Direction

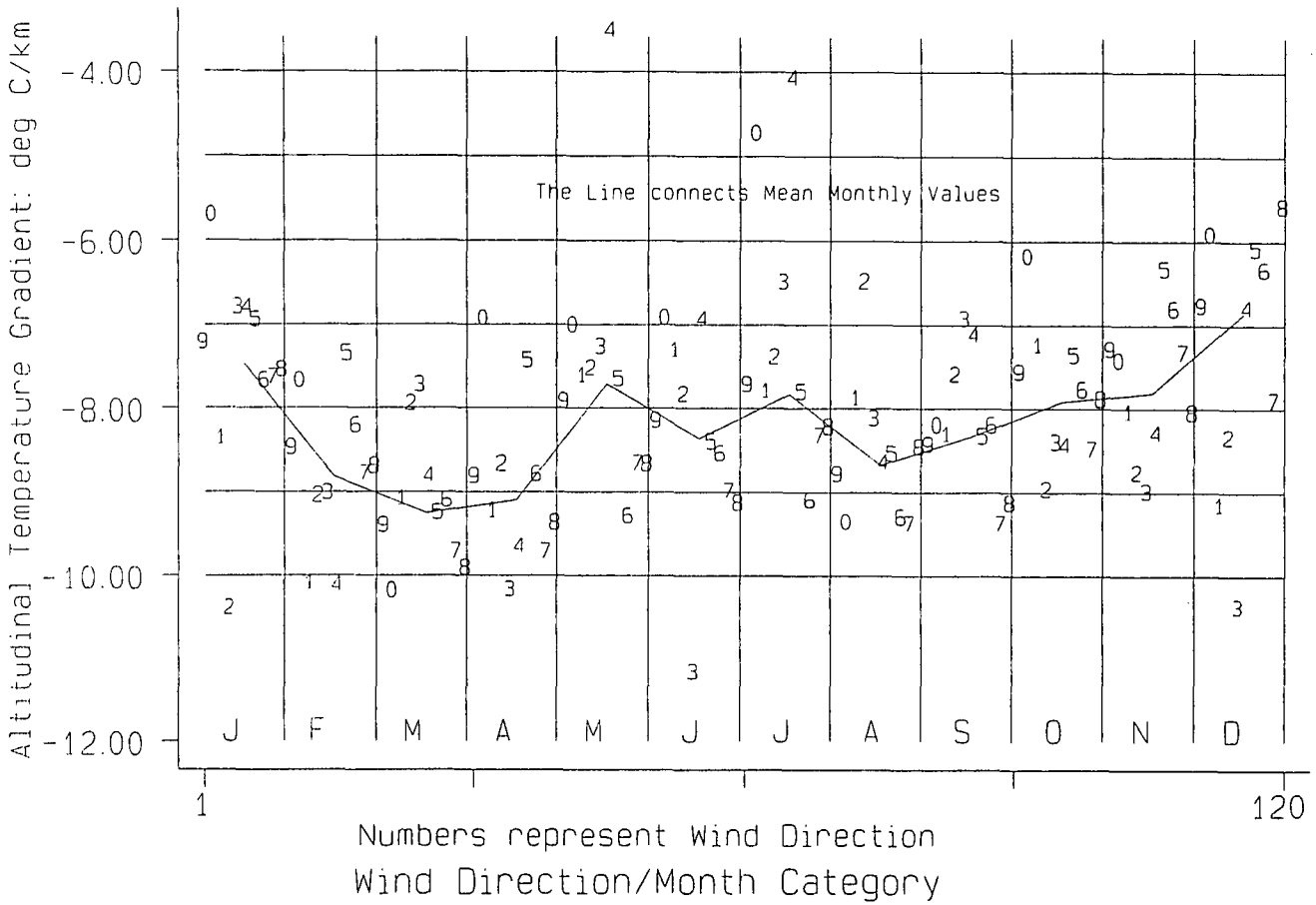

superadiabatic rate is experienced in January but values from May to September are below **-8°C/km**. Instability of north-easterly flows in winter probably arises due to warming of intensely cold air leaving Eurasia. Warming of surface layers will increase the lapse rate with intensely cold air aloft. In contrast, air in summer from Eurasia and Scandinavia is cooled as it moves towards northern England, leading to greater stability. In summary, superadiabatic lapse rates seem likely with blocked conditions in winter, spring or early summer.

Northerly flows (1) are similar to north-easterlies in that they show steepest lapse rates in winter and early spring. Cold arctic air moving south in winter and spring will warm and develop instability. By summer, long hours of sunshine in the Arctic mean that the air is not much colder than polar maritime air and northerly outbreaks become relatively stable.

Not all airflows show steepest lapse rates in winter. The normal pattern for southerlies (5), south-westerlies (6) and westerlies (7) is for winter rates to be shallower than spring and summer ones. For example, rates for southerly (5) flow peak in March and between June and September. Southerlies are often associated with tropical maritime air. In summer this appears to become unstable as it is heated rapidly. The December rate is only **-6.17°C/km**. Air moving north is often subject to cooling from beneath and temperature inversion formation is possible, especially if the flow is weak. The annual cycle of lapse rates for south-westerlies (6) peaks in March-May and July-August with a slight decrease in June. Westerlies (7) show the double peak and trough pattern with peaks at the equinoxes and troughs at the solstices (described in Chapter 5). The trough in summer is weak. Lapse rates are usually steep with westerly flow, i.e. higher than the monthly average. Because south-westerlies and westerlies are the most common airflows the "double peak and trough" pattern extends to the mean monthly lapse rates (solid line in Figure 8.1). North-westerlies (8) are usually associated with unstable polar maritime air and the steep rate (nearly **-10°C /km**) in March is expected.

Calm conditions (0) are associated with some interesting results. In late autumn

and winter (when solar input is low), **a** is also low, because of the tendency for radiation inversions. Since daily maxima are being used to derive the lapse rate, the effects of inversions must last throughout the day on many occasions to account for this. Calm conditions produce some of the lowest rates, including **-5.78°C/km** in January. Mid-summer values are also low, e.g **-4.81°C/km** in July, indicating the effectiveness of heating in the upland atmosphere under calm conditions with a strong radiation input. Advection of the free air is limited when conditions are calm and high maxima occur.

The variation of **a** in Figure 8.6 is summarised in Table 8.3:

Table 8.3: Annual trends in mean lapse rates for differing airflows

Wind Direction	Annual Lapse Rate Cycle
N/NE	Peak in winter - more stable in summer
E/SE	Very irregular. Some extremely high and low values. Superadiabatic rates most common with easterlies in winter and spring
S	Stable, especially in winter
SW	Less stable than southerlies. Winter minimum
W	Consistently high lapse rates, especially around the equinoxes. Lower at the solstices
NW	Peak in spring -trough in winter
CALM	Shallow rates due to temperature inversion in winter and upland heating in summer. Spring and autumn have higher lapse rates

8.3.3 ii) Latitudinal Coefficient

Results for the latitudinal coefficient, **b**, are shown in Figure 8.7. The latitude effect is more negative in summer than winter. This is unusual since the increase in daylength with latitude in summer may be thought to decrease the meridional

Figure 8.7. Variation of the Latitudinal Coefficient in the Daily Maxima Regressions According to Month and Airflow Direction

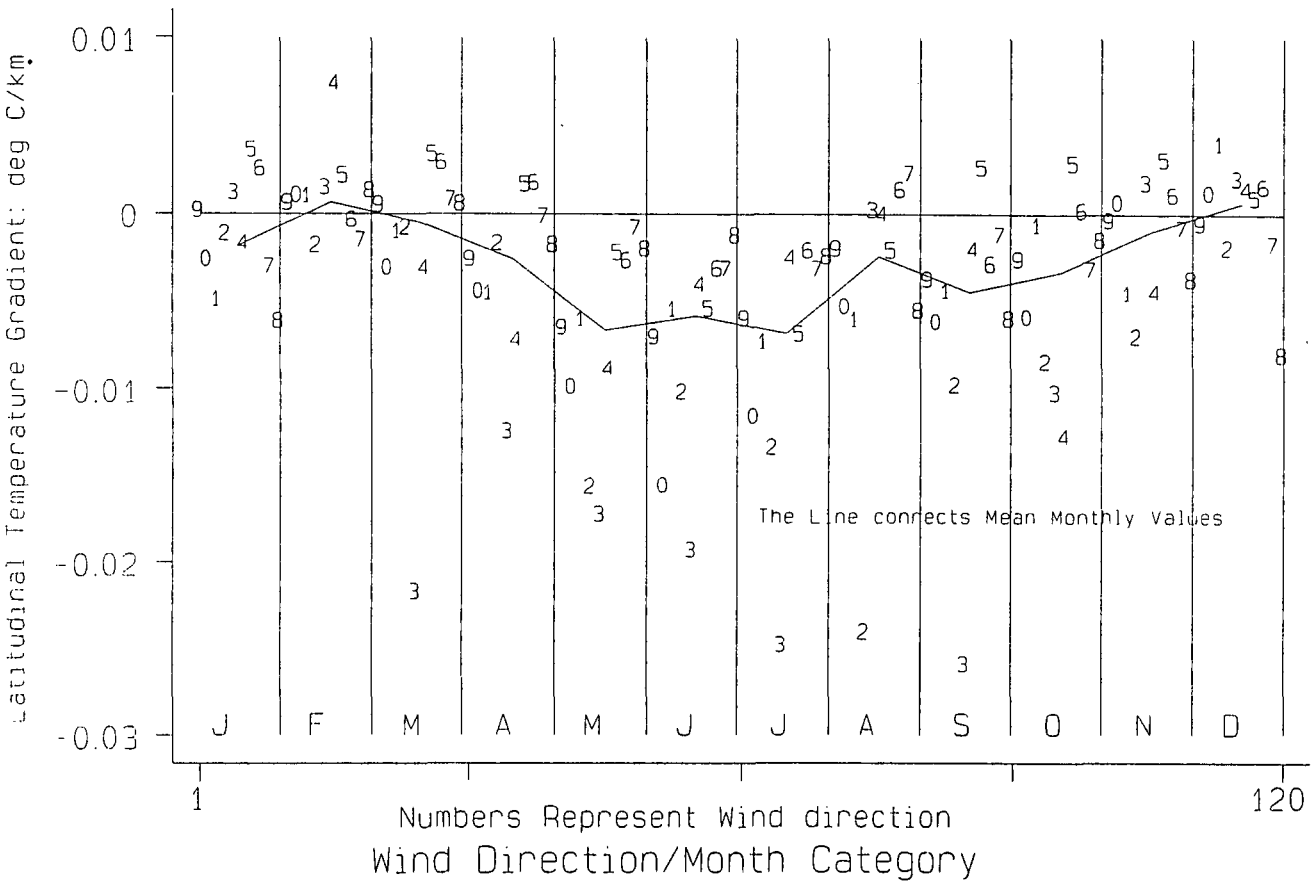

temperature gradient. Instead continental influences ensure that the gradient is stronger in summer. Duncan (1991) compared the Central England Temperature series with a record of similar length at Edinburgh. Temperature differences were greatest in summer, indicating a stronger latitudinal temperature gradient. The south of England is more continental than the north and the coldest winters at sea level occur in the south-east midlands (Manley 1952). Therefore from November to March **b** is sometimes weakly positive such as for south-easterly (4) flow in February. In such cases, proximity to the continent is the important factor. Southerlies (5) are associated with positive values of **b** from September to April.

The steepest latitudinal temperature gradients are associated with easterly flow (3), especially in summer (e.g. **-26°C/1000 km**). This gradient only applies within the study area. Calm conditions also encourage steep temperature gradients between May and July when solar input is strong. If summer conditions were to become more frequently anticyclonic, with much more continental air from the east or even north-east, the latitudinal temperature gradient would increase, southern England becoming considerably warmer than the north. Alternatively, progressive summers with winds from the south-west or west (Lumb 1993) would increase the latitudinal temperature gradient.

The latitudinal effect for westerlies (7) is positive in March but negative all the rest of the year (weaker than **-5°C/1000 km**). South-westerlies (6) show the most negative values in summer but from October to April **b** is positive or negligible, suggesting an increase in temperature in the north under outbreaks of tropical maritime or returning polar maritime air. Northerly (1) flow on the other hand is associated with steep negative gradients, reaching nearly **-10°C/1000 km** between May and August. North-westerlies (8) are anomalous as values of **b** reach their most negative in winter.

Finally, calm (0) conditions allow a marked latitudinal decrease in summer maxima, **b** in June reaching **-15.9°C/1000 km**. Values from November to February are negligible or weakly positive. The continental nature of the southern part of the region, low daytime maxima occurring under calm conditions in winter accounts this.

It is reassuring that **b** shows regular patterns with wind direction. However, altitude accounts for most of the variation in maximum temperature and **b** (along with **c**) explains only a small proportion of the overall variation.

8.3.3 iii) Longitudinal Coefficient

The longitudinal coefficient (**c**) (Figure 8.8) shows a much more consistent relationship with wind direction. Westerly (7) and south-westerly (6) flows consistently produce the strongest west-east temperature increases, while north-easterly (2) and easterly (3) flows produce the strongest west-east temperature decreases. Daytime maxima increase away from the onshore coast (to the west if winds are easterly and to the east if winds are westerly). The pattern of **c** associated with each airflow direction over the course of the year is very marked even though longitude is relatively unimportant in explaining temperature variation as a whole.

Calm conditions (0) are associated with a negative gradient (temperature increase to the west) in the early part of the year but a positive gradient from July onwards, reflecting the fact that the North Sea is cooler than the land from February to July, but warmer from August to January. The east of the region is relatively cold in spring and warm in late summer and autumn. The seasonal variation in **c** is subdued for calm conditions relative to other airflows because the longitudinal effect depends solely on horizontal advection, controlled by airflow movement.

Northerlies (1) show negative values of **c**, i.e. a temperature decrease to the east, except in November and December when the North Sea is relatively warm. In May and June values approach **-20°C/1000 km**, equivalent to a decrease of 5°C from the west to the east coast. North-easterlies (2) have a more pronounced effect. The gradient in May reaches **-38.5°C/1000 km,** equivalent to a 10°C difference between the west and east coasts. Easterlies (3) show a similar pattern. Advective cooling in the north-east is therefore one of the major features supported by Figure 8.8 (see Caton 1957, Catchpole 1966).

Figure 8.8. Variation of the Longitudinal Coefficient in the Daily Maxima Regressions According to Month and Airflow Direction

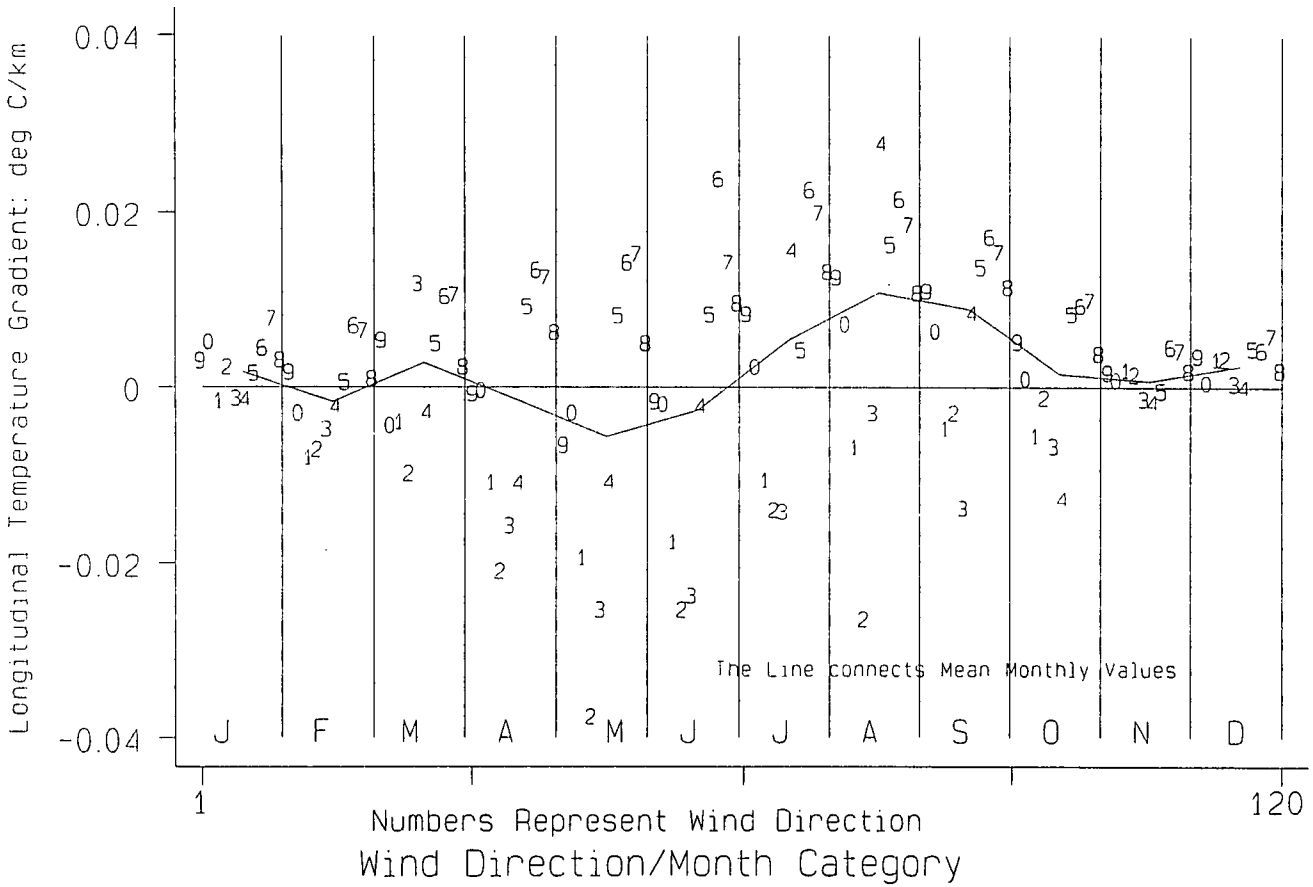

South-easterlies (4) are unusual in that they show a sudden change from negative values of **c** in May and June to positive ones in July and August. Southerlies (5), south-westerlies (6), westerlies (7) and north-westerlies (8) show positive longitudinal coefficients with higher maximum temperatures in the lee of the Pennines. The steepest gradients are seen in late summer (especially July, August and September) and the shallowest in winter when air crossing the cold land surface has little opportunity to be warmed. The increase from west to east is less for north-westerlies (8) than for the other progressive airflow directions. Values peak at **+12.4°C/1000 km** in July as opposed to **+21.7°C/1000 km** for south-westerlies in the same month.

Whatever the wind direction, from November to January **c** is negligible. Westerlies produce the highest values in December and January but these are still low, e.g. **+4.9°C/1000 km** in December.

8.3.3 iv) The Success of the Regressions

Figure 8.9 assesses the overall success of the 108 multiple regressions by presenting R^2 values, i.e. the proportion of temperature variation explained by altitude, latitude and longitude combined. Values over 0.9 (90% explanation) are common, especially from September to April. During these eight months even the worst R^2 values are around 0.8 (for calm conditions). Local temperature inversions are the problem, meaning that local factors need to be taken into account. From May to August R^2 is often poorer. Solar input is extremely important but is local in its effects. On a day of intermittent cloud cover, wherever the sun shines maximum temperatures will be raised considerably above those of neighbouring stations. This local heating is most important when air is calm and when the circulation is slack (often south-easterly flow). Hence the low R^2 for these categories in May, June and July. In spring and autumn even R^2 values for calm conditions are above 0.9. Highest values are associated with south-westerly (6) and westerly (7) airflows, especially in winter.

Further development of equations with poor R^2 would need to concentrate on local factors such as aspect and exposure. The inclusion of a continentality factor could

Figure 8.9. R2 in the Daily Maxima Regressions
According to Month and Airflow Direction

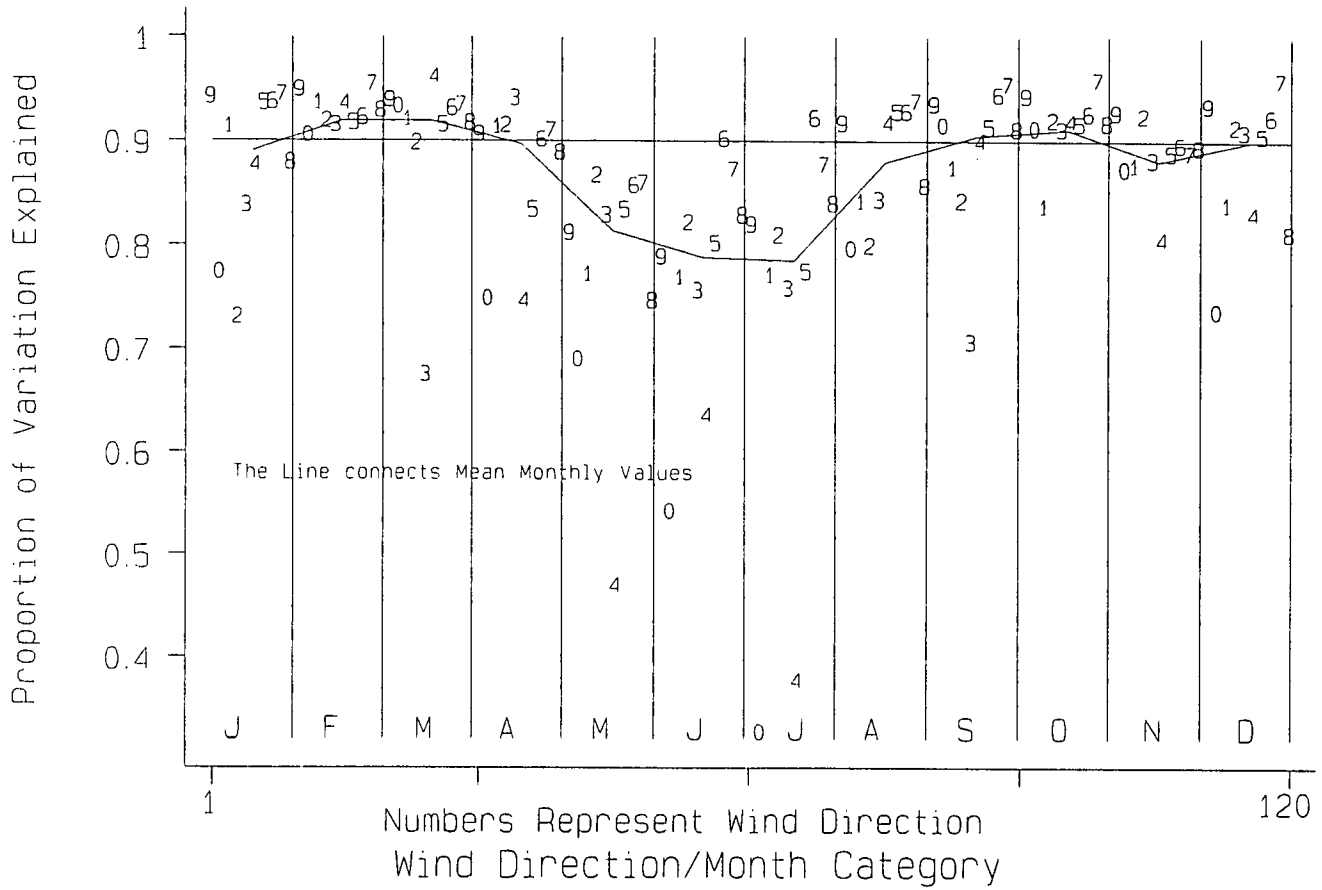

be useful.

For a particular airflow estimates of average daily maximum temperatures at any location can be produced by applying the appropriate regression. The constant term represents temperature at sea level at zero latitude and longitude. In the model this location is in the southern Irish Sea.

8.4 Results: Minimum Temperatures

A similar analysis to that for maxima was performed for minimum temperatures. Results were less satisfactory because minima are more dependent on local factors such as exposure and aspect, especially when conditions are calm (Hawke 1944, Harding 1978).

8.4.1 Seasonal Effects

Table 8.4 gives values of **a**, **b** and **c**, the altitudinal, latitudinal and longitudinal coefficients in each month. As in Table 8.1, **a** is given in °C/km and **b** and **c** in °C/1000 km.

a is lower (less negative) than in the maximum temperature regressions, indicating shallower night-time lapse rates and increased stability. The formation of temperature inversions by night encourages this. **a** in November is only **-5.08°C/km**, the long nights being conducive to stability. **a** is plotted against month in Figure 8.10. Compared with values for maximum temperatures (Figure 8.1), the steepest rate in March (**-6.96°C/km**) is approximately equal to the shallowest rate for maximum temperatures seen in December (**-6.85°C/km**)! The peak in lapse rate in March is the same as for maxima and there is again a secondary peak in August, although this is not as strong as that for maximum temperatures. The lowest values of **a** are experienced in late autumn and winter. Air-mass character is likely to be an important influence on lapse rate (Manley 1952), as the critical solar elevation theory discussed in Chapter 5 is unlikely to be important at night.

Figure 8.10. The Monthly Variation of the Altitudinal Coefficient (Representative of Lapse Rate) in the Multiple Regression Equations of Daily Minima

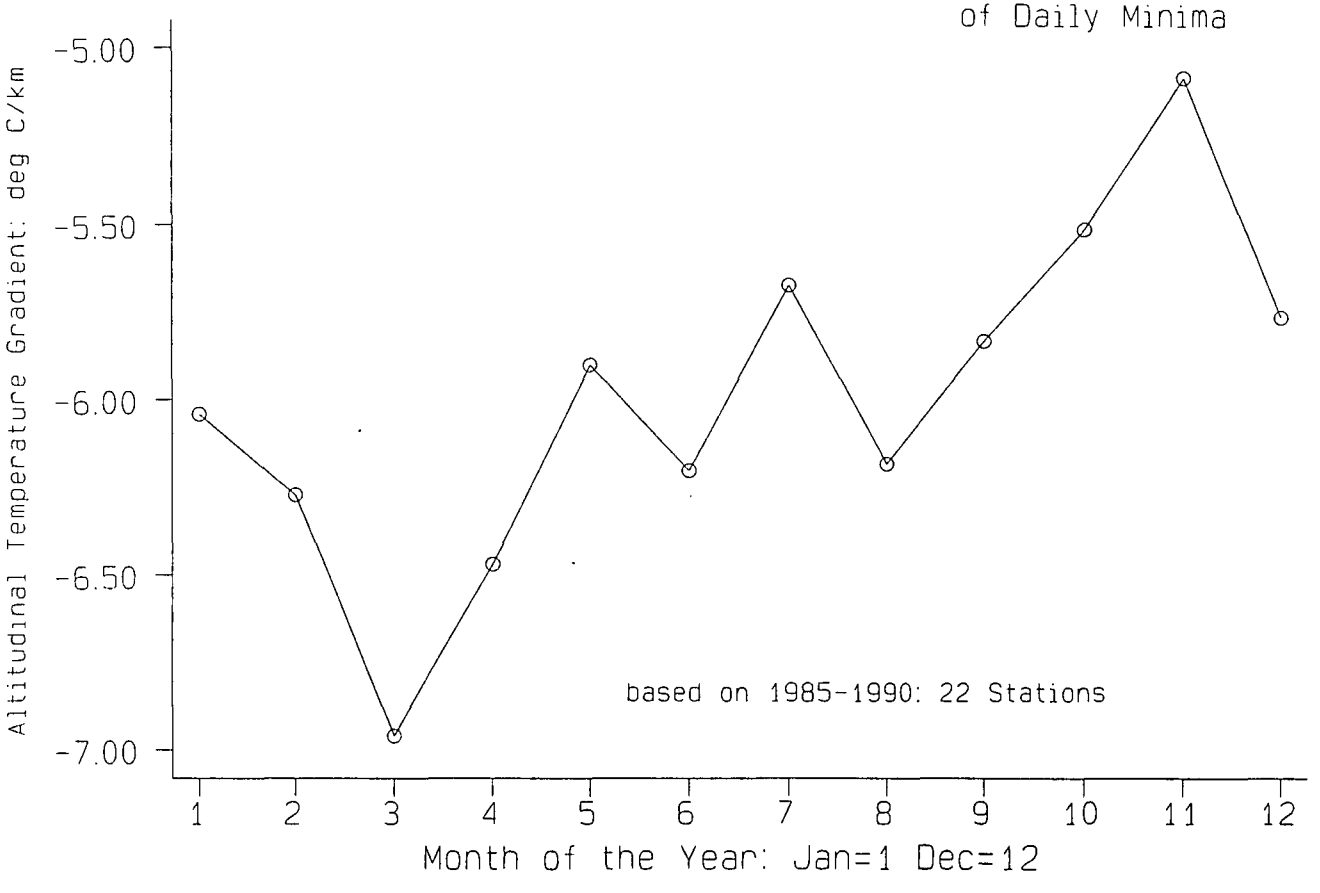

Table 8.4: Altitudinal, latitudinal and longitudinal coefficients in the monthly regressions of daily minimum temperatures.

	a	b	c	const	R^2
J	-6.04	-2.88	-5.69	2.33	0.770
F	-6.27	-2.89	-3.62	1.95	0.768
M	-6.96	-5.80	-2.45	3.52	0.841
A	-6.47	-5.19	-2.33	4.93	0.810
M	-5.90	-10.36	-3.36	8.49	0.726
J	-6.20	-7.62	-2.56	10.37	0.738
J	-5.67	-8.66	-1.47	12.76	0.707
A	-6.18	-6.62	0.35	12.10	0.771
S	-5.83	-8.17	0.76	9.89	0.639
O	-5.51	-7.89	-0.87	8.46	0.601
N	-5.08	-4.66	0.68	3.77	0.595
D	-5.76	-5.72	-1.64	3.98	0.718
YEAR	-5.85	-6.18	-2.01	6.88	0.725

Figure 8.11 shows **a**, **b** and **c** plotted against month. The rate of decrease of minimum temperature with latitude ranges from **-10.36°C/1000 km** in May to **-2.88°C /1000 km** in January. The latitudinal gradient is therefore strongest between May and September, and weakest in winter, broadly similar to the pattern for maximum temperatures.

The longitudinal coefficient, **c**, is not very important in explaining minimum temperature, except perhaps in January and February (when the latitudinal coefficient is less important). **c** reaches **-5.69°C/1000 km** in January, representing a decrease in minima of about 1.4°C from the west to the east coast. By February, **c** has fallen to **-3.62°C/1000 km** and it remains around **-2.5°C/1000 km** from March to June. The influence of the North Sea surface temperature on **c** is negligible, unlike for maximum temperatures. From August to November **c** fluctuates around zero but by December it

Figure 8.11. Monthly Variation in Altitudinal, Latitudinal and Longitudinal Coefficients: Daily Minima Regressions

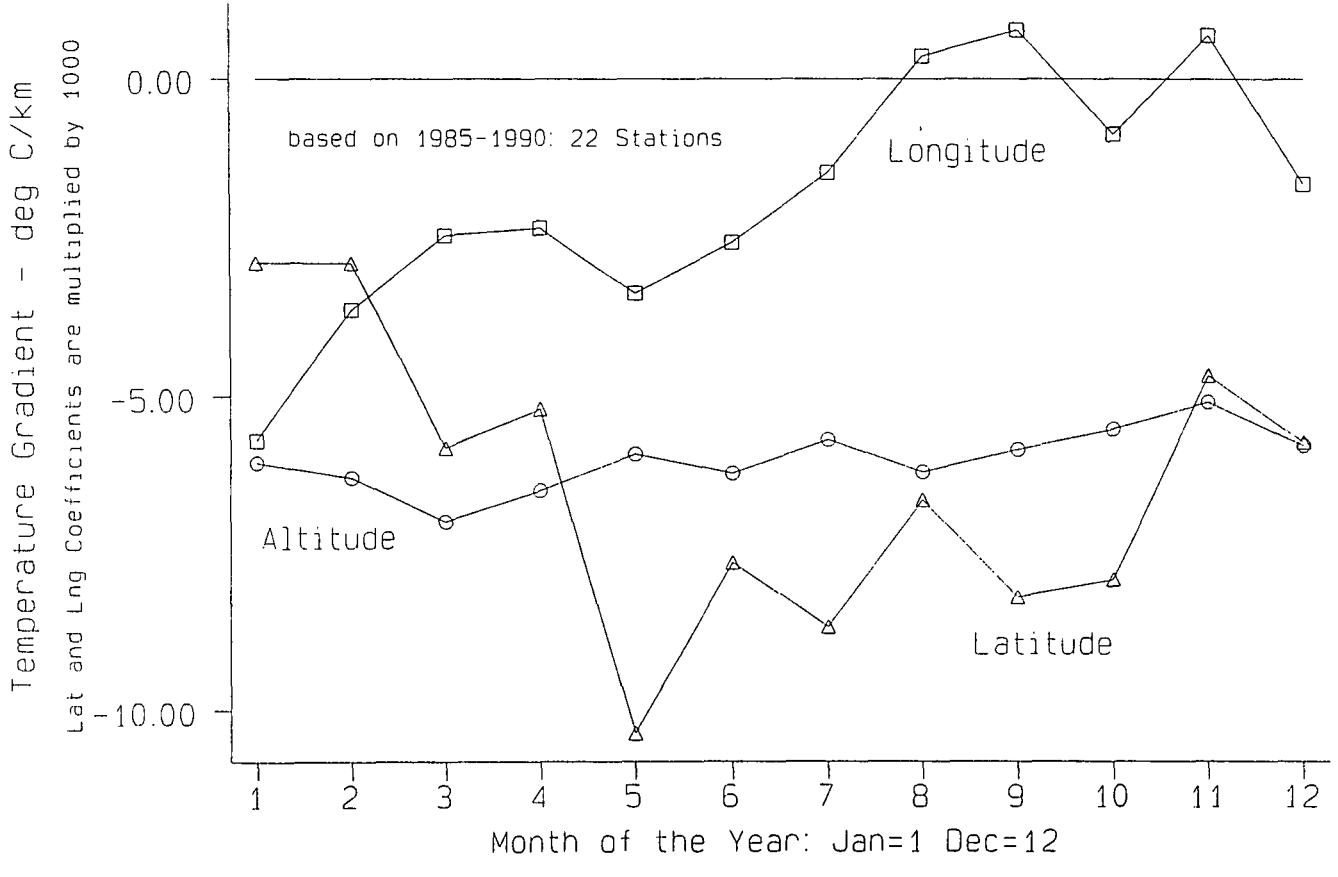

has again turned negative.

Examining R^2 values, the inclusion of longitude is often superfluous. The adjusted R^2 value is higher if longitude is excluded, except in January and February. Values vary from **0.841** in March to **0.595** in November. The success of the regression model largely depends on the strength of the altitudinal coefficient, the other two factors being less helpful.

8.4.2 Airflow Effects

Regressions were performed for each wind direction. The altitudinal coefficient is plotted in Figure 8.12.

The mean lapse rate under calm conditions is less than for all other airflows (**-4.07°C/km**), due to the tendency for temperature inversion formation on calm nights, caused either by intense longwave radiation loss or trapping of cold air by topography.

Again, the steepest lapse rates are associated with easterly (3) and westerly (7) airflows, similar to the pattern for maximum temperatures, although absolute values are less. Southerlies (5) and northerlies (1), being parallel to the relief trend, lead to more stable conditions. Figure 8.13 shows altitudinal (**a**), latitudinal (**b**) and longitudinal (**c**) coefficients plotted against wind direction. **b** is negative ranging from **-11.11°C/1000 km** for calm conditions to **-5.13°C/1000 km** for south-westerly flows. The steep meridional temperature gradient for calm conditions reflects changes in night length. Although minimum temperatures usually occur at night, it is the changing influence of net radiation totals (which vary primarily with latitude) which contribute to this steep gradient. The latitudinal temperature gradient is also strong for winds with an easterly component and is probably associated with the cloud-free nature of such air. Progressive airflows with winds from between south and north-west tend to be cloudy, which decreases any latitudinal temperature gradient.

c is positive for north-westerly (8), northerly (1) and north-easterly (2) flows,

Figure 8.12. Variation of the Altitudinal Coefficient in the Daily Minima Regressions According to Airflow Direction

Figure 8.13. Variation of the Altitudinal, Latitudinal and Longitudinal Coefficients in the Daily Minima Regressions According to Airflow

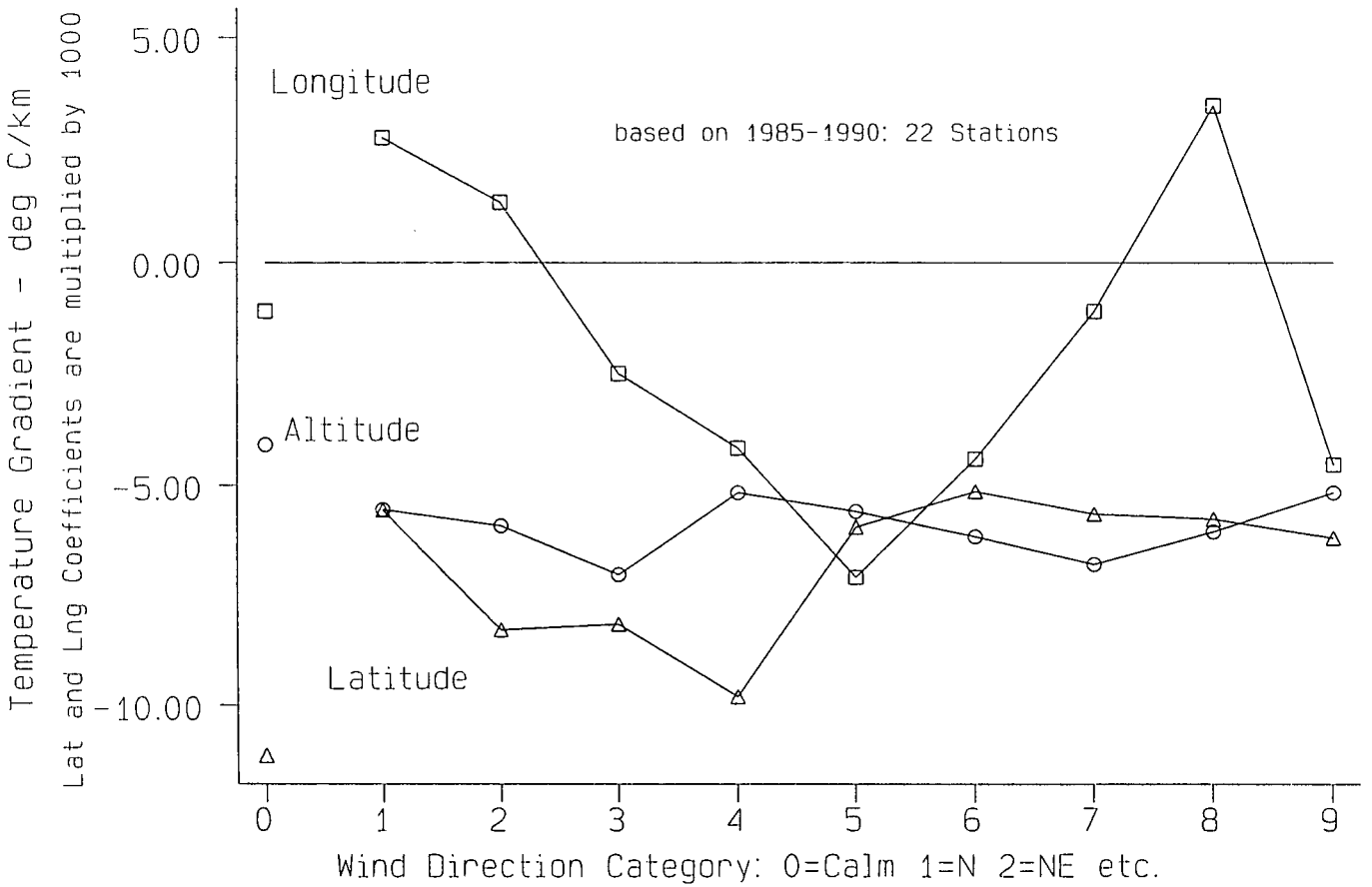

indicative of an increase in minimum temperatures with longitude for these airflows. The gradient is **3.52°C/1000 km** for north-westerly flow. For all other airflows **c** is negative, especially for southerlies (**-7.08°C/1000 km**). Longitude contributes little to the final regression. Values of R^2 range from around 0.7 to only 0.42 for calm conditions (local site variables are influential in the latter case).

8.4.3 Combined Seasonal and Airflow Effects

The analysis for all airflows in all months shows that different airflows have different seasonal trends in coefficients.

8.4.3 i) Altitudinal Coefficient

Values of **a** are given in Table 8.5. Altitudinal, latitudinal and longitudinal coefficients are listed in Appendix 6. Underlined figures are based on 21 stations.

Table 8.5 : The altitudinal coefficient, **a**, (°C km^{-1}) for each airflow in each month.

a	CALM	N	NE	E	SE
J	-3.64	-5.88	-4.63	-6.87	-5.35
F	-3.73	-6.24	-7.20	-7.95	-7.92
M	-5.16	-6.85	-4.80	-7.94	-8.73
A	-5.20	-6.22	-6.71	-7.15	-8.56
M	-3.90	-6.05	-5.38	-6.95	-4.01
J	-5.26	-6.16	-6.84	-7.49	-4.07
J	-3.57	-6.49	-4.63	-4.90	-2.33
A	-4.12	-5.32	-7.70	-5.78	-3.50
S	-4.67	-5.03	-4.44	-7.32	-4.60
O	-3.51	-4.79	-5.29	-6.22	-6.60
N	-4.36	-5.35	-6.61	-6.07	-6.01
D	-3.98	-7.01	-5.83	-7.13	-7.07

Table 8.5: continued

a	S	SW	W	NW	MEAN
J	-6.05	-6.57	-7.16	-5.53	-6.04
F	-6.43	-6.27	-6.59	-7.02	-6.27
M	-7.58	-6.80	-7.78	-6.94	-6.96
A	-5.17	-6.89	-5.86	-7.09	-6.47
M	-4.19	-6.81	-7.37	-6.46	-5.90
J	-5.61	-6.82	-6.36	-5.87	-6.20
J	-4.68	-6.47	-6.04	-6.81	-5.67
A	-5.63	-7.29	-7.07	-6.59	-6.18
S	-5.93	-5.83	-7.06	-6.23	-5.83
O	-5.90	-5.90	-5.98	-7.86	-5.51
N	-5.79	-5.85	-5.64	-3.83	-5.08
D	-6.80	-5.80	-7.04	-4.02	-5.76

a is plotted against month in Figure 8.14 , the number indicating wind direction class (as in Figures 8.6 to 8.9). The line connects the median altitudinal coefficients for each month (different from the mean coefficient shown in the table). Because altitudinal temperature gradients are always negative, steepest lapse rates appear at the bottom of Figure 8.14 and the shallowest at the top. The most noticeable feature is that calm conditions (0) have very shallow lapse rates of minima, averaging only **-4°C/km** due to frequent temperature inversions, especially between October and February.

Some wind directions are associated with unusual seasonal patterns in lapse rate. Northerlies (1) are most stable from August to November. The graph for north-easterlies (2) is very irregular as rates are based on only a few observations. Easterlies (3) have high lapse rates, especially early in the year. South-easterlies (4) show a large variation, being most unstable from February to April (**a** greater than **-8°C/ km**). **a** is only **-4°C/km** in May and **-2.33°C/km** in July, as a summer heat source develops over the uplands. From October to December south-easterlies are again associated with steep

Figure 8.14. Variation of the Altitudinal Coefficient in the Daily Minima Regressions According to Month and Airflow Direction

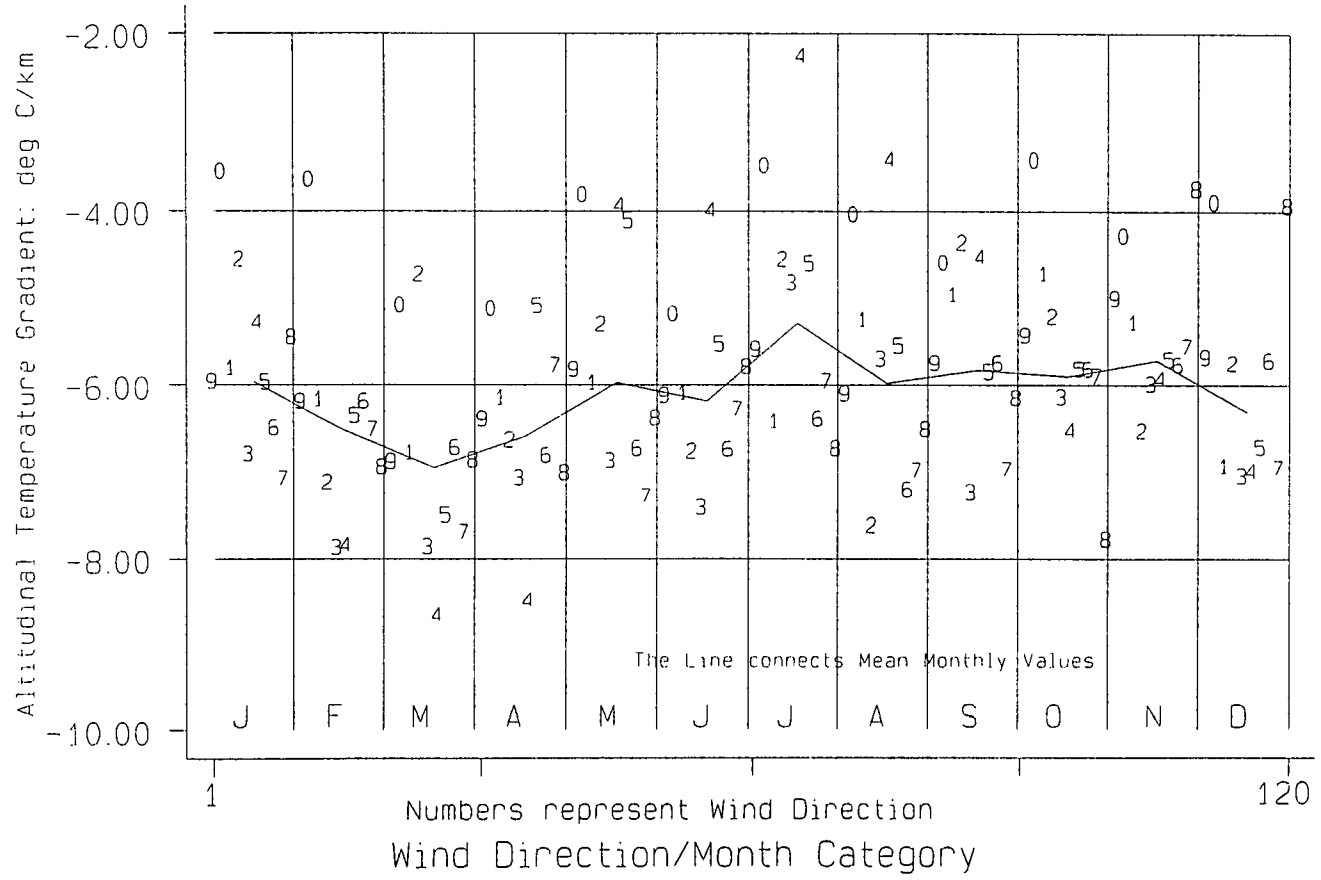

lapse rates of minimum temperature.

Southerlies (5) appear to be more stable in summer. South-westerlies (6) show little seasonal change, **a** remaining between **-6** and **-7°C/km**. Westerlies (7) also have uniformly high lapse rates. The pattern is similar to that for maxima, suggesting relatively little diurnal change in lapse rate for westerly flow. Finally, north-westerlies (8) show remarkably high stability in winter, the reason for which is unclear. Overall, north-westerly flows favour shallow lapse rates in winter, south-easterlies in summer and calm conditions all year.

8.4.3 ii) Latitudinal Coefficient

The latitudinal effect, **b**, is shown in Figure 8.15. As for maxima, summer gradients are consistently stronger (more negative) than winter ones. The pattern between wind directions is more subtle for minimum temperatures because of local effects. **b** is invariably strong for calm conditions with temperatures at night related to parameters such as daylength. **b** reaches **-20°C/1000 km** in March and September. In winter the shallowest meridional gradients in minimum temperature are associated with blocked anticyclonic conditions (airflow between north and south-east). The main trends in **b** are listed in Table 8.6:

Table 8.6: The seasonal cycle in the latitudinal coefficient for different airflows

Airflow Type	Seasonal Cycle of Latitudinal Coefficient
North	negligible in winter, negative in summer
East	negligible in winter, strongly negative in summer
South	steeper gradient in summer
West	moderate gradient throughout the year

Overall, **b** shows double peaks in May and September, but values remain strongly negative throughout the summer.

Figure 8.15. Variation of the Latitudinal Coefficient in the Daily Minima Regressions According to Month and Airflow Direction

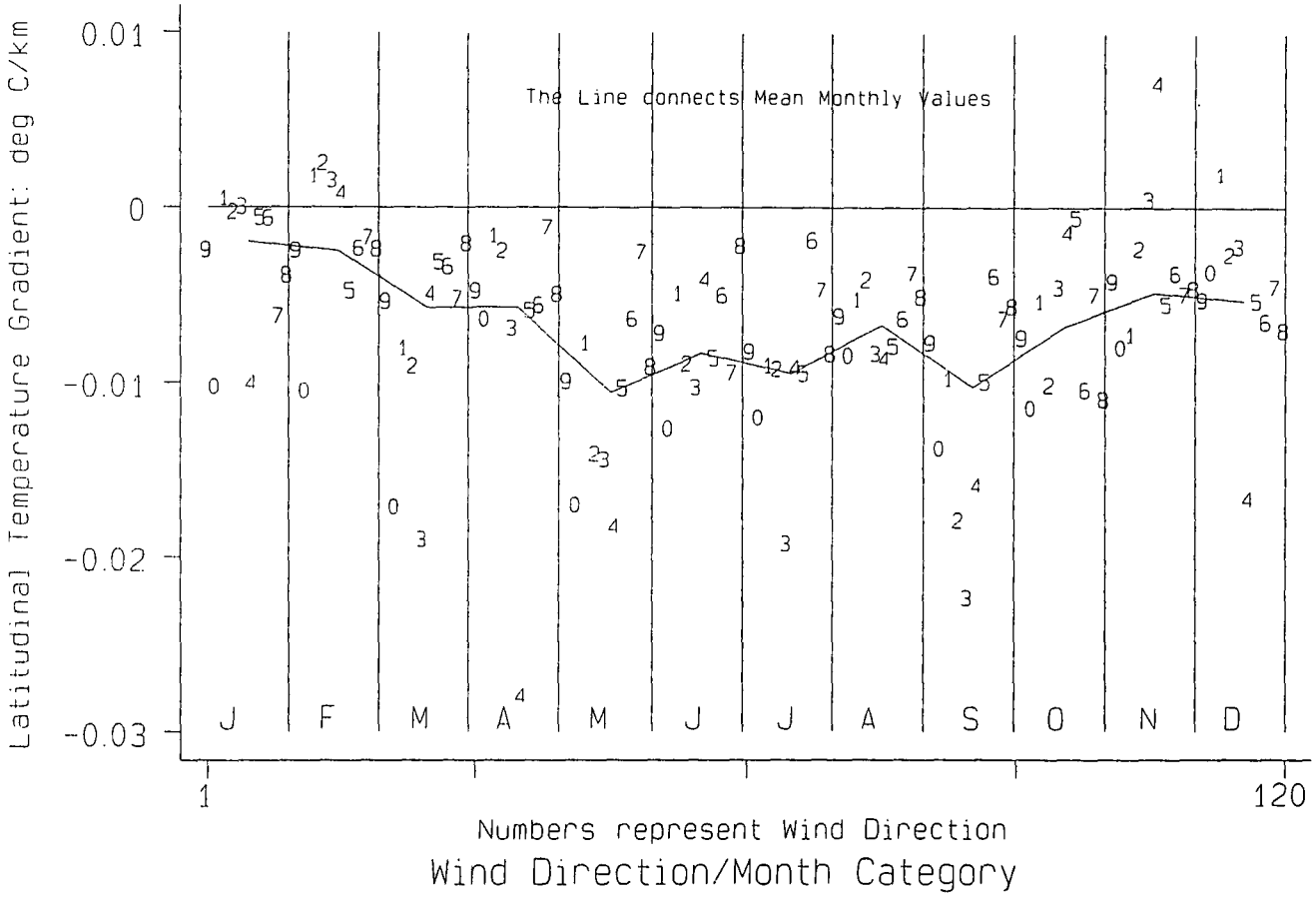

8.4.3 iii) Longitudinal Coefficient

The longitudinal effect (**c**) is plotted in Figure 8.16. Values are negative apart from in autumn when the North Sea is relatively warm. Northerlies (1) and north-westerlies (8) favour higher minima to the east of the Pennines, especially in autumn. Values of **c** for north-easterlies (2) are also usually positive, even between January and March. However, in April and May **c** turns negative. Southerly airflows encourage **c** to be negative all year whereas south-westerlies (6) and westerlies (7) produce a decrease in minima to the east in winter but not in summer. Westerly flows are likely to be cloud-free in the east, leading to lower minima in the lee of the Pennines in winter. Calm conditions produce unremarkable values of **c**.

The effects of altitude, latitude and longitude are weaker than in the maximum temperature regressions because of local temperature variation due to factors such as aspect and exposure. Wide variations in minima can occur within a small area (Waco 1968). It is important whether a site is in a frost pocket or north-facing, for example.

8.4.3 iv) The Success of the Regressions

Figure 8.17 shows R^2 for all regressions. A low R^2 means that local influences are important. The range in R^2 is much greater than for maximum temperatures and it falls below 0.1 in a few cases. Values between 0.7 and 0.9 (indicating reasonable success) are common, especially between February and June. There is a sharp drop in R^2 values during September, followed by a slow recovery. Local influences on minima are most noticeable in autumn (Manley 1952), solar elevation being relatively low and the air calm. All R^2 are below 0.7 in September; the highest is for westerlies (0.701). Mean autumn values are around 0.5!

R^2 for calm conditions are universally poor, nine months recording values below 0.5. Easterly and south-easterly flows show low R^2 in summer, values for south-easterlies falling below 0.1 in July and August. In this case there seems to be absolutely no relationship between the three macroscale site variables and minimum temperature.

Figure 8.16. Variation of the Longitudinal Coefficient in the Daily Minima Regressions According to Month and Airflow Direction

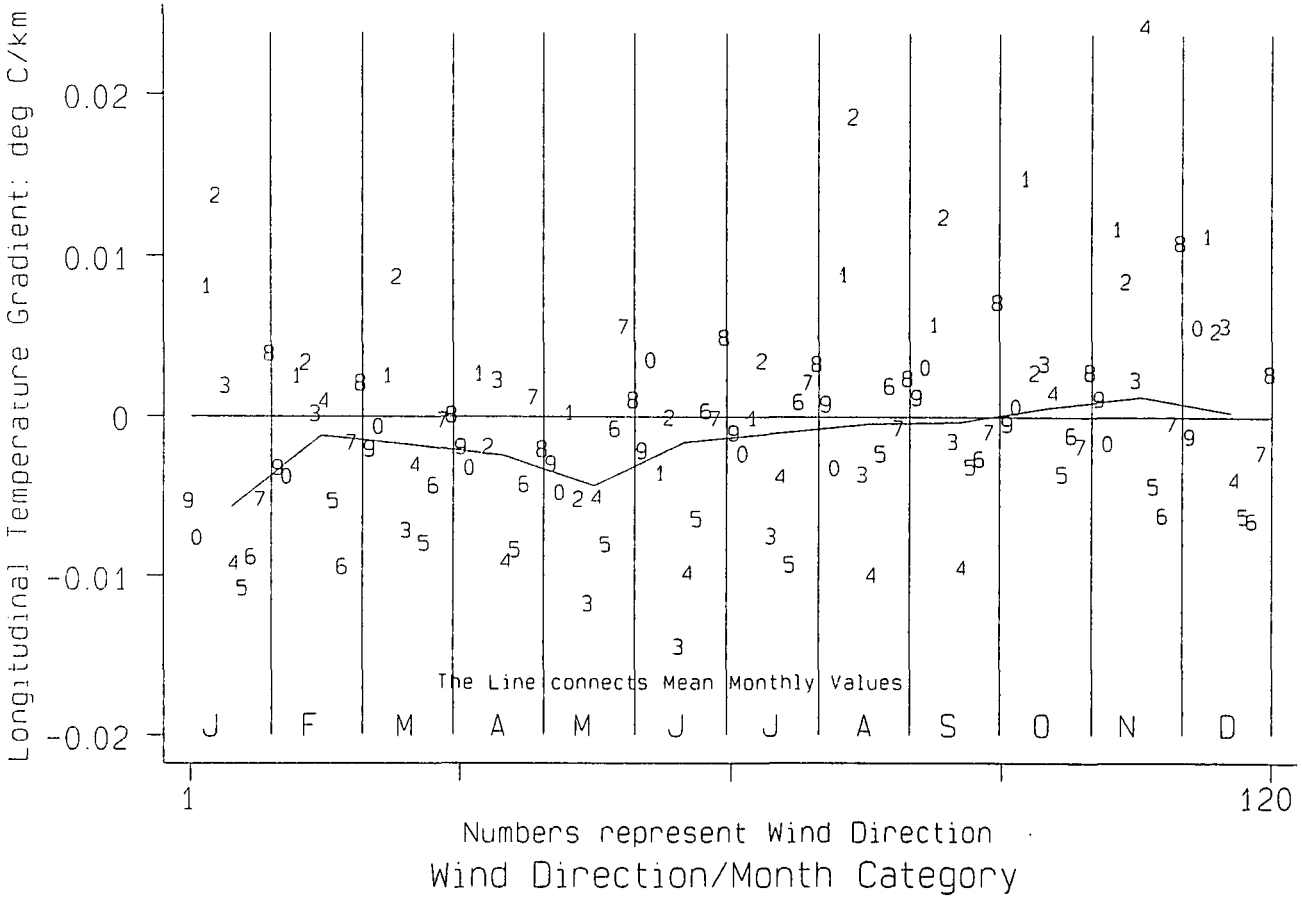

Figure 8.17. R2 in the Daily Minima Regressions
According to Month and Airflow Direction

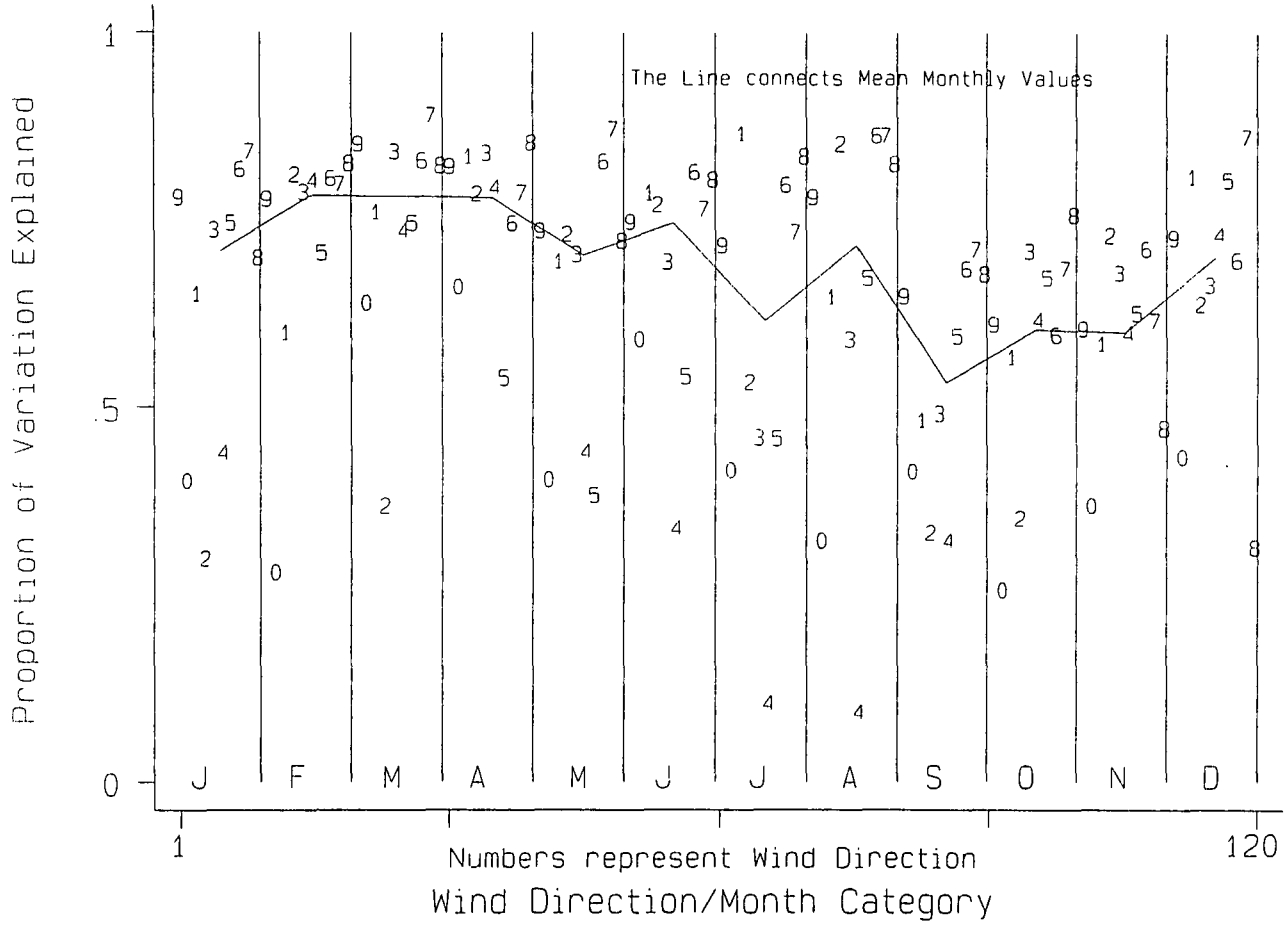

Westerlies and south-westerlies show the most consistent R^2 values, although even these drop in September.

The root-mean-square error (Figure 8.18) in a regression takes into account the sample size of the regression and the amount of temperature variability. Errors peak in September and there is a gradual decrease throughout the autumn. Worst errors are connected with calm conditions, southerly and easterly flows in summer, and with south-easterlies at any season.

8.5 The Development of Circulation Indices and Their Relationship with Regression Coefficients

Coefficients derived from an analysis of temperatures recorded during a historical month, can be related to the airflow patterns experienced during that month through use of circulation indices which were derived for each month between January 1985 and December 1990 (Figure 8.19). Murray & Lewis (1966) assessed daily weather patterns through calculation of indices representative of progressiveness, southerliness, meridionality and cyclonicity in the circulation pattern and used these to relate circulatory characteristics to weather parameters, i.e. winter temperatures with progressiveness. Indices, similar to those of Murray and Lewis, were created for the Durham wind data.

To measure southerliness, wind directions were assigned scores as follows:

Wind direction	**S**	**SW/SE**	**W/E**	**NW/NE**	**N**
Value	**+2**	**+1**	**0**	**-1**	**-2**

Scores were summed over the month concerned and divided by the number of days in that month. A completely southerly month would record an S index of +2 and a completely zonal one (i.e. constant westerly flow), an index of zero.

Similarly to measure westerliness, wind directions were assigned scores as

Figure 8.18. The Root Mean Squared Error in the Daily Minima Regressions According to Month and Airflow Direction

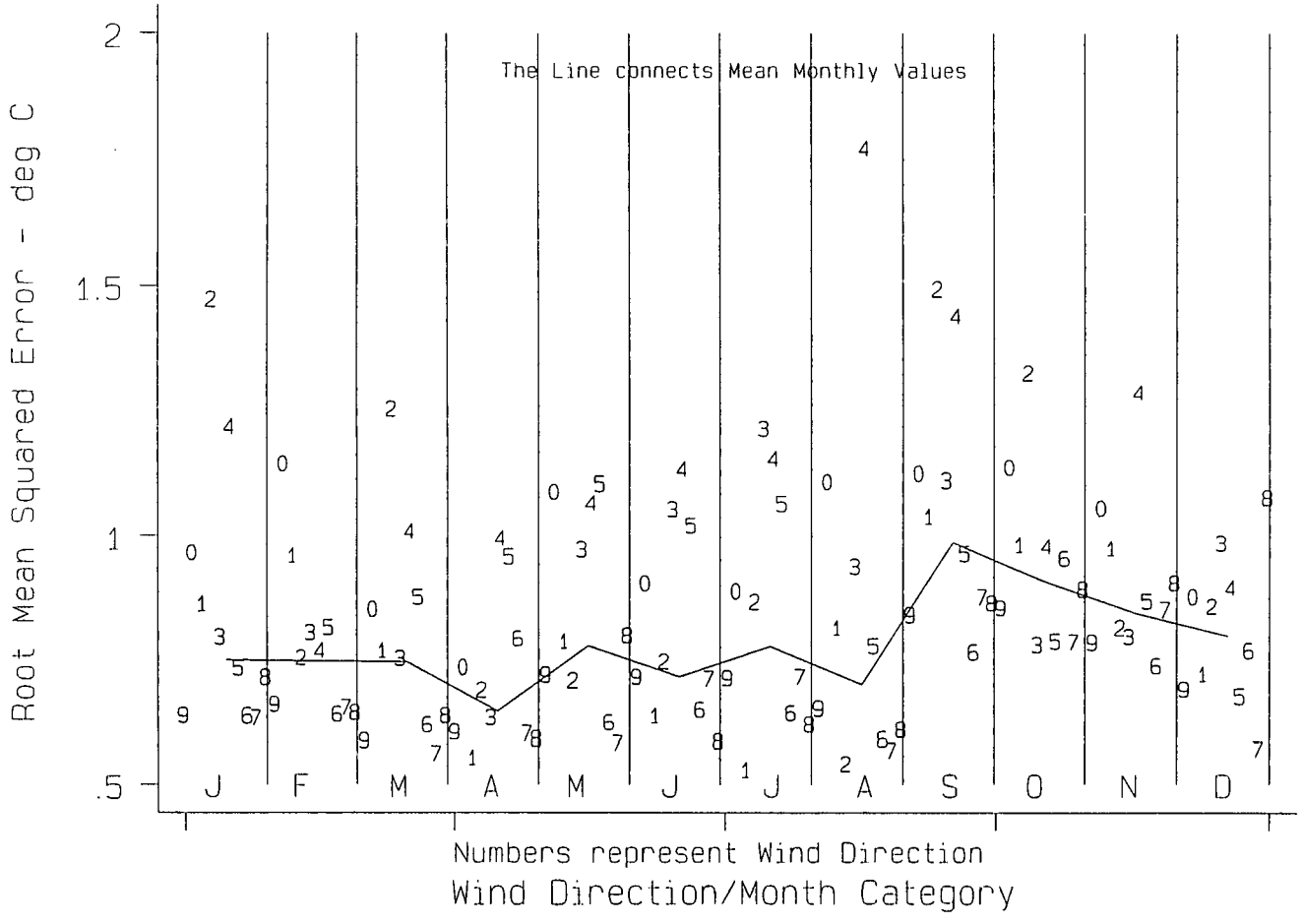

Figure 8.19. Time Series of Three Circulation Indices of Southerliness, Westerliness and Meridionality, 1985-1990

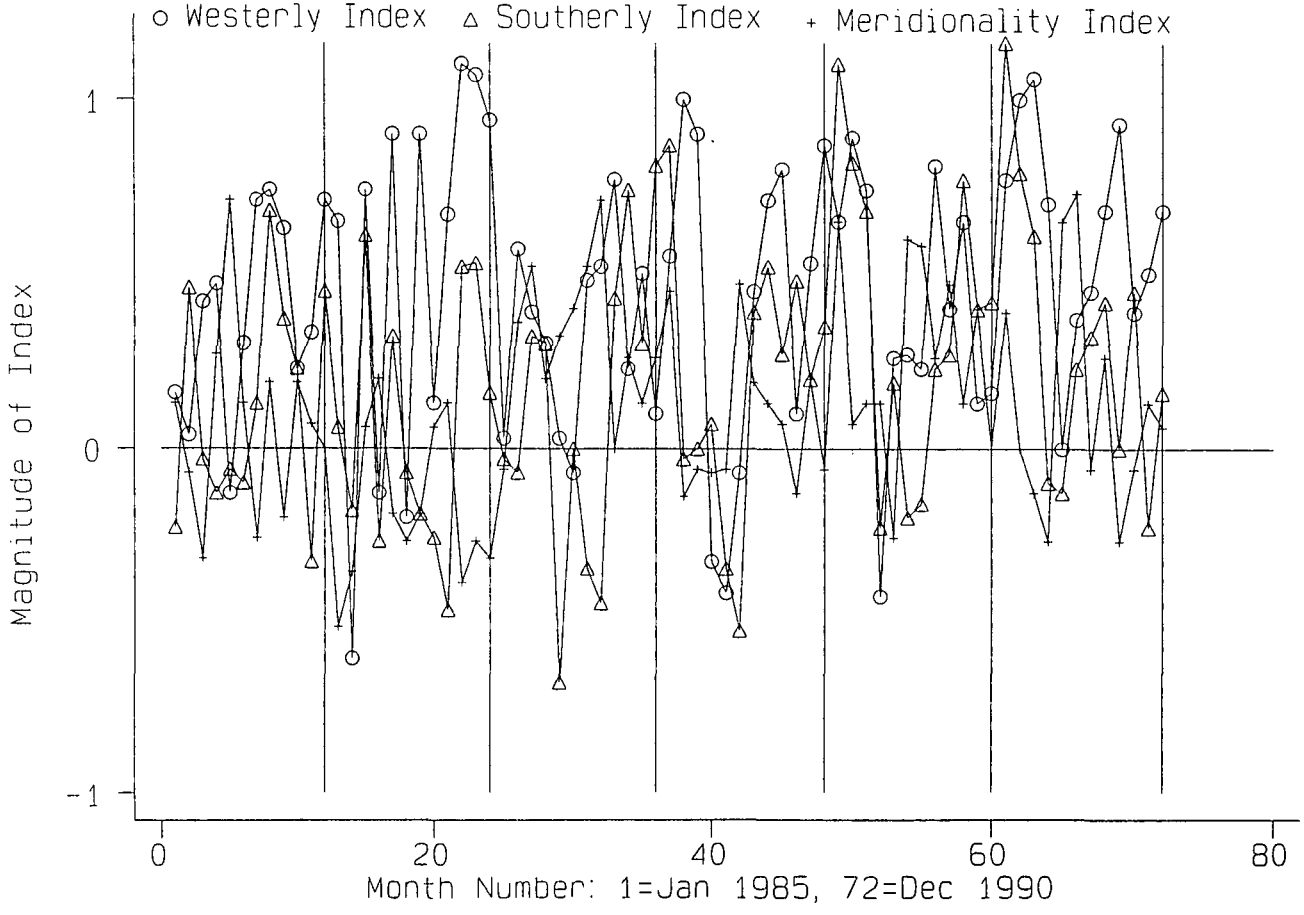

follows:

Wind direction	W	NW/SW	N/S	NE/SE	E
Value	+2	+1	0	-1	-2

Finally, to measure meridionality, categories were assigned as follows:

Wind direction	N/S	NE/SE/SW/NW	W/E
Value	+2	0	-2

Calculated indices in Figure 8.19 vary between -2 and +2. Long-term trends are hard to identify. Values greater than 1 are occasionally recorded but those below -1 are not, illustrating the predominance of southerly and westerly winds.

The variation of the three indices by month is shown in Figure 8.20. Westerliness (Figure 8.20 a) peaks in winter and late summer (August/September) with a distinct trough between April and June. The building of the Scandinavian anticyclone to the north and east of Britain in spring means that eastward progress of Atlantic air is often temporarily checked. Another period with a tendency towards blocking is October. There are extreme variations in the westerly index in any month. In February 1986 the index fell below -0.5, a month uncharacteristically dominated by easterly airflows. In May 1986 the movement of depressions from west to east continued and the westerly index was unusually high.

The southerly index is shown in Figure 8.20 b. From April until July there is a tendency for more northerly outbreaks. In contrast, values are positive from August to March (but with no pronounced peak in any individual month). Some very high southerly indices are recorded during January (>1).

Meridionality (Figure 8.20 c) shows an erratic variation, peaking in summer (especially during June). A lack of meridionality is seen for February when major airflows are zonal. There is a large inter-annual variation in meridionality.

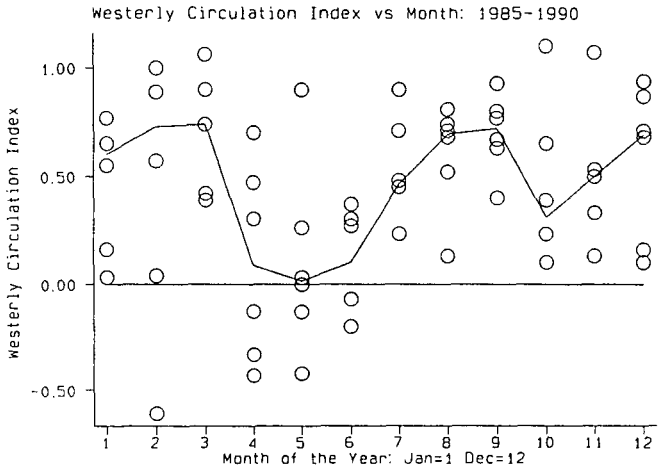

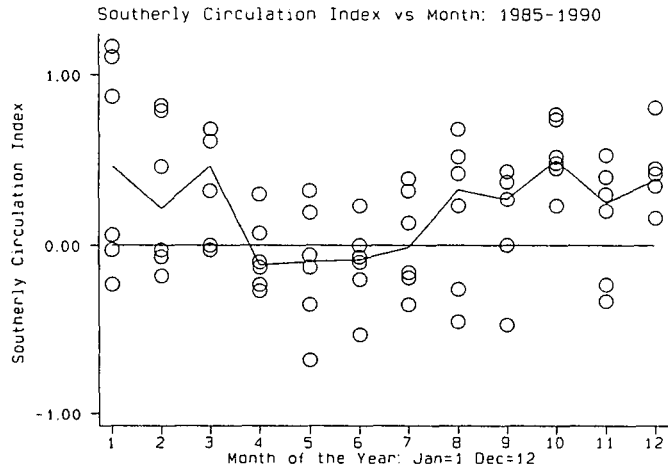

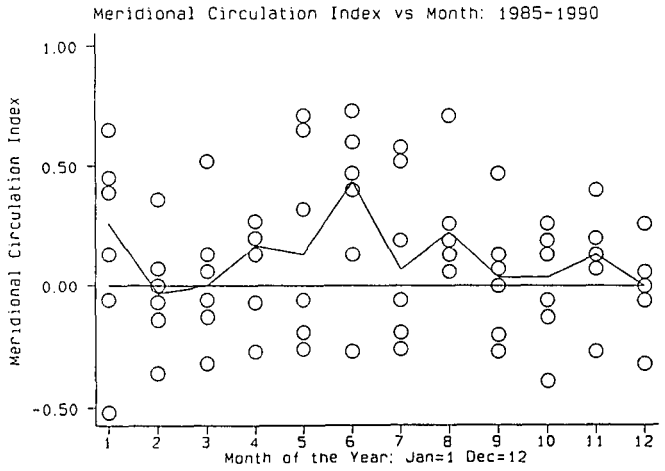

Figure 8.20. Monthly Variation in Circulation Indices, 1985-1990

8.5.1 Correlations between Circulation Indices and Regression Coefficients

The three circulation indices can be correlated with regression coefficients in the regressions of mean temperature against altitude, latitude and longitude. The mean temperature regression was obtained by taking the average of the maximum and minimum temperature regressions, described in sections 8.3 and 8.4 respectively. These correlations are useful since they describe relationships between the spatial distribution of mean temperature and the circulation pattern. On an annual timescale seven out of fifteen correlations are significant at the 10% level. At the 1% level there is a positive correlation between the latitudinal coefficient and southerliness (0.393). In strong southerly flow the meridional temperature gradient becomes indistinct (less negative). The strongest correlation is positive, between the longitudinal coefficient and westerliness (0.556), i.e. under progressive conditions the east is warmer than the west. Finally, a positive correlation (0.427) between the southerly and westerly indices is significant (at 1%). This is not surprising since prevailing winds are south-westerly. The altitudinal coefficient is negatively correlated with westerliness at the 10% level. Mean lapse rates would therefore increase under a progressive scenario. Other significant correlations on an annual basis include those between the westerly index and latitudinal coefficient, the southerly index and longitudinal coefficient, and the westerly and meridional indices (negative).

In certain months different relationships become important. For example, the strongest January correlation is the negative one between the altitudinal coefficient and westerliness (-0.862). As there are only 6 years in the sample, a correlation in an individual month has to be above the thresholds in Table 8.7 to be significant. Those significant at 1% include those between the longitudinal coefficient and westerliness in May (0.957) and between the meridional and westerly indices in November (-0.918). The former correlation indicates that a more progressive circulation dominated by westerly flow would increase the longitudinal coefficient and thus benefit temperatures in the east of the region. This relationship is also significant in January, February, April and between May and August. In autumn the relationship is weaker, presumably because the warmer North Sea eradicates the need for heat advection from the west.

Table 8.7: Threshold values of **r** required for significance.

Significance Level	**Critical r (n=70)**	**Critical r (n=6)**
10 %	0.1982	0.7293
5 %	0.2352	0.8114
1 %	0.3059	0.9172

A few correlations are unstable, switching sign between different months, suggesting that a larger sample is desirable. Relationships between airflow indices and spatial temperature distribution according to latitude are important in winter. Both meridional and southerly circulations increase the latitudinal coefficient (weaken the north-south temperature gradient) in December and January, whereas increased westerliness does the opposite in December. The effects of increased meridionality are unclear.

In summary, increased progressiveness increases mean lapse rates, especially in winter, while an increased southerly bias, as suspected to be occurring in recent years by Murray (1993), decreases the north-south temperature gradient (see Figure 8.21 a). Increased progressiveness would favour the east of the country. Any warming would be amplified by lee effects of the Pennines. The correlation between the westerly index and longitudinal coefficient for all months between 1985 and 1990 is shown in Figure 8.21 b. Numbers represent month. The correlation turns negative in December (12) and January (1), presumably because of a cooling effect of the land in mid-winter.

The latitudinal temperature gradient is expected to weaken on an annual scale, under a more progressive circulation. This is a negative feedback process since the decreased north/south temperature gradient, initiated by increased zonality, is equal to a weakening in the latitudinal temperature contrast which drives the zonal circulation. Overall effects of increased meridionality (i.e. blocking) on temperature gradients are unclear, specific effects depending on the season. The effects of changes in airflow direction will be investigated in more detail using **uni-directional airflow scenarios** in

Figure 8.21. Correlation between Circulation Indices and Regression Coefficients

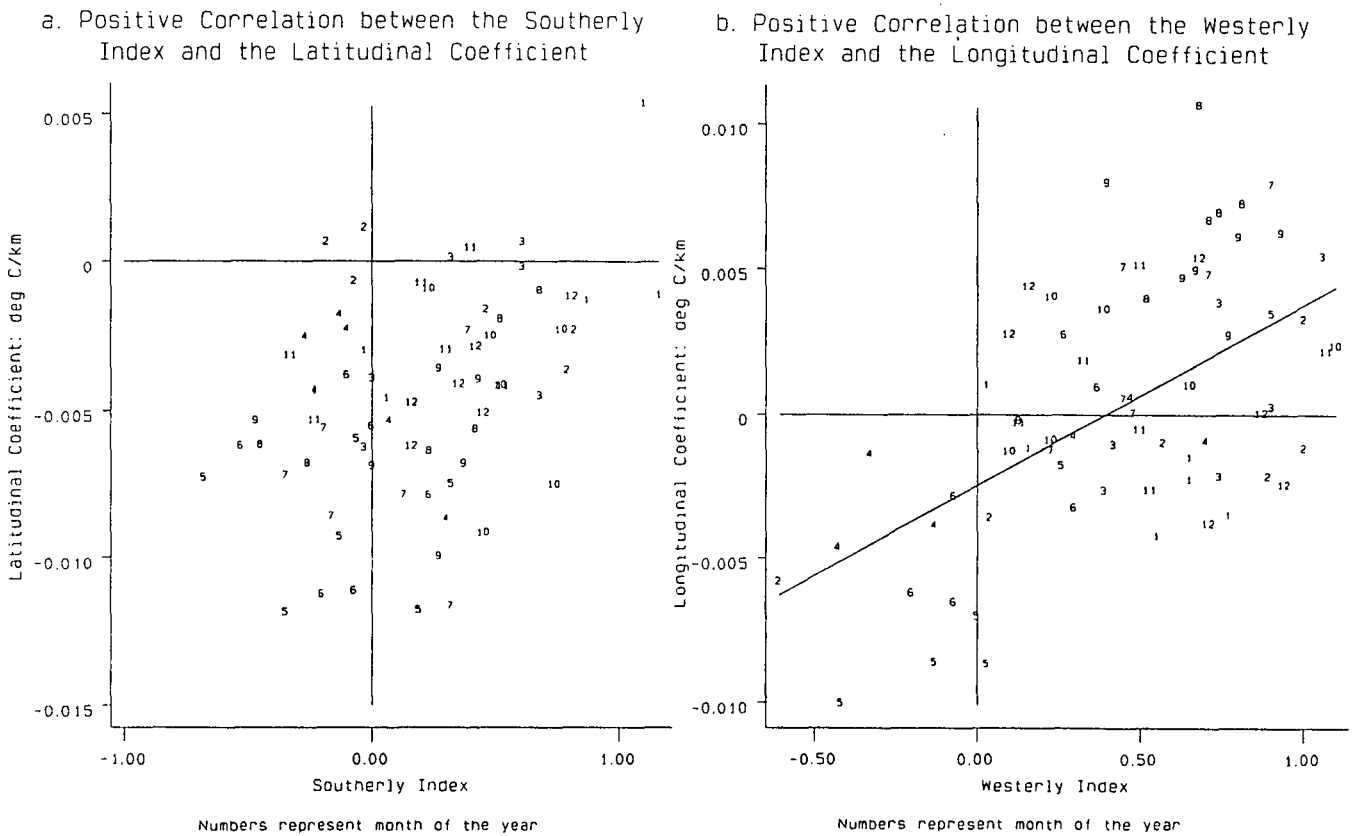

8.5.2 Correlations between Circulation Indices and Mean Temperatures

Mean temperatures recorded at any location can be related to progressiveness, southerliness and meridionality (Kozuchowski & Marciniak 1988, Jones et al. 1993). By examining the spatial variation of such relationships one analyses the sensitivity of temperature to changes in the general circulation.

Mean monthly temperatures at each location are correlated with westerliness in each month using historical data. Most locations show strong positive correlations between mean daily temperature and westerliness in January and February when the contrast between mild Atlantic air and cold continental air is great. By April only stations in the east of the region show this relationship. In Sunderland it remains until May, due to the coastal cooling effect. Some Cumbrian stations record a negative relationship between mean daily temperature and westerliness in July, westerly Atlantic air often leading to cool weather.

Mean monthly temperatures are correlated with wind indices at four locations in Table 8.8.

Most significant correlations with westerliness occur from January to March while southerliness is important in April and September. Meridionality is of no use when attempting to devise an index related to mean monthly temperatures. The relationships listed in Table 8.8 show that a decrease in westerly flow could lead to colder winters at all sites, while changes in southerly flow would be most critical in spring and autumn. As there are numerous possible correlations, one would expect a few to be significant even if there were no relationships at all between circulation indices and temperature. Thus it is sensible to concentrate on the relationships significant at 1%, i.e. southerliness in January, April and September, and westerliness in February.

Table 8.8: Strong correlations between mean monthly temperatures and circulation indices.

Month	Place	Index	r	Signfce Level
January	Durham	W	0.787	10 %
January	Durham	S	0.954	1 %
January	Ambleside	W	0.824	5 %
January	Ambleside	S	0.966	1 %
January	Gt Dun Fell	S	0.920	1 %
January	Eskmeals	W	0.841	5 %
January	Eskmeals	S	0.972	1 %
February	Durham	W	0.956	1 %
February	Ambleside	W	0.958	1 %
February	Gt Dun Fell	W	0.898	5 %
February	Eskmeals	W	0.892	5 %
March	Durham	W	0.795	10 %
March	Ambleside	W	0.840	5 %
March	Gt Dun Fell	W	0.910	5 %
March	Eskmeals	W	0.797	10 %
April	Durham	S	0.900	5 %
April	Ambleside	S	0.938	1 %
April	Gt Dun Fell	S	0.778	10 %
April	Eskmeals	S	0.842	5 %
June	Gt Dun Fell	S	0.739	10 %
September	Durham	S	0.809	10 %
September	Ambleside	S	0.926	1 %
September	Eskmeals	S	0.857	5 %

8.6 Robustness of the Regressions

Generally, the effects of removal of individual data points are insignificant, meaning that most equations are fairly robust.

As an example the regression for maximum temperatures under westerly flow in July will be used:

$$X=(-0.00841alt)-(0.00353lat)$$
$$+(0.01906lng)+18.111....r^2=0.870 \quad ----(2)$$

The influence of an individual point on regression coefficients can be analysed in many ways (Belsley, Kuh & Welsch 1980). The simplest measures are **dfbetas**. These can be produced for each point in the data set and for each coefficient (in this case altitude, latitude and longitude). The dfbeta coefficient expresses how the coefficient concerned varies when the data point concerned is removed, i.e. they measure the differences between the regression coefficients when each observation is included and excluded, the difference being scaled by the estimated standard error of the coefficient.

In Table 8.9, which shows dfbetas for the above example, the first three columns list dfbetas for altitude, latitude and longitude. Belsley, Kuh & Welsch (1980) suggest that a critical threshold value for dfbetas deserving special attention is:

$$abs(dfbeta)=2/\sqrt{(n)} \quad ----(3)$$

where **n** is the number of data points.

In this case the threshold is 0.43 since **n**=22. Bollen & Jackman (1990) suggest a threshold of 1, meaning that inclusion of the data point has shifted the coefficient by

at least one standard error. Using the more conservative threshold, notable dfbetas are underlined. Overall there are few points with great influence (all dfbetas are below 1).

Table 8.9: Measures of influence of individual stations in the regression of daily maxima for westerly flow in July.

Place	DFalt	DFlat	DFlng	leverage	Cook's dist
Ambleside	-0.13	-0.22	-0.27	0.13	0.05
Appleby	-0.01	-0.05	-0.04	0.05	0.01
Aspatria	0.01	-0.01	0.04	0.18	0.00
Carlisle	0.14	-0.17	0.17	0.17	0.02
Carlton-in Cleveland	-0.00	-0.02	0.03	0.21	0.00
Carlton-in Coverdale	0.12	-0.30	0.14	0.18	0.04
Durham	-0.03	0.03	0.12	0.11	0.01
Eskmeals	0.35	0.42	0.62	0.27	0.19
Gt Dun Fl	0.07	-0.00	-0.00	0.66	0.00
Hartburn	0.05	0.03	-0.10	0.16	0.01
Haydon Br	-0.11	0.25	0.00	0.11	0.03
Hgh Close	-0.00	0.38	0.52	0.13	0.14
Keswick	-0.31	-0.05	-0.93	0.13	0.25
Kielder	0.03	0.46	-0.11	0.25	0.07
Leeming	0.00	0.01	-0.01	0.22	0.00
Lw Ether	0.00	-0.01	0.08	0.08	0.00
Newcastle	0.13	-0.21	-0.19	0.17	0.03
Redesdale	-0.08	-0.54	0.00	0.25	0.09
Sunderland	0.06	-0.09	-0.14	0.17	0.01
Warcop	-0.08	0.07	0.02	0.06	0.01
Whasdyke	0.00	0.04	0.03	0.13	0.00
Widdybank	-0.14	0.01	-0.01	0.20	0.01

Observations at Kielder Castle and Redesdale strongly affect the latitudinal coefficient. Kielder increases it (dfbeta is positive), whereas Redesdale decreases it. The longitudinal coefficient is most strongly affected by Keswick. The anomalous warmth of Keswick (in the west of the study area) decreases the coefficient. Eskmeals has the opposite effect. There are no individual observations which notably affect the altitudinal coefficient, showing that the equation is robust.

Robustness is also analysed through indices such as leverage and Cook's Distance. **Leverage** (column 4) describes the influence of one particular point in contributing to the regression equation. If a point is an outlier, lying far away from the rest of the data, it has high leverage. In Figure 8.22 mean July maxima under westerly flow are plotted against altitude. Great Dun Fell (point 9) has high leverage because it is an outlier, explaining the value of 0.66 in Table 8.9. The addition of Great Dun Fell does not in this case significantly alter the regression coefficients (despite having high leverage). **Cook's distance** (Cook 1977) estimates the overall influence of each point on results. The distance depends on the size of the residual and leverage.

An accepted cutoff for notable values of Cook's distance is:

$$c=4/n \quad \text{----(4)}$$

In this case the threshold is 0.182. Thus Eskmeals and Keswick have a significant effect. Great Dun Fell has a low Cook's distance, despite high leverage, while the leverage for Keswick is low. The same regression is shown below, omitting Keswick and Eskmeals:

$$X=(-0.00840alt)-(0.00465lat) +(0.02012lng)+18.126....r^2=0.921 \quad \text{----(5)}$$

The altitudinal coefficient has barely changed and the biggest change is in the

Figure 8.22. July Mean Daily Maxima Under the Influence of Westerly Flow versus Altitude

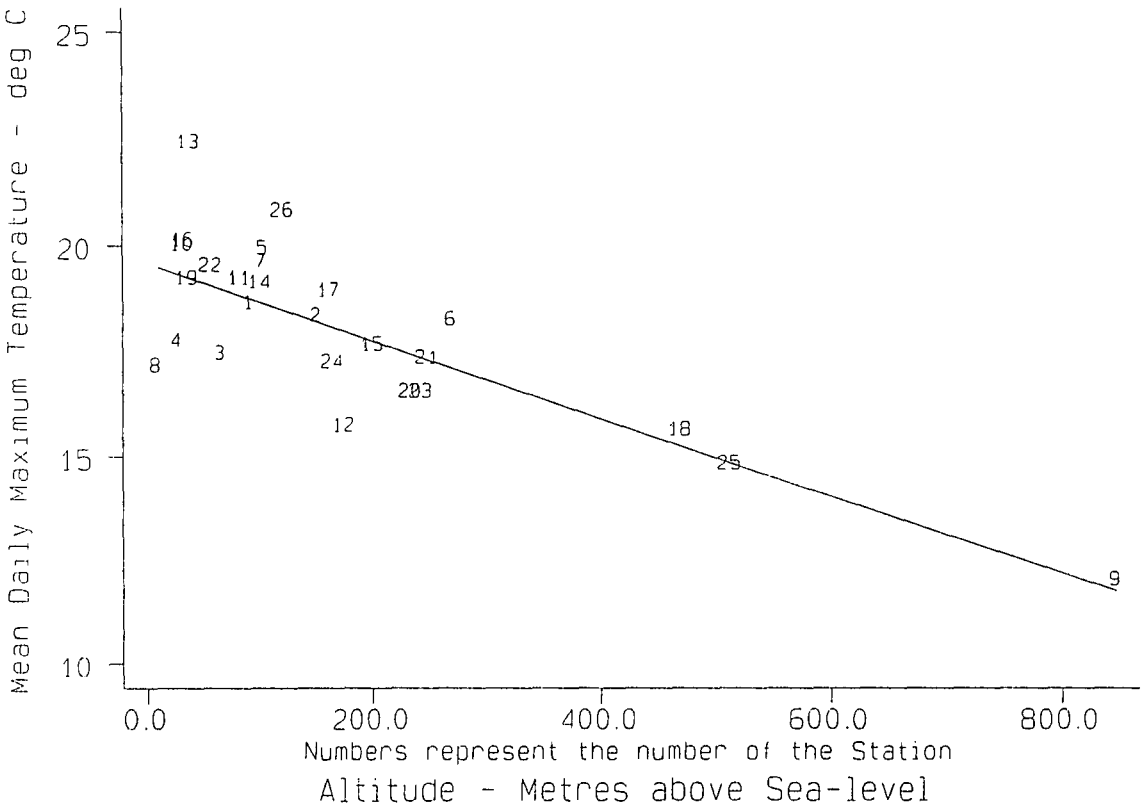

latitudinal coefficient. Temperatures predicted for this new regression differ by less than a tenth of a degree and so the original regression was fairly robust.

The same is true for the majority of the other regressions, showing that the data are remarkably well-behaved. Occasionally, significant changes in the latitudinal and longitudinal coefficients occur when certain points are removed. This occurs because altitude accounts for the "lion's share" of the temperature variation, with latitude and longitude "scrabbling about" for the remaining variation.

Robustness measures are shown below for the north-easterly regression of maximum temperatures in August. This is expected to be the least robust since it is based on data from one day only. Dfbetas exceed 1 for Redesdale (latitude) and Widdybank Fell (altitude). Because no value exists for Great Dun Fell, Widdybank Fell has a strong influence, decreasing the altitudinal coefficient (i.e. increasing the mean lapse rate). Great Dun Fell was **masking** the effect of Widdybank Fell. When the regression is recalculated without Redesdale and Widdybank Fell (Cook's distance is greater than 0.18 for these stations) the change in coefficients is small.

Table 8.10: Measures of influence of individual stations in the regression of daily maxima for north-easterly flow in August.

Place	**DFalt**	**DFlat**	**DFlng**	**leverage**	**Cook's dist**
Ambleside	-0.10	-0.19	-0.23	0.13	0.04
Appleby	0.01	-0.02	-0.02	0.06	0.00
Aspatria	0.20	-0.14	0.46	0.18	0.09
Carlisle	0.17	-0.17	0.17	0.19	0.03
Carlton-in Cleveland	-0.02	-0.08	0.15	0.21	0.01
Carlton-in Coverdale	0.04	-0.05	0.02	0.24	0.00
Durham	-0.04	0.05	0.16	0.11	0.01
Eskmeals	0.11	0.10	0.15	0.29	0.01

Table 8.10: continued

Place	DFalt	DFlat	DFlng	leverage	Cook's dist
Gt Dun Fl	.	.	.	.	.
Hartburn	-0.16	-0.08	0.25	0.18	0.03
Haydon Br	0.17	-0.36	-0.00	0.11	0.06
Hgh Close	-0.12	0.26	0.35	0.13	0.08
Keswick	-0.19	-0.04	-0.72	0.13	0.17
Kielder	0.04	0.15	-0.04	0.26	0.01
Leeming	0.09	0.14	-0.12	0.23	0.01
Lw Ether	-0.05	0.02	-0.15	0.08	0.01
Newcastle	0.10	-0.12	-0.11	0.19	0.01
Redesdale	0.44	1.08	-0.01	0.28	0.35
Sunderland	0.06	-0.07	-0.11	0.18	0.01
Warcop	-0.17	0.06	0.02	0.10	0.02
Whasdyke	0.07	-0.27	-0.22	0.13	0.05
Widdybank	-1.01	0.03	-0.03	0.58	0.28

The new regression is:

$$X=(-0.00658alt)-(0.02979lat)$$
$$-(0.02721lng)+23.386....r^2=0.803 \quad ----(6)$$

leading to a change of less than 0.1°C in predicted temperatures.

Conclusions concerning robustness are listed below:

1. Great Dun Fell, as an outlier, has great leverage, although the effect on the altitudinal coefficient is often small;

2. Eskmeals, Sunderland and Carlisle show significant effects, especially under calm conditions. These stations are influenced by coastal circulations which create locally enhanced spatial temperature gradients. The coastal influence can on occasion affect the latitudinal and longitudinal coefficients since temperatures at the coastal stations do not fit in with inland spatial temperature variation;

3. Keswick and Kielder Castle sometimes have a strong influence, especially on the longitudinal and latitudinal coefficients respectively;

4. the regressions appear fairly robust and the original equations can be used for further work in the rest of the thesis. Altitudinal coefficients are especially robust.

8.7 The Use of Regression Models to Describe Spatial Temperature Variation: An Overview

Many authors have used multiple regression to study spatial temperature distributions. Although regression is widely used, the intricacies of statistics involved are not easily understood (see section 8.5). When more controlling variables are added unusual changes can occur in the coefficients of existing controlling variables, especially if the regression is poor or if there is collinearity (significant correlation between controlling variables). In this case collinearity between altitude, latitude and longitude is not serious (Table 8.11), no correlations being significant.

Table 8.11: Collinearity matrix for altitude, latitude and longitude (22 stations).

22 Stations	Altitude	Latitude	Longitude
Altitude	-	0.020	-0.049
Latitude	0.020	-	0.048
Longitude	-0.049	0.048	-

Temperature varies relatively smoothly in space (Hopkins 1977), at least when compared with rainfall which has a very spotty distribution (Sharon 1972, 1974). A

smooth spatial pattern leads to high inter-station coefficients when the inter-station distance is small (Yamamoto 1980), whereas a more spotty distribution, such as rainfall from scattered convective clouds, shows low inter-station correlation. Multiple regression is usually more successful for describing smooth fields such as temperature. Despite this, multiple regression models of rainfall have been successful (Gregory 1965, Kutiel 1988).

Many statistical temperature models in the USA are based on regression. A fine example is the analysis of Pielke & Mehring (1977) of surface temperatures in the mountains of West Virginia, using data from 1958 to 1973. The regression of mean temperature on altitude was stronger in summer, air-mass contrasts being less marked. In winter the formation of temperature inversions weakened the relationship between temperature and altitude. A linear temperature/altitude relationship is the backbone of this type of model. Hennessy (1979) suggested fitting a polynomial function to describe a curved trend in the altitude/temperature relationship. Konovalov et al. (1991) also found the variation of temperature with altitude to be curvilinear in their numerical estimation of meteorological variables in mountainous areas in Russia. Landform type will affect the temperature/altitude relationship. Thus Hess (1969) developed separate regression equations for convex and concave landforms in the Polish Carpathians.

The temptation to use more and more complex controlling variables to increase the coefficient of determination (R^2) can lead to controlling factors with no physical meaning. This is the case for White & Smith (1982) who produced maps of climatic properties in Britain (including temperature) based on multiple regression equations.

Regressions of maxima based on spatial variables are more successful than those of minima. The latter are highly spatially variable and can be strongly affected by local topography (Harding 1978). Nearly always, lapse rates of maxima with altitude are steeper and better defined than those of minima (e.g. Lambert & Chitrakar 1989), especially when conditions are calm and conducive to temperature inversion formation (Austin 1957, Trilsbach 1988). Airflow within incised topographic canyons can become uncoupled from that at the mesoscale (Sommers 1976). This decreases the accuracy of

interpolated temperature values based on regression.

More complex statistical models attempt to take local temperature variation into account. Walts and Pochop (1977) related temperatures between known locations in an attempt to extrapolate temperature predictions to new points using second order polynomials. McCutchan (1976) simulated diurnal temperature variation through harmonic analysis. A bias condition function, specific to the location, took time of day, synoptic situation and elevation into account. In a later paper (McCutchan 1979) the diurnal cycle of temperature in mountainous terrain in California was described by Fourier analysis and found to be largely independent of site factors such as elevation, aspect and slope. The only two inputs needed to explain 93.6% of the temperature variation were the mean daily temperature and diurnal temperature range.

In simple regression models it is difficult to include effects of local influences. Examples include coastal sea-breezes (Brittain 1978), reservoirs (Gregory & Smith 1967), urban areas (Chandler 1965), incised topography (Waco 1968), sea fret (Catchpole 1966), local cloud (Caton 1957) and lee effects (Lockwood 1962). All of the above are relevant in northern England, especially coastal effects.

Attempts have been made by authors to include such local influences. Running et al. (1987) included slope and aspect effects and cold-air drainage in their spatial extrapolation of meteorological data for estimation of evapotranspiration and photosynthesis. In this case the regression model was used to simulate a background climate, which in turn was used to simulate changes in plant growth. Examples of regression baseline climates used in modelling are numerous, e.g. Urban et al. (1993).

8.8 Limitations of Regression Models in Northern England

Coastal influences complicate the spatial temperature distribution and often result in an enhanced spatial temperature gradient in the immediate coastal strip. Temperatures at coastal stations do not fit in with the spatial pattern of maxima and minima inland (section 8.5).

A related problem is that regression requires relationships between the controlling variables and the predictand to be linear. A curvilinear trend, such as an increase in temperature gradient as one approaches the coast or at high altitude, is modelled badly and will reduce R^2.

Despite these inadequacies, the multiple regressions are applied to the analysis of growing season variation with altitude in the second half of the thesis. It is important to include Great Dun Fell as it has an altitude of 847 m. It is debatable whether the altitudinal temperature decrease is linear up to and including this altitude. Great Dun Fell records higher temperatures than would be expected from a purely linear relationship and influences the altitudinal coefficient, reducing it in some cases. Regression diagnostics, however, shows that the influence is not large.

8.9 Conclusions

This chapter has described 108 regression equations which predict daily maximum and minimum temperatures at any location from altitude, latitude and longitude, for any airflow in any month. R^2 values are good, especially for maxima. Altitude is the dominant effect. All three coefficients showed systematic variation with airflow and season, although different airflows showed different seasonal cycles in coefficients. The analysis of robustness showed up the influence of coastal stations (Eskmeals, Carlisle and Sunderland) and Great Dun Fell.

Results from the regressions in this chapter will be used to define a baseline climate. This is summarised in Chapter 9 which draws from the regression model to provide a detailed description of climate in northern England, with special reference to the decrease of temperature with altitude. The resulting **altitudinal zonation** of climate in the Pennines is described and compared with that in other mountain ranges.

ALTITUDINAL ZONATION OF MEAN TEMPERATURE IN THE PENNINE UPLANDS: SOME COMPARISONS WITH OTHER MOUNTAIN RANGES

9.1 Introduction

The multiple regression models described in the last chapter describe the spatial variation of temperature in northern England under variable airflow conditions. This chapter uses results from these regressions to describe the altitudinal zonation of temperature resources in the Pennines, offering comparisons with other mountain ranges, and concludes the discussion and evaluation of the regression models.

9.2 Regressions of Mean Temperature

Mean daily temperature regressions can be predicted using the average of the maximum and minimum temperature regressions. The coefficients in the mean temperature regressions are simply the mean of the coefficients in the relevant maximum and minimum temperature regressions (Chapter 8). Setting latitude and longitude to their mean values, one can derive a temperature representative of a given altitude.

Table 9.1 and Figure 9.1 show predicted mean monthly maximum, mean and minimum temperatures for a range of altitudes. At sea-level, mean temperatures are often 6°C higher than at 800 m in the same month. The horizontal lines in Figure 9.1 represent threshold temperatures of 0°C and 6°C, the freezing point and the threshold for plant growth respectively. There is a contrast in the amount of time that temperatures are above these thresholds according to altitude (section 9.4).

Figure 9.1. Predicted Monthly Maximum, Mean and Minimum Temperatures at a Range of Altitudes (Sea-level to 800 m), using Multiple Regression Models

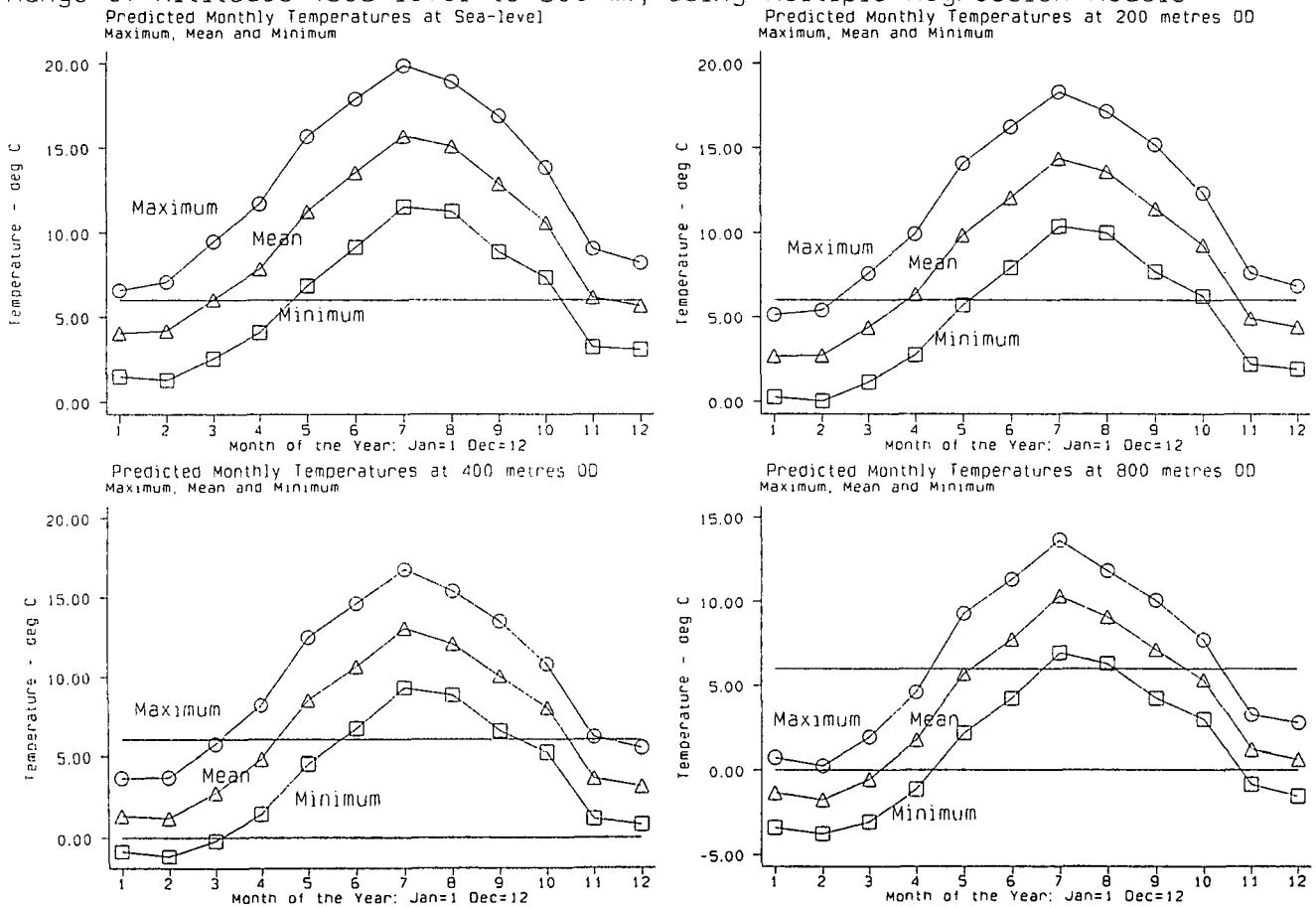

Table 9.1: Predicted mean monthly temperatures (°C) at representative altitudes. Winter = December to March inclusive.

Month	Sea-level	100 m	200 m	400 m	600 m	800 m	Great Dun Fell
Jan	4.04	3.37	2.70	1.37	0.03	-1.30	-1.60
Feb	4.19	3.45	2.71	1.23	-0.26	-1.74	-2.08
Mar	6.03	5.21	4.39	2.74	1.10	-0.55	-0.95
Apr	7.89	7.12	6.35	4.81	3.28	1.74	1.39
May	11.28	10.58	9.89	8.50	7.11	5.72	5.42
Jun	13.54	12.82	12.09	10.65	9.21	7.77	7.44
Jly	15.70	15.03	14.35	13.01	11.66	10.31	9.96
Aug	15.10	14.35	13.59	12.09	10.59	9.08	8.67
Sep	12.89	12.17	11.45	10.02	8.58	7.15	6.75
Oct	10.61	9.95	9.29	7.98	6.66	5.34	5.01
Nov	6.16	5.54	4.92	3.67	2.43	1.18	0.88
Dec	5.67	5.04	4.41	3.15	1.89	0.63	0.32
Annual	9.43	8.72	8.01	6.60	5.19	3.78	3.43
Winter	4.98	4.27	3.55	2.12	0.69	-0.74	-1.08

9.3 Variation of Lapse Rates in the Mean Temperature Regressions

The variation of the altitudinal coefficient in the maximum and minimum temperature regressions has been analysed in detail, so this section is brief.

Lapse rates of mean temperatures are steep by global standards, ranging from -8.22°C/km in March to -6.23°C/km in November (Figure 9.2). In a cool cloudy summer, in which a succession of Atlantic depressions cross northern England from west to east, lapse rates will be steep, as suggested by high values of the altitudinal coefficient under westerly flows. Manley (1952) quotes examples of such cool and cloudy summer months, including August 1946 when mean monthly temperatures were

Figure 9.2. Monthly Variation of the Altitudinal Coefficient (Representing Lapse Rate) in the Regressions of Maximum, Mean and Minimum Temperatures

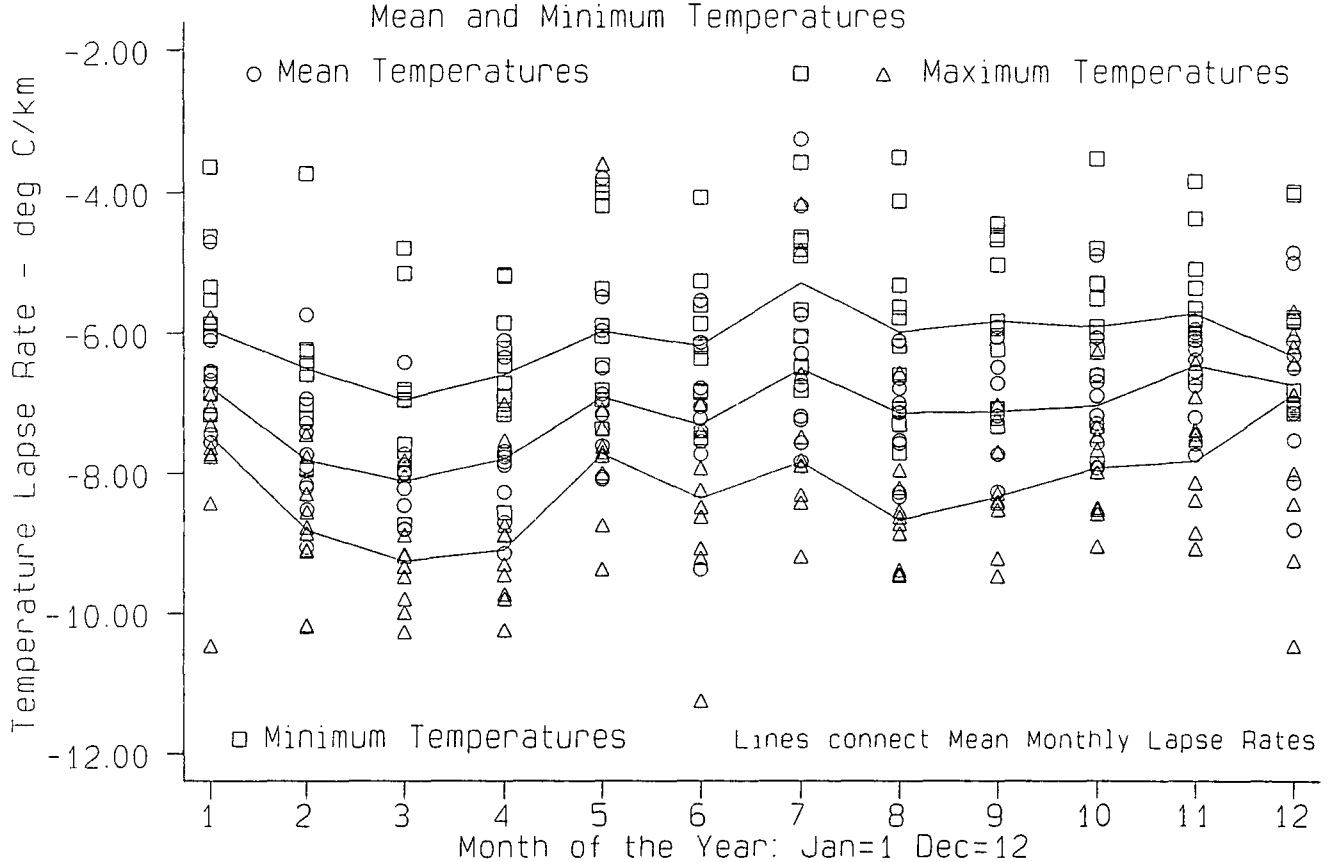

-1.6°F below normal at Penrith but -2.7°F below at Moor House (560 m). Within the data period studied here, August 1985 was such a month dominated by westerlies, with steep mean temperature lapse rates. The benefit in upland areas is proportionally greater in calm settled anticyclonic weather, especially in summer when mean temperatures at high altitude can approach those in the lowlands more closely (Tabony 1985, Flohn 1953). Given calm cloud-free conditions, upland heating is often considerable, especially on plateaux, and low mean temperature lapse rates are recorded for calm conditions. Shallow lapse rates also occur under "blocked" synoptic conditions (usually easterly or south-easterly flow). In June 1940 (an anticyclonic month), temperatures were 6.7°C warmer than average at Moor House but only 4.7°C warmer at Penrith (Manley 1952). At any season there is benefit for the uplands in times of anticyclonic weather because of temperature inversion formation. Other anticyclonic months include March 1933 and December 1935 (Manley 1942). Lapse rates of mean temperature are also different for northerly and southerly flows, the latter being more stable. The temperature contrast between the two airflows increases at high altitudes.

The circulation pattern is a critical control of upland temperatures. The major cause of low air temperatures in mountains is the advection of free air. In Colorado, the advection of cold air at the 700 mb level at Niwot Ridge (> 3000 m) prevents summer air temperatures from rising very high (Barry 1973, Le Drew 1975). Cold air advection is also experienced at Great Dun Fell, especially in windy weather, often associated with a strong zonal (westerly) circulation.

Steep lapse rates (Harding 1979a), especially in moist westerly airflows, can allow snow to fall above 400 m as late as May. Severe falls in April, during the lambing season, are common. The recent fall of several cm at 300 m on 14 May 1993 is testimony to the sometimes rapid altitudinal temperature decrease in spring. Spring temperatures are extremely variable. Because solar input is strong, calm anticyclonic conditions produce maxima over 20°C, even above 500 m (e.g. 20.7°C on 30 April 1990 at Widdybank Fell). On the other hand the steep lapse rates under some conditions cause low temperatures. Above 200 m the predicted mean temperature for March is lower than for December (Table 9.1). The number of months with mean temperature

greater than 6°C (assumed to be critical for grass growth) varies from 9 at sea-level to 4 at Great Dun Fell. This rapid decline in growth potential underlies the rapid transition to tundra-like ecosystems above 300 m (see Chapter 10).

9.4 Climatic Zonation in Northern England

The elevations of annual and monthly isotherms will be derived to define ecological zones in the Pennines. The isotherms include 0°C (the freezing limit), 6°C (the growth limit) and 10°C (the timberline limit in summer) (Hollermann 1985). The seasonal fluctuation in isotherm elevations aids definition of altitudinal zones relevant to physical processes. The classification used is similar to that of Del Barrio et al. (1990), which was undertaken for the Pyrenees. In their study 7°C was taken as the growth threshold (instead of 6°C). The three critical altitudinal limits from their study, reproduced here (Figure 9.3), are:

1. the 0°C mean winter air temperature (MWAT) (December to March inclusive);

2. the mean annual 0°C isotherm (MAAT);

3. the 10°C July isotherm (MJAT).

Above the 0°C MWAT isotherm, most winter precipitation is assumed to fall as snow and permanent winter snow cover is expected (Rijckborst 1967, Garcia-Ruiz et al. 1985). The lower limit of individual frosts is below this. The 10°C MJAT isotherm approximates to the upper forest limit or treeline (Tranquillini 1979, Hollermann 1985, Leffler 1981) as well as the lower limit of active solifluction. Above the 0°C MAAT isotherm, freeze-thaw cycles are common.

The situation in any one month will be represented by six isotherms (Figure 9.4) including the three of Del Barrio et al. (1990) and listed in Table 9.2. Many isotherms occur at elevations above the highest Pennine summits, especially in summer, and are therefore theoretical.

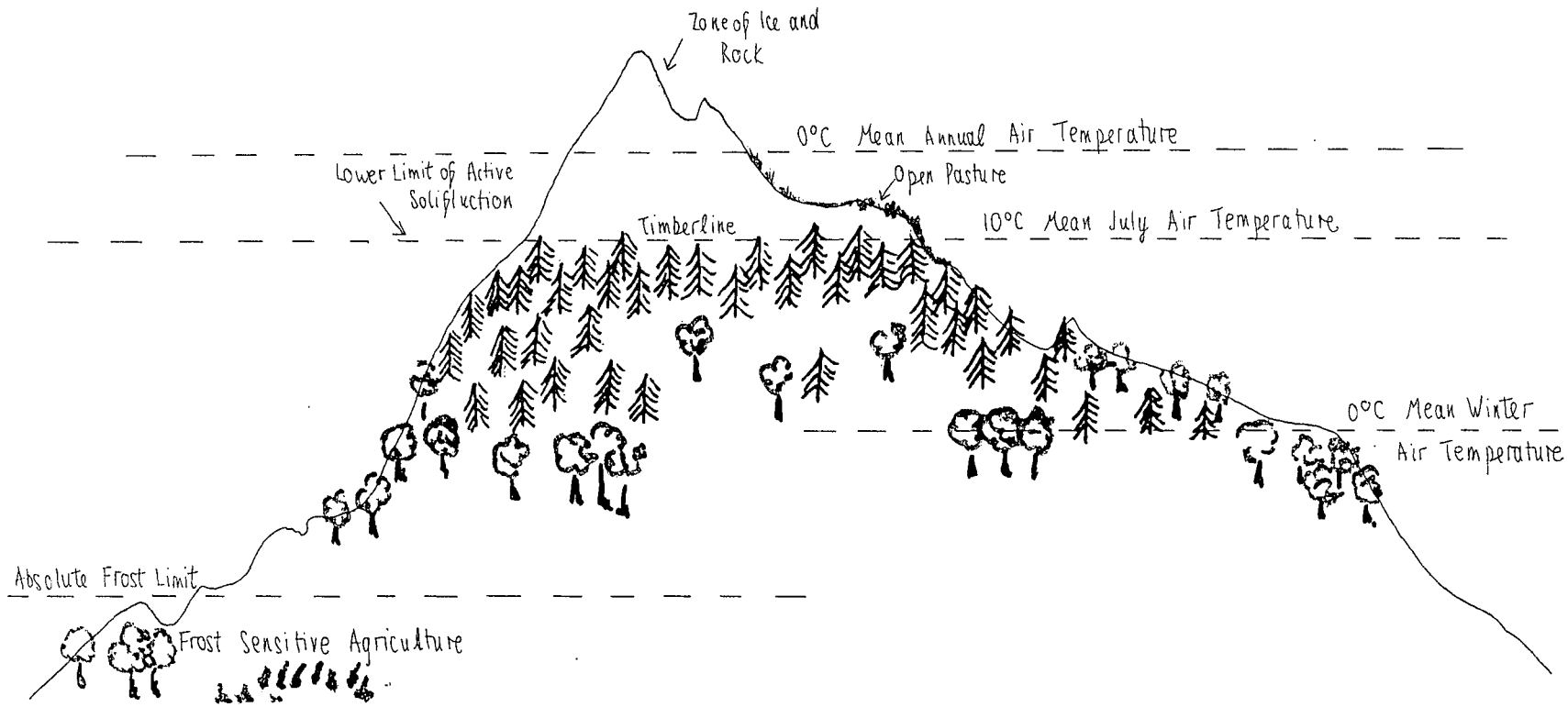

Figure 9.3. Theoretical Model of Altitudinal Zonation based on Isotherm Elevations (based on that of Del Barrio et al (1990))

Figure 9.4. Monthly Variation in the Elevations of Critical Isotherms in Northern England: Altitudinal Zonation

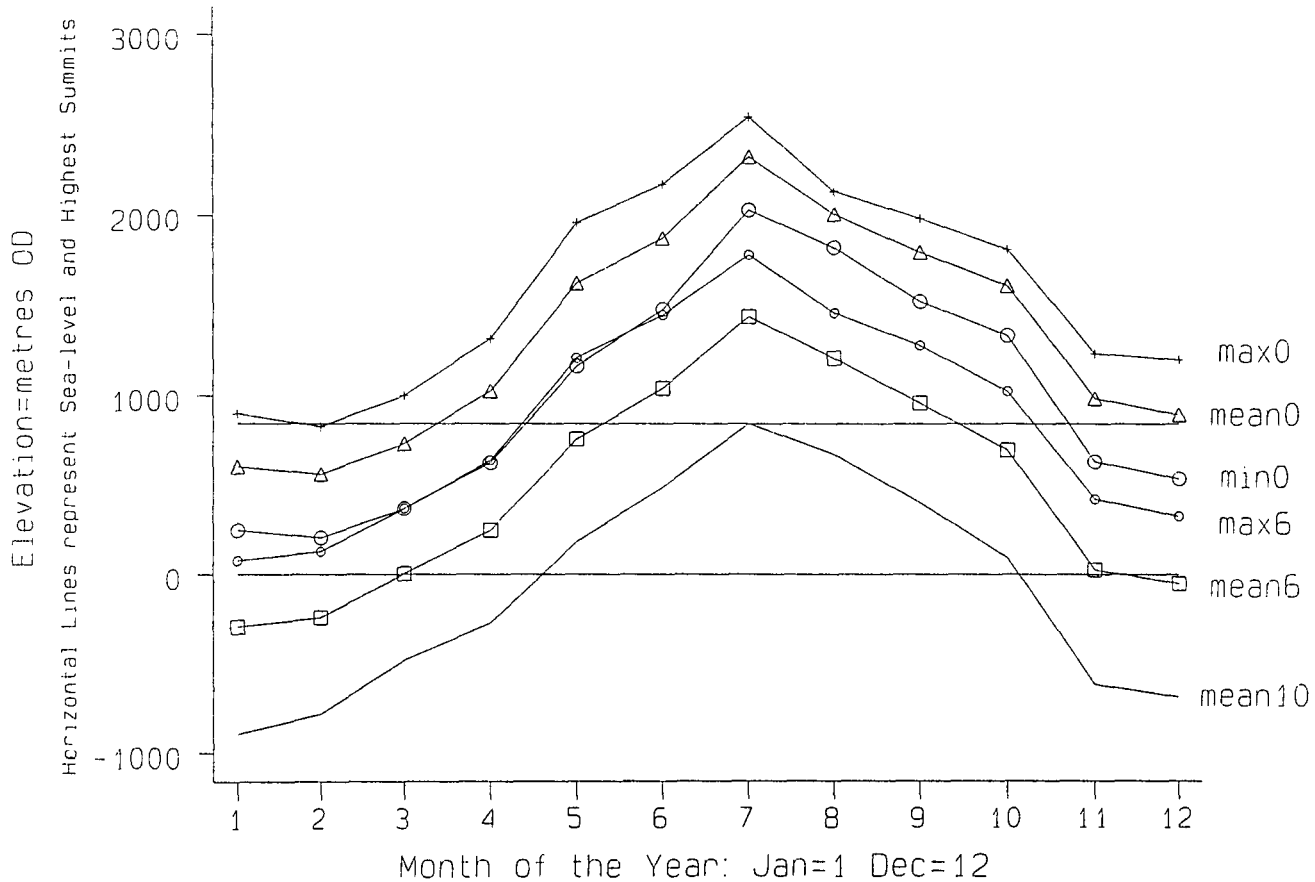

Table 9.2: Monthly elevations of critical isotherms (metres above sea-level).

Month	MMAX 0	MMEAN 0	MMIN 0	MMAX 6	MMEAN 6	MMEAN 10
Jan	900	606	248	78	-294	-894
Feb	830	565	204	129	-244	-784
Mar	1001	734	369	368	4	-483
Apr	1317	1027	629	642	246	-275
May	1960	1623	1164	1210	760	184
Jun	2175	1875	1479	1446	1044	490
Jly	2550	2329	2030	1781	1439	846
Aug	2137	2008	1822	1459	1210	678
Sep	1985	1798	1523	1280	961	403
Oct	1812	1612	1336	1027	701	93
Nov	1236	989	634	422	26	-616
Dec	1203	899	538	327	-52	-686
Annual	1595	1336	985	856	485	-81
Winter	939	696	337	221	-143	-702

Column 4 lists the 0°C isotherm of mean minimum temperature (MMIN0). Above this altitude nocturnal frost is a significant hazard. This level will be defined as the frost limit. Mean minima fall to freezing at 204 m in February. The lapse rate is -6.27°C/km. Freeze-thaw processes will be common above this level in this month, i.e. in most upland areas. MMIN0 rises to over 2000 m in July, implying that frosts would occur down to this level in mid-summer if the uplands were high enough.

Between the 0°C mean minimum and 0°C mean temperature (MMEAN0) isotherms, daytime temperatures above freezing offset the frost accumulation at night. This zone applies to much of the Pennines in winter. Precipitation is expected to be snow when mean temperatures fall below 0°C (i.e. above MMEAN0). This limit will be called the snow limit and occurs at 565 m in February (Table 9.2). The land above

this is expected to be snow-covered. The highest passes in the Pennines top 600 m, including Hartside (589 m) and Killhope (626 m), and rise above the snow limit in February. From November to April MMEAN0 lies below 1000 m (below the highest summits in the region).

The isotherm of 0°C mean maximum temperature (MMAX0) indicates the limit to the permanent ice zone (the ice limit), above which temperatures remain constantly below freezing. Freeze-thaw processes are commonest between the ice and frost limits. The ice zone extends down to 830 m in February but only 939 m for winter as a whole (December to March inclusive). The Pennines do not have a well-defined ice zone and only the highest summits such as Cross Fell are subject to severe freezes. In July the theoretical ice limit is 2329 m! Many Alpine passes and Pyrenean peaks are above this elevation but are snow-free in summer; in Britain there would be permanent ice at this level because of the maritime climate.

Annually, MMEAN0 averages 1336 m, i.e. the snow limit is equivalent to the height of many Scottish summits. Ben Nevis (1406 m) in western Scotland lies above this level. Although the snow-line depends on precipitation as well as temperature, one conservative estimate of the present-day climatological snow-line is the annual MMAX0 altitude (1595 m). Average day-time temperatures below freezing would allow little snow melt. There is much debate about the existence of permanent snow beds on sheltered parts of Ben Nevis (1406 m) and Cairngorm (1245 m). The latter summit lies just below the proposed snow-line. Manley (1952) estimated the height of the present snow-line to be 5300 ft (1615 m) in Scotland and 5900 ft (1798 m) in Cumbria. In the Pennines it may be higher because of slightly greater continentality. The 1595 m (5233 ft) estimate derived from the data is slightly lower than Manley's estimates. Between the frost and ice limits the mean maximum is above freezing and the mean minimum below. Thus freeze-thaw cycles are likely to be strong. This zone covers much of the Pennines in winter (337-939 m) and remains on high summits in spring.

The 6°C mean temperature isotherm (MMEAN6) represents the theoretical limit to plant growth. In winter, MMEAN6 occurs at negative altitude and no net growth

occurs anywhere. By March MMEAN6 has risen to 4 m. April is the most critical month for growth with this growth limit at 246 m. By May MMEAN6 has risen to 760 m. Thus sustained grass growth is not likely on the highest summits until June! In the autumn the decline of MMEAN6 with altitude is much more rapid, falling from 701 m in October to 26 m in November. Thus the delay in growth with altitude is more marked in spring than in autumn. Largest contrasts between upland and lowland occur in April and May. In mid-summer (July) growth would be expected up to 1439 m. However, there is no effective growing season at this level. Plants could not flourish with mean temperatures of 6°C in the warmest month only.

The 6°C maximum temperature isotherm (MMAX6) indicates the sporadic growth limit. Temperatures above 6°C are expected at the warmest part of the day. In July MMAX6 falls at 1781 m, low compared with the Pyrenees where pastureland is found above this altitude. In the French Alps, the village of St.Veran in the Parc du Queyras (based on pastoral farming) is sited at over 2000 m. In winter MMAX6 falls to only 78 m in northern England. Coastal areas may experience sporadic grass growth throughout the winter, with mean daily maxima remaining above 6°C.

The 10°C July isotherm (MMEAN10) is representative of the climatological treeline (Del Barrio et al. 1990). Although variations in treeline elevation occur due to exposure, drainage, aspect and soil type (Taylor 1965), summer mean temperatures control limits to tree growth as tree-ring studies have shown (Bednarz 1984). In the Pennines MMEAN10 rises to 846 m in the warmest month (July). A mean temperature of 10°C in one month alone is not sufficient for tree growth and the 10°C isotherm for June to September inclusive should be considered. Taken for these months, MMEAN10 falls at around 600 m, approximating the height of the present treeline (Plate 10). Where exposure is great or drainage is poor the treeline is depressed below this level, as on many steeper slopes and in wetter parts of Cumbria (Plate 11). Evidence of tree growth at 800 m during the Climatic Optimum (5000 BC) implies that mean summer temperatures (between June and September) were at least 10°C. A temperature difference of at least +1.4°C between then and now is postulated. Taylor (1965) gives evidence of treelines in Wales above 600 m during the Climatic Optimum and relates

changes in the treeline to changes in the continentality of the climate. He suggests that the depression of the present treeline is due to an increased maritime influence.

On Figure 9.4 the frost limit (MMIN0) is usually at least two hundred metres above the sporadic growth limit (MMAX6), apart from in spring. Between March and June the difference is negligible. In May the frost limit falls below the sporadic growth limit! Thus frost occurring within the sporadic growth zone can be a problem at this time, causing damage to young plants. Apart from the relative depression of the frost limit in spring, the spacing of the isotherms remains fairly constant throughout the year.

9.5 Comparison of the Pennines with the Pyrenees: A Continental Mountain Range

In comparison with other mountain ranges the altitudinal decline in the temperature resource is extremely steep in northern England. The unexpectedly low treeline (Pearsall 1950) is a result of the steep decrease in accumulated temperatures with altitude (see Chapter 10). In the Central and Eastern Pyrenees the 10°C July isotherm (MMEAN10) falls at 2438 m (Del Barrio et al. 1990), derived using stations between 0° 30' W and 2° 30' E. This is 1600 metres higher than in the Pennines, suggesting that summer temperatures are at least 10°C warmer at an equivalent altitude in the Pyrenees (assuming a conservative mean lapse rate of -6.25°C/km). Higher summer temperatures are encouraged by the lower latitude of the Pyrenees but also by increased continentality with clearer summers characterised by much more insolation. The timberline falls between 2000 and 2400 m, slightly lower than MMEAN10 in July, since one month alone with a mean temperature of 10°C is insufficient for tree growth.

In winter the mean 0°C isotherm (MMEAN0) occurs at 1694 m. Stable winter snow cover is therefore characteristic of the upper montane forest belt between 1694 and 2438 m. The difference between the timberline and the winter snow limit is 744 m. In Northern England the equivalent winter MMEAN0 (December to March) falls at 696 m, lower than in the Pyrenees by 1000 m. The difference between the July MMEAN10 and winter MMEAN0 isotherms is only 150 m (20% of the difference in the Pyrenees) and the zone characterised by stable winter snow cover and summer

growth present in the Pyrenees is severely restricted in northern England. The limit of stable winter snow cover (696 m) lies above the Pennine timberline and the marginal nature of the Pennines is therefore due not to cold winters but to cool and cloudy summers. Global warming scenarios in which winters become milder but summers experience little change (Houghton et al. 1990, 1992) could increase the maritime nature of northern England and do little to improve upland cultivation. If Pyrenean snow cover above the snow limit (1694 m) were to melt in milder winters, this could only increase the length of the growing season. Pfister (1985) shows that a change in weather "types" will have contrasting effects on snow cover at differing altitudes. Milder winters dominated by westerly airflows would increase snow at high altitudes but allow more rain (and snow melt) at low levels. Anticyclonic conditions with pronounced temperature inversions would maintain winter snow cover in the lowlands but permit melt above the inversion, especially on south-facing slopes.

The mean annual 0°C isotherm (MMEAN0) falls at 2726 m in the Pyrenees. Although this is high there is still land above this limit, whereas the Pennines are not high enough to reach this zone (> 1336 m). Therefore the Pyrenees possess a wider range of habitats due to the much wider range in altitude. Del Barrio et al. (1990) calculate the length of the vegetative growth period (VGP) at important sites, i.e the period for which mean temperatures are above 7°C. At Goritz (2160 m) the VGP is 128 days and the mean temperature during this period is 10.8°C. Using 7°C in the Pennines mean VGP is only 105 days at 800 m (interpolated from Figure 9.4). Great Dun Fell (847 m) records a shorter (and colder) growing season than sites above 2000 m in the Pyrenees! Growing conditions on the summit are approximately equal to those at 2500 m in the Pyrenees.

9.6 Comparison with the Tatra Mountains

Another comparison is made with the Tatra (near the border of Poland and Slovakia). Although the Tatra are further south than the Pennines, the latitudinal difference is small. The Tatra are approximately at the latitude of Northern France. A recent study by Niedzwiedz (1992) and numerous articles by Hess (1965, 1969, 1974)

ensure that climatic data are now available up to the highest summits (above 2000 m). The highest climate station is Lomnicky Stit (2635 m).

Hess divided the mountains into five zones according to mean annual temperature (Table 9.3).

Table 9.3: Mean annual air temperatures in the Polish Tatra.

Mean Annual Temperature /°C	Level of Isotherm/ N slope: m	Level of Isotherm S slope:m	Life Zone Class
-2	2200	2350	Snow line
0	1850	2050	Sub-Alpine
2	1550	1650	Timberline
4	1150	1200	Agricultural Limit
6	650	700	Lowland

Source: Hess (1974).

The -2°C isotherm of mean annual temperature (MMEAN-2) was taken by Hess to represent the snow-line. This falls above 2000 m in the Tatra, in comparison with the estimate of 1595 m in the Pennines. Differences in aspect appear important in the Tatra with a difference in 150 metres between north and south facing slopes. The O°C isotherm (MMEAN0) was defined by Hess as the limit of the sub-alpine zone. MMEAN0, at around 2000 m, is lower than in the Pyrenees (2726 m) but higher than in the Pennines (1336 m), despite severer winters than both mountain ranges. The 0°C mean winter air temperature isotherm falls below 700 m because of intense temperature inversion at low levels (Niedzwiedz 1992). Stations below this altitude in the Tatra record mean January temperatures as low as -5°C!

In the Tatra, a mean annual temperature of 2°C is coincident with the treeline (both occurring at 1600 m), while the agricultural and mixed forest limit falls at 1200

m (coincident with a mean annual temperature of 4°C). Mean annual temperatures in treeless parts of the Pennines are higher than this showing that mean annual temperature alone is not a good indicator of potential for tree and plant growth. The 10°C July isotherm in the Tatra (at 1650 m) is a better indicator of the natural treeline. Warmer summers in the Tatra raise the treeline to more than twice its respective altitude in northern England (846 m) whereas mean annual temperatures are similar at sea-level in both regions at 9°C. Hess (1969) developed the following regression equation for mean annual temperature in the Tatra:

$$T_a = 9.2 - (0.0048 alt) \quad ----(1)$$

The lapse rate of -4.8°C/km is much lower than values in northern England (Chapter 8). The shallow rate, along with warmer summers, raises life zones in the Tatra above those in the Pennines, despite severer winters. The growing season becomes negligible at 2500 m but it is still 190 days at 844 m.

Contrasts between the Pennines and Tatra are due to continentality effects (warmer summers and shallower lapse rates in the latter range). For the Tatra the World Meteorological Organisation (WMO) predicts a rise of 100 m in life zones under a warming of 1°C (WMO 1986), yet an increase in westerly flow (see section 8.5), as postulated by Niedzwiedz (1992), may lower life zones because of a reduced annual temperature range. The comparison with the maritime Pennine climate is informative.

9.7 Other Comparisons

The mountain station of Fanaråken (approximately 2000 m) in southern Norway exhibits greater continentality than northern England. Temperatures on the summit are about 10°C lower than on Ben Nevis in winter but only slightly lower in summer. The altitudinal difference is 600 metres. Temperatures at the same altitude are higher than in northern England in summer, leading to a slightly higher treeline (Manley 1949). The contrast in altitudinal zonation between continental and maritime mountain ranges

is also evident within Washington state, USA (Price 1978). The timberline is almost 1000 m higher in the continental Wallowas than in the maritime Cascades (2700 m compared with 1700 m). Contrasts in zonation due to continentality are not confined to the temperate zone. Life zones are consistently higher on dry subtropical mountains than on wetter equatorial ones (Messerli & Winiger 1992). Thus rice cultivation reaches its highest elevations in the Himalayan system (2700 m in the Jumla valley) and not in equatorial areas such as Indonesia, where it only reaches 1400 m (Uhlig 1978).

9.8 Conclusions

This chapter has illustrated the altitudinal zonation of the temperature resource in northern England, the Pyrenees and the Polish Tatra. Differences in the relative altitudes of critical isotherms and in the rate of change in the temperature resource with altitude have been identified.

In summary, major causes of the marginal nature of the British uplands include:

1. low summer temperatures. The mean temperature of the warmest month barely reaches 10°C above 800 m;

2. a steep altitudinal decrease in temperature, especially in spring.

Other known reasons for marginality include:

3. windy conditions due to exposure to the Atlantic westerlies;

4. cloudy conditions and a lack of insolation, even in summer;

5. high precipitation, leading to poor drainage and waterlogging, exacerbated by a lack of evaporation.

The second part of the thesis will explore the consequences of the steep

altitudinal decline in temperature in more detail.

a. The altitudinal variation in "environmental potential" is described by examining the altitudinal variation of growing season length and strength (measured by accumulated temperatures) and frost risk (Chapters 10-12).

b. The temperature resource under the influence of each airflow type is simulated to examine the altitudinal decline of growth potential under different synoptic influences (Chapters 13-14). The relationship with the circulation pattern is important since effects of changes in relative frequencies of airflows on growth conditions can then be described.

c. Past variation of growth parameters within the region is examined, using a time series from Durham University Observatory (1801-1990) and effects are extrapolated to the uplands (Chapter 15).

d. The variability of daily temperatures around a mean value for each airflow is introduced, allowing a more accurate determination of growth and frost parameters (Chapters 16-17).

e. Temperatures associated with different airflows are modified under global warming scenarios, derived from GCM output data (Chapter 18). Warming radically alters the growth potential and temperature resource, illustrating the sensitivity of the Pennines to climatic change.

THE ALTITUDINAL VARIATION OF ACCUMULATED TEMPERATURES IN THE NORTH OF ENGLAND

10.1 Introduction

The thesis is not concerned with attempts to predict the effects of future climatic change on agriculture (and hence land use) per se. It is immediately apparent that to do so it would be necessary to model changes in climatic factors other than temperature, such as windiness, precipitation and insolation, as well as the influence of edaphic, topographic, social and economic factors. Nevertheless, indicators based on temperature can be used to illustrate the sensitivity of maritime uplands (such as the Pennines) to climatic fluctuation.

This chapter investigates the variation in growing season quality with altitude over a sample six year period (1985-1990). The rapid decrease in accumulated temperatures with altitude is a fundamental characteristic of a climate dominated by steep lapse rates and maritime air. Low summer temperatures are the restricting factor for cultivation and tree growth in many parts of northern England. Later in the thesis this is used as a baseline upon which the results of recent GCM (General Circulation Model) temperature simulations are placed. The methodology shows how global scale GCM model output can be applied to illustrate changes in climate within a small area through the use of synoptic climatology.

The relationship of the chosen parameters to changes in airflow frequencies is important since it is only when the synoptic climatology of an individual area has been fully described that it is possible to speculate about the local effects of climate change. Climate is composed of day to day variations in weather: it is airflow variations that control that weather. Variations in airflow frequencies can be predicted for future global warming scenarios (Hulme et al. 1993) and so it is important to relate such airflow variations to resultant temperature change. With more detailed information on other climatic indices (e.g. the number of freeze-thaw cycles for weathering applications, or the accumulated temperatures and precipitation required for a specific crop), similar

methodology could be used to show the change in the expected spatial distribution of the indices under the influence of climate change.

10.2 Estimation of Growing Season Strength

Daily maximum and minimum temperatures were obtained at 26 locations in northern England (for a description of these sites and a map see Chapter 4). Most of the high altitude stations are sited in the Alston massif (Great Dun and Widdybank Fell), Northumberland (Kielder and Redesdale), or the Upper Eden valley (Warcop and Shap). The bias towards lowland localities and accessible sites was discussed in Chapter 4. The chosen data period (1985-1990) includes cold winters (1985,1986), cool summers (1985), mild winters (1989,1990) and warm summers (1989, 1990). At four locations (Houghall, Nenthead, Shap and Wycliffe Hall) data were only available for part of the period and these locations have been omitted from some analyses.

Growing season strength is measured by accumulating daily mean or maximum temperatures above a critical threshold. The actual threshold temperature and the temperatures used to calculate the excess depend on the application concerned.

Various forms of accumulated temperatures have been used in scientific study (Thom 1954, Shellard 1959). For example, accumulated temperatures were related to potential for crop growth by Petr (1991) in the Czech Republic and by Carter et al. (1991a) in Europe. Heat resources were evaluated by Guoyu (1991) for China and the United States and were found to be among the highest in the temperate zone. Accumulated temperatures were used by Hess et al. (1984) to evaluate the spatial variation of "thermal potential" in the Carpathians. In many crop and forestry models, limits set to species were defined by accumulated temperatures. Changes in accumulated temperatures predicted from GCMs were used to predict changes in species' distributions (Carter et al. 1991b, Botkin & Nisbet 1992, Urban et al. 1993). Accumulations below a threshold have also been used to represent winter severity in the USA (Assel 1980) and heating requirements (Aceituno 1979). Specific examples are listed in Table 10.1.

Table 10.1: Growing season calculations based on accumulated temperatures.

APPLICATION	PLACE	THRES -HOLD	TEMPER- ATURE	CRITICAL VALUE	AUTHOR
General Crops	U.S.A	>6°C	Mean Daily	1000	Dept of Ag
Heating Estimates	U.S.A	<18°C	Mean Daily	N/A	American Engineer
Cotton	South U.S.A	>60°F 15.5°C	Mean Daily	1900	Ahrens (1991)
Wheat	Indiana	>40°F 4.5°C	Mean Daily	2100	Ahrens (1991)
Peas	North U.S.A	>40°F 4.5°C	Mean Daily	1100	Ahrens (1991)
Oats	Lammer- muir Hills	>4.4°C	Mean Daily	1050- 1250	Parry (1981)
Mountain Hemlock	Oregon	>6°C	Maximum Daily	183	Urban et al.(1993)
Ponderosa Pine	Oregon	>6°C	Maximum Daily	600	Urban et al.(1993)
General Crops	Britain	>6°C	Maximum Daily	N/A	Shellard (1959)

In the first example mean daily temperatures in excess of 6°C are summed to obtain an annual estimate of growth potential. Mean monthly temperatures could be used if daily temperatures were unavailable but would lead to serious differences in the calculated value.

A threshold of 6°C was taken in this study to represent the lower limit for realistic plant growth. This is the most widely quoted figure by British authors (Scott 1884, Manley 1952, Taylor 1967b). An accumulation of 1000 degree days (d°C) above 6°C was taken to be a lower limit for profitable agricultural cultivation. Parry (1978) used the 1150 d°C isopleth as critical for oat cultivation in the Lammermuir Hills but the threshold temperature was lower (4.4°C) and he considered land between 1050 d°C

and 1250 d°C to be marginal. The limit chosen here is somewhat arbitrary. However, the method is more important than the absolute accumulated temperature limit chosen.

Daily mean temperatures were calculated by taking the arithmetic average of daily maxima and minima. 6°C was subtracted to obtain the degree days contribution for that particular day. Negative values were ignored and positive values were summed to give the total growing season strength for each of the six years (Table 10.2). Days with missing data would by default record an accumulation of zero with the software used. To allow for this, annual totals were corrected by multiplying them by **k** where:

$$k = 365 / \textit{number of days with data} \quad \text{----(1)}$$

k is always greater than or equal to unity. In most cases corrections are negligible but at Great Dun Fell corrections are very important since temperatures are unavailable at weekends. If missing data are concentrated at a certain season an anomalous result occurs because of the implicit assumption that the missing days have a degree day contribution equal to the average daily contribution over the whole year. Cases where this leads to incorrect accumulations are mentioned in the text.

Table 10.2: Growing season strength in degree days, calculated using actual mean daily temperatures.

Place	**1985**	**1986**	**1987**	**1988**	**1989**	**1990**	**alt**
Ambl	1222	1169	1268	1403	1554	1532	90
App	1324	1169	1259	1337	1357	1332	150
Asp	1292	1195	1291	1392	1586	1558	64
Clsle	1366	1268	1354	1485	1709	1672	26
CClv	1378	1291	1337	1406	1638	1665	103
CCov	1028	935	994	983	1233	1236	270
Dur	1289	1222	1281	1385	1534	1557	102

Table 10.2: continued

Place	1985	1986	1987	1988	1989	1990	alt
Esk	1371	1268	1372	1440	1676	1730	8
GDF	417	251	379	314	600	530	847
Htbn	1312	1188	1227	1333	1514	1567	31
Hay	1316	1240	1271	1376	1553	1550	82
Hghcl	1045	1014	1091	1161	1281	1574	175
Hughl	-	-	-	-	-	1369	36
Kes	1558	1437	1513	1563	1654	1739	100
Kield	911	774	937	1006	1200	1236	201
Leem	1411	1339	1421	1494	1710	1775	32
Lweth	1164	1070	1108	1178	1394	1462	162
Nent	-	-	1061	792	978	982	470
Nwcs	1425	1345	1371	1484	1695	1735	35
Rdsd	927	802	869	927	1053	1067	235
Shap	-	-	-	1015	1130	1159	249
Sund	1405	1319	1346	1515	1736	1812	56
War	1122	951	1071	1109	1320	1213	244
Whas	1169	1115	1227	1297	1474	1434	165
Wid	675	594	667	711	874	842	513
Wy	-	-	-	-	1586	1310	120

Most locations report their coldest year in 1986, accumulated temperatures ranging from 251 d°C at Great Dun Fell, to 1437 d°C at Keswick. The warmest years are 1989 and 1990. Sunderland on the east coast reports 1812 d°C in 1990 and Great Dun Fell manages 600 d°C in 1989 (over twice the amount recorded there in 1986). The inter-annual variation in accumulated temperatures is over 100% at this high altitude. The figure of 1574 d°C for High Close in 1990 appears anomalously high and results because of the correction process, required to compensate for missing data.

10.3 The Linear Relationship between Accumulated Temperatures and Altitude

Figure 10.1 plots growing season strength against altitude between 1985 and 1990. A critical accumulation of 1000 d°C will be taken as the lower limit for successful agricultural cultivation in a particular year. In a bad year, such as 1986, 5 or 6 stations record temperature accumulations below 1000 d°C (including Kielder Castle, Redesdale and Carlton-in-Coverdale), whereas in 1989 only 3 stations (Nenthead, Widdybank Fell and Great Dun Fell) fall below, the first station only slightly so. Values for Nenthead are unavailable for 1985 and 1986.

In 1985 Keswick and Warcop exhibit higher accumulated temperatures than expected given the altitude. The Warcop value is misleadingly high due to the correction process. Keswick shows high accumulations in all years, suggesting that local factors are important. The extremely sheltered south-facing location means that the site is warm. Straight lines are fitted to the relationship between accumulated temperatures and altitude. Subsequent analysis suggests slight curvilinearity, upland stations producing higher accumulations than would be expected from a linear relationship, although the lack of high altitude stations makes the curved trend difficult to substantiate.

In 1988 there is very little correlation between altitude and growing season below 100 m. This may be a consequence of summer cooling at coastal locations, associated with a reduced diurnal temperature range and lower mean temperatures (Linacre 1982).

Linear regressions summarizing the relationship between growing season strength and altitude are shown. The altitude at which the regression line crosses 1000 d°C is a crude estimate of the critical altitudinal limit to crop growth in that year. Microclimatic variations due to topography will elevate or depress this limit in many areas. This theoretical limit is listed in the first column of Table 10.3, and varies from 236 m in 1986 to 463 m in 1989. This variation is similar in magnitude to the 200 metre decline in the cultivation limit described by Parry (1978) for the Lammermuir

Figure 10.1. Growing Season Strength, Measured by Annual Accumulated Temperatures (deg-days), versus Altitude, 1985-1990: Modelled by a Linear Relationship Using 22 Stations in Northern England

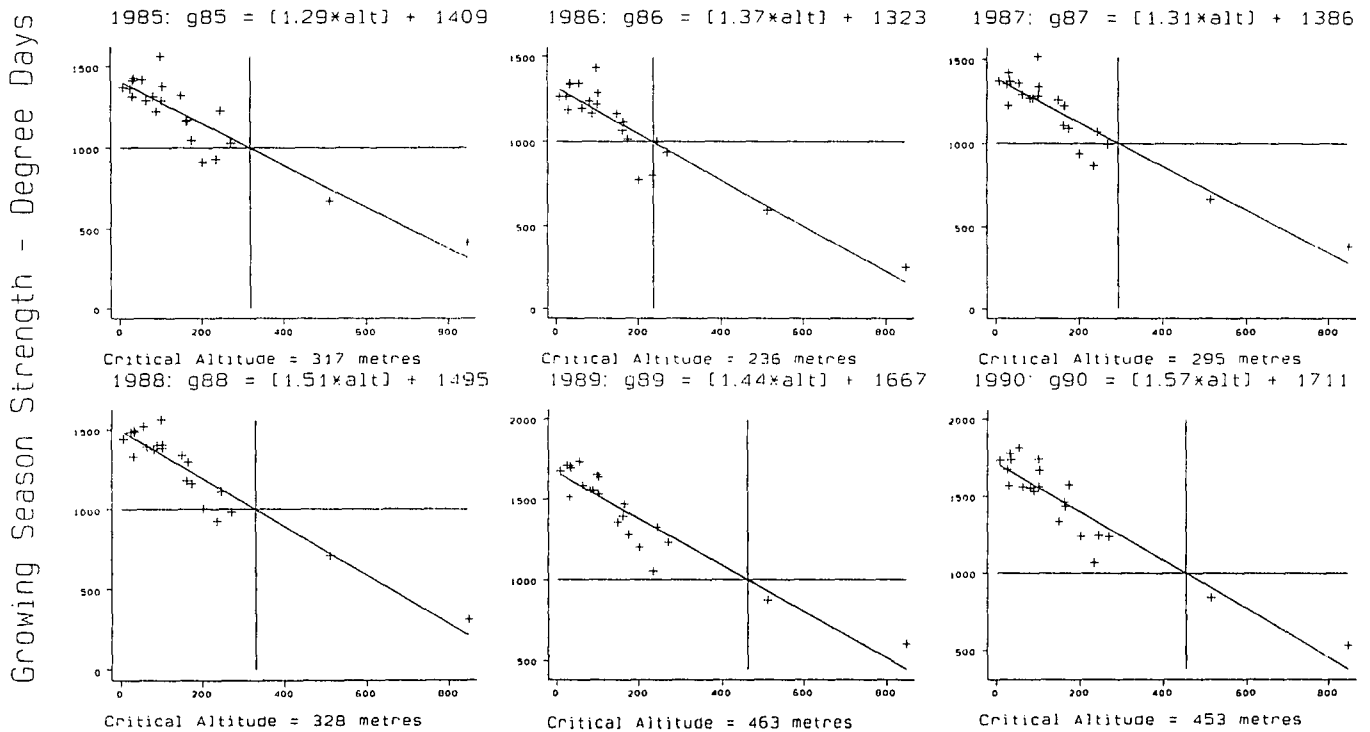

Hills (from 425 to 225 m). Therefore, inter-annual variation is considerable within this six-year period. Considerable areas of land between 236 and 463 m will be suitable for agricultural development in warm years such as 1989, but not in colder years such as 1986. This large amount of "marginal" land includes much of Upper Teesdale, Upper Weardale, the Shap/Brough area and Upper Eden Valley, and large areas in Kielder Forest and the North Yorkshire Moors (Figure 10.2).

Table 10.3: Linear regressions between growing season strength and altitude.

	critical alt (metres)	gradient (d°C/metre)	constant (d°C)
1985	317	1.29	1409
1986	236	1.37	1323
1987	295	1.31	1386
1988	328	1.51	1495
1989	463	1.44	1667
1990	453	1.57	1711
average	351	1.42	1499

The gradient, shown in the second column of Table 10.3, indicates the characteristic drop in degree days per unit increase in altitude. This varies from 1.29 d°C/m in 1985 to 1.57 d°C/m in 1990. The rate is steeper in warmer years such as 1989 and 1990, although the percentage change in growing season with altitude may be steeper in cooler years. The third column gives the constant term, representing predicted growing season strength at sea level. This varies by nearly 400 d°C between years.

If the mean growing season strength over the six year period is related to altitude, the gradient of the regression line is 1.42 d°C per metre, the predicted growing season at sea-level is 1499 d°C, and the critical altitude is 351 m (for an accumulation of 1000 d°C). This altitudinal limit will have fluctuated dramatically in the past, especially as it varies between 236 m and 463 m in such a short period.

Figure 10.2. Marginal Land (between 236 and 463 Metres above Sea-level)
Derived by Extrapolation of 1000 deg day Cultivation Limits in Fig. 10.1

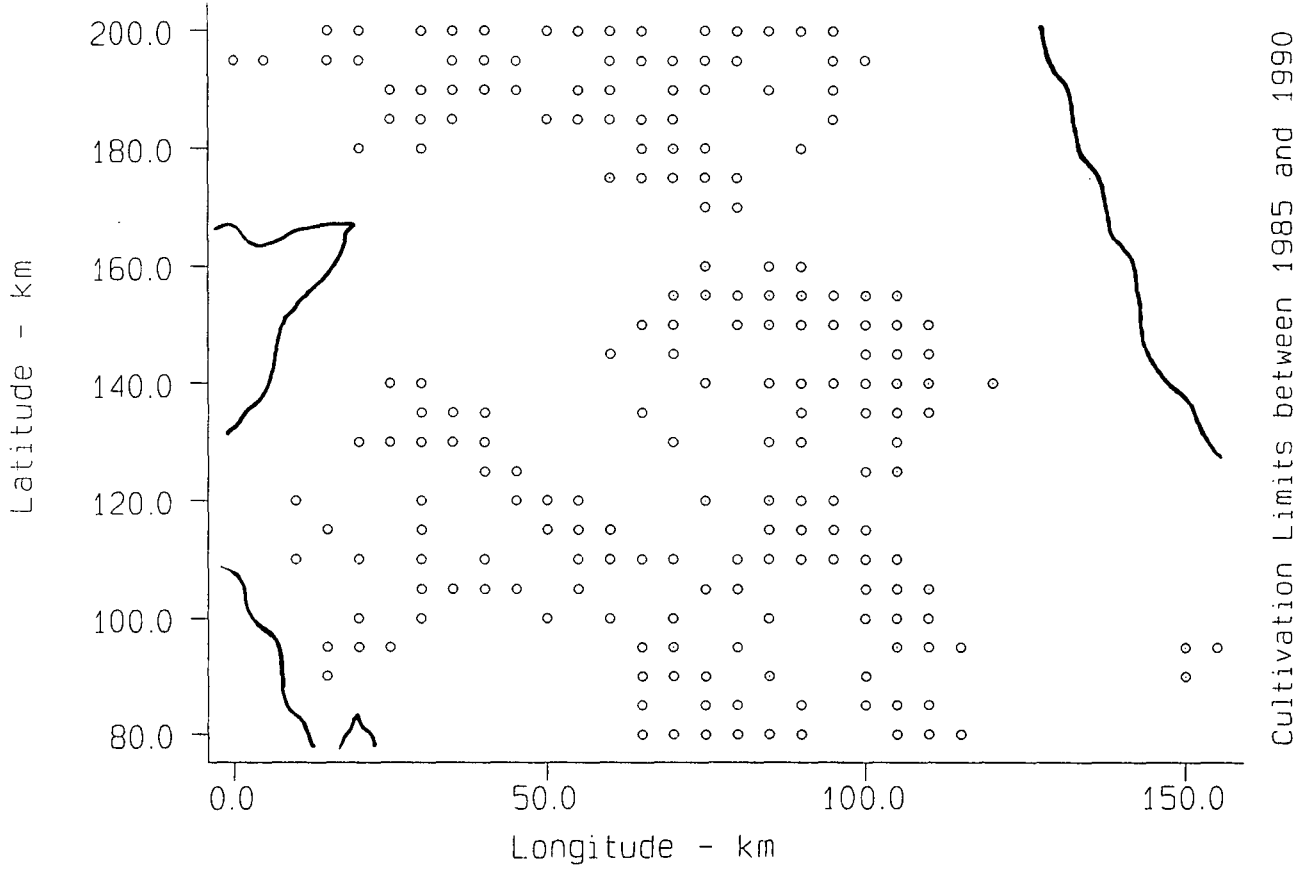

Many studies have illustrated such systematic changes in growing season length or strength over many timescales and in contrasting regions of the world. Davis (1972) examined the variation in the onset of spring in Britain. The first day of spring, defined by maximum temperatures, was found to be related to:

1. ice cover in the Baltic and the Iceland area;

2. the sea temperature pattern in the North Atlantic;

3. the circulation at 500 mb;

4. atmospheric circulation indices.

Moran & Morgan (1977) investigated change in growing season indices in Wisconsin, finding that fluctuations in the length and strength of the growing season were not necessarily correlated with changes in mean annual Northern Hemisphere temperature. Skaggs & Baker (1985) carried out a similar study using five rural Minnesota stations with data from 1899 to 1982. A general warming trend was discovered. Suckling (1989) used a climate departure index (CDI) to study the variability of growing season length in the south-eastern USA. The 1980s had a greater climate variability with unusual spring and autumn freeze dates. There are numerous, often contradictory, findings concerning historical fluctuation in growing season parameters, because of the contrasting indices used to define growing season. The fluctuation of the theoretical cultivation limit created for this study will be examined over the last two centuries by referring to the Durham meteorological record (Kenworthy 1985) (Chapter 15).

10.4 The Use of an Exponential Model to Relate Growing Season Strength with Altitude

r^2 for the linear regressions between altitude and accumulated temperatures varies from 0.895 (1988) to 0.806 (1987). If an exponential function is fitted, r^2

increases in most cases to over 0.9. Consideration of a simple annual temperature curve, represented by a sine-wave (Figure 10.3), suggests that, given a constant rate of increase in mean annual temperature, the area bounded by the curve and a certain critical threshold temperature will increase at a non-linear rate. Mathematical proof of this is given in section 10.5, supporting the idea that an exponential regression is more appropriate to model the altitudinal decrease in accumulated temperatures.

The exponential relationship is as follows:

$$growing\ season(g) = g_0 \times e^{(-k \times a)} \quad ----(2)$$

$\mathbf{g_0}$ is the predicted growing season at sea-level, **a** represents altitude in metres and **k** is a coefficient. Thus:

$$\ln g = (\ln g_0) - (k \times a) \quad ----(3)$$

Growing season values need to be transformed using natural logarithms. The logarithm of growing season strength is then regressed against altitude using a straight

Table 10.4: Exponential regressions between growing season strength and altitude.

YEAR	ln g_0	g_0 d°C	k	critical altitude	r^2
1985	7.3	1480.3	-0.0015	261	0.905
1986	7.27	1436.6	-0.0019	191	0.927
1987	7.282	1453.9	-0.0014	267	0.855
1988	7.382	1606.8	-0.0018	264	0.945
1989	7.454	1726.8	-0.0013	420	0.926
1990	7.466	1747.6	-0.0014	399	0.903
average	7.366	1581.3	-0.0016	286	0.945

Figure 10.3. Simplified Annual Temperature Curve (a Sine Wave) in Relation to a 6 deg C Threshold Temperature

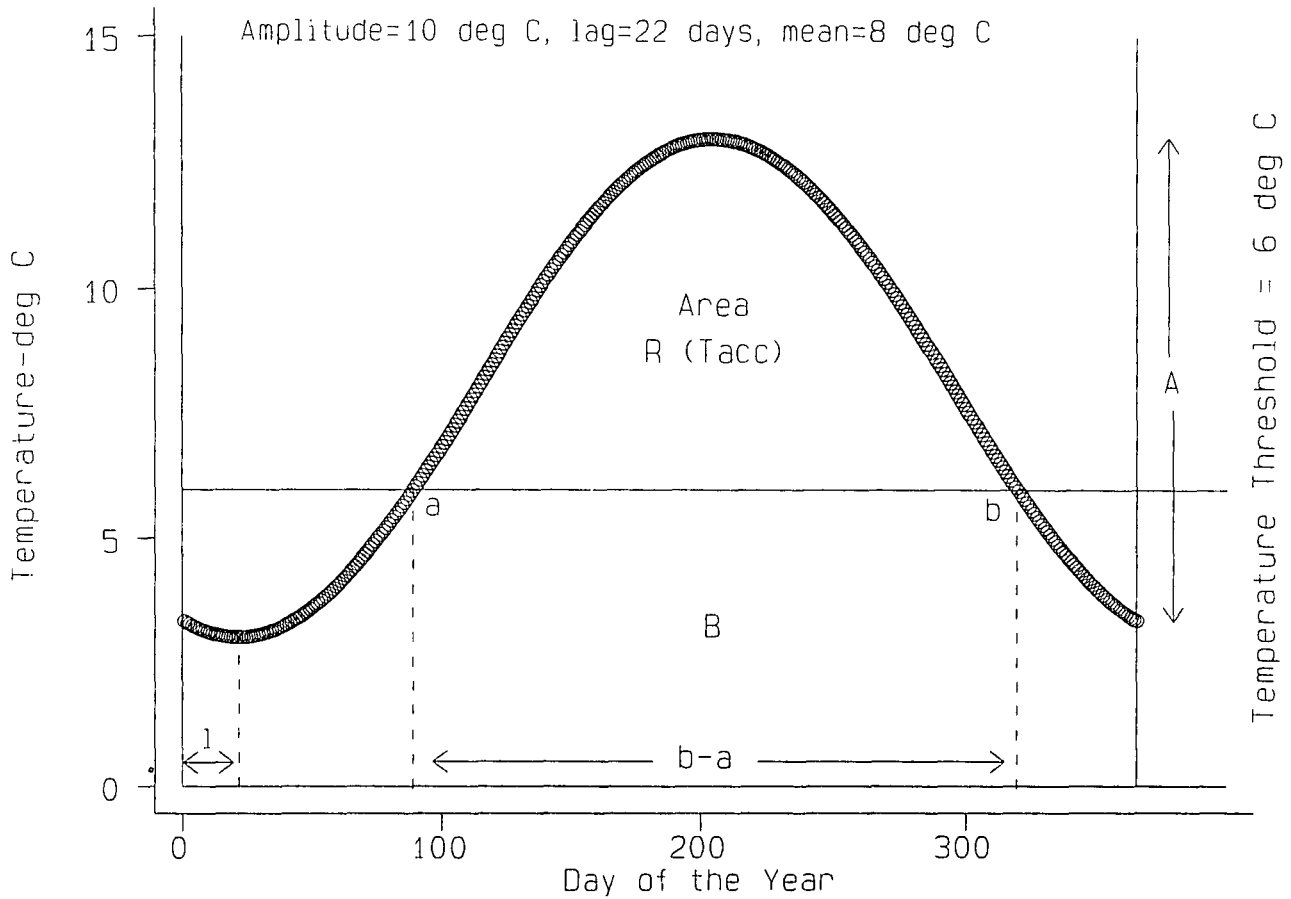

line with gradient **k** and intercept equal to ln g_0. In Table 10.4 values of ln g_0, $\mathbf{g_0}$, **k** and the new cultivation limit using exponential regression are given for 1985-1990.

Curves are shown in Figure 10.4, each year on a separate graph as in Figure 10.1. In general, r^2 is higher for the exponential function. Values for the four stations with incomplete data (Houghall, Nenthead, Shap and Wycliffe Hall) are included in the analysis. The low r^2 of 0.855 (in 1987) is partly due to the anomalously high residual belonging to Nenthead in that year which arises due to missing data. Otherwise r^2 is always above 0.9. Thus an exponential relationship more accurately describes the altitudinal decrease in accumulated temperatures than a linear relationship. The lack of high altitude stations means that the robustness of the regressions is fairly low (section 10.6). Predicted values of sea-level growing season strength, g_0, vary from 1436.6 d°C in 1986 to 1747.6 d°C in 1990. Accumulations are higher than in the linear model because of the increased growing season gradient simulated at low altitude. **k** varies from -0.0013 in 1989 to -0.0019 in 1986. There is no strong relationship between **k** and the linear gradient. For example, the linear gradient is steeper in 1989 than in 1986, but this is not so for **k**.

Critical altitudinal limits to cultivation in the exponential model are lower than in the linear model, ranging from 191 m in 1986 to 420 m in 1989. The amount of variation is still large and critical altitudes interpolated using this exponential model are 40-60 metres lower than equivalent linear limits. The difference is represented on Figure 10.5, which shows both exponential and linear regressions for the average growing season strength between 1985 and 1990. The critical cultivation limit (an accumulation of 1000 d°C) in the exponential regression is 286 m whereas in the linear case it is 351 m. It is at very low and very high altitudes that the exponential model predicts higher temperature accumulations than the linear model. The exponential model takes into account the extra warmth experienced at lowest altitudes, often due to coastal influences, and the relative (not absolute) warmth on the highest summits. This may be the result of temperature inversions (Hennessy 1979), or the heating of upland plateaux in summer (Tabony 1985).

Figure 10.4. Growing Season Strength, Measured by Annual Accumulated Temperatures (deg days), versus Altitude, 1985-1990: Modelled by an Exponential Relationship

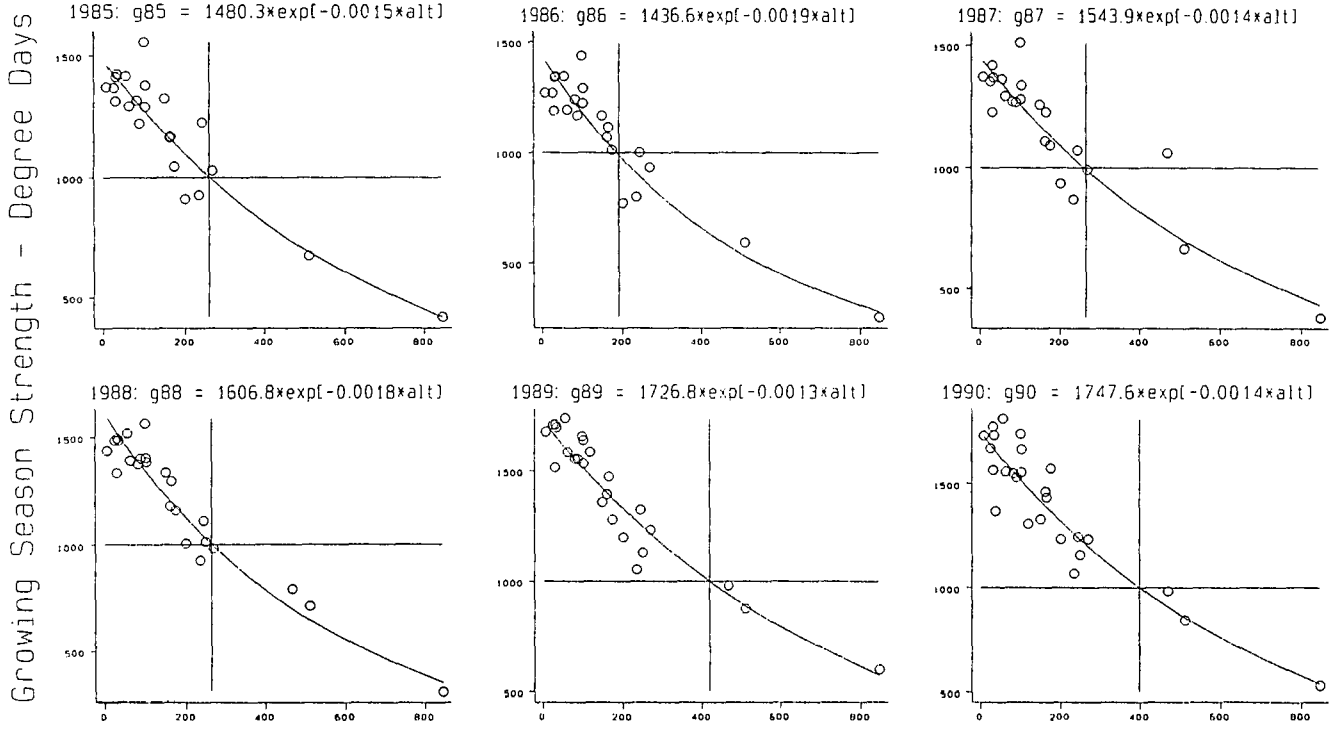

22-26 Stations-depending on year

Altitude - Metres above Sea-level

Figure 10.5. Exponential and Linear Models of Mean Growing Season Strength (deg days) from 1985-1990 versus Altitude

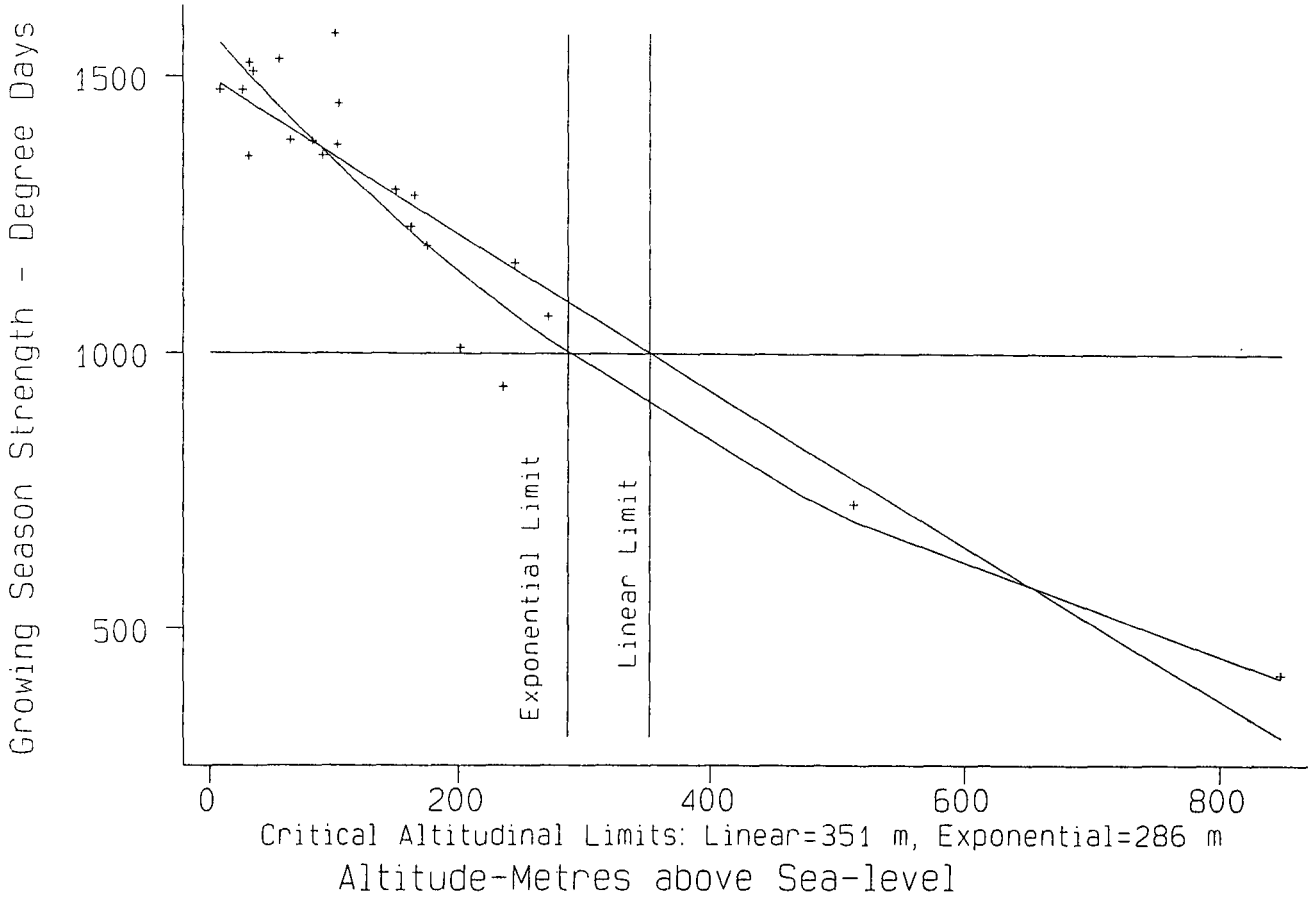

10.5 An Analytical Investigation into the Altitudinal Decline in Growing Season Strength: Linear or Exponential?

The shape of the altitudinal decline in growth potential, as measured by accumulated temperatures, will be approached analytically. The annual temperature fluctuation is represented as a sinusoidal curve with amplitude **A** equal to the annual temperature range and mean temperature **m** equal to the mean annual temperature (Figure 10.3). The area of the curve (**R**) above the critical threshold, marked as **d**, is representative of growing season strength. The length of the growing season is marked as **l**.

As the critical temperature threshold is altered the area **R** will change. The same effect is obtained if the annual temperature curve is moved (i.e. mean annual temperature **m** is changed) or if the amplitude **A** (mean annual temperature range) is altered.

The annual temperature curve can be described by:

$$t=(A/2)\times[\sin((2\pi/365)\times(x-91.25-l))]+m \quad ----(4)$$

where **A** = amplitude, **m** = mean annual temperature, **l** = the lag in the minimum point of the curve in days after December 31, and **x** = the day of the year (between 1 and 365). 2*_pi/365 is a factor allowing conversion from days in the year to radians. For any day in the year (a given value of **x**) the expected mean temperature can be obtained if **l**, **A** and **m** are known.

For example: Let **A** = 10°C, **m** = 9°C and **l** = 22 days.

On 22 Jan (x=22) the expected temperature is 4°C. On 22 Apr (x=112) the temperature expected is 8.89°C.

To obtain the beginning and end dates of the growing season, equation 4 is set equal to 6°C:

$$x=(365/2\pi)\times\arcsin([2\times(6-m)/A]+91.25+l) \quad ----(5)$$

The value of **x** produced is typically the start day of the season (**a**). To obtain the last day (**b**), which is equidistant from the warmest day of the year (a sine curve is symmetrical), the following equations are used:

$$warmest\ day(w)=l+(365/2) \quad ----(6)$$

Therefore:

$$b=2(l+(365/2))-a = 2w-a \quad ----(7)$$

The length of the growing season in days is equal to **b-a**.

Notes: - if b>365 the last day of the growing season will fall in January of the following year;

- if m-(A/2) >=6, the length of the growing season is 365 days since the curve never dips below 6°C;

- if m+(A/2) <=6, there is no growing season since the curve never rises above 6°C.

Accumulated temperatures T_{acc} during the growing season are obtained by calculation of the area under the sine curve between **a** and **b**, minus area **B** (Figure 10.3).

Thus:

$$T_{acc}=\int_a^b (A/2)\times[\sin((2\pi/365)\times(x-91.25-l))]+m\ dx$$
$$-6(b-a)\quad ----(8)$$

The area **B** [=6(b-a)] represents the area between **a** and **b** below the threshold and must be subtracted from the integral to get the required area **R**.

$$T_{acc}=(A/2)\int_a^b[\sin((2\pi/365)\times(x-91.25-l))]\ dx+\int_a^b m\ dx\ -6(b-a)$$

$$=(365/2\pi)\times A/2\int_a^b 2\pi/365[\sin((2\pi/365)\times(x-91.25-l))]\ dx$$
$$+\ m(b-a)-6(b-a)$$

$$=(365A/4\pi)\times[-\cos((2\pi/365)(x-91.25-l))]_a^b+(m-6)\times(b-a)$$

$$=(365A/4\pi)\times[-\cos((2\pi/365)\times(b-91.25-l))$$
$$+\cos((2\pi/365)\times(a-91.25-l))]+(m-6)\times(b-a)\quad ---(9)$$

Once **A**, **a**, **b**, **l** and **m** are known the annual temperature accumulation can be calculated. This can be done for each station using historical temperature data. Alternatively, arbitrary values of **A**, **l** and **m** can be created. In the following section, expected accumulated temperatures at each location are derived through Fourier analysis.

10.6 Fourier Analysis of Recorded Temperature Data

The Fourier curve (i.e. the sine curve representing annual variation in mean temperature) was extracted at each station using mean daily temperatures recorded for

all years between 1985 and 1990.

The yearly march of temperature was modelled by a sine curve with a phase lag ϕ, plus a constant m:

$$y=m+((A/2)\sin(t+\phi)) \quad ----(10)$$

where **t** is the day of the year.

A sine wave with a phase lag is obtained by the addition of a cosine and sine wave:

$$y=m+(A/2)\times[\cos\phi\sin\alpha+\sin\phi\cos\alpha] \quad ----(11)$$

If b1 = (A/2)*cos(ϕ) and b2 = (A/2)*sin(ϕ):

$$phase=\phi=\arctan[b2/b1] \quad ----(12)$$

Such a curve was fitted by regressing mean daily temperatures against the sine and cosine of the Julian date. Sin(day) and cos(day) were generated from the day number, which varied between 1 and 365. Leap years were treated as any other calendar year.

Table 10.5: Fourier analysis of mean daily temperatures, 1985-1990.

Place	high	low	amp	phase	r2	rms error (°C)
Amblsd	14.76	2.63	12.1	-19.7	0.706	2.765
Applby	14.50	2.15	12.4	-20.7	0.674	3.043
Asptra	14.57	3.21	11.4	-24.2	0.671	2.810
Clisle	14.68	3.23	11.5	-25.0	0.669	2.840
Crlclv	15.07	3.02	12.0	-26.0	0.672	2.977
Crlcov	13.43	1.51	11.9	-26.1	0.682	2.874
Durham	14.69	3.01	11.7	-26.2	0.696	2.726
Eskmls	14.84	3.88	11.0	-28.4	0.684	2.631
Gtdnfl	9.30	-2.20	11.5	-30.4	0.676	2.815
Hartbn	14.58	2.93	11.6	-26.4	0.676	2.847
Haydon	14.63	2.99	11.6	-24.6	0.665	2.922
Hghcls	13.64	2.54	11.1	-23.4	0.695	2.598
Houghl	13.95	4.31	9.6	-12.4	0.606	2.786
Kswick	15.37	3.95	11.4	-20.7	0.693	2.686
Kieldr	12.93	1.54	11.4	-23.4	0.670	2.870
Leemng	15.45	3.10	12.4	-24.7	0.690	2.928
Lwethr	14.13	2.22	11.9	-25.8	0.686	2.848
Nenthd	12.34	1.39	10.9	-22.2	0.662	2.774
Nwcstl	15.13	3.70	11.4	-27.5	0.689	2.715
Rdsdle	12.66	1.44	11.2	-25.6	0.679	2.724
Shap	12.89	2.93	10.0	-24.1	0.587	2.895
Sundld	15.06	4.11	11.0	-29.9	0.682	2.640
Warcop	13.58	2.34	11.2	-26.1	0.648	2.925
Whasdy	14.35	2.73	11.6	-23.8	0.693	2.735
Widdyb	11.68	0.02	11.7	-27.4	0.686	2.786
Wyclfe	14.71	2.97	11.7	-23.3	0.701	2.616

The phase lag in the annual curves varies between -12.39 days (the minimum temperature is expected on Jan 12) at Houghall, to -30.38 days at Great Dun Fell. The figures refer to the occurrence of the minima in days after Jan 1. Houghall data are unreliable because of the extremely short time period. Stations in the north-east experience a longer temperature lag behind solar radiation input than those in the north-west (Figure 10.6). The lag also increases towards the coasts, reaching nearly 30 days at Sunderland on the east coast and over 28 days at Eskmeals on the west coast. More surprising is the increase in lag at high altitude, illustrated in Figure 10.7 a. The mountain summit of Great Dun Fell records the longest lag, unexpected at high altitude, where traditionally the response to solar heating is thought to be extremely rapid due to the strong dependence of temperature on direct solar radiation. The relationship between phase lag and altitude is complex because both mountain stations (high altitude) and coastal stations (low altitude) show large lags, but for contrasting reasons.

There is a strong relationship between station exposure and lag (Figure 10.7 b). The outlying value of Great Dun Fell distorts the graph somewhat but phase lag decreases with increasing shelter (a higher exposure value). All stations with a short lag are sheltered inland sites where a lack of air movement encourages rapid response to solar heating. Phase lag is plotted against the distance from the nearest coast in Figure 10.7 c. One may expect the phase lag to decrease with increasing distance inland, because surface temperatures lag less behind solar radiation input in continental areas (Trenberth 1983). The actual relationship is not strong because of the effect of high altitude stations inland. The altitudinal effect outweighs any continental effect. If stations above 200 m are highlighted, they nearly all fall in the same region of Figure 10.7 d, confusing the relationship between phase lag and continentality.

Both phase lag and amplitude of the annual temperature signal are used as measures of continentality (Driscoll & Yee Fong 1992, Trenberth 1983, Prescott & Collins 1951) and the two should be correlated (Figure 10.7 e). Inclusion of the four stations with incomplete data (marked as 0) produces unusual values but when these are omitted (Figure 10.7 f), there is a weak negative relationship (phase lag increases as amplitude decreases).

Figure 10.6. Map of Phase Lag in the Annual Temperature Signal:
Mean Daily Temperatures

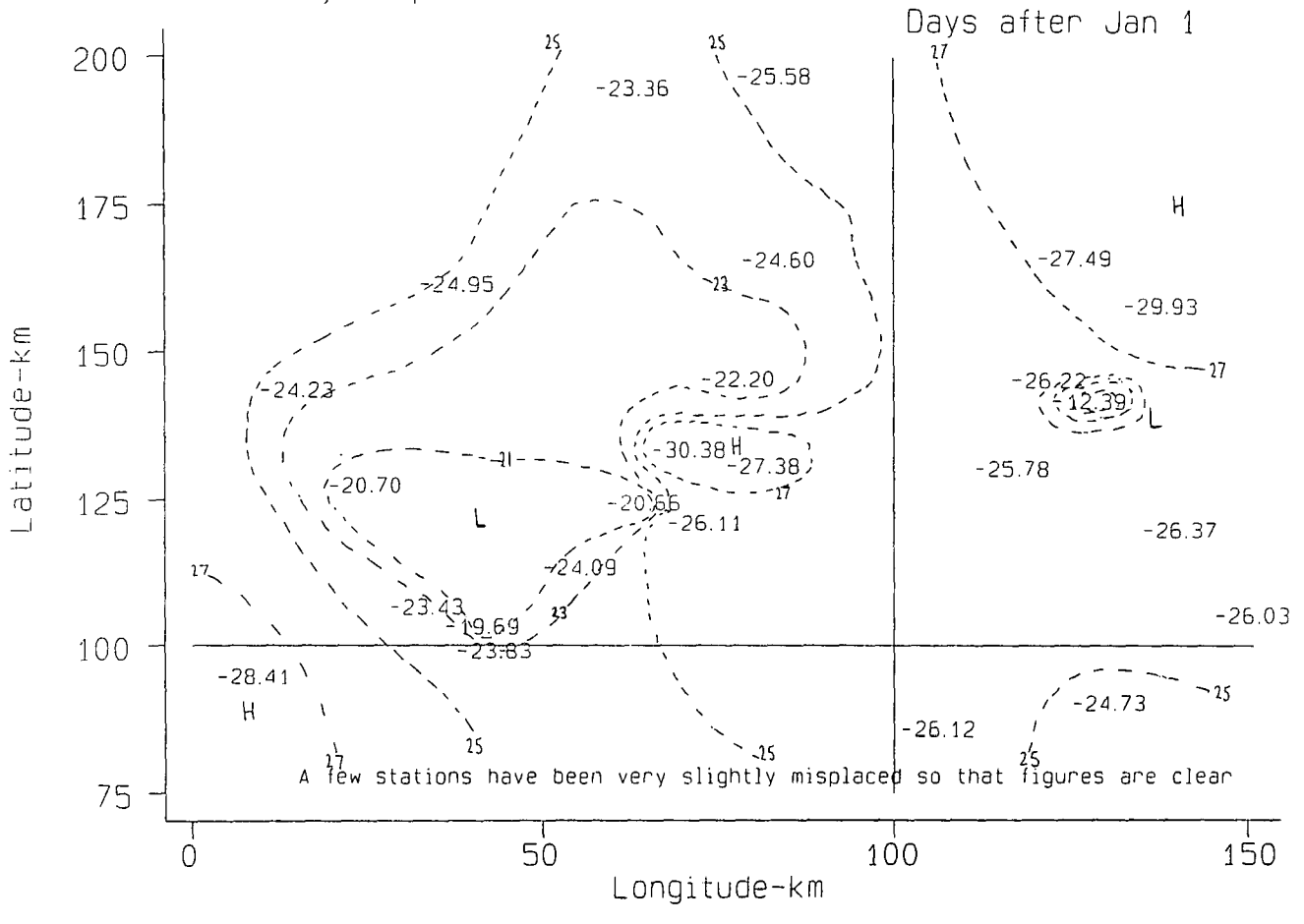

Figure 10.7. Relationships between Phase Lag in the Annual Temperature Signal and Environmental Factors

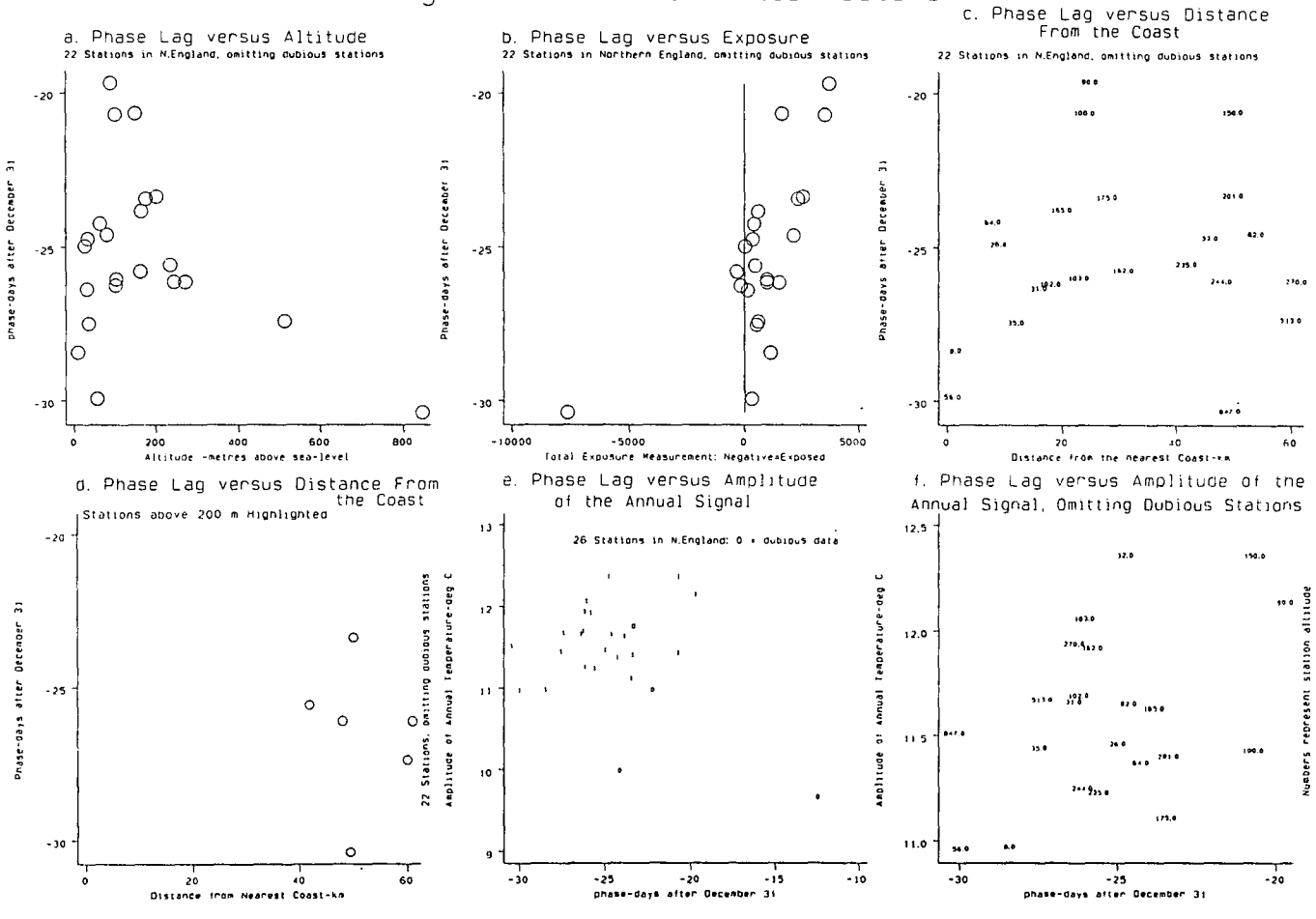

Table 10.6 lists starting and ending dates of the growing season (the period for which mean temperatures are 6°C or above) together with growing season length and strength for all locations (obtained from equations 5-9).

Table 10.6: Growing season parameters obtained via Fourier curves.

Place	Start Day	End Day	Season Length	Season Strength
Amblsd	84.2	320.2	236.0	1267.3
Applby	89.5	316.8	227.4	1193.2
Asptra	84.5	329.0	244.5	1274.8
Clisle	84.7	330.2	245.5	1295.2
Crlclv	86.5	330.6	244.1	1347.2
Crlcov	102.9	314.3	211.5	981.9
Durham	87.9	329.6	241.7	1281.2
Eskmls	81.3	340.5	259.2	1373.8
Gtdnfl	147.2	278.6	131.4	282.5
Hartbn	89.0	328.7	239.7	1256.8
Haydon	86.6	327.6	241.0	1269.5
Hghcls	92.3	319.6	227.4	1072.5
Houghl	62.6	327.2	264.6	1254.1
Kswick	71.5	334.9	263.3	1473.0
Kieldr	101.9	309.8	207.9	902.7
Leemng	83.5	331.0	247.4	1418.5
Lwethr	95.3	321.2	225.9	1135.5
Nenthd	104.2	305.2	200.9	801.9
Nwcstl	81.5	338.4	256.9	1409.7
Rdsdle	105.9	310.3	204.4	854.9
Shap	92.5	320.7	228.2	970.3
Sundld	79.7	345.2	265.4	1432.4
Warcop	96.7	320.6	223.9	1050.8

Table 10.6: continued

Place	Start Day	End Day	Season Length	Season Strength
Whasdy	88.8	323.9	235.1	1204.2
Widdyb	120.1	299.6	179.5	650.2
Wyclfe	85.2	326.3	241.2	1281.8

As altitude increases, mean annual temperature decreases at a rate of 6.85°C/km, the first date of the growing season gets later by 79.3 days/km, the last date of the growing season gets earlier by 68.4 days/km, and accumulated temperatures

Table 10.7: Regression of growing season parameters against altitude.

Parameter	Gradient	Constant	r2	error
max temp	-0.00689	15.17	0.879	0.475
min temp	-0.00681	3.72	0.854	0.522
mean temp	-0.00685	9.45	0.916	0.386
start day	0.0793	77.84	0.836	6.522
end day	-0.0684	334.32	0.836	5.624
season length	-0.148	256.48	0.884	9.943
season strength	-1.385	1387.02	0.879	95.56

above 6°C decrease by -1.385 d°C/m (Table 10.7). The delay in the start of the growing season in spring (with increasing altitude) is more rapid than the foreshortening in autumn. Thus the season is shifted to slightly later in the year at high altitude. Steep lapse rates in maritime air in spring are associated with the steep decrease in growth potential. For example, the first date of the growing season occurs around 20th March at Sunderland near the coast, whereas the equivalent date is 27th May at Great Dun Fell (847 m).

r^2 for all relationships in Table 10.7 is high (mostly well above 0.8). Over 80% of the variation in mean temperature, growing season length and strength is thus accounted for by altitude alone.

The length of the growing season is defined as the period of time over which the annual temperature curve is above the threshold (**b-a** in Figure 10.3). Length is plotted against altitude in Figure 10.8. There is a strong negative relationship. At sea-level a growing period of 256.5 days (over 8.5 months) is expected, falling to about 130 days (just over 4 months) at Great Dun Fell (847 m).

Growing season strength, derived from integration of the Fourier curve above the threshold (equation 9), is plotted against altitude in Figure 10.9. An annual accumulation of 1000 d°C is expected at 278 m. In order to reduce the expected accumulation to 500 d°C one must move up to 638 m. The altitude at which the accumulation would become zero, assuming a linear decrease, would be 998 m (i.e. approximately 1000 m). In reality temperatures commonly exceed 6°C at much higher altitudes than 1000 m in Scotland, as recorded on Cairngorm (Barton 1987) and Ben Nevis (Omond 1910). One of the disadvantages of the Fourier approach therefore is that it is possible for temperatures (especially during the day and at sites with a large diurnal temperature range) to exceed the threshold while the mean temperature signal remains below.

10.7 Application of Fourier Analysis to Examination of the Relationship between Growing Season Strength and Altitude

Arbitrary Fourier curves with set values of amplitude and mean temperature can be used to define the expected relationship between growing season strength and altitude. Two families of curves were created with amplitudes of 10°C and 20°C, representative of maritime and continental climates respectively. Accumulated temperatures were calculated for curves differing in mean temperature by 1°C. **m** was increased in 1°C steps from 0°C to 15°C in the maritime case (**A**=10°C) and from -8 °C to 20°C in the continental case (**A**=20°C).

Figure 10.8. Growing Season Length, Predicted From Fourier Analysis, versus Altitude

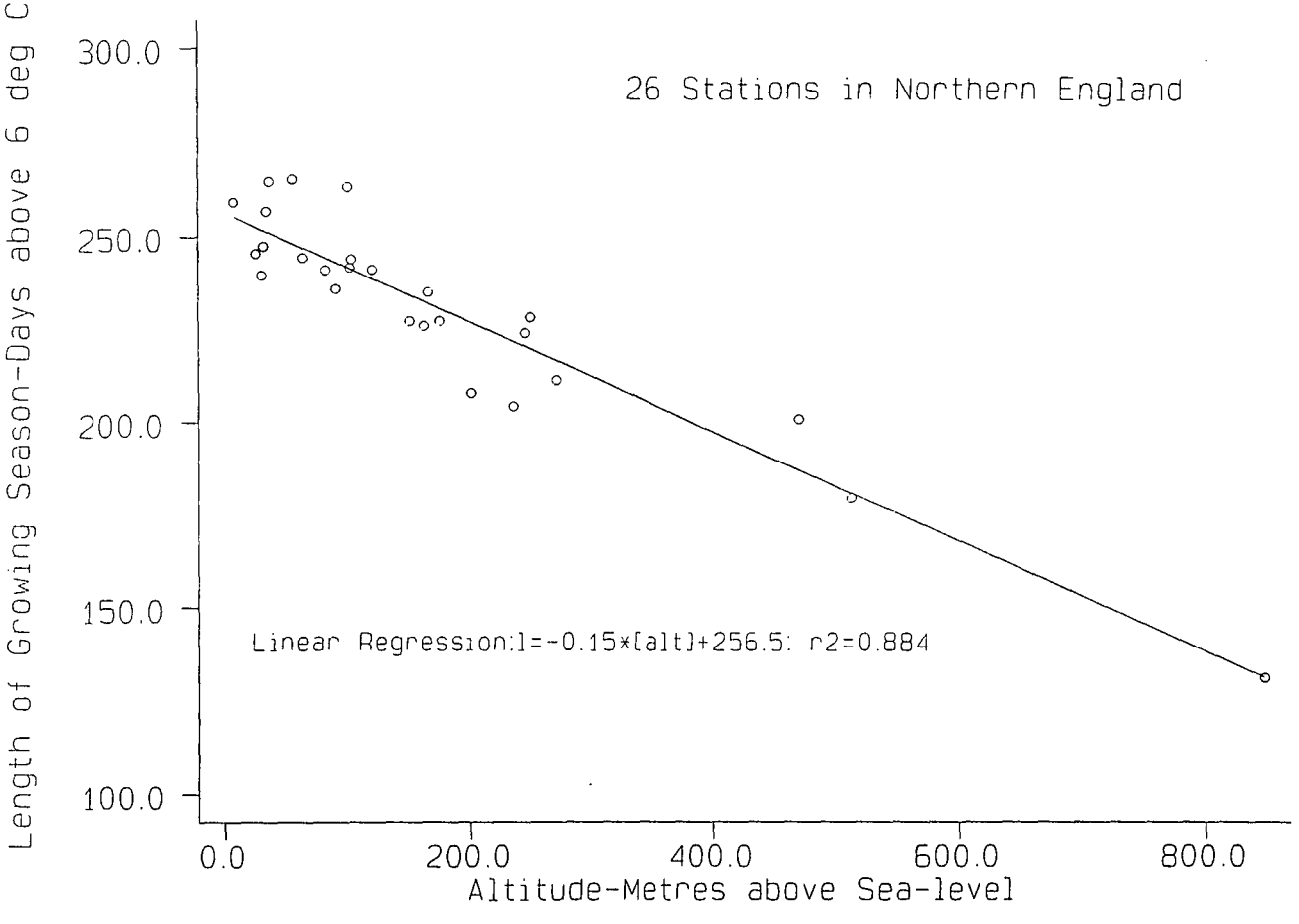

Figure 10.9. Growing Season Strength, Predicted From Fourier Analysis, versus Altitude

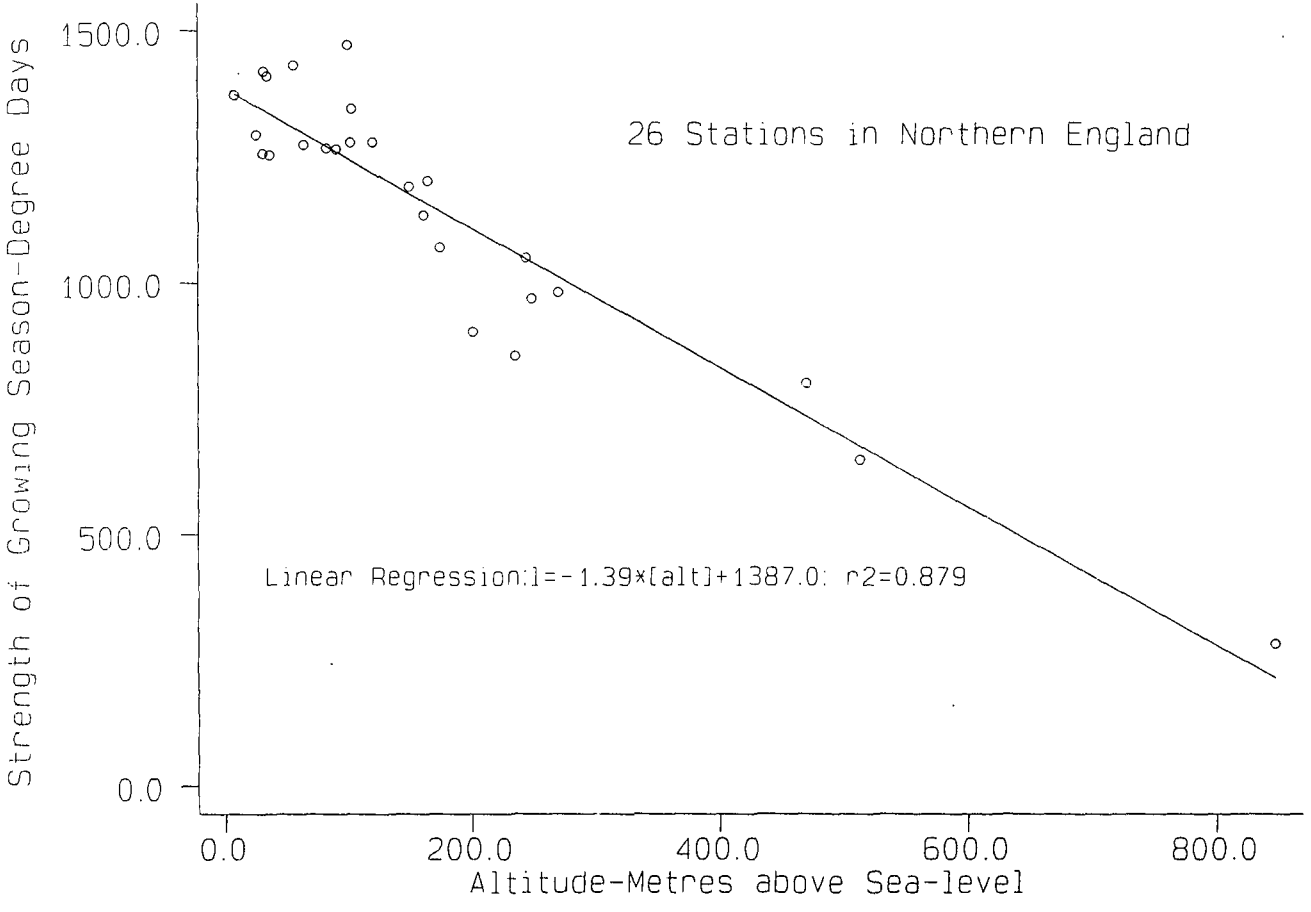

The change in growing season length as mean temperature increases is shown in Figure 10.10. The critical threshold is 6°C. A constant change in mean temperature can be assumed to be representative of changing altitude (assuming a constant lapse rate). When the mean annual temperature is 6°C the growing season is 182.5 days in length, irrespective of amplitude. The rate of change of growing season length with change in mean annual temperature is steeper in the maritime case, accounting for the rapid decrease in growth potential in the maritime uplands of Western Europe. In continental climates the effect of a given change in mean temperature on growing season length is less and mean annual temperature can stray further above or below 6°C before the growing season extends throughout the year or ceases to occur respectively. Thus maritime areas are more sensitive to global climate change (changes in mean annual temperature). The rate of increase in growing season length is very steep in the upper and lower portions of each curve. If **A**=10°C the change in growing season length between mean annual temperatures of 10 and 11°C is over 70 days.

The variation in growing season strength (measured by accumulated temperatures above 6°C) in relation to a constant rate of change of mean annual temperature is shown in Figure 10.11. Given any mean annual temperature, annual temperature accumulation is higher in a more continental climate because of the warmer summer. With mean annual temperatures at 6°C, the difference between the maritime (**A**=10°C) and continental (**A**=20°C) cases is over 500 d°C. As mean annual temperature rises above 6°C, the amplitude (representing continentality) of the temperature signal becomes less influential and the relative benefits of a continental climate diminish. At a mean temperature of 16°C both amplitudes create an annual degree-day accumulation of 3650 d°C. Mean annual temperature can be extremely low in a climate with a large annual temperature range and there is still an annual accumulation above 0 d°C. For example, in parts of Siberia the mean annual temperature range approaches 60°C and a mean annual temperature as low as -20°C would still produce a little growth in the short summer period with mean temperatures peaking at 10°C.

It follows that the rate of decrease in growing season strength with decreasing

Figure 10.10. Change in Growing Season Length as Mean Annual Temperature Changes, Given Two Contrasting Signal Amplitudes

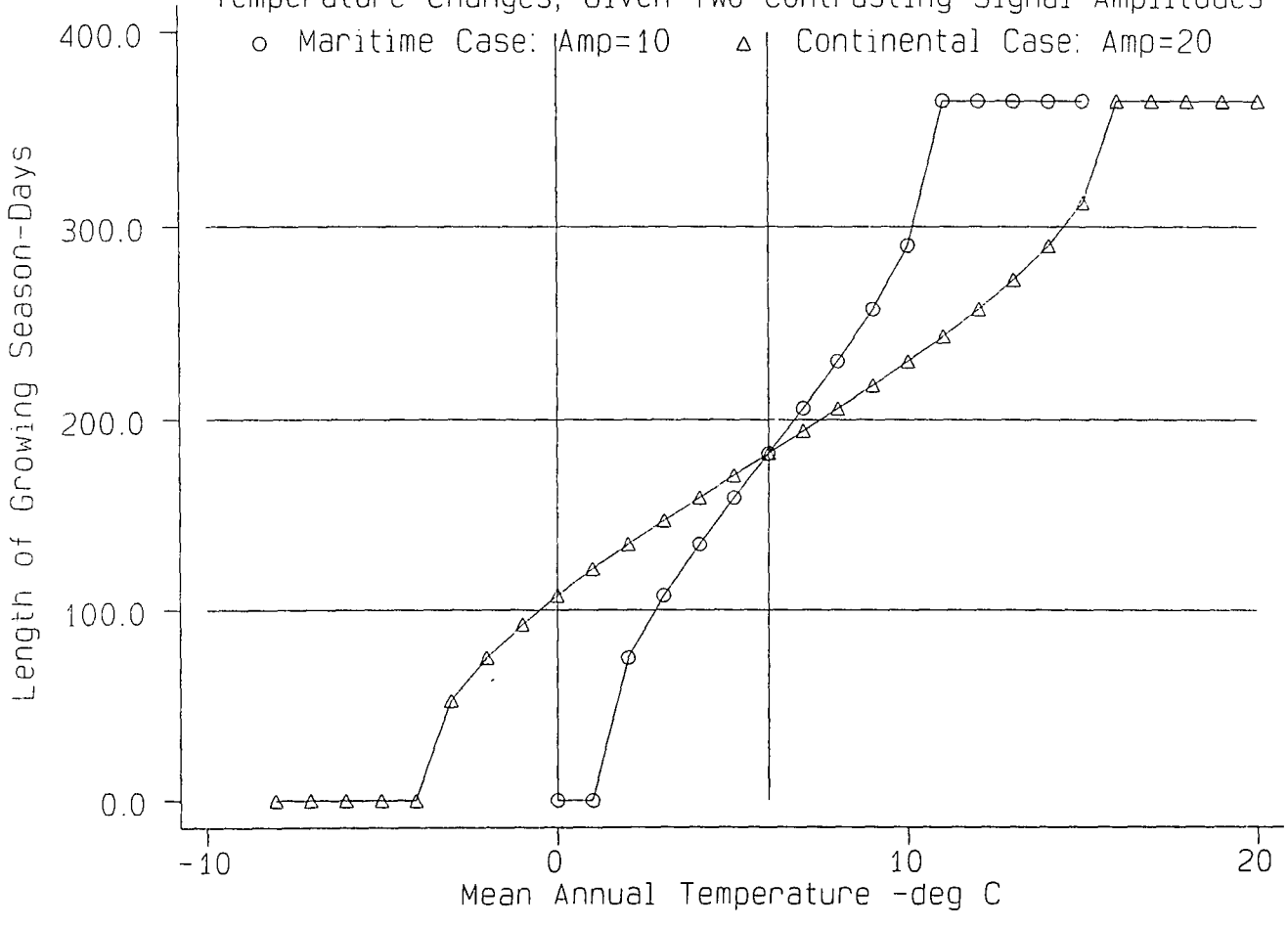

Figure 10.11. Change in Growing Season Strength as Mean Annual Temperature Changes, Given Two Contrasting Signal Amplitudes

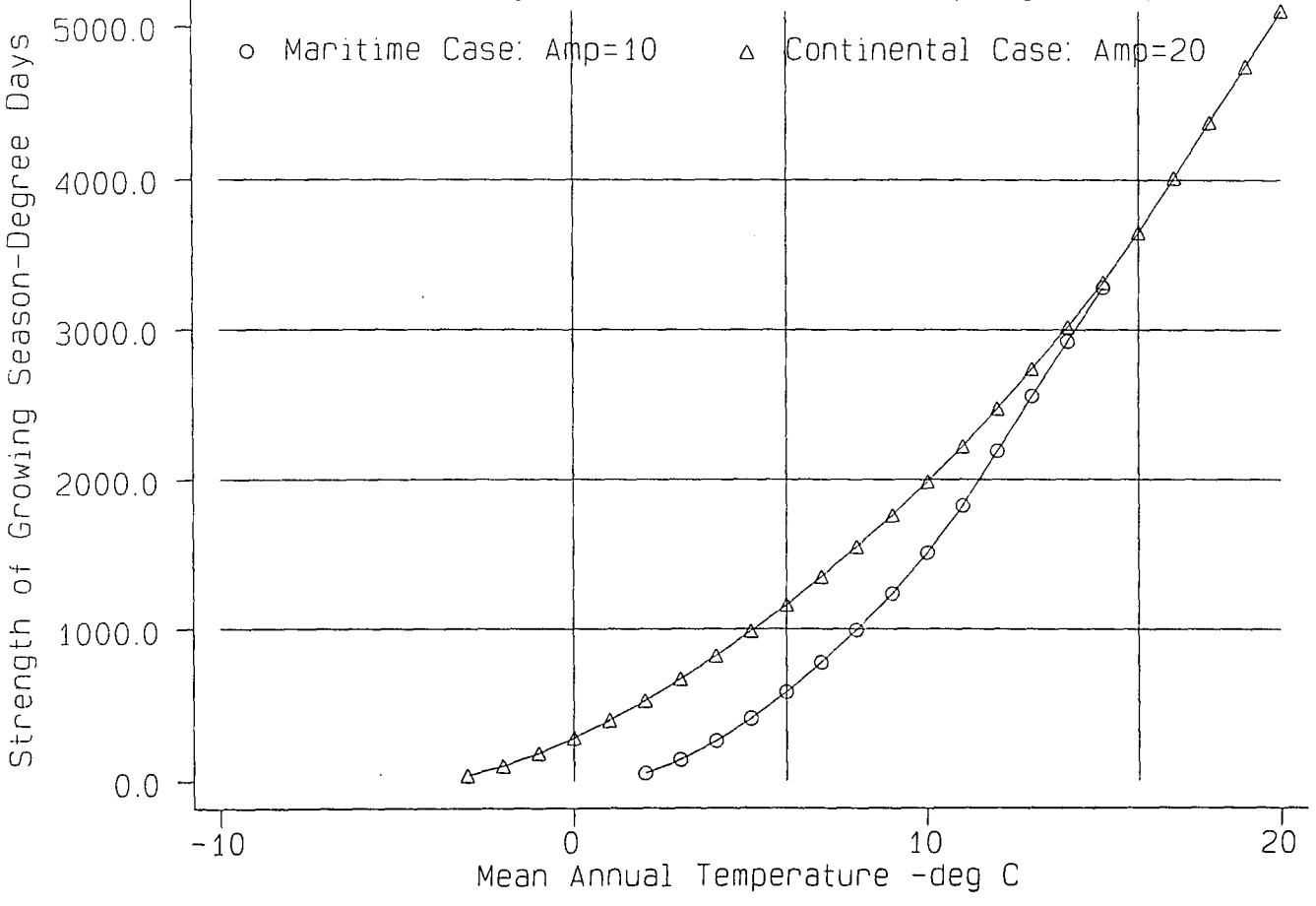

mean annual temperature is steeper in a maritime climate, especially when mean annual temperature is above the critical growth threshold. Thus the altitudinal decline in growing season strength is more rapid in parts of western Europe than in mainland Europe, despite similar mean annual temperatures. As mean annual temperature continues to decrease towards the threshold, the rate of decrease in growing season strength also decreases, supporting an exponential (or at least a form of non-linear) relationship between altitude and growing season strength. The decrease in mean temperature with altitude is assumed to be linear.

10.8 Robustness of the Growing Season/Altitude Regression

It is helpful to examine the robustness of individual regressions of accumulated temperatures versus altitude. Figure 10.12 shows five different regressions using the same data (mean accumulated temperatures over the six years versus altitude). Linear (1) and exponential (2) models have been described previously. The calculation of the dfbeta for altitude (DFalt), leverage and Cook's distance (Table 10.8) highlights the strong influence of Great Dun Fell.

Table 10.8: Robustness measures for the growing season strength/ altitude regression.

Place	DFalt	leverage	Cook's distance
Ambleside	0.01	0.05	0.00
Appleby	-0.00	0.05	0.00
Aspatria	0.03	0.06	0.00
Carlisle	-0.02	0.07	0.00
Carlton-in-Cleveland	-0.08	0.05	0.03
Carlton-in-Coverdale	-0.06	0.06	0.01
Durham	-0.02	0.05	0.00
Eskmeals	0.02	0.08	0.00

Figure 10.12. Five Different Regression Models of Mean Annual Accumulated Temperatures (deg days) versus Altitude (1985-1990)

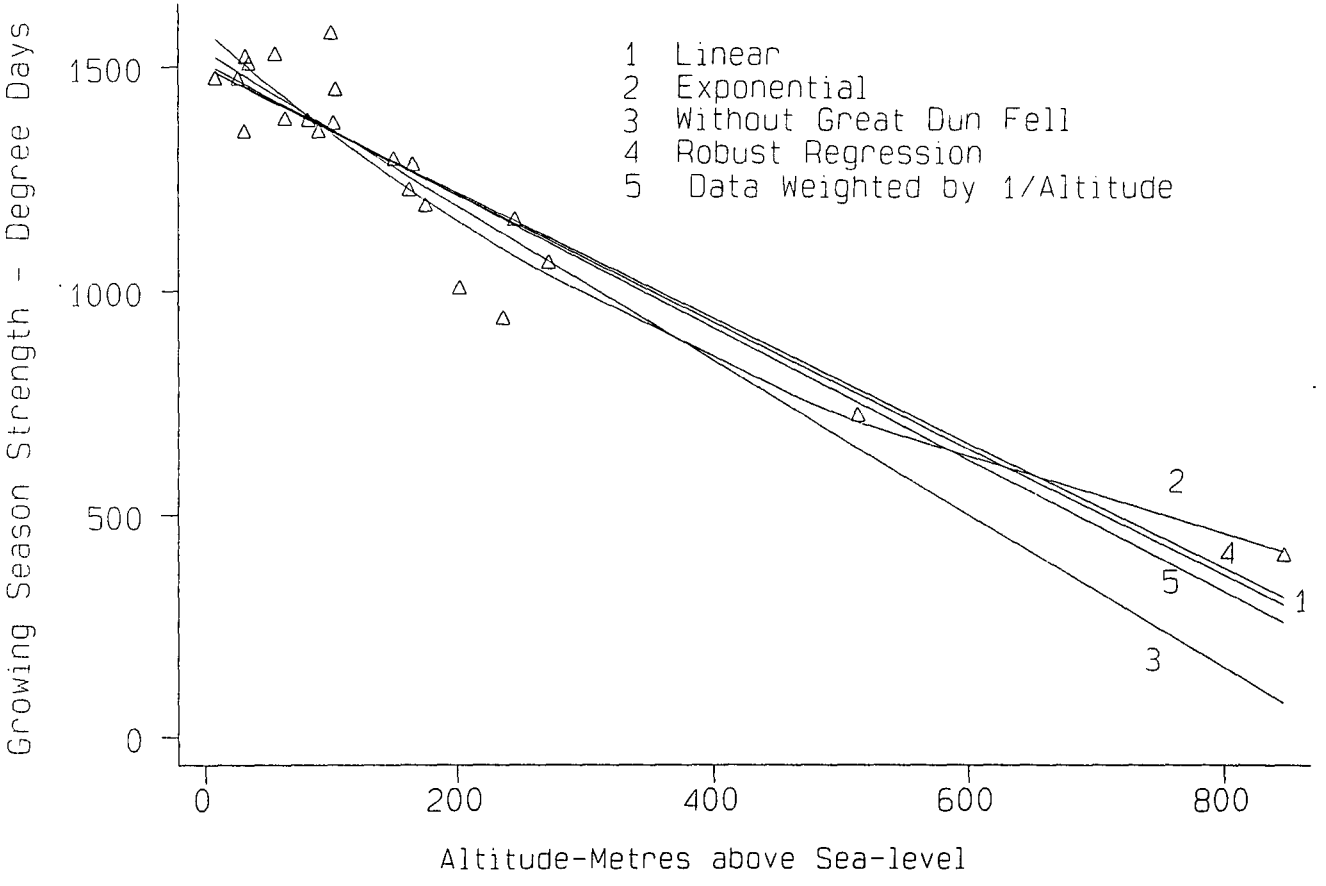

Table 10.8: continued

Place	DFalt	leverage	Cook's distance
Great Dun Fl	2.83	0.66	3.68
Hartburn Gr	0.16	0.07	0.04
Haydon Br	-0.00	0.06	0.00
High Close	-0.00	0.05	0.01
Keswick	-0.20	0.05	0.13
Kielder	-0.09	0.05	0.10
Leeming	-0.12	0.07	0.02
Low Etherley	0.00	0.05	0.00
Newcastle	-0.10	0.07	0.01
Redesdale	-0.20	0.05	0.14
Sunderland	-0.15	0.06	0.04
Warcop	0.01	0.05	0.00
Whasdyke Fm	-0.00	0.05	0.00
Widdybank	-0.22	0.20	0.03

Omission of Great Dun Fell produces regression line number 3, with a gradient of -1.72 d°C/m, as opposed to -1.42 d°C/m for the original regression. This change highlights the strong influence of the relatively high accumulated temperatures at Great Dun Fell in reducing the altitudinal gradient in accumulated temperatures. Robust regression (4) and a regression on weighted data in inverse proportion to altitude (5) give slightly different results. The remarkable warmth of Great Dun Fell raises questions about its representativeness. It is possible that the exposed nature of the station increases accumulated temperatures recorded because of the increased advection of relatively warm free air, especially in winter. It is therefore postulated that this relative warmth is widespread at high altitude. A mathematical approach (section 10.5) has already suggested the increased suitability of an exponential relationship between growing season strength and altitude. The steep gradient of -1.72 d°C/m, obtained

without Great Dun Fell, is considered to be too high.

10.9 Limitations of the Use of Accumulated Temperatures to Indicate Growth Potential

a) The use of a 6°C threshold temperature is simplistic. Studies of plant physiology indicate that different threshold temperatures are relevant for different crops. In the Pennine uplands there is little arable farming and the main land use is sheep grazing. The grass upon which sheep feed does not grow in a normal year until late April or even May. It would be useful to know the critical threshold temperature(s) for this grass, in order to create a more realistic set of growth conditions.

b) Growth indices using accumulated temperatures (e.g. Primault 1969) usually implicitly assume that the response of plant growth to temperatures above the threshold is linear, i.e. the rate of growth is proportional to the excess above the threshold. A few authors have developed more complex indices based on relationships between growth rate and temperature. The response of growth rate to a wide range of temperatures is not usually linear (Figure 10.13 a) but can be represented by an asymmetric bell-like curve (Figure 10.13 b) (Sutcliffe 1977). Three cardinal temperatures, i.e. the minimum (T_{min}) and maximum (T_{max}) temperatures at which growth can occur, and the optimum range of temperature over which the highest growth rate is maintained (T_{opt}) can be defined. T_{max} for most plants is over 35°C and in northern England growth rates usually increase up to the highest temperatures recorded (around 30°C). Thus the linear relationship can often be assumed when considering growth in a temperate climate. T_{min} is below zero for most plants and for many alpine species can be less than -7°C (Larcher 1975). T_{opt} for alpines is often in the range 10-20°C.

Methods for dealing with the complex relationship between plant growth rate and temperature are variable. Tyldesley (1978) represented a plant growth/temperature curve as a series of straight line segments. Accumulated temperatures relevant to an individual plant could be calculated using given formulae. The example given concerned

Figure 10.13 Responses of Plant Growth to Temperature

T_{min} represents the threshold which is usually taken as 6°C

The linear response does not take the adverse effect of extremely high temperatures into account.

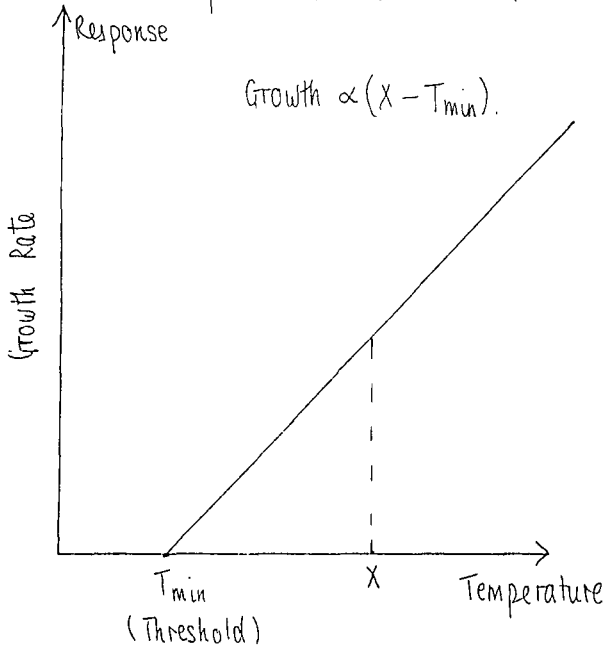

a. Simple Linear Response.

The bell-shaped curve is the most accurate representation of the growth rate (see Sutcliffe 1977).

T_{min} = Threshold Temperature

T_{opt} = Optimum Growth Temperature

T_{max} = Highest Temperature for which Growth Occurs

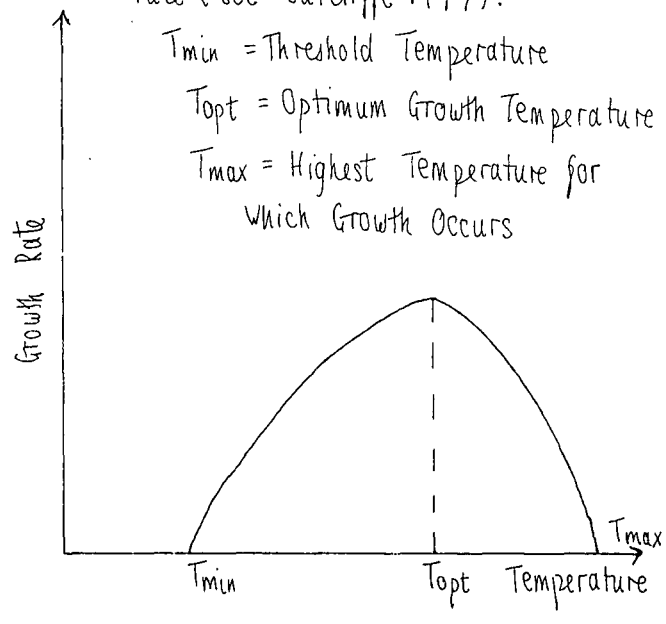

b. Asymmetric Bell-Shaped Response

The logistic curve can be used to approximate the rising limb of the growth curve between T_{min} and T_{opt}. The decline above T_{opt} is not modelled.

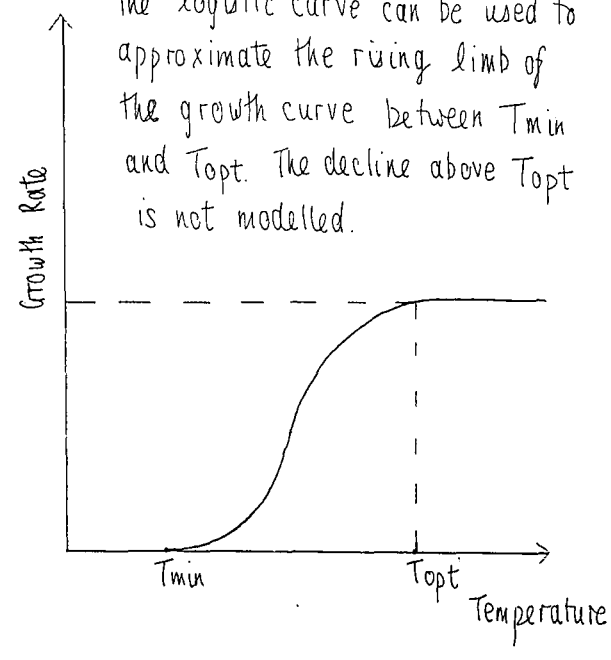

c. Logistic S-Shaped Approximation

the sporulation of a wheat fungus. Utaaker (1968) weighted temperature excess above the critical threshold according to the relative respiration rate at that temperature compared with that at 10°C. Accumulated temperatures calculated in this manner for Norway spruce (Picea aries) showed that the decrease in "growth potential" with altitude was steepest in spring. One warm day in spring was seen to have a larger beneficial effect than a week of warm weather in autumn.

Another method involves fitting a logistic S-shaped curve to growth rate variation (Figure 10.13 c). Plant response, after a poor start, increases rapidly in the central temperature range and then slows as higher temperatures are reached. The turning point A is half way between T_{min} and T_{opt}. The dotted part of the curve is often irrelevant in northern England since heat stress is virtually unknown, especially in the uplands. Hence the logistic approximation is suitable.

c) Using a threshold temperature, below which growth is assumed to cease, tells us nothing about the periods of time for which temperatures are above or below the threshold. The amount of time with temperatures above the threshold on a daily basis can vary, given a similar mean daily temperature, depending on diurnal temperature range. A mean daily temperature of 6°C may be calculated from a daily maximum of 10°C and a minimum of 2°C. The temperature would be above the critical threshold for about half of the day (probably during daylight). Any analysis based on degree days alone would assign no growth to that day because of the mean temperature of 6°C. A similar problem is evident when mean monthly maxima or minima are used. A mean daily maximum of 5°C over a month may conceal several days when the maximum temperature rose above 6°C. The overall accumulated degree day figure would be negative. In any cumulative analysis, fluctuation above and below the threshold on a timescale less than the unit of analysis (in the last example the month) is ignored. The final accumulation is the sum of all positive excesses above the threshold and deficits. Negative values will often cancel out some positive contributions, leading to an erroneous answer as only positive values above the threshold should contribute to the result (Thom 1954).

10.10 Conclusions

There is a wide inter-annual fluctuation in growing season strength in northern England. In the linear model, growing season strength decreases by between 1 and 1.5 d°C per metre increase in altitude. Taking 1000 d°C as the critical limit for tree and plant growth, land between 236 and 463 m is referred to as marginal because accumulations only exceed 1000 d°C in some years. Calculations using a digital terrain model (DTM), described in Chapter 4, show that approximately 30% of the land in northern England lies between these altitudes (Figure 10.2). The variation of over 200 metres in the theoretical cultivation limit between years is on the same scale as the decline in critical cultivation altitudes over 300 years within the Lammermuir Hills, documented by Parry (1978). Thus, the study area is extremely sensitive to small inter-annual changes in mean temperature.

In the exponential model land between 191 and 420 m is marginal (about 35% of the total land area). This model appears to perform slightly better than a simple linear model and leads to lower limits. Both linear and exponential models of the altitudinal decrease in growing season strength lead to large amounts of marginal land. It is therefore interesting but not crucial to decide which is the more realistic. The absence of many high level stations makes this difficult since evidence for the exponential trend is based largely on observations at Widdybank Fell and Great Dun Fell (section 10.7). A mathematical approach suggests superiority of the exponential relationship (section 10.5).

Accumulated temperatures are only one indicator, although probably the single most useful measure, of what may be loosely termed "climate potential". Therefore the following two chapters concentrate on the length of the growing season and frost occurrence respectively.

OTHER MEASURES OF GROWTH POTENTIAL

11.1 Introduction

In Chapter 10 "growth potential" was estimated by accumulating the excess of daily mean temperatures above 6°C. The problem with the use of degree days, however, is that calculations are sensitive to the time period of measurement and the length of the growing season is ignored. It may be important whether the period of time with temperatures above the threshold is continuous or interrupted.

11.2 Calculation of Growing Season Length

In calculating the length of the growing season, growth was assumed to occur if the daily maximum temperature rose above 6°C. A binary categorical variable was created for each station equal to 1 (signifying a "growing day") if the daily maximum temperature was above 6°C, and 0 otherwise. For each year from 1985 to 1990, days were numbered from 1 to 365 (1 to 366 in 1988) and the following indicators of growth occurrence were calculated:

a. first growing day;
b. last growing day;
c. total number of growing days;
d. first consecutive growing day in spring;
e. last consecutive growing day in autumn (i.e. all days between **d** and **e** are growing days);
f. number of consecutive growing days (calculated as **(e-d)+1**).

Mean values calculated over six years are shown in Table 11.1 for a few locations.

Table 11.1: Growth indicators (1985-1990).

Place	a	b	c	d	e	f
Amb	7 Jan	30 Dec	313	1 Apr	16 Nov	229
App	8 Jan	29 Dec	305	12 Apr	18 Nov	222
Dur	7 Jan	29 Dec	315	31 Mar	19 Nov	234
Esk	2 Jan	31 Dec	332	24 Mar	22 Nov	244
GDF	12 Mar	9 Dec	191	7 Jun	24 Sep	110
Htbn	8 Jan	29 Dec	314	5 Apr	15 Nov	225
Kield	8 Jan	29 Dec	289	19 Apr	14 Nov	211
Nwc	7 Jan	29 Dec	315	15 Apr	19 Nov	219
Sund	3 Jan	30 Dec	322	4 Apr	19 Nov	230
Wid	11 Jan	27 Dec	245	7 May	23 Oct	170

The mean date of the first growing day is nearly always near the beginning of January, as growth occurs sporadically throughout the winter. For a similar reason, the last growing day is nearly always near the end of December. In many years dates are similar at many locations, e.g. Jan 9 and Dec 30 in 1986 and Jan 1 and Dec 31 in 1988. Great Dun Fell is an exception, the first growing day not occurring on average until March 12. The relevance of the first and last growing days is limited since after the first growing day there is always a return to cold conditions. The first and last dates with maxima above 6°C would be more meaningful in a continental climate with a large seasonal variation in temperature. In northern England days with maxima over 6°C occur throughout the winter, especially in lowland and coastal areas.

Table 11.2 lists regression coefficients for indicators **c** to **f** against altitude (Figure 11.1).

Figure 11.1. Relationships between Growing Season Length and Altitude (Metres above Sea-level)

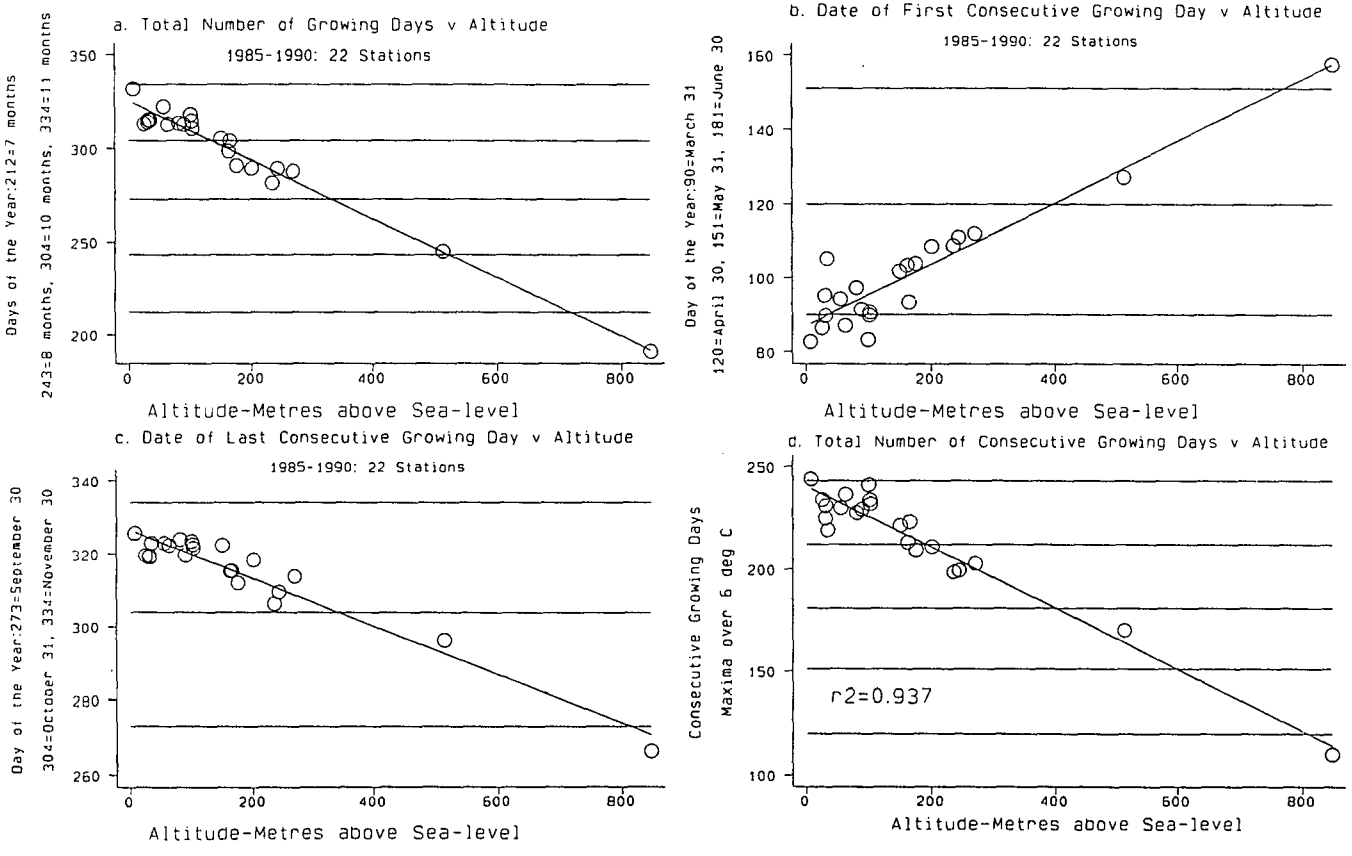

Table 11.2: Regression parameters for growth indicators **c**, **d**, **e** and **f** against altitude.

Indicator	Gradient	Constant	r^2
c	-0.157	325.3	0.971
d	0.083	86.9	0.880
e	-0.066	326.4	0.922
f	-0.149	240.5	0.937

The constant term represents the predicted value of the growth indicator at sea-level. The total number of growing days (**c**) decreases with altitude (Figure 11.1 a). r^2 for the linear regression is very strong (0.971). The total number of growing days ranges from 332 at Eskmeals on the west coast (equivalent to 11 months) to 191 at Great Dun Fell (just over 6 months). Most lowland areas record about 300 growing days per annum. There is a mean decrease of one day for every 6.4 metres rise in altitude. The number of consecutive growing days (**f**) must be used to define the length of the continuous growing season. The average date of the first consecutive growing day (**d**) is plotted against altitude in Figure 11.1 b). At sea-level, dates at the end of March or in early April are expected. This is delayed to late April at 200 m, early May at Widdybank Fell (513 m), and early June at Great Dun Fell (847 m). There is a two month contrast between Great Dun Fell and sea-level. A similar relationship is shown for the mean date of the last consecutive growing day (**e**) (Figure 11.1 c) which occurs in late September at Great Dun Fell, late October at Widdybank Fell and mid-November in lowland areas. The rate of change is one day per 15 metres, less than the rate of one day delay per 12 metres at the beginning of the consecutive growing season.

The total number of consecutive growing days (**f**) decreases from 244 at Eskmeals (a growing season of 8 months) to 110 days at Great Dun Fell (below 4 months). Thus the length of the growing season is more than halved at Great Dun Fell in comparison with sea-level. The relationship (Figure 11.1 d) is strong with r^2 equal to 0.937 and a gradient of 1 day per 6-7 metres. The number of consecutive growing

days (**f**) is usually about 90 days fewer than the total number of growing days (**c**).

Values may show a considerable range between years. Regression lines for **f**, the number of consecutive growing days plotted against altitude, are slightly different in each year (Figure 11.2). The altitudinal decrease in season length was twice as steep in 1990 as in 1985. Thus conditions in 1990 were beneficial in lowland areas but not at Great Dun Fell. The variation in the altitudinal gradient of growing season length is related to synoptic patterns. 1985 was a year with a wet cool summer but devoid of cold snaps in spring and autumn. As a result the length of the growing season was 4.5 months at Great Dun Fell, a better than average figure, but the season failed to reach 8 months at coastal locations. In 1990 a mild winter at low levels extended the season beyond 9 months at Sunderland while cold snaps in early June and September at Great Dun Fell reduced the season to 99 days. The altitudinal gradient in season length was very steep in 1990.

An alternative approach would be to calculate the period of the year when daily maximum temperatures are expected to be above 6°C from a seasonal curve of mean maxima, extracted by Fourier analysis (Conrad & Pollak 1950). Using this method, a number of stations give the consecutive growth period as 365 days because mean daily maxima never fall below 6°C (Eskmeals, Haydon Bridge, Keswick, Newcastle and Sunderland). The Fourier method overestimates growing season length due to its reliance on mean daily maximum temperatures.

11.3 The Conversion of Growth Occurrence to the Probability of Growth

The occurrence of growing days around the calendar year can be converted to probabilities that express the chance on that calendar date that the maximum temperature will be above 6°C. It is possible that on any calendar date growth occurs in any number of years between 0 and 6. For each day a variable was created, consisting of the number of years in which growth occurred, divided by 6. Growth in all six years leads to a value of 1 and no growth, to a value of 0. The variable, a crude estimate of growth probability, was averaged within five day bands (pentads) to provide

Figure 11.2. Annual Linear Regressions (1985-1990) of the Length of the Consecutive Growing Season versus Altitude

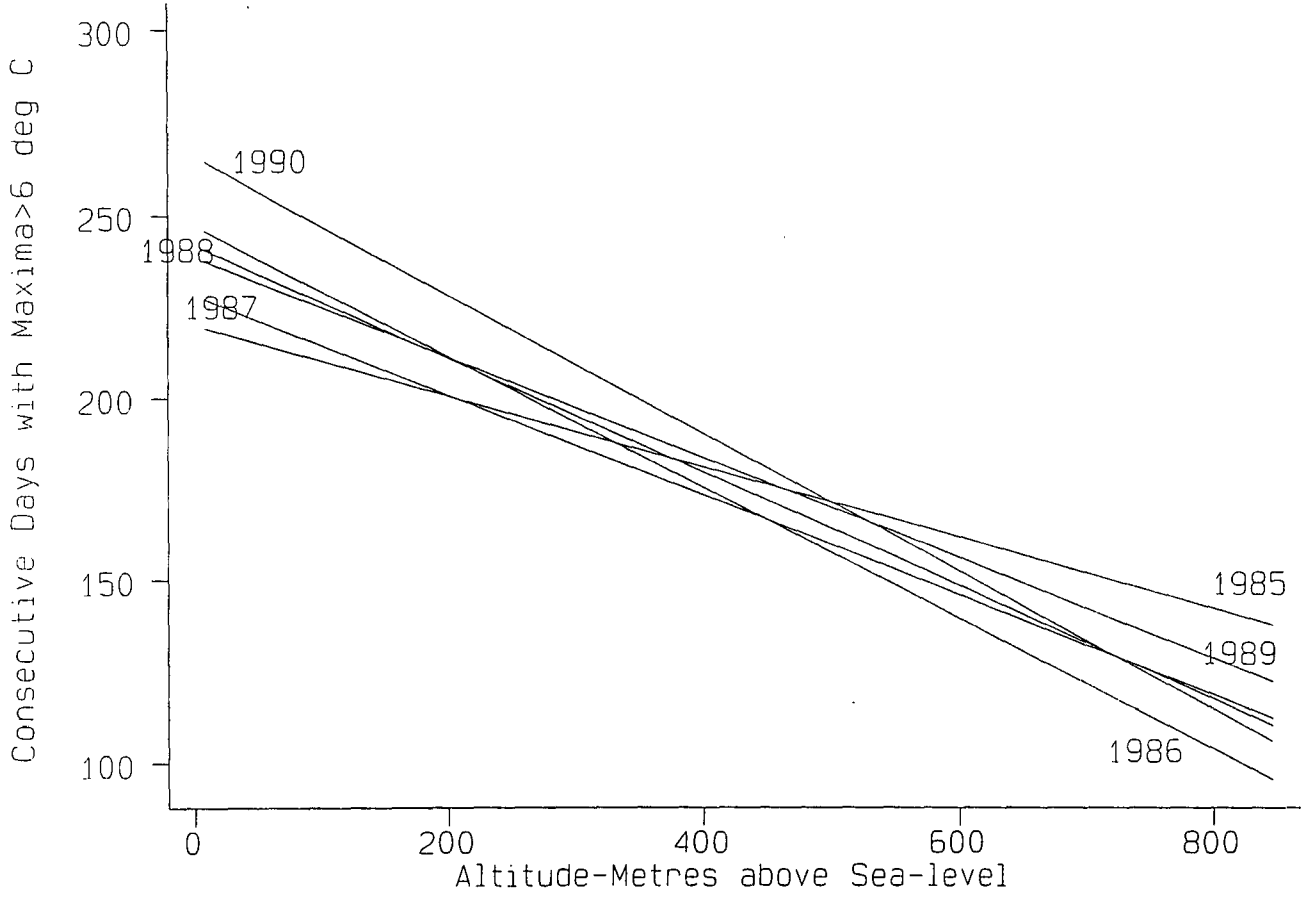

stability. Figure 11.3 plots this estimate for four locations; Great Dun Fell, Widdybank Fell, Appleby and Sunderland. Great Dun Fell shows low probabilities of growth (near zero) from December to March and a short period with high growth probability from mid-June to mid-August. By September the probability has fallen to 0.9 (90%). Lines on Figure 11.3 join the median values in each month. At Widdybank Fell the consecutive growing season (with growth probability equal to 1) lasts over 4 months. Probabilities of maxima over 6°C in winter fall to about 0.2 (20%). Sunderland is sited on the coast and has a period of over six months when the growth probability is 1. Probabilities in November and December are still high due to the warming influence of the North Sea. Even in mid-winter probabilities are over 50%. Finally, Appleby exhibits a long consecutive growth period but low probabilities in winter, typical of an inland valley site.

Inter-diurnal variability often masks any smooth annual trend in growth probability. This can be eradicated by smoothing. **Robust locally weighted regression** with Cleveland's (1979) tricube weighting function was used, variously called lowess or loess (Hamilton 1992). The **bandwidth**, which controls the amount of smoothing, was set at 0.5, i.e. half the "data length" (six months). Thus when a probability is derived for a particular date, values up to three months either side of that date affect the result. Smoothing on one year's data (running from day 1 to 366) means that the probability on day 366 can be very different from the probability on day 1! At Sunderland there is a considerably higher growth probability at the end of December than at the beginning of January. A solution is to replicate the data and place copies fore and aft, thereby creating three identical years. The smoothed curve for the middle year will "wrap round", with the probability on day 366 connecting smoothly to that on day 1.

Resulting growth probability curves are shown for all locations, using a similar probability scale, in Figure 11.4. Four curves are irregular, being based on less than six years data (Houghall, Nenthead, Shap, Wycliffe Hall). Growth probabilities approach 1 during summer at all sites. Probabilities at Great Dun Fell are considerably lower than at other locations for much of the year, falling to 0.1 in mid-winter. Figure

Figure 11.3. Occurrence of Growing Days (Maxima>=6 deg C) by Pentads, Expressed as a Growth Probability

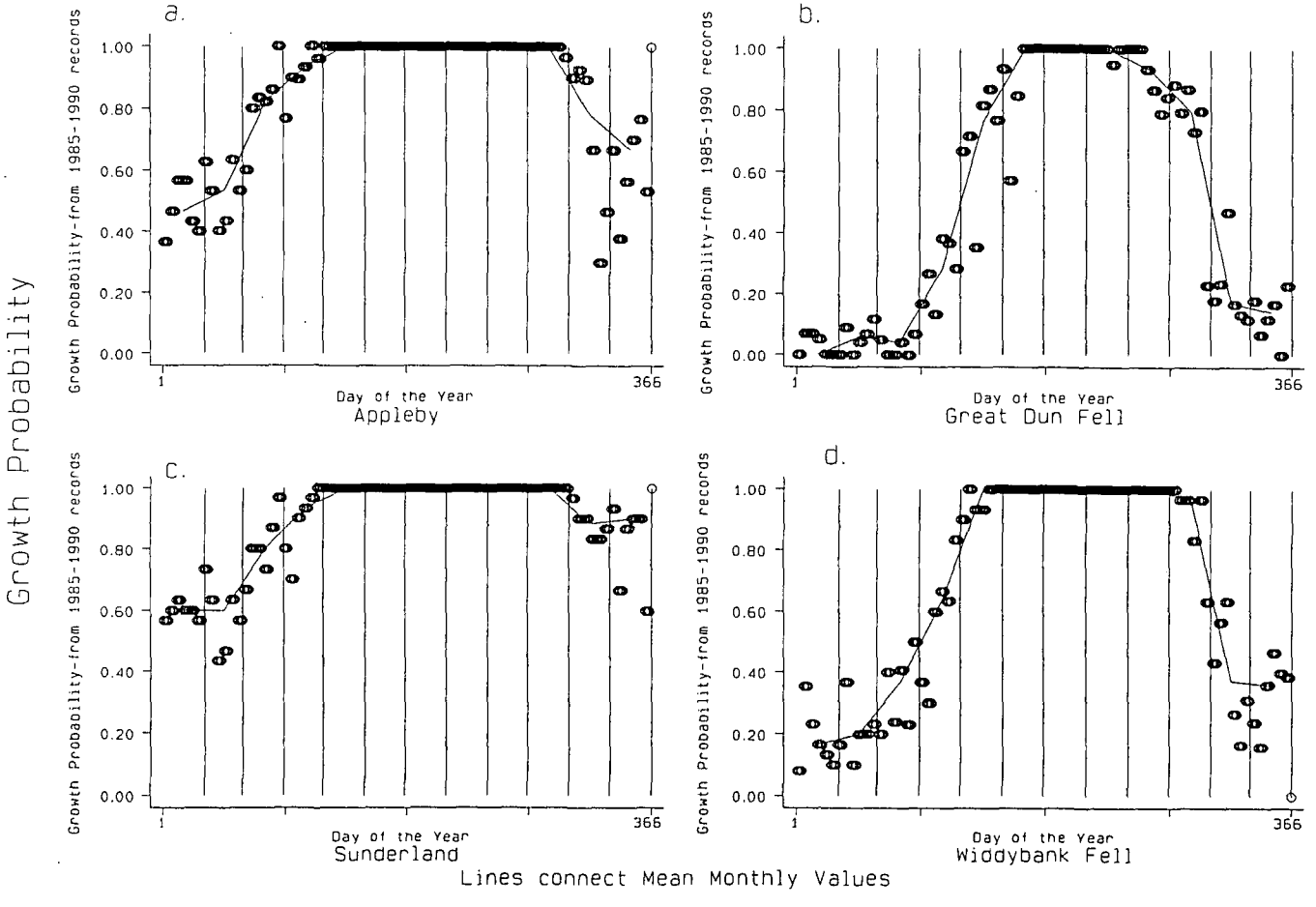

Figure 11.4. Curves of Growth Probability for all 26 Stations

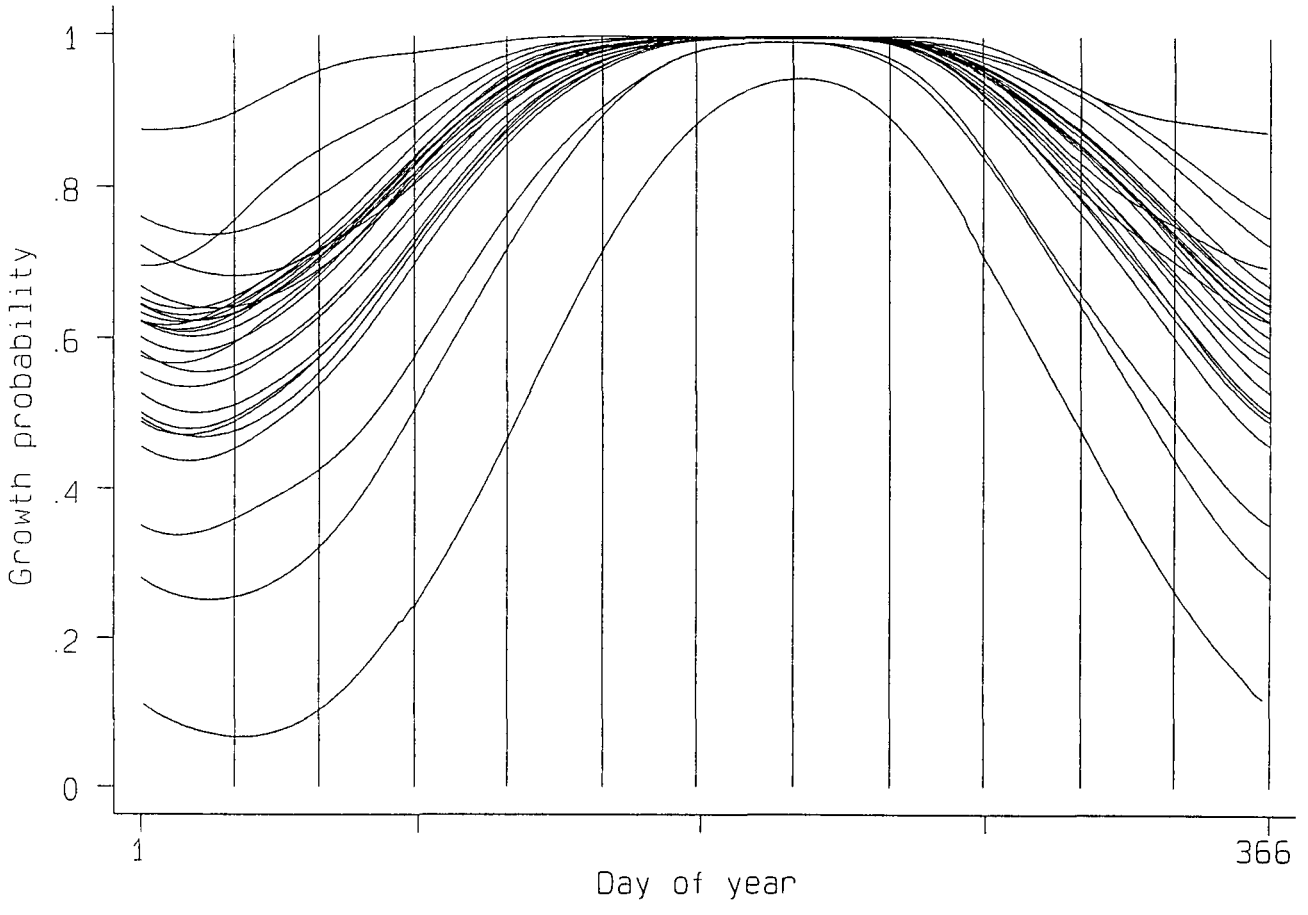

11.4 could be especially useful for prediction as growth probability can be interpolated for any calendar date.

Growth probability curves for a selection of stations are shown in Figure 11.5 along with the original data. The discussion below applies to Great Dun Fell. Maximum growth probability of 0.944 is recorded on August 3 and the minimum of 0.068 is recorded on February 3. By coincidence these extremes appear six calendar months apart. The curve does not have to be symmetrical or even smooth as a few kinks in Figure 11.4 indicate. Temperature singularities (Lamb 1950) may be to blame. To calculate the amount of time that the growth probability function is above or below certain thresholds is possible. Table 11.3 gives examples at Great Dun Fell and Ambleside. The bracketed figures represent the proportion of a year of 366 days.

Table 11.3: Periods above growth probability thresholds.

	Days above threshold	
Prob Threshold	Great Dun Fell	Ambleside
10 %	312 [0.85]	366 [1]
25 %	245 [0.67]	366 [1]
50 %	178 [0.49]	366 [1]
75 %	112 [0.31]	262 [0.72]
90 %	56 [0.15]	185 [0.51]
95 %	- [0]	153 [0.42]
99 %	- [0]	103 [0.28]
99.9 %	- [0]	51 [0.14]

85% of the year at Great Dun Fell has a probability of growth over 0.10 (10%) but less than half the year (49%) has a growth probability over 50%. The probability function never reaches 0.95 in summer and there is no period applicable to the last three probabilities in the table. At Ambleside growth probability is always above 0.5. The lowest value (0.608) is recorded on January 15 and the highest (0.999+) on July

Figure 11.5. Smoothed Growth Probability Curves at Four Sites

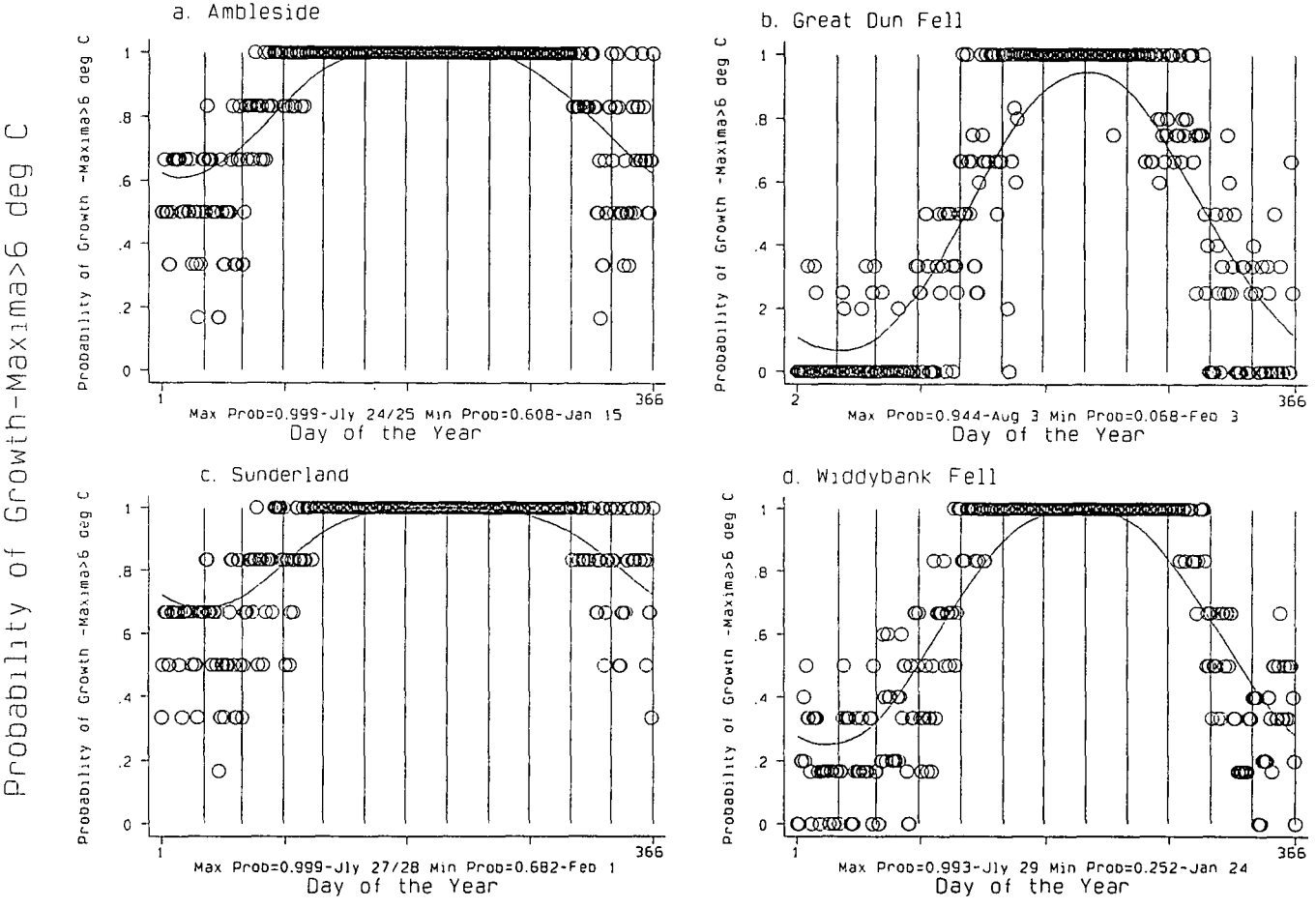

bandwidth=six months All Curves are smoothed by Lowess and are wrapped round

24/25. Probabilities remain above 0.999 for 51 days (14% of the year) and over half the year is associated with probabilities above 0.9. The curve is subjective, especially with regard to extreme values, since the smoothness of the curve depends on the bandwidth chosen. If bandwidth is decreased there is less smoothing and extreme probabilities are amplified.

A useful way of plotting the "growth probability function" is against days away from the winter solstice (Figure 11.6) (Beck 1992). The variable plotted on the x-axis varies from 1 at the winter solstice to 183 at the summer solstice. The value for both equinoxes is around 91. This x-axis variable is a proxy for noon solar elevation, in turn a proxy for solar radiation input. The year is plotted as a curve which forms a closed loop. For the growth function the loop must be followed anticlockwise. A marked lag in growth probability behind solar forcing is shown. Growth probabilities in spring are much lower than corresponding values in autumn and the curve exhibits hysteresis. The area enclosed by the curve relates to the lag in maxima behind solar radiation. If lag is non-existent the loop simplifies to a linear relationship between day value and growth probability.

Many stations show evidence of pointedness at the summer solstice, indicating uniformly high growth probabilities at this time (e.g. Ambleside). In contrast, at Great Dun Fell, growth probability increases a fair amount after the summer solstice. At Sunderland the lowest probability (below 0.7) is delayed until well after the winter solstice. There is a large contrast between probabilities on the rising and falling limbs at 50 days from the winter solstice. The two upland localities show similar patterns at both solstices. Lowland sites exhibit a steeper change in growth probability per day at the winter solstice than at the summer solstice. Growth probability at the autumnal equinox can be nearly as high as at the summer solstice (e.g. at Sunderland) and the probability at the vernal equinox almost as poor as at the winter solstice (e.g. Great Dun Fell and Sunderland). Slight kinks in the Great Dun Fell graph in April and September may be connected with temperature singularities (Lamb 1950).

Figure 11.6. Growth Probability Plotted Against Days Away from the Winter Solstice

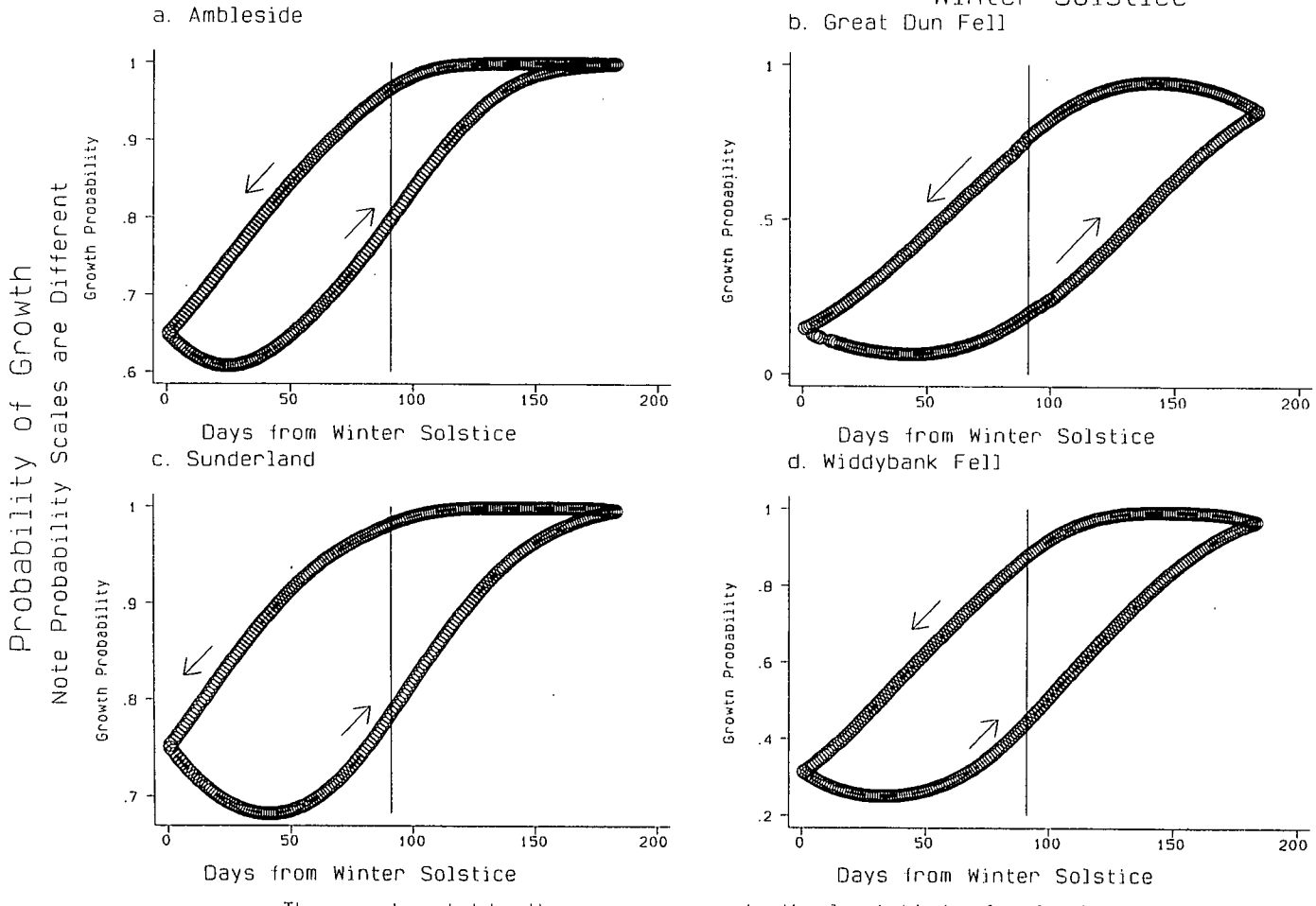

The area bounded by the curve represents the lag behind solar forcing

11.4 Conclusions

This chapter has illustrated the altitudinal gradient in growing season length in northern England, concentrating on the occurrence of growing days with maxima above 6°C. The total number of (consecutive) growing days shows a strong negative correlation with altitude, although actual dates of the first and last (consecutive) growing days often do not show such a close fit with altitude. The graphic techniques employed here will be used in the following chapter to investigate frost probability. Then growth and frost probabilities will be compared.

MEASURES OF FROST RISK

12.1 Introduction

Previous chapters introduced the concepts of **growing season strength** and **length**, describing their altitudinal variation within northern England. The third climatic measure to be investigated is the risk of frost. The growing season itself is sometimes defined as the interval between the last "killing" frost of spring and first "killing" frost of autumn because the most serious threat to agricultural development in many areas is low minimum temperatures occurring in spring and autumn. The length of the frost-free period has often been used as an indicator of growth potential (Hess et al. 1976). Vedin (1990) examined changes in the frost-free period in Northern Sweden using air threshold temperatures of 3°C and 0°C, taking account of the fact that ground minima are always lower than air minima. Nkemdirim & Venkatesan (1985) examined the frost-free season in Canada, east of the Rockies, delimiting three regions. The length decreased from east to west. The frost-free period was also used to define growing season length in Wisconsin (Moran & Morgan 1977), Minnesota (Skaggs & Baker 1985) and the south-eastern USA (Suckling 1989).

In temperate environments fluctuations of air temperature around freezing point are also of interest as they control **freeze-thaw** processes. Freeze-thaw cycles may increase in frequency up to a certain altitude but then decrease above this as temperatures fall consistently below freezing. This is the case in the Rockies (Fahey 1973) and Carpathians (Hess et al. 1976).

At very high altitudes in the tropics frost can occur on every night of the year and there is no frost-free period. At intermediate altitudes, such as the higher parts of the Nilgiri Hills in Southern India, radiation frost is restricted to the dry season. Frost is feared by tea cultivators above 1800 m from October until April (Lengerke 1978). Frost is also common in dry subtropical mountains where there is a large diurnal temperature range. For example, frost frequency increases from 39 per annum at Tamanrasset (1376 m) to 114 per annum at Asekreme (2706 m) in the Ahaggar

mountains of the Sahara (Yacono 1968). In temperate mountains such as the Pennines the total frost frequency will increase with altitude but at least there is a clearly defined frost-free season, although this may be short. Frost is extremely common at high altitudes in northern England, especially during winter, but also in spring and autumn, depending on altitude.

Because frost can be extremely damaging for agriculture, and is relevant for prediction of road icing (Rayer 1987, Lindqvist 1992), there have been many attempts to predict frost in mountain areas. Unfortunately, this is made difficult by the fact that the altitudinal increase in frost occurrence encouraged by lower ambient air temperatures is often offset by nocturnal tendencies for cold air to collect in valleys. Minimum temperatures are extremely variable, depending on topographical influences (Harding 1978). Bootsma (1976) estimates climatological freeze risk in hilly terrain and finds topography to be extremely important. Waco (1968) shows how incised topography in the Santa Monica Mountains of Southern California leads to isolated areas prone to radiation frost while upper slopes remain frost-free. Favoured **frost-hollows** can experience temperatures 10°C lower than immediate surrounding areas even in the normally cloudy and windy British climate. Hawke (1944) cites the example of the Rickmansworth frost hollow in the Chilterns. The occurrence of low minima in valley bottoms means that **thermal belts** form on the valley slopes above, where frosts are less frequent than on summits above and in the valleys beneath (Chickering 1884). The thermal belts of the Appalachians in North Carolina are exploited by fruit growers (Dunbar 1966).

It follows that the frost-free period is highly dependent on local topography and landform as well as absolute altitude (Hess et al. 1984). Thus relationships between frost parameters and altitude are less precise than the relationships involving growth parameters in Chapters 10 and 11 and the regressions for minimum temperatures in Chapter 8 are relatively poor.

12.2 Definition of Frost Parameters

An air frost was said to occur if the daily minimum temperature was 0°C or below. As temperature at the ground surface is usually below that of the air at screen level, a damaging ground frost can occur when the air minimum remains above 0°C. Thus the frost risk at the ground is underestimated when using air temperatures.

For each year from 1985 to 1990 the following indicators of frost occurrence were extracted:

a. first autumn frost;
b. last spring frost;
c. total number of frosts;
d. length of frost-free season (calculated as **(a-b)-1** in days).

Average values are shown in Table 12.1 for a variety of locations.

Table 12.1: Mean frost dates at a selection of locations (1985-1990).

Location	a	b	c	d
Amb	19 Oct	23 Apr	55	179
App	2 Oct	14 May	79	140
Dur	6 Nov	20 Apr	52	199
Esk	3 Nov	27 Apr	44	190
GDF	2 Oct	27 May	154	127
Htbn	10 Oct	5 May	59	157
Kield	19 Sep	2 Jun	108	108
Nwc	23 Nov	11 Apr	30	225
Sund	30 Nov	27 Mar	25	247
Wid	22 Oct	19 May	96	155

The date of the first autumn frost (**a**) is usually in October or November. At mild coastal locations the first frost may be delayed, the most marked effect being seen at Sunderland where the first frost is expected on 30 November. At Great Dun Fell, 2 October is the likely date (almost two months earlier). Appleby also expects its first frost on 2 October while Kielder Castle records its first frost on 19 September! The altitude of Kielder is only 201 m, compared with 847 m at Great Dun Fell, and severe **frost hollow** characteristics are shown at this site. The relationship between the date of the first autumn frost and altitude is poor, the regression having an r^2 of 0.01. Increasing altitude has no discernable effect in bringing forward the average date of the first autumn frost.

Frosts in late spring can damage young crops. Late frosts are a serious problem in northern England until June (Manley 1952) (Table 12.1). The last frost at Great Dun Fell is expected on 27 May and at Widdybank Fell on 19 May. In the Kielder frost hollow, 2 June is likely. In many lowland locations, especially near the coast, the frost risk recedes quickly. At Durham the last frost is expected around 20 April and at Sunderland on 27 March. Thus the relationship of the last spring frost with altitude is stronger than the relationship in autumn. The increase in frost risk with altitude is more strongly defined than in autumn, although r^2 is still low (0.352).

The above dates are the average first and last frosts recorded over six years. Frosts will have occurred earlier in autumn and later in spring. Extreme dates of occurrence (Table 12.2) show that the frost risk is still above zero outside the average dates of first and last frosts. The period between extreme frosts in Table 12.2 is therefore shorter than the average frost-free period (**d**) shown in Table 12.1.

Extremely early frosts have occurred in August at Great Dun Fell and Kielder. As a result, the totally frost-free season at Great Dun Fell is reduced to 69 days. At Kielder the period is 78 days. Frosts surveyed over a longer period would reduce these figures even more. The Kielder season is extremely short compared with Sunderland (190 days) and the frost-free period increases by 275% between Great Dun Fell and Sunderland. "Spring" frosts have occurred on 13 June at Kielder and Widdybank Fell.

Data for Great Dun Fell are missing on this occasion so the latest recorded frost date is 7 June. It is impossible to correct for missing data.

Table 12.2: Extreme frost dates (1985-1990).

Location	First/Autumn	Last/Spring	Frost-Free
Amb	11 Sep	4 May	129
App	10 Sep	12 Jun	89
Dur	23 Oct	30 Apr	175
Esk	30 Oct	10 May	172
GDF	16 Aug	(7 Jun)	69
Kield	31 Aug	13 Jun	78
Sund	3 Nov	26 Apr	190
Wid	2 Oct	13 Jun	110

Figure 12.1 shows frost occurrence plotted against the calendar date at six locations. Sporadic frosts occur in August and September at Great Dun Fell, Kielder and Appleby. The only frost-free month is July. The mean frost-free period, taken from column **d** of Table 12.1, varies from 247 days (8 months) at Sunderland to 108 days (less than 4 months) at Kielder Castle. This is plotted against altitude in Figure 12.2 a. r^2 is poor (0.223) because of the short period at Kielder and long periods at Sunderland and Newcastle. Frost free periods of 6 months are common at low altitude, decreasing to about 4 or 5 months in frost hollows. The relationship of frost-free period with altitude is much weaker than that of the consecutive growing season (Chapter 11) because the period is based on minimum temperatures which are more strongly related to topography than to absolute altitude (Harding 1978).

The relationship between total frost occurrence (**c**) and altitude is strong (Figure 12.2 b) with r^2 equal to 0.735. At sea-level the expected annual frost frequency is 41. This rises by one day for just under 8 metres altitudinal increase. Great Dun Fell records a mean of 154 frosts per annum, about 50 more than Kielder. The increase in

Figure 12.1. Frost Occurrence Around the Year at Six Locations (1985-1990)

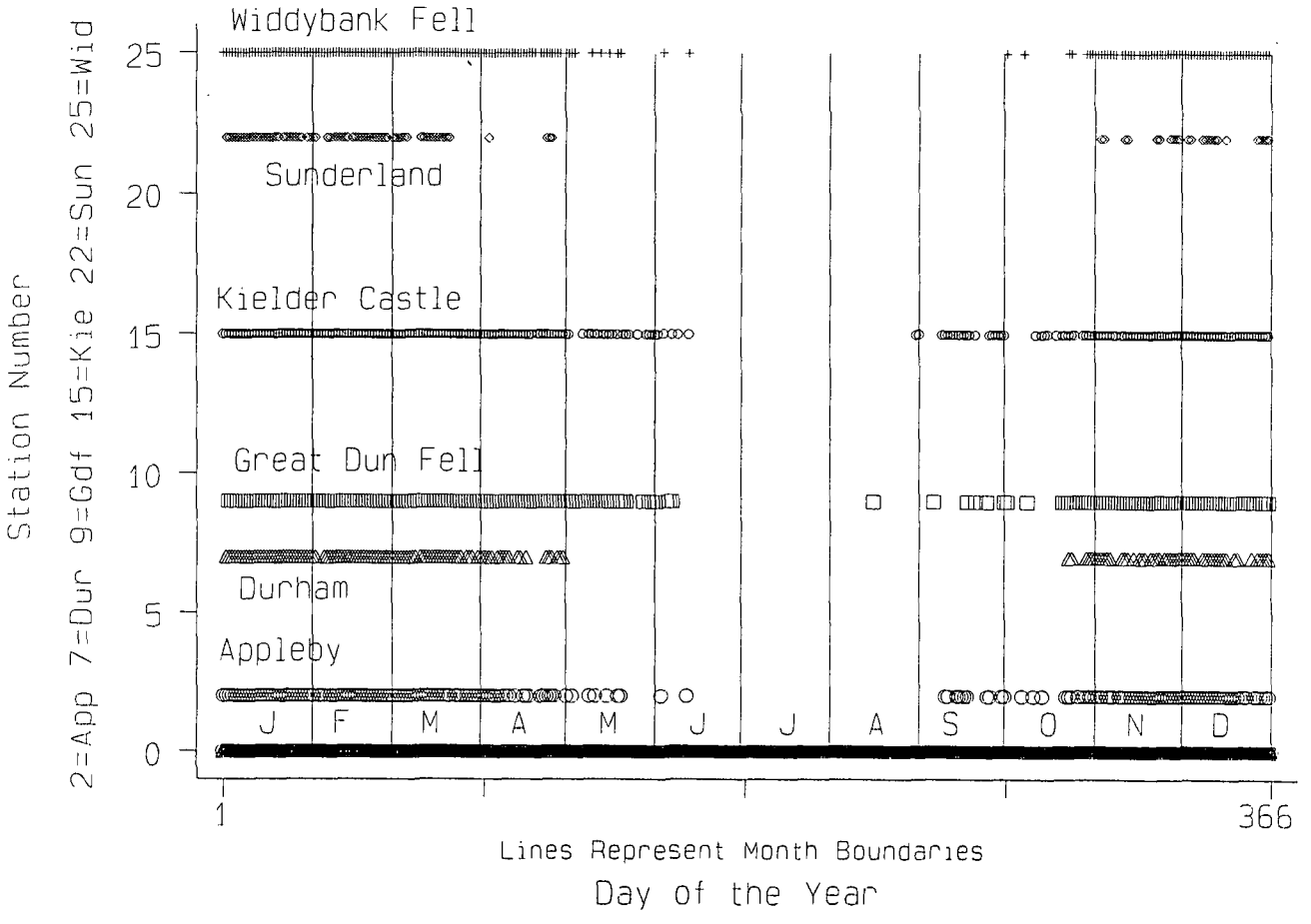

Figure 12.2. Relationships between Frost Parameters and Altitude (Metres above Sea-level)

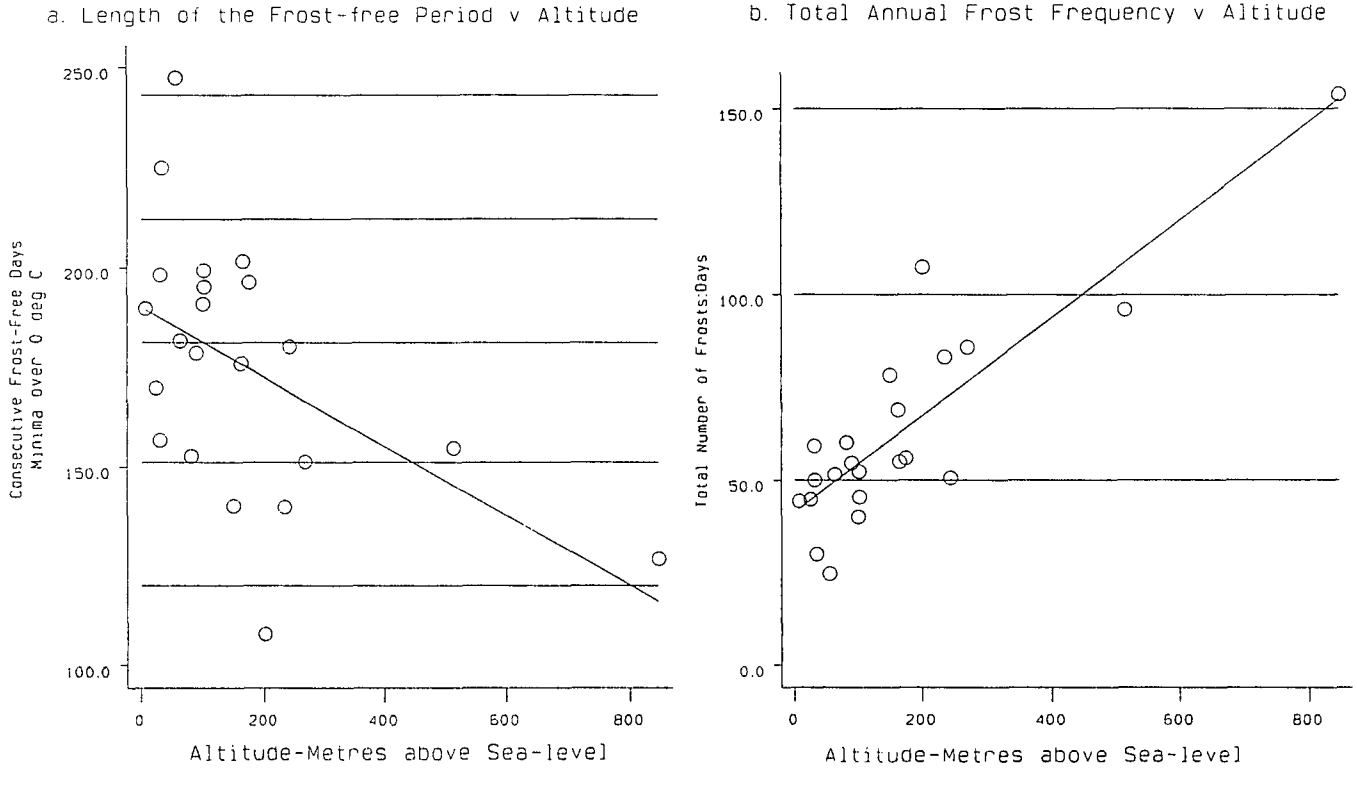

22 Locations in N.England [1985-1990]

total frost occurrence is about threefold from sea-level to 800 m. Coastal locations record few frosts. Sunderland records an average of 25 and Newcastle only 30. At high altitude the length of the frost-free season is similar to that in lowland frost hollows but the total number of frosts is much higher. In winter the temperature at 800 m in the free air is likely to be below 0°C, resulting in advection frost on windy nights. At lower elevations clear calm nights are required for an air frost to occur. This radiation frost may occur well into spring or in autumn if the air is calm and the sky is clear. Lowland frosts are therefore more sporadic and do not occur on all nights throughout the winter.

12.3 Calculation of Frost Probability

In an examination of frost risk in Florida by Waylen (1988), **frost probability curves** were derived showing the frost probability on each day of the year. A similar approach is followed here. Dividing the number of frosts recorded on each calendar date between 1985 and 1990 by six produces a crude estimate of the probability of frost on that date. Figure 12.3 shows such probabilities (averaged by pentad or five day period) at four localities; Great Dun Fell, Kielder Castle, Sunderland and Widdybank Fell. Lines connect median monthly frost probabilities. At Great Dun Fell the frost

Table 12.3: Mean monthly frost probabilities (multiplied by 100).

	J	F	M	A	M	J	J	A	S	O	N	D
Amb	39	44	28	14	01	00	00	00	02	03	27	24
App	54	51	39	18	04	01	00	00	07	08	35	40
Dur	39	46	31	14	00	00	00	00	00	04	19	21
Esk	30	34	23	11	01	00	00	00	00	02	24	22
GDF	89	88	89	68	28	06	00	01	04	13	69	75
Kie	58	60	49	40	15	03	00	01	12	18	47	48
Sun	25	25	15	02	00	00	00	00	00	00	06	10
Wid	60	71	58	41	05	01	00	00	00	05	34	41

Figure 12.3. Occurrence of Frost (Minima<=0 deg C) by Pentads, Expressed as a Frost Probability

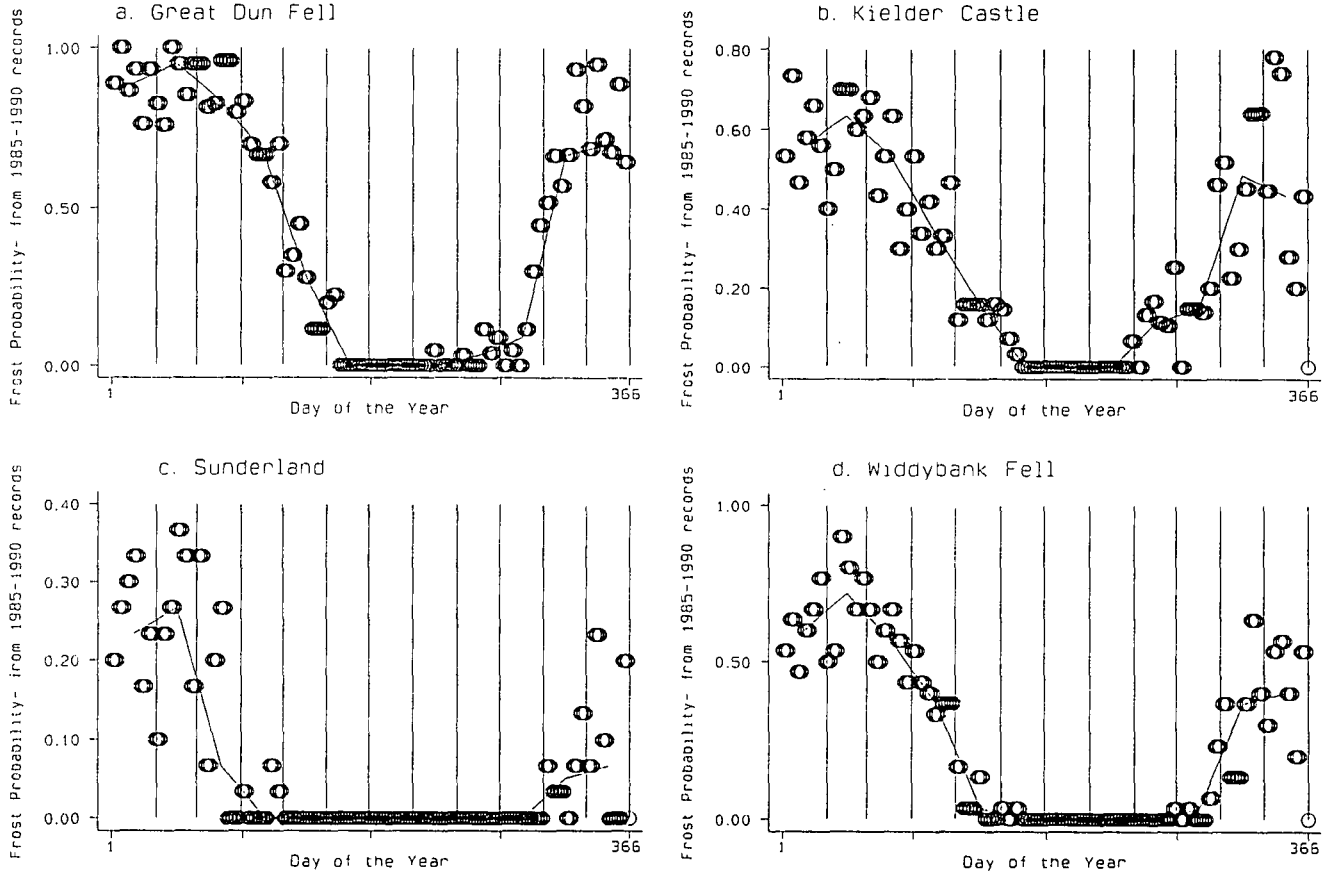

Lines connect Mean Monthly Values

probability approaches 1 in winter. Mean probabilities are 0.88 in February and 0.89 in January and March (Table 12.3). Peak winter probabilities range from 0.89 at Great Dun Fell to 0.25 at Sunderland. Probabilities fall to zero in July.

Great Dun Fell (Figure 12.3 a) has a short frost-free season between mid-June and mid-August. Kielder Castle (Figure 12.3 b) is sited in a frost hollow and although winter probabilities range between 0.6 and 0.8, the major feature is the extremely short frost-free season. By September the frost probability is approaching 0.2. By contrast, Sunderland (Figure 12.3 c) has a six month frost-free period and peak winter frost probabilities are below 0.4. Finally, the graph for Widdybank Fell (Figure 12.3 d) shows winter probabilities above 0.5 but a longer frost-free season in summer than Kielder, even though Kielder is 300 metres lower.

Cleveland's smoothing procedure (1979) is used to eradicate inter-pentad variability and derive a smooth representation of frost probability variation around the year. Results using a bandwidth of six months are shown in Figure 12.4. Four curves are irregular due to missing data (Houghall, Nenthead, Shap and Wycliffe Hall). Nearly all the curves approach zero in July and August, although this limit is not reached unless the period between the first and last extreme frosts (Table 12.2) is greater than the bandwidth.

More detailed curves are shown for selected stations in Figure 12.5. Frost probability at Great Dun Fell reaches a maximum of 0.876 on February 3 and a minimum of 0.019 on August 5. A smaller bandwidth would widen the extreme probabilities recorded. In this case the greatest frost probability occurs on the same date (February 3) as the lowest growth probability (Chapter 11). The curve for Kielder Castle reaches a maximum of 0.551 on January 23 but only falls to 0.033 (3.3%) on July 24, higher than at Great Dun Fell on the same date. An isolated frost in July appears more likely at Kielder than on Great Dun Fell when using this wide bandwidth.

Table 12.4 compares frost probabilities at Great Dun Fell and Ambleside. Bracketed figures represent the proportion of a year of 366 days.

Figure 12.4. Curves of Frost Probability for all 26 Stations

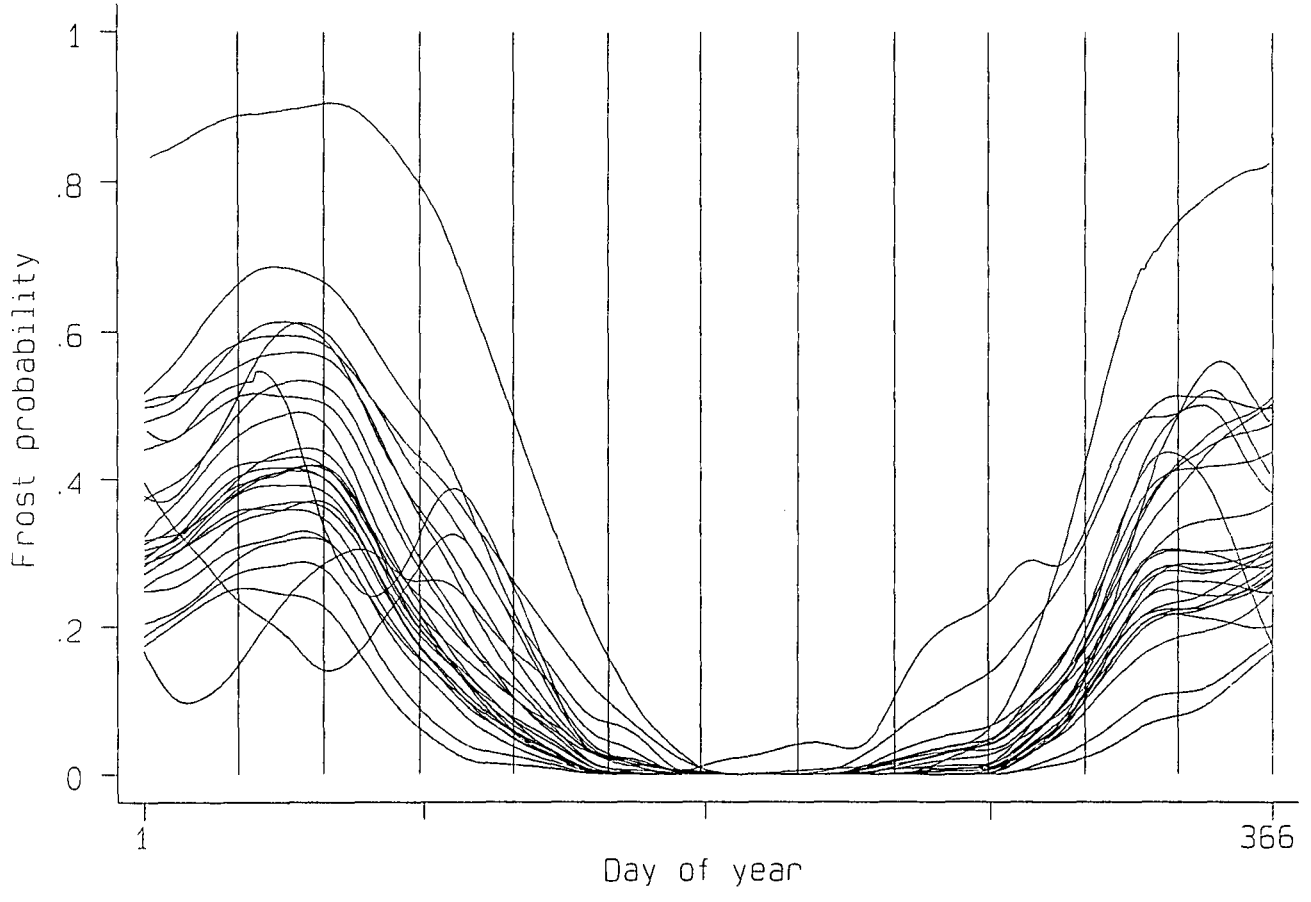

Figure 12.5. Smoothed Frost Probability Curves at Three Sites

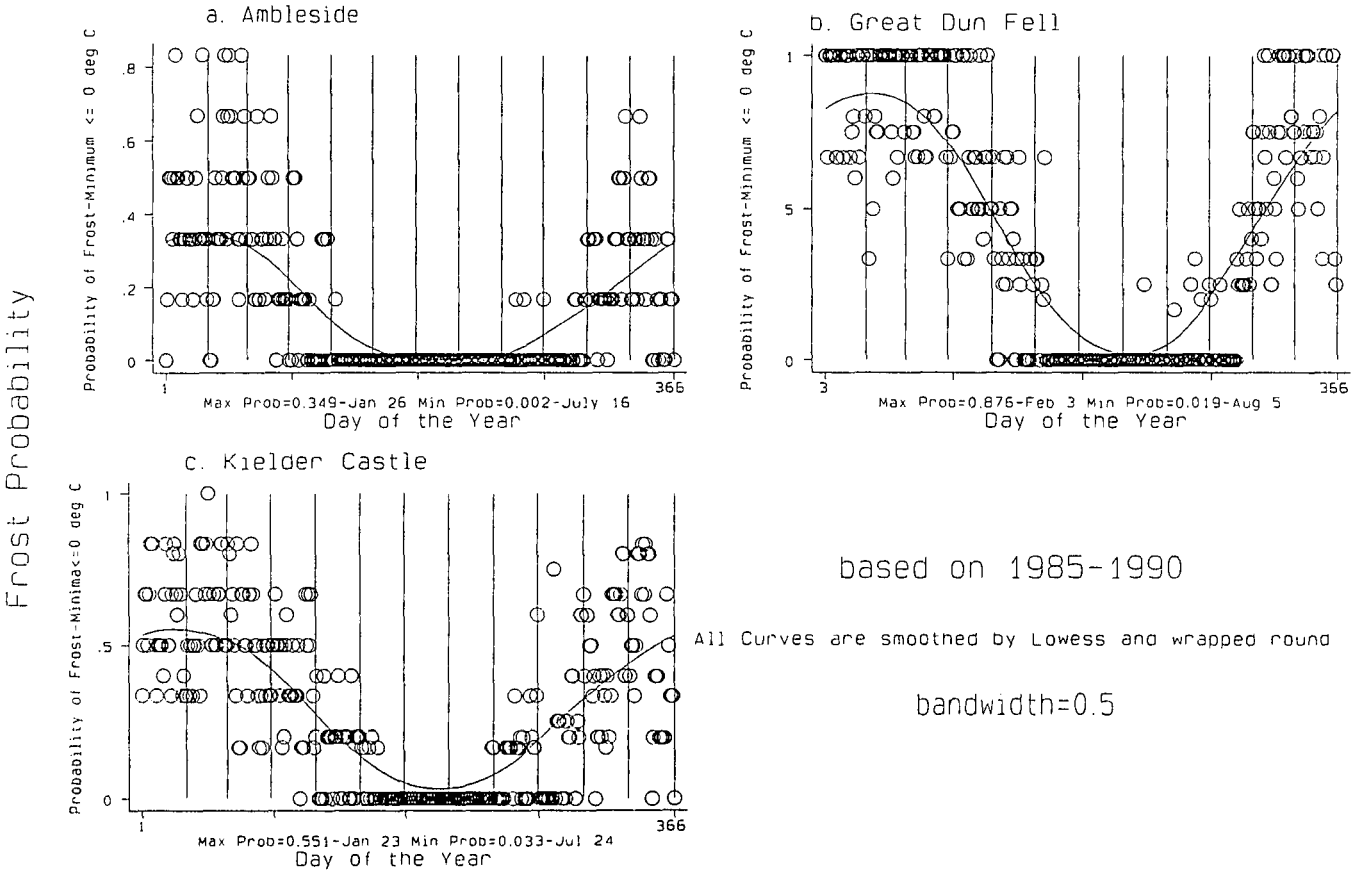

Table 12.4: Proportions of the year with frost risk above certain thresholds.

	Period of days above threshold	
Threshold	**Great Dun Fell**	**Ambleside**
75 %	96 [0.26]	- [0]
50 %	171 [0.47]	- [0]
25 %	237 [0.65]	108 [0.30]
10 %	287 [0.78]	203 [0.55]
5 %	315 [0.86]	241 [0.66]
2 %	356 [0.97]	278 [0.76]
1 %	366 [1]	299 [0.82]
0.5 %	366 [1]	319 [0.87]

At Great Dun Fell 47% (nearly half) of the year has a frost probability over 50%. At Ambleside only 30% of the year has a probability over 25% and the risk never reaches 50%. Kielder Castle has figures (not shown) similar to Great Dun Fell. The presence of Kielder reservoir a few kilometres to the south-east does not reduce the frost hazard, despite the fact that modification of air temperatures near a reservoir is likely (Gregory & Smith 1967).

The **frost probability function** is plotted against days away from the winter solstice in Figure 12.6. Vertical scales of individual graphs are not comparable. The loop must be followed clockwise unlike the growth probability function. Again, graphs show marked **hysteresis**, with greatest frost probabilities occurring after the winter solstice, especially at Sunderland and Widdybank Fell. Frost probability at the vernal equinox is much greater than at the autumnal equinox. The curve for Great Dun Fell is fairly symmetrical with similar changes in probability around both solstices. Frost probability at the autumnal equinox is nearly as low as at the summer solstice and that at the vernal equinox is nearly as high as at the winter solstice. The difference in probability between the equinoxes is over 0.5.

Figure 12.6. Frost Probability Plotted Against Days Away From Winter Solstice

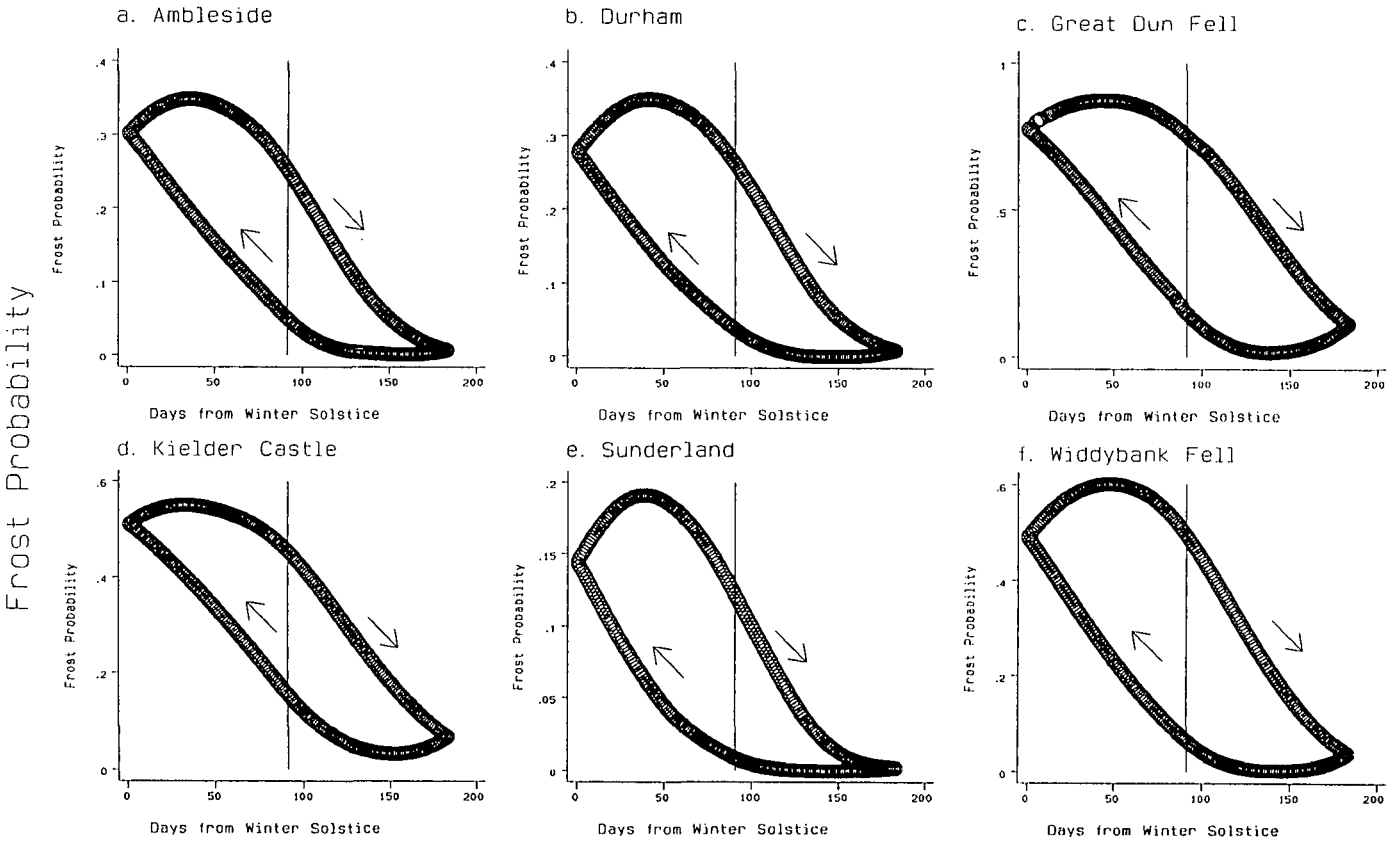

Note: Vertical Scales are Different

The area bounded by the curve represents lag behind solar forcing

The curve for Kielder is also symmetrical and fairly flat throughout winter and summer. The lowest frost probability is relatively high (3.3%). The loop for Sunderland is pointed in summer and has a flat bottom, indicative of a long frost-free period. It is not until October that the probability starts to rise substantially. By the winter solstice the probability is still less than 15% but it reaches almost 20% by the end of January. By May, probabilities are again negligible. The loop for Widdybank Fell shows a strong lag behind solar forcing. The rate of change of frost probability is greater at the winter solstice than at the summer solstice.

12.4 A Comparison of the Growing and Frost-Free Periods

This section combines the growth and frost probability functions. Serious problems for agriculture occur when the probability of growth and frost risk are simultaneously high. In this situation fresh growth can be damaged by frost. If the consecutive growing season [indicator **f** in Chapter 11] is longer than the average frost-free period [indicator **d** in Chapter 12] there will be days within the growing season at risk from frost. An estimate of the number of days at risk (**risk days**) is gained by subtracting the average frost-free period from the average consecutive growing season.

Figure 12.7 a shows the number of "risk days" plotted against altitude. There is a tendency for a decrease in risk day frequency with altitude because minima are often less severe (compared with maxima) at high altitudes. At Great Dun Fell the number of risk days is -20. The only other locations with negative risk were Newcastle and Sunderland, both urban locations near the coast. Growth is therefore less likely to be disturbed by frost in coastal localities (not surprising) and on Pennine summits (surprising). Many lowland sites show around 50 risk days in an average year although inter-annual variability is high. Durham recorded 23 risk days in 1985, a year in which the frost free season was nearly as long as the period of continuous growth. Overall, minima were relatively high and maxima were relatively low in this unsettled cloudy year. A reduced diurnal temperature range, often associated with an increase in altitude (Linacre 1982), will decrease the number of risk days. In 1990 Durham recorded 55 risk days (more than twice the amount in 1985). Figures at Great Dun Fell are -9 in

Figure 12.7. The Number of 'Risk Days' Related to Environmental Factors

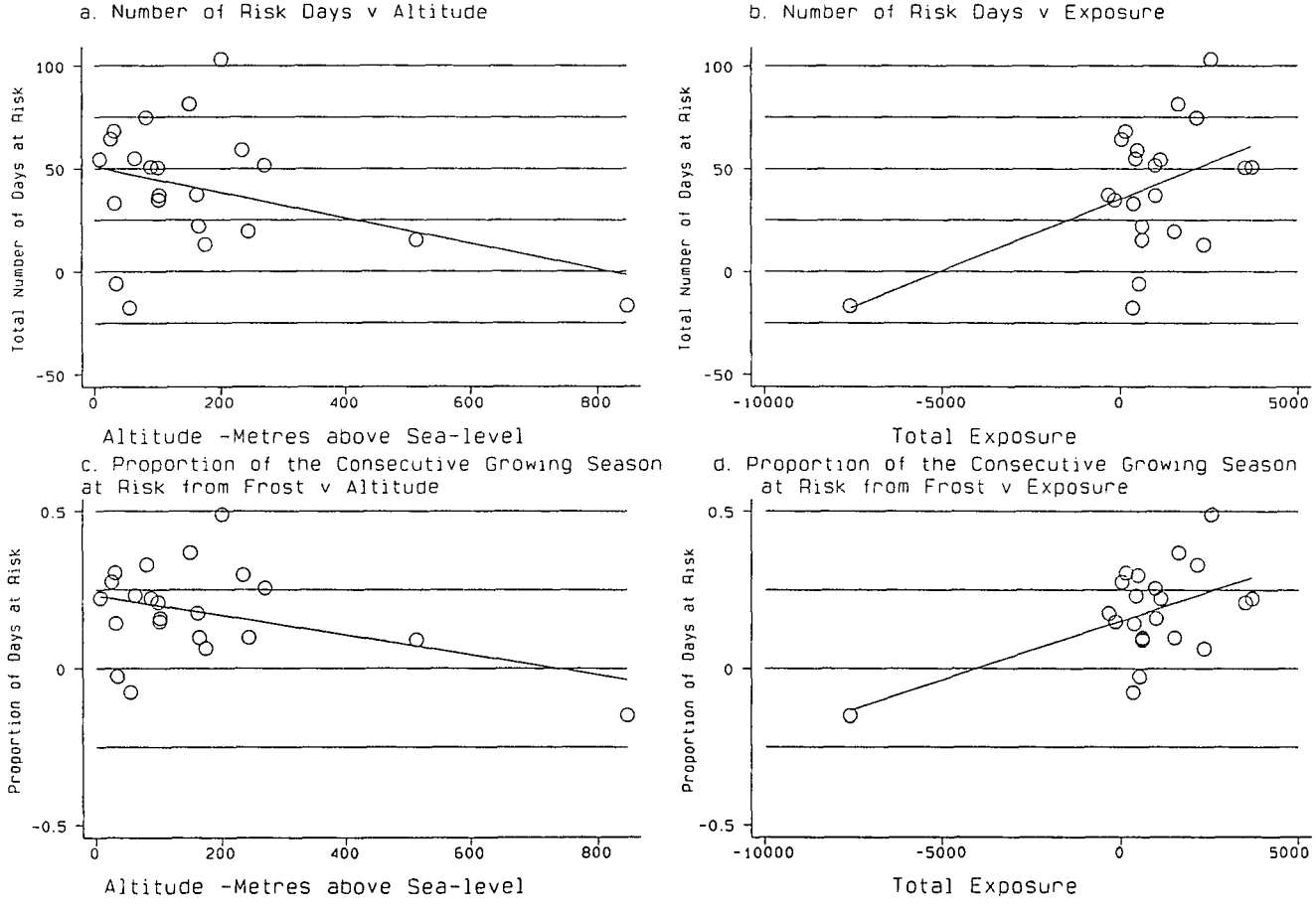

1985 but 2 days in 1990. Houghall only recorded data in 1990 and 222 risk days suggest that the site has an extreme frost problem. Even Kielder recorded only 106 such risk days in 1990. It is ironic that Houghall agricultural college appears to be sited where there is an extremely high risk to frost-sensitive plants.

Risk days are plotted against station **exposure** in Figure 12.7 b). As shelter increases so does the number of risk days. Great Dun Fell, which is very exposed, has a frost-free period longer than the consecutive growth period, while Kielder, which is sheltered, has over 100 risk days. Even without Great Dun Fell (an outlier with very low exposure) there is quite a strong relationship between exposure and risk days.

Dividing the number of "risk days" by the length of the consecutive growing season gives the proportion of the growing season at risk (Figure 12.7 c). This decreases with altitude. The proportion of the season at risk at Kielder Castle approaches 0.5 (50%). Typical values range between 0.2 and 0.3. At upland locations values are lower despite shorter growing seasons. At Great Dun Fell and Sunderland the risk is non-existent. Figure 12.7 d relates the proportion of the season at risk with exposure. Sheltered areas have a greater proportion of the consecutive growing season at risk from frost as expected. Data for Houghall in 1990 is not shown but 79% of the season at risk in this case. In comparison, at Kielder the figure was only 46%. The above proportions are conservative since they are based on the average (not the shortest) frost-free period. Additionally, when deriving the above proportion it is implicitly assumed that the whole frost-free period falls within the consecutive growth period (if the latter is longer). This is often, but not always, true.

Growth probability and frost risk are superimposed on one graph for Great Dun Fell in Figure 12.8 a. Between November and April frost probability is greater, whereas from May to October the opposite is true. The difference between the two probabilities is represented by the third curve. This third curve is, however, not the best indicator of overall risk. Problems for agricultural cultivation are greater when both growth and frost probabilities are high. Table 12.5 lists the possible combinations of frost and growth probability and resultant overall risk:

Figure 12.8. Combination of Growth and Frost Probabilities: Great Dun Fell

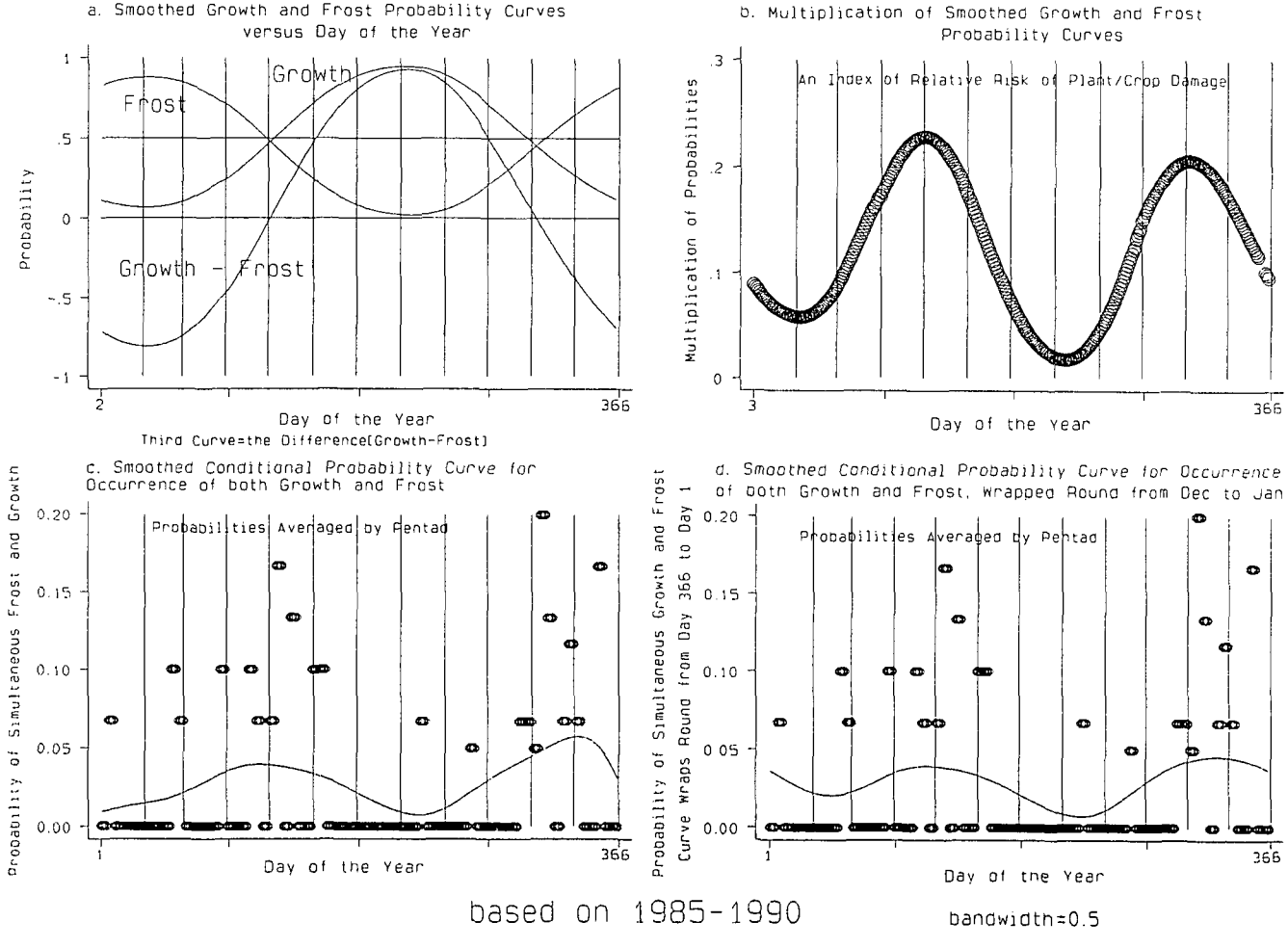

Table 12.5: Combinations of frost and growth probabilities and overall risk:

Frost Probability		**Growth Probability**	
		High	Low
	High	+	o
	Low	o	-

+ = high risk, o = medium risk, - = low risk.

The two probabilities could normally be multiplied to obtain an overall risk estimate (Figure 12.8 b) but since the two probabilities are not independent, conditional probabilities provide better results. The multiplied probability peaks at the end of April and at the end of October (roughly the changeover periods of the growth and frost probabilities in Figure 12.8 a). The daily risk appears to exceed 20% at the beginning of May but the autumn peak is lower. Conditional probabilities for each day of the year were derived by creating categorical variables for both growth and frost occurrence and setting the conditional probability equal to 1 if both growth and frost occurred on the same day. The conditional probability was averaged over the six years and then over pentads to reduce short-term variability and is smoothed over a year in Figure 12.8 c, peaking at 0.057 in early December. A curve which "wraps round" from December to January (see section 11.3, p 195) (Figure 12.8 d) has the highest probability of 0.046 in November, although late April and early May is also a critical period (the probability reaches 0.039). Because growth and frost are dependent and their occurrences are negatively correlated, the conditional probabilities in Figure 12.8 d are much lower than the erroneous values derived through multiplication (Figure 12.8 b). Nevertheless, peaks in late spring and late autumn are shown in both cases.

12.5 Conclusions

Frost risk in northern England has been evaluated. Although the total number of frosts shows an increase with altitude, the length of the frost-free period is not strongly correlated with altitude. The risk of frost during the consecutive growing season decreases with altitude because of a reduced diurnal temperature range.

Therefore coastal and mountain areas are the least prone to damaging frosts during the growing season.

Following chapters (13-14) attempt to predict how probabilities of growth and frost would change if the circulation pattern over Britain were to alter. Changes in the relationships of the probabilities with altitude are examined. The relative lengths of the consecutive growth period and frost-free period will change, depending on airflow type. Thus changes in the circulatory pattern will alter the thermal potential of the Pennine area. Relatively small changes could have great environmental effects since there is much marginal land.

THE DEVELOPMENT OF AIRFLOW SCENARIOS TO PREDICT CHANGES IN THE TEMPERATURE REGIME AT DIFFERING ALTITUDES FROM CHANGES IN THE CIRCULATION PATTERN OVER THE BRITISH ISLES

13.1 Introduction

Smith (1965) has predicted the general effects on agriculture of changing weather in each season. Problems would occur if winters were longer and springs were colder and therefore later. Warmer summers would be beneficial, especially in upland areas. Such weather changes must be related to changes in the circulation pattern if the underlying processes are to be understood. Future climate change will involve changes in the relative frequencies of weather types as well as changes in conditions associated with individual weather types. It is therefore necessary to understand the effects of contrasting synoptic situations on the upland temperature regime.

The contrast between the two components of climate change is illustrated by Perry & Barry (1973) for the British Isles, using "weather types" devised by Lamb (1972). The weather experienced in Britain at any one time depends on the airflow pattern and the time of year. Perry & Barry separate changes in air temperature between 1925-35 and 1957-67 into those due to changes in the frequency of weather types (between-type climate change) and those due to warming or cooling of specific weather types (within-type climate change). They found that for every month, apart from January, most temperature change was due to changes within weather types. Despite this result (which may have arisen partly because of classification problems) the variation in frequency of weather-types around the year is critically important in determining surface climate.

There is considerable evidence (contrary to Perry & Barry 1973) to show that the majority of climatic change is connected with between-type climate change. Analysis by Sowden & Parker (1981) suggests that most inter-decadal temperature variability can be accounted for by circulation changes. Even within airflow types most long-term variability is assigned to subtle changes in airflow direction which would not be picked up by the airflow classification. For example, warming in westerly flows is

attributed to an increasing southerly bias. A few significant changes, however, cannot be accounted for in this manner, namely warming trends for both westerly and anticyclonic days in October, significant at 1%.

The most well-known attempt to describe airflow patterns in a quantitative manner is that of Murray & Lewis (1966), who devised indices of progressiveness, southerliness, cyclonicity and meridionality based on airflow direction. The importance of similar indices in determining the surface temperature field in the Pennines was discussed in Chapter 8. Examples abound of the use of such indices to relate observed surface weather to circulation patterns. January and July temperatures in Europe are strongly correlated with changes in the circulation pattern (Kozuchowski & Marciniak 1988). Weather anomalies over Britain are related to circulation tendencies by Perry (1969). Mean temperatures are strongly correlated with indices of progressiveness and southerliness in different ways depending on season. The strongest correlations are positive between temperature and progressiveness in winter and positive between temperature and southerliness in spring and autumn. Evidence for such correlation is examined for England and Wales back to 1781 (Kington 1976). A good example of an extreme month is August 1912 which is both the coldest and the most cyclonic in the record. In northern Scotland airflow direction (as measured by PSCM indices) is crucially important in determining weather contrasts between western and eastern coasts (Mayes 1991). Murray (1990) relates the climate of Skye to airflow types.

As a result of such relationships, changes in the mean pressure pattern over Europe alone could cause significant climatic changes. For example, if the circulation were to become more zonal (with increased progressiveness), as suggested by Lumb (1993), western coasts of Britain would become even milder and wetter while the east would become drier. Glasspoole (1954) produces evidence of an increase in westerlies during the first half of this century, relating this to a 5-10% increase in precipitation in western regions of Britain, especially in winter. Murray (1993) gives evidence that southerly synoptic types have increased in frequency over Britain since 1980, especially in spring and autumn, explaining part of the warming trend in these seasons. Long-term trends in Lamb's catalogue of daily weather types are analysed using principal

components analysis by Briffa et al. (1990). There is a recent decline in westerly types and increase in pure cyclonic and anticyclonic types (up to 1987), suggesting a trend towards more variable weather with concentrated wet and dry spells. Warmer autumns are suggested, with an increase in southerly types, supporting Murray's view (1993).

A critical consequence of a change in the circulation pattern may be contrasting effects at differing altitudes, due to a steepening or lessening of mean free-air lapse rates. This idea has been largely uninvestigated, however, at least in Britain. Pfister (1985) in his study of snowlines in Europe makes this important point for snow cover. A more westerly winter circulation would bring more rain at lower altitudes, accompanied by snow melt, while heavy snow would fall at higher altitudes. A more anticyclonic circulation with frequent temperature inversions could maintain lowland snow cover but permit melt on higher south-facing slopes above the inversion. Thus the altitudinal variation in snow cover depends largely on airflow patterns. The frequency of blocking anticyclones in the vicinity of Britain, as examined by Sumner (1959), is important in determining altitudinal trends in climatic elements.

Temperature differences between individual weather types are necessary if between-type change is to be influential. In the newest GCMs these differences must be simulated along with within-type changes related to greenhouse forcing. Hulme et al. (1993) illustrate the ability of a GCM control simulation to emulate local "synoptic climatology" over Britain for the UKHI Met Office model (Viner & Hulme 1992). According to the GCM temperature differences between weather types become insignificant in summer, although winter contrasts are good.

Changes in airflow character and frequency will occur together and statistical methods are required to separate the resultant effects of each (Comrie 1992). This usually involves examination of each weather type separately as a first stage. This chapter concentrates solely on the potential effects of changes in airflow frequency (between-type climate change) on temperature parameters. Thus climate is viewed as a result of mixing fixed conditions associated with various wind patterns.

13.2 The Use of Uni-directional Airflow Scenarios

The effects of changes in relative airflow frequencies on the temperature resource in northern England is modelled by examining each airflow separately. Assuming one airflow direction (or weather type) to persist over the region continually for a whole year, and that the temperature distribution conforms to that predicted for the particular airflow in Chapter 8, the effects of this airflow on temperature can be analysed. Spatial distribution of surface temperature will change according to month, so an approximate seasonal cycle associated with the airflow in question must be modelled. The scenarios will be called **uni-directional wind scenarios** since they examine the seasonal temperature cycle for one airflow type in isolation. There are a number of objections to this:

1. The dominance of one airflow at the expense of all others for a year is unrealistic. The circulation of the atmosphere is complex.

The use of one airflow alone gives an idea of the contribution of that airflow type to surface climate, relative to other airflows. The use of airflows in isolation provides examples of extreme cases. The real climate is due to a combination of many airflows and will be more moderate.

2. Airflows will change character if they persist over one region.

This is known to be true in some cases. In anticyclonic conditions with calm surface winds, temperatures are likely to rise progressively in summer and fall in winter. A northerly outbreak of polar air will often intensify with time, lowering surface temperatures further. The opposite occurs if the strength of the northerly flow declines or if arctic air is gradually replaced by another airflow (not possible in the uni-directional scenarios). Temperatures may increase or decrease with the persistence of many airflows but it is thought best to simulate the temperature of an individual airflow throughout the year by using the present mean temperature distribution. A possible exception is the calm scenario. Conditions will eventually depart markedly from those

experienced under anticyclonic conditions in each individual month (described by the regression equations) because of the continued absence of horizontal advection. Surface temperature would be strongly controlled by radiation input and it is likely that winter temperatures would drop progressively lower at this high latitude (55°N). In the persistent Siberian anticyclone at a similar latitude, temperatures as low as -50°C are recorded, although this is in a continental location. In summer a positive net radiation balance would encourage a progressive rise in temperature.

3. Airflows do not fall into discrete categories described by surface winds.

There are two slightly different issues here. The first concerns the validity of using surface wind direction to classify airflow types and the second concerns whether it is possible to determine discrete airflow types. First, wind direction at the surface will differ from that in the upper air by around 20-30° because of the effects of surface friction (Ekman 1904). However, surface temperature is more strongly related to surface wind direction than to upper air direction, because of the directional influences of surface features (e.g. coastlines and topography). Second, the division of airflows into classes, although subjective, allows a comparison of conditions under airflows with a broadly similar character.

4. The spatial temperature distribution for an airflow will change over time, i.e. temperature fields described by regressions based on 1985-1990 are inadequate.

This is valid and scenarios produced in this chapter ignore within-type climate change. Nevertheless, we can speculate about the effects of changes in relative airflow frequencies alone on the future temperature resource of the region.

Despite such objections, the uni-directional scenario approach is useful because it tells us about the comparative influences of different airflows on climate by examining airflow influences in isolation. The scenarios describe the extreme cases of dominance by one airflow alone. The real climate varies between such extremes.

13.3 Temperature Prediction Under Individual Airflow Types

The multiple regression equations predicting daily maximum and minimum temperatures from altitude, latitude and longitude for each wind direction in each month of the year (108 cases), using data from 1985-1990, and described in Chapter 8, were assumed to describe the expected temperature distribution for individual airflows, e.g. a westerly flow in January. To simulate constant westerly flow the temperature distribution in each month was assumed to be controlled by the appropriate equation.

Altitude accounts for most of the temperature variation in all equations (Chapter 8). Setting station latitude and longitude to their mean values (130.6 and 80.2 respectively), the expected mean monthly maximum, minimum and mean temperatures for any altitude can be derived:

$$X=(a\times alt)+(b\times 130.6)+(c\times 80.2)+k \quad ----(1)$$

where X = the predicted mean temperature, a, b and c are the altitudinal, latitudinal and longitudinal coefficients from the relevant equation, and k is the appropriate constant. Expected mean temperatures were derived by averaging expected maxima and minima.

13.4 Results

Predicted mean temperatures at sea level are given in Table 13.1 overleaf.

Growing season strength for a particular airflow is calculated from:

$$T_{acc}=n\times(x-6) \quad -----(2)$$

where **n** is the number of days in the month and x is the simulated mean temperature. This crude figure ignores temperature variability around the predicted mean (see

Table 13.1: Expected mean temperatures at sea-level (°C).

°C	CALM	N	NE	E	SE
JAN	1.95	2.32	1.32	0.54	0.93
FEB	2.37	2.57	2.29	0.90	0.53
MAR	4.17	5.06	2.78	5.16	3.90
APR	7.58	6.35	6.79	6.03	6.68
MAY	11.93	9.78	11.10	11.33	11.29
JUN	14.28	12.02	13.18	15.27	13.40
JLY	17.10	15.62	15.76	16.03	16.94
AUG	14.68	12.78	15.37	13.03	17.88
SEP	12.12	11.23	11.15	13.52	12.08
OCT	9.19	9.88	9.50	11.28	11.40
NOV	5.69	4.46	6.18	5.49	7.82
DEC	4.19	3.17	4.58	5.02	5.03
	S	SW	W	NW	MEAN
JAN	4.99	5.45	5.43	3.07	4.04
FEB	5.27	5.92	5.13	3.51	4.19
MAR	7.18	6.58	6.79	5.52	6.03
APR	10.29	9.53	8.42	7.55	7.89
MAY	11.95	12.14	11.67	10.27	11.28
JUN	14.11	14.44	13.27	12.97	13.54
JLY	16.10	15.86	15.36	14.87	15.70
AUG	15.99	15.68	15.22	15.14	15.10
SEP	13.75	14.03	13.29	11.95	12.89
OCT	11.72	10.92	10.66	9.83	10.61
NOV	7.48	8.15	6.50	4.03	6.16
DEC	6.87	6.37	6.72	4.02	5.67

Chapter 16 for a stochastic approach). In the above case the contribution is negative. Results for sea-level and 800 m are shown in Figures 13.1 and 13.2 respectively.

Figure 13.1. Predicted Growing Season Strength (Accumulated Temperatures) for Uni-directional Wind Scenarios at Sea-level: Monthly Accumulations

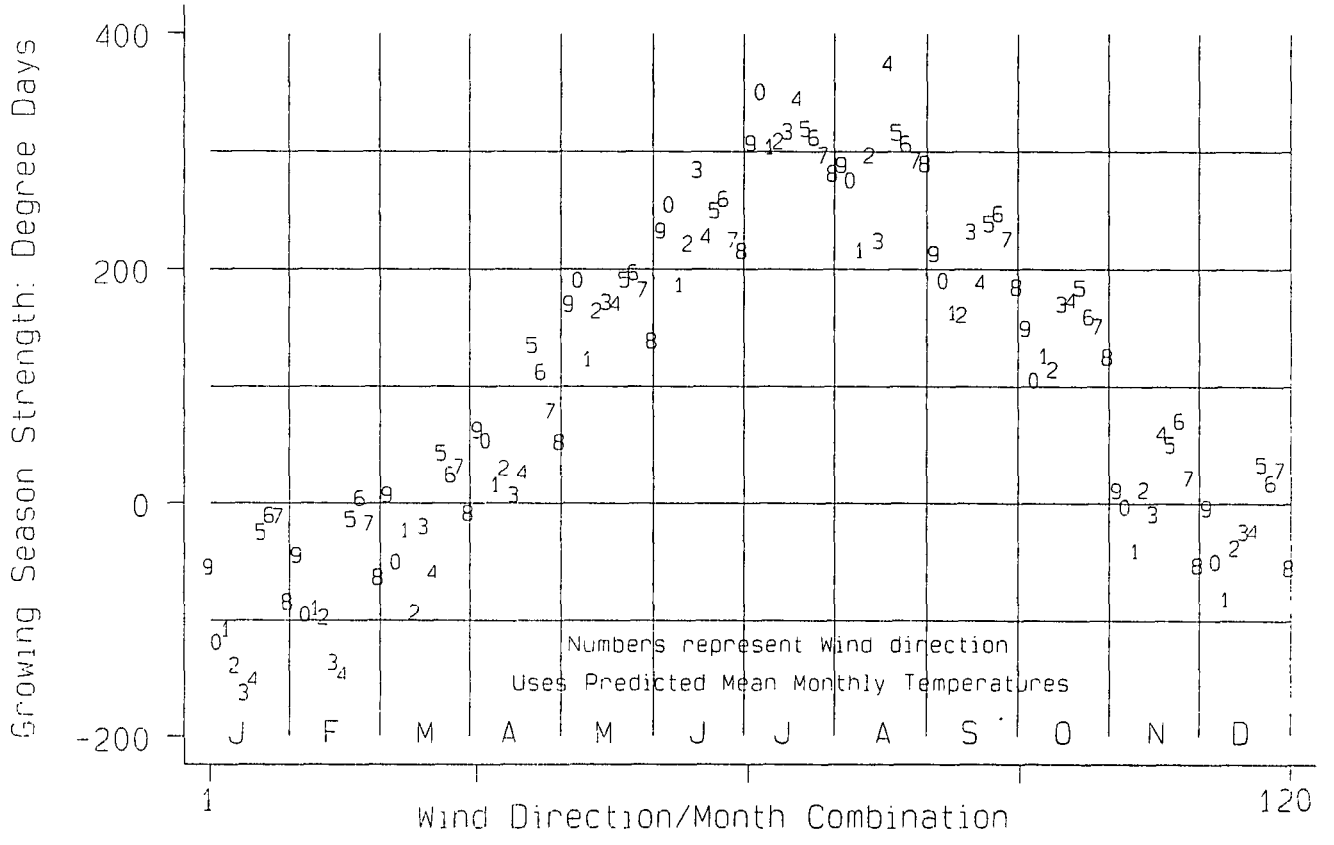

Figure 13.2. Predicted Growing Season Strength (Accumulated Temperatures) for Uni-directional Wind Scenarios at 800 Metres above Sea-level: Monthly Accumulations

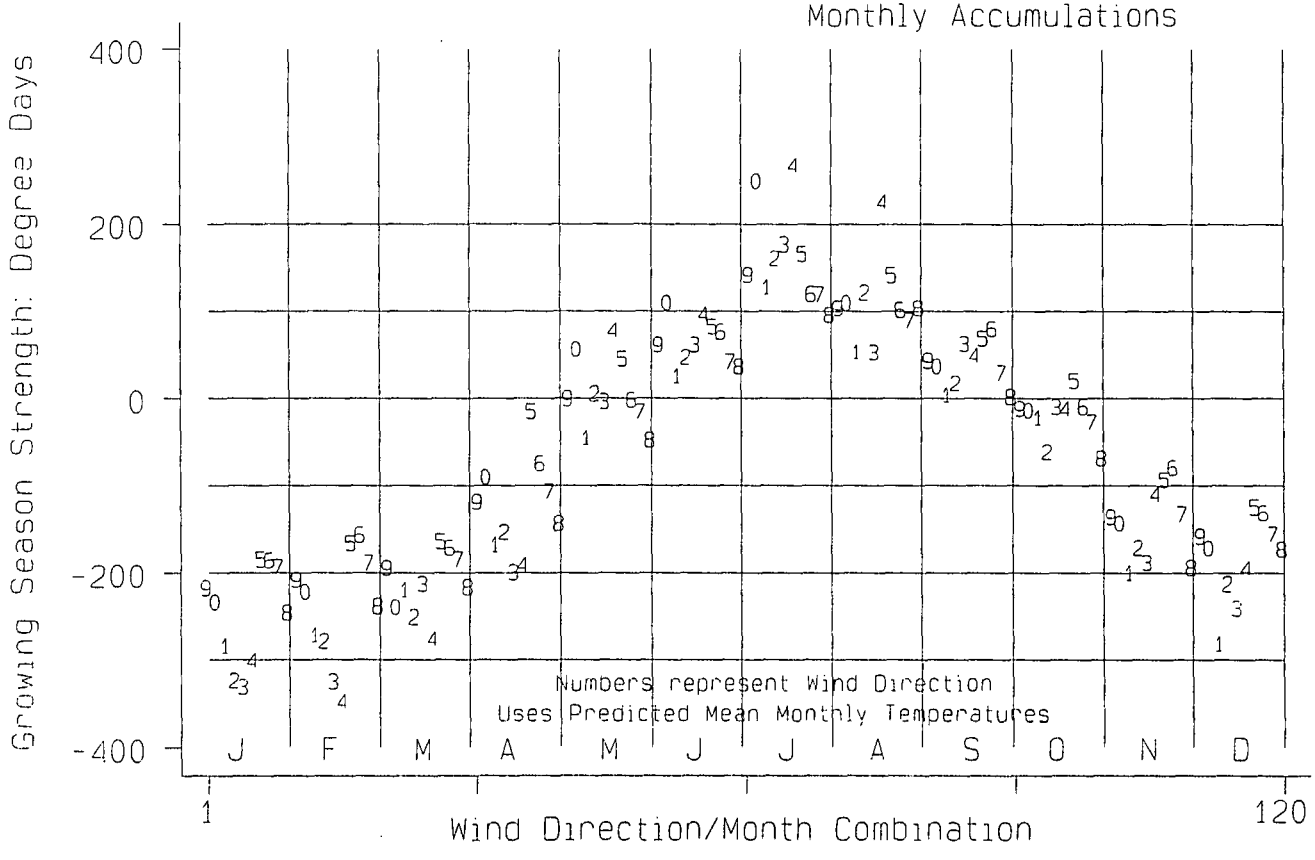

Accumulated temperatures associated with calm conditions (wind=0) at sea-level are negative between November and March inclusive and, compared with other wind directions, are low in winter and high in summer. The July accumulation is over 350 d°C. South-easterly flow (4) shows an extreme seasonal variation with accumulations in July and August above 300 d°C, while values in January and February are below -150 d°C. Accumulations for northerly flows (1) are usually at least 100 d°C lower than those for southerly flows (5) in the same month. Westerlies (7) show a subdued seasonal variation.

Figure 13.2 shows similar data for 800 m above sea-level. Accumulations are usually negative from November to April inclusive. Calm conditions (0) give relatively high temperature accumulations, especially in summer (e.g. July). From January to March values are below -200 d°C despite frequent temperature inversions. Accumulations for northerly (1) airflows are low, especially in the second half of the year. Southerlies (5), by contrast, give much higher accumulations with positive accumulations in six months (nearly 200 d°C in July). Easterlies (3) show a larger seasonal fluctuation in accumulated temperatures than westerlies (7), which although mild in winter, barely contribute 100 d°C in summer due to steep lapse rates characteristic of maritime air. South-easterly accumulations are the most extreme, ranging from -350 d°C in February to nearly 300 d°C in July!

13.5 Derivation of Growing Season Strength for Uni-directional Airflow Scenarios

13.5.1 Annual Accumulated Temperatures, G_y: One Estimate of Growing Season Strength

Figure 13.3 and Table 13.2 show annual accumulated growing season strength for each airflow at certain altitudes, i.e. accumulated temperatures for the uni-directional wind scenarios. The results assume that one airflow direction (e.g. westerlies or easterlies) dominates the region for the whole year. Negative accumulations in months with mean temperatures below 6°C are included, reducing this annual accumulation (G_y). A constant westerly flow, associated with extreme progressiveness

Figure 13.3. Predicted Annual Growing Season Strength, Gy, for Uni-directional Wind Scenarios at Various Altitudes: Annual Accumulations

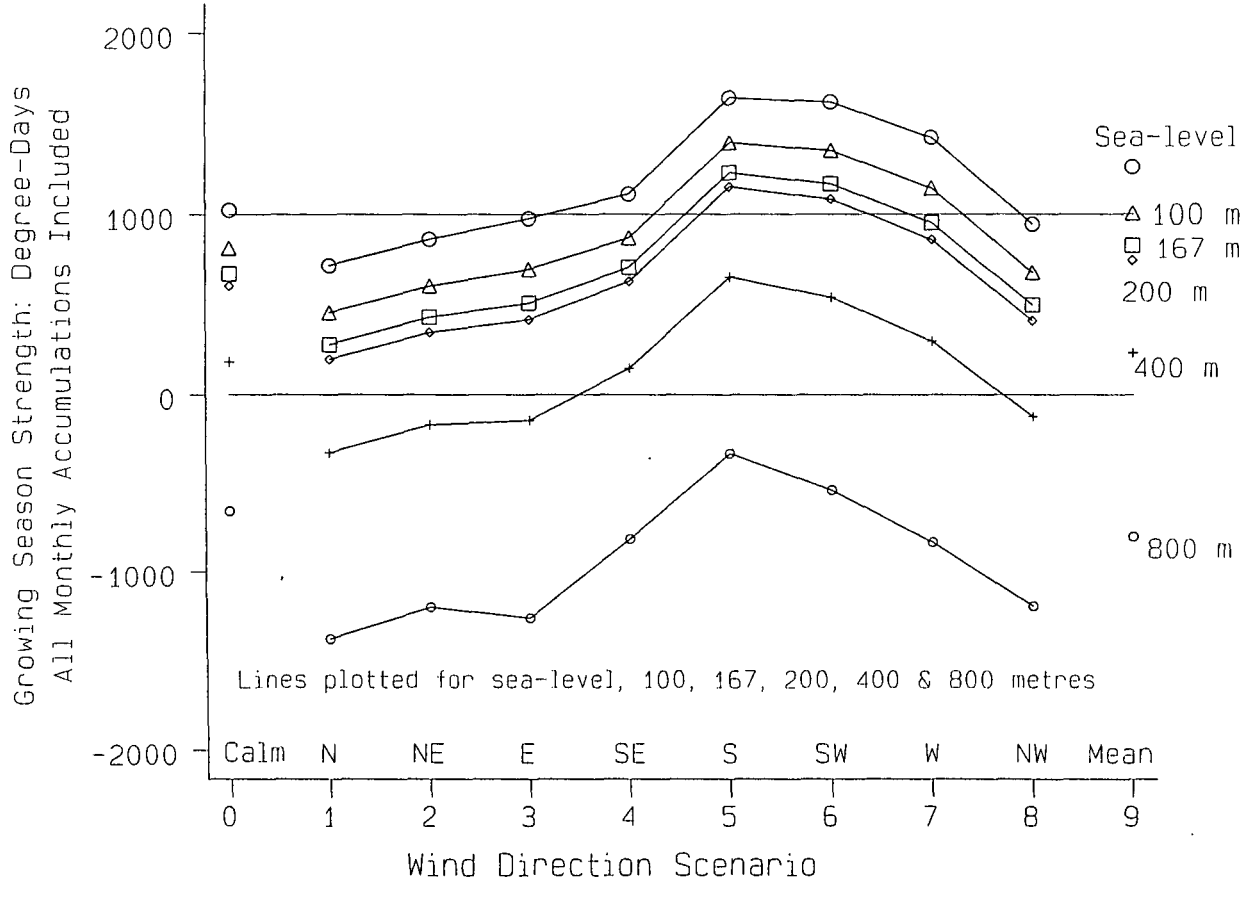

in the circulation, would produce a growing season strength of 1425.6 d°C at sea-level, falling to below 1000 d°C at 167 m and below 0 d°C at 800 m. The steep decline arises partly because of strong negative contributions in winter.

Table 13.2: Simulated annual growing season strength, $\mathbf{G_y}$, (including negative values) for uni-directional wind scenarios.

alt	0	100	167.8	200	400	800
Calm	1026.0	816.0	673.2	606.0	186.0	-655.2
N	721.2	458.4	280.8	196.8	-327.6	-1375.2
NE	865.2	607.2	433.2	349.2	-166.8	-1198.8
E	978.0	698.4	508.8	418.8	-140.4	-1258.8
SE	1112.4	872.4	709.2	631.2	150.0	-812.4
S	1645.2	1398.0	1231.2	1152.0	657.6	-328.8
SW	1623.6	1353.6	1170.0	1083.6	543.6	-535.2
W	1425.6	1143.6	952.8	861.6	297.6	-829.2
NW	948.0	680.4	499.2	412.8	-121.2	-1190.4
Mean	1262.4	1005.6	830.4	747.6	232.8	-796.8

At 800 m above sea-level, accumulations are always negative because of mean annual temperatures below 6°C. The rate of decrease in annual growing season strength G_y with altitude depends on the lapse rates simulated. Steep lapse rates in westerly and north-westerly airflows encourage a large difference in accumulated temperatures between 800 m and sea-level. At sea-level, wind direction has an important effect on G_y, there being a variation of over 200% between 1645.2 d°C (for southerly flow) and 721.2 d°C (for northerly flow). For northerly, north-easterly and easterly winds annual totals are below 1000 d°C, even at sea-level. The high altitude (800 m) value for westerly winds is surprisingly severe (-829.2 d°C). This is lower than G_y for south-easterly winds at the same altitude (not the case at sea-level). The relative warmth of southerly winds is enhanced at 800 m because they commonly have a shallow lapse rate and the strong temperature contrast between southerly and westerly winds at 800 m is

largely absent at sea-level. Since winds from between these two directions will be extremely common in a climate dominated by an Atlantic circulation, greater sensitivity of temperature and growing season parameters to wind direction is suggested at high altitude. Variability in the upland temperature resource would increase in a climate dominated by streams of maritime Atlantic air (both polar and tropical) approaching from between west and south. Finally, calm conditions are associated with a higher annual temperature accumulations at 800 m than expected, due to the influence of temperature inversion formation at low levels.

13.5.2 Warm Season Accumulated Temperatures, G_p

Figure 13.4 and Table 13.3 list annual accumulated temperatures when negative contributions from months with mean temperatures below 6°C are ignored. The resulting annual accumulation (G_p) depends on warmth in the warm season alone. The period of positive temperature accumulation (above 6°C) is 10 months at sea-level under southerly winds but only 3 months at 800 m under northerly airflows.

Table 13.3: Simulated annual growing season strength, G_p, for the warm season for uni-directional wind scenarios.

Alt	0	100	167.8	200	400	800
Calm	1376.2	1253.7	1170.4	1131.2	912.6	518.5
N	1094.1	960.0	876.6	837.0	589.8	183.6
NE	1258.4	1106.7	1022.4	982.2	735.6	313.6
E	1362.2	1227.6	1136.4	1093.2	825.6	320.0
SE	1518.4	1377.6	1296.4	1257.9	1049.4	675.5
S	1697.0	1490.0	1363.2	1312.0	1019.2	472.8
SW	1642.0	1429.6	1304.8	1245.6	890.4	344.4
W	1467.0	1238.3	1125.6	1071.7	759.0	245.2
NW	1243.2	1078.0	965.3	915.6	633.6	211.5
Mean	1384.2	1225.7	1122.8	1073.8	804.6	316.8

Figure 13.4. Predicted Warm Season Growing Season Strength, Gp,
for Uni-directional Wind Scenarios at Various Altitudes

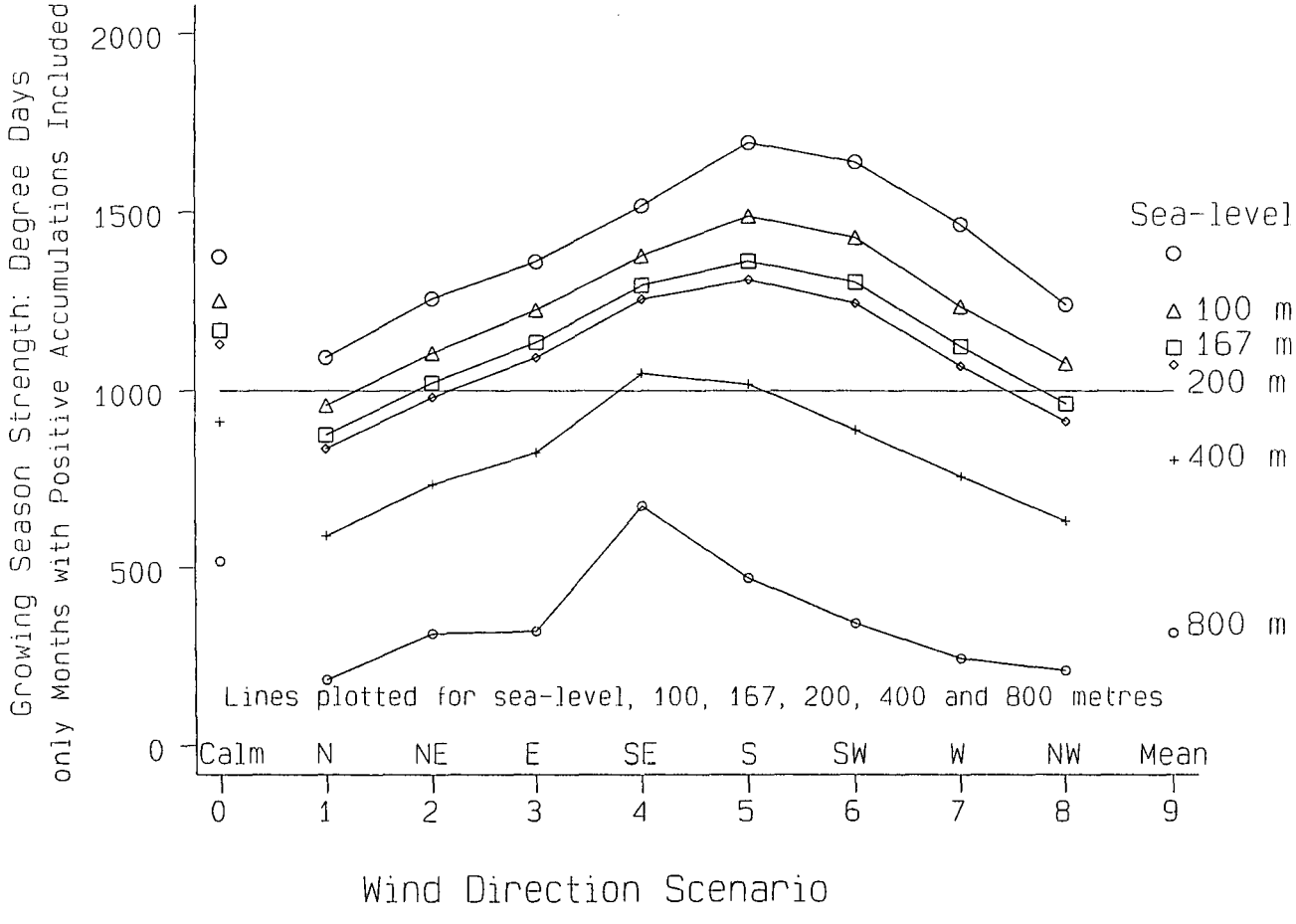

Southerly winds are associated with the highest growing season strength (nearly 1700 d°C) at sea-level. At very high altitudes, however, south-easterly flows produce a higher value of G_p. Warm, stable (and often anticyclonic) air from the continent blows into the region from the south-east and shallow lapse rates ensure that this air is warmer than southerly air at 800 m. The relative warmth of south-easterly flows at high altitude is clear in Figure 13.4.

The threshold of 1000 d°C (the theoretical cultivation limit in Chapter 10) is exceeded at 400 m under both southerly and south-easterly flow. On the other hand, warm season temperature accumulations G_p for south-westerly and westerly winds deteriorate more rapidly with altitude. At 800 m the accumulation for south-westerly flows is only half of that for south-easterlies, whereas at sea-level the south-westerly accumulation is higher. Temperature accumulations for different airflows do not stay in relative proportion as altitude increases because of the contrasts in lapse rates. The altitudinal decrease in G_p is not linear because the number of months with mean temperatures above 6°C (months that contribute to the warm season accumulation) also decreases.

Northerly and north-westerly winds lead to cold seasons at sea-level. At 100 m a harvest could fail if northerly winds were to prevail throughout the year (assuming a critical accumulation to be 1000 d°C). Under a scenario dominated by polar maritime air from the north-west, the 1000 d°C elevation falls below 167.8 m (the mean altitude of the stations).

The altitudinal decrease in growing season strength is steeper when lapse rates are high. Thus in the westerly scenario the predicted growing season strength at 800 m is only 16.7 % of that at sea-level (Table 13.4).

Table 13.4: Ratio and difference of annual growing season strength, G_p, at 800 m compared with sea-level.

Airflow Scenario	Difference(d°C)	Ratio (800/sea-l)
Calm	857.7	0.377
N	910.5	0.168
NE	944.8	0.249
E	1042.2	0.235
SE	842.9	0.445
S	1224.2	0.279
SW	1297.6	0.210
W	1221.8	0.167
NW	1031.7	0.170
Mean	1067.4	0.229

The mean ratio of G_p at 800 m to G_p at sea-level is 0.23 but the variation in this ratio (Figure 13.5) between different airflows is considerable, from 44.5% for south-easterly flow to 16.7% for westerly flow. This is because south-easterly flows have the shallowest temperature lapse rates. Even in northern England lapse rates would be lowered under the constant influence of continental air. The relative effectiveness of change in growing season strength with altitude under maritime conditions has already been illustrated by Manley (1945a). A particular location such as northern England is only oceanic or maritime in its climate because of the prevailing airflows present. Thus, if air from the continent were to dominate northern England the Pennine climate would become more similar to that of nearby continental uplands (e.g. Central Norway). The eastern seaboard of North America, although in close proximity to the ocean, has a continental climate because of prevailing westerlies bringing air to the region from inland. Moreover, the deterioration of accumulated temperatures with altitude is less rapid under such conditions than on the more maritime Pacific coast due to shallower mean lapse rates (Wolfe 1990).

Figure 13.5. Warm Season Growing Season Strength, Gp, at 800 Metres above Sea-level as a Proportion of that at Sea-level, for Uni-directional Wind Scenarios

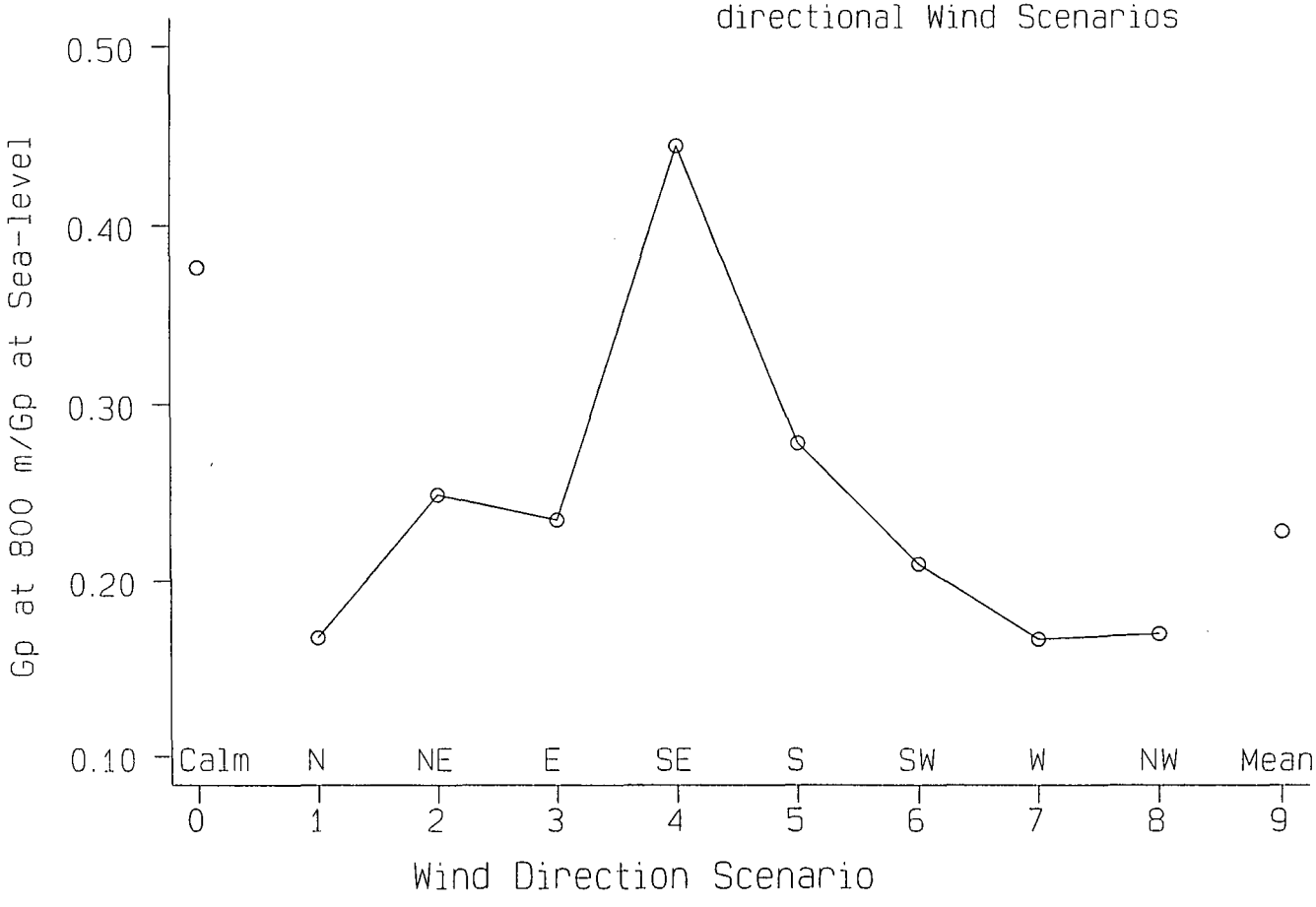

The ratio between G_p at 800 m and sea-level for northerly winds is low, partly because absolute accumulations are low anyway. For westerlies and north-westerlies the ratio is also low, but with higher absolute accumulations. Finally, calm conditions would have benefits in upland areas, the ratio being 0.377. At 800 m the calm scenario allows a temperature accumulation of 518.5 d°C, more than double the accumulation for westerlies (245.2 d°C) and bettered only by south-easterly winds.

The contrasting effects of airflows at differing altitudes such as these have not really been taken into account in scenarios regarding local climate change. Changes in accumulated temperatures will not be coincident at differing altitudes. Hence the pattern of temporal change at the 400 m level will be different from that at sea-level, a similar change in airflow types having contrasting effects at high and low altitudes.

The absolute difference in the simulated warm season temperature accumulation (G_p) between sea-level and 800 m is shown in Figure 13.6. This is largest for south-westerly and westerly flows, despite a similar G_p ratio as northerly flow. Annual temperature accumulations G_y, which include negative winter contributions (not shown in tabular form), are also shown as the upper line in this diagram. For G_y the benefit of calm conditions is even more marked with a simulated drop of only 1681.2 d°C from sea-level to 800 m, compared with an average difference of over 2000 d°C. Frequent temperature inversions in winter anticyclones are responsible. Airflows perpendicular to the Pennines (i.e. westerlies and easterlies) have an enhanced overall lapse rate (Chapter 8), creating a larger altitudinal contrast in annual growing season strength.

13.6 Generation of 1000 d°C Cultivation Limits for Uni-directional Wind Scenarios

Using the uni-directional wind scenarios described above one can interpolate the elevation at which 1000 d°C are expected. The annual total (G_y) includes the influence of winter conditions and so is less useful than G_p when considering temperature accumulations relevant to the growing season. Both accumulations are examined here, illustrating the differences in results. When using annual totals (G_y), critical "cultivation

Figure 13.6. Absolute Differences in Warm Season (Gp) and Annual (Gy) Growing Season Strengths between 800 Metres above Sea-level and Sea-level for Uni-directional Wind Scenarios

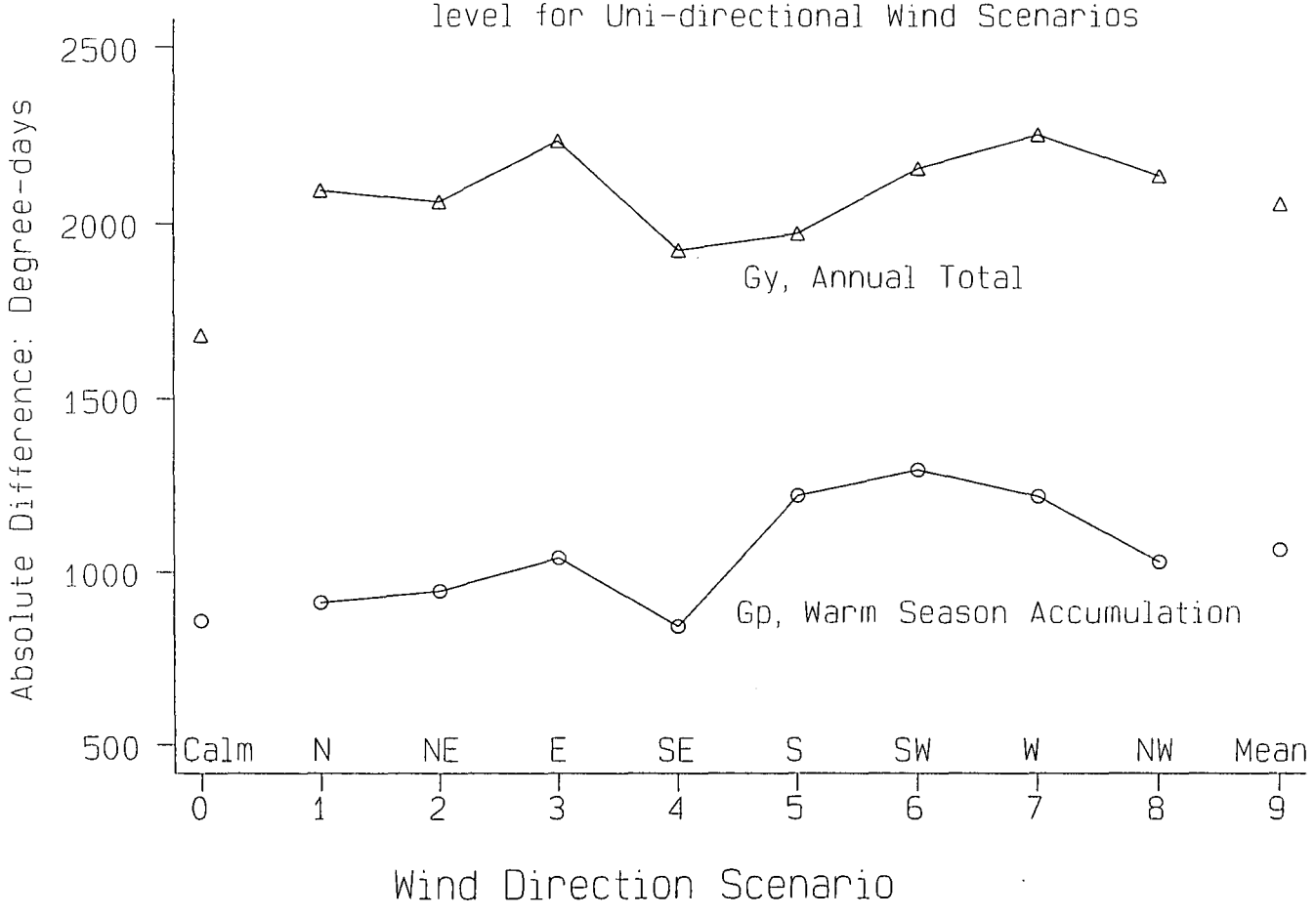

Figure 13.7. Variation of Annual Growing Season Strength, Gy, with Altitude, in all Uni-directional Wind Scenarios

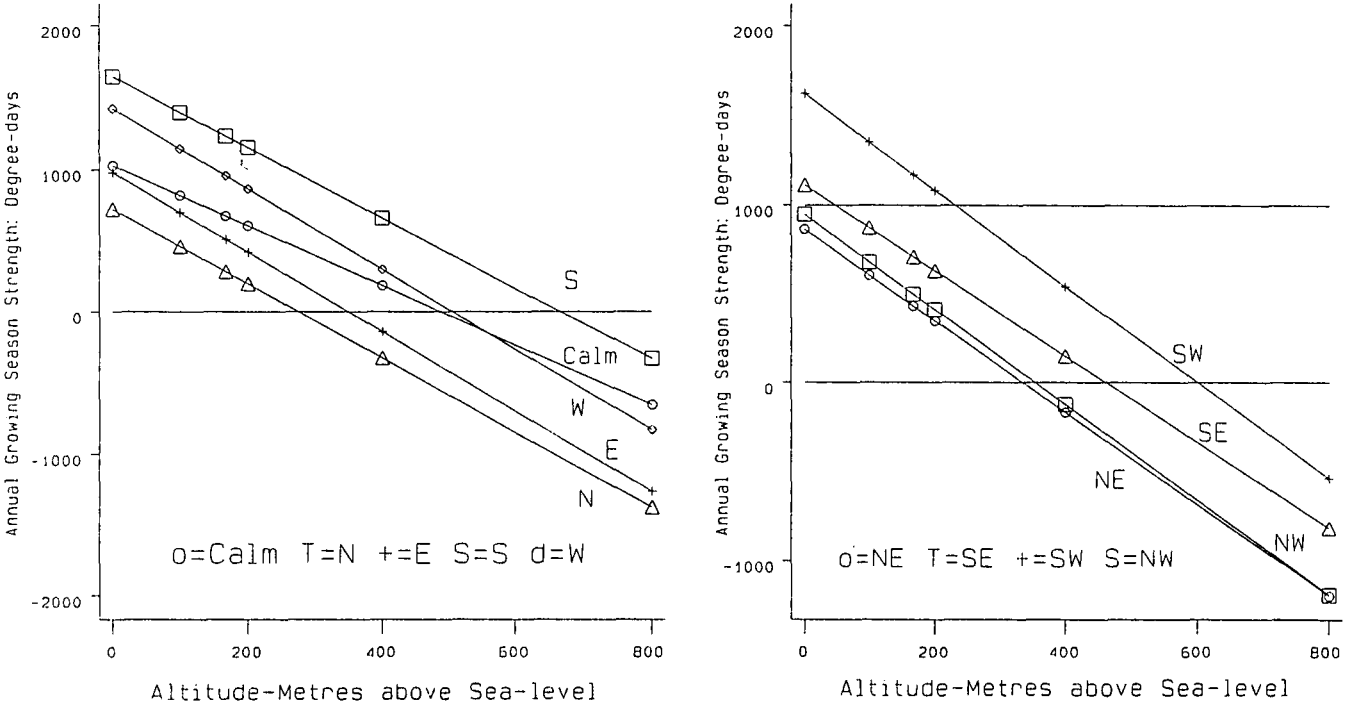

limits" are low because of low annual accumulations. The linear variation of G_y with altitude is shown in Figure 13.7. Winds from between north-west and east record accumulations below 1000 d°C at sea-level (e.g. only 721 d°C for constant northerly winds). For calm conditions the interpolated critical altitude only rises to 12 m. Table 13.5 lists elevations of the interpolated 1000 d°C limits for all the uni-directional wind scenarios.

Table 13.5: Critical altitudes (m) at which the predicted degree day accumulation ($\mathbf{G_y}$ or $\mathbf{G_p}$) is 1000 d°C.

Airflow scenario	Crit level (yearly total-G_y)	Crit level (warm season total-G_p)
Calm	12	320
N	<0	70.2
NE	<0	185.7
E	<0	269.6
SE	46.8	452.8
S	261.4	414
SW	231.0	338.2
W	150.9	245.8
NW	<0	146.9
Mean		254.8

For a south-easterly flow the critical elevation at which G_y equals 1000 d°C is 46.8 m. Under westerly flow this limit reaches 150.9 m. Highest limits occur for mild southerly (261.4 m) and south-westerly (231.0 m) flows. There is a fair amount of variation in the 1000 d°C cultivation limit between different airflows. In terms of the proportion of land above or below this limit, only 32.9% of land lies above 261 m (the southerly airflow cultivation limit) but in the poorer scenarios all the land is unsuitable. The gradient in degree days varies from -2.82 d°C/m for westerlies (the simulated lapse rate is steep) to -2.10 d°C/m for calm conditions. These gradients are steeper than those in Chapter 10. This is because G_y is used instead of a daily temperature

accumulation G_d.

As stated previously, G_y is less useful than G_p in calculations relating to changes in growing potential. When warm season accumulations (G_p) alone are used, however, linear interpolation can only be used locally (i.e. between values immediately above and below 1000 d°C in Figure 13.8) to derive a cultivation limit, as the simulated decrease of G_p with altitude is not linear. Calculation of interpolated critical 1000 d°C limits (in the right hand column of Table 13.5) for G_p is derived from local linear interpolation. Limits are comparable with those calculated from the baseline climate data for 1985-1990 in Chapter 10, G_p being a better approximation to a daily temperature accumulation. The variation between uni-directional scenarios is large, from 70.2 m for northerly flow to 452.8 m for south-easterly flow. In the first case only 23.2% of the land in northern England is below the limit. This is restricted to low lying areas around the Tyne, Tees and the Solway Firth. In the south-easterly scenario, however, 90.1% of the land is suitable for cultivation using the same thermal criterion, including most of Stainmore and lower slopes of the Pennines. The 1000 d°C limit for the calm scenario is fairly high at 320 m. Despite colder winters, summers would be fairly warm. Although the highest altitudinal limit is recorded in the south-easterly scenario, the highest temperatures at sea-level are associated with southerlies because of the steeper altitudinal decrease in G_p for the latter airflow. South-westerly and westerly simulations lead to low cultivation limits (e.g. 245.8 m for westerly flow) due to steep lapse rates. Polar maritime air, which would be present in the north-westerly scenario, lowers the 1000 d°C elevation to below 150 m, illustrating the effectiveness of maritime air-masses in increasing the altitudinal gradient of "growth potential" (Manley 1945a).

Theoretical cultivation limits for the uni-directional wind scenarios above will be compared with limits calculated from the 1985-1990 data. Using a linear model of degree days versus altitude (Chapter 10, section 3), the 1000 d°C limit varied from 236 m in 1986 to 463 m in 1989. The 1986 value is within the range of values simulated for the uni-directional wind scenarios. However, the limit in 1989 (and the value of 453 m in 1990) are both slightly above the limit for the warmest airflow (452.8 m),

Figure 13.8. Variation of Warm Season Growing Season Strength, Gp, with Altitude, in all Uni-directional Wind Scenarios

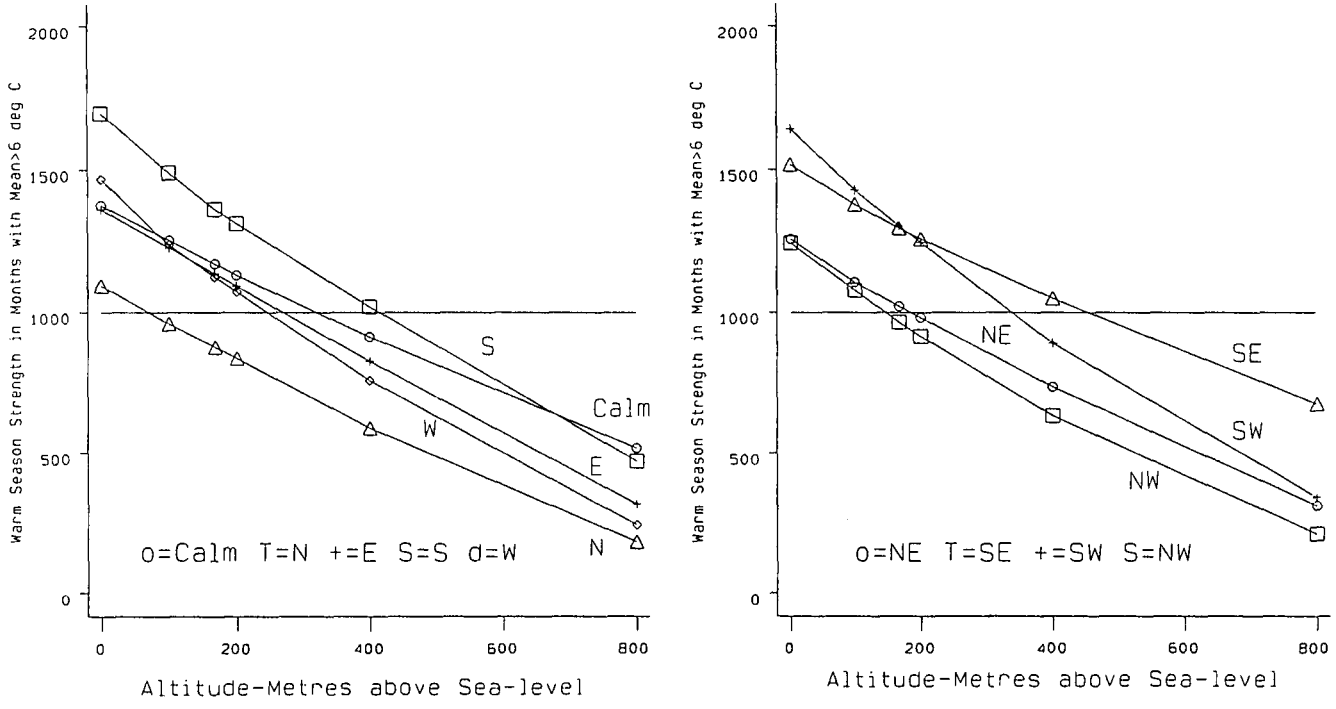

confirming that 1989 and 1990 were both exceptionally warm. Certain airflows are required to be warmer than the average conditions expected (derived from 1985-1990) in 1989 and 1990 to account for the extremely high cultivation limits experienced.

An exponential model was also used to describe the variation of growing season strength with altitude and was supported by mathematical theory (Chapter 10, section 4). Cultivation limits interpolated using this model were lower than in the linear case, varying between 191 m and 420 m. Reassuringly, these values are well within the range 70-453 m specified for the individual uni-directional wind scenarios, although they lie near the upper end of the range (especially the warm years of 1989 and 1990).

13.7 Complex Wind Scenarios

A mix of airflows in any month could be simulated to make the scenario more realistic. To calculate predicted mean monthly temperatures under a combination of wind directions requires a weighted average of the two or more appropriate regression equations. For example, to simulate the mean temperature in a month with **n** days of northerlies and **e** days of easterlies (the month has **m** days (**n+e=m**)) the resulting equation is:

$$X = \frac{n}{m}[a_n(alt) + 130.6b_n + 80.2c_n + k_n]$$
$$+ \frac{e}{m}[a_e(alt) + 130.6b_e + 80.2c_e + k_e] \quad ----(3)$$

The subscript n applies to the coefficients a, b and c and constant k, in the northerly regression and subscript e to the equivalent coefficients in the easterly regression. If **n=e** the result simplifies to:

$$X=\frac{n}{m}[a_n+a_e]\,alt+\frac{n}{m}[b_n+b_e]\,130.6$$
$$+\frac{n}{m}[c_n+c_e]\,80.2+\frac{n}{m}[k_n+k_e] \quad ----(4)$$

In this special case the new coefficients are simply the average of the coefficients from the two relevant regressions. A calculation could be carried out for any combination of winds in any proportions, although it becomes more complicated for three or more wind directions. Using weighted averages for the coefficients in the relevant regression equations, it is theoretically possible to generate the predicted temperatures for any combination of winds. A mean scenario for a calendar month is calculated by deriving the average of the altitudinal coefficients (lapse rates) for all nine airflow types (including calm) and this leads to the same results as the bottom row of Table 13.3.

13.8 Conclusions

The relationship between growing season strength and changes in the circulation pattern has been illustrated. The sensitivity of accumulated temperatures in the uplands to changing airflow patterns is greater than in adjacent lowland areas, with a wider percentage variation between the airflow scenarios at 800 m. The contrast in the altitudinal gradient of growing season strength between maritime and continental airflows arises because of the contrast in lapse rates (Chapters 5, 6 and 8). A more continental influence (such as in the south-easterly scenario) would be beneficial to upland areas, while increased progressiveness (associated with a more zonal westerly circulation) would be detrimental. Maps of the change in growing season strength for maritime and continental scenarios are given in Chapter 18.

The uni-directional wind scenarios created in this chapter are used to investigate the influence of the circulation on growing season length and frost occurrence in following chapters.

THE RELATIONSHIP OF THE LENGTH OF THE FROST-FREE PERIOD AND GROWING SEASON TO THE CIRCULATION PATTERN OVER THE BRITISH ISLES

14.1 Introduction

In the previous chapter mean daily temperatures simulated in different airflow scenarios were used to calculate growing season strength (G_p) at all altitudes for nine uni-directional wind scenarios. The other indices of "climatic potential", such as the number of (consecutive) growing days and frost occurrence (Chapters 11 and 12), cannot be simulated directly for these scenarios. Such parameters must first be related to mean daily temperature. If frost probability can be predicted from mean daily temperature it is then possible to determine the effects of a change in mean daily temperature on frost occurrence. The first section examines relationships between mean daily temperature, growing days and frost occurrence using logit regression.

14.2 Logit Regression: Relating Growing Days and Frost Occurrence to Mean Daily Temperature

Frost occurrence and the occurrence of growing days can both be described by categorical variables with two outcomes, those of occurrence (1) and non-occurrence (0). As mean daily temperature decreases, a frost (minimum $< 0°C$) is more likely and a growing day (maximum $>6°C$) less likely to occur. An S-shaped curve, produced by **logit** regression (Hamilton 1992), is most appropriate to model such binary variables.

Logistic curves show the occurrence of growing days for representative sites in Figure 14.1. The probability of a day with a maximum above 6°C rises steeply from zero when the monthly mean daily temperature is 0°C to nearly 1 when the mean daily temperature is 6°C. The curve is only a model so there is the slightly erroneous probability of a non-growing day when the mean temperature is 6°C! Subtle differences arise between different locations. Eskmeals shows an above zero probability of a growing day at a mean daily temperature of 0°C whereas High Close and Great Dun

Figure 14.1. Logistic Curves Relating Growth Occurrence (Maximum>=6 deg C) with Mean Daily Temperature for Representative Locations

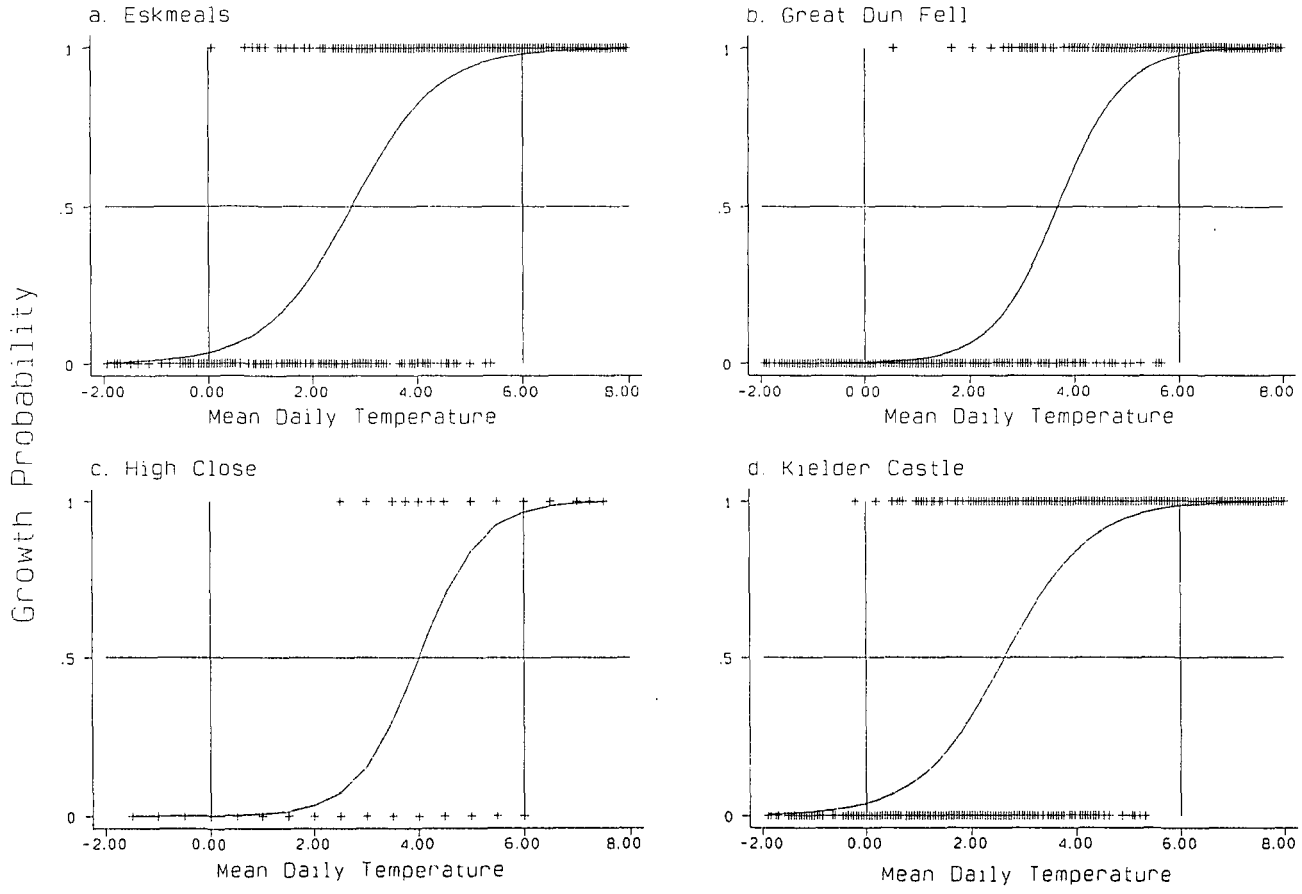

All graphs are shown between -2 and 8 deg C

Fell do not. The logistic curve for Great Dun Fell is steep due to the small diurnal temperature range experienced. A site with a large diurnal temperature range (such as Kielder) will show a shallower logistic curve. Thus small changes in the mean temperature of a particular airflow will alter growth probabilities at a faster rate at exposed sites with a small diurnal temperature range. The rate of change of growth probability also depends on absolute temperature; a decrease in mean daily temperature from 6°C to 5°C usually has less effect on growth probability than the equivalent decrease from 4°C to 3°C.

The logit function **L** is defined by coefficients **a** and **b**, where **L=ax+b**. **x** is mean daily temperature (°C). The probability of a frost or growing day at any mean daily temperature is:

$$probability(P) = 1/(1+e^{-L}) \quad ----(1)$$

where **L** is the logit function. If **L** equals zero the probability is 0.5. At a mean temperature of 0°C, **L** = **b** and the probability of growth is:

$$probability(P) = 1/(1+e^{-b}) \quad ----(2)$$

b will be negative for the growth probability as the probability of a growing day should be extremely low when x is 0°C. **b**, representative of the probability of a growing day when x=0°C, is listed in Table 14.1. At Great Dun Fell a value of **-5.85** corresponds to a growth probability of **0.0029**. In contrast, **b** is **-3.23** at Kielder, corresponding to a probability of **0.038 (3.8 %)**. This is more than ten times that at Great Dun Fell, illustrating the effect of an increased diurnal temperature range.

a, the coefficient of mean daily temperature, is related to the rate of increase in growth probability when mean daily temperature increases above 0°C. **a** is high at exposed locations such as Great Dun Fell (**1.594**), High Close (**1.681**) and Warcop

Table 14.1: Regression coefficients (**a** and **b**) in the logistic growth probability function.

place	**a**	**b**	r^2	**x(°C) (L=0.5)**
Durham	1.428	-4.36	0.73	3.40
Eskmeals	1.215	-3.33	0.68	3.15
Great Dun Fl	1.594	-5.85	0.81	3.98
Haydon Br	1.211	-3.51	0.70	3.31
High Close	1.681	-6.73	0.75	4.3
Houghall	1.477	-3.63	0.54	2.8
Kielder	1.225	-3.23	0.69	3.04
Nenthead	2.669	-10.29	0.85	4.04
Sunderland	1.767	-6.69	0.76	4.07
Warcop	1.957	-7.09	0.80	3.88
Wycliffe Hl	1.268	-3.32	0.65	3.01

(**1.957**). The value of **2.669** for Nenthead relates to the dramatic increase in probability above 0°C, suggesting that this site is unusual in some way. Sheltered sites such as Kielder, Wycliffe Hall and Haydon Bridge have low values of **a**.

To calculate the mean daily temperature x_c for which **L** is 0.5:

$$x_c = (0.5 - a)/b \quad ----(3)$$

The growing day probability corresponding to a logit of 0.5 is 0.622. Values of the x_c range from **2.8°C** at Houghall to **4.3°C** at High Close. Kielder requires a mean daily temperature of only **3.04°C**.

The success of the logistic curves can be assessed by the pseudo r^2 value, which represents the proportion of variation in growth occurrence explained by mean daily

temperature. r^2 is relatively high in most cases, ranging from **0.54** at Houghall to **0.85** at Nenthead. Nearly all values are above 0.7.

Logistic curves were also derived relating frost probability to mean daily temperature (Figure 14.2). **a** is negative, indicating a decrease in frost probability with increasing mean temperature, and **b** is positive, meaning that frost probability at a mean daily temperature of 0°C is nearly equal to 1. **b** varies between **5.46** at Eskmeals (probability= **0.996**) to **2.52** at Hartburn Grange (probability=**0.926**) (Table 14.2). Frost probability decreases rapidly above 0°C at Great Dun Fell (**a = -1.472**) and Eskmeals (**-1.534**), as expected of such exposed summit and coastal locations. Frost probabilities were calculated for a mean daily temperature of 5°C (as well as 0°C). Houghall shows a high probability of **0.47 (47%)**! This is followed by **32.7%** at Wycliffe Hall and **31.2%** at Kielder. The corresponding probability for Great Dun Fell is only **0.023 (2.3%)**.

The mean daily temperature for which **L** is 0.5 ranges from **3.93°C** at Houghall to **1.90°C** at Newcastle and Warcop. This difference of 2°C in mean daily temperature given a similar frost probability means that great local variations in frost risk occur. 2°C can be the difference between mean temperatures of two consecutive months, especially in a maritime climate (Manley 1952)!

Pseudo r^2 is often lower than for growth curves, averaging between 0.6 and 0.7. The worst value is **0.39** at Houghall (caused by insufficient data), while the best is **0.8** at Great Dun Fell. The success of the model at the upland summit suggests a stronger dependence of frost occurrence on mean daily temperature there.

Figure 14.2. Logistic Curves Relating Frost Occurrence (Minimum <=0 deg C) with Mean Daily Temperature for Representative Locations

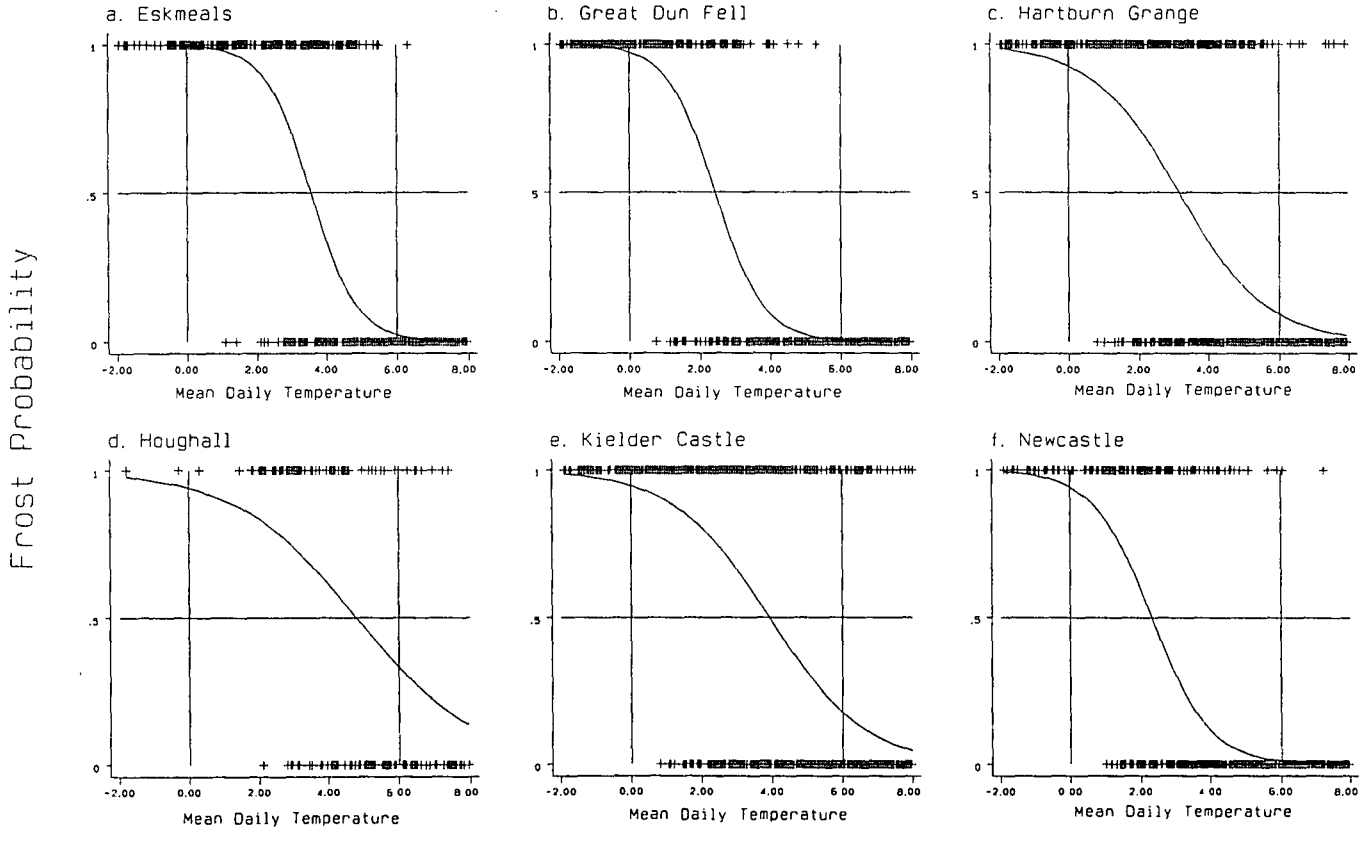

All graphs are shown between -2 and 8 deg C

Table 14.2: Regression coefficients (**a** and **b**) in the logistic frost probability function.

place	a	b	r^2	prob (x=5°C)	x(°C) (L=0.5)
Durham	-0.941	2.80	0.61	0.130	2.44
Eskmeals	-1.534	5.46	0.74	0.099	3.23
Great Dun Fl	-1.472	3.59	0.80	0.023	2.10
Hartburn Gr	-0.800	2.52	0.56	0.185	2.53
High Close	-1.241	3.76	0.67	0.080	2.63
Houghall	-0.580	2.78	0.39	0.470	3.93
Kielder	-0.736	2.89	0.56	0.312	3.25
Nenthead	-1.398	4.06	0.71	0.051	2.55
Sunderland	-1.483	3.55	0.72	0.021	2.06
Warcop	-1.440	3.24	0.74	0.019	1.90
Wycliffe Hl	-1.096	4.76	0.67	0.327	3.89

14.3 Use of Logistic Curves to Estimate the Total Number of Growing Days and Frosts in the Uni-directional Wind Scenarios

14.3.1 Growing Days

The mean daily temperatures predicted in Chapter 13 for individual airflows will be converted to the number of growing days or frosts expected per annum, using the logistic curves. Durham (102 m) and Great Dun Fell (847 m) are used as examples. Predicted mean daily temperature and the associated frost and growth probabilities for each airflow in each month at Durham are represented in Figure 14.3. The top two graphs relate to probability of a growing day. Figure 14.3 a shows the simulated growing day probability for each airflow. This is then converted into the number of growing days expected per month (Figure 14.3 b). Numbers represent wind direction.

There is a large variation in winter growth probabilities according to airflow,

Figure 14.3. Simulated Number of Growing Days and Frosts for Uni-directional Wind Scenarios using Logistic Curves: Durham Monthly Accumulations

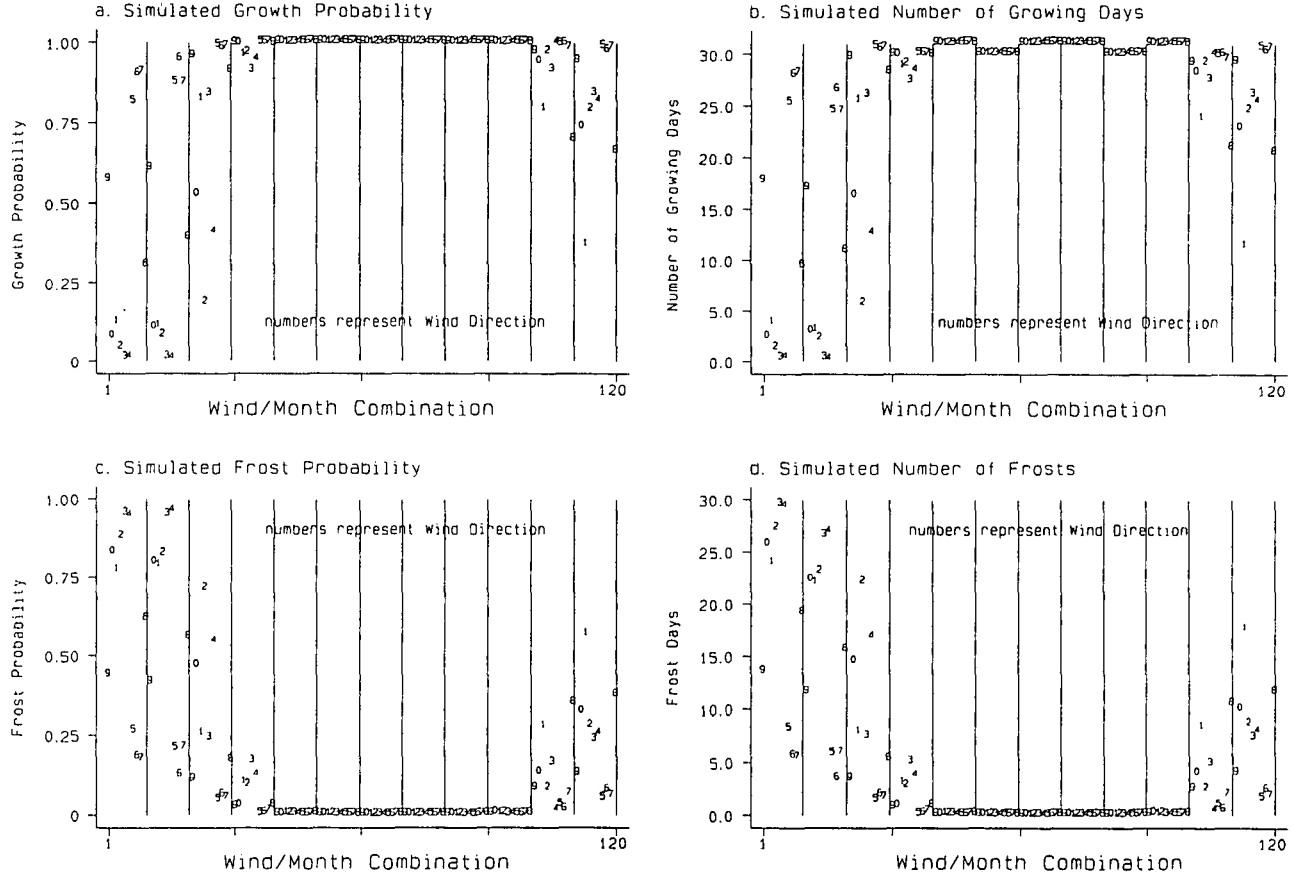

especially between January and March. Mean daily temperatures often fall between 0°C and 6°C in these months and resultant contrasts in growth probability are great. For example, the January growth probability is 1% for easterly and south-easterly flows (mean temperatures below freezing), but 90% for south-westerly and westerly flows (mean temperatures are 4.6°C). The number of growing days expected in January therefore varies from 0.3 to 28.1, depending on airflow. From December to March, winds between north-west (8) and south-east (4) produce low probabilities. Easterlies and south-easterlies are coldest in January and February while northerlies and north-westerlies are coldest in November and December. Between May and October wind direction becomes irrelevant, all airflows being associated with maxima above 6°C. Calm conditions produce low growth probabilities (10%) in January and February. The importance of mild airflows from the south and west at Durham in encouraging growing days to occur throughout the winter must be acknowledged (Figure 14.3 b).

The annual total number of growing days (G_T) for the uni-directional airflow scenarios is shown in Table 14.3 and Figure 14.4.

Table 14.3: Annual growing days ($\mathbf{G_T}$) and frosts ($\mathbf{F_T}$) at Durham and Great Dun Fell for uni-directional wind scenarios.

Wind direction	Growdays Durham	Growdays GDF	Frosts Durham	Frosts GDF
Calm	286.8	184.8	76.8	164.4
N	280.8	165.6	82.8	184.8
NE	276.0	163.2	86.4	186.0
E	291.6	178.8	80.4	181.2
SE	280.8	182.4	85.2	174.0
S	355.2	213.6	18.0	130.8
SW	358.8	190.8	14.4	139.2
W	357.6	174.0	16.8	170.4
NW	303.6	146.4	62.4	190.8
Mean	337.2	180.0	36.0	172.8

Figure 14.4. The Simulated Annual Total of Growing Days and Frosts for Uni-directional Wind Scenarios at Durham and Great Dun Fell

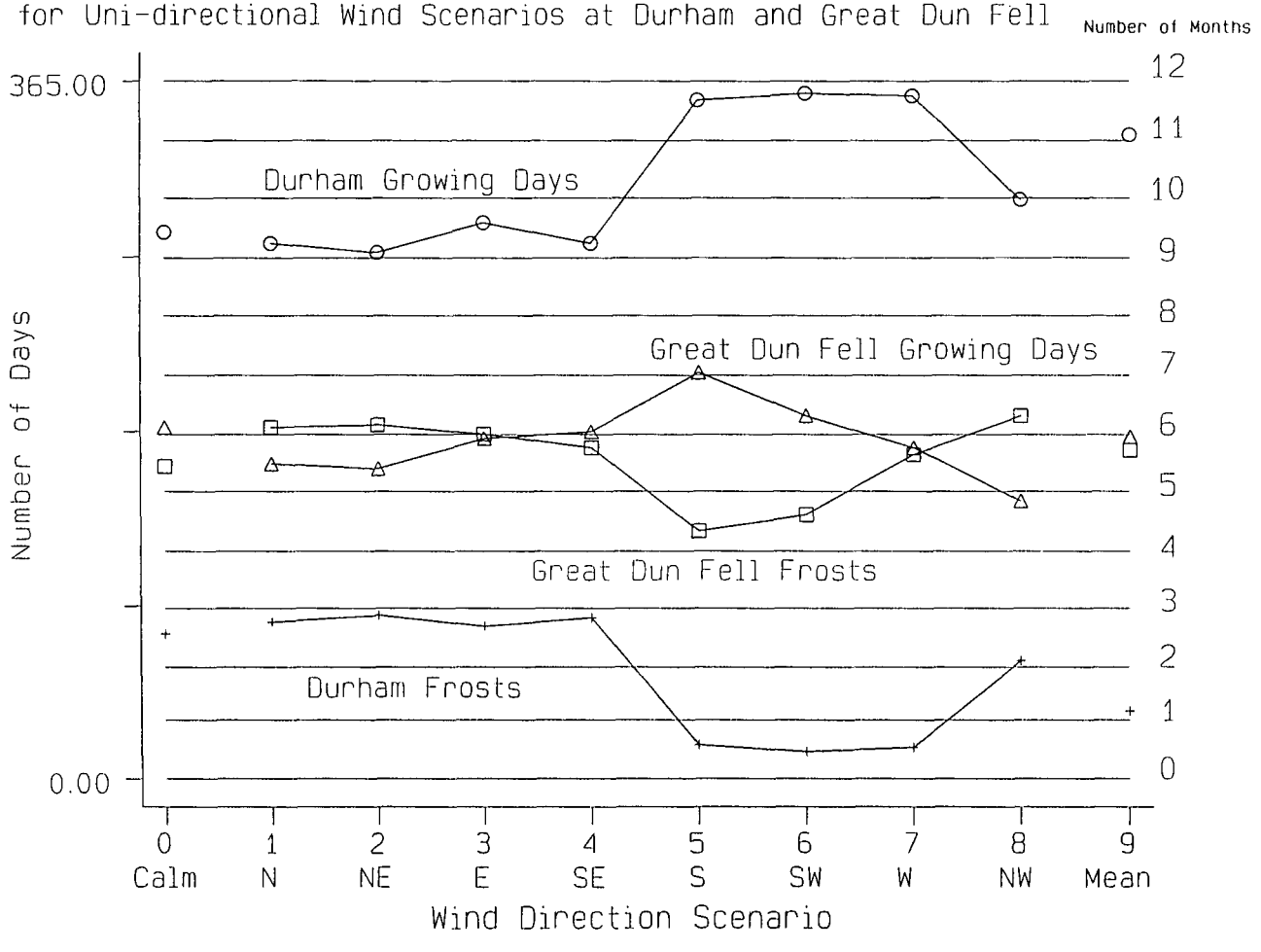

The annual number of growing days predicted for Durham ranges from 276 for north-easterly flow to 358.8 for south-westerly flow. The contrast between continental north-easterly flow and mild Atlantic air from the south and west is 70-80 growing days per annum. The difference in the annual total occurs due to winter differences.

Simulated temperatures are the mean for the particular airflow. Unfortunately this can lead to bias. For example, if the mean is near 6°C growth probability is likely to be overestimated, and if the mean is well below 6°C the probability is likely to be underestimated, because the simulation ignores exceptionally mild and cold spells (Hamilton 1987). When temperature thresholds are involved the simulation of extreme conditions can be as critical as that of mean conditions (see Chapter 16).

Mean daily temperatures predicted for Great Dun Fell were also converted to frost and growth probabilities for each airflow. There is less contrast in winter growth probabilities and wind direction is largely irrelevant. Between November and March all the simulated mean temperatures are below 0°C and growth is negligible. Between May and October growth probabilities are high, mean daily temperatures being above 6°C. Only in April is there a significant contrast, between zero growth probability for easterly flow (mean temperature of -1.29°C) and a growth probability of 0.878 under southerly flow (mean temperature of 4.91°C). Annual totals (G_T) range from 163.2 growing days for north-easterly flow to 213.6 days for southerly flow (Figure 14.4). Numbers are lower than at Durham but the range between airflow types is also less, at only 50 days (compared with over 80 at Durham).

To conclude, the contrast in the annual number of growing days G_T between mild airflows from the south and west, and continental air from between east and north, is great in lowland areas, but less significant in the uplands. Durham gains extra warmth in the lee of the Pennines due to föhn effects in westerly flows. At Great Dun Fell monthly contrasts in the number of growing days are more influential than contrasts due to airflows, although the latter becomes important in April.

14.3.2 Frosts

Frost probabilities associated with the uni-directional wind scenarios are shown for Durham in Figures 14.3 c and d. Between January and March frost probability depends strongly on airflow. In January frost probability is 17.2% for westerly and 17.9 % for south-westerly flow, but 94.5% for south-easterly and 95.1% for easterly flow. Similar contrasts arise in February and March. Winds between north-west (8) and south-east (4) have high frost probabilities in winter. Frosts are uncommon between May and October inclusive (Figure 14.3 d) in all airflow types. Predicted variation in winter according to airflow is considerable, e.g from 5 to 30 days in January. The circulation pattern is therefore important in controlling winter frost occurrence in lowland areas.

Cumulative annual frost days (F_T) (Table 14.3 and Figure 14.4) vary by 500% between airflows. North-easterlies will produce 86.4 frosts per annum, whereas south-westerly flow would produce only 14.4. This illustrates the dramatic reduction in frost associated with mild southerly and westerly winds. The contrast between the southerly, south-westerly and westerly airflows and others is strong, the next lowest annual total being 62.4 for the north-westerly scenario. Advection of mild air from the Atlantic prevents frosts, explaining why the growing season is much longer in lowland areas facing southern and western coasts, such as Galloway, Dyfed, Cornwall and even north-western Scotland (Bilham 1938, Taylor 1967a). Sub-tropical plants can flourish as far north as Inverewe on the north-western coast of Scotland (Manley 1952) due to the lack of frost.

Annual frost totals (F_T) at the summit of Great Dun Fell are much higher than at Durham. Simulated daily temperatures below freezing for all airflows in winter mean that advection frost is inevitable from November to March. Exceptionally mild conditions which occasionally occur are not simulated. By April, the frost probability falls to 0.026 for southerly flow but is still 0.996 for easterly flow. A month later the highest probability is only 0.119 (for north-westerly flow). April is therefore the only month when there is a large variation in frost probability according to airflow. The

circulation in April is thus critical for both growth and frost occurrence in the uplands. Likewise, in November there is a well-marked contrast in frost probabilities between 0.382 for south-westerly flow and 0.996 for northerly flow.

Overall, there is less dependence of frost occurrence on airflow direction at Great Dun Fell than at Durham. Annual totals F_T (Table 14.3) vary from 190.8 days for north-westerlies to 130.8 days for southerlies and 139.2 days for south-westerlies. The annual frost total for westerlies (170.4 days) is almost as high as for other wind directions, due to relatively steep lapse rates simulated. The recorded frost frequency at Great Dun Fell averages 154 days between 1985 and 1990 so the scenarios are fairly realistic. The variation in F_T between wind scenarios amounts to 60 days, much less than at Durham (in both absolute and relative terms).

Because the effect of airflow direction appears subordinate to the annual fluctuation in air temperature at Great Dun Fell when evaluating frost and growth probabilities, one may expect changes in the general circulation pattern alone to have less influence on annual frequencies of frosts and growing days at high altitude. The effect of a change in the circulation is moderated by the advective effect of the free air which is largely independent of wind direction. Small temperature changes which arise due to changes in relative airflow frequencies would be more significant in terms of growth and frost occurrence in lowland areas for most of the year. Absolute changes in temperature are likely to be similar at Great Dun Fell but the significance of these changes is less. The increased sensitivity of the lowlands contrasts with the impression obtained when the percentage variation in accumulated temperatures was examined (Chapters 10 and 13) which was greater in upland areas. Thus, the sensitivity of the climatic environment to changes in the circulation pattern increases or decreases with altitude, depending on the parameters under investigation. Although synoptic (between-type) causes of variation in accumulated temperatures are increasingly important at high altitude, variation in the occurrence of growing days and frosts becomes less dependent on synoptic controls and more dependent on season in the uplands.

14.4 The Conversion of Growing Days and Frosts to the Number of Consecutive Growing Days and the Length of the Frost-free Period Respectively.

14.4.1 Growing Days

The total number of frosts or growing days is not the most useful climatic indicator. The length of the consecutive growing season (the number of consecutive growing days) and length of the frost-free season, discussed in Chapters 11 and 12, are more useful. Unfortunately, there is no direct way of calculating these quantities for the scenarios. However, the length of the consecutive growing season can be related statistically to the total number of growing days and the frost-free period to the total number of frosts, using data from 1985-1990. Then the number of growing days (G_T) can be converted to a corresponding number of consecutive growing days (G_C), and likewise for frosts.

The relationship between the number of consecutive growing days $\mathbf{G_C}$ and the total number of growing days $\mathbf{G_T}$ is modelled well by linear regression (Figure 14.5 a):

$$G_c = (0.948 G_T) - 67.8 \quad r^2 = 0.968 \quad ----(4)$$

This equation is based on mean values of G_C and G_T derived for 22 locations in the study area. The intercept should be zero because if there are no growing days there is, by definition, no growing season. The negative constant obtained indicates underestimation of G_C at low values of G_T. The lowest number of growing days is about 200 (Great Dun Fell) so this is not a serious problem if extrapolation beyond the range of the data used to develop the regression is not attempted. G_C is expected to increase much more rapidly as G_T approaches 365. There is little evidence, however, of a curved trend in Figure 14.5 a.

The relationship between G_C and G_T at an individual location is subtly different, depending on station altitude and exposure. Adding local exposure (Chapter 4) to the

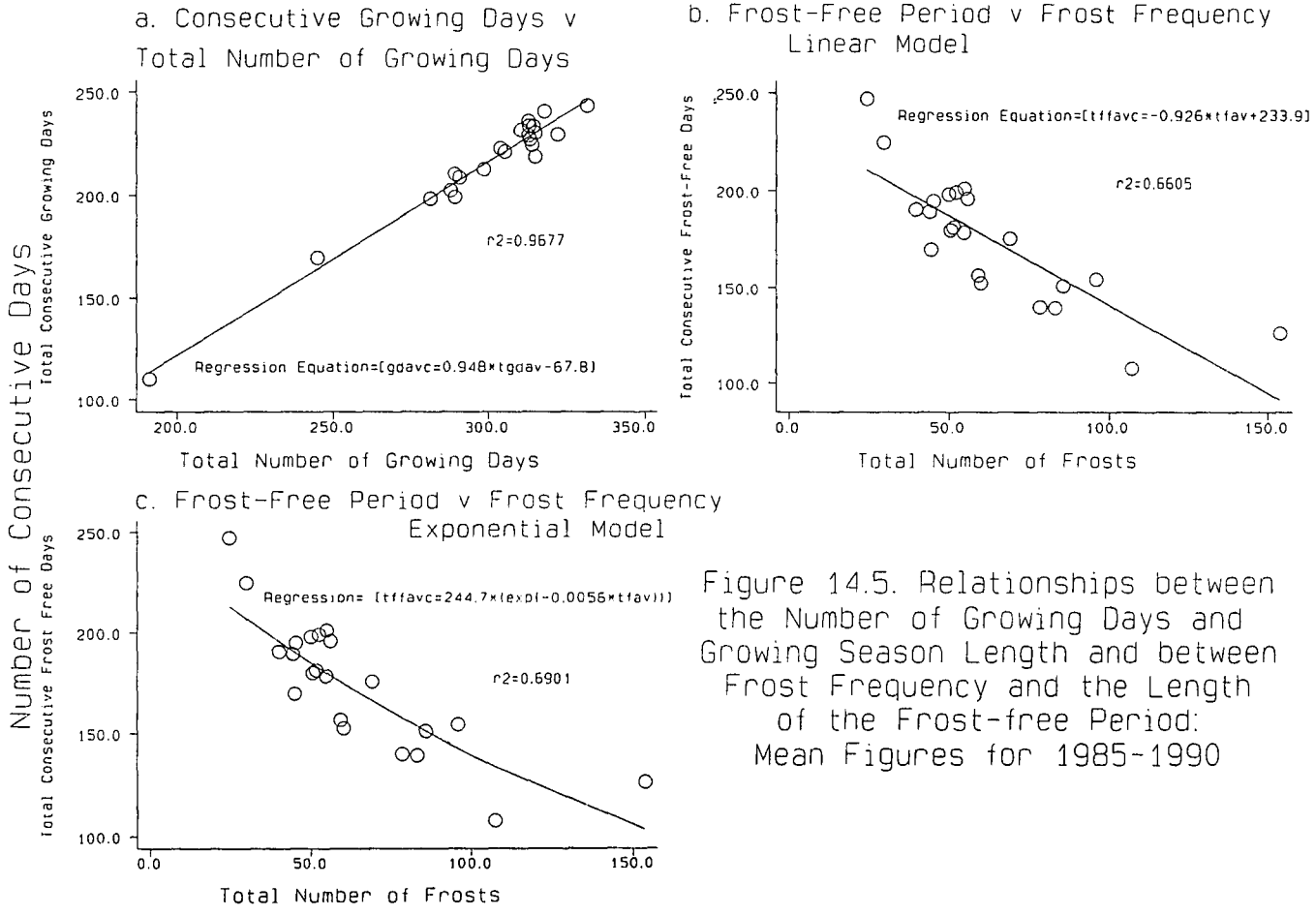

Figure 14.5. Relationships between the Number of Growing Days and Growing Season Length and between Frost Frequency and the Length of the Frost-free Period: Mean Figures for 1985-1990

regression increases R^2 slightly to 0.971. Separate equations can then be produced for each location.

$$G_c = (0.894 G_T) + (0.007 l) - 51.86 \quad \text{----(5)}$$

l represents exposure at the local scale and is high in sheltered locations. For a given value of G_T , G_C is higher in a sheltered location. At Great Dun Fell (l = -1051):

$$G_c = (0.894 G_T) - 59.22 \quad \text{----(6)}$$

while at Durham (l = -199) :

$$G_c = (0.894 G_T) - 53.25 \quad \text{----(7)}$$

G_C is about six days longer at Durham than at Great Dun Fell for a given number of grow days G_T due to increased shelter.

The predicted length of the growing season (G_C) at Durham varies from 193.5 days for constant north-easterly flow (just over 6 months) to 267.5 days for south-westerly flow (nearly 9 months) (Table 14.4). The length of the season at Great Dun Fell is shorter, ranging from 71.7 days for north-westerly flow to 131.7 days for southerly flow. The difference between these two extremes amounts to over 2 months and in percentage terms the difference is more significant than at Durham. At Durham there is an appreciable contrast between airflows running clockwise from north-west to south-east (yielding seasons of around 200 days) and the values of over 260 days predicted for southerly, south-westerly and westerly airflows. At Great Dun Fell the contrast is less extreme, with 103.8 days simulated for south-easterly flow, 131.7 days for southerly flow and 111.4 days for south-westerly flow (Table 14.4 and Figure

14.6).

One drawback to this approach is the assumption that the relationship between G_T and G_C remains constant, irrespective of airflow. A mild airflow may allow sporadic growing days to occur in winter but this would not increase G_C unless the extra days were immediately before or after the original growing season.

Table 14.4: The length of growing and frost-free seasons at Durham and Great Dun Fell for uni-directional wind scenarios.

place	Growing Season Durham	Growing Season GDF	Frost-Free Period Durham	Frost-Free Period GDF
Calm	203.1	106.0	154.2	104.7
N	197.8	88.8	144.1	70.5
NE	193.5	86.7	138.1	68.5
E	207.4	100.6	148.2	76.5
SE	197.8	103.8	140.1	88.6
S	264.3	131.7	252.8	161.0
SW	267.5	111.4	258.8	146.9
W	266.4	96.3	254.8	94.6
NW	218.2	71.7	178.3	60.4
Mean	248.2	101.7	222.6	90.6

14.4.2 Frosts

Similar techniques were used to predict the length of the frost-free period (F_C) from the total annual number of frosts (F_T) (Figure 14.5 b):

$$F_C = (-0.926 F_T) + 233.9 \ldots . r^2 = 0.66 \text{ ----(8)}$$

Figure 14.6. Simulated Lengths of the Consecutive Growth Period and Frost-Free Period for Uni-directional Wind Scenarios at Durham and Great Dun Fell

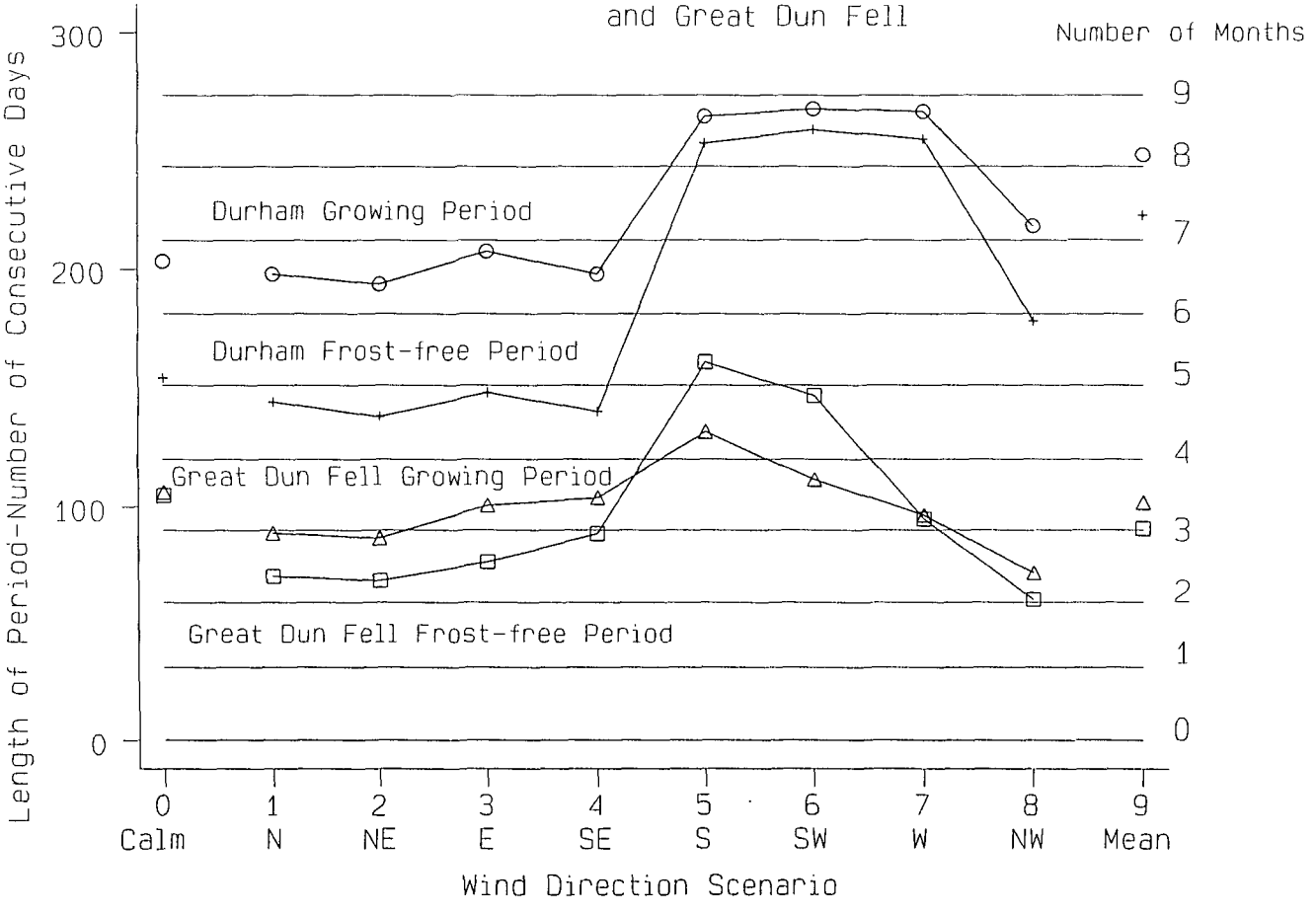

r^2 is only 0.66 and there is evidence of a curvilinear trend, F_C decreasing less rapidly as F_T continues to increase. This is common sense since further frost occurrence in a region of already high risk is just as likely to be realised in increased winter frequencies as in more unseasonal frosts which reduce the length of the frost-free period. At Great Dun Fell, F_C still averages more than four months despite a mean F_T of 154. An exponential model was fitted but r^2 still remained low, at 0.69 (Figure 14.5 c):

$$\ln F_C = 244.7 \times e^{-0.0056 F_T} \quad ----(9)$$

Adding station altitude and micro-exposure to the linear regression, however, increased R^2 to 0.87:

$$F_C = (-1.676 F_T) + (0.105 alt) - (0.109 micro) + 261.2 \quad ----(10)$$

Thus:

$$F_C = (-1.676 F_T) + 282.92 \quad ----(11) \quad (Durham)$$

$$F_C = (-1.676 F_T) + 380.22 \quad ----(12) \quad (Great\ Dun\ Fell)$$

The constants in equations 11 and 12 represent the expected frost-free period when there are no frosts, extrapolated from the observed data. This should be equal to 365/366 days. The Great Dun Fell value is near this but that for Durham is well below, highlighting the inaccuracies in extrapolating regression equations outside the range upon which they were developed.

F_C at Durham (Table 14.4 and Figure 14.6) ranges from 138.1 days (about 4.5

months) for north-easterly flow to 258.8 days (about 8.5 months) for south-westerly flow. The variation of 120 days between airflows is large. The frost-free period is not as long as the consecutive growing period ($F_C < G_C$) in all scenarios. The difference is greatest for northerly and easterly airflows. Thus there is a greater risk of frost at Durham during the growing season in the scenarios in which the circulation is dominated by northerly and easterly surface flow. Increased anticyclogenesis over Scandinavia is one cause of more frequent northerly and easterly surface flows, especially in spring (Lamb 1950). According to the above analysis, frost risk during the growing season would increase for such a scenario with F_C becoming much shorter than G_C.

At Great Dun Fell F_C ranges from 60.4 days (2 months) for north-westerly flow to 161 days for southerly flow. This percentage variation of 267% is greater than the variation in G_C. The growth period (G_C) is often longer than the frost-free one (F_C) although the difference between the two is less than at Durham. Thus there is less relative frost risk during the consecutive growing season at the mountain summit. Under mild southerly and south-westerly flows F_C is longer than G_C!

14.5 The Calculation of 'Risk Days' for the Uni-directional Wind Scenarios

Mean daily temperatures for the uni-directional wind scenarios of Chapter 13 were converted into probabilities of growth and frost using logistic curves, enabling the length of the growing season (G_C) and frost-free period (F_C) to be simulated. There is a wide variation in both G_C and F_C between airflows. At Great Dun Fell, the frost-free period is longer than the growth period for southerly and south-westerly flows, while for all other airflows the opposite is true. In Durham the growing season is always longer than the frost-free period, although the difference is reduced for maritime airflows from the south and west. Frost is therefore likely to be present during the growth period, especially in the lowlands towards the beginning and end of the growing season.

The number of 'risk days' were calculated for each scenario by subtracting F_C

from G_C (as in Chapter 12). A negative result means that there is no frost risk during the consecutive growing season (Table 14.5).

Table 14.5: Number of risk days at Great Dun Fell and Durham for uni-directional wind scenarios.

scenario	riskdays Great Dun Fell	riskdays Durham	riskdays /G_C GDF	riskdays /G_C Durham
Calm	1.3	48.9	0.0123	0.2408
N	18.3	53.7	0.2061	0.2715
NE	18.2	55.4	0.2099	0.2863
E	24.1	59.2	0.2396	0.2854
SE	15.2	57.7	0.1464	0.2917
S	-29.3	11.5	-	0.0435
SW	-35.5	8.7	-	0.0325
W	1.7	11.6	0.0177	0.0435
NW	11.3	39.9	0.1576	0.1829
Mean	11.1	25.6	0.1091	0.1031

The highest number of risk days is 59.2, for easterly flow at Durham. Dividing the number of risk days by the length of the consecutive growing season gives an estimate of the proportion of the season at risk (columns 4 and 5). This varies from zero to 29%, the latter figure applying to south-easterly flow at Durham.

14.6 Conclusions: An Assessment of the Sensitivity of Climate Potential in Northern England to Circulation Changes

Changes in the relative frequencies of airflow types alone have important effects on growth and frost parameters in northern England. Changes in growing season length and frost risk do not necessarily mirror accompanying changes in growing season strength, discussed in Chapter 13.

For example, it has been shown that westerly and south-westerly airflows would encourage a rapid altitudinal decrease in growing season strength, accumulated temperatures at 800 m falling to 17% of those at sea-level (Table 13.4). The decrease was associated with steep lapse rates simulated for westerly flows. Work in this chapter has shown that in the westerly scenario the frost-free period becomes longer than the consecutive growth period, and despite the steep altitudinal reduction in accumulated temperatures, the upland growing season would be frost-free. On the other hand, larger upland temperature accumulations under blocked conditions (e.g. the south-easterly scenario) coincide with the frost-free period becoming shorter than the growth period ($F_C < G_C$). The number of risk days is 15.2 at Great Dun Fell for south-easterly flow. This is ironic since it is this airflow that experiences the highest warm season accumulated temperatures at 800 m. Despite high accumulated temperatures, continental air (in the south-easterly scenario) leads to a short frost-free period relative to the growth period.

These two examples show how parameters measuring growing season strength, length and frost risk must be examined together to gain an overall picture of changes in "climate potential" associated with each airflow type.

THE GROWING SEASON IN THE DURHAM METEOROLOGICAL RECORD 1801-1990 AND IMPLIED ALTITUDINAL LIMITS TO CROP GROWTH

15.1 Introduction

Previous chapters describe potential changes in the altitudinal variation of growing season strength, length and frost occurrence which would be experienced were airflow frequencies to alter. Each airflow scenario represents the influence of one airflow in isolation and in this way relative characteristics of airflow types are compared, although such an approach tells us little about recorded temporal changes in the relevant parameters which result from a combination of airflow changes. Extreme sensitivity of the growth and frost parameters to changes in airflows is suggested. To help assess whether such inter-annual contrasts are likely to occur, this chapter uses climatic data from Durham Observatory to illustrate the inter-annual variation in growing season strength in the region recorded over the last two centuries. By relating the historical variation of growing season strength to extrapolated cultivation limits, using relationships developed in Chapter 10 between growing season strength and altitude, small changes in mean annual temperature are shown to have had marked effects on the environment of northern England.

15.2 Data Sources

Temperature records from Durham Observatory (102 m) belong to one of the longest continuous meteorological time series in Britain. Daily data extend back to 1847 but mean monthly temperatures were reconstructed by Manley back to 1801 (Kenworthy 1985, Cox 1993a). The Durham record is the only reliable temperature series for the whole of the 19th and much of the 20th century in north-eastern England. The nearest comparable series is that constructed by Manley (1946) for Lancashire. The Radcliffe Observatory record in Oxford extends further back, to 1815, but is less relevant to the Pennines. Unlike Oxford, there has been relatively little urbanisation in the vicinity of Durham Observatory in the last two centuries and the record is fairly homogeneous, after changes in instrumental exposure and observing practice have been

taken into account. Manley carried out corrections to screen temperatures, necessitated by changes in the location of thermometers (Manley 1941, Kenworthy 1985) and these are accounted for in the data. Recent articles concerning the Durham record include an analysis of variations in temperature and rainfall (Harris 1985), the use of smoothing methods (Cox 1993b) and a comparison with data from the nearby village of Heighington (Pepin 1994).

15.3 Calculation of Growing Season Strength

An immediate problem is that many subtly different methods can be used to calculate accumulated temperatures, depending on the data available:

1. Annual accumulated temperatures (G_d), obtained from summing daily excesses of mean temperature above 6°C, reflect temperature variation on a daily timescale. These were related to altitude in Chapter 10 for the recent period.

2. The annual accumulated temperatures (G_y) calculated using mean monthly temperatures are lower than G_d, because winter months (when mean temperatures are below 6°C) contribute negative values to the annual total, cancelling out some of the positive accumulation.

3. The sum of accumulations within months with mean temperatures above 6°C (G_p) approaches the daily value G_d more closely.

4. The sum of April to October accumulations (G_w) is approximately equal to G_p in most years and is easier to calculate.

The four different estimates are summarised in Table 15.1, calculated at Durham for 1985 to 1990.

Table 15.1: Comparison of different accumulated temperature measures (d°C) (1985-1990). The threshold temperature is 6°C.

YEAR	G_d	G_y	G_w	G_p
1985	1288	777.45	1219.40	1219.40
1986	1222	762.85	1097.90	1166.90
1987	1282	872.35	1182.85	1188.85
1988	1385	1171.65	1270.30	1310.60
1989	1533	1343.20	1392.50	1432.70
1990	1556	1383.35	1365.20	1450.70
MEAN	1378	1052	1255	1295

Daily data are unavailable during the early years of the Durham record and mean monthly temperatures (yielding G_y, G_w or G_p) must be used to calculate growing season strength. Accumulated temperatures for a month with **n** days are estimated as **n(m-6)** where **m** is the mean monthly temperature. The result is negative if $\mathbf{m < 6}$, i.e. if the mean monthly temperature is below 6°C. Leap years were treated as ordinary years. G_y, G_p and G_w were calculated over the 190 years of the record. G_p and G_w are more indicative of growth potential, concentrating solely on the effective growing season. G_y also depends on winter conditions.

15.4 The Historical Variation in Growing Season Strength

15.4.1. Introduction

Any data series which are based on a temporal (or spatial) progression can be smoothed to identify possible trends in data structure. Good reviews of **time-series analysis** (Conrad & Pollak 1950, Holloway 1958, Lewis 1960, Chatfield 1975) make the point that the approach is full of traps. For example Lewis (1960) illustrates that when moving averages are used for smoothing, a random set of numbers can produce apparent periodicities. This **Slutsky-Yule** effect is often a valid objection to be raised when a "trend" is identified.

A good example of time-series analysis is given by the Uppsala record in Sweden which dates back to 1722. Bergström (1990) smoothed the wind records, showing that westerly winds were more frequent in the early 18th century. This would explain the cooler summers and milder winters experienced at this time. Anomalous years in the record are shown to affect filtered time series in unusual ways, especially when running means, rather than medians, are used (Bärring & Mattsson 1992). This is because running means are not resistant to outliers. The influence of extreme observations on smoothing results should be an important area of concern.

15.4.2 Smoothing of Accumulated Temperatures

G_y (section 15.3) is shown in Figure 15.1, smoothed using cubic splines connecting running medians (Hamilton 1992). The resulting curve depends on the method used and is somewhat arbitrary (Chatfield 1975). Cubic splines are based on numerous locally-weighted regression curves calculated at intervals along the series (Cox 1993b). The resulting curve is therefore largely resistant to outliers. There is a large inter-annual variation in G_y. Temperature accumulations in the warmest years are more than five times those recorded in the coldest years. The lowest annual total (255.5 d°C) occurred in 1879 at the end of a cold period, and has been connected with disastrous harvests reported at this time. In East Anglia corn was still being gathered in at Christmas (Lamb 1982). The 1879 summer Central England Temperature (CET) was only 13.7°C (Manley 1974), more than 1.5°C below the 1961-1990 average (15.37°C) (Parker, Legg & Folland 1992). The Durham record is therefore consistent with this. Other poor years evident in Figure 15.1 include 1816 (270.1 d°C), which has been nicknamed the 'year without a summer' due to the influence of the eruption of Mt. Tambora in 1815 (Lamb 1982). The highest annual accumulated temperature occurred in 1990 (1383.4 d°C). The warmth of the last two years in the record is striking. 1989 appears as the third warmest and 1990 as the warmest year. The smoothed curve indicates cold periods at the end of the 19th century and in the late 1960s and 1970s, along with a warm period around 1950. A recent increase in warmth is shown. These trends are also shown in other analyses (Perry & Barry 1973, Manley 1974, Parker, Legg and Folland 1992) and it is reassuring that the Durham record is in agreement.

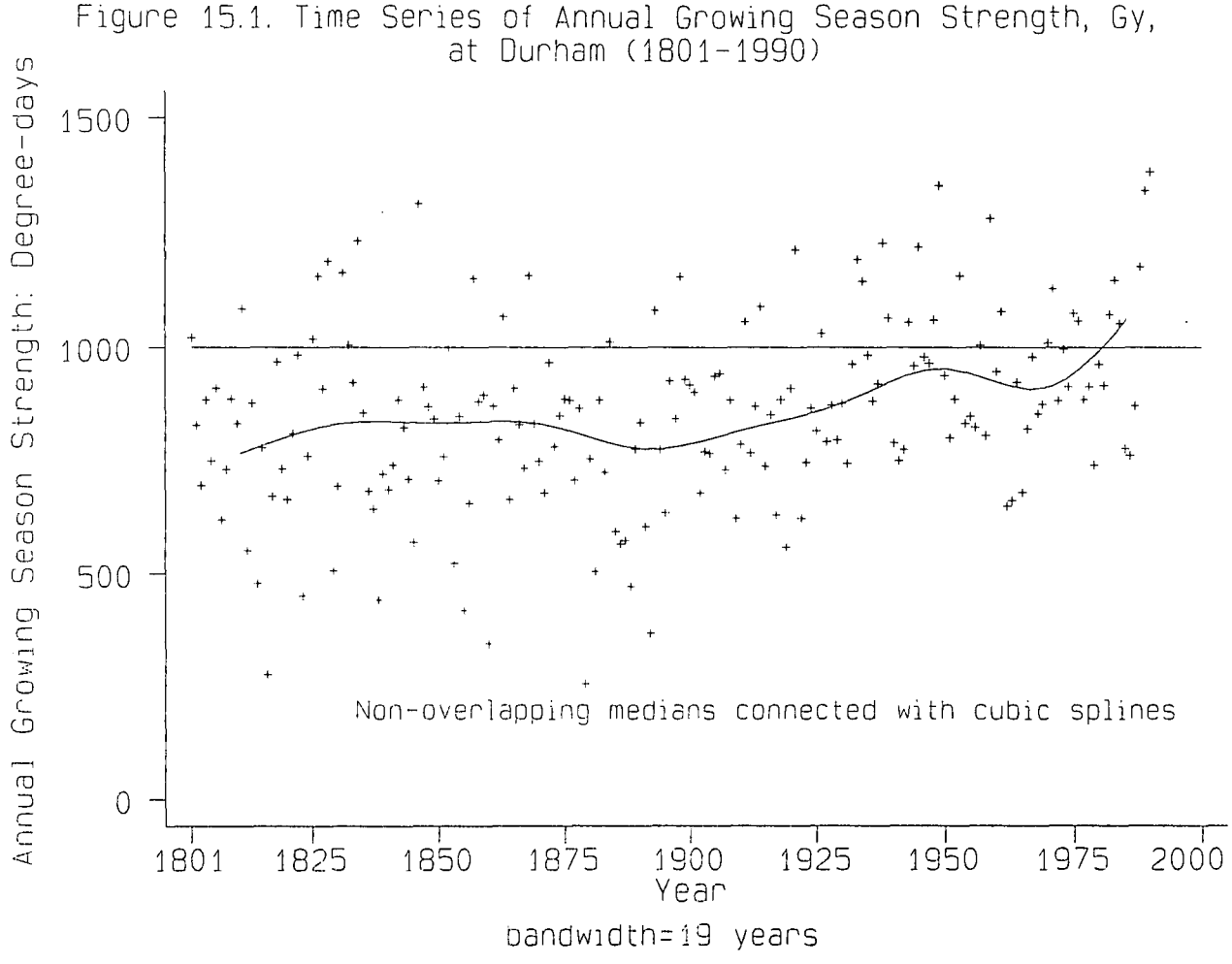
Figure 15.1. Time Series of Annual Growing Season Strength, Gy,
at Durham (1801-1990)
Annual Growing Season Strength: Degree-days
1500
1000
500
0
Non-overlapping medians connected with cubic splines
1801
1825
1850
1875
1900
1925
1950
1975
2000
Year
bandwidth=19 years

G_p (Figure 15.2) is more representative of warmth in the growing season since it is not affected by winter weather. Accumulations above 1500 d°C are common, especially in the 1930s and 1940s. Other warm seasons are evident in the first half of the 19th century, e.g. 1826 and 1846. These two summers were also very warm in the CET series, 1826 being the hottest summer in the record (Manley 1974). 1989 and 1990 warm season accumulations were less outstanding, with values around 1400 d°C, confirming that it is largely mild winters that led to increased high G_y values in 1989 and 1990.

Annual values of G_y and G_p were also smoothed using a running line least-squares smoothing method with Cleveland's (1979) tricube weighting function, variously known as 'lowess' and 'loess'. The amount of smoothing was controlled by setting the bandwidth **b**, which could vary between 0 and 1. The larger the bandwidth the more the smoothing. If b were equal to 1, the time-series would be fitted by simple linear regression (Computing Resource Center 1992).

Annual temperature accumulations (G_y) are smoothed using three different bandwidths. With **b** equal to 0.8 (152 years) there is a steady increase in G_y from around 800 d°C in 1800 to almost 1000 d°C in 1990 (Figure 15.3 a). Using a reduced bandwidth of 0.5 (90 years) produces a sharp upturn in the last decade (Figure 15.3 b). The low bandwidth of 0.2 (38 years) makes the recent increase appear dramatic (Figure 15.3 c). Warm periods appear around 1800, 1830-40, 1910 and in the 1940s. These trends must be treated with caution since production of spurious oscillations in smoothing analysis is common (Burroughs 1980).

G_p is smoothed using lowess (Figure 15.4). Most values fall above 1000 d°C, the assumed critical limit to cultivation in Chapter 10. A bandwidth of 0.8 is associated with a levelling off of the curve over the last 20 years, a feature not evident in other graphs. A bandwidth of 0.5 produces a decrease throughout the 19th century, followed by an increase to around 1300 d°C in the 20th century. With a bandwidth of 0.2, the warming in the 1930s and 1940s, cooling in the 1960s and a recent increase in warmth are shown. The early part of the 19th century appears to have been warmer than the

Figure 15.2. Time Series of Warm Season Growing Season Strength, Gp, at Durham (1801-1990)

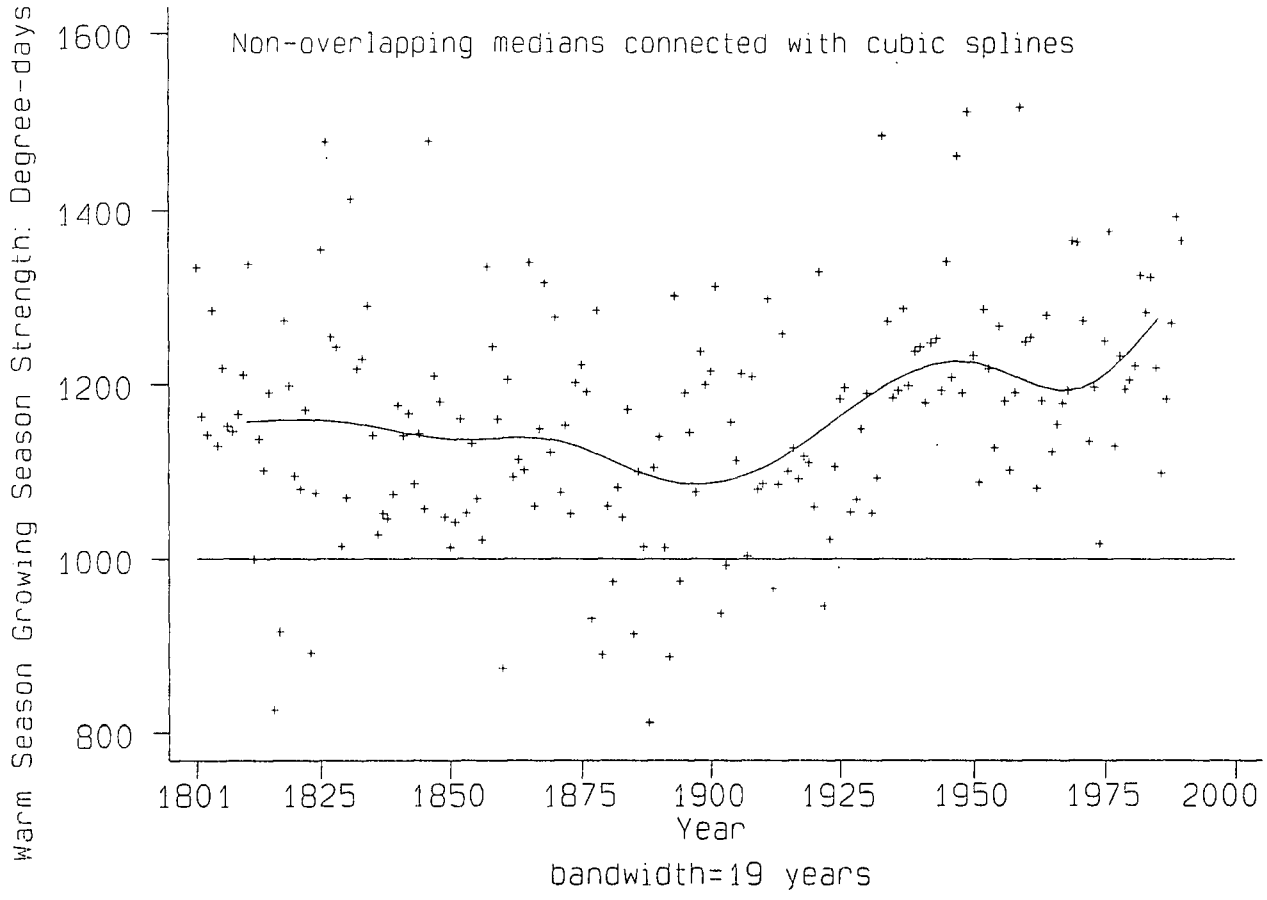

Figure 15.3. Time Series of Annual Growing Season Strength, Gy, at Durham (1801-1990), Smoothed by 'Lowess' at Three Different Bandwidths

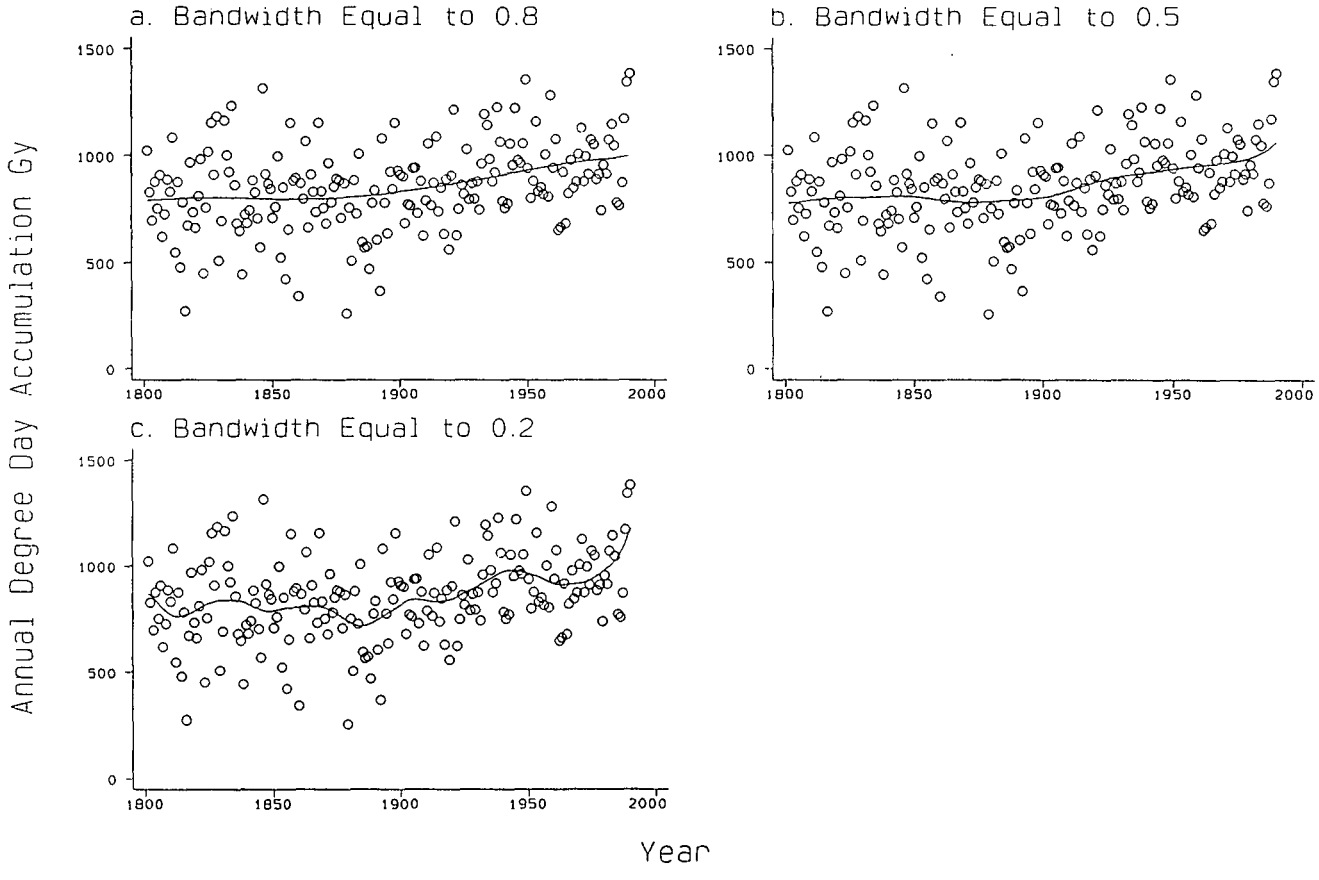

Figure 15.4. Time Series of Warm Season Growing Season Strength, Gp, at Durham (1801-1990), Smoothed by 'Lowess' at Three Different Bandwidths

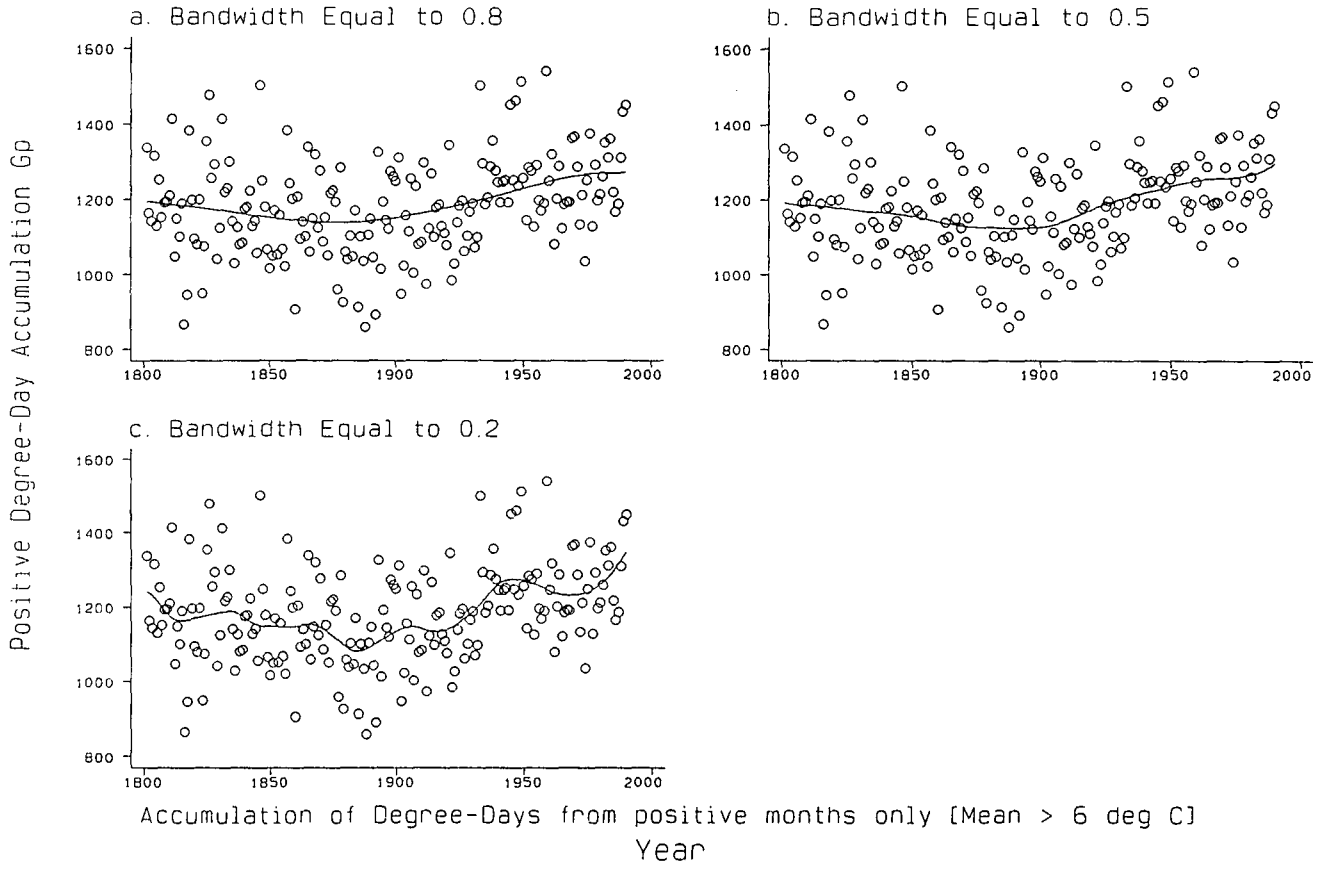

latter part. Comparison with Figure 15.3 c suggests that at the beginning of the 19th century warmer summers were often offset by colder winters.

15.5 Comparison of Historical Growing Season Strength with the Theoretical Accumulated Temperatures Derived in the Uni-directional Wind Scenarios of Chapter 13

Growing season strength can be predicted specifically for Durham (102 m) for the uni-directional wind scenarios in Chapter 13 using the regression equations for each airflow type in each month (Table 15.2). For example, the warm season temperature accumulation (G_p) would be 1018.8 d°C in the north-easterly scenario. Annual accumulated temperatures (G_y) would be 512.4 d°C.

Table 15.2: Durham temperature accumulations (d°C) for uni-directional wind scenarios.

Airflow Scenario	Predicted G_p	Predicted G_y
Calm	1224.3	765.6
N	912.6	414.0
NE	1018.8	512.4
E	1102.2	552.0
SE	1362.9	810.0
S	1476.0	1372.8
SW	1490.4	1406.4
W	1302.4	1209.4
NW	1112.3	723.6
Mean	1217.3	988.8

Accumulated temperatures are similar to those predicted at 100 m (Tables 13.2 and 13.3) since Durham has a similar elevation. Accumulations are lower than those predicted for 100 m under easterly flow because longitudinal and latitudinal coefficients

are negative at Durham. In contrast, accumulations for south-westerly and westerly flows are higher than the value for 100 m. An accumulation of over 1300 d°C is predicted under the westerly scenario for Durham, compared with 1238.3 d°C at 100 m.

G_y varies between 414 d°C for constant northerly flow and 1406.4 d°C for constant south-westerly flow at Durham. In the historical climate record, 186 out of 190 annual values (nearly 98 %) fall within these limits. G_y averages 853.04 d°C and ranges from 255.5 to 1383.35 d°C. The four historical G_y values falling outside the scenario extremes are all lower than 414 d°C, occurring in the 19th century (Table 15.3).

Table 15.3: Historical values of G_y and G_p falling outside predicted extremes for uni-directional wind scenarios. Figures in parenthesis represent these extremes.

G_y (414-1406.4 d°C)			**G_p (912.6-1490.4 d°C)**		
Year	**Value**	**Higher /Lower**	**Year**	**Value**	**Higher /Lower**
1816	270.1	L	1816	867.0	L
1860	339.5	L	1846	1501.7	H
1879	255.5	L	1860	906.5	L
1892	365.0	L	1888	859.9	L
			1892	891.6	L
			1933	1502.1	H
			1949	1512.2	H
			1959	1540.7	H

Two values occur in well-known cold years (1816 and 1879). 1860 and 1892 also appear as cold in the CET series. For G_y to fall below the predicted accumulation under the northerly scenario, certain airflows must have been associated with colder conditions than those recorded for 1985-1990. In other words, within-type climate change is necessary to account for this climatic variation (Barry 1967, Perry & Barry

1973, Comrie 1992). Fluctuations in growing season strength at Durham are too large to be explained by reference to circulation changes alone. G_y never exceeds 1406.4 d°C, the accumulation associated with the south-westerly scenario and the highest value is 1383.4 d°C (1990).

Historical G_p values will also be compared with predicted extremes (912.6 d°C for the northerly scenario and 1490.4 d°C for the south-westerly scenario). G_p varies between 859.9 and 1540.7 d°C. Thus values rise above and fall below these limits. The four years below (all in the 19th century) include 1816, 1860 and 1892, but not 1879. The four years above are mostly in the 20th century but include the hot summer of 1846, referred to as exceptional by the Durham Chronicle on Friday 19 June of that year:

> It is so melting hot this week
> that, though our readers flout us,
> The truth we must in conscience speak,
> We've scarce our wits about us (Kenworthy 1985, p 23).

Warmer and colder conditions than those recorded in 1985-1990 for individual airflow types are required to account for the historical fluctuation of G_p. Within-type climatic change (with reference to the 1985-1990 base period) is thus necessary to explain the extremely warm and cold years.

15.6 Seasonal Variations in Accumulated Temperatures

Seasonal accumulated temperatures have been smoothed using a bandwidth of 0.5 (Figure 15.5). In spring (March-May) total accumulated temperatures average around 100 d°C but are negative in a few years. The lowest value is -121.5 d°C (in 1837). In the warmest springs, the accumulation nears 300 d°C. The last three decades of the 19th century were dominated by cold springs, as was 1800-1810. The warming trend over the last two centuries is illustrated by counting the number of springs with negative temperature accumulations in each decade (Table 15.4).

Figure 15.5. Seasonal Time Series of Accumulated Temperatures at Durham, 1801-1990

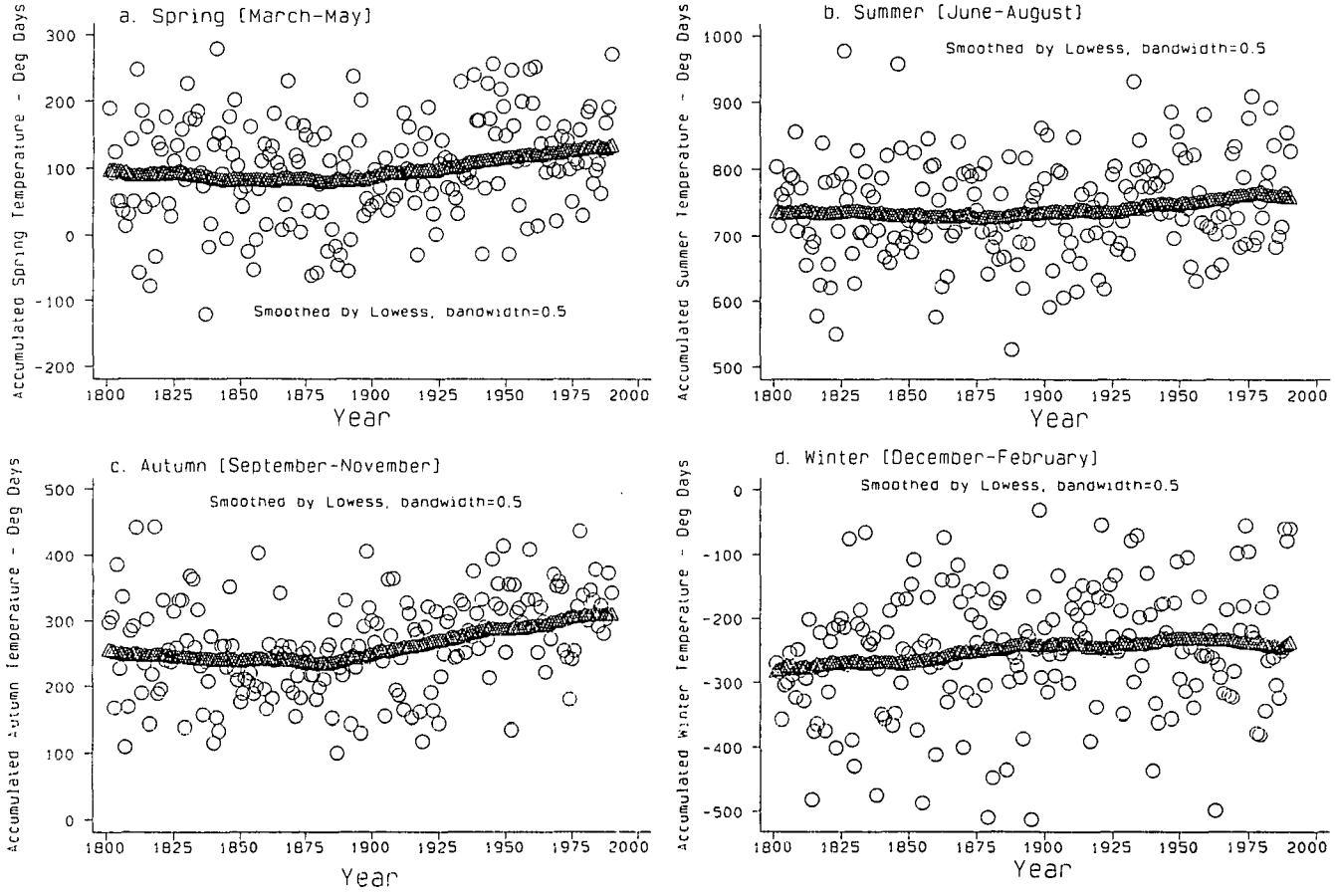

Table 15.4: The number of springs with negative accumulated temperatures in each decade (1801-1990).

Decade	N of neg years	1891-1900	2
1801-1810	-	1901-1910	-
1811-1820	3	1911-1920	1
1821-1830	-	1921-1930	-
1831-1840	2	1931-1940	-
1841-1850	1	1941-1950	1
1851-1860	3	1951-1960	1
1861-1870	-	1961-1970	-
1871-1880	2	1971-1980	-
1881-1890	4	1981-1990	-

The relative absence of years with negative spring accumulations in the 20th century is marked. This will have benefits in upland areas since the importance of warmth early in the year should not be underestimated (Taylor 1967a).

Summer (June-August) accumulations (Figure 15.5 b) show reduced percentage variability, ranging from 526 d°C in 1888 to 976 d°C in 1826. 700-750 d°C is typical, although the best summers exhibit nearly twice the warmth of the worst. Little temporal trend can be seen, in contrast to other seasons.

Autumn (September-November) accumulated temperatures exhibit a steady increase since the 1870s. Mean values of around 250 d°C in the 1870s increase to about 300 d°C in the 1980s. Accumulations below 200 d°C were common in the 19th and early 20th centuries, but there have been only two such seasons since 1950 (1952 and 1975).

Winter (December-February) values increase gradually throughout the record. A cooling in the 1960s and 1970s is shown. Despite recent warming, all values are well

below zero because a mean temperature above 6°C for the three winter months is extremely unlikely.

In conclusion, spring and autumn have become milder, possibly leading to an earlier start to the growing season and a later finish. Winters have also become milder but summer temperatures show little change. A change in spring warmth will have the most benefit, especially in upland areas where the delayed rise of temperature in spring is a major feature of the maritime climate. One warm day in spring is said to be worth a week in late summer or autumn for this reason (Utaaker 1968).

Examination of April temperatures tells an interesting story. Conditions in April are critical for growth and frost occurrence and in upland areas the month is marginal in growing terms. Mean accumulated temperatures at Durham are below 50 d°C (Figure 15.6), negative accumulations occurring in a third of years. Contrasts in frosts and growing days are at their greatest, especially in the uplands, depending on the circulation pattern (Chapter 14). April is also the month when lambing occurs in northern England and the effect of weather on growth of spring grass is especially important. If April is cold, grass growth will not begin until May and lambs require imported hay. Cold April weather can also cause fatalities among young lambs, especially if conditions are also wet (Starr 1981).

The smoothed graph of April accumulated temperatures shows little evidence of a historical increase, although a warming trend between 1900 and 1960 may be postulated. The smoothed curve lies almost at the same level in 1990 as in the middle of the 19th century. The reasons behind this are unclear. Increased advection of cold air drawn from the North Sea would explain low temperatures, especially in the north-east, especially if low sea surface temperatures (SST) were involved. Any explanation for sea-surface temperature variation must be connected to changes in SSTs outside British waters. A change in oceanic circulation would also account for some temperature changes within individual airflow types. These are necessary to account for the temporal variation in growing season strength since 1801.

Figure 15.6. Smoothed April Accumulated Temperatures at Durham, 1801-1990

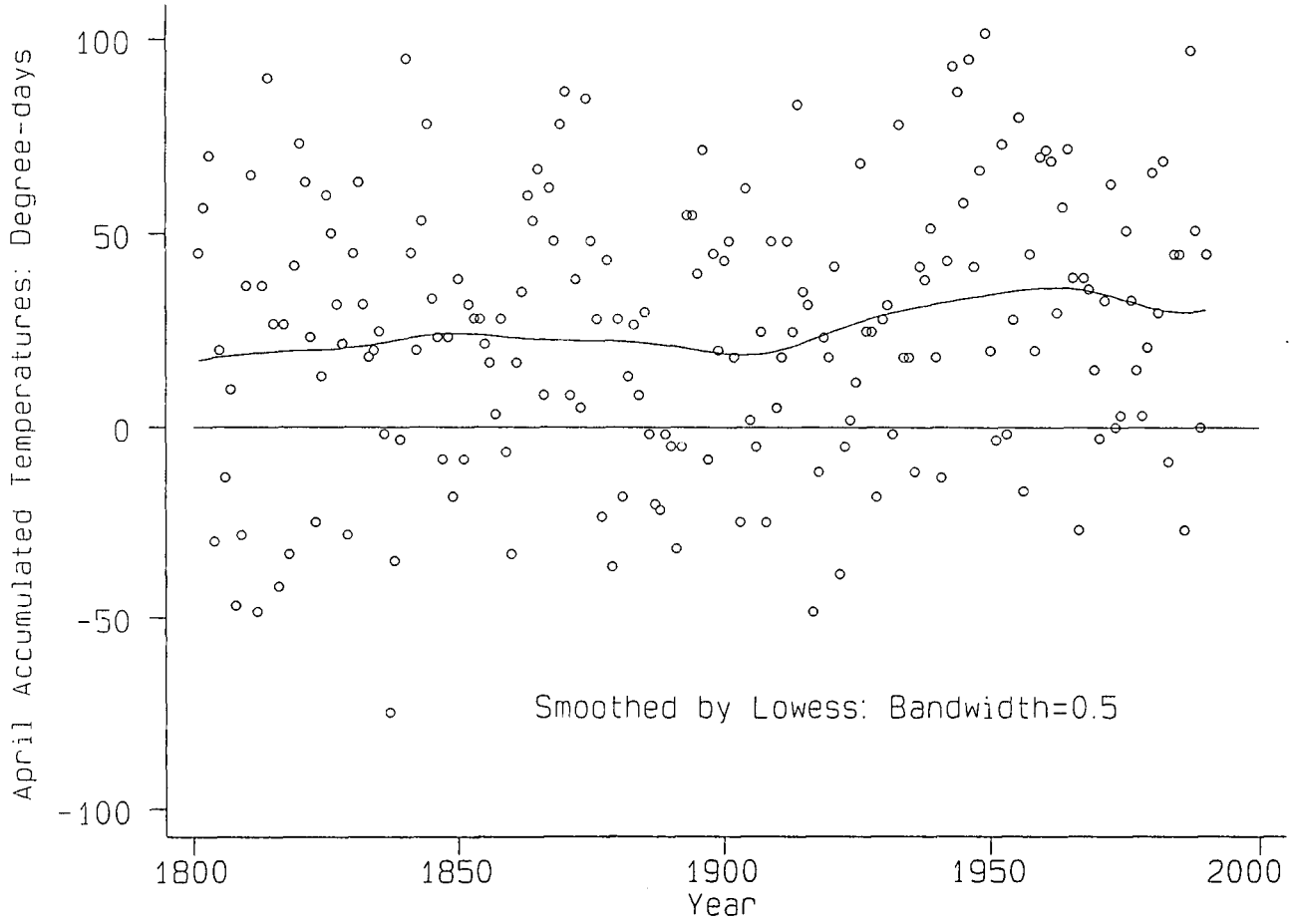

15.7 The Application of Linear and Exponential Models of the Altitudinal Decline in Growing Season Strength to the Calculation of Critical Cultivation Limit Altitudes

Fluctuations in growing season strength (as illustrated for Durham) will result in shifting altitudinal limits for agricultural cultivation and plants. When growing season strength averaged over 1985-1990 was regressed against altitude, the gradient of the resultant line was -1.42 d°C/m, the predicted sea-level growing season was 1499 d°C, and the critical altitude (at which 1000 d°C is expected) was 351 m (Chapter 10). Removal of Great Dun Fell increased the gradient to -1.72 d°C/m. The cultivation limit is expected to have fluctuated widely in the past, especially as it varies between 236 m and 463 m in the sample period (1985-1990). Assuming the gradient of -1.42 d°C/m to be representative of the rate of decrease of accumulated temperatures with altitude in an average year, the elevation of the 1000 d°C cultivation limit can be estimated for any year back to 1801, by referring to G_p in the Durham record. G_p is used as the best approximation to G_d, the daily temperature accumulation.

The estimated limit is given by:

$$crit\ level(c) = 102 + ((G_p - 1000)/1.42) \ldots . m \quad ----(1)$$

Because G_p is on average only 94% of G_d (Table 15.1), 940 d°C could be used as an equivalent limit to 1000 d°C. In this case critical altitudes would be 42 metres higher than the figures quoted below. The 1000 d°C critical limit, **c**, varies from 3.3 m in 1888 to 482.8 m in 1959 (Figure 15.7). 90% of northern England in the digital terrain model falls between these elevations and is expected to have experienced an accumulation greater than 1000 d°C in some years but not in others. **c** is dependent on the value chosen for the altitudinal gradient in accumulated temperatures. Assuming a gradient of -1.57 d°C/m (the steepest recorded between 1985 and 1990), **c** ranges from 12.8 m to 446.4 m. Using a gradient of -1.29 d°C/m (the shallowest recorded between 1985 and 1990) **c** ranges from -6.6 m to 521.1 m (over 95% of northern England falls

Figure 15.7. Extrapolated 1000 Degree Day Cultivation Limit Altitudes, 1801-1990, Assuming a Linear Decrease of 1.42 Degree-Days per Metre

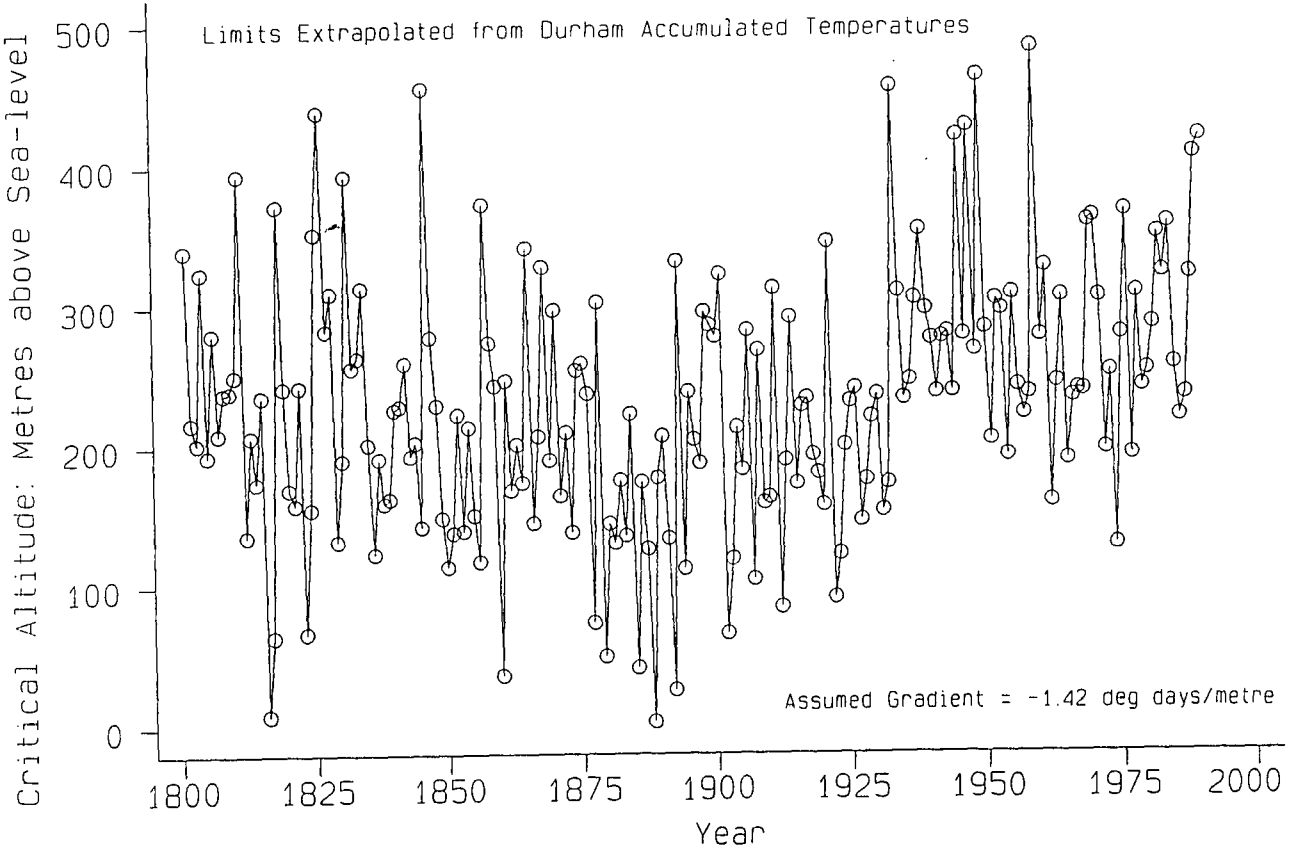

between these elevations). The limit falls below sea-level in 1888! Uncertainty in the gradient accounts for an error in the upper critical cultivation limit of nearly 80 metres and of 20 metres in the lower limit. However, these errors are small when compared with the inter-annual variation in the cultivation limit (from near sea-level to nearly 500 m), suggesting that the model is not overly sensitive to the gradient chosen.

An exponential model relating accumulated temperatures and altitude was discussed in Chapter 10, although the lack of high altitude stations meant that relative merits of the linear and exponential models were difficult to evaluate. The gradient of the exponential curve derived for the 1985-1990 mean growing season (Table 10.4) can also be used to estimate the critical 1000 d°C limit back to 1801. Assuming a curve:

$$g = g_0 \times e^{(-0.0016a)} \quad ----(2)$$

ln (g) has a gradient of -0.0016/m. The critical limit **c** is therefore:

$$c = 102 + (\ln(G_p/1000))/0.0016 \ldots . m \quad ----(3)$$

where G_p is the historical growing season strength.

If G_p is greater than 1000 d°C at Durham, **c** will be above 102 m. Estimates of **c** using the exponential model vary from 7.7 m in 1888 to 372.1 m in 1959 (Figure 15.8). Values are more conservative than in the linear case but still encompass more than 80% of the land in northern England within their range. Using a low gradient (0.0013), **c** varies between -14.1 m and 434.5 m. Using a steep gradient (0.0019), values range from 22.6 m to 227.5 m. Interestingly, the upper limit is more variable than the lower. It is also to be noted that the change in critical limits is not linearly related to changes in **k** because of the exponential nature of the model. Limit altitudes are more sensitive to **k** than in the linear model. Differences in the 1959 limit exceed 200 m due to uncertainty in the rate of exponential decline in growing season strength

Figure 15.8. Extrapolated 1000 Degree Day Cultivation Limit Altitudes, 1801-1990, Assuming an Exponential Decline of Degree-Days with Altitude

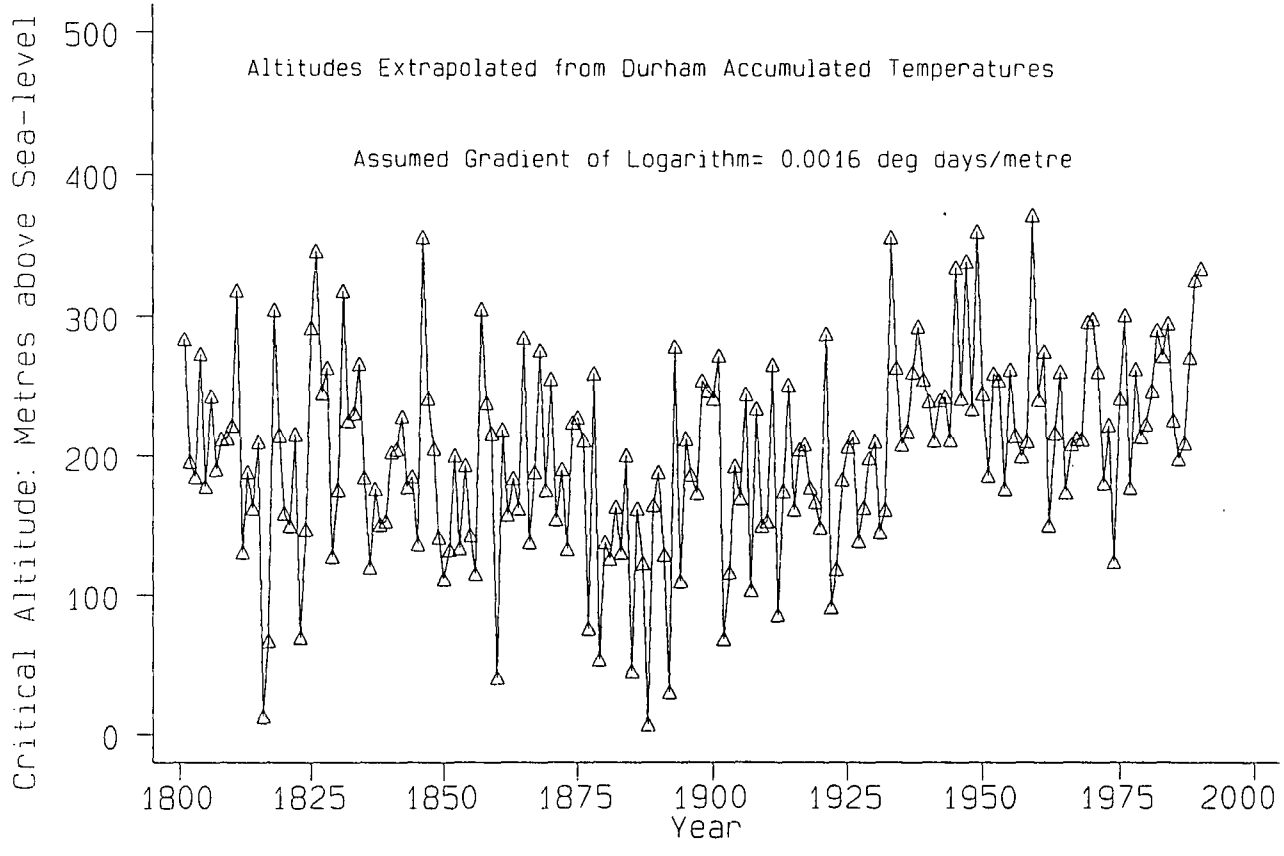

with altitude. For this reason use of the linear model is to be preferred, extrapolated limits being less sensitive to the gradient chosen.

15.8 Critical Cultivation Limit Altitudes in the Uni-directional Wind Scenarios

Theoretical annual temperature accumulations for the airflow scenarios could be used to predict critical cultivation limit altitudes if the relationship between growing season strength and altitude had been defined. Predicted accumulated temperatures at Durham are listed in Table 15.2 for the uni-directional wind scenarios. Assuming the annual temperature accumulation to be 912.6 d°C in a year of constant northerly flow, the linear model relating growing season strength and altitude (gradient = -1.42 d°C/m) produces a cultivation limit of 40.5 m and the exponential model (gradient = -0.0016/m) an altitude of 44.8 m (Table 15.5). Estimates assume that accumulated temperatures at Durham for each airflow are representative of those at 102 m.

Critical limit altitudes extrapolated using both linear and exponential models (gradients of -1.42 d°C/m and -0.0016/m respectively) (Table 15.5 overleaf) are shown on Figure 15.9. The contrast between airflow scenarios is strong.

Extrapolation of cultivation limits using linear and exponential models of altitudinal growing season decline outside the period on which the models are based may lead to inaccuracies since the extrapolation assumes that relationships defined for 1985-1990 remain unchanged.

To eradicate the dependence of the limits on the historical accumulated temperatures at Durham, estimates for an airflow scenario can be gained directly from the relevant monthly regressions. Mean temperatures were described for each airflow type in each month in Chapter 8. Setting latitude and longitude to their mean values, representative accumulated temperatures were calculated for given altitudes (Table 13.3). 1000 d°C limits were interpolated for each uni-directional wind scenario using this information (Table 13.5). These regression limits are listed again in the last column of Table 15.5. The westerly and south-westerly regression limits are lower than limits

Figure 15.9. Extrapolated 1000 Degree Day Cultivation Limit Altitudes for Uni-directional Wind Scenarios, Assuming Both Linear and Exponential Declines

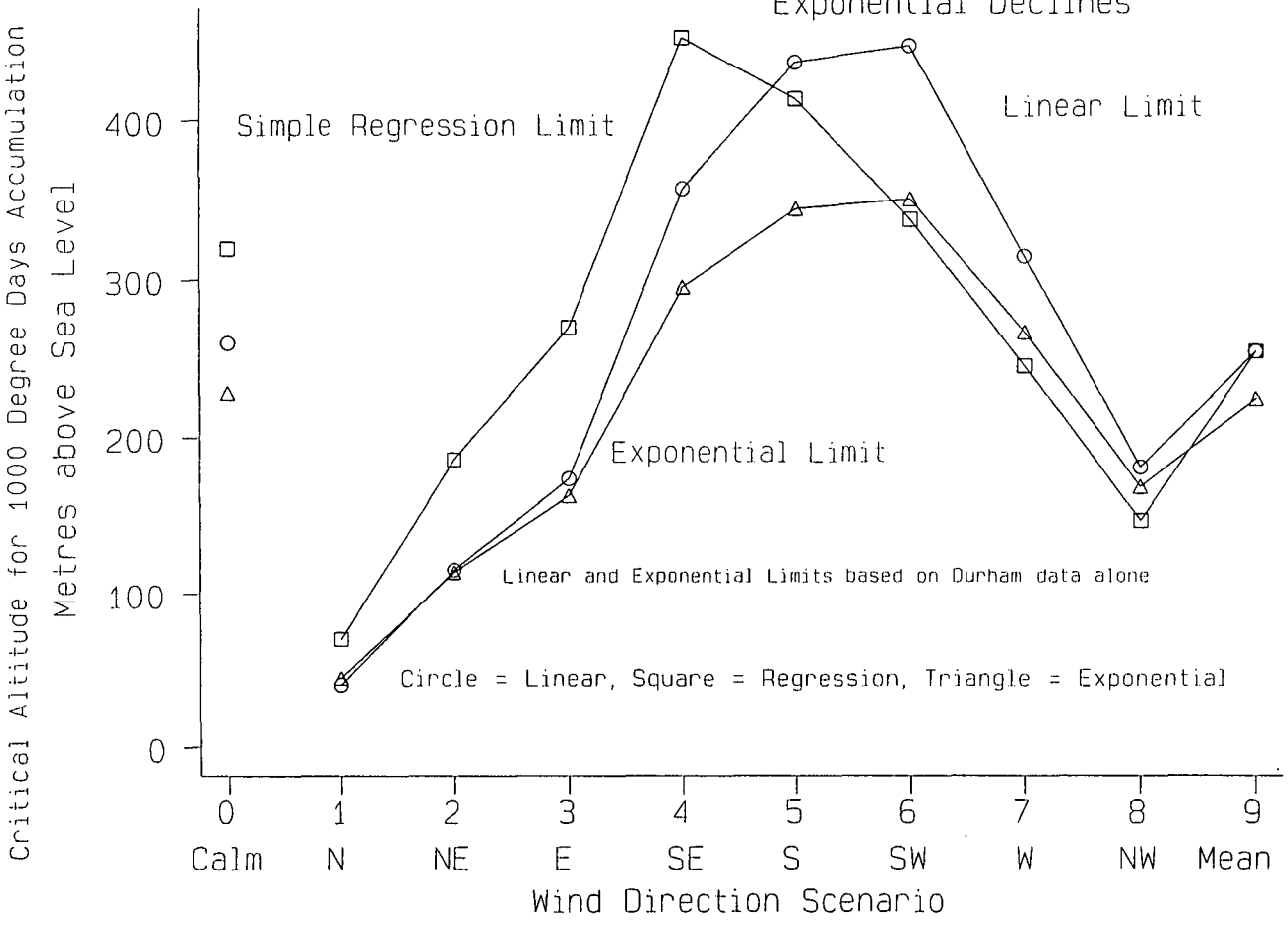

based on extrapolation from Durham data in this chapter. The overall range in limits between airflows is less for the regression limits (by 24.3 m).

Table 15.5: Critical altitudes (m) (1000 d°C accumulation) for uni-directional wind scenarios.

Airflow Scenario	Linear Critical Limit	Exponential Critical Limit	Regression Limit
Calm	260.0	228.5	320.0
N	40.5	44.8	70.2
NE	115.2	113.6	185.7
E	174.0	162.8	269.6
SE	357.6	295.5	452.8
S	437.2	345.3	414.0
SW	447.4	351.4	338.2
W	315.0	267.1	245.8
NW	181.1	168.5	146.9
Mean	255.0	224.9	254.8

Nevertheless, the variation in regression 1000 d°C cultivation limits according to airflow is still wide, illustrating the sensitivity of the Pennines to changes in relative airflow frequencies, even when each airflow remains unchanged with respect to 1985-1990. About 70% of northern England in the study area lies between 70.2 and 452.8 m (the extreme altitudes). The advantage of the limits in the right hand column of Table 15.5 is that they are interpolated instead of extrapolated and depend on temperatures at all sites, not just at Durham. The simple regression limits are therefore to be preferred.

15.9 Summary of Results

a) There is a wide variation in annual accumulated temperatures at Durham

between 1801 and 1990. An inter-annual variation of over 500%, between 255 d°C and 1384 d°C, is shown for the annual accumulation (G_y), while the variation in warm season accumulations (G_p) is over 200%. The pattern of variation agrees with other time-series such as the CET index (Manley 1974). The warmth of 1989 and 1990 is largely due to mild winters in these years, G_p being unremarkable. Spring, autumn and winter show more consistent warming trends than summer. Uni-directional wind scenarios, based on multiple regressions of mean daily temperature for different airflow types, create a range in predicted accumulated temperatures from 913 d°C to 1490 d°C for G_p and 414 d°C to 1406 d°C for G_y. Nearly all historical temperature accumulations fall within these limits. G_y has been lower than 414 d°C in four years, while G_p has fallen both above and below the predicted extremes. Changes within the character of airflows are therefore necessary to account for this variation.

b) Temporal variation of the theoretical 1000 d°C cultivation limit was extrapolated back to 1801 by using Durham accumulated temperatures and assuming the relationships between growing season strength and altitude defined in Chapter 10 to remain constant. The inter-annual variation in limits is extremely large, 90% of northern England falling between the extreme altitudes recorded. The choice of the gradient between growing season strength and altitude when using a linear model did not have undue influence on extrapolated cultivation limits.

c) The application of the above methodology to simulated temperature accumulations in the uni-directional wind scenarios of Chapter 13 showed that critical cultivation limits varied by over 400 metres between different airflows. Extreme sensitivity of temperature accumulations to airflow types is demonstrated. Small changes in the circulation pattern connected with global climate processes may have dramatic consequences for growing season strength in the study area with an equally strong influence on the altitudinal zonation of the Pennines. Of particular interest is the contrast between the northerly scenario (air from the Arctic) and the south-easterly scenario (continental air).

15.10 Problems Encountered and Areas for Further Research

Extrapolation using regression equations outside the range upon which they are based is undesirable because relationships defined between growing season strength (accumulated temperatures) and altitude for 1985-1990 cannot be assumed to hold for all time. Because of this, contrasting values of the gradient between growing season strength and altitude were tested to illustrate the effect of temporal change in the growing season/altitude relationship. Differences in cultivation limit elevations due to changes in the gradient were considerably less than the range between wind scenarios, at least when the linear model was employed. This is reassuring but does not eradicate the problem.

High or low cultivation limits in individual years are not as important as any temporal trend in the 1000 d°C limit. It would require more than one failed harvest to lead to crop abandonment and more than one good year to encourage crop development at higher altitudes. The probability of runs of good or bad years could be investigated (Parry 1976).

It is unrealistic to assume that lapse rates and temperatures within airflow-types remain constant. Changes in climate processes will alter airflow character as well as encourage variations in relative airflow frequencies. For example, a cooling of westerly flows may occur due to a diversion of Atlantic ocean currents, reducing warm-air advection in winter. Work is required to assess the effects of such changes in airflow quality. With changes within airflow properties, i.e. within-type climate change, which has been shown to be necessary to explain the range of climatic behaviour present at Durham, the consequences for "climatic potential" in the High Pennines could be marked. It is significant that the actual cultivation limits in the Lammermuir Hills were observed to fall by 200 metres in around 300 years (a mean rate of 2 metres every 3 years), at a time when the rate of climatic change was slower than predicted for the near future (Parry 1978).

Subsequent work could attempt to analyse possible changes in mean temperature

and lapse rates within airflows. Such expected changes could soon be extracted from GCMs (Viner & Hulme 1992). The most recent GCMs are attempting to estimate changes in airflow quality which can then be combined with the predicted changes in relative frequencies to produce a realistic climatic scenario. Unfortunately, such data are as yet unobtainable. The effects of arbitrary changes within airflows are examined in Chapter 18 using recent GCM data.

Before attempting this, the next chapter introduces the concept of **internal variability** of airflows. Up to the present, airflows have been treated as invariable, possessing a constant surface temperature, i.e. the temperature on a day with a particular airflow in a particular month has been simulated as invariable. In reality there will be a random variation of mean daily temperatures around this expected value in any airflow. It is more realistic to think of mean daily temperatures under the influence of a particular airflow as forming a normal Gaussian distribution around the mean value predicted for the airflow.

THE SIMULATION OF CLIMATIC VARIABILITY TO IMPROVE ESTIMATES OF ACCUMULATED TEMPERATURES

16.1 Introduction

Previous climate scenarios are based on the prediction of mean temperatures for each airflow type. All airflows show fluctuation in daily temperatures around the mean and many climatic indicators, including accumulated temperatures, will be affected by such variability. The range of climatic behaviour expected in a particular airflow is particularly important when converting the simulated mean temperatures into the length of the growing or frost-free season (Chapter 14). For example, the number of growing days and length of the growing season are underestimated when the mean temperature is well below 6°C, because warm spells are not simulated. Likewise when the mean temperature is above 6°C the temperature will nonetheless fall below the threshold on cold days. Inter-diurnal temperature variability will be simulated for each airflow to allow such cases to be taken into account.

16.2 Estimates of the Variability of Mean Daily Temperature (σ)

Standard deviations (σ) of mean daily temperatures in each month were calculated for each location. The standard deviation of mean daily temperatures (σ) falls consistently between 2°C and 4°C. σ reaches 3.78°C at Carlisle in December, whereas the lowest value (not including Houghall, Nenthead, Shap and Wycliffe Hall) is 2.09°C at Sunderland in July. These calculated deviations represent the variability of mean daily temperatures within the relevant month. σ shows a strong relationship with altitude in many months (Table 16.1), although the sign of the relationship is inconsistent.

Table 16.1: Relationship of standard deviation (σ) of mean daily temperatures (°C) with altitude (metres above sea-level): σ = a(alt) + b.

Month	Mean σ	a	b	r	GDF	Dur
Jan	3.05	-0.00062	3.310	-0.476	2.78	3.25
Feb	3.28	-	-	-0.015	3.28	3.28
Mar	2.79	-	-	-0.196	2.79	2.79
Apr	2.91	0.00058	2.876	0.642	3.37	2.94
May	2.57	0.00091	2.407	0.642	3.18	2.50
Jun	2.77	-	-	0.333	2.77	2.77
Jly	2.41	0.00087	2.230	0.742	2.97	2.32
Aug	2.48	-	-	0.056	2.48	2.48
Sep	2.51	-	-	-0.020	2.51	2.51
Oct	2.57	-	-	0.057	2.57	2.57
Nov	2.86	-	-	-0.222	2.86	2.86
Dec	2.97	-0.00112	3.259	-0.636	2.31	3.14

The final two columns represent σ extrapolated to the relevant altitudes for Great Dun Fell (847 m) and Durham (102 m). In seven months no systematic change of σ with altitude was found and mean values were assumed to be representative at all altitudes. In some summer months (e.g. July) σ increases strongly with altitude (Figure 16.1 a). There is greater temperature variation at high altitudes, σ increasing from 2.3°C at sea-level to nearly 3°C at Great Dun Fell. σ also increases with altitude in April and May. Points marked with '1' on the July and December graphs are for the stations with missing data. These were ignored when calculating regression lines. In December and January there is a distinct decrease in temperature variability with altitude (Figure 16.1 b). Temperature inversions occur frequently in winter, causing a greater variability of temperature at low altitudes. Such areas experience mild conditions on days with no inversion but cold temperatures on days with inversions (Figure 16.1 c). Above the inversion, temperatures will be less variable. The gradients of all regression lines are slight (Table 16.1). The steepest gradient (December) is

Figure 16.1. Relationships between the Standard Deviation of Mean Daily Temperatures and Altitude in July and December

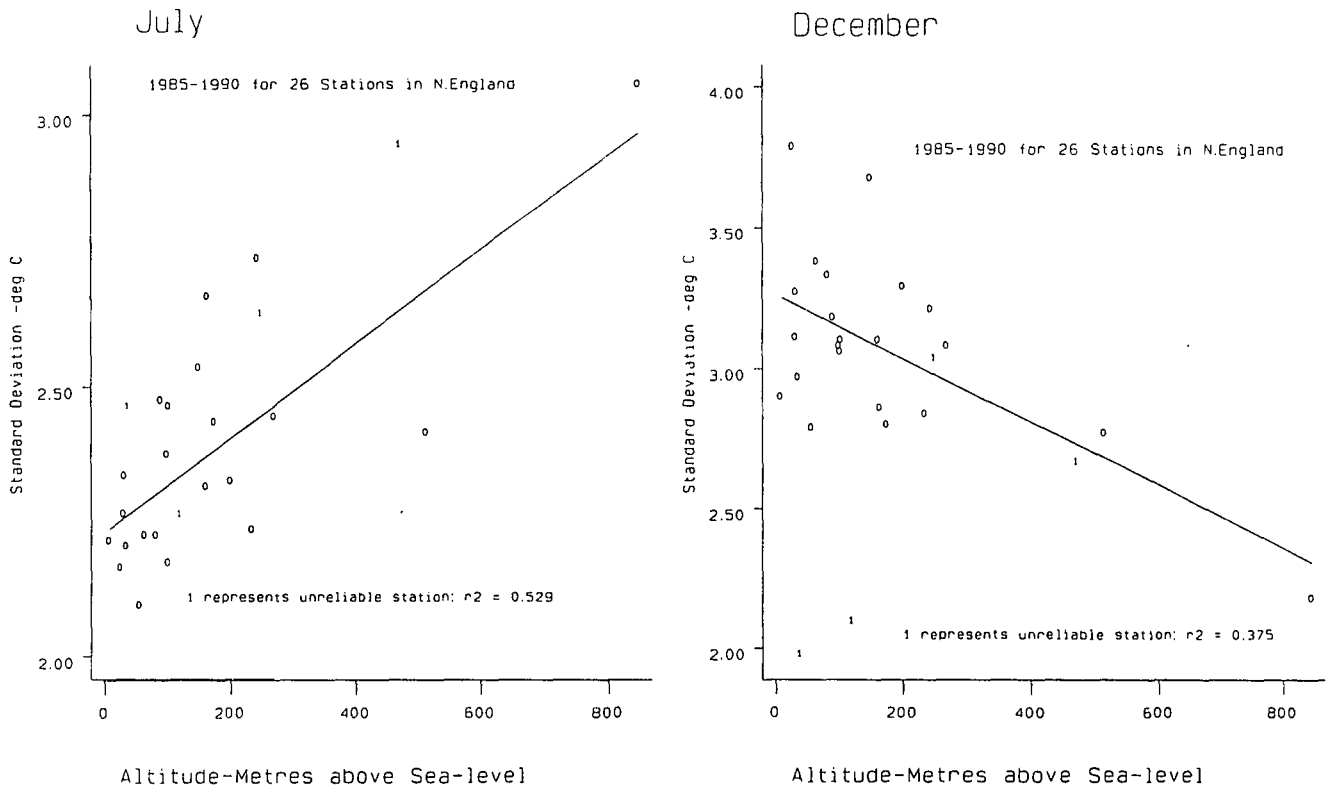

-0.00112°C /m. σ is thus expected to be 3.26°C at sea-level, 3.14°C at Durham, but only 2.31°C on Great Dun Fell.

16.3 Simulation of Daily Time Series

The mean daily temperature (μ) and the standard deviation (σ) of mean daily temperature in an airflow scenario can be used to generate a random series of daily temperatures. Stochastic simulations are often used in climate impact studies (e.g. Chia 1991). By perturbing the parameters of a stochastic model in a way consistent with results of GCM experiments, the streams of synthetically generated data can be regarded as climate change scenarios (Woo 1992). The problems behind this type of approach are discussed by Mearns (1989). For example, it is difficult to relate randomly generated temperature, precipitation and insolation data so that they make physical sense when compared, e.g. insolation should vary inversely with precipitation.

In Table 16.1 σ can be used to estimate the expected variability of daily temperatures. All airflows in a particular month will be assumed to show similar variability (this assumption is dropped later). Assuming inter-diurnal temperature variability to remain fairly constant in future climates, σ will range from 2.5°C in summer to over 3°C in winter. In some months σ is expected to decrease or increase with altitude.

In Chapter 13 mean daily temperatures were predicted for any airflow in any month at a given altitude, e.g. the predicted sea-level January mean daily temperature is 4.04°C (Table 13.1), assuming all airflows to show equal weighting. To improve this scenario a time series of mean daily temperatures will be generated with a mean (μ) of 4.04°C and σ equal to that expected for sea-level (3.31°C). A computer program developed to produce normal or Gaussian random numbers with a mean of zero and a standard deviation of one [N(0,1)] was used (Hamilton 1992). 31 cases were simulated (a month's figures). Ten random simulations are shown (Figure 16.2). Values simulated by the program (**y**) were transformed by:

Figure 16.2. Ten Random Number Simulations with a Mean of Zero and a Standard Deviation of One

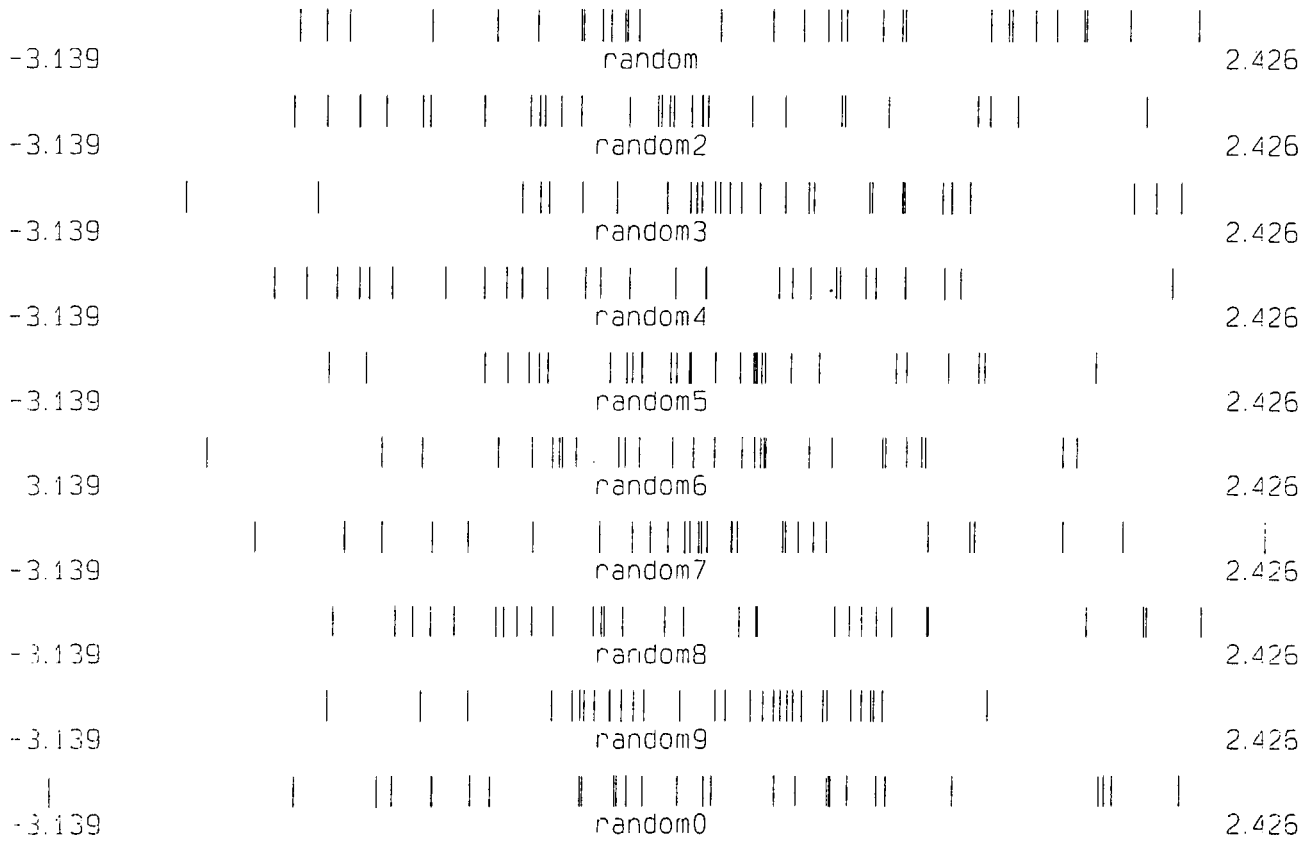

Oneway Line Graphs show the Simulated Distributions

$$y_t = \mu + (\sigma \times y) = 4.04 + (3.31y) \quad ----(1)$$

where μ was the scenario mean and σ the scenario standard deviation. This produces a time series applicable to the scenario in question:

$$y_t = [N(4.04, 3.31)] \quad ----(2)$$

The actual mean **x** and standard deviation **s** in the random series are different to those expected since each series is only a sample of values from the original distribution. In a longer series, **x** and **s** should tend towards μ and σ respectively.

Table 16.2: Two random daily temperature series for sea-level: relevant parameters and resulting accumulated temperatures. **n** represents the number of growing days.

	Run A				Run B			
Mth	x	s	n	d°C	x	s	n	d°C
Jan	4.59	3.80	12	29.3	3.58	2.27	4	2.5
Feb	4.73	3.77	12	27.6	3.74	2.25	5	2.8
Mar	6.49	3.21	17	50.5	5.64	1.92	15	18.8
Apr	8.37	3.31	23	84.8	7.49	1.98	24	52.5
May	11.68	2.77	31	176.1	10.95	1.66	31	153.5
Jun	14.00	3.18	31	240.0	13.16	1.90	31	214.8
Jly	16.07	2.56	31	312.2	15.39	1.53	31	291.1
Aug	15.51	2.85	31	294.8	14.76	1.70	31	271.6
Sep	13.30	2.88	31	219.0	12.54	1.72	31	196.2
Oct	11.03	2.95	29	156.6	10.25	1.77	30	132.0
Nov	6.63	3.29	18	52.3	5.76	1.96	16	20.6
Dec	6.21	3.75	17	52.9	5.22	2.24	14	16.5
Tot				1696				1373

Table 16.2 shows the results of two runs of the program for sea-level. A series was generated for each month using values of μ and σ from previous scenarios and Table 16.1 respectively.

n is the number of days recorded with mean temperatures above 6°C, i.e. growing days. Accumulated temperatures (**d°C**) in months with less than 31 days have been corrected to allow for this. Accumulated temperatures vary between the two runs, from 1696.01°C in run A to only 1372.81°C in run B. The difference between the two runs is entirely due to random variation. Both totals are realistic daily accumulations (G_d) for northern England. In previous scenarios accumulations were based on mean monthly figures (G_p) (Chapter 13). However, when using this approach, if the standard deviation of a weather element can be estimated, a daily temperature accumulation can be simulated using mean monthly figures alone. This approach could be applied to the early years of the Durham record but many samples would be required to reduce the high variability of results.

The number of growing days (**n**) varies according to the series. In January **n** is 12 in run A but only 4 in run B (Table 16.2). Results from ten simulations are shown in Table 16.3. The runs described in Table 16.2 are runs 1 and 9. In run 1 the sample mean is above μ, whereas the opposite is the case in run 9 (run B). The sample standard deviation is very low (i.e. much lower than σ) in run 9, whereas it is above that predicted in run 1.

The most extreme individual daily values are typically about two real standard deviations (σ) away from the mean, although in run 10 the minimum daily value was more than 3 standard deviations lower ($-3.139*\sigma$), and is an outlier on Figure 16.2.

Table 16.3: Values of x and s for 10 runs of random numbers: real mean (μ) = 0, real standard deviation (σ) = 1. Runs 1 and 9 were described in Table 16.2.

Run No	Mean(x)	St Dev(s)	Min	Max
1 (A)	0.165	1.149	-1.972	2.122
2	-0.371	0.993	-2.000	1.884
3	0.174	1.008	-2.506	2.042
4	-0.408	1.083	-2.097	1.999
5	-0.124	0.805	-1.839	1.650
6	-0.130	0.906	-2.412	1.561
7	-0.031	1.010	-2.191	2.426
8	-0.083	1.079	-1.825	2.130
9 (B)	-0.139	0.687	-1.852	1.160
10	-0.165	1.188	-3.139	2.025

According to the Central Limit Theorem, the mean of the simulation means (x) should approximate to the true mean (μ) as all simulations are samples from the true population, individual observations are independent and are drawn from a parent population which is normal. The standard deviation of the sample means s_x is:

$$s_x = \sigma / (n)^{0.5} \quad ----(3)$$

where **n** = 31. In January:

$$s_x = 3.31/(31)^{0.5} = 0.59 \quad ----(4)$$

One method of determining the expected annual temperature accumulation would involve calculating accumulated temperatures in as many simulations as practical and taking the mean result. Alternatively, knowledge of normal distributions can be used

to predict this accumulation analytically.

16.4 An Analytical Approach to Improve Estimates of Accumulated Temperatures

To calculate the probability that a single daily temperature will rise above the threshold (6°C), the threshold temperature must be converted to a **z**-score, where:

$$z = (x - \mu) / \sigma \quad ----(5)$$

For January sea-level mean daily temperatures, μ is 4.04°C and σ is 3.31°C. Thus:

$$z = (6 - 4.04) / 3.31 = 0.592 \quad ----(6)$$

The probability of 6°C being exceeded on any one day is therefore 0.277 (from tables of the standard normal random variable). 8.59 growing days are therefore expected in a month of 31 days. Figure 16.3 shows an imaginary normal distribution with mean μ and standard deviation σ. The vertical line represents the z-score corresponding to a temperature of 6°C (the threshold). The shaded area to the right of the line represents the probability of 6°C being exceeded. Table 16.4 shows growth probabilities in all months, calculated in this way.

Figure 16.3. Normal (Gaussian) Distribution
with Mean μ and Standard Deviation σ

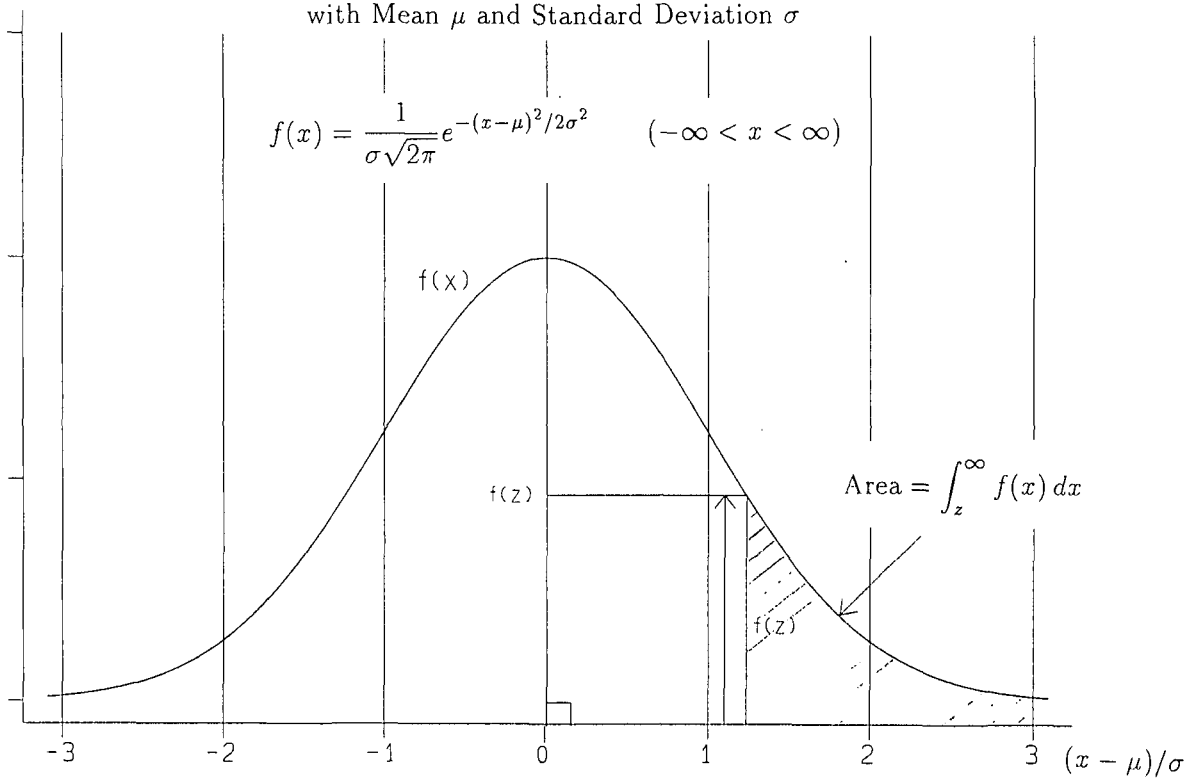

The average or expectation of x, given that $x \geq z$, is

$E(x \mid x \geq z) = f(z) / \int_z^\infty f(x)\,dx$ if $\mu = 0$ and $\sigma = 1$.

In general, multiply this by σ and then add μ.

Table 16.4: Probability of a mean daily temperature above 6°C at sea-level, assuming normality.

Month	μ	σ	z(6)	p(>z)	np
Jan	4.04	3.31	0.592	0.277	8.59
Feb	4.19	3.28	0.552	0.291	8.12
Mar	6.03	2.79	-0.011	0.504	15.62
Apr	7.89	2.88	-0.656	0.744	22.32
May	11.28	2.41	-2.191	0.986	30.57
Jun	13.54	2.77	-2.722	0.997	29.91
Jly	15.70	2.23	-4.350	1.000	31.00
Aug	15.10	2.48	-3.669	1.000	31.00
Sep	12.89	2.51	-2.745	0.997	29.91
Oct	10.61	2.57	-1.794	0.964	29.85
Nov	6.16	2.86	-0.056	0.522	15.66
Dec	5.67	3.26	0.101	0.460	14.26

The annual total growing days simulated at sea-level is 266.8. This compares with 130.8 days at 800 m. According to **hazard theory** (Thom 1954, Pitman 1993) the average expectation of temperature, given that temperatures are above the threshold, is:

$$E(x|x \geq z) = [1/\sqrt{(2\pi)}] \times e^{(-z^2/2)} / prob(x \geq z) \quad ----(7)$$

This assumes the distribution to be standard normal, i.e. x = N (0,1). Otherwise, the result (derived by inserting a value for **z**) is the **z**-score of the average expected temperature. This is multiplied by σ and added to μ to provide an estimate of the mean excess temperature:

$$T_{ex} = (E \times \sigma) + \mu \quad ----(8)$$

By definition, T_{ex} is greater than 6°C. As μ increases, T_{ex} tends towards the mean of the distribution (μ) since z becomes increasingly negative and more and more observations rise above the threshold. If T_{ex} is known the expected degree day accumulation is:

$$T_{acc} = n_m \, p(T_{ex} - 6) \quad ----(9)$$

where $\mathbf{n_m}$ is the number of days in the month and **p** the probability that $x > 6$°C. The computer program used to generate $\mathbf{T_{acc}}$ is listed in Appendix 7.

Table 16.5 gives monthly results at sea-level and 800 m.

Table 16.5: $\mathbf{T_{ex}}$ and $\mathbf{T_{acc}}$ for mean temperature scenarios.

Month	**T_{ex} °C sea-level**	**T_{acc} d°C sea-level**	**T_{ex} °C 800 m OD**	**T_{acc} d°C 800 m OD**
Jan	8.04	17.53	6.87	0.12
Feb	8.06	16.74	7.05	0.24
Mar	8.24	34.97	6.75	0.09
Apr	9.13	69.99	7.61	4.64
May	11.37	164.05	8.44	35.07
Jun	13.57	226.28	9.13	68.02
Jly	15.70	300.70	10.76	136.68
Aug	14.68	269.08	9.55	99.09
Sep	12.91	206.77	8.43	49.63
Oct	10.82	144.07	7.97	24.80
Nov	8.34	36.68	7.13	1.41
Dec	8.48	35.41	6.78	0.24

In summer T_{ex} approaches μ at 800 m. T_{acc} at sea-level ranges from over 300 d°C in July to only 16.74 d°C in February. At 800 m T_{acc} is negligible between November and April. March yields a disappointing T_{acc} value due to a low σ (only 2.79°C) and steep lapse rate. Annual total accumulated temperatures reach 1535.28 d°C at sea-level but only 420 d°C at 800 m.

The above figures are better than those in Chapter 13 since they are based on daily (as opposed to monthly) temperature data. Variability of temperature within a month has been taken into account and results are sensitive to σ.

16.5 Individual Airflow Scenarios

Figure 16.4 a shows predicted mean excess temperatures above 6°C, T_{ex}, for all airflows in each month. Every airflow within a particular month is assumed to show a standard deviation of daily temperatures equal to that listed in Table 16.4. As μ increases, T_{ex} tends towards the simulated mean (μ). The dependence of T_{ex} on σ is shown in Figure 16.4 b which plots T_{ex} against **z**. The graph exhibits banding according to month (represented by number), all airflows in a particular month having similar σ. Changing σ alters the curve between **z** and T_{ex}. Given a negative z-score, T_{ex} is lower if σ is smaller. The opposite is true when **z** is positive.

Figure 16.5 presents sea-level results for all airflows. σ is determined by month alone, e.g. all March airflows have a standard deviation of 2.79°C. Figure 16.5 a shows μ (numbers represent wind direction) and σ for all scenarios. Figure 16.5 b shows simulated T_{acc} values. These are nearly always greater than zero, even in winter, most airflows showing a small probability of a growing day.

Table 16.6 shows results for sea-level and 800 m accumulated over the year for each airflow type (similar to the uni-directional wind scenarios in Chapter 13). Sea-level T_{acc} varies between 1191 d°C for northerly flow and 1818.72 d°C for southerly flow, a 152.7% variation.

Figure 16.4. Mean Temperature Excess above 6 deg C versus Mean Temperature and Z-score

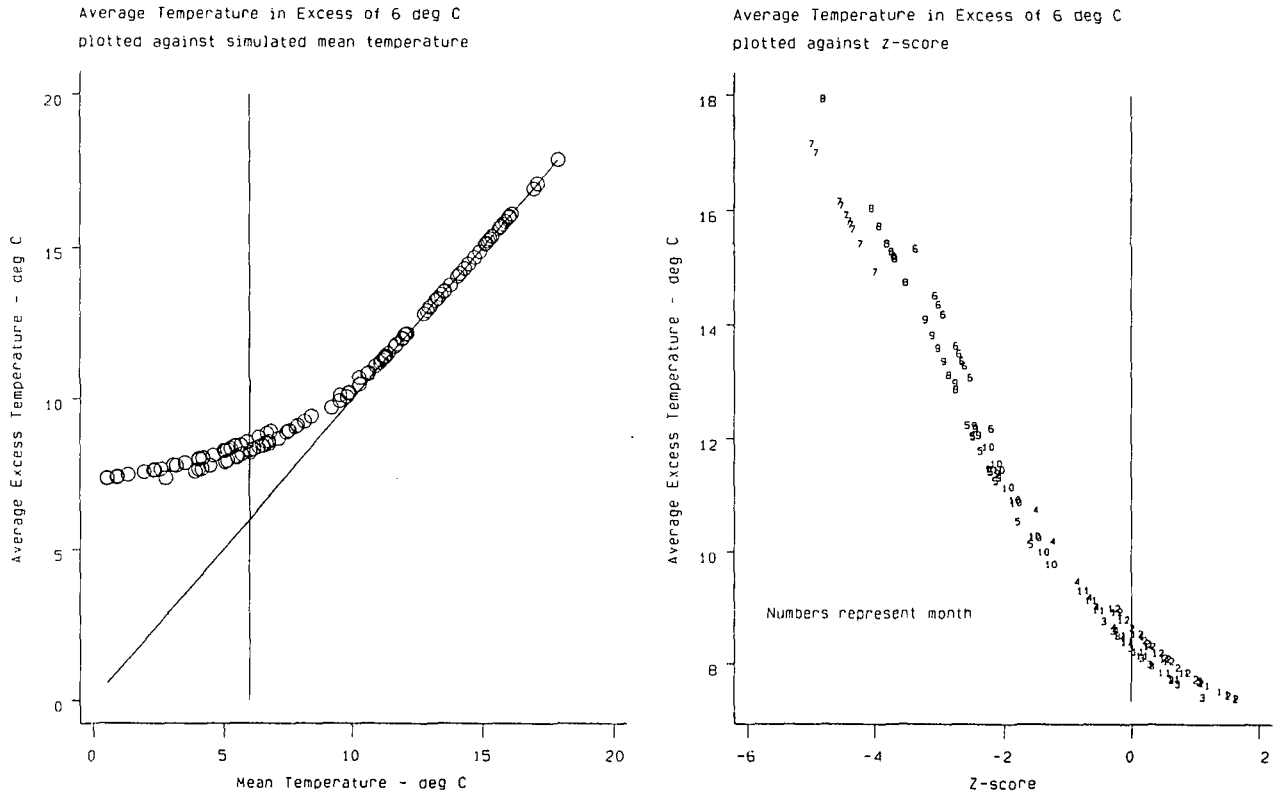

Figure 16.5. Simulated Parameters for Mean Daily Temperature Simulations

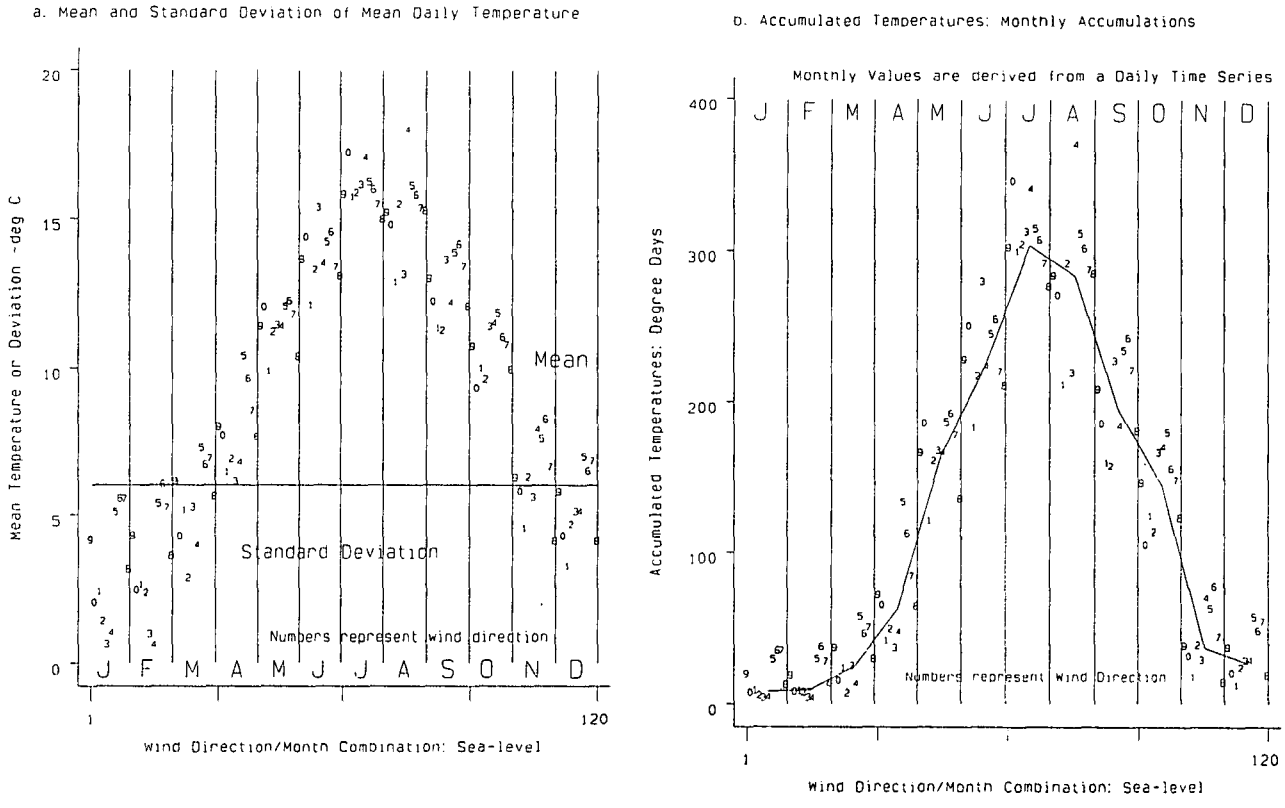

Table 16.6: Simulated T_{acc} at sea-level and 800 m for uni-directional wind scenarios (T_{acc} is an estimate of G_d).

Wind	T_{acc} d°C sea-level	T_{acc} d°C 800 m OD	800m/sea-l Ratio	Difference
Calm	1468.68	598.32	0.407	870.36
N	1191.00	295.92	0.248	895.08
NE	1355.40	412.44	0.304	942.96
E	1479.00	418.92	0.283	1060.08
SE	1601.16	738.60	0.461	862.56
S	1818.72	580.92	0.319	1237.80
SW	1788.96	450.48	0.252	1338.48
W	1618.08	353.28	0.218	1264.80
NW	1342.92	301.56	0.225	1041.36
Mean	1535.28	420.00	0.274	1115.28

At 800 m T_{acc} is much lower, ranging from 738.6 d°C for south-easterly flow to 295.92 d°C for northerly flow (i.e. by 249.6%). The absolute difference between airflows is 442.68 d°C, less than the 627.72 d°C contrast at sea-level. At high altitude the absolute difference in growing season strength between airflows decreases but the relative (percentage) variation is much greater. Calculating T_{acc} at 800 m as a percentage of that at sea-level produces similar results to Chapter 13, values ranging from 46.1% for continental south-easterly flow to 21.8% for westerly flow. The contrast in the rate of altitudinal decline in "growth potential" between continental and maritime airflows is marked.

16.6 The Influence of Temperature Variability (σ): A Sensitivity Analysis

The above results are affected by the selection of σ. It is simplistic to assume that the variability of temperature within any one airflow is the same as that within the month as a whole and errors in σ are likely. A sensitivity analysis of the influence of σ on T_{acc} was undertaken to assess the importance of such errors.

In any month some airflows will be inherently more variable than others. For example, south-westerly flows may be extremely variable because of the alternating influences of tropical maritime and returning polar maritime air-masses. σ was derived for all airflows at Durham and Great Dun Fell in each season from the data. Results, to the nearest 0.25°C, are listed in Tables 16.7 a and b.

South-easterly flow in spring at Great Dun Fell is highly variable, temperatures having a standard deviation of 4.75°C. This falls to 4.50°C in summer. In winter westerly flows are associated with a wider temperature variation than easterly ones, possibly due to the contrast between polar and tropical maritime air. Winter is the most variable season at Great Dun Fell and spring at Durham.

Table 16.7 a): Actual standard deviations of mean daily temperatures at Durham (°C), (1985-1990).

Airflow	Spring	Summer	Autumn	Winter
Calm	2.50	2.75	2.75	2.75
N	2.00	2.00	1.50	1.75
NE	2.00	2.25	2.00	1.75
E	1.75	1.50	1.75	1.75
SE	2.25	3.50	1.00	2.50
S	3.00	2.75	2.50	3.00
SW	2.50	2.25	2.50	3.50
W	2.25	1.75	2.25	2.75
NW	2.50	2.50	2.25	3.00
Mean	2.75	2.50	2.50	3.25

Table 16.7 b): Actual standard deviations of mean daily temperatures at Great Dun Fell (°C), (1985-1990).

Airflow	Spring	Summer	Autumn	Winter
Calm	3.25	2.25	2.50	3.25
N	2.50	2.50	1.75	1.25
NE	2.50	2.50	2.50	1.25
E	3.25	2.75	2.00	1.50
SE	4.75	4.50	1.00	3.50
S	3.50	3.00	2.25	2.50
SW	2.75	2.25	2.50	2.50
W	2.25	2.25	2.50	2.25
NW	2.75	2.00	2.50	1.75
Mean	3.00	2.75	2.75	2.75

Figure 16.6 plots sea-level T_{acc} using the actual recorded standard deviations for each airflow at Durham, against T_{acc} derived using monthly estimates of σ (Table 16.1). There is little difference in the values, especially in summer. In winter differences arise when the mean daily temperature is close to 6°C. A mean temperature near the threshold increases the sensitivity of T_{acc} to σ. In Figure 16.7 a, which shows the number of growing days at sea-level for all airflows using the two estimates of σ, the greatest change is from 28.97 to 22.1 growing days for south-easterly flow in November. A similar graph for 800 m (Figure 16.7 b) illustrates a marked change in growing days for south-easterly flow in September and October.

A formal estimate of the **sensitivity** of T_{acc} to changes in σ is obtained by dividing the change in T_{acc} by the change in σ:

$$sensitivity\ (s) = \Delta T_{acc} / \Delta \sigma \quad ----(10)$$

Sensitivity ratios (s) were derived for sea-level and 800 m. Mean values were

Figure 16.6. Accumulated Temperatures, Tacc, Simulated for Sea-level Using Two Different Standard Deviation Estimates

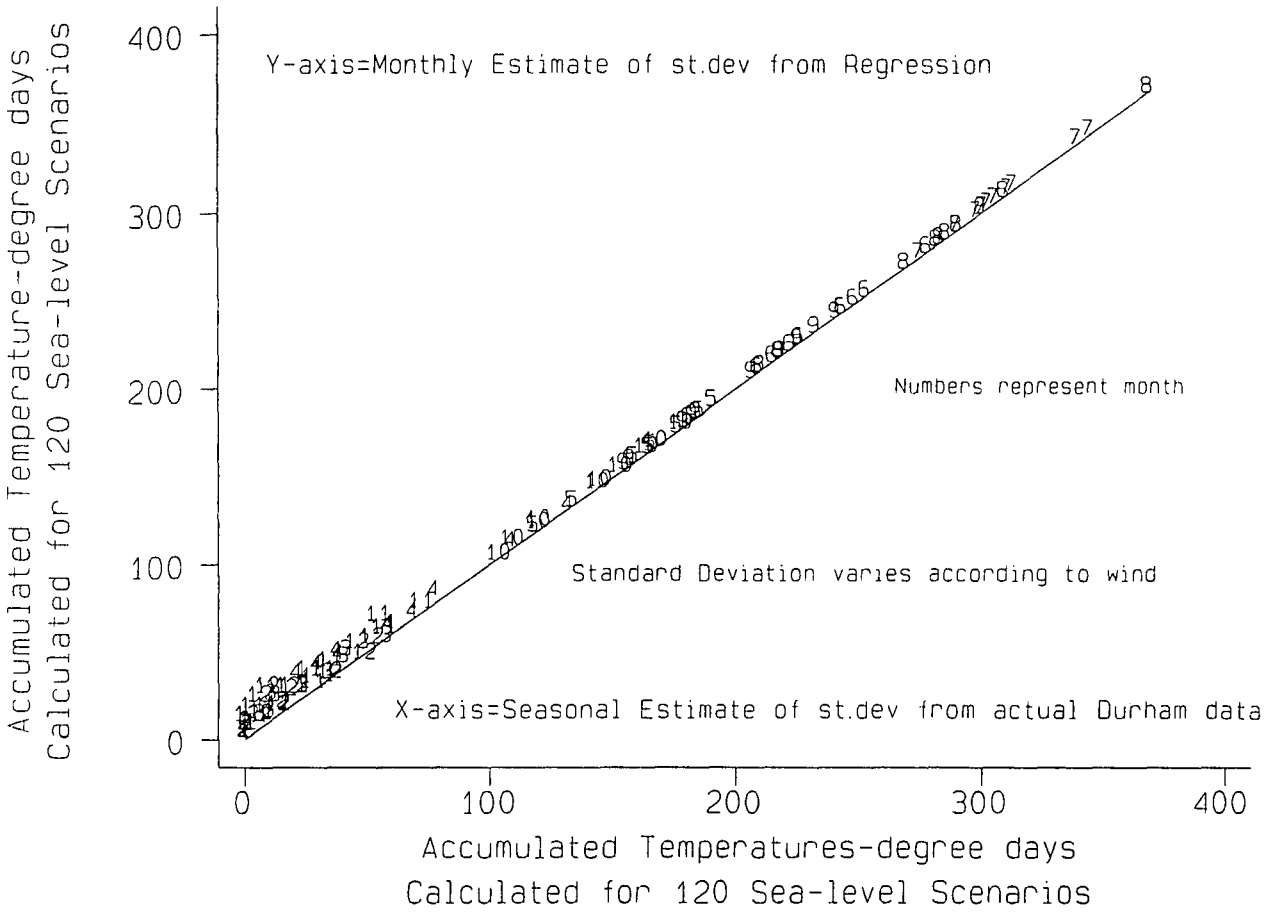

Figure 16.7. The Simulated Number of Growing Days per Month at Sea-level and 800 Metres above Sea-level using Two Different Standard Deviations

a. Sea-level

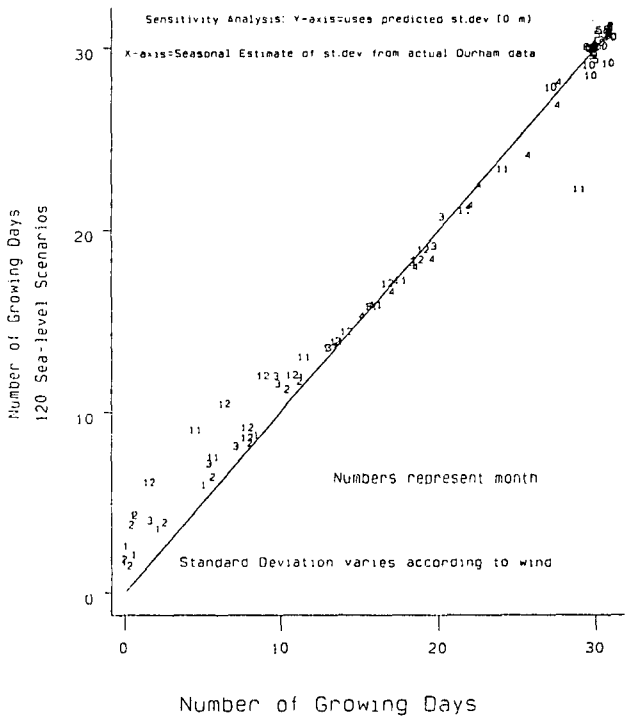

b. 800 Metres above Sea-level

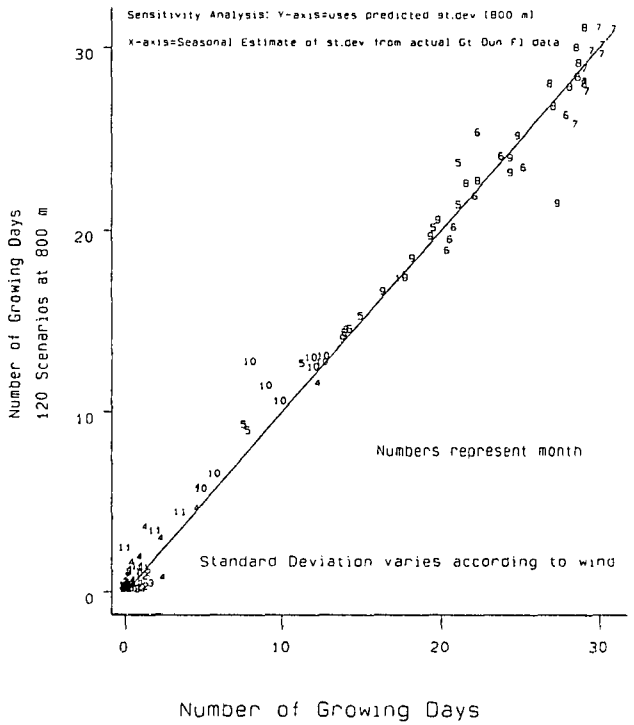

One figure is plotted for each of the 120 airflow/month combinations

4.92 d°C/°C at sea-level rising to 5.40 d°C/°C at 800 m, suggesting that high altitude accumulated temperatures are more sensitive to change in climatic variability. Maximum sensitivities are 12.29 d°C/°C at sea-level for south-westerlies in December and 26.82 d°C/°C at 800 m for southerlies in April. At sea-level (Figure 16.8 a) in summer ΔT_{acc} is negligible. An increase in variability would result in similar accumulated temperatures. In spring and autumn ΔT_{acc} is linearly related to $\Delta\sigma$. At 800 m (Figure 16.8 b) a similar relationship holds although in winter there is little variation in T_{acc}. Presumably this is because mean temperatures at 800 m fall below the growth threshold.

Figure 16.8 c plots sensitivity at sea-level against that at 800 m for each airflow in each month. Numbers represent month.

Table 16.8: Monthly mean values of s (d°C/°C), the sensitivity of T_{acc} to changes in σ.

Month	Lowlands (0 m)	Uplands (800 m)
January	7.01	0.41
February	6.72	0.54
March	10.61	0.62
April	9.33	5.45
May	1.24	11.47
June	0.25	9.46
July	0.00	3.31
August	0.03	5.75
September	0.35	10.20
October	2.35	10.95
November	10.32	2.17
December	10.87	1.18

Both sensitivity ratios are positive, showing that increased variability in surface temperature always leads to increased accumulated temperatures. This is not obvious

Figure 16.8. Sensitivity Analysis: Relationship of Change in Tacc to Change in Simulated Standard Deviation

a. Sea-level Sensitivity

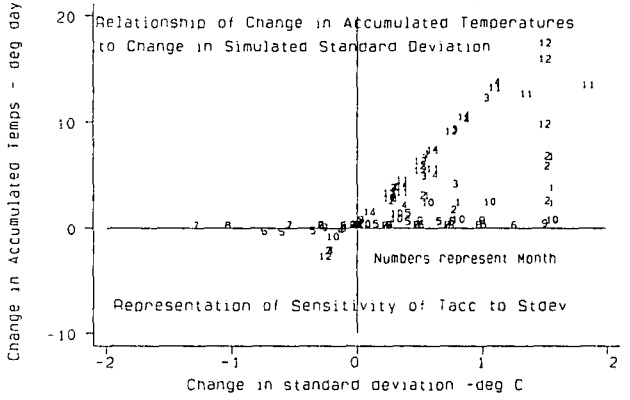

b. 800 Metres Sensitivity

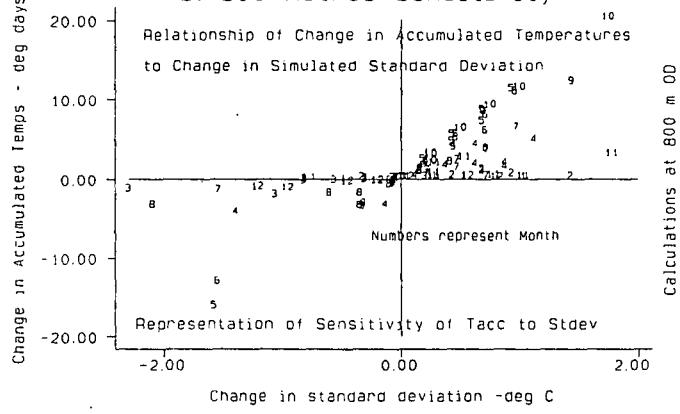

c. Relationship between Sensitivities at Sea-level and 800 Metres for each Airflow in each Month

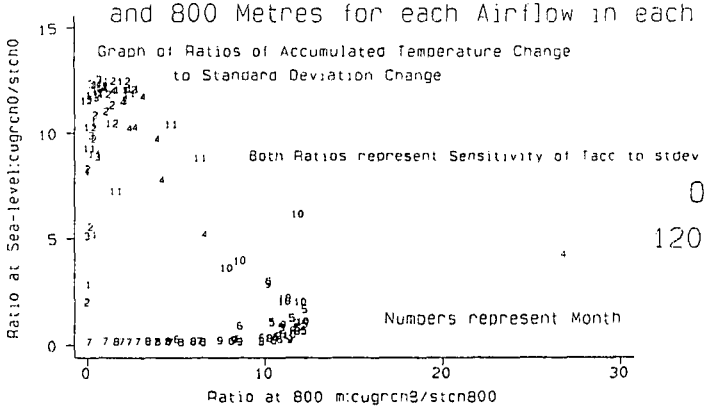

One figure is plotted for each of the 120 airflow direction/month combinations

from consideration of temperature distributions. More variable temperatures lead to wider extremes and in summer the warmer days outweigh the cooler days which would also arise. In winter, some of the warmer days rise above 6°C. Higher accumulated temperatures occur at both sea-level and 800 m under increased variability.

January sensitivity of T_{acc} to σ is higher in the lowlands (mean monthly values of s are given in Table 16.8 and are shown in Figure 16.9) reaching 7.01 d°C/°C. Upland sensitivity is low because 6°C is well above temperatures experienced. By March, sensitivity in the lowlands has peaked at 10.61 d°C/°C, mean daily temperatures being close to 6°C. Individual airflows show ratios as high as 12 d°C/°C, this being a definite upper limit. Upland sensitivity in March is only 0.62 d°C/°C, but rises in April as conditions become warmer. By May s reaches 11.47 d°C/°C at 800 m although sea-level sensitivity has fallen. The most sensitive month is March at sea-level, April at intermediate altitudes, and May in the uplands.

Throughout the summer upland sensitivity remains high, only falling to 3.31 d°C/°C in July. By September s has risen again to 10.20 d°C/°C and 10.95 d°C/°C is recorded in October. In the lowlands the autumn peak occurs in November and December. The most sensitive upland periods occur later in spring and earlier in autumn. Any increase in temperature variability associated with climate change (Houghton et al. 1990) will have a greater effect on growing season strength in upland areas because sensitivity is greater at 800 m from May to October.

Mean sensitivities for individual airflow types at sea-level and 800 m are shown in Table 16.9 overleaf.

Northerly flows are associated with great sensitivity in the uplands. Similar trends are seen for north-easterly and easterly flows. Temperature variation within such polar and arctic air-masses is therefore critically important in the uplands and in a climate dominated by a blocked (meridional) circulation, growing potential in the uplands would be extremely sensitive to changes in temperature variability. Under continental air-mass influences from the south-east, the sensitivity is less. A larger

Figure 16.9. Monthly Variations in Mean Sea-level and 800 Metres Sensitivities of Tacc to Standard Deviation

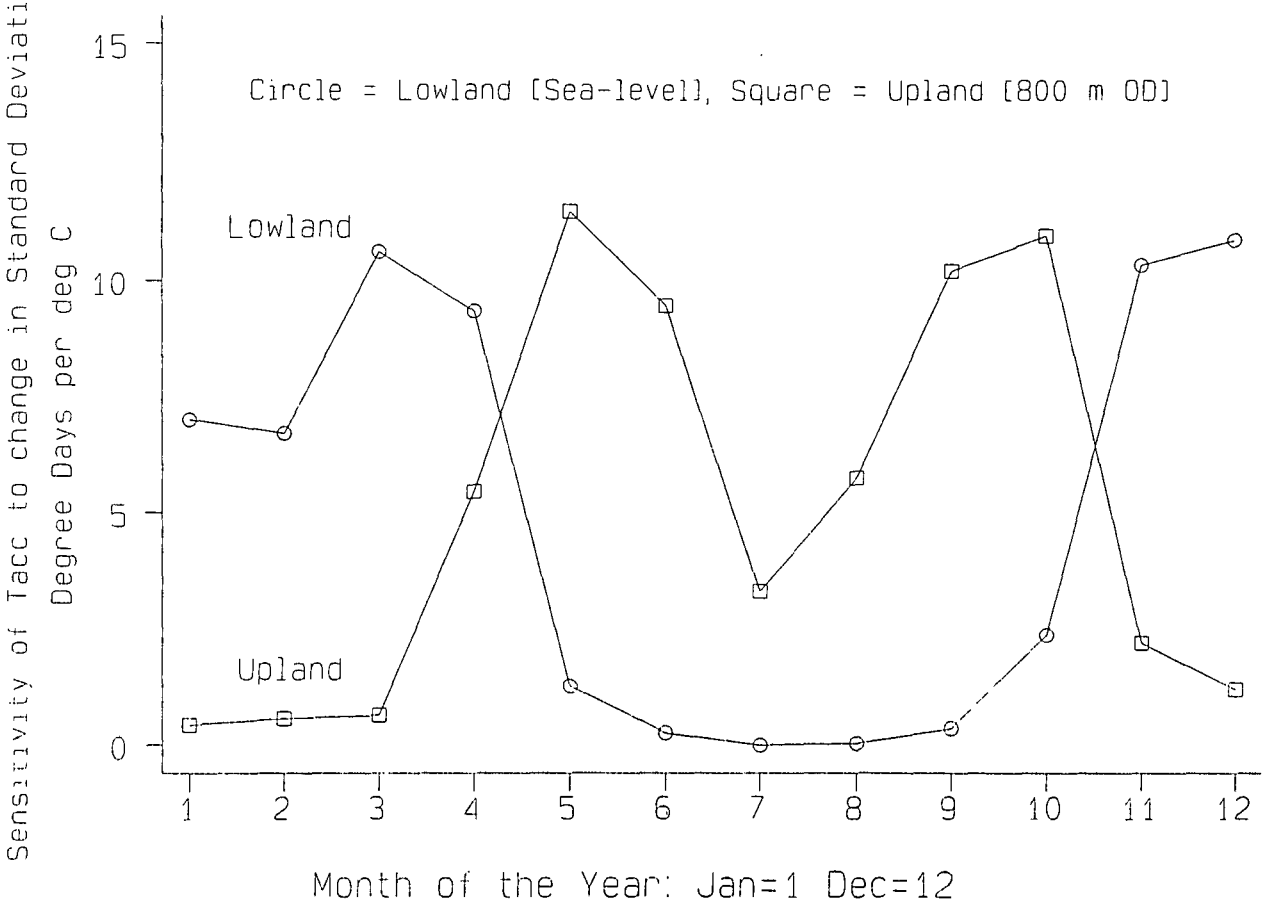

annual swing in mean temperature means that variability within this airflow is less important. Sensitivity at 800 m peaks at 7.09 d°C/°C for southerly flows. The only two airflows for which sensitivity is higher at sea-level are westerlies and north-westerlies, because polar maritime air often produces temperatures near 6°C in winter at sea-level.

Table 16.9: Mean values of s (d°C/°C) at sea-level and 800 m for each airflow.

Airflow	Lowlands (0 m)	Uplands (800 m)
Calm	5.01	4.23
N	4.44	6.87
NE	4.20	5.90
E	4.22	5.72
SE	3.82	4.03
S	5.22	7.09
SW	5.33	5.72
W	5.73	5.48
NW	5.38	4.66
Mean	5.87	4.77

16.7 Conclusions

The simulation of accumulated temperatures using a time series of daily mean temperatures derived from a specified normal distribution allows a more accurate estimate of growth potential. This accounts for inter-diurnal variability in air temperatures. Parameters such as the number of frosts or growing days, which formerly required a logistic function to relate their probability to mean daily temperature (Chapter 14), can be simulated directly.

Annual accumulated temperatures can be calculated given a mean and standard deviation for the daily temperature series as long as the distribution is normal. In Britain this assumption usually holds true. Slight skewness in the distribution (positive

in summer and negative in winter) could occur due to relatively infrequent spells of hot or cold weather. For a particular airflow, however, temperatures are likely to be normally distributed. Another assumption, which is less valid, is that successive daily temperatures are mutually independent. Cold and warm spells tend to occur (Hamilton 1987), successive days recording above or below normal temperatures. The probability distribution of temperature on day **n** depends in part on the temperature recorded on the previous day (Jolliffe 1990). Useful results were obtained using this assumption, despite possible inaccuracies.

The growth estimates produced (T_{acc}) estimate G_d, the sum of daily temperature excesses above 6°C, and not G_p or G_y, as in Chapter 13. Results for uni-directional wind scenarios confirm previous findings, showing that the circulation pattern is important in controlling the altitudinal gradient in growth potential. In the uplands the percentage variation in accumulated temperatures between airflows is greater and the environment is more sensitive to synoptic changes. Continental air from the south-east and calm anticyclonic conditions benefit the uplands through increased stability, decreased lapse rates and higher temperatures. Maritime air has the opposite effect, reducing T_{acc} at 800 m to around 20% of that at sea-level.

Regional predictions concerning possible benefits of global warming in upland areas depend therefore on the relative influences of continental and maritime airflows. Effects shown in this chapter will be magnified if airflows themselves change character, in terms of either mean temperature or variability. Many GCMs forecast changes in temperature variability as well as mean temperature increases (Houghton et al. 1990), and there is evidence that absolute temperatures and temperature variability are related in many climates (Rind 1991). Changes in variability could be at least as influential as changes in mean temperatures, especially when temperatures are close to a critical threshold.

THE SIMULATION OF CLIMATIC VARIABILITY TO IMPROVE FROST ACCUMULATION ESTIMATES

17.1 Introduction

Simulation of climatic variability using normally-distributed random data will be used to investigate frost parameters in this chapter. A logistic function was used in Chapter 14 to relate frost occurrence with mean daily temperature. The relationship was site-dependent and of variable strength, R^2 varying from 0.39 at Houghall to 0.8 at Great Dun Fell. An alternative method involves assuming that consecutive daily minima are normally distributed and independent of one another. Once the standard deviation (σ) of daily minima is known, this is combined with the mean to create a time series of daily minima. This is similar to the procedure employing daily mean temperatures (Chapter 16).

Values of σ in the original data were examined and it was assumed that variability would remain constant in a future climate, despite changes in mean minima. Recorded values of σ were used as the simulated standard deviation, as in Chapter 16.

17.2 Variability of Daily Minimum Temperatures (σ)

The standard deviation of daily minimum temperatures within each month was calculated: σ ranged from 4.51°C at Carlisle in December to 1.89°C at Sunderland in July. The extreme values correspond with those for mean daily temperatures. Since mean temperatures depend in part on minima, this is not surprising. Relationships between σ, altitude and exposure (on three spatial scales) were examined. In all months (except from April to June) there is a relationship with one parameter, although this is sometimes weak (Table 17.1). Micro-exposure (on a scale of 250 metres or less) is most influential in five months, whereas altitude is influential in July, November and December, and local exposure (on a scale of 1 km) in September. The total (macroscale) exposure was never the most important site factor.

Table 17.1: Relationship of standard deviation of daily minima (σ) (°C) with station altitude (metres above sea-level) and exposure: σ = a (alt or exp) + b.

Month	Mean σ	a	b	indep	r	σ at GDF	σ at Dur
Jan	3.53	0.00248	3.59	micro	0.497	3.53	3.53
Feb	3.78	0.00201	3.83	micro	0.432	3.78	3.78
Mar	3.27	0.00177	3.31	micro	0.555	3.27	3.27
Apr	3.01	-	-	texp	0.125	3.01	3.01
May	2.65	-	-	alt	0.194	2.65	2.65
Jun	2.85	-	-	local	0.183	2.85	2.85
Jly	2.36	0.00057	2.27	alt	0.432	2.75	2.33
Aug	2.63	0.00139	2.66	micro	0.429	2.63	2.63
Sep	3.20	0.00065	3.19	local	0.488	3.20	3.20
Oct	3.22	0.00214	3.27	micro	0.497	3.22	3.22
Nov	3.36	-0.00131	3.58	alt	-0.516	2.47	3.45
Dec	3.55	-0.00139	3.78	alt	-0.594	2.60	3.64

The final two columns show σ extrapolated to the altitudes of Great Dun Fell (847 m) and Durham (102 m). When altitude was not the controlling factor the mean standard deviation was assumed to be representative of all sites. Figures 17.1 a), b) and c) show the strongest relationships. Stations represented by "1" were not included to calculate the regression line, being based on less than six years of data.

In March (Figure 17.1 a) σ increases with micro-exposure, i.e. at sheltered sites temperature variability increases due to frequent air stagnation. High Close shows the lowest variability, σ being only 2.59°C. At the other extreme, Kielder (prone to low minima and frost hollow effects) shows a standard deviation of 3.72°C.

In September (Figure 17.1 b) there is a weak relationship between σ and local exposure, sheltered locations such as Keswick and Kielder showing great variability. Appleby and Kielder have standard deviations of around 4.00°C, whereas Great Dun

Figure 17.1. Relationships between the Standard Deviation of Minimum Daily Temperatures and Environmental Factors

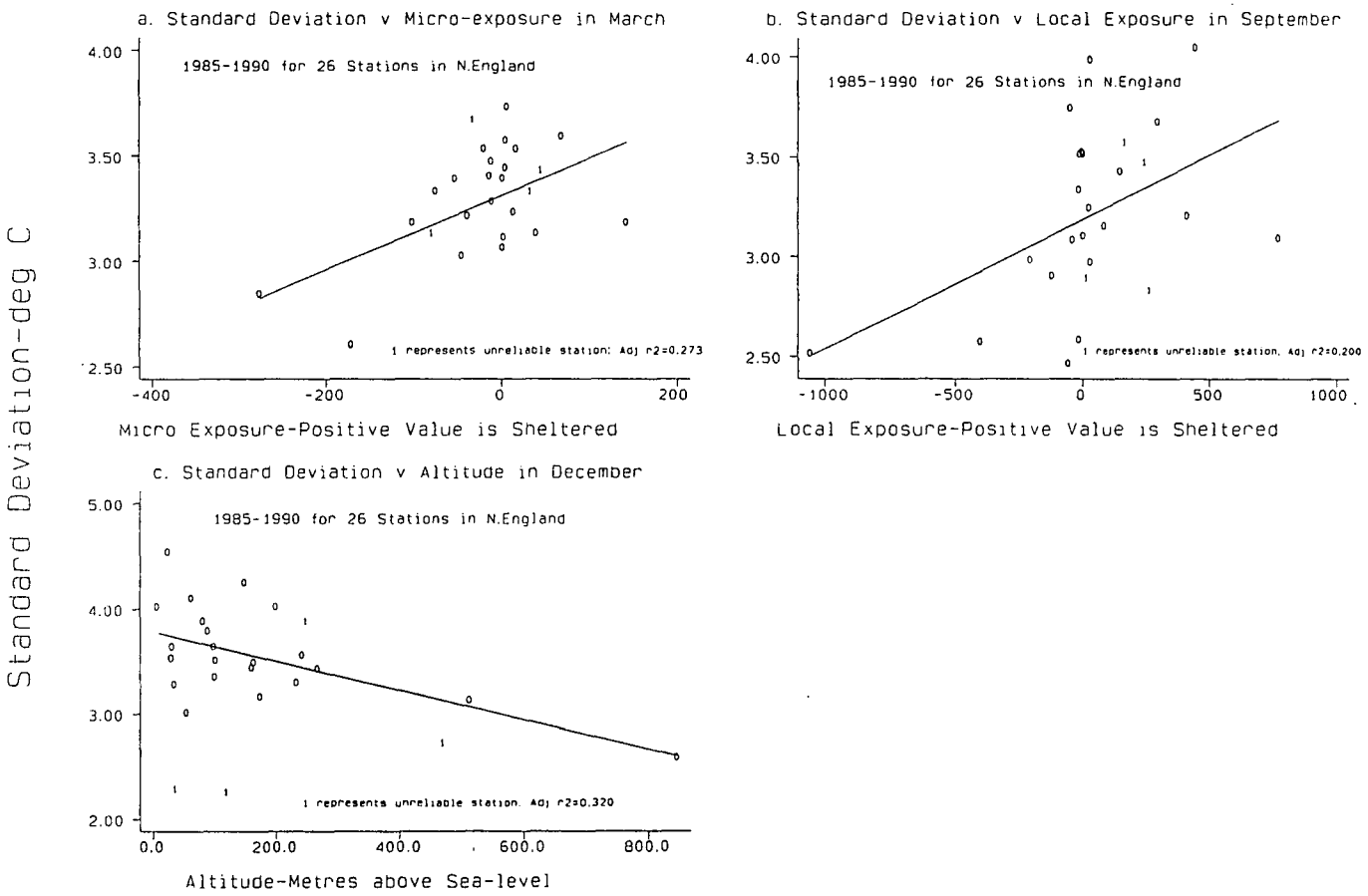

Fell (a very exposed summit site) has a value of 2.50°C. Newcastle and Sunderland record low variability in minima because of the moderating influence of the North Sea.

The strongest relationship of σ with site factors in any month is the inverse one with altitude in December (Figure 17.1 c). Minima are strongly influenced by temperature inversions, especially in December when nights are long. In lowland areas minima vary considerably between nights with and without surface inversions. Above the inversion level temperatures are less variable, being independent of its formation. Upland areas are frequently above the inversion level in mid-winter so σ decreases with altitude.

Generally, inter-diurnal variation in minima is greatest in winter when temperature inversions are common. σ averages 2.36°C in July but rises to 3.78°C in February. In most months σ increases with increasing exposure values. The relationship with altitude is negative between August and March. However, there is a weak altitudinal increase in σ between April and July. The absence of a strong relationship suggests that it is an altitudinal increase in the variability of daily maxima which underlies the strong positive summer correlations between altitude and σ of mean daily temperature.

17.3 Simulation of Daily Time Series

Using the same ten random number simulations in Figure 16.2, daily time series of minimum temperatures were created for sea-level using the mean (μ) predicted for the relevant scenario and the standard deviation (σ) from Table 17.1. In each run the predicted number of frosts (minima below 0°C) is shown in Table 17.2.

Corrections are required in months of less than 31 days. With these necessary corrections, annual frost frequencies vary from 29.1 days (run 3) to 74.9 days (run 4). The mean annual number of frosts simulated is 49.3. No frosts occur in June, July and August and only one frost occurs in both May and September (run 10). The largest number of frosts simulated within a single month is 16 in January (run 4).

Table 17.2: The number of frosts at sea-level simulated in ten time-series.

Number of Frosts Simulated per Month (Minima < 0 deg C)													
Run	J	F	M	A	M	J	J	A	S	O	N	D	T
1	12	13	6	4	0	0	0	0	0	0	5	6	46
2	14	14	11	7	0	0	0	0	0	0	9	11	66
3	7	7	5	2	0	0	0	0	0	1	3	5	30
4	16	16	13	7	0	0	0	0	0	0	12	13	77
5	10	12	7	2	0	0	0	0	0	0	5	7	43
6	12	13	8	3	0	0	0	0	0	1	5	7	49
7	8	9	6	4	0	0	0	0	0	0	6	6	39
8	14	14	10	4	0	0	0	0	0	0	9	10	61
9	12	13	4	2	0	0	0	0	0	0	3	4	38
10	13	14	8	6	1	0	0	0	1	1	8	8	60

Table 17.3 shows the first simulation in more detail.

Table 17.3: Frost occurrence and severity in run 1.

Month	**x (°C)**	**s (°C)**	**μ (°C)**	**σ (°C)**	**n**	**sv (°C)**	**d°C**
Jan	2.08	4.06	1.50	3.53	12	-5.46	25.56
Feb	1.90	4.34	1.28	3.78	11.7	-6.17	31.59
Mar	3.11	3.76	2.57	3.27	6	-3.88	13.62
Apr	4.57	3.46	4.07	3.01	4	-1.87	4.56
May	7.31	3.05	6.87	2.65	0	-	-
Jun	9.64	3.27	9.17	2.85	0	-	-
Jly	11.88	2.61	11.51	2.27	0	-	-
Aug	11.69	3.02	11.26	2.63	0	-	-
Sep	9.41	3.68	8.88	3.20	0	-	-
Oct	7.89	3.70	7.36	3.22	0	-	-
Nov	3.81	4.11	3.22	3.58	4.8	-3.84	12.50
Dec	3.72	4.34	3.10	3.78	6	-4.35	14.94

The sample mean **x** is greater than μ and the sample deviation **s** is greater than σ. **sv** indicates the severest frost simulated (-6.17°C in February). The final column shows the 'frost degree days' or accumulation of daily minimum temperatures below freezing. This has been used as an index of winter severity as by Assel (1980) and gives an idea of likely frost damage.

The annual frost accumulation amounts to -99.16 d°C. The expected accumulation could be calculated by repeating the process as many times as possible and taking the mean accumulation. This will approach the true accumulation, assuming the minima to be normally distributed (Central Limit Theorem).

17.4 An Analytical Approach to Improve Frost Accumulation Estimates

A quicker method to calculate the expected frost frequency and accumulation involves using standard normal distributions (Table 17.4).

Table 17.4: Probability of a minimum daily temperature less than 0°C in each month at sea-level, assuming normality.

Month	n	μ (°C)	σ (°C)	z(0)	p(<z)	np
Jan	31	1.50	3.53	-0.425	0.336	10.41
Feb	28	1.28	3.78	-0.339	0.367	10.28
Mar	31	2.57	3.27	-0.786	0.216	6.71
Apr	30	4.07	3.01	-1.352	0.088	2.65
May	31	6.87	2.65	-2.592	0.005	0.15
Jun	30	9.17	2.85	-3.218	0.001	0.02
Jly	31	11.51	2.27	-5.070	0.000	0.00
Aug	31	11.26	2.63	-4.281	0.000	0.00
Sep	30	8.88	3.20	-2.775	0.003	0.08
Oct	31	7.36	3.22	-2.286	0.011	0.35
Nov	30	3.22	3.58	-0.899	0.185	5.54
Dec	31	3.10	3.78	-0.820	0.206	6.38

The method is similar to that used in the previous chapter to calculate expected growth accumulation (see section 16.4). Again the critical frost temperature (0°C) is converted into a **z**-score. **z** will be negative since all predicted mean minima are greater than 0°C. The probability of frost at sea-level in January is 33.6% (using tables of the standard normal random variable). This is converted to the expected monthly frost frequency by multiplying by **n**, the number of days in the month. The mean annual number of frosts predicted for sea-level is 42.6 by this method.

F_{ex}, the mean frost temperature, will be below 0°C and frost accumulation F_{acc} is negative. Monthly results are shown in Table 17.5 for sea-level and 800 m. The mean annual frost accumulation at sea-level is -92.16 d°C. Most occurs between November and April and the summer months only contribute -0.59 d°C!

Table 17.5: $\mathbf{F_{ex}}$ and $\mathbf{F_{acc}}$ in each month (see also Table 17.4).

Month	$\mathbf{F_{ex}}$ **°C sea-level**	$\mathbf{F_{acc}}$ **°C sea-level**	$\mathbf{F_{ex}}$ **°C 800 m OD**	$\mathbf{F_{acc}}$ **°C 800 m OD**
Jan	-2.34	-24.32	-4.42	-113.49
Feb	-2.59	-26.68	-4.84	-113.57
Mar	-1.87	-12.52	-4.04	-102.91
Apr	-1.39	-3.69	-2.85	-55.11
May	-0.83	-0.12	-1.50	-9.70
Jun	-0.77	-0.01	-1.26	-2.64
Jly	-0.42	-0.00	-0.88	-0.15
Aug	-0.56	-0.00	-0.87	-0.22
Sep	-0.96	-0.08	-1.50	-4.20
Oct	-1.10	-0.38	-1.75	-9.72
Nov	-1.95	-10.82	-2.31	-44.01
Dec	-2.13	-13.58	-2.73	-60.73

F_{ex} is always negative although during the summer it approaches 0°C. It never

approaches the mean minimum temperature at sea-level because the probability of frost never reaches 1. At 800 m, however, F_{ex} approaches the mean minimum in winter as frost probabilities are over 0.95. F_{acc} at sea-level reaches -26.68 d°C in February but this is negligible compared with T_{acc} in Chapter 16. In contrast, at 800 m the winter frost accumulation F_{acc} is larger than summer growth accumulation T_{acc}! From January to March -329.97 d°C of frost compare with 303.79 d°C of growth between June and August. Equivalent figures at sea-level are -63.52 (F_{acc}) and 796.06 (T_{acc}). The simulated high and low altitude climates could not be more contrasting in terms of the relative magnitudes of winter frost and summer growth.

All results are sensitive to σ. Using mean standard deviations in months when no relationship of σ with altitude was found could lead to errors. Additionally, different airflows show different inter-diurnal variability and should also have different values of σ.

17.5 Annual Frost Accumulations Under Differing Airflow Influences

As for the growth accumulation T_{acc}, predicted frost frequencies and frost accumulations were calculated for each airflow in each month, assuming σ to be determined by month alone. Figures 17.2 a and 17.2 b show frost frequency at sea-level and 800 m respectively. The frequency varies rapidly over the year, especially at 800 m. In winter, upland frost frequencies are high, ranging from 30.1 days for easterly flow to 23.59 days for southerly flow in January. Frequencies remain high until March or even April and then only fall slowly. Even in May, 13.06 frosts are expected with a north-westerly flow. July is the only frost-free month. Sea-level frequencies reach 21.89 days for north-easterlies in January. Otherwise values are low, mostly below 1 frost per month between May and October. Wind direction has a greater influence on winter frost frequencies at sea-level than at 800 m where air frosts occur anyway, due to the advection of the free air. Only in April and May is airflow direction critical at 800 m.

Table 17.6 lists annual frost frequencies and accumulations for each airflow at

Figure 17.2. Predicted Monthly Frost Frequencies

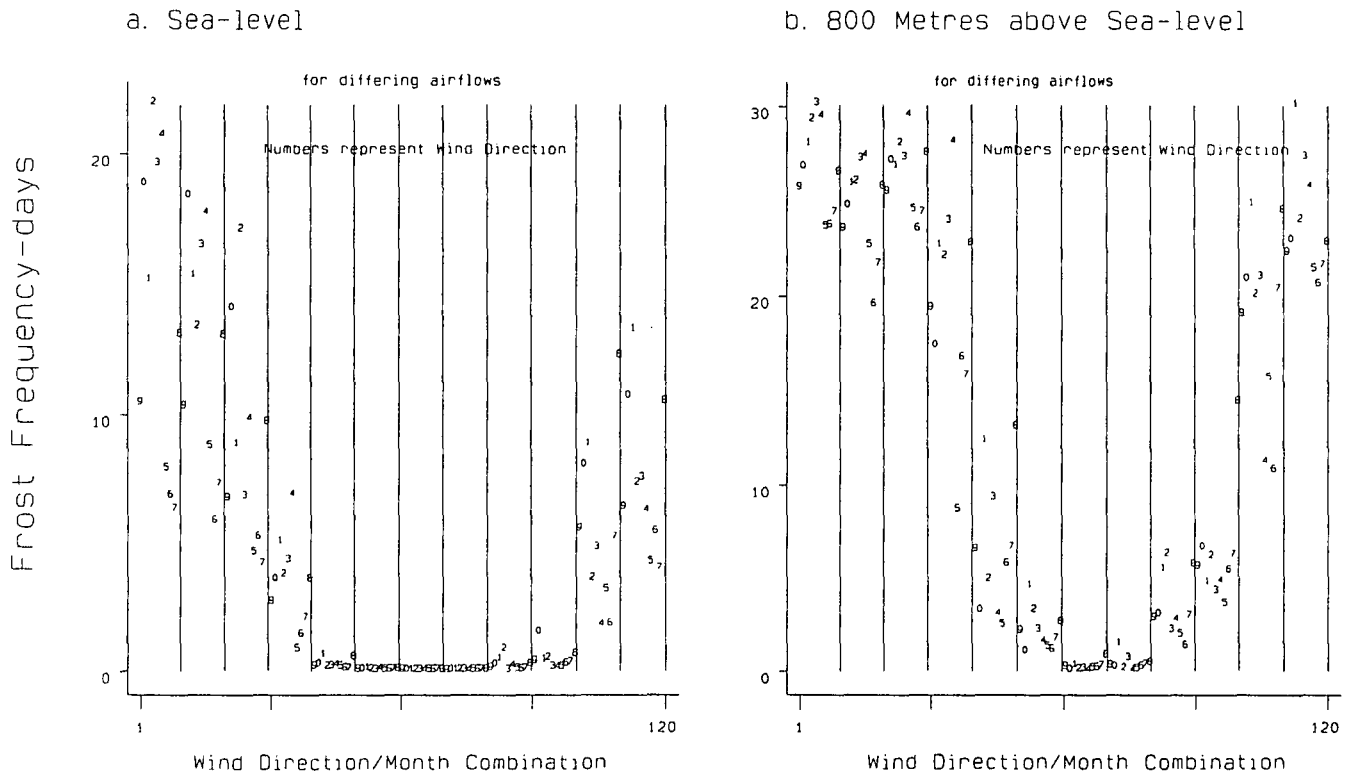

sea-level and 800 m, assuming the airflow to dominate for the whole year (as in uni-directional wind scenarios).

Table 17.6: Frost frequencies and accumulation F_{acc} (d°C) at sea-level and 800 m for uni-directional wind scenarios.

Wind	Frost n Sea-level	Frost n 800 m OD	F_{acc} Sea-lvl	F_{acc} 800 m OD	Ratio 800m/Sea
Calm	75.36	153.72	213.46	565.92	2.65
N	67.92	187.20	175.20	777.60	4.44
NE	68.40	170.04	195.72	696.00	3.56
E	59.76	175.32	164.88	802.68	4.87
SE	63.60	163.56	183.00	828.72	4.53
S	29.64	125.64	60.24	406.92	6.75
SW	26.76	128.52	51.12	387.84	7.59
W	29.28	145.80	56.28	459.12	8.16
NW	63.24	186.60	155.88	692.04	4.44
Mean	42.60	152.52	92.16	516.48	5.60

At sea-level the annual frost frequency averages 75.36 under calm conditions. This is the highest figure out of all airflows because of the tendency towards low minima on calm "radiation" nights. Colder airflows such as northerly flow produce 67.92 frosts per annum, while milder flows such as south-westerlies only produce 26.76, leading to a threefold variation in frequency. There is a large contrast between mild winds between west and south and the other airflows. At 800 m calm conditions do not produce the highest frequency. This is achieved by northerly flows (187.2) and then north-westerly flows (186.6), illustrating the severity of polar maritime air at this elevation.

Frost accumulations (F_{acc}) at 800 m are not correlated with frequencies. Surprisingly, south-easterlies produce the severest frost accumulation (-828.72 d°C), despite shallow lapse rates. An invasion of continental air would therefore increase frost

risk in winter as well as increase summer growth accumulations (Chapters 13 and 16). Severest conditions are experienced between January and April, the latter month recording -140.88 d°C! Severe winter and spring frosts would combine with the improved growing season, producing uncertain environmental consequences. The smallest frost accumulations occur for airflows from between south and west, with annual totals around -400 d°C. At sea-level, all accumulations are relatively low, being highest for calm conditions (-213.48 d°C) and lowest for south-westerly flow (-51.12 d°C). The frost risk would become negligible at sea-level under a progressive zonal circulation dominated by southerly and westerly flows, but would worsen to over -200 d°C under anticyclonic conditions. The sensitivity of results to σ is similar to the previous chapter.

17.6 Conclusions

Under a continental south-easterly scenario the growth accumulation at 800 m would be high, at 738.6 d°C (46.1% of the sea-level value). However, frost accumulation would also be high (-828.72 d°C) and more than four times that at sea-level. The bulk of this occurs in winter but considerable accumulations occur in March and April. The more continental climate represented by the south-easterly scenario would include a severer frost regime as well as improved summer warmth because of increased diurnal and annual temperature ranges. With frosts on 163.56 days the growing season would be shortened but also strengthened. In contrast, an increase in mild oceanic weather types decreases frost occurrence but also lowers summer accumulated temperatures to between 580.92 d°C (southerly) and 353.28 d°C (westerly). Incorporation of temperature variability has substantiated the results of Chapters 13 and 14, showing that daily variation is just as important as changes in mean conditions.

The next chapter employs climatic output from recent GCMs to alter the mean temperatures of airflow types. Using the altered temperatures, new estimates of accumulated growth and frost are interpolated over the study area. Changes in climate are related to "potential" for crop growth. In all scenarios, 3°C is used as an estimate

of the standard deviation of daily temperatures. Sensitivity analyses in Chapter 16 have shown that an error of 1 °C in estimating σ leads to an error of 12 degree-days (d°C) per month at the most, at the most sensitive seasons. Possible errors from this source are small, compared with the accumulations involved.

THE USE OF GCM SCENARIO OUTPUT TO ILLUSTRATE EFFECTS OF FUTURE CLIMATE CHANGE ON ACCUMULATED TEMPERATURES AND FROST RISK

18.1 Introduction

There is much speculation about the possible effects of climatic change on land-use in the UK and Europe using recent GCM predictions (Hulme et al. 1993b). The airflow scenarios developed in this thesis are now compared with such GCMs. Current estimates of future temperature change are converted into attendant changes in climatic potential (measured by accumulated temperatures, frost frequency and frost accumulation).

Previous research has been concerned particularly with possible agricultural changes in marginal regions (Parry et al. 1988) and the response of grain crops to warming (Nuttonson 1955, Nield et al. 1979). Notable studies include an investigation into a northward shift in grain maize limits in the Northern Hemisphere (Parry et al. 1990, Carter et al. 1991a) and a shift of sunflowers into southern Britain (Carter et al. 1991b). Shifts in natural species distributions will be complicated by mountains which restrict latitudinal movement by acting as physical barriers to migration, often remaining unsuitable for cultivation despite increased warmth. Mountain regions are useful for studying the responses of ecosystems to climate change since many "climatic zones" (representative of those over a wide latitudinal range) exist in a small area. Warming or cooling will cause these altitudinal zones to shift either up or down slope. The shifting of altitudinal belts has been used as evidence of past climatic change (Messerli & Winiger 1992). The Pennines are especially interesting because they lie close to the present northern limits of grain cultivation in western Europe. The lack of summer warmth causes much land to be marginal (Parry 1976) and effects of warming supported by time-series analysis (Manley 1974, Parker & Jones 1991, Parker et al. 1992), and that predicted by GCMs, are likely to be considerable in northern England.

Most recent climate models predict that warming will occur in Britain over the next half-century (Houghton et al. 1992). However, many scenarios are not particularly

impact-orientated (Robinson & Finkelstein 1991). Accumulated temperatures are extremely useful as a measure of growing season strength and temperature thresholds are also important for assessment of climatic risks, e.g. frost probability. Such variables are rarely simulated directly as GCM output and must be calculated from temperature predictions.

Theoretical altitudinal limits to cultivation in the northern Pennines vary considerably between uni-directional airflow scenarios (Chapter 13). There is therefore great sensitivity in response to between-type climate change. Within-type changes are also considered in some of the following scenarios (see Lamb 1972, Comrie 1992, Hulme et al. 1993a).

18.2 The Construction of Future Climatic Change Scenarios

Changes in "climate potential" for five scenarios will be compared:

a) **The control situation**, as described by the regression models of Chapter 8 and associated with the altitudinal zonation described in Chapter 9.

b) **Warm and cold analogues**. Temperatures experienced during an exceptionally warm year (1989) and a cold year (1986) are used to represent the variability inherent in the present climate.

c) **Uni-directional airflow scenarios**, as introduced in Chapters 13 and 14. These simulate the cumulative annual effect of a sustained airflow from one direction, without any change in the quality of that airflow from that between 1985 and 1990. Airflow temperatures are defined by the appropriate regressions in Chapter 8. Such simulation of climate differences due to variation in airflows makes sense because changes in the circulation pattern have occurred in the past (Briffa et al. 1990, Mayes 1994) and are predicted for the future (Lumb 1993, Murray 1993).

d) **Arbitrary warming scenarios**, whereby a constant temperature increase is applied

to the control climate. The three figures applied are +1°C, +2°C and +4°C. The biggest increase approaches that suggested by many GCMs. Arbitrary temperature increases have been applied to investigate effects of temperature change on European agriculture (Carter et al. 1991a).

e) **Two GCM simulations**; the UKHI (United Kingdom Meteorological Office High Resolution GCM Equilibrium Experiment) (Viner & Hulme 1992) and GISS (Goddard Institute for Space Studies) (Hansen et al. 1984) GCMs. Both are equilibrium climate models and simulate mean temperatures for a control (baseline) climate (1 * CO_2) and for a world in which the carbon dioxide content is twice present levels (2 * CO_2). UKHI is a high resolution experiment to study the equilibrium response of climate to CO_2 doubling (Viner & Hulme 1992), and is being developed by the Hadley Centre, part of the British Meteorological Office. Models of this type are widely quoted in climate impact studies (Mitchell et al. 1990, Carter et al. 1991b, Warrick & Barrow 1991, Hulme et al. 1993b).

Because simulated control climates (1 * CO_2) do not provide an accurate baseline for the Pennine region, the difference between the 2 * CO_2 and 1 * CO_2 simulations is used to estimate temperature change to be applied to the baseline (control) climate, described here by ground station data.

18.3 Definitions of Climatic Potential

The same procedure for calculation of "climate potential" (accumulated temperatures and frost parameters) is followed in all scenarios. First, the mean temperature (for growth parameters) or mean minimum temperature (for frost parameters) is calculated for each month for each cell of a digital terrain model (Chapter 4), covering the whole of northern England at a resolution of 5 by 5 kilometres. Mean monthly temperatures are calculated directly for the control and airflow scenarios from the appropriate regression equations in Chapter 8. Continental and maritime airflow scenarios are created using appropriate south-easterly or westerly airflow regressions in each month respectively.

Mean monthly temperatures are then interpolated to all 800 grid points using the equations. Grid temperatures are converted into expected accumulated temperatures T_{acc}. T_{acc} can be calculated accurately if the mean and standard deviation of the expected mean monthly temperature is known (Chapter 16). Assuming σ to be 3°C leads to the results discussed below.

Twelve individual monthly T_{acc} values are summed, giving the annual total for each grid point. A map is then drawn of annual growth potential. A categorical variable **L** was created, based on annual T_{acc} values.

Table 18.1: Categorisation of annual accumulated temperatures, T_{acc}.

Land Potential Category (L)	**T_{acc} range of values(d°C)**
1	<500
2	500-749
3	750-999
4	1000-1199
5	1200-1399
6	1400-1599
7	1600-1799
8	1800-1999
9	2000-2499
10	>2500

Classes 1 to 3 are sub-marginal, accumulated temperatures being below the critical limit of 1000 d°C, assumed necessary for cultivation (Chapters 1 and 10). Class 4 is marginal, because although T_{acc} is above the critical 1000 d°C, it is below 1200°C and may show deficiencies in colder years. Classes 5 and above are non-marginal.

18.4 Methods Involved in Individual Scenarios

Before results are discussed, equations and methods used to construct individual scenarios are outlined.

The south-easterly uni-directional wind scenario is chosen to represent the continental airflow scenario. A warmer summer and colder winter result. Mean lapse rates are shallower and the uplands benefit in relative terms. Conversely, the westerly scenario is chosen to represent the most maritime situation. Steeper lapse rates and a reduced seasonal swing in temperature result.

1986 is taken to be the cold analogue. Mean monthly temperatures are calculated using the multiple regression equations appropriate to that year. The warm analogue is represented by the year 1989. The use of past conditions to represent variability is common (Lamb 1982, Webb & Wigley 1985, Barry 1990).

The three arbitrary scenarios are self-explanatory, illustrating the response of the area to set increases in temperature.

Monthly temperature corrections for the GISS 2 * CO_2 scenario are given by Houghton et al. (1992), calculated from the global sensitivity to doubling carbon dioxide and are listed below:

Winter	Spring	Summer	Autumn
+4.5°C	+3.5°C	+3.5°C	+3.75°C

Warming is expected to be concentrated in winter (December-February). The mean increase is 3.81°C.

Temperature corrections for the UKHI 2 * CO_2 scenario are calculated by taking the arithmetic mean of the difference between control and perturbed simulation temperatures for two grid squares relevant to the study area, 49 and 63 in the

European window, (Viner & Hulme 1992) (Table 18.2). Grid square 49 covers the area north of the Tyne and square 63 most of the Pennine region and much of Central England. The dimensions of a grid square are 250 km by 250 km.

Table 18.2: Corrections to mean temperatures (°C) in the UKHI 2 * CO_2 scenario.

Grid Square	JAN	FEB	MAR	APR	MAY	JUN
49	+7.82	+7.07	+5.89	+3.52	+3.93	+2.51
63	+6.55	+6.53	+5.58	+3.30	+4.24	+2.93
Mean	+7.19	+6.80	+5.74	+3.41	+4.09	+2.72
	JLY	AUG	SEP	OCT	NOV	DEC
49	+2.17	+2.99	+3.15	+3.25	+3.62	+4.71
63	+2.86	+3.45	+3.77	+3.39	+3.09	+4.45
Mean	+2.52	+3.22	+3.46	+3.32	+3.36	+4.58

The 2 * CO_2 scenario is not fixed in time, depending on the rate at which carbon dioxide increases in the future. The global mean temperature rise for a doubling of CO_2 (the climate sensitivity) can be related to the spatial change in that particular climatic element to provide a local estimate of climate change. In order to convert such estimates to a prediction fixed in time the output can be linked with output from the STUGE model (Sea-Level and Temperature Under the Greenhouse Effect) (Viner & Hulme 1993).

In both GCMs, predicted temperature increases are greater in winter than in summer, in line with other models (Schlesinger & Mitchell 1985). Accumulated temperature increases will not be as strong as they would be if warming were concentrated in summer. The annual temperature range is predicted to decrease and the climate may become more maritime.

One of the major problems in simulating **mesoscale** climatic change from **macroscale** GCMs is that of downscaling predictions so that they are relevant to a local

area (Giorgi & Mearns 1991, Robock et al. 1993). It is important that regional scale climatic features are included within the scenarios. In the UKHI model there are only two grid squares relevant to the whole of the study area and the mean temperature change predicted for these squares is applied over the detailed baseline climate. This could be unrealistic as the amount of warming is not expected to be similar in all areas.

18.5 The Control Climate

The control situation (Figure 18.1) represents the present climate (Chapters 10-12). Numbers represent **L**, the land potential category (Table 18.1). Out of 715 land pixels, with altitudes ranging from sea-level to 847 m, 553 (74.6 %) are class 4 or above and can be considered as **cultivable** land. 169 (22.8 %) of pixels are **marginal** (class 4) and 188 (25.37 %) of pixels are class 3 or below (**sub-marginal**). The sub-marginal land includes most of the high Pennines, Yorkshire Dales, Kielder Forest and Cumbrian Fells. Higher parts of the Vale of Eden, Tyne Gap and much of Kielder are classified as marginal. A large amount of land has accumulated temperatures too low for agricultural production, in part explaining the large areas of uncultivated moorland.

18.6 Results for Climate Change Scenarios: Accumulated Temperatures

Maps drawn for other scenarios (Figure 18.2) show surprising contrasts in the relative amounts of cultivable, sub-marginal and marginal land. Results are compared in Table 18.3. Figures are derived from 741 pixels, including values interpolated for the 26 climate stations. Station values are omitted on the maps.

Column 1 lists the scenarios. This is followed by mean annual accumulated temperatures above 6°C (T_{acc}), the maximum and minimum pixel accumulations and the ratio **R** between these two. The second half of the table lists percentages of land in sub-marginal (column 6), marginal (column 7), non-marginal (column 8) and cultivable categories (column 9). Cultivable land includes marginal but not sub-marginal land. The percentage of cultivable land which is marginal is given in the far right hand column. This figure gives an idea of the fragility of the agricultural resource base. Percentages

Figure 18.1. Land Potential, as Measured by Accumulated Temperatures, Gd, in Northern England for the Control Climate

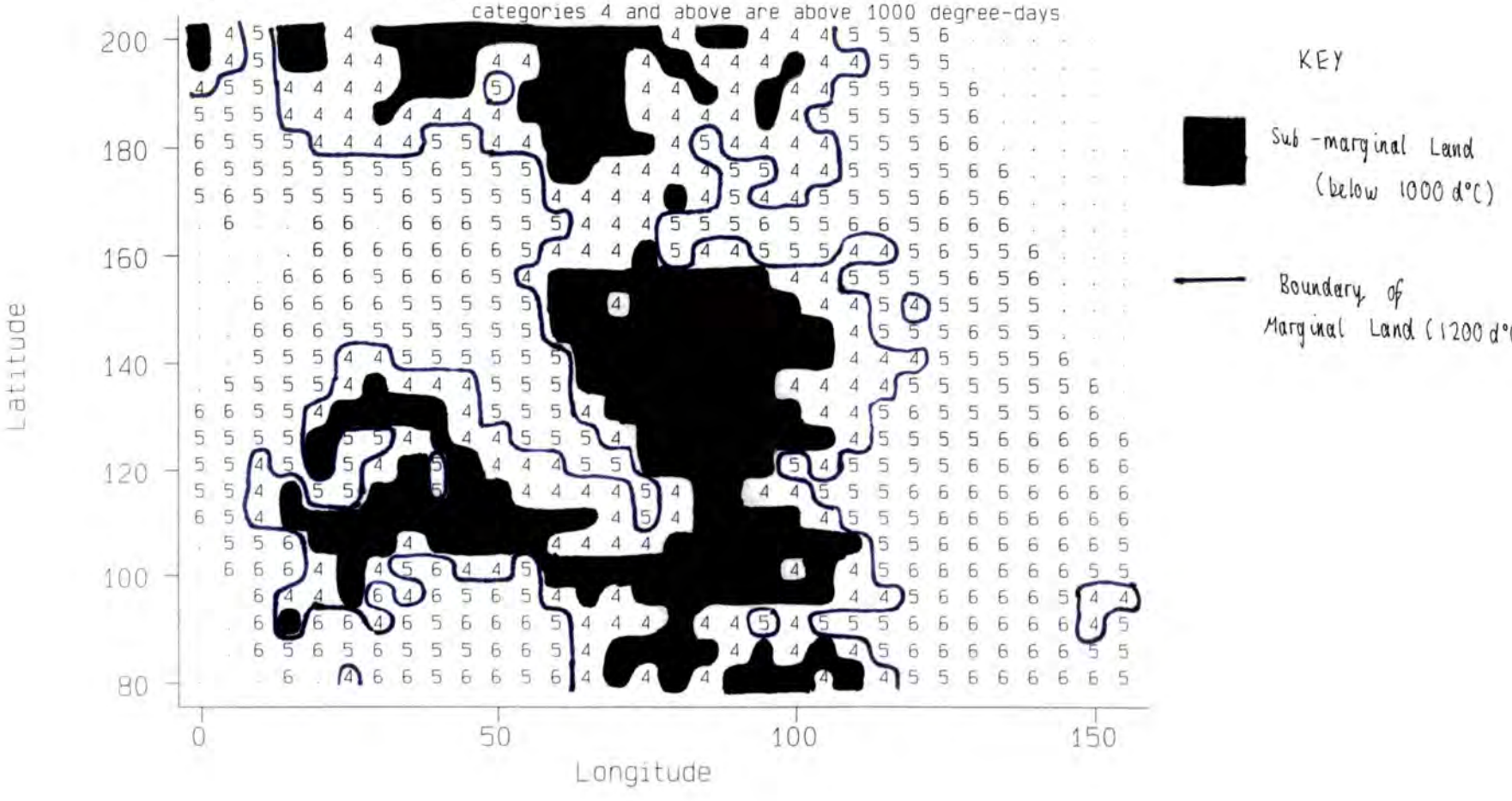

Figure 18.2. Land Potential Category (L) in Northern England
Under Nine Scenarios

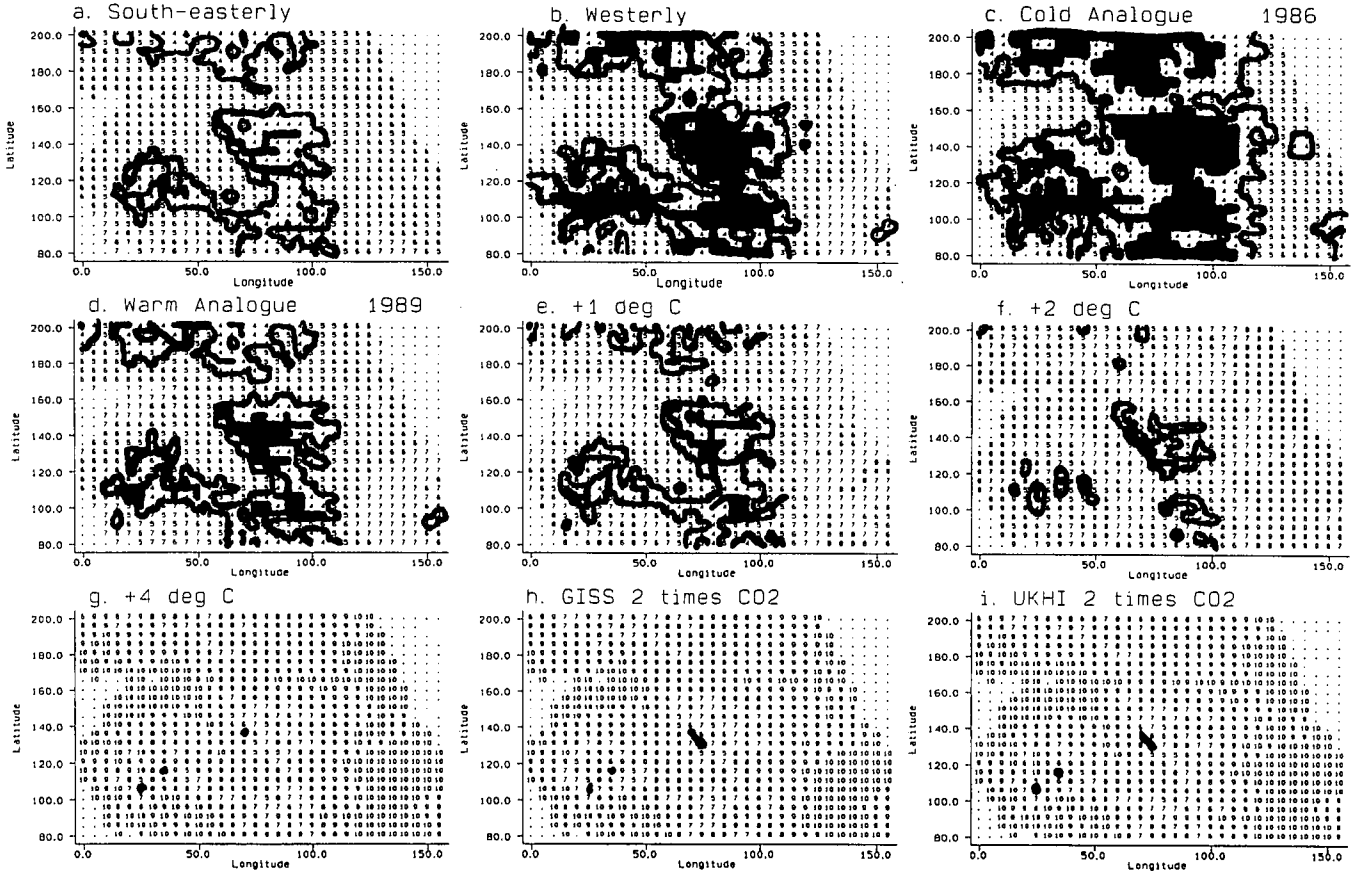

KEY

Sub-marginal Land (below 1000 d°C)

Boundary of Marginal Land (1200 d°C)

Based on Accumulated Temperatures in Degree Days
categories 4 and above are above 1000 degree-days

do not always add up to 100 due to rounding errors.

Table 18.3: Scenario results based on 741 pixels. T_{acc} is measured in d°C.

Scenario	Mean T_{acc}	Max T_{acc}	Min T_{acc}	Max/Min
Control	1175.8	1589.6	387.0	4.11
SE	1326.9	1713.1	711.0	2.41
W	1198.0	1743.4	311.3	5.60
1986 (Cold)	1052.1	1462.7	301.5	4.85
1989 (Warm)	1317.5	1759.6	495.2	3.55
+1°C	1414.3	1867.9	519.7	3.59
+2°C	1677.2	2168.7	675.8	3.21
+4°C	2270.0	2824.8	1058.2	2.67
GISS	2193.1	2750.2	984.3	2.79
UKHI	2287.1	2871.3	970.4	2.96

Table 18.3: continued: Figures below are percentages.

L (1-3) sub-mgl	L (4) marginal	L (> =5) non-mgl	L (> =4) cultivable	L(4/> =4)
25.4	22.8	51.8	74.6	30.6
5.3	22.5	72.2	94.7	23.8
28.1	17.7	54.3	71.9	24.6
38.2	28.5	33.3	61.8	46.1
14.2	19.3	66.5	85.8	22.5
8.6	15.3	76.1	91.4	16.7
2.0	5.8	92.2	98.0	5.9
-	0.5	99.5	100.0	0.5
0.1	0.5	99.3	99.9	0.5
0.1	0.5	99.3	99.9	0.5

Most scenarios lead to an increase in the amount of cultivable land. Given a circulation dominated by continental south-easterlies, 94.7% of the land becomes cultivable, illustrating the relative benefit of such an airflow in the uplands. T_{acc} would increase to 711 d°C on the highest summit in the grid and to over 1700 d°C in lowland areas. The increase is greatest in the uplands due to the decrease in lapse rates. The ratio between the highest and lowest accumulations of 2.4 is the lowest among all scenarios. In contrast, a westerly regime decreases the amount of cultivable land, although the amount of marginal land (class 4) also decreases to 17.7%, illustrating the steepening of the altitudinal gradient in T_{acc}. This accompanies steep lapse rates in maritime airflow. The ratio between T_{acc} at sea-level and the highest summit rises to 5.6.

The cold analogue, not surprisingly, causes a decrease in cultivable land to around 60%. Mean T_{acc} is only 1052.1 d°C. In contrast, the warm analogue leads to 85.8% of land being cultivable. These two cases illustrate the contrast between good and bad years. The risk is too great for widespread agricultural development in many areas, because of this inter-annual variation. Extreme inter-annual contrast will be even greater, the two analogues being taken from a six-year period.

Changes accompanying arbitrary temperature increases are surprising. An increase of 1°C would increase cultivable land to 91.36% of the total, with only 7% of this being marginal. T_{acc} exceeds 1800 d°C in the warmest areas. A 2°C increase has even more dramatic effects, confining sub-marginal land to 2% of northern England. This confirms Manley's suggestions (1942) concerning the rapid changes in upland environment which would be associated with small fluctuations in mean temperature. An increase of 4°C would eradicate all sub-marginal land and allow cultivation up to the highest summits, assuming other climate factors (other than temperature) to be favourable. There would be enough warmth on the summit of Cross Fell to grow grain crops such as oats, which require an annual accumulated temperature sum of 1000 d°C (Parry 1975, 1981).

Both 2 * CO_2 GCM scenarios, expected to apply to the year 2050, produce

similar results to the +4°C increase in temperature. Virtually all sub-marginal and marginal land is eradicated with the exception of the highest areas above 800 m (0.5% of the land area is still marginal). The mean T_{acc} is over 2000 d°C in both cases, values approaching 3000 d°C in the warmest areas. This is comparable with present day values in parts of central Europe.

R represents the percentage decrease in growing season strength between sea-level and the highest summits. The contrast between the continental and maritime scenarios has already been mentioned. **R** in other scenarios falls between these two extremes. Because of higher accumulated temperatures in GCM scenarios **R** falls to between 2.5 and 3.0 in these cases.

The above results cannot be turned into a prediction of land-use change (Hossell 1992, Hulme et al. 1993b). They show a change in only one climatic parameter (accumulated temperatures), albeit one important for plant and crop growth. Attendant changes in frost occurrence are discussed in section 18.7.

The change in accumulated temperatures can be measured by comparing climate potential categories (**L**). Table 18.4 shows the percentage of pixels that increased, decreased or stayed the same (in terms of **L**) for each scenario (compared with the control scenario). For the two GCMs and the +2°C and +4°C arbitrary scenarios all pixels increased, most by more than one category. Many increased by three or more categories, equivalent to at least a 600 d°C increase in T_{acc}. The mean increase is calculated by comparing the mean T_{acc} for the scenario with that for the control (1175.8 d°C). Increases of 1000 d°C are normal for the +4°C scenario and the two GCM simulations.

Table 18.4: Changes in **L** -the climate potential category, in each scenario. % up represents the percentage of pixels for which **L** increased.

Scenario	% up	% down	% same	% up1	% up2	% up3+
SE	71.4	-	28.6	70.2	1.2	-
W	20.9	8.1	71.0	20.9	-	-
1986	-	57.1	42.9	-	-	-
1989	69.2	-	30.8	69.2	-	-
+1°C	96.1	-	3.9	74.1	22.0	-
+2°C	100.0	-	-	3.9	44.1	52.0
+4°C	100.0	-	-	-	-	100.0
GISS	100.0	-	-	-	0.3	99.7
UKHI	100.0	-	-	-	0.3	99.7

Changes represented by the UKHI and GISS scenarios appear unrealistically large but they illustrate the extreme sensitivity of the climatic resource in this marginal area to warming. Many other factors (edaphic, topographic, economic, political etc.) will reduce the efficiency of the conversion of this increase in "climate potential" to land-use change. Changes in farming methods and, more importantly, active attempts at conservation of upland ecosystems are both likely to delay the spread of agricultural cultivation. Additionally, much land will remain unsuitable for cultivation in other ways, especially in areas with highly acidic soils and/or steep slopes. Changes in precipitation are also important since waterlogging is a problem in many areas. It is unlikely that warming will increase this problem, unless rainfall undergoes a similar increase to temperature, because of increased evapotranspiration (Warrick & Barrow 1991). Wind exposure and lack of solar radiation are other climatic constraints which will also alter. Results on possible responses of such elements to CO_2-induced change are even more scarce than that on temperature (Houghton et al. 1990, 1992) but will be briefly discussed in Chapter 19.

18.7 The Frost Hazard

Frost risk is expected to decrease in warming scenarios, especially since minima are predicted to increase at a faster rate than maxima (Cao et al. 1992, Karl 1993). However, changes in frost risk are not always positively correlated with those in accumulated temperatures, as in the continental scenario of Chapter 14. In this case annual accumulated temperatures increased but frost risk also increased. Calculations of annual frost frequency (in days) and annual frost accumulation were carried out for the control, continental and maritime airflow, GCM and +1°C scenarios. Regression models for minimum temperatures (Chapter 8), upon which the scenarios are based, are less satisfactory than those for mean temperatures because a linear relationship of minima with altitude ignores the effects of temperature inversions (Pielke & Mehring 1977, Hennessy 1979) and topography (Manley 1943, Harding 1978). R^2 was lower and results (Table 18.5) are therefore to be treated with caution. F_{acc} represents the frost accumulation (accumulated temperature deficit below 0°C).

Table 18.5: Frost hazard based on 741 pixels.

Scenario	Mean F_{acc} d°C	Max F_{acc} d°C	Min F_{acc} d°C	Max/ Min	Freq (days)
Control	-141.2	-560.9	-52.2	10.75	64.5
SE	-295.1	-890.2	-125.1	7.12	93.1
W	-96.1	-505.4	-28.1	17.99	48.7
+1°C	-86.9	-411.9	-27.6	14.92	44.6
UKHI	-5.0	-58.4	-0.8	73.0	4.1
Max Freq	**Min Freq**	**Freq <30(%)**	**Freq 30-60**	**Freq 60-90**	**Freq >90**
162.5	31.2	-	54.0	31.9	14.2
170.1	52.2	-	2.4	49.9	47.6
157.3	19.2	21.6	51.6	20.4	6.5
135.4	18.6	24.0	55.2	17.6	3.2
35.7	0.8	99.7	0.3	-	-

The control situation is represented in Figures 18.3 (frost frequency F_o) and 18.4 (frost accumulation F_{acc}). As for accumulated temperatures, pixels were categorised according to their F_{acc} and F_o values (Table 18.6).

Table 18.6: Categorisation of annual frost frequency, $\mathbf{F_o}$, and accumulation, $\mathbf{F_{acc}}$.

Frequency Category	**F_o range (days)**	**Accumulation Category**	**F_{acc} range (d°C)**
1	0-14.9	1	<50
2	15.0-29.9	2	50-99
3	30.0-44.9	3	100-199
4	45.0-59.9	4	200-299
5	60.0-74.9	5	300-399
6	75.0-89.9	6	400-499
7	90.0-119.9	7	500-599
8	120.0-149.9	8	600-799
9	150.0-179.9	9	800-999

Much of the highest land in the Pennines and on the Cumbrian fells experiences more than 90 frosts per annum. The total rises above 150 in the worst areas. A frequency of 162.5 days is extrapolated for Great Dun Fell. Much of the lowlands show a mean frequency of less than 60 days (class 4 or below). Frost accumulations (F_{acc}) are shown in Figure 18.4. The -100 d°C isotherm lies at approximately 100 metres above sea-level and accumulations rise to -500 d°C on Great Dun Fell (category 7).

Maps of frost occurrence and accumulation for other scenarios are shown in Figures 18.5 and 18.6 respectively. Given a 1°C increase the mean annual number of frosts decreases by approximately 20 and the average frost accumulation falls to 62% of the original value. Frost occurrence and severity are extremely sensitive to small temperature changes, frost being essentially an extreme event (Parry 1976, Wigley 1985).

Figure 18.3. Annual Frost Occurrence for the Control Climate

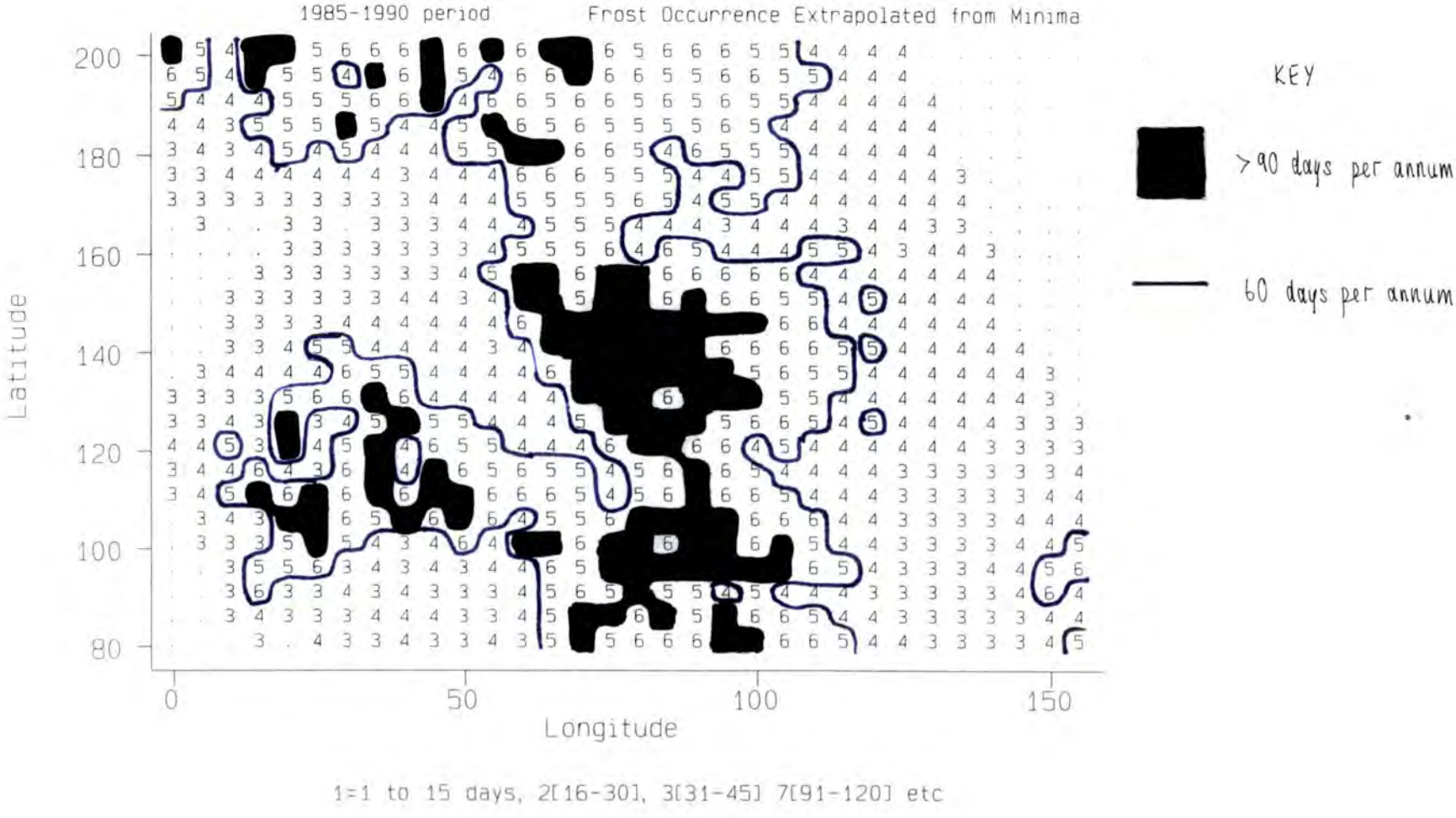

Figure 18.4. Annual Frost Accumulation for the Control Climate

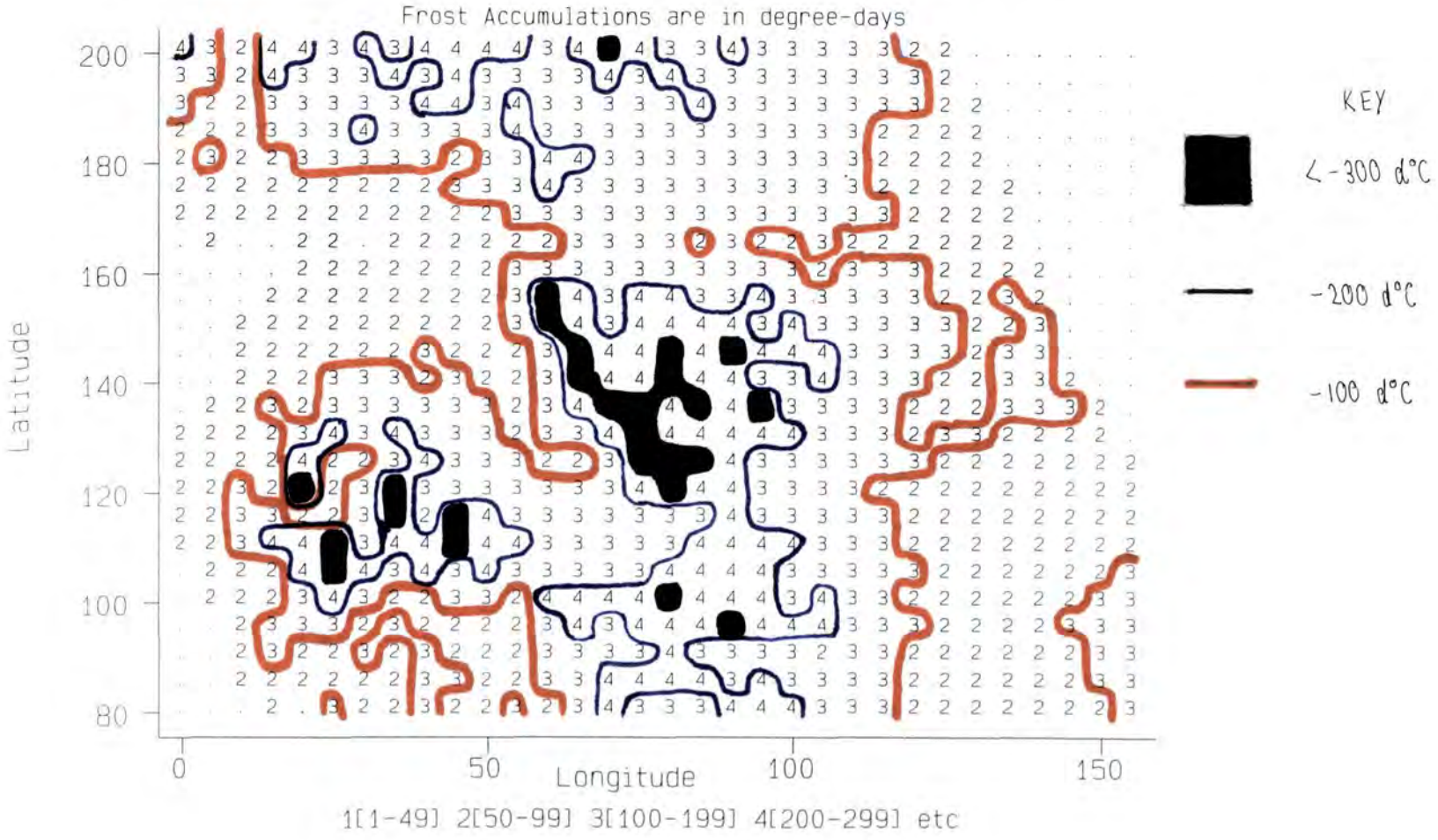

Figure 18.5. Annual Frost Occurrence in Northern England: Four Scenarios

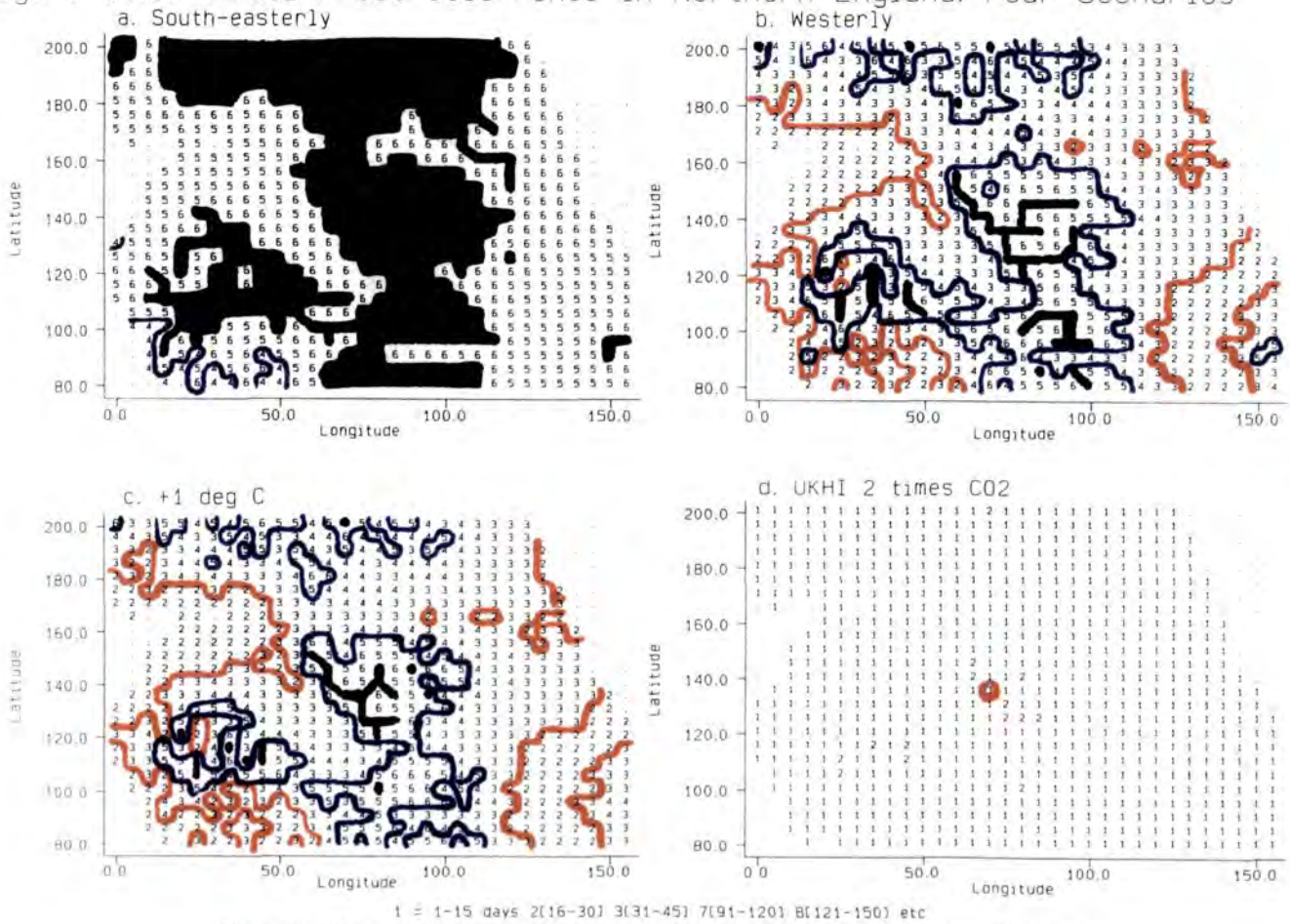

Figure 18.6. Annual Frost Accumulation in Northern England: Four Scenarios

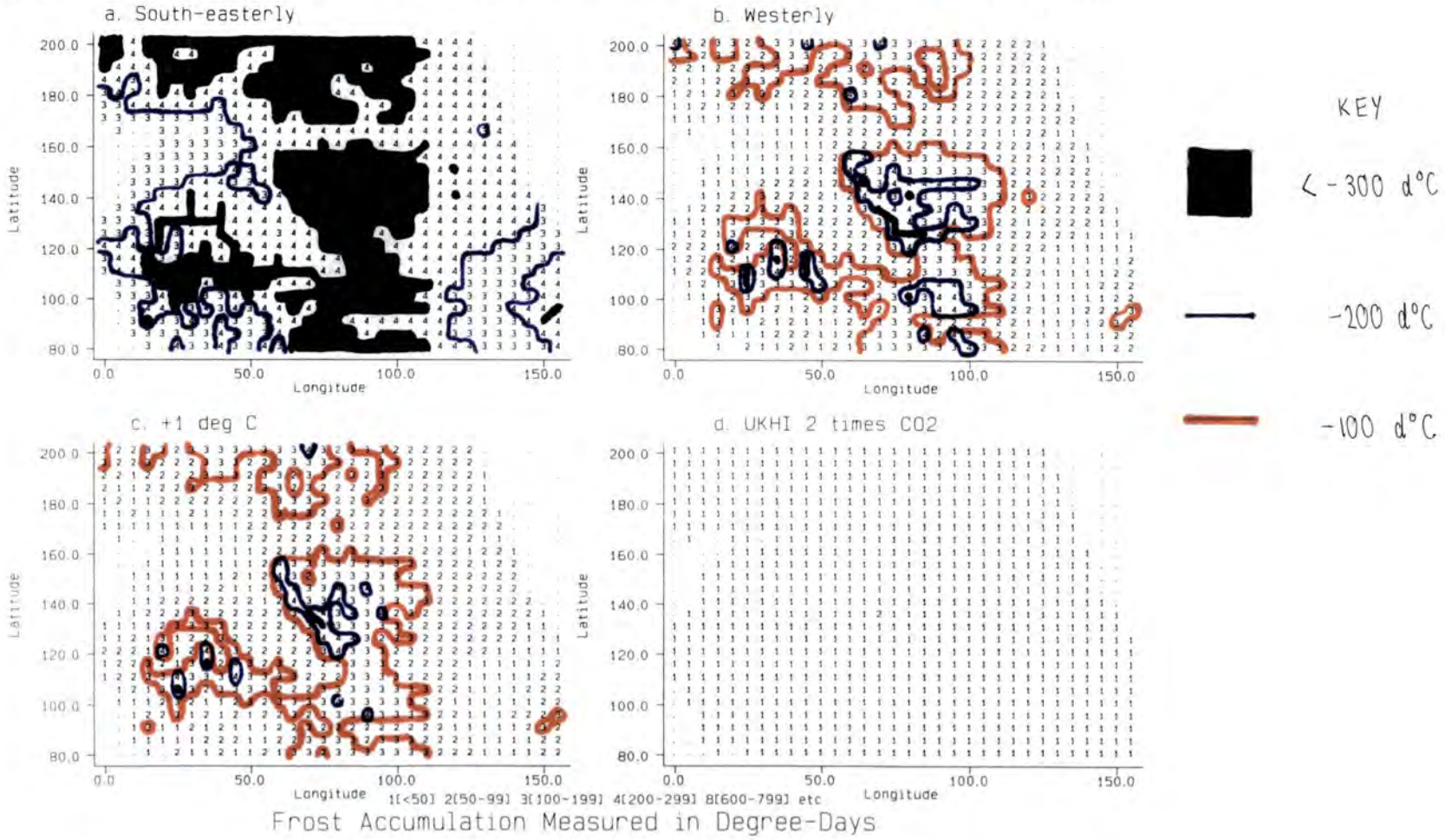

The continental (SE) and maritime (W) scenarios reveal startling differences. In the continental case the mean annual frost frequency increases to 93.1 days (equivalent to over three months). However, the increase in the highest value to 170.1 days is less than the increase in the lowest value, suggesting that the most rapid increase in frost occurrence would be in agriculturally productive lowland areas. The ratio between summit and sea-level frost accumulations falls to 7.12, despite an accumulation of -890.2 d°C on the highest summit. Only half of the land records an annual occurrence of less than 90 days. A continental scenario therefore increases frost risk and doubles the mean annual frost accumulation, despite simultaneously increasing accumulated temperatures in the growing season. Consequences for plant-life are unclear. In contrast, the maritime (W) scenario results in a mean annual frost accumulation of less than -100 d°C and a mean frequency of 48.7 days. Both figures are similar to the +1°C scenario. In terms of frost risk, the maritime scenario would be beneficial, especially in the lowlands.

R^2 is higher in the westerly equations (Figure 8.18) and thus the maritime scenario is more reliable. The south-easterly equations are poor because of the tendency for temperature inversions, especially when conditions are anticyclonic. In summer, R^2 falls very low and there is little confidence in frost predictions at this time. Fortunately, summer frosts do not contribute much to the annual total (on average only 2.4% of frosts occur between May and October), so poor summer predictions have little influence on annual results.

The UKHI 2 * CO_2 scenario is obtained by adding the following temperature corrections to mean minimum temperatures (Table 18.7). Corrections are the average of those over grid squares 49 and 63.

Predicted warming is greater in winter, especially between January and March. Because of this, the predicted minima are lowest in November and April for the UKHI 2 * CO_2 scenario. This is highly unrealistic as a "coreless" winter with mean minimum temperatures remaining fairly constant throughout five or six months is predicted. The only locations which experience such "coreless" winters are in polar latitudes where

there is a complete absence of insolation for part of the year.

Table 18.7: Corrections to mean minima (°C) in the UKHI 2 * CO_2 scenario.

Grid Square	JAN	FEB	MAR	APR	MAY	JUN
49	+8.36	+7.76	+6.31	+3.96	+4.18	+2.76
63	+6.60	+6.22	+5.60	+3.23	+4.29	+3.06
Mean	+7.48	+6.99	+5.96	+3.60	+4.24	+2.91
	JLY	AUG	SEP	OCT	NOV	DEC
49	+2.97	+3.05	+3.46	+2.87	+3.48	+4.64
63	+3.10	+3.39	+3.81	+3.39	+2.77	+4.15
Mean	+3.04	+3.22	+3.64	+3.13	+3.13	+4.40

The frost risk in the UKHI 2 * CO_2 scenario becomes negligible in lowland areas, totals rising to 35.7 days per annum on the highest summits (such as Great Dun Fell). Mean frost frequency is 4.1 days per annum and the mean accumulation is only -5 d°C! Due to such low figures, 99.7% of pixels record a frequency of less than 30 days and the ratio between the highest and lowest accumulation soars to 73. Frost becomes restricted to upland areas by 2050 and even in these areas there are sharp decreases. Freeze-thaw processes, which at present are a major geomorphological force in Britain, are likely to become less important as freezing temperatures become infrequent. Because warming is concentrated in mid-winter, the length of the frost-free period may remain relatively constant, meaning that sporadic spring and autumn frosts will still be a problem, perhaps even more so due to the largely frost-free winter.

18.8 The Comparison of Frost with Accumulated Temperatures

Monthly mean frost accumulation F_{acc} and growth accumulation T_{acc} for the control and UKHI scenarios are shown in Figure 18.7, allowing comparison of the two. From April to October T_{acc} is well above F_{acc} in both the control and the UKHI scenarios. In the UKHI scenario this is the case for the whole year. Monthly

Figure 18.7. Simulated Frost and Growth Accumulations for Control and UKHI 2 * CO2 Scenarios: Monthly Mean Values over the Grid

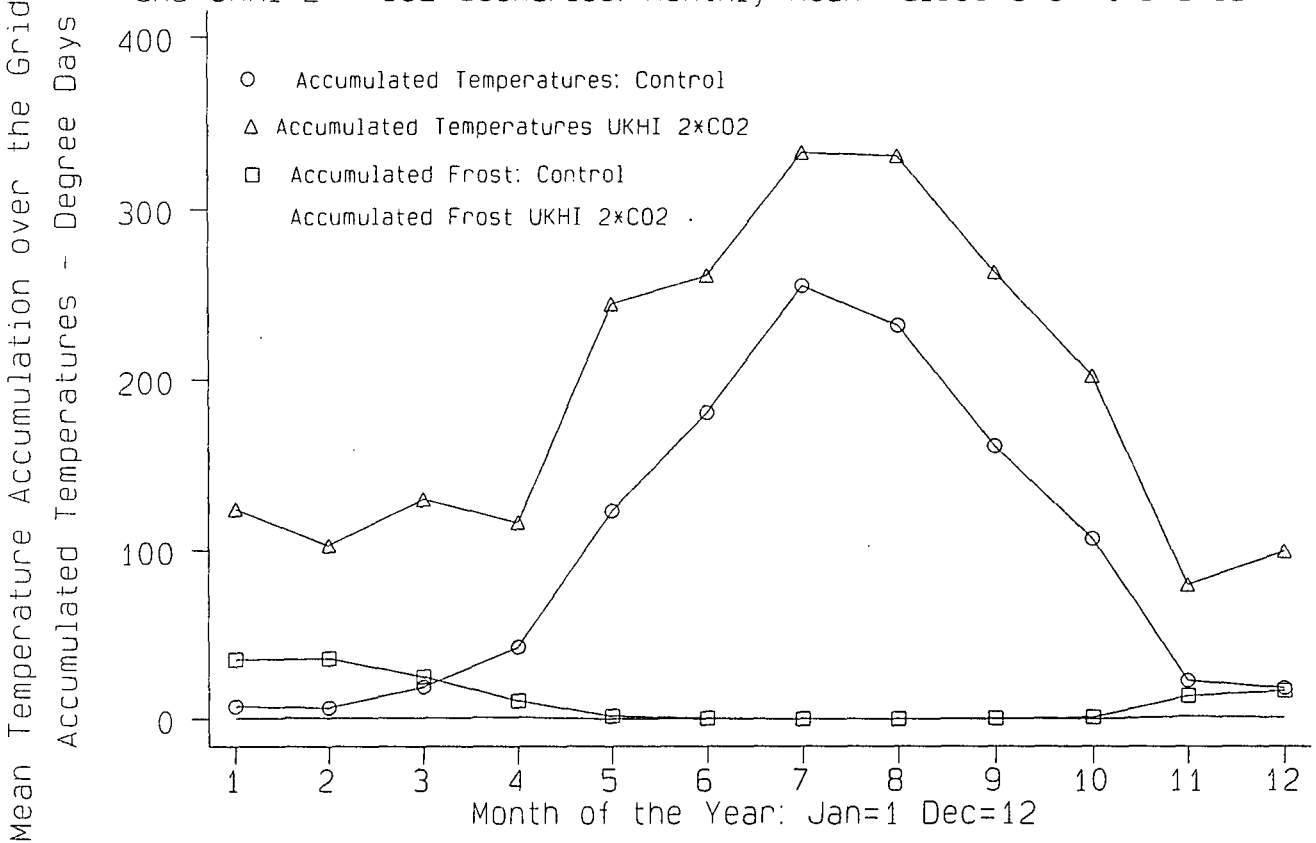

Mean Monthly Accumulated Temperatures and Frost for UHKI 2*CO2 and Control Scenarios

accumulated temperatures remain above 100 d°C, even in winter, remarkably high compared with the control situation, and frost accumulations are negligible. Under the control climate F_{acc} exceeds T_{acc} from January to March and is similar in November and December.

Figure 18.8 shows frost and growth accumulations for the five contrasting scenarios. Figures given are mean values over the digital terrain model. The control situation is again shown (on the top left hand graph) and UKHI on the bottom right. In the south-easterly scenario F_{acc} exceeds T_{acc} from December to April. There is a relatively short but warm summer with a sudden increase in T_{acc} in July and August. The late summer peak increases the annual growth accumulation. In contrast, the westerly scenario shows smoother seasonal transitions with moderate T_{acc} values in summer and values similar to F_{acc} throughout the winter. F_{acc} for the +1°C scenario is very similar to that under the westerly scenario although T_{acc} is much higher.

18.9 Conclusions

This chapter has applied the results of different climate scenarios to a study of change in "climate potential" in northern England. "Climate potential" is represented by accumulated temperatures above 6°C, frost occurrence and frost accumulation (below 0°C). Changes in all three parameters are considerable. If the scenarios are accurate, changes in land-use due to movement in altitudinal limits to cultivation upslope may result by 2050. This highlights the fragility of upland ecosystems, which would be "squeezed" onto less land.

One of the most detailed and successful climatic impact assessments was the **MINK** study carried out for the Great Plains States of **M**issouri, **I**owa, **N**ebraska and **K**ansas (Rosenberg 1993). Different studies concentrated on agriculture, forestry, water resources and the economy. The assumed spatial homogeneity in proposed climate change was largely valid because of the absence of any marked topography within the study area (this was the major reason for the choice of the area in the first place). In contrast, the effects of altitude and topography are shown to be considerable in this

Figure 18.8. Simulated Growth and Frost Accumulation for Five Scenarios: Monthly Mean Values over the Grid

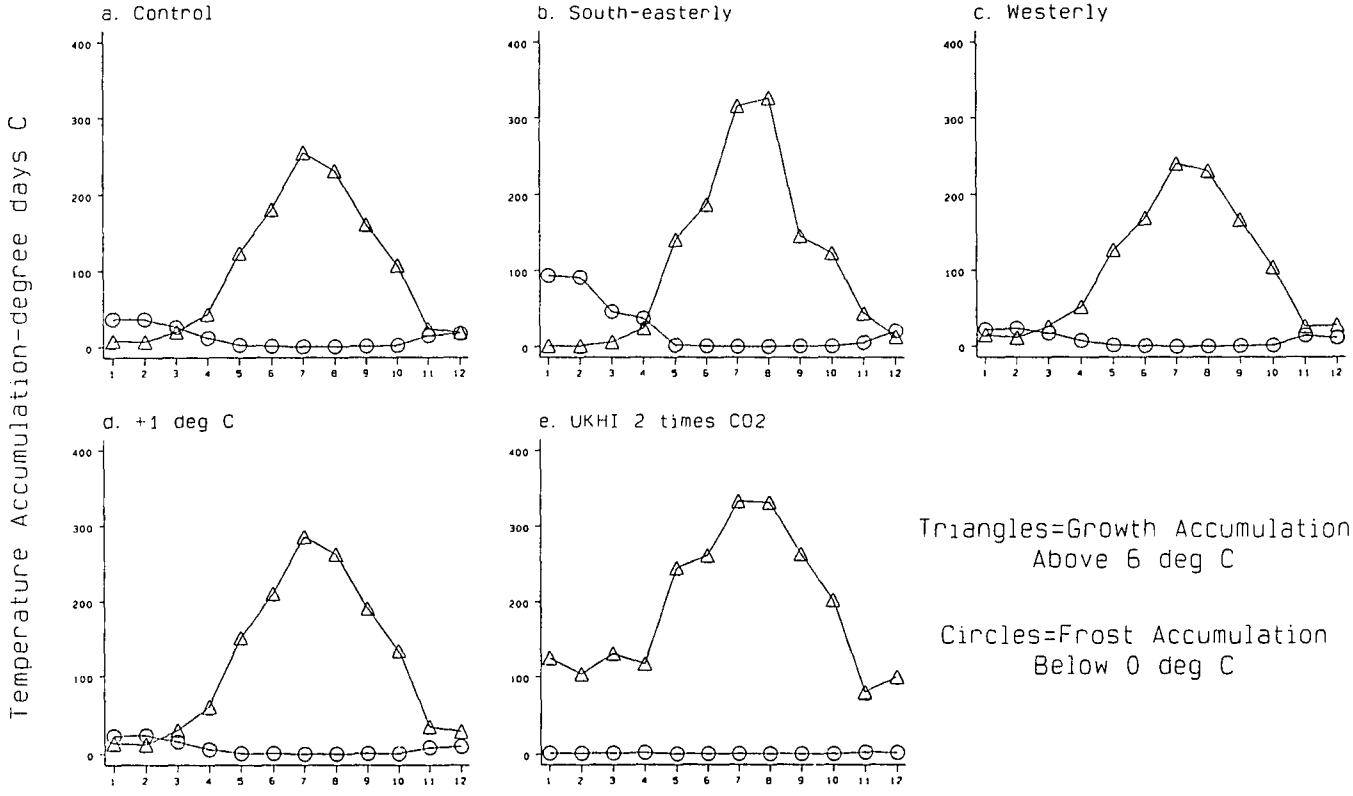

study and will alter in a changed climate, changing the spatial temperature distribution.

The effects of global warming on changes in free-air lapse rates and altitudinal temperature gradients calculated from ground-based stations (Schlesinger & Mitchell 1985) have not been considered here, except implicitly in the contrasts between airflow scenarios. A lapse rate change will alter the altitudinal gradient in growth potential and changes in the uplands may be more or less marked than in the lowlands. There is already tentative evidence that increased lapse rates associated with more progressive conditions (Lumb 1993) are limiting the benefits of recent warming in the Scottish mountains (McClatchey 1993). Lapse rates are now being calculated in GCMs, albeit tentatively, by comparing 850 mb temperatures with those at ground level in both control and 2 * CO_2 simulations. Data from the UHKI model could be considered in this way to investigate the possible lapse rate changes and their relationships with changing daily airflow patterns. At present the data required for such an investigation are unavailable due to practical restrictions concerning the GCMs themselves. Predicted changes in lapse rates within individual airflow types under conditions of increased carbon dioxide will, however, be an important area for future study as information becomes available. Such lapse rate changes will have profound effects on the altitudinal component of climate in the study area and so will be an important focus for future work.

PREDICTED CHANGES IN CLIMATE ELEMENTS OTHER THAN TEMPERATURE FOR THE UKHI MODEL AND EFFECTS ON THE PENNINE ENVIRONMENT

19.1 Introduction

The temperature regime is only one, albeit a very important, component of the climatic environment. GCMs are also concerned with predicting changes in other weather elements. Although this thesis is not primarily concerned with other climatic variables, GCM predictions for net radiation, cloudiness, wind direction components, humidity and precipitation are examined in this penultimate chapter, considering the probable effects of changes in such elements on the environmental changes predicted to occur in northern England as a result of temperature change. The environmental response to temperature change will be moderated by changes in other climatic (precipitation, insolation and windiness) and non-climatic (edaphic, topographical, social and economic) factors and so it is important to assess whether such changes are likely to complement the temperature effects or reduce them.

19.2 Predicted Changes in Weather Elements in the UKHI GCM

Mean monthly changes in weather parameters (other than air temperature) were calculated for grid squares 49 and 63 of the UKHI (United Kingdom High Resolution) General Circulation Model. Differences exist between change in each grid square, showing that predicted climate change is not spatially homogeneous. The expected changes in six elements are discussed below with special reference to whether such influences are likely to support or oppose the changes in "climate potential" predicted for the UKHI model.

Predicted changes in net surface radiation are shown in Figure 19.1 for each grid square and as a mean value. A change is calculated by subtracting the baseline (1 times CO_2) monthly mean from the 2 times CO_2 value. Increases in net radiation are expected, especially in summer in grid square 63 and in winter in grid square 49. It is not clear whether increases are due primarily to increased solar input, a decrease in

Figure 19.1. Predicted Monthly Changes in Net Surface Radiation for Grid Squares 49 and 63 between the 1 times CO2 and 2 times CO2 Simulations of the UKHI Model

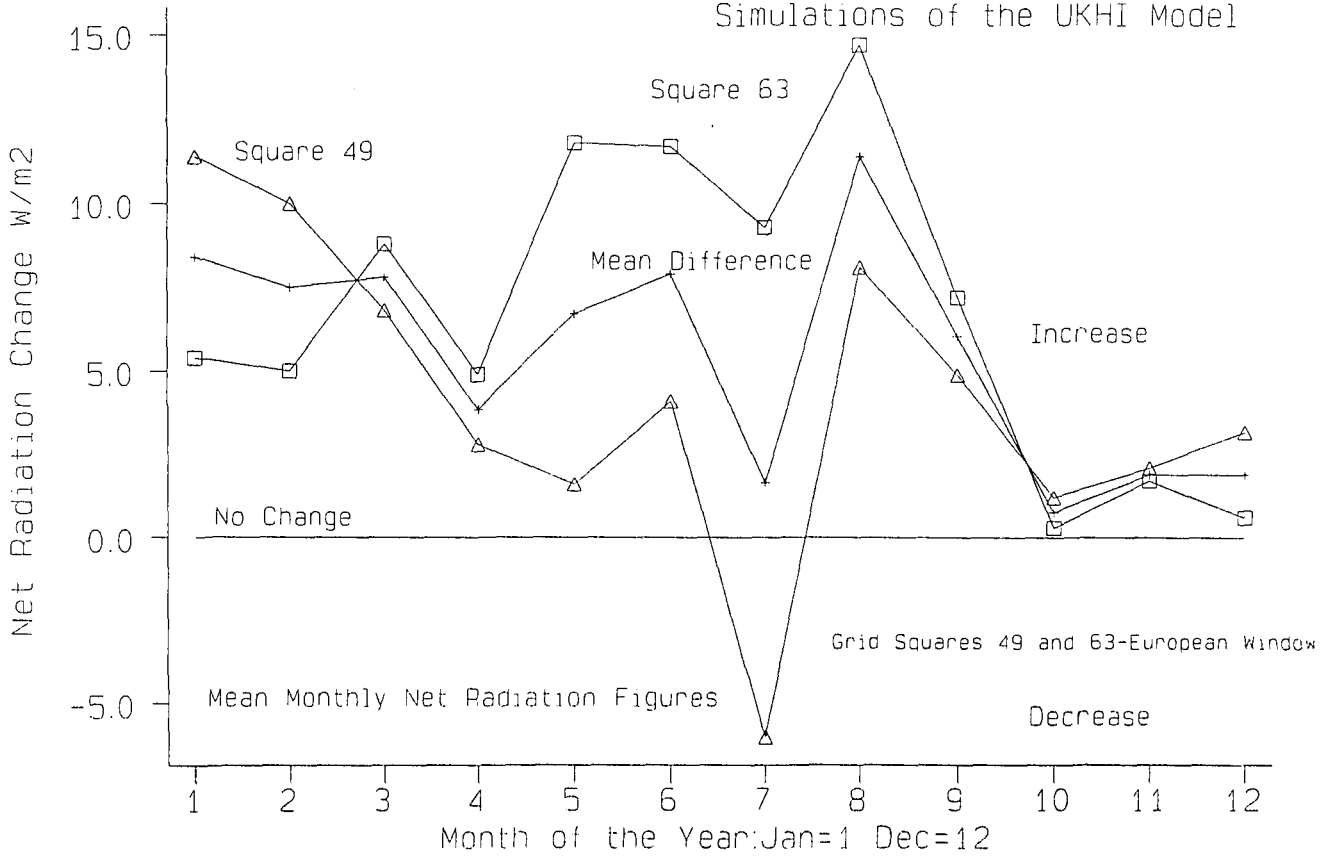

albedo or a decrease in longwave radiation loss. An increase in direct insolation would be most beneficial in agricultural terms. An increase in net radiation will increase air temperature (Chapter 7) but only an increase in solar radiation will provide more energy for photosynthesis. In July there is a decrease simulated for square 49 (the northern part of the region). This is the time when solar radiation input is most important in upland areas, temperatures being warm enough for plant growth. The increase in winter net radiation simulated is likely to be associated with increased advection of mild air and increased cloudiness (thereby reducing the mean longwave radiation loss). Square 49 shows an increase of over $+10$ W/m^2 in January. Smallest increases in net radiation occur between October and December in both grid squares.

As seen in Chapter 7, the relationship between net radiation and temperature change is complex, because of the variation in solar inefficiency, ψ. ψ generally increases with altitude. The increase of 10 W/m^2 simulated for January could be expected to lead to an additional warming of 0.66°C, assuming ψ to be 15.12 W/m^2°C (the mean value at Durham). This appears a sensible estimate. More direct solar radiation is required in upland areas, incessant cloudy conditions meaning that there is a large sunshine deficit. Unfortunately, increases in net radiation are predicted to be smallest in mid-summer when they would be most beneficial and it is largely increased winter cloudiness which accounts for the net radiation increases.

Changes in cloudiness (Figure 19.2) will be connected with changes in net radiation, extra cloud cover increasing net radiation in winter and at night and decreasing it by day in summer. The predicted change in cloudiness is similar in both grid squares with a rapid increase in winter, especially in January and February. More frequent and vigorous winter depressions would account for this. The increase in winter cloudiness would decrease frost risk and fit in with the increase in net radiation simulated at this time. In summer, changes are less distinct. In grid square 63 (the south of the region) summer cloudiness is expected to show a weak decrease, suggesting a shifting northward of depression tracks such that the climate would become very slightly more influenced by the high pressure belt to the south (the Azores high). Changes are, however, likely to be minimal. The summer north-south gradient in

Figure 19.2. Predicted Monthly Changes in Cloudiness for Grid Squares 49 and 63 between the 1 times CO2 and 2 times CO2 Simulations of the UKHI Model

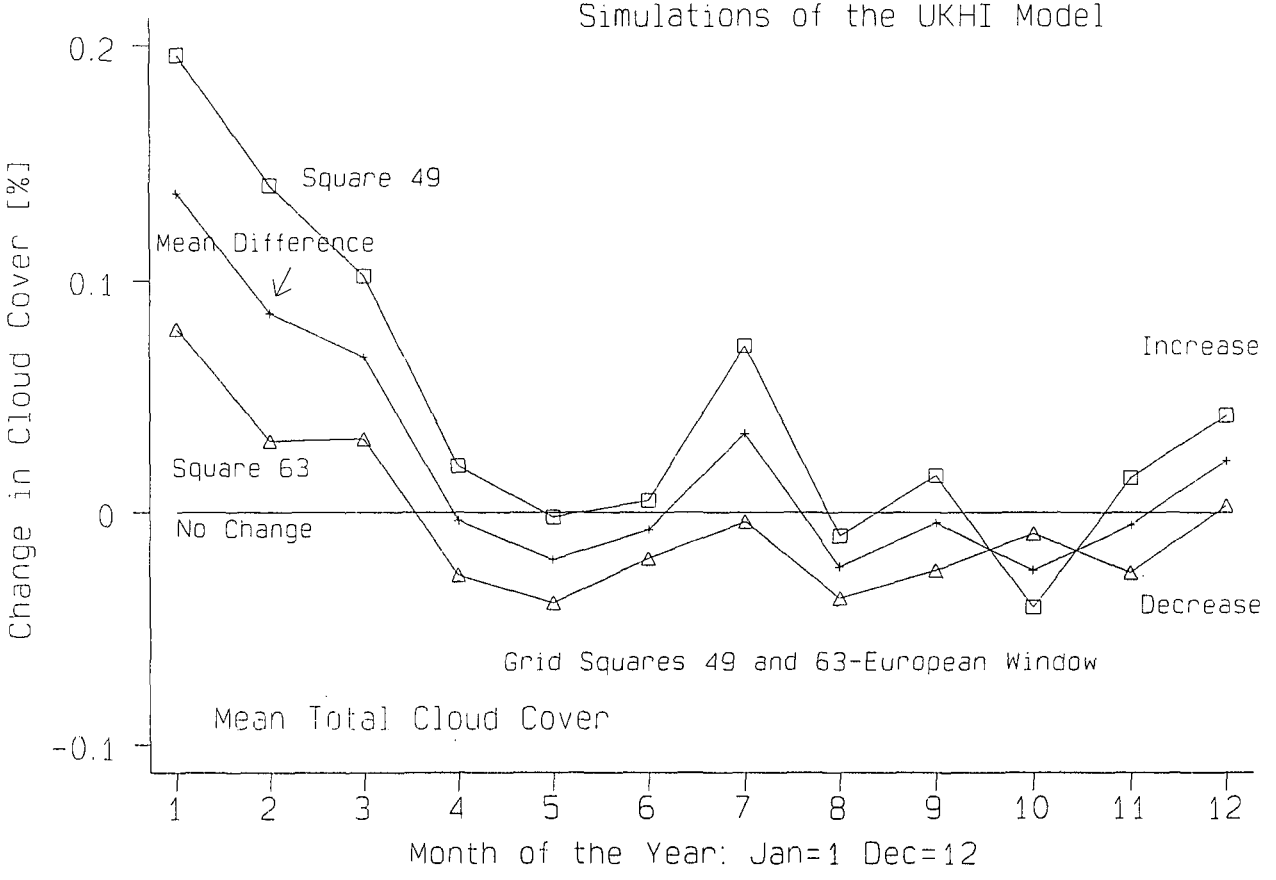

cloudiness would be enhanced over the region with southern areas experiencing more sunshine at a time when it is most required.

An examination of airflow components (Figures 19.3 and 19.4) is extremely useful since it indicates predicted trends in the circulation pattern. The mean x-wind component, representing the strength of zonal flow (i.e. westerliness), exhibits an increase throughout the year in square 63 except in August and September. The strong increase in zonal flow in winter supports the view that winter storminess over Britain will increase (Lumb 1993) with stronger and more frequent depressions. In summer the increase in zonal flow is weaker and blocking becomes more frequent in late summer in the south of the region.

Chapters 13 and 14 were concerned with analysing the effects of such airflow changes on the spatial distribution of temperature in northern England. The tendency toward blocking in late summer would favour greater warmth at the end of the growing season, especially in the uplands. This would be beneficial in cool areas where crops often do not ripen until late in the year (Manley 1952). Anticyclonic blocking would also be associated with a decrease in cloudiness and more insolation, especially in the uplands. Increased westerliness favours a smaller annual temperature range with milder winters, and steep lapse rates in most months. Changes in the y-wind component representative of southerliness (meridionality) are more irregular with decreases predicted for April and July-August, meaning that more northerly outbreaks are favoured at these times of year. The April singularity, whereby air flows south over Europe associated with an increasing meridional temperature gradient (Lamb 1950), is therefore likely to strengthen. In winter, southerliness is expected to increase, i.e. the advection of mild Atlantic air from the south (and west) is expected to be concentrated in winter. Increased southerliness will allow frost occurrence and accumulation to decrease. Frost would become a rarity in lowland areas (Chapter 17).

The increase in absolute humidity in the 2 * CO_2 simulation is uniform throughout the year, varying from 10 to 18 kg water/kg air (Figure 19.5). Higher air temperatures will encourage higher absolute humidities. Not surprisingly the increase

Figure 19.3. Predicted Monthly Changes in the X-Wind Component for Grid Squares 49 and 63 between the 1 times CO2 and 2 times CO2 Simulations of the UKHI Model

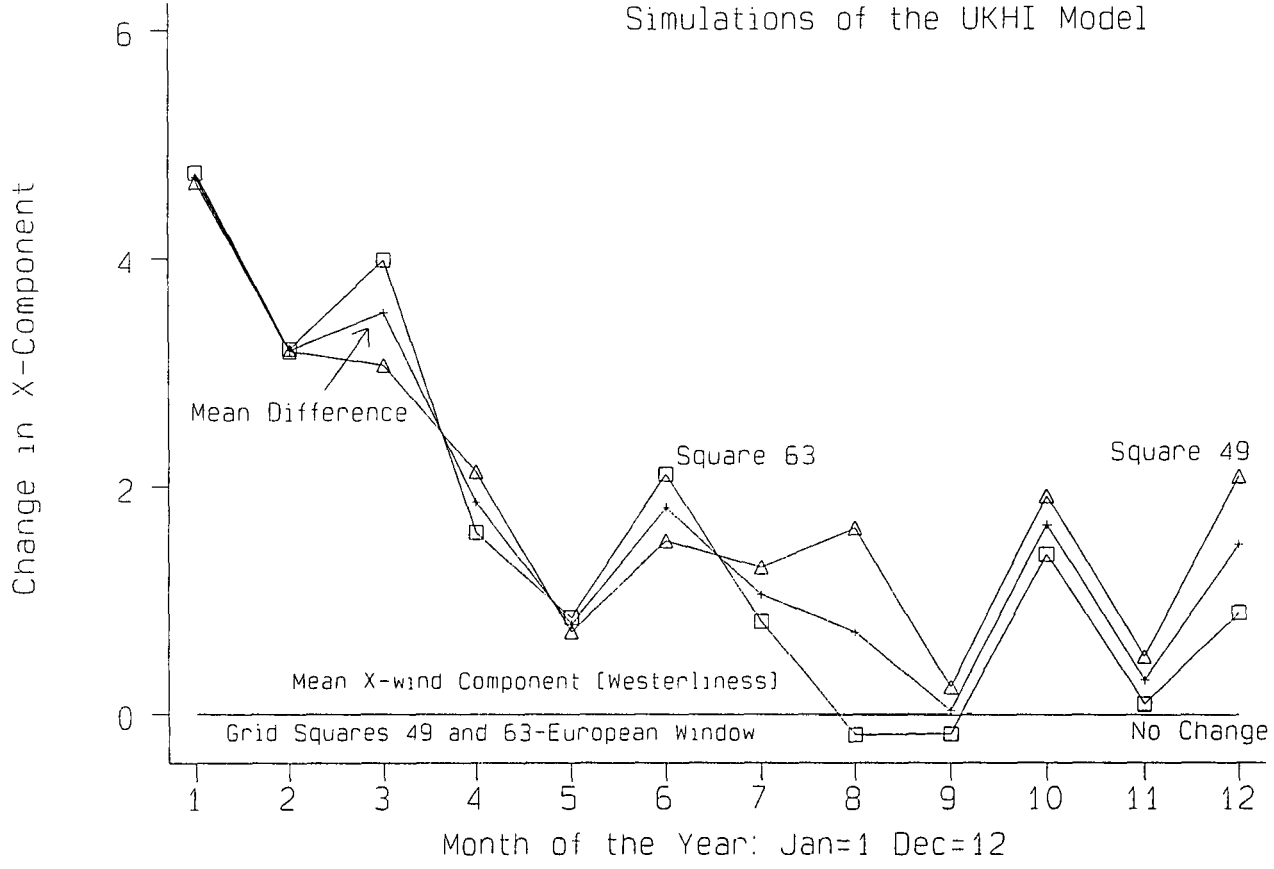

Figure 19.4. Predicted Monthly Changes in the Y-Wind Component for Grid Squares 49 and 63 between the 1 times CO2 and 2 times CO2 Simulations of the UKHI Model

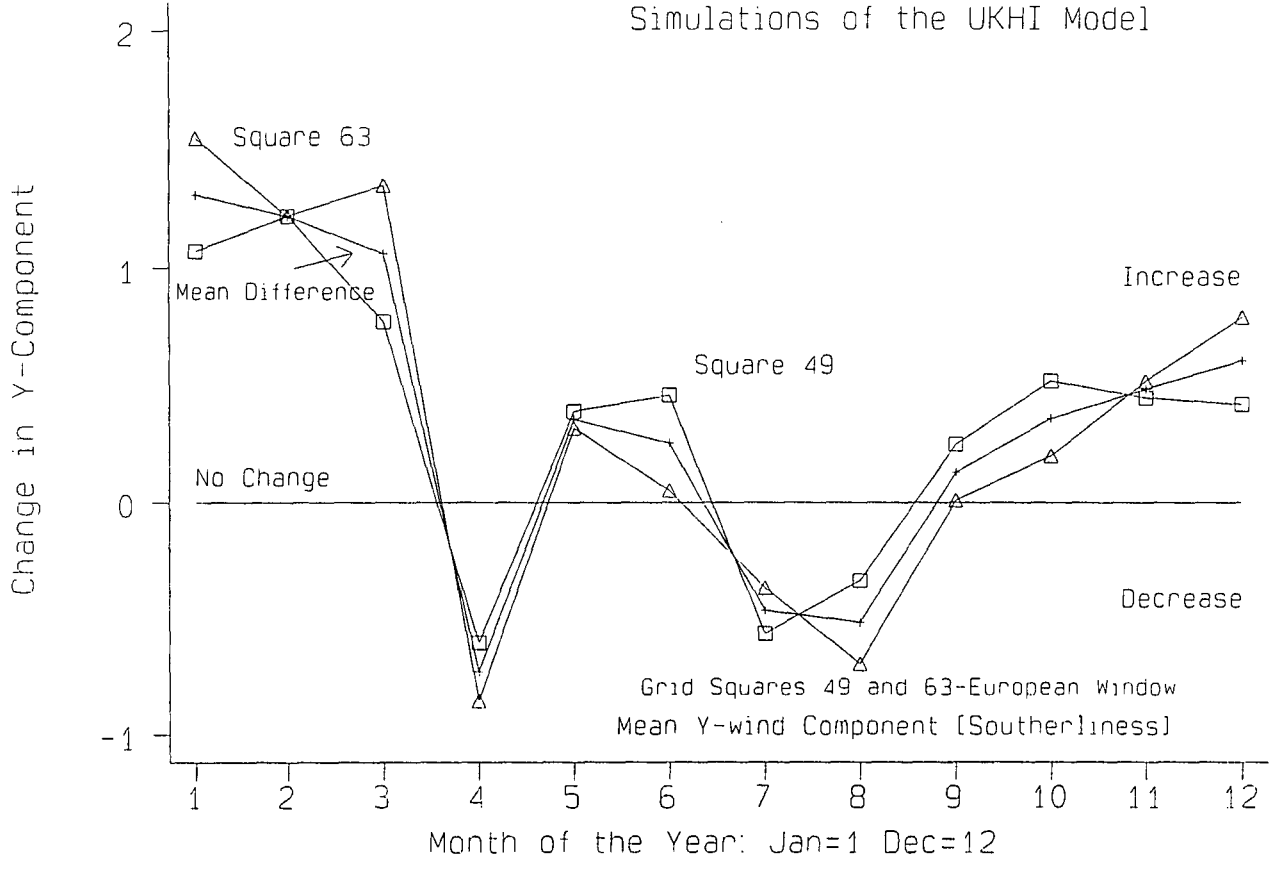

Figure 19.5. Predicted Monthly Changes in Absolute Humidity for Grid Squares 49 and 63 between the 1 times CO2 and 2 times CO2 Simulations of the UKHI Model

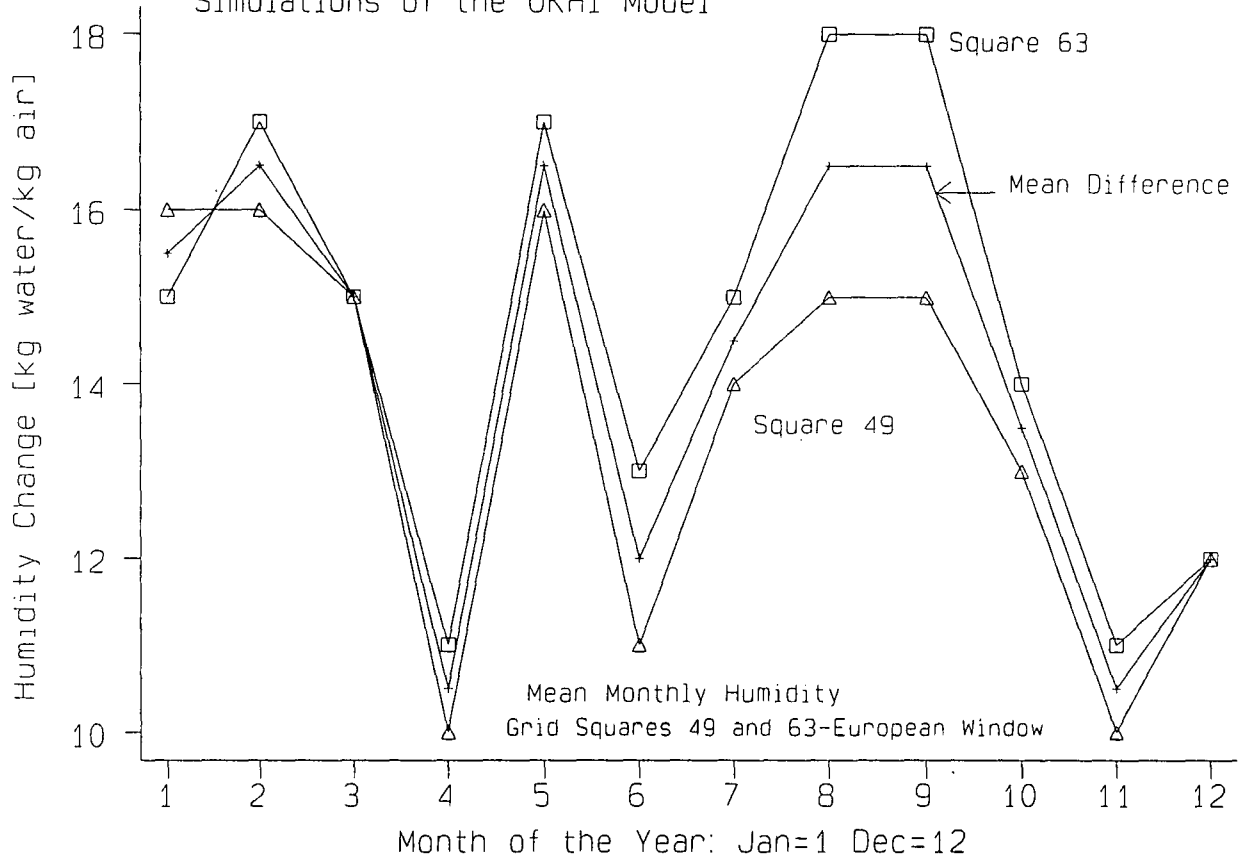

in both is predicted to be less in the north of the region (square 49). Higher humidities do not necessarily encourage increases in monthly precipitation. However, there does appear to be a parallel increase in precipitation, especially in the north of the region (square 49) in winter (Figure 19.6). The January increase of around 40 mm (1.5 inches) is substantial. Wetter winters suggest an association with increased cyclogenesis and a more mobile zonal circulation. Increase in summer rainfall is less distinct, especially between July and September when decreases appear possible. The enhanced role of convection may be outweighed by the tendency for anticyclogenesis building up from the Azores or southern Europe in summer, connected with a displacement of depression tracks to the north. An enhanced seasonal variation in rainfall with a winter maximum (as seen presently in the Mediterranean) is therefore supported.

It is reassuring that the model predictions for individual weather elements fit in well with one another, suggesting a more mobile zonal winter circulation with more frequent (and stronger) depressions crossing over, or to the north of, the region. Thus precipitation will increase, especially in upland areas. Airflow will have stronger westerly and southerly components and wind speeds are likely to increase, along with cloudiness and net radiation. Under this more unsettled winter regime, frost risk will decrease substantially, and although winter temperature will be higher at all altitudes, it is lowland areas which will reap the greatest benefit from these changes.

In summer, especially during August, increases in zonality are less distinct and an increase in anticyclonic blocking, building up from the south, will decrease rainfall and cloudiness and increase insolation. Such changes are predicted for square 63 only, and thus meridional gradients in late summer rainfall, insolation and cloudiness may increase. The increase of northerly outbreaks in April and July/August does not easily fit in with the other predictions. Any anticyclonic blocking in late summer will increase accumulated temperatures especially in the uplands, which will gain the greatest benefit from these summer changes.

Figure 19.6. Predicted Monthly Changes in Precipitation for Grid Squares 49 and 63 between the 1 times CO2 and 2 times CO2 Simulations of the UKHI Model

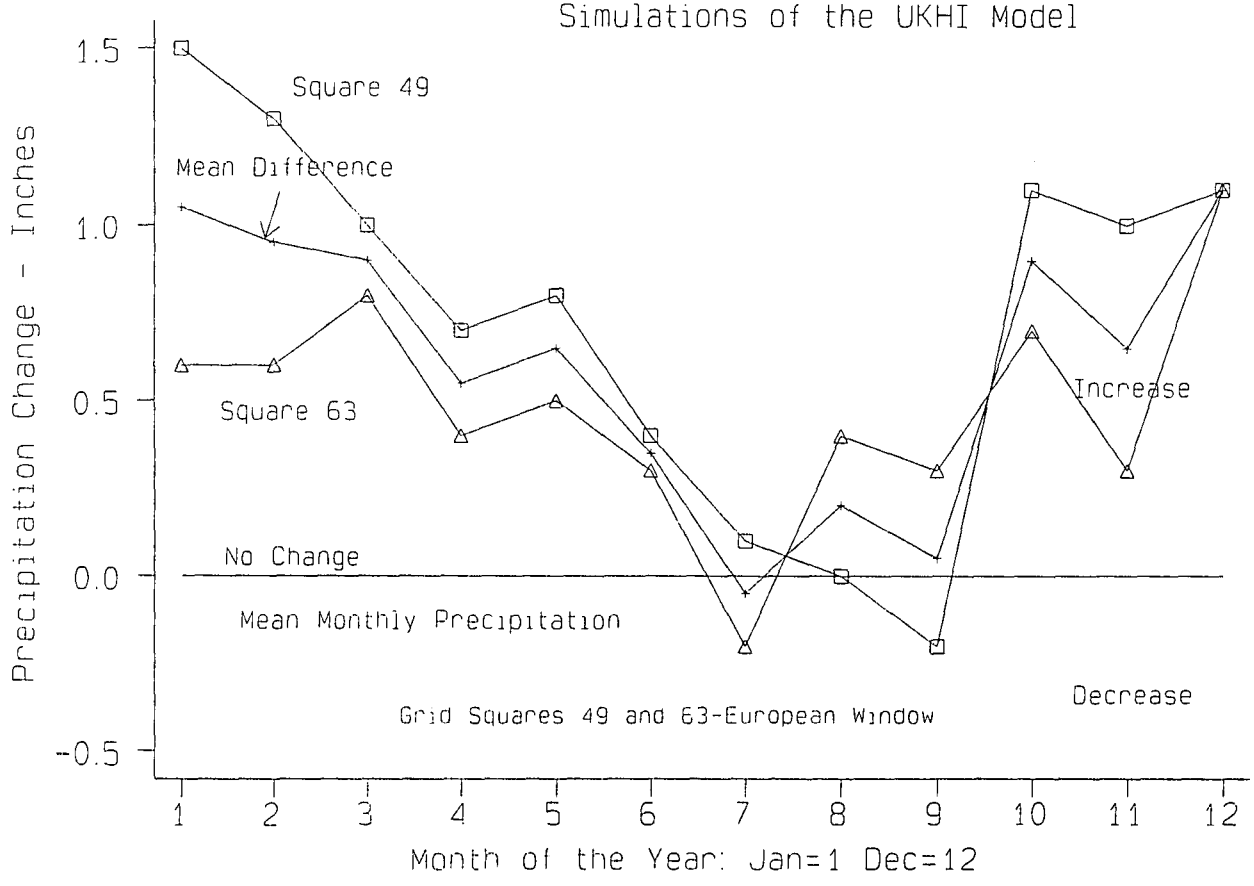

19.3 Summary of the Consequences of These Simulated Changes

All the simulated changes in weather elements for the summer season complement the effects of increased warmth predicted for the Pennine uplands. Relatively drier and warmer summers with increased insolation and reduced precipitation and cloudiness are predicted, especially in the south of the region and such conditions have a proportionally greater benefit in the uplands (Manley 1942). Lapse rates are likely to decrease under a blocked influence, as temperatures on the plateau approach more closely those at low levels (Tabony 1985). An increase in insolation is often cited as beneficial for further agricultural expansion in this maritime upland environment (Manley 1952) and the reduction in summer precipitation is unlikely to lead to water stress, except perhaps on well-drained south-facing slopes used for pasture (Bell, pers comm 1993). Increased winter precipitation will reduce summer water stress by raising up the surface water table, although in lowland areas irrigation may be required in exceptional years, as is normal in many parts of southern and eastern England at present (Penman 1948, Pearl et al. 1954). On the other hand, problems of waterlogging on plateaux during the growing season may be reduced.

Increases in westerly and southerly flow components are expected to be concentrated in winter. However, slight increases are predicted during some summer months. Westerly flows are associated with the steepest lapse rates (Chapter 8) and thus any increased zonality will cause the altitudinal gradient in temperature resources to increase (Chapters 13, 18). Under an increased zonal flow, areas sheltered from the west are likely to see the greatest benefit. For example, the north-eastern lowlands would experience a greater increase in climate potential than the lowlands of Cumbria. Because increases in westerliness are indistinct in summer, it is unclear whether the growing season in the uplands would suffer. Late summer may see a decrease in westerliness which would increase upland growing season strength. The other factor is that of wind speed. Increased windiness would make it difficult for development of widespread upland cultivation even if conditions were warmer and drier, because of exposure. Unfortunately, no details are given in the UKHI model of wind speed changes but since strongest winds usually come from the south and west, mean speeds

are expected to increase in winter and show little change in summer. Cloudiness is expected to show a modest decrease in summer which would be beneficial, increasing insolation.

No predictions are given for snow cover and changes in surface runoff. The occurrence of discrete events, such as freeze-thaw cycles and frost, is also difficult to predict under the 2 * CO_2 scenario (Chapters 14, 17). Often it is frequencies of extreme events which are more important than changes in mean values of precipitation, insolation, cloudiness and wind components. Nevertheless, this investigation into changes in weather elements other than temperature has shown that the benefits of temperature increases are likely to be complemented by decreased cloudiness, precipitation and windiness and increased insolation in late summer (July-September) in upland areas if more anticyclonic blocking were to occur as predicted. Opposite changes are predicted for winter when a stronger zonal circulation is predicted. The milder, wetter conditions will lead to a reduction of frost in lowland areas. Upland areas could remain bleak although this has little impact on cultivation in the growing season.

A strong distinction can be drawn between the effects of a mobile zonal westerly circulation (increases in precipitation, cloudiness, wind speed and decreases in insolation, especially in the uplands) and the opposite effects of a more blocked anticyclonic circulation. The contrast between the two is reinforced at high altitudes. Thus growing season accumulated temperatures T_{acc} are strongly correlated with other climate factors. A continental influence would benefit <u>all</u> relevant weather elements simultaneously, supporting predictions concerning changes in land suitability (using T_{acc}) in Chapter 18.

SUMMARY

Note: Numbers refer to the chapter in which the point is discussed

Introduction

1.1 The maritime environment of northern England, with steep lapse rates in the prevailing polar maritime air masses and a subdued seasonal temperature fluctuation, means that small changes in temperature can produce marked changes in the growing season. There is a rapid altitudinal decrease in "climatic potential" for cultivation, resulting in a low treeline and much marginal land. The lack of summer warmth prevents widespread agricultural cultivation (Parry 1976).

1.2 Numerous analyses of global temperature data illustrate a steady temperature increase of about 0.5°C between 1900 and 1990 (Manley 1974, Parker et al. 1992, Mintzer 1992). This warming trend is expected to continue due to anthropogenic emissions of greenhouse gases, such as carbon dioxide, which enhance the natural greenhouse effect. The context is complicated by the supposition that natural climate fluctuations are also related to solar output variations (Tavakol 1979) and that without anthropogenic influences there would be a cooling.

1.3 The thesis examines the altitudinal decrease in climatic potential in northern England, illustrating the sensitivity of relevant parameters to airflow variations and climate change. Due to 1.1 and 1.2, effects of climate changes may be pronounced.

Relevant literature on lapse rates is reviewed, factors behind the variation of air temperature are discussed, and data sources are described in Chapters 2-4.

Lapse Rate Analysis

5.1 The temporal and spatial variation of ground-based lapse rates is examined using data from 7 meteorological stations. The lapse rate is important since the altitudinal

temperature decline controls that in climatic potential. The rate between Durham (102 m) and Widdybank Fell (513 m) shows a strong seasonal fluctuation, peaking at the equinoxes. A solar hypothesis is outlined to account for this. There are also lapse rate variations according to airflow direction, the rate increasing under downslope (westerly) airflow.

6.1 Examination of lapse rates on several slopes of the Pennines shows that each rate has different relationships with season and airflow direction. Lapse rates tend to peak in spring, due to the instability of polar maritime air at this season, and are shallowest in winter, due to temperature inversion formation. Lee slope rates are steeper than windward ones due to föhn effects. Air mass affects ground-based lapse rate through stability contrasts, but air-mass type is difficult to separate from airflow direction since the two are strongly linked. Radiosonde data for the free-air are unavailable on a scale relevant to surface climate (in the lowest 1000 metres of the atmosphere) so it is not possible to compare free-air and ground-based lapse rates empirically in the region.

7.1 Net radiation estimates can be used to predict air temperature. A physical model relating surface temperature change with net radiation shows solar efficiency (net radiation/temperature change) to be extremely variable. Efficiency can be predicted from solar elevation, wind speed, wind direction and relative humidity, leaving 33% of its variation unexplained.

8.1 Mean lapse rates are calculated for each airflow in each month for daily maximum, mean and minimum temperatures using multiple regression involving twenty-two stations, against altitude, latitude and longitude. The statistical models are highly successful and robust, especially for maxima. Minima show a poorer relationship with altitude because of topographical influences. Altitude accounts for most of the temperature variation in the successful regressions.

9.1 The regression models are used to describe the spatial variation of temperature in northern England under varying conditions. Altitudinal zonation in the Pennines, based on the varying altitudes of critical isotherms of mean temperature, is described and

compared with the Pyrenees and Polish Tatra. Differences exist in the relative elevations of isotherms between the three mountain ranges. Summer isotherms are extremely low in northern England, explaining the low treeline and marginal nature of the uplands.

The Present Climate

10.1 "Climatic potential" is described by several parameters, all based on temperature: annual accumulated temperatures above 6°C (T_{acc}) (growing season strength); the length of the growing season (number of growing days per annum and the dates of the first and last growing days); frost occurrence/frequency and accumulation below 0°C (F_{acc}).

10.2 The variation in growing season strength (annual accumulated temperatures above 6°C) is described for 1985-1990 within the study region. A wide inter-annual fluctuation is shown. Mean growing season strength varies from around 415 d°C at Great Dun Fell (847 m) to 1577 d°C at Keswick (100 m), an anomalously warm site. The altitudinal gradient in T_{acc} can be modelled well by both linear and exponential relationships. Positive skewness in station altitudes means that it is difficult to decide whether the linear or exponential model is preferable. Both lead to similar results. A deductive approach suggests superiority of the exponential relationship. Taking 1000 d°C (degree-days) to be a critical accumulation for cultivation, land between 236 and 463 metres above sea-level is considered as marginal (about 30% of the land area of northern England), since accumulations exceed 1000 d°C in some years but not in others (using the linear model).

11.1 Growing season length shows a negative correlation with altitude. The total number of (consecutive) growing days is strongly correlated with altitude, although dates of the first and last growing days are more variable. Mean growing season length is 244 days at Eskmeals (8 m) but only 110 days at Great Dun Fell. The presence or absence of growing days (days with maxima of 6°C or above) is used to construct a growth probability curve relative to day of the year.

12.1 A similar process is undertaken for frost occurrence (minima of 0°C or below). The relationship of frost occurrence and probability with altitude is weak, minima being less dependent on altitude than maxima. The frost-free period averages 69 days on Great Dun Fell, but rises to 190 days at Sunderland, near the east coast.

12.2 A comparison of growing and frost-free seasons shows that frost during the growing season is more likely at low elevations. Coastal and mountain areas are least prone to damaging frosts during the growth period, having fewer "risk days".

13.1 "Uni-directional airflow scenarios" are created from the multiple regression equations to simulate the effects of a sustained airflow from one direction. Because different lapse rates are simulated for each airflow, the effects of a particular airflow are altitudinally selective. Airflows are assumed to retain their 1985-1990 characteristics. The sensitivity of T_{acc} to the circulation pattern (airflow type) is high in upland areas, there being a wide percentage variation in accumulated temperatures between airflow scenarios. A continental influence (south-easterly flow) increases T_{acc} at high altitude while a more maritime (westerly) influence has the opposite effect, steepening the altitudinal gradient in growing season strength.

14.1 The occurrence of growing days and that of frost are related to mean daily temperature using logit regression so that changes in growing season length and the frost-free period can be determined in each airflow scenario. Changes in these parameters do not mirror those in T_{acc}. For example, despite high accumulated temperatures in the south-easterly scenario, the frost-free period becomes short relative to the growth period and the risk of frost damage becomes great. Frost occurrence is lowest in the south-westerly and westerly scenarios, although growing season length at high altitude is relatively poor. Many parameters must be examined to gain an idea of the changes in climatic potential associated with each airflow type. Changes in the circulation pattern alone are shown to have far-reaching effects on many indices measuring climatic potential.

16/17.1 Introduction of the daily variability of temperature within airflows allows a

more accurate estimation of climatic potential. Once the mean and standard deviation of daily temperature are obtained, parameters such as the number of frosts or growing days can be simulated directly for that scenario, assuming that observations are normally distributed and independent.

The Past Climate

15.1 Past variation in climatic potential is analysed by examining annual variations in accumulated temperatures at Durham back to 1801. There is an inter-annual variation of over 500%, between 255 and 1384 d°C for annual accumulations (above 6°C). Spring, autumn and winter show more consistent warming trends over the 190 year record than summer. Extrapolation of 1000 d°C cultivation limits back to 1801, assuming the linear and exponential relationships between growing season strength and altitude described in 10.2, produces a wide inter-annual variation in elevations. About 90% of northern England falls between the extreme elevations recorded. Application of the above methodology to simulated temperature accumulations in the uni-directional wind scenarios shows cultivation limits to vary by over 400 metres between different airflows. Thus climatic potential is extremely sensitive to between-type climate change, small circulation changes causing large changes in the amount of marginal land.

The Future Climate

18.1 Contrasts between airflows in the altitudinal gradient of climatic potential will increase if airflows themselves experience within-type climate change. This is investigated by using General Circulation Model (GCM) output in which all airflows undergo warming.

18.2 The two GCMs examined are GISS (Goss Institute for Space Studies) (Hansen et al. 1984) and UKHI (United Kingdom Meteorological Office High Resolution Equilibrium Experiment) (Viner & Hulme 1992). Both simulate surface climate for a doubled carbon dioxide concentration (assumed to be representative of 2050). For comparison, effects of continental (south-easterly) and maritime (westerly) airflow

scenarios and arbitrary temperature increases are also analysed.

18.3 Annual temperature accumulations (T_{acc}), interpolated over a 5 * 5 km digital terrain model of northern England, are extremely high in the GCM doubled carbon dioxide scenarios. Sub-marginal (< 1000 d°C) and marginal (1000-1200 d°C) areas are largely eradicated, and there is enough warmth at the highest elevations for some cultivation (e.g. oats). Frost is unusual in lowland areas in both GCM simulations.

18.4 Such considerable changes in climate potential will not necessarily result in rapid land-use change due to the restrictions of other climatic (precipitation, windiness, lack of insolation) and non-climatic (soils, slopes, drainage, economic) factors. The extreme sensitivity in upland areas to changes induced by global warming illustrates the fragility of the present mountain environment. The contrast between continental and maritime airflow scenarios is small compared with changes predicted by the GCMs.

18.5 Changes in lapse rates and temperatures within individual airflows are being simulated in the latest GCMs. At present the required data are unavailable, but they will become so in the near future and the effects of such changes could be investigated in a sequel to this thesis.

19.1 Predicted change in other weather elements forecast in the UKHI model (precipitation, net radiation, cloudiness, airflow components and humidity) is described. The changes are likely to complement the effects of increased temperature. Decreased precipitation, cloudiness and a more blocked circulation, predicted for late summer, will be beneficial for upland cultivation. For winter a stronger zonal flow is suggested, leading to greater precipitation, cloudiness and higher net radiation, as well as increased warmth. Lowland areas would benefit most, with frost occurrence being substantially reduced.

Conclusions

The thesis methodology and the statistical methods employed (regression, Fourier

analysis, significance testing) have been applied to the analysis of variations in climatic potential based on temperature. Temperature data are widely available and it is fairly certain that temperatures will increase under greenhouse forcing. Moreover, temperature is the main limiting factor for agricultural expansion in much of the region under the present climatic regime. It would be equally possible, however, to apply the methodology to analyse any climate-based index or phenomenon, e.g. water deficit, winter snow pack, evaporation, freeze-thaw weathering, air pollution, wind resources and indices relevant to mountain ecology.

The use of synoptic climatology (examining the relationship between surface climate and circulation patterns) helps to explain past changes in the climatic environment and to convert GCM predictions concerning circulation change into local or regional climate changes. This is especially so in mountainous areas where the role of altitude is crucial, lapse rates of all weather elements varying according to airflow type. Response to particular circulation changes is altitudinally selective and altitude is the differentiating factor. In flat areas a similar methodology could be applied but the differentiating factors in response to airflows would be latitude, longitude or distance from the coast. Unless a strong relationship is found, results will be less satisfactory. The techniques employed in the thesis are equally applicable to other mountain and high altitude regions, although they are not restricted to such areas.

It is expected that the methodology would be less useful in the tropics where in many areas air-mass contrasts are subdued and variation in airflow patterns throughout the year is less influential. In low latitudes the diurnal cycle of weather dominates the climate, with local convective regimes being more important than the migration of synoptic scale pressure systems and changes in air-mass, at least in many areas. Changes in precipitation are predicted to be considerably more important (but less predictable) than those of temperature in the tropics (Houghton et al. 1990, Mitchell et al. 1990). Such changes will be primarily related to changes in local weather conditions on a sub-synoptic scale.

In contrast the methodology is likely to be useful in polar and sub-polar

latitudes, especially near the limits of extensive sea-ice. In such areas wind direction (and hence airflow type) is extremely important in affecting surface climate conditions through advective influences, especially in summer. For example, a strong dependence of mean temperatures on airflow direction is experienced at Churchill on the fringe of Hudson Bay, offshore winds bringing relatively high summer temperatures (Hare & Hay 1974). Most polar areas, with the exceptions of Greenland and Antarctica, are at low altitude and so distance from the coast or sea-ice boundary is the usual differentiating factor. It is easiest to assume that relationships between the spatial distribution of weather elements and airflow type remain constant in a future climate, but this is not necessary since within-type climate change can be incorporated into the study.

In conclusion, the use of synoptic climatology is most useful:

a) in mountainous areas;

b) where air-mass contrasts are great and the influence of the pressure pattern is important;

c) where advective effects are strong, i.e. at a sea-ice boundary or on a coastline.

In such areas future climatic changes due to changes in the general circulation pattern are likely to be strong, as illustrated by the strong inter-diurnal variability of climate elements in such areas at present.

An area which would be interesting to investigate is the Rocky Mountain area of the United States. This temperate mountain range is well-endowed with meteorological stations and is sited in a continental climatic regime, providing a contrast with Northern England. The contrasts between polar, tropical and maritime air-masses from the Pacific are well documented (Barry 1973, Court 1974) and are expected to result in a wide variation of lapse rates. Subjects of interest include the response of the mountain snow pack (its accumulation, depth, spatial and temporal variation) to circulation changes, the potential for agricultural development on the lower slopes of the Colorado Front Range under conditions of global warming, the viability of solar and wind energy as natural resources in such a semi-arid high altitude

environment, and the effects of global warming upon the diversity of mountain species (Grabherr et al. 1994) and migration of existing species into high altitude areas (Beerling & Woodward 1994). Relevant indices to be analysed include accumulated temperatures, effective precipitation, cloudiness, water deficit, solar radiation receipt, snow accumulation, frost frequency and freeze-thaw cycles, runoff and wind chill.

The methodology has importance in its own right and could be applied to any area other than northern England, any time period or for any application, within the limits discussed above.

BIBLIOGRAPHY

Aceituno, P. (1979). Statistical Formulae to Estimate Cooling or Heating Degree Days, Agric.Met. 20, 227-232.

Aguado, E. (1985). Snowmelt Energy Budgets in Southern and East-Central Wisconsin, Annals Assoc.Amer.Geog. 75, 203-211.

Ahrens, C.D. (1991). Meteorology Today: An Introduction to Weather, Climate and the Environment, West Publishing Company, St.Paul, 576 pp.

Alonso, W. (1968). Predicting Best With Imperfect Data, Jnl Amer. Inst. Planners 34, 248-255.

Ångstrom, A. (1924). Solar and Terrestrial Radiation, Quart.Jnl Roy.Met.Soc. 50, 121-126.

Assel, R.A. (1980). Maximum Freezing Degree Days as a Winter Severity Index for the Great Lakes, 1897-1977, Mon.Weather Rev. 108, 1440-1445.

Austin, J.M. (1957). Low-Level Inversions, Final Report, M.I.T. DA. 19-129 QM, 377 pp.

Axelrod, D.I. (1966). A Method of Determining the Altitudes of Tertiary Floras, Paleobotanist 14, 144-171.

Bagnall, D. (1982). The Effect of Temperature and Radiation on Crop Growth in Australia, Proceedings Seminar on Farmers and the Weatherman, Sydney, Australian Institute of Agricultural Science, 47-59.

Ballantyne, C.K. (1983). Precipitation Gradients in Wester Ross, North-West Scotland, Weather 38, 379-387.

Bärring, L. & Mattsson, J.O. (1992). Influence of Anomalous Years on Filtered Time Series of the Annual Temperature from Uppsala, Sweden, Geogr.Ann. 74 A(2-3), 275-282.

Barry, R.G. (1967). The Prospect for Synoptic Climatology: A Case Study, in Steel, R.W. & Lawton, R. eds, Liverpool Essays in Geography, Longmans, London, pp. 85-106.

Barry, R.G. (1973). A Climatological Transect on the East Slope of the Front Range, Colorado, Arctic & Alpine Res. 5, 89-110.

Barry, R.G. (1978). H.B. de Saussure: The First Mountain Meteorologist, Bull.Amer.Met.Soc. 59, 702-705.

Barry, R.G. (1990). Changes in Mountain Climate and Glacio-Hydrological Responses, Mountain Research and Development 10, 161-170.

Barry, R.G. (1992a). Mountain Climatology and Past and Potential Future Climate Changes in Mountain Regions: A Review, Mountain Research and Development 12, 71-86.

Barry, R.G. (1992b). Mountain Weather and Climate, 2nd edition, Routledge, London & New York, 402 pp.

Barton, J.S. (1987). Weather Observations on Cairn Gorm Summit 1979-1986, Met.Mag. 116, 346-353.

Beck, R.A. (1992). An Improved Format for Showing Temperature Time Series?, Weather 47, 346-349.

Bednarz, Z. (1984). The Comparison of Dendroclimatological Reconstructions of Summer Temperatures from the Alps and Tatra Mountains from 1741-1965, Dendrochronologia 2, 63-72.

Beerling, D.J. (1993). The Impact of Temperature on the Northern Distribution Limits of the Introduced Species Fallopia japonica and Impatiens glandulifera in North-West Europe, Jnl Biogeography 20, 45-53.

Beerling, D.J. & Woodward, F.I. (1994). Climate Change and the British Scene, Jnl Ecology 82, 391-397.

Belasco, J.E. (1952). Characteristics of the Air Masses over the British Isles, Geophysical Memoir 11 (No.87), Meteorological Office, 34 pp.

Bellamy, D. & Quayle, B. (1989). England's Last Wilderness: A Journey through the North Pennines, Penguin Books Ltd, Middlesex, 192 pp.

Belsley, D.A., Kuh, E. & Welsch, R.E. (1980). Regression Diagnostics, John Wiley & Sons, New York, 292 pp.

Beran, D.W. (1967). Large Amplitude Lee Waves and Chinook Winds, Jnl Appl.Met. 6, 865-877.

Bergström, H. (1990). The Early Climatological Records of Uppsala, Geogr.Ann. 72 A(2), 143-149.

Berliand, T.A. (1970). Solar Radiation and Radiation Balance Data, Hydrometeorology Publishing House, Leningrad.

Bilham, E.G. (1938). The Climate of the British Isles, Macmillan and Co. Limited, London, 347 pp.

Birse, E.L. (1971). Assessment of Climatic Conditions in Scotland: 3. The Bioclimatic Sub-Regions, Map and Explanatory Pamphlet, The Macaulay Institute for Soil Research, Aberdeen.

Blumenstock, D.I. & Price, S. (1967). The Climate of Hawaii, in Climates of the States Vol 2, Water Information Center, Port Washington, pp. 614-639.

Bollen, K.A. & Jackman, R.W. (1990). Regression Diagnostics: An Expository Treatment of Outliers and Influential Cases, in Fox, J. & Long, J.S. eds, Modern Methods of Data Analysis, Sage Publications, Newbury Park, pp. 257-291.

Bootsma, A. (1976). Estimating Minimum Temperature and Climatological Freeze Risk in Hilly Terrain, Agric.Met. 16, 425-443.

Borisov, A.M., Grudzinski, M.E. & Khrgian, A.Kh. (1958). O Meteorologicheskikh Usloviakh Vysokogornogo Tian-Shanya (Meteorological Conditions of the High Tien-Shan), Trudy Tsentr. Aerol.Obs. 21, 175-199.

Botkin, D.B. & Nisbet, R.A. (1992). Forest Response to Climatic Change: Effects of Parameter Estimation and Choice of Weather Patterns on the Reliability of Projections, Climatic Change 20 (2), 87-111.

Brazel, A.J. & Marcus, G.M. (1991). July Temperatures in Kashmir and Ladakh, India: Comparisons of Observations and General Circulation Model Simulations, Mountain Research and Development 11, 75-86.

Briffa, K., Jones, P.D. & Kelly, P.M. (1990). Principal Component Analysis of the Lamb Catalogue of Daily Weather Types: Part 2, Seasonal Frequencies and Update to 1987, Int.Jnl Clim. 10, 549-563.

Brittain, O.W. (1978). Forecasting Sea-Breezes at Eskmeals, Met. Mag. 107, 88-96.

Bücher, A. & Dessens, J. (1991). Secular Trend of Surface Temperature at an Elevated Observatory in the Pyrenees, Jnl Climate 4, 859-868.

Budyko, M.I. (1974). Climate and Life, Academic Press, New York, pp. 189-192.

Burbidge, F.E. (1951). The Modification of Continental Polar Air over Hudson Bay, Quart.Jnl Roy.Met.Soc. 77, 365-374.

Burroughs, W.J. (1980). Quasi-Cycles in Meteorology, Weather 35, 156-161.

Calder, I.R. (1990). Evaporation in the Uplands, Wiley, Chichester, 148 pp.

Cao, H.X., Mitchell, J.F.B. & Lavery, J.R. (1992). Simulated Diurnal Range and Variability of Surface Temperature in a Global Climate Model for Present and Doubled CO_2 Climates, Jnl Climate 5, 920-943.

Carter, T.R., Parry, M.L. & Porter, J.H. (1991a). Climatic Change and Future Agroclimatic Crop Potential in Europe, Int.Jnl Clim. 11, 251-269.

Carter, T.R., Porter, J.H. & Parry, M.L. (1991b). Climatic Warming and Crop Potential in Europe: Prospects and Uncertainties, Global Env.Change 1, 291-292.

Catchpole, A.J.W. (1966). Climatic Studies in North-East England, PhD Thesis, University of Durham, unpublished.

Caton, P.G.F. (1957). Occurrence of Low Layer-Type Cloud Over Eastern England in Relation to Synoptic Situation, Met.Mag. 86, 161-169.

Cayan, D.R. (1980). Large Scale Relationships Between Sea Surface Temperature and Surface Air Temperature, Mon.Weather Rev. 108, 1293-1301.

Cengiz, H.S., Gregory, J.M. & Sebaugh, J.L. (1981). Solar Radiation Prediction from other Climatic Variables, Trans.Amer. Soc.Agric.Engineers 24, 1269-1272.

Chandler, T.J. (1965). The Climate of London, Hutchinson, London, 292 pp.

Chatfield, C. (1975). The Analysis of Time Series: Theory and Practice, Chapman and Hall, London, 263 pp.

Chen, L., Ritter, E.R. & Feng, Z. (1985). The Atmospheric Heat Source Over the Tibetan Plateau, May-August 1979, Mon.Weather Rev. 113, 1771-1790.

Chia, E. (1991). Stochastic Simulation of Daily Weather Sequences at a Single Site: An Appraisal of the State of the Art, Singapore Jnl Tropical Geography, 12(1), 31-43.

Chickering, J.W.Jr. (1884). Thermal Belts, Amer.Met.Jnl 1, 213-218.

Cleveland, W. (1979). Robust Locally Weighted Regression and Smoothing Scatterplots, Jnl Amer.Stat.Assoc. 74, 829-836.

Computing Resource Center. (1992). Stata Reference Manual: Release 3, 5th edition, Santa Monica, California, 1165 pp.

Comrie, A. (1992). A Procedure for Removing the Synoptic Climate Signal from Environmental Data, Int.Jnl Clim. 12, 177-183.

Conrad, V. & Pollak, L.W. (1950). Methods in Climatology, 2nd edition, Harvard University Press, Cambridge, Massachussetts, 459 pp.

Cook, R.D. (1977). Detection of Influential Observations in Linear Regression, Technometrics 19, 15-18.

Court, A. (1974). The Climate of the Conterminous United States, in Bryson, R.A. & Hare, F.K. eds, Climates of North America, World Survey of Climatology Volume 11, Elsevier, Amsterdam, pp. 193-266.

Cowley, J.P. (1978). The Distribution over Great Britain of Global Solar Irradiation on a Horizontal Surface, Met.Mag. 107, 357-373.

Cox, N.J. (1993a). Climatic Averages 1961-1990: Maximum and Minimum Temperatures, in Goldie, H. ed., Durham University Observatory:Daily Meteorological Observations 1992, Department of Geography, University of Durham, pp. 34-41.

Cox, N.J. (1993b). Temperatures at Durham 1801-1990: A Preliminary Analysis Using Smoothing Splines, in press.

Craddock, J.M. (1951). The Warming of Arctic Air Masses Over the Eastern North Atlantic, Quart.Jnl Roy.Met.Soc. 77, 355-364.

Davies, J.A. (1967). A Note on the Relationship between Net Radiation and Solar Radiation, Quart.Jnl Roy.Met.Soc. 93, 109-115.

Davis, N.E. (1972). The Variability of the Onset of Spring in Britain, Quart.Jnl Roy.Met.Soc. 98, 763-777.

Del Barrio, G., Creus, J. & Puigdefabregas, J. (1990). Thermal Seasonality of the High Mountain Belts of the Pyrenees, Mountain Research and Development 10, 227-233.

de Quervain, A. (1904). Die Hebung der Atmosphärischen Isothermen in der Schweizer Alpen und ihre Beziehung zu deren Höhengrenzen, Gerlands Beitr.Geophys. 6, 481-533.

de Saussure, H.B. (1796). Voyages dans les Alpes, Précédes d'un Essai sur l'histoire Naturelle des Environs de Genève, vol. 4, chapters V-IX, L.Fauche Borel, Neuchatel.

Dewey, K. (1977). Daily Maximum and Minimum Temperature Forecasts and the Influence of Snow Cover, Mon.Weather Rev. 105, 1594-1597.

Dirmhirn, I. (1951). Untersuchungen Der Himmelstrahlung in den Ostalpen mit Besonder Berücksichtigung ihrer Höhenabhängigkeit, Arch.Met.Geophys.Biokl. B, 2, 301-346.

Doesken, N.J., Brown, T.J. & Barry, R.G. (1989). Differences in Recent Climate Trends between High Plains and the Colorado Rockies, in preparation.

Driscoll, M. & Yee Fong, J. (1992). Continentality: A Basic Climatic Parameter Re-Examined, Int.Jnl Clim. 12, 185-192.

Dunbar, G.S. (1966). Thermal Belts in North Carolina, Geog.Rev. 56, 516-526.

Duncan, K. (1991). A Comparison of the Temperature Records of Edinburgh and Central England, Weather 46, 169-173.

Eden, P. (1991). Gunby, Lincs.; Putting the Record Straight, Weather 46, 330-331.

Eide, O. (1948). On the Temperature Difference Between Mountain Peak and Free Atmosphere at the Same Level II, Gaustatoppen-Kjeller, Met.Ann. 2(3), 183-206.

Ekhart, E. (1948). De la Structure Thermique et de l'Atmosphère dans la Montagne, La Météorologie (Ser. 4), 9, 3-26. Translated in Whiteman, C.D. & Dreiseitl, E. eds, (1984). Alpine Meteorology, PNL-5141, ASCOT-84-3, Batelle, Pacific Northwest Laboratories, Richland, Washington, pp. 73-93.

Ekman, V.W. (1902). Om Jordrotationens Inverkan på Vindströmmer i Hafvet, Nyt. Mag.Naturv. 40, 1-22.

Evans, M. (1980). Housing, Climate and Comfort, Architectural Press, London.

Fahey, B.D. (1973). An Analysis of Diurnal Freeze-Thaw and Frost Heave Cycles in the Indian Peaks Region of the Colorado Front Range, Arctic & Alpine Res. 5 (3), 269-281.

Fitter, A.H. & Hay, R.K.M. (1981). Environmental Physiology of Plants, Academic Press, London, 355 pp.

Fliri, F. (1971). Neue Klimatologische Querprofile der Alpen - ein Energiehaushalt, Ann.Met., N.F. 5, 93-97.

Flohn, H. (1953). Hochgebirge und allgemeine Zirkulation. II. Die Gebirge als Wärmequellen, Arch.Met.Geophys.Biokl. A, 5, 265-279.

Fritschen, L.J. (1967). Net and Solar Radiation Relations over Irrigated Field Crops, Agric.Met. 4, 55-62.

Garcia-Ruiz, J.M., Creusnovau, J. & Puigdefabregas, J. (1985). Los Recursos Hidricos Superficiales del Alto Aragón, Instituto de Estudios Alto Aragoneses 2, 224 pp.

Giorgi, F. & Mearns, L. (1991). Approaches to the Simulation of Regional Climate Change: A Review, Rev. Geophysics 29, 191-216.

Glasspoole, J. (1954). New Climatological Averages For Great Britain, Met.Mag. 83, 44-48.

Goldie, H. (1992). ed., Durham University Observatory:Daily Meteorological Observations 1992, , Department of Geography, University of Durham, 42 pp.

Grabherr, G., Gottfried, M. & Pauli, H. (1994). Climate Effects on Mountain Plants, Nature 369, p. 448.

Green, F.H.W. & Harding, R.J. (1979). The Effect of Altitude on Soil Temperature, Met.Mag. 108, 81-91.

Green, F.H.W. & Harding, R.J. (1980). The Altitudinal Gradients of Air Temperature in Southern Norway, Geogr.Ann. 62 A(1-2), 29-36.

Gregory, S. (1965). Rainfall over Sierra Leone, Research Paper No. 2, Department of Geography, University of Liverpool, 58 pp.

Gregory, S. & Smith, K. (1967). Local Temperature and Humidity Contrasts Around Small Lakes and Reservoirs, Weather 22, 497-505.

Gruber, A. & Chen, T.S. (1988). Diurnal Variation of Outgoing Longwave Radiation, Jnl Clim. 8, 1-16.

Guoyu, R. (1991). A New Discovery in the Comparison of the Heat Resources of Temperate Areas between China and the United States, Bull.Amer.Met.Soc. 72, 239-241.

Hamilton, L.C. (1990). Statistics with Stata, Brooks/Cole Publishing Company, Pacific Grove, California, 171 pp.

Hamilton, L.C. (1992). Regression With Graphics: A Second Course in Applied Statistics, Brooks/Cole Publishing Company, Pacific Grove, California, 363 pp.

Hamilton, M.G. (1987). Very Warm Spells and Very Cold Spells at Edgbaston, Birmingham, During 1920-1979, Weather 42, 2-8.

Hann, J. (1906). Lehrbuch der Meteorologie, C.H.Tauchnitz, Leipzig.

Hann, J. von. (1913). Die Berge kälter als die Atmosphäre, Ein Meteorologisches Paradoxon, Met.Zeit. 30, 304-306.

Hanna, L.W. & Siam, N. (1981). The Empirical Relation Between Sunshine and Radiation and its Use in Estimating Evaporation in North-East England, Jnl Clim. 1, 11-19.

Hansen, J., Lacis, S., Rind, D., Russel, L., Stone, P., Fung, I., Ruedy, R. & Lerner, J. (1984). Climate Sensitivity Analysis of Feedback Mechanisms, in Hansen, J. & Takahashi, T. eds, Climate Processes and Climate Sensitivity, Geophys.Mono.Ser. 29, 130-163, AGU Washington.

Harding, R.J. (1978). The Variation of the Altitudinal Gradient of Temperature Within the British Isles, Geogr.Ann. 60 A(1-2), 43-49.

Harding, R.J. (1979a). Altitudinal Gradients of Temperature in the Northern Pennines, Weather 34, 190-202.

Harding, R.J. (1979b). Radiation in the British Uplands, Jnl Appl.Ecol. 16, 161-170.

Hare, F.K. & Hay, J.E. (1974). The Climate of Canada and Alaska, in Bryson, R.A. & Hare, F.K. eds, Climates of North America, World Survey of Climatology Volume 11, Elsevier, Amsterdam, pp. 49-134.

Harris, R. (1985). Variations in the Durham Rainfall and Temperature Record, 1847-1981, in Tooley, M.J. & Sheail, G.M. eds, The Climatic Scene, Allen and Unwin, London, pp. 39-59.

Harrison, S.J. (1974). Problems in the Measurement and Evaluation of the Climatic Resources of Upland Britain, in Taylor, J. ed., Climatic Resources and Economic Activity, David & Charles, Newton Abbot, pp. 47-63.

Harrison, S.J. (1975). The Elevation Component of Soil Temperature Variation, Weather 30, 397-409.

Hastenrath, S.L. (1968). Der Regionale und Jahrzeitliche Wandel des Vertikalen Temperaturgradienten und seine Behandlung als Wärmhaushaltsproblem, Met.Rdsch. 21, 46-51.

Hawke, E.L. (1944). Thermal Characteristics of a Hertfordshire Frost Hollow, Quart.Jnl Roy.Met.Soc. 70, 23-48.

Hennessy, J.P.Jr. (1979). Comments on "Use of Mesoscale Climatology in Mountainous Terrain to Improve the Spatial Representation of Mean Monthly Temperatures", Mon.Weather Rev. 107, 352-353.

Hess, M. (1965). Vertical Climatic Zones in the Polish Western Carpathians, Zeszyty Nauhowe UJ - Prace Geograficzne, Kraków, 11, 267 pp.

Hess, M. (1969). Principal Climatological Problems of the Carpathians, Zeszyty Naukowe UJ-Prace Geograficzne, Kraków, 25, pp. 4-47.

Hess, M. (1974). Vertical Climatic Zones in the Tatra Mountains, Czasopismo Geograficzne 45(1), 75-95.

Hess, M., Niedzwiedz, T. & Obrebska-Starkel, B. (1976). An Attempt at the Application of the Frostless Period as a Guiding Criterion in the Typology of Mesoclimatic Conditions in the Mountains, Geographia Polonica 33, 73-85.

Hess, M., Niedzwiedz, T. & Obrebska-Starkel, B. (1984). A Method of Characterizing the Thermal Relations in Mountainous Areas/ The Lower Beskid Range in the Polish Carpathians as an Example, Geojournal 3, 251-257.

Hollermann, P. (1985). The Periglacial Belt of Mid-Latitude Mountains from a Geoecological Point of View, Erdkunde 39, 259-270.

Holloway, J.L. (1958). Smoothing and Filtering of Time Series and Space Fields, Advances in Geophysics 4, 351-388.

Hopkins, J.S. (1977). The Spatial Variability of Daily Temperatures and Sunshine over Uniform Terrain, Met.Mag. 106, 278-292.

Hossell, J.E. (1992). Global Warming and the British Landscape: The Sensitivity of Land-Use and Vegetation in Britain to Climatic Change, PhD Thesis, University of Birmingham, unpublished.

Houghton, J.T., Jenkins, G.J. & Ephraums, J.J. (1990). eds, Climate Change: The IPCC Scientific Assessment, Press Syndicate, Cambridge, 365 pp.

Houghton, J.T., Callander, B.A. & Varney, S.K. (1992). eds, Climate Change 1992: The Supplementary Report to the IPCC Scientific Assessment, Cambridge University Press, 200 pp.

Hoyt, D.V. (1977). Percent of Possible Sunshine and the Total Cloud Cover, Mon.Weather Rev. 105, 648-652.

Hoyt, D.V. (1980). Variations in Sunspot Structure and Climate, Climatic Change 2, 79-92.

Hu, H.C. & Lim, J.T. (1983). Solar and Net Radiation in Peninsular Malaysia, Jnl Clim. 3, 271-283.

Hulme, M., Briffa, K.R., Jones, P.D. & Senior, C.A. (1993). Validation of GCM Control Simulations Using Indices of Daily Airflow Types Over the British Isles, Climate Dynamics, in press.

Hulme, M., Hossell, J.E. & Parry, M.L. (1993). Future Climate Change and Land-Use in the United Kingdom, Geographical Jnl 159, 131-147.

Hurry, D.G.W. (1969). Meteorological Survey of Glen Nevis - Summer 1968, Weather 24, 214-221.

Idso, S.B., Baker, D.G. & Blad, B.L. (1969). Relations of Radiation Fluxes over Natural Surfaces, Quart.Jnl Roy.Met.Soc. 95, 244-257.

Ilko, J. (1991). Trends in the Course of Temperature According to Long Term Measurements on Ten Stations between Altitudes from 100 to 3000 m above Sea-level, Mountain Meteorology, Climatology & Aerology of the Lower Layers of Troposphere, Slovak Hydrometeorological Institute, Bratislava, pp. 55-66.

Iversen, J. (1944). Viscum, Hedera and Ilex as Climate Indicators, Geol.För.Stockh. Förh. 66, 463-483.

Johnson, R.C. (1985). Mountain and Glen Climatic Contrasts at Balquhidder, Jnl Met. 10, 105-108.

Jolliffe, I.T. (1990). Lengths of Very Warm and Very Cold Spells at Edgbaston, Int.Jnl Clim. 10, 407-411.

Jones, P.D., Hulme, M. & Briffa, K.R. (1993). A Comparison of Lamb Circulation Types with an Objective Classification Scheme, Int.Jnl Clim. 13, 655-663.

Jones, P.D., Wigley, T.M.L. & Wright, P.B. (1986). Global Temperature Variations between 1861 and 1984, Nature 322, 430-434.

Karl, T.R., Jones, P.D., Knight, R.W., Kukla, G., Plummer, N., Razuvayev, V., Gallo, K.P., Lindseay, J., Charlson, R.J. & Peterson, T.C. (1993). Asymmetric Trends of Daily Maximum and Minimum Temperature, Bull.Amer.Met.Soc. 74, 1007-1023.

Katsoulis, B.D. & Leontaris, S.N. (1981). The Distribution over Greece of Global Solar Radiation on a Horizontal Surface, Agric. Met. 23, 217-229.

Kenworthy, J.M. (1985). The Durham University Observatory Record and Gordon Manley's Work on a Longer Time Series for North-East England, in Tooley, M.J. & Sheail, G.M. eds, The Climatic Scene, Allen & Unwin, London, pp. 17-38.

Kington, J.A. (1976). An Introduction to an Examination of Monthly and Seasonal Extremes in the Climatic Record of England and Wales Using Historical Daily Synoptic Weather Maps from 1781 Onward, Weather 31, 72-78.

Klinedinst, P.L., Wilhite, D.A., Hahn, G.L. & Hubbard, K.G. (1993). The Potential Effects of Climate Change on Summer Season Dairy Cattle Milk Production and Reproduction, Climatic Change 23, 21-36.

Konovalov, V.G., Karandaeva, L.M. & Ratsek, I.V. (1991). Numerical Estimation of the Fields of Meteorological Elements in Mountains for Glaciation Regime Computations, Int.Symp.Glac-Ocean-Atmosphere Interactions Proc. 1990, St.Petersburg, 208, 529-541.

Kozuchowski, K. & Marciniak, K. (1988). Variability of Mean Monthly Temperatures and Semi-Annual Precipitation Totals in Europe in Relation to Hemispheric Circulation Patterns, Jnl Clim. 8, 191-199.

Kutiel, H. (1988). The Relationship of Rainfall Patterns in the Galilee, Israel, to Regional Circulation Patterns, PhD Thesis, University of Utah, 117 pp., unpublished.

Lamb, H.H. (1950). Types and Spells of Weather Around the Year in the British Isles: Annual Trends, Seasonal Structure of the Year, Singularities, Quart.Jnl Roy.Met.Soc. 76, 393-438.

Lamb, H.H. (1972). British Isles Weather Types and a Register of the Daily Sequence of Circulation Patterns, 1861-1971, Geophysical Memoir 116, HMSO, London, 85 pp.

Lamb, H.H. (1982). Climate, History and the Modern World, Methuen, London, 387 pp.

Lambert, L. & Chitrakar, B.D. (1989). Variation of Potential Evapotranspiration with Elevation in Nepal, Mountain Research and Development 9, 145-152.

Lapen, D.R. & Martz, I.W. (1993). The Measurement of Two Simple Topographic Indices of Wind-Sheltering Exposure from Raster Digital Elevation Models, Computers & Geosciences 19, 769-779.

Larcher, W. (1975). Physiological Plant Ecology, Springer-Verlag, Berlin, 252 pp.

Lauer, W. (1975). Klimatische Grundzüge der Höhenstufung Tropischer Gebirge, in Tagungsbericht und Wissenschaftliche Abhandlungen, 40 Deutscher Geographentag, Innsbruck, F.Steiner, Innsbruck, pp. 76-90.

Lawrence, E.N. (1960). Variation of Surface Wind Velocity with Height in Hilly Terrain, Met.Mag. 89, 287-292.

Le Drew, E. (1975). The Energy Balance of a Mid-Latitude Alpine Site During the Growing Season, 1973, Arctic and Alpine Res. 7, 301-314.

Lee, D.O. (1979). Contrasts in Warming and Cooling Rates at an Urban and a Rural Site, Weather 34, 60-66.

Leffler, R.J. (1981). Climate and the Timberline in the Appalachians, Weatherwise 34, 116-119.

Lengerke, H.J.Von. (1978). On the Short-Term Predictability of Frost and Frost Protection -A Case Study on Dunsandle Tea Estate in the Nilgiris (South India), Agric.Met. 19, 1-10.

Lewis, P. (1960). The Use of Moving Averages in the Analysis of Time Series, Weather 15, 121-126.

Linacre, E.T. (1968). Estimating the Net Radiation Flux, Agric. Met. 5, 49-63.

Linacre, E.T. (1982). The Effect of Altitude on the Daily Range of Temperature, Jnl Clim. 2, 375-382.

Linacre, E.T. (1992). Climate Data and Resources: A Reference and Guide, Routledge, London, 366 pp.

Linacre, E.T. & Hobbs, J.E. (1977). The Australian Climatic Environment, Wiley, Jacaranda, 354 pp.

Lindqvist, S. (1992). Local Climatological Modelling for Road Stretches and Urban Areas, Geogr.Ann. 74 A(2-3), 265-274.

Lockwood, J.G. (1962). Occurrence of Föhn Winds in the British Isles, Met.Mag. 91, 57-65.

Lowry, W.P. (1980). Clear-Sky Direct-Beam Solar Radiation Versus Altitude: A Proposal For Standard Soundings, Jnl Appl.Met. 19, 1323-1327.

Ludecke, C. & Kuhle, M. (1991). Comparison of Meteorological Observations at Mt Everest and K2: Examples of the 1984 and 1986 Expeditions, Met. & Atmos. Physics 47(1), 55-60.

Lumb, F.E. (1961). Seasonal Variations of the Sea Surface Temperature in Coastal Waters of the British Isles, Met.Office Sci.Paper No. 6, MO 685.

Lumb, F.E. (1993). A Stormy Prospect For Next Century, Weather 48, 159-160.

McCulloch, J.S.G. (1965). Tables for the Rapid Computation of the Penman Estimate of Evaporation, East African Agricultural and Forestry Journal 3, 286-295.

McCutchan, M.H. (1976). Diagnosing and Predicting Surface Temperature in Mountainous Terrain, Mon.Weather Rev. 104, 1044-1051.

McCutchan, M.H. (1979). Determining the Diurnal Variations of Surface Temperature in Mountainous Terrain, Jnl Appl. Met. 16, 571-584.

McCutchan, M.H. (1983). Comparing Temperature and Humidity on a Mountain Slope and in the Free Air Nearby, Mon.Weather Rev. 111, 836-845.

McCutchan, M.H., Fox, D.G. & Furman, R.W. (1982). San Antonio Mountain Experiment (SAMEX), Bull.Amer.Met.Soc. 83, 1123-1131.

McIlveen, J.F.R. (1992). Fundamentals of Weather and Climate, Chapman and Hall, London, 497 pp.

McKay, D.C. & Thurtell, G.W. (1978). Measurements of the Energy Fluxes Involved in the Energy Budget of a Snow Cover, Jnl Appl. Met. 17, 339-349.

Malberg, H. (1973). Comparison of Mean Cloud Cover Obtained by Satellite Photographs and Ground-Based Observations over Europe and the Atlantic, Mon. Weather Rev. 101, 893-897.

Manley, G. (1935). Some Notes on the Climate of North-East England, Quart.Jnl Roy. Met.Soc. 61, 405-410.

Manley, G. (1936). The Climate of the Northern Pennines: The Coldest Part of England, Quart.Jnl Roy.Met.Soc. 62, 103-113.

Manley, G. (1939). On the Occurrence of Snow Cover in Great Britain, Quart.Jnl Roy.Met.Soc. 65, 2-27.

Manley, G. (1941). The Durham Meteorological Record, 1847-1940, Quart.Jnl Roy.Met.Soc. 67, 363-382.

Manley, G. (1942). Meteorological Observations on Great Dun Fell, A Mountain Station in Northern England, Quart.Jnl Roy.Met.Soc. 68, 151-165.

Manley, G. (1943). Further Climatological Averages for the Northern Pennines, with a Note on Topographical Effects, Quart. Jnl Roy.Met.Soc. 69, 251-261.

Manley, G. (1945a). The Effective Rate of Altitudinal Change in Temperate Atlantic Climates, Geogr.Rev. 35, 408-417.

Manley, G. (1945b). The Helm Wind over Cross Fell, Quart.Jnl Roy. Met.Soc. 71, 197-215.

Manley, G. (1946). Temperature Trend in Lancashire, 1735-1945, Quart.Jnl Roy. Met.Soc. 72, 1-13.

Manley, G. (1947). A Remarkable Winter Day on the High Pennines, Weather 2, 6-8.

Manley, G. (1949). Fanaråken: The Mountain Station in Norway, Weather 4, 352-354.

Manley, G. (1952). Climate and the British Scene, Collins, London, 314 pp.

Manley, G. (1974). Central England Temperatures: Monthly Means 1659-1973, Quart. Jnl Roy.Met.Soc. 100, 389-405.

Manley, G. (1978). Meteorological Observations on Royal Deeside, Weather 33, 457-459.

Manley, G. (1980). The Northern Pennines Revisited: Moor House, 1932-78, Met. Mag. 109, 281-292.

Marshall, W.A.L. (1954). Comparison of the Wind Recorded by the Anemograph with the Geostrophic Wind, Professional Notes 108, Meteorological Office.

Mayes, J.C. (1991). Contrasting Weather in Northern Scotland 1988-90 in Relation to Regional Airflow Types, Weather 46, 16-21.

Mayes, J.C. (1994). Recent Changes in the Monthly Distribution of Regional Weather Types in the British Isles, Weather 49, 156-162.

Mearns, L.O. (1989). The Simulation of Meteorological Time Series for Climatic Change Scenario Development, EPA Meeting, Aug 31 1989, Boulder, Colorado, U.S.A..

Messerli, B. & Winiger, M. (1992). Climate, Environmental Change, and Resources of the African Mountains from the Mediterranean to the Equator, Mountain Research and Development 12, 315-336.

Mintzer, I.M. (1992). Living in a Warming World, in Mintzer, I.M. ed., Confronting Climate Change: Risks, Implications and Responses, Cambridge University Press, pp. 1-14.

Mitchell, J.F.B., Manabe, S., Meleshko, V. & Tokioka, T. (1990). Equilibrium Climate Change and Its Implications for the Future, in Houghton, J.T., Jenkins, G.J. & Ephraums, J.J. eds, Climate Change: The IPCC Scientific Assessment, Cambridge University Press, pp. 131-172.

Monteith, J.L. (1973). Principles of Environmental Physics, Arnold, London, 241 pp.

Monteith, J.L. & Szeicz, G. (1961). The Radiation Balance of Bare Soil and Vegetation, Quart.Jnl Roy.Met.Soc. 87, 159-170.

Monteith, J.L. & Szeicz, G. (1962). Radiative Temperature in the Heat Balance of Natural Surfaces, Quart.Jnl Roy.Met.Soc. 88, 496-507.

Monteith, J.L. & Unsworth, M.H. (1990). Principles of Environmental Physics, 2nd edition, Edward Arnold, London, 228 pp.

Moran, J.M. & Morgan, M.D. (1977). Recent Trends in Hemispheric Temperature and Growing Season Indices in Wisconsin, Agric.Met. 18, 1-8.

Morecroft, M.D., Marrs, R.H. & Woodward, F.I. (1992). Altitudinal and Seasonal Trends in Soil Nitrogen Mineralisation Rate in the Scottish Highlands, Jnl Ecol. 80, 49-56.

Murray, R.M. & Lewis, R.P.W. (1966). Some Aspects of the Synoptic Climatology of the British Isles as Measured by Simple Indices, Met.Mag. 95, 193-203.

Murray, R.M. (1990). Estimating the Continental Component in the Maritime Climate of Skye, Weather 45, 255-261.

Murray, R.M. (1993). Bias in Southerly Synoptic Types in Decade 1981-90 over the British Isles, Weather 48, 152-154.

Nadelhöffer, K.J., Giblin, A.E., Shaver, G.R. & Laundre, J.A. (1991). Effects of Temperature and Substrate Quality on Element Mineralisation in Six Arctic Soils, Ecology 72, 242-253.

Niedzwiedz, T. (1992). Climate of the Tatra Mountains, Mountain Research and Development 12, 131-146.

Nield, R.E., Richman, H.N. & Seeley, M.W. (1979). Impacts of Different Types of Temperature Change on the Growing Season for Maize, Agric.Met. 20, 367-374.

Nkemdirim, L.C. (1970). Empirical Methods for the Assessment of Insolation and Evaporation in Southern Scotland, Arch.Met. Geophys.Biokl. B, 18, 131-141.

Nkemdirim, L.C. & Venkatesan, D. (1985). The Nature of the Distribution in Space and Time of the Annual Frost-Free Season in Canada, East of the Rockies, Geogr.Ann. 67 A(1-2), 1-12.

Nuttonson, M.Y. (1955). Wheat-Climate Relationships and the Use of Phenology in Ascertaining the Thermal and Photo-Thermal Requirements, Amer.Inst.Crop Ecol., Washington D.C.

O'Hare, G. & Sweeney, J. (1993). Lamb's Circulation Types and British Weather: An Evaluation, Geography 78 (1), 43-60.

Ohmura, A. (1982). Climate and Energy Balance of the Arctic Tundra, Jnl Clim. 2, 65-84.

Oke, T.R. (1987). Boundary Layer Climates, 2nd edition, Methuen, London, 435 pp.

Olecki, Z. (1989). Solar Radiation Balance in the Upper Vistula Basin, Rozprawy Habilitacyjne U.J. Kraków 157, 126 pp.

Oliver, H. (1991). Studies of Surface Energy Balance of Sloping Terrain, Int.Jnl Clim. 12, 55-68.

Oliver, J. (1960). Upland Climates in South Wales, in Taylor, J.A. ed., Hill Climates and Land Usage with Special Reference to the Highland Zone of Britain, Memorandum No.3, Aberystwyth.

Omond, R.T. (1910). Large Differences of Temperature Between the Ben Nevis and Fort William Observatories, Trans.Roy.Soc.Edinb. 44, 702-705.

Osborn, H.B. (1984). Estimating Precipitation in Mountainous Regions, Jnl Hydr.Engin. 110, 1859-1863.

Paltridge, G.W. & Platt, C.M.R. (1976). Radiative Processes in Meteorology and Climatology, Elsevier, Amsterdam, 318 pp.

Parker, D.E., & Jones, P.D.(1991). Global Warmth in 1990, Weather 46, 302-311.

Parker, D.E., Legg, T.P. & Folland, C.K. (1992). A New Daily Central England Temperature Series, 1772-1991, Int.Jnl Clim. 12, 317-342.

Parry, M.L. (1972). Secular Climatic Change and Marginal Land, Inst.Brit.Geogr. Conference Paper, Aberdeen.

Parry, M.L. (1975). Secular Climatic Change and Marginal Agriculture, Trans.Inst. Brit.Geogr. 64, 1-18.

Parry, M.L. (1976). The Significance of the Variability of Summer Warmth in Upland Britain, Weather 31, 212-217.

Parry, M.L. (1978). Climatic Change, Agriculture and Settlement, Studies in Historical Geography Series, Dawson Books, Folkestone, UK, 214 pp.

Parry, M.L. (1981). Evaluating the Impact of Climatic Change, in Smith, C.D. & Parry, M.L. eds, Consequences of Climatic Change, Department of Geography, University of Nottingham, pp. 3-16.

Parry, M.L., Carter, T.R. & Konijn, N.T. (1988). The Impact of Climatic Variations on Agriculture, Vol. 1: Assessments in Cool Temperate and Cold Regions, Kluwer Academic Publishers, Dordrecht, 876 pp.

Parry, M.L., Carter, T.R. & Porter, J.H. (1990). The Greenhouse Effect and the Future of UK Agriculture, Jnl Roy.Agric.Soc. England 150, 120-131.

Parry, M.L. (1990). Climatic Change and World Agriculture, Earthscan, London, 165 pp.

Parton, W.J. & Logan, J.A. (1981). A Model for Diurnal Variation in Soil and Air Temperature, Agric.Met. 23, 205-216.

Pavlov, A.V. (1962). Izv.Akad.Nauk.Geophys.Series 6, p. 94.

Pearl, R.T. et al. (1954). The Calculation of Irrigation Need, Tech. Bull. No.4, Min. Agric. Fish and Food, HMSO. London, 35 pp.

Pearsall, W.H. (1950). Mountains and Moorlands, Collins' New Naturalist, London, 415 pp.

Pedgley, D. (1979). Mountain Weather: A Practical Guide for Hillwalkers and Climbers in the British Isles, Cicerone Press, Cumbria, 112 pp.

Penman, H.L. (1948). Natural Evaporation From Open Water, Bare Soil and Grass, Proc.Roy.Soc. A, 193, 120-145.

Pennell, I. (1992). An Investigation of the Occurrence of Unusually Severe Winter Weather in Britain, and the Reasons For It, BSc Dissertation, Department of Environmental Science, University of Lancaster, 63 pp.

Pepin, N.C. (1990). A Comparison of Climatic Conditions at Two Meteorological Stations on the Dip Slope of the Pennines: Widdybank Fell (513 m OD) and Durham Observatory (102 m OD), BSc Dissertation, Department of Geography, University of Durham, 146 pp.

Pepin, N.C. (1992). The Spatial and Temporal Variation of the Altitudinal Temperature Gradient in Northern England, Graduate Discussion Paper 92/5, Department of Geography, University of Durham, 32 pp.

Pepin, N.C. (1993). Assessment of the Meteorological Impact of the A167 London-Edinburgh-Thurso Trunk Road: Cock O' The North to Aycliffe Improvement, Report for W.A.Fairhurst & Partners, Department of Geography, University of Durham, 60 pp.

Pepin, N.C. (1994). Analysis of the Chevallier Meteorological Record: Heighington 1870-1884, Weather, in press.

Peppler, W. (1931). Zur Frage des Temperaturunterschiedes Zwischen den Berggipfeln und der Freien Atmosphäre, Beitr.Phys. Frei.Atmos. 17, 247-263.

Perry, A.H. (1968). Summer Days in the British Isles, Weather 23, 212-214.

Perry, A.H. (1969). The PSCM Index and Regional Anomalies of Temperature, Rainfall and Sunshine, Weather 24, 225-228.

Perry, A.H. (1976). Synoptic Climatology, in Chandler, T.J. & Gregory, S. eds, The Climate of the British Isles, Longman, London, pp. 8-38.

Perry, A.H. & Barry, R.G. (1973). Recent Temperature Changes due to Changes in the Frequency and Average Temperature of Weather Types over the British Isles, Met.Mag. 102, 73-82.

Petr, J. (1991). Weather and Yield, Elsevier, Amsterdam, 288 pp.

Pfister, C. (1985). Snow Cover, Snowlines and Glaciers in Central Europe Since the 16th Century, in Tooley, M.J. & Sheail, G.M. eds, The Climatic Scene, Allen & Unwin, London, pp. 154-174.

Pielke, A. & Mehring, P. (1977). Use of Mesoscale Climatology in Mountainous Terrain to Improve the Spatial Representation of Mean Monthly Temperatures, Mon. Weather Rev. 105, 108-112.

Pitman, J. (1993). Probability, Springer-Verlag, New York, 559 pp.

Polavarapu, R.J. (1968). Some Studies of Sensible and Latent Heat Fluxes at Waltair, South-Eastern Coast of India, Agric.Met. 5, 255-268.

Prescott, J.A. (1940). Evaporation From a Water Surface in Relation to Solar Radiation, Trans.Roy.Soc.South Australia 64, 114-125.

Prescott, J.A. & Collins, J.A. (1951). The Lag of Temperature Behind Solar Radiation, Quart.Jnl Roy.Met.Soc. 77, 121-126.

Price, L.W. (1978). Mountains of the Pacific North West: A Study in Contrast, Arctic & Alpine Res. 10(2), 465-478.

Priestley, C. & Taylor, R.J. (1972). On the Assessment of Surface Heat Flux and Evaporation Using Large-Scale Parameters, Mon. Weather Rev. 100, 81-92.

Primault, B. (1969). D'une Application Pratique des Indices Bio-Météorologiques, Agric.Met. 6, 71-96.

Rao, C.R.N. & Bradley, W.A. (1983). Estimation of the Daily Global Solar Irradiation at Corvallis, Oregon (U.S.A.) from the Hours of Bright Sunshine, the Daily Temperature Range and Relative Humidity, Jnl Clim. 3, 179-185.

Rayer, P.J. (1987). The Meteorological Office Forecast Road Surface Temperature Model, Met.Mag. 116, 180-191.

Reiter, E.R. & Heuberger, H. (1960). A Synoptic Example of the Retreat of the Indian Summer Monsoon, Geogr.Ann. 42 A, 17-35.

Reynolds, G. (1956). Local Temperature Variations in Wirral, Weather 11, 15-17.

Richardson, W.E. (1954). Temperature Differences in the South Tyne Valley, near Alston, Cumberland, Weather 9, 82-85.

Richner, H. & Phillips, P.D. (1984). A Comparison of Temperatures from Mountain Tops and the Free Atmosphere - Their Diurnal Variation and Mean Difference, Mon.Weather Rev. 112, 1328-1340.

Rider, N.E. & Robinson, G.D. (1951). A Study of the Transfer of Heat and Water Vapour Above a Surface of Short Grass, Quart.Jnl Roy.Met.Soc. 77, 375-401.

Rijckborst, H. (1967). Hydrology of the Upper Garonne Basin (Valle de Aran, Spain), Leidse.Geol.Meded. 40, 74 pp.

Rind, D. (1991). Climate Variability and Climate Change, in Schlesinger, M.E. ed., Greenhouse Gas Induced Climatic Change: A Critical Appraisal of Simulations and Observations, Elsevier, Amsterdam, pp. 69-78.

Ripley, E.A. (1963). Private Communication to McCulloch (1965).

Robinson, P.J. & Finkelstein, P.L. (1991). The Development of Impact-Orientated Climate Scenarios, Bull.Amer.Met.Soc. 72, 481-490.

Robock, A., Turco, R.P., Harwell, M.A., Ackerman, T.P., Andressen, R., Chang, H.S. & Sivakumar, M.V.K. (1993). Use of General Circulation Model Output in the Creation of Climatic Change Scenarios for Impact Analysis, Climatic Change 23, 293-335.

Rosenberg, N.J. (ed.) (1993). Towards an Integrated Impact Assessment of Climate Change: The MINK Study, Climatic Change 24 (1-2), 173 pp.

Rouse, W.R., Mills, P.F. & Stewart, R.M. (1977). Evaporation in High Latitudes, Water Resources Research 13, 909-914.

Running, S.W., Nemani, R.R. & Hungerford, R.D. (1987). Extrapolation of Synoptic Meteorological Data in Mountainous Terrain and Its Use for Simulating Forest Evapotranspiration and Photosynthesis, Can.Jnl Forest.Res. 17, 472-483.

Samson, C.A. (1965). A Comparison of Mountain Slope and Radiosonde Observations, Mon.Weather Rev. 95, 327-330.

Sauberer, F. & Dirmhirn, I. (1958). Das Strahlungsklima, in Steinhauser, F., Eckel, O. & Lauscher, F. eds, Klimatographie von Osterreich, Springer, Vienna, pp. 13-102.

Schlesinger, M.E. & Mitchell, J.F.B. (1985). Model Projections of the Equilibrium Climatic Response to Increased Carbon Dioxide, in McCracken, M.C. & Luther, F.M. eds, Projecting the Climatic Effects of Increasing Carbon Dioxide, DOE/ER 0237, U.S. Dept of Energy, Washington D.C., pp. 81-147.

Scott, R.H. (1884). Cumulative Temperature, Quart.Jnl Roy.Met. Soc. 10, 296-302.

Sharon, D. (1972). The Spottiness of Rainfall in a Desert Area, Jnl Hydrology 17, 161-175.

Sharon, D. (1974). On the Modelling of Correlation Functions for Rainfall Studies, Jnl Hydrology 22, 219-224.

Shaw, E. (1962). An Analysis of the Origins of Precipitation in Northern England, 1956-1960, Quart.Jnl Roy.Met.Soc. 88, 539-547.

Shellard, H.C. (1959). Averages of Accumulated Temperature and Standard Deviation of Monthly Mean Temperature over Britain, 1921-1950, Professional Notes 125, Meteorological Office.

Siegel, A.F. (1988). Statistics and Data Analysis: An Introduction, Wiley & Sons, New York, 518 pp.

Skaggs, R.H. & Baker, D.G. (1985). Fluctuations in the Length of the Growing Season in Minnesota, Climate Change 7, 403-414.

Slatyer, R.O. & McIlroy, I.C. (1961). Practical Climatology, UNESCO, pp 3-54.

Smith, L.P. (1950). Variations of Mean Air Temperature and Hours of Sunshine on the Weather Slope of a Hill, Met.Mag. 79, 231-233.

Smith, L.P. (1952). Variations in Air Temperature and Humidity on the Weather Slope of a Coastal Hill, Met.Mag. 81, 102-104.

Smith, L.P. (1965). Possible Changes in Seasonal Weather, in Johnson, C.G. & Smith, L.P. eds, The Biological Significance of Climatic Changes in Britain, Academic Press, London & New York, pp. 187-191.

Smithson, P.A. (1970). Influence of Topography and Exposure on Airstream Rainfall in Scotland, Weather 25, 379-386.

Snow, J.W. (1975). The Climates of Northern South America, M.S. Thesis, University of Wisconsin, Madison, 238 pp.

Sommers, W.T. (1976). On the Accuracy of Interpolated LFM Forecasts and their Use in Predicting Surface Conditions in Mountainous Terrain, Mon.Weather Rev. 104, 1573-1582.

Sowden, I.P. & Parker, D.E. (1981). A Study of Climatic Variability of Daily Central England Temperatures in Relation to the Lamb Synoptic Types, Jnl Clim. 1, 3-10.

Starr, J.R. (1981). Weather and Lamb Mortality in a Commercial Lowland Sheep Flock, Agric.Met. 24, 237-252.

Suckling, P.W. (1989). Application of a Climate Departure Index to the Study of Freeze Dates and Growing Season Length in the South-Eastern United States, Int.Jnl Clim. 9, 383-394.

Sumner, E.J. (1959). Blocking Anticyclones in the Atlantic-European Sector of the Northern Hemisphere, Met.Mag. 88, 300-311.

Sutcliffe, J. (1977). Plants and Temperature, Arnold, London, 57 pp.

Tabony, R.C. (1985). The Variation of Surface Temperature with Altitude, Met.Mag. 114, 37-48.

Tavakol, R.K. (1979). Solar Variability, C^{14} and Climatic Change, Climate Monitor 8 (3), 76-81.

Taylor, J.A. (1965). Climatic Change as Related to Altitudinal Thresholds and Soil Variables, in Johnson, C.G. & Smith, L.P. eds, The Biological Significance of Climatic Changes in Britain, Academic Press, London & New York, pp. 37-50.

Taylor, J.A. (1967a). Weather and Agriculture, Pergamon Press, London, 225 pp.

Taylor, J.A. (1967b). Economic and Ecological Productivity under British Conditions, in Weather and Agriculture, Pergamon Press, London, pp. 137-145.

Taylor, J.A. (1976). Upland Climates, in Chandler, T.J. & Gregory, S. eds, The Climate of the British Isles, Longman, London, pp. 264-287.

Thom, H.C.S. (1954). The Rational Relationship Between Heating Degree Days and Temperature, Mon.Weather Rev. 82, 1-6.

Tranquillini, W. (1979). Physiological Ecology of the Alpine Timberline, Springer-Verlag, Berlin-Heidelberg-New York, 137 pp.

Trenberth, K. (1983). What are the Seasons?, Bull.Amer.Met.Soc. 64, 1276-1282.

Trilsbach, A. (1988). Temperature Inversions in the Vale of Pickering, Report Submitted to the Chief Health and Housing Officer for Ryedale D.C., University of Durham, 26 pp.

Turner, H. (1958). Maximal Temperaturen oberflächennaher Bodenschichten an der Alpinen Waldgrenze, Wetter u. Leben 10, 1-12.

Tyldesley, J.B. (1978). A Method of Evaluating the Effect of Temperature on an Organism when the Response is Non-Linear, Agric.Met. 19, 137-153.

Uhlig, H. (1978). Geoecological Controls on High-Altitude Rice Cultivation in the Himalayas and Mountain Regions of South-East Asia, Arctic & Alpine Res. 10, 519-529.

Urban, D., Harmon, M. & Halpern, C. (1993). Potential Response of Pacific North-Western Forests to Climatic Change, Effects of Stand Age and Initial Composition, Climatic Change 23, 247-266.

Utaaker, K. (1968). A Temperature-Growth Index - The Respiration Equivalent - Used in Climatic Studies on the Mesoscale in Norway, Agric.Met. 5, 351-359.

Vedin, H. (1990). Frequency of Rare Weather Events During Periods of Extreme Climate, Geogr.Ann. 72 A(2), 151-155.

Viner, D. & Hulme, M. (1992). Climate Change Scenarios for Impact Studies in the UK: General Circulation Models, Scenario Construction Methods and Applications for Impact Assessment, Report Prepared for the U.K. Dept of Environment, Climatic Research Unit, Norwich, 70 pp.

Viner, D. & Hulme, M. (1993). Construction of Climate Change Scenarios by Linking GCM and STUGE Output, Technical Note No. 2 (March 1993), Produced for U.K. Dept of Environment, Climatic Research Unit, Norwich, 20 pp.

Voloshina, A.P. (1966). Teplovoi Balans Poverkhnosti Vysokogornykh Lednikov V. Letnii Period, Izdat.Nauka, Moscow.

Waco, D. (1968). Frost Pockets in the Santa Monica Mountains of Southern California, Weather 23, 456-461.

Wallén, C. (1970). Climates of Northern and Western Europe, Elsevier, Amsterdam, 253 pp.

Walter, A. (1967). Notes on the Utilization of Records from Third Order Climatological Stations for Agricultural Purposes, Agric. Met. 4, 137-143.

Walter, A. (1969). A Relation Between Incoming Solar Radiation and Degree Hours of Temperature, Agric.Met. 6, 435-438.

Walts, D. & Pochop, L. (1977). Operational Objective Temperature Forecasts at Non-MOS Stations, Mon.Weather Rev. 105, 3-8.

Warrick, R.A. & Barrow, E.M. (1991). Climate Change Scenarios for the U.K. Trans. Inst.Brit.Geogr. 16, 387-399.

Waylen, P. (1988). Statistical Analysis of Freezing Temperatures in Central and Southern Florida, Jnl Clim. 8, 607-628.

Webb, J.D.C. & Meaden, G.T. (1993). Britain's Highest Temperatures by County and by Month, Weather 48, 282-291.

Webb, T. & Wigley, T.M.L. (1985). What Past Climates Can Indicate About a Warmer World?, in McCracken, M.C. & Luther, F.M. eds, Detecting the Climatic Effects of Increasing Carbon Dioxide, DOE/ER 0237, U.S. Dept of Energy, Washington D.C., pp. 237-258.

White, E.J. & Smith, R.I. (1982). Climatological Maps of Great Britain, NERC Institute of Terrestrial Ecology, Cambridge.

Wigley, T.M.L. (1985). Impact of Extreme Events, Nature 316, 106-107.

Wigley, T.M.L., Angell, J.K. & Jones, P.D. (1985). Analysis of the Temperature Record, in McCracken, M.C. & Luther, F.M. eds, Detecting the Climatic Effects of Increasing Carbon Dioxide, DOE/ER 0237, U.S. Dept of Energy, Washington D.C., pp. 55-90.

W.M.O. (1986). Report of the International Conference of the Assessment of the Role of Carbon Dioxide and of other Greenhouse Gases in Climate Variations and Associated Impacts, Villach, Austria, October 1985, W.M.O. No. 661, 78 pp.

Wolfe, J.A. (1990). An Analysis of Present Day Terrestrial Lapse Rates in the Western Conterminous United States and their Significance to Paleoaltitudinal Estimates, U.S. Geol.Survey Bulletin, 35 pp.

Woo, M.K. (1992). Application of Stochastic Simulation to Climate Change Studies, Climate Change 20, 313-330.

Yacono, D. (1968). L'Ahaggar, Essai sur le Climat de Montagne au Sahara, Travaux de l'Institut de Recherches Sahariennes 27, Université d'Alger.

Yamamoto, R.(1980). Variability of Northern Hemisphere Mean Surface Air Temperature During the Recent Two Hundred Years, in Ikeda, S., Suzuki, E., Uchida, E. & Yoshino, M.M. eds, Statistical Climatology, Elsevier, Amsterdam, pp. 307-325.

Yeh, D.Z. (1982). Some Aspects of the Thermal Influences of Qinghai-Tibetan Plateau on the Atmospheric Circulation, Arch.Met. Geophys.Biokl. A, 31, 205-220.

Yoshino, M.M. (1966). Some Aspects of Air Temperature Climate of the High Mountains in Japan, Jap.Prog.Clim., November, pp. 21-27.

APPENDIX 1
PHOTOGRAPHIC PLATES

Plate 1. The Summit of Cross Fell (893 m), the highest point of the Pennines. The Cross Fell range is viewed from across the largely treeless, tundra-like landscape of the Alston block. Cross Fell is the summit on the right.

Plate 2. The area of Upper Teesdale. This area lies in the vicinity of the tree line, the hay meadows at about 450 metres above sea-level being amongst the highest in the country. Higher slopes are open moorland.

Plate 3. Fog trapped below a Temperature Inversion. The existence of a cloud layer is evidence of a temperature inversion, humid air being trapped below on this still winter morning.

Plate 4. Durham Observatory Building (102 m).

Plate 5. The Stevenson Screen at Durham Observatory.

Plate 6. Widdybank Fell Climatological Station (513 m). The Cross Fell range is shown in the distance.

Plate 7. Great Dun Fell (847 m). The weather station is marked by a white dome on the left-hand summit of the three. The site is extremely exposed.

Plate 8. Appleby in the Vale of Eden. The sheltered site is prone to temperature inversions.

Plate 9. The Pennine Escarpment, rising above the Vale of Eden. Great Dun Fell is indicated by the presence of the Radar station (white dome).

Plate 10. Coniferous Plantation at nearly 600 m above Sea-level in the Alston Massif. The present treeline lies at around 600 m, as in this photograph looking towards the Cross Fell range. Trees thrive better where there is shelter from the prevailing westerly airflows.

Plate 11. The Low Treeline on the Exposed South-Westerly Facing Slopes of Skiddaw in Cumbria. In wetter areas such as this the treeline is much lower than in more 'continental' areas further east (Plate 10).

APPENDIX 2
CALCULATION OF THE SATURATION VAPOUR PRESSURE GRADIENT

The saturation vapour pressure at temperature T is given by:

$$e_s(T) = e_o \times \exp(-\lambda M_w / RT) \quad ----(1)$$

where e_o is a constant (at least over a restricted temperature range), λ is the latent heat of vaporisation of water ($2511.6 * 10^3$ J/kg), M_w is the molecular weight of water (=18), R is the molar gas constant, which is 8.314 $Jmol^{-1}K^{-1}$, and T is the absolute temperature in Kelvin. By differentiating with respect to T it can be shown that

$$\Delta = \lambda \times M_w \times e_s(T) / (R \times T^2) \quad ----(2)$$

Note that Δ is the gradient of the saturation vapour pressure/temperature curve. Now:

$$e_s(T) = e_s(T^*) \times \exp[A \times (T - T^*) / (T - T')] \quad ------(3)$$

where A = 17.27. T^* = 273 K ($e_s(T^*)$ = 6.1 hPa), and T' = 36 K. Thus

$$e_s(T) = 6.1 \times \exp[(17.27 \times (T - 273)) / (T - 36)] \quad ---(4)$$

Converting T in Kelvin to T in Celsius the equation becomes

$$e_s(T) = 6.1 \times \exp[(17.27 \times T) / (T + 237)] \quad ----(5)$$

λ varies only slightly with temperature and can be approximated by

$$[(-12/5) \times T] + 2501 \ldots . Jg^{-1} \quad ----(6)$$

with T in Celsius. Thus we derive equation 9:

$$\Delta = ([(-12/5) \times T + 2501] \times 18 \times (6.1 \times \exp[(17.17 \times T) / (T + 237)])) / (8.314 \times (T + 273)^2) \quad -----(7)$$

APPENDIX 3
DEFINITION OF SPECIFIC HUMIDITY

Specific Humidity can be expressed as a function of total air pressure p and vapour pressure e. For the vapour component,

$$e=\chi\times(R/M_w)\times T-----(8)$$

where χ is the absolute humidity. Thus:

$$\chi(gm^{-3})=M_w e/RT---(9)$$

The dry air has pressure **p - e** and therefore, by the equation of state, has a density of

$$\rho_a=M_a(p-e)/RT----(10)$$

where M_a = 29 $gmol^{-1}$. The density of moist air is the sum of the dry air and vapour densities. Thus

$$\rho=[(M_w\times e)+M_a\times(p-e)]/RT----(11)$$

Thus specific humidity can be defined as

$$shumid=\chi/\rho=(\epsilon\times e)/[(p-e)+(\epsilon\times e)]----(12)$$

where ϵ = 0.622 = M_w/M_a. This is equivalent to equation 15 assuming the total air pressure p to be 1000 mbars.

APPENDIX 4
FILE SHOWING EQUATIONS TO ESTIMATE DAILY NET IRRADIATION AND SURFACE ENERGY BALANCE CALCULATIONS ASSUMING ISOBARIC WARMING/COOLING.

The model requires daily values of maximum temperature, minimum temperature, sunshine hours, day number, wet bulb, dry bulb, wind direction and snow cover.

Lines preceded by an asterisk (*) are comment lines and do not form part of the running model. The model is written in Stata language.

```
*Define the conversion factor from degrees into radians
macro define convfact=2*_pi/360
*Calculate the noon solar elevation for each day of the year
gen decl=23.45*sin(0.986*(day-80)*%convfact)
gen solar=35+decl
*Calculate the daylength
macro define mitanA=-sin(55*%convfact)/cos(55*%convfact)
gen x=%mitanA*(sin(decl*%convfact)/cos(decl*%convfact))
gen daylngth=abs((-_pi/2)+atan(x/sqrt(1-x*x)))/(%convfact*7.5)
*Generate expression for mean daily temperature
gen meanD=(maxD+minD)/2
*Define station altitudes
macro define altD=102
*Calculation of Penman constants
gen const1D=0.42+(0.011*(meanD))+(3*(10^-5)*%altD)
gen const2D=1-const1D
*Calculate gradient of saturation vapour pressure curve (against temperature). The mean
*daily temperature is used.
gen satvapD=6.1*exp((17.27*meanD)/(meanD+237))
gen satvap9D=6.1*exp((17.27*dryD)/(dryD+237))
gen satgradD=(((-12/5)*(meanD)+2501)*18*satvapD)/(8.314*((meanD+273)^2))
*Calculate psychrometer "constant"
gen psychroD=(satgradD/const1D)-satgradD
*Calculate vapour pressure at 9 am
gen vapD=(6.1*exp((17.27*wetD)/(wetD+237)))-(psychro*(dryD-wetD))
*Calculate relative humidity
gen rhumidD=(vapD)/(6.1*exp((17.27*dryD)/(dryD+237)))
*Convert this to specific humidity
gen shumidD=((0.622*vapD)/((1000-vapD)+(0.622*vapD)))*1000
*Calculate the overall transmissivity of the solar beam
*Calculate the amount of precipitable water. Note 9.81 is acceleration due to gravity
gen wD=(shumidD*1000)/(500*9.81)
*Expression for transmissivity due to water vapour
gen transwD=0.896-(0.0636*log(wD*(1/sin(solar*%convfact))))
*Expression for transmissivity due to aerosols
gen transa=exp[-0.1*(1/sin(solar*%convfact))]
*Overall transmissivity
```

```
gen transD=transwD*transa
*Hence calculate the maximum potential instantaneous solar irradiance at noon
gen maxiradD=1380*(transD)*sin(solar*%convfact)
*Calculate total potential (clear-sky) irradiance for the daylight period
*Assume a sinusoidal variation in the irradiance curve
gen iradDp=(2/_pi)*daylngth*3600*maxiradD
*Estimate proportion of time the sky is clear
gen skyD=sunD/daylngth
*Linacre's (1992) estimate of actual total irradiance, including diffuse and direct
*components
gen iradD=iradDp*(0.36+0.64*skyD)
*Calculate daily temperature range at screen level
gen rangeD=maxD-minD
*Assume minimum to occur at dawn
*Alternative formulae for total irradiance
gen iradD2=(0.048*iradDp)-(3.5*rangeD)+(0.029*iradDp*rangeD)+24
*Calculate total incoming radiation that is absorbed at the ground surface, allowing for
*albedo
gen iradDb=iradD*(1-0.2)
replace iradDb=iradD*(1-0.7) if snowD==1
*Estimate average cloud cover
gen cloudD=8*(daylngth-sunD)/daylngth
*Calculate downwards longwave radiation for cloudy sky
gen QldcD=(208+(6*((maxD+minD)/2)))*(1+(0.0034*(cloudD^2)))
*Estimate black-body radiation loss upwards
gen QluD=0.97*((((maxD+minD)/2)+273)^4)*5.67*(10^-8)
*Estimate net longwave exitance over 24 hours
gen exitD2=(QluD-QldcD)*24*3600
*Alternative formula for net longwave exitance over the 24 hour period (Linacre 1992)
gen exitnceD=(107-(meanD)-(9*cloudD))*24*3600
*Calculate net irradiation at the earth's surface
gen netiradD=iradDb-exitnceD
*Alternative estimate of net daily irradiation*/
gen netirdD2=iradDb-exitD2
*Calculate total heat input (joules) during the time of temperature increase from the
*minimum at dawn to the maximum (0.6*daylength) after dawn
gen heatD=((iradDb*0.655)-(exitnceD*daylngth*0.6/24))
*Hence calculate the apparent heat capacity of the air (ψ)- i.e. rate of heat input
*required per temperature increase of 1°C: Units = Wm^-2°C^-1
gen acapacD=(heatD/rangeD)/(3600*daylngth*0.6)
*In reality some of this heat goes into heating the ground, and the remainder is lost due
*to convection (heats the air) or through evaporation. Advection can also add or take
*away heat.
```

APPENDIX 5
ALTITUDINAL,LATITUDINAL AND LONGITUDINAL COEFFICIENTS FOR ALL WIND DIRECTIONS IN ALL MONTHS:MAXIMA

month= month of the year January=1
December=12
wind=wind direction

KEY TO WIND: 0 = calm 1=N 2=NE 3=E 4=SE
5=S 6=SW 7=W 8=NW 9=mean for month

alt22=altitudinal coefficient (°C per kilometre)

lat22=latitudinal coefficient (°C per kilometre)

lng22=longitudinal coefficient (°C per kilometre)

r2=coefficient of determination in regression
(alt lat lng)

		a	b	c		
month	**wind**	**alt22**	**lat22**	**lng22**	**r2**	
1	9	-7.30	-0.00021	0.00213	0.935	
1	0	-5.78	-0.00298	0.00427	0.767	
1	1	-8.43	-0.00523	-0.00232	0.907	
1	2	-10.48	-0.00152	0.00144	0.724	*
1	3	-6.87	0.00081	-0.00208	0.831	
1	4	-6.87	-0.00204	-0.00217	0.870	
1	5	-7.03	0.00322	0.00073	0.929	
1	6	-7.76	0.00215	0.00357	0.930	
1	7	-7.72	-0.00340	0.00690	0.937	
1	8	-7.63	-0.00649	0.00222	0.872	
2	9	-8.55	0.00023	0.00085	0.942	
2	0	-7.76	0.00066	-0.00377	0.898	
2	1	-10.17	0.00066	-0.00869	0.930	
2	2	-9.12	-0.00216	-0.00786	0.912	
2	3	-9.09	0.00110	-0.00555	0.908	
2	4	-10.20	0.00704	-0.00294	0.929	
2	5	-7.44	0.00176	-0.00030	0.910	
2	6	-8.29	-0.00074	0.00611	0.915	
2	7	-8.86	-0.00190	0.00553	0.947	
2	8	-8.77	0.00093	0.00012	0.922	
3	9	-9.48	0.00013	0.00446	0.932	
3	0	-10.27	-0.00344	-0.00515	0.926	
3	1	-9.15	-0.00136	-0.00467	0.914	
3	2	-8.03	-0.00116	-0.01058	0.891	
3	3	-7.81	-0.02206	0.01102	0.668	*
3	4	-8.88	-0.00342	-0.00359	0.955	
3	5	-9.33	0.00298	0.00407	0.908	

3	6	-9.18	0.00251	0.00949	0.924
3	7	-9.80	0.00041	0.00969	0.927
3	8	-9.99	0.00019	0.00144	0.910
4	9	-8.89	-0.00297	-0.00157	0.899
4	0	-7.01	-0.00480	-0.00120	0.742
4	1	-9.30	-0.00486	-0.01156	0.907
4	2	-8.74	-0.00204	-0.02178	0.908
4	3	-10.25	-0.01281	-0.01659	0.934
4	4	-9.73	-0.00756	-0.01162	0.740
4	5	-7.52	0.00126	0.00833	0.827
4	6	-8.87	0.00135	0.01253	0.894
4	7	-9.80	-0.00056	0.01165	0.903
4	8	-9.45	-0.00213	0.00538	0.882
5	9	-8.00	-0.00686	-0.00737	0.805
5	0	-7.09	-0.01027	-0.00372	0.683
5	1	-7.69	-0.00637	-0.02020	0.766
5	2	-7.61	-0.01598	-0.03849	0.860
5	3	-7.35	-0.01761	-0.02623	0.822
5	4	-3.59	-0.00922	-0.01154	0.463
5	5	-7.74	-0.00258	0.00730	0.827
5	6	-9.37	-0.00305	0.01339	0.850
5	7	-8.74	-0.00120	0.01436	0.852
5	8	-8.74	-0.00238	0.00411	0.740
6	9	-8.23	-0.00741	-0.00246	0.782
6	0	-7.00	-0.01593	-0.00276	0.535
6	1	-7.39	-0.00579	-0.01838	0.763
6	2	-7.92	-0.01056	-0.02622	0.815
6	3	-11.25	-0.01969	-0.02460	0.750
6	4	-7.01	-0.00439	-0.00294	0.629
6	5	-8.48	-0.00579	0.00738	0.795
6	6	-8.62	-0.00350	0.02292	0.895
6	7	-9.07	-0.00352	0.01335	0.865
6	8	-9.21	-0.00160	0.00873	0.822
7	9	-7.80	-0.00635	0.00746	0.813
7	0	-4.81	-0.01194	0.00142	0.319
7	1	-7.87	-0.00766	-0.01130	0.765
7	2	-7.47	-0.01372	-0.01480	0.803
7	3	-6.57	-0.02509	-0.01499	0.752
7	4	-4.15	-0.00285	0.01489	0.370
7	5	-7.89	-0.00723	0.00335	0.768
7	6	-9.18	-0.00247	0.02170	0.915
7	7	-8.41	-0.00353	0.01906	0.870
7	8	-8.30	-0.00279	0.01237	0.833
8	9	-8.86	-0.00236	0.01172	0.910
8	0	-9.44	-0.00565	0.00633	0.790
8	1	-7.95	-0.00639	-0.00750	0.836
8	2	-6.56	-0.02435	-0.02729	0.793 *
8	3	-8.20	-0.00018	-0.00374	0.837

8	4	-8.72	-0.00038	0.02700	0.911
8	5	-8.62	-0.00245	0.01547	0.921
8	6	-9.38	0.00096	0.02065	0.921
8	7	-9.46	0.00189	0.01772	0.931
8	8	-8.54	-0.00588	0.00992	0.850
9	9	-8.51	-0.00410	0.01013	0.928
9	0	-8.28	-0.00654	0.00551	0.908
9	1	-8.38	-0.00473	-0.00543	0.868
9	2	-7.68	-0.01016	-0.00372	0.836
9	3	-7.01	-0.02622	-0.01461	0.700
9	4	-7.20	-0.00238	0.00764	0.893
9	5	-8.41	0.00221	0.01287	0.906
9	6	-8.28	-0.00324	0.01637	0.937
9	7	-9.46	-0.00159	0.01460	0.947
9	8	-9.21	-0.00635	0.01060	0.904
10	9	-7.65	-0.00297	0.00428	0.936
10	0	-6.26	-0.00626	0.00012	0.905
10	1	-7.32	-0.00100	-0.00624	0.831
10	2	-9.04	-0.00882	-0.00202	0.913
10	3	-8.48	-0.01061	-0.00750	0.904
10	4	-8.51	-0.01310	-0.01347	0.912
10	5	-7.45	0.00246	0.00748	0.909
10	6	-7.86	-0.00022	0.00845	0.919
10	7	-8.57	-0.00357	0.00905	0.951
10	8	-7.97	-0.00184	0.00294	0.910
11	9	-7.37	-0.00074	0.00083	0.920
11	0	-7.51	0.00026	-0.00004	0.866
11	1	-8.12	-0.00487	0.00118	0.870
11	2	-8.84	-0.00737	0.00061	0.917
11	3	-9.07	0.00137	-0.00218	0.875
11	4	-8.37	-0.00479	-0.00253	0.799
11	5	-6.41	0.00267	-0.00128	0.881
11	6	-6.89	0.00068	0.00370	0.889
11	7	-7.42	-0.00119	0.00323	0.881
11	8	-8.13	-0.00409	0.00098	0.887
12	9	-6.85	-0.00094	0.00269	0.927
12	0	-6.00	0.00080	-0.00034	0.730
12	1	-9.23	0.00363	0.00243	0.833
12	2	-8.42	-0.00229	0.00240	0.907
12	3	-10.46	0.00162	-0.00043	0.902
12	4	-6.87	0.00106	-0.00080	0.824
12	5	-6.17	0.00051	0.00352	0.898
12	6	-6.42	0.00116	0.00337	0.916
12	7	-7.99	-0.00210	0.00494	0.951
12	8	-5.67	-0.00841	0.00108	0.805

* only 21 stations

APPENDIX 6

ALTITUDINAL,LATITUDINAL AND LONGITUDINAL COEFFICIENTS FOR ALL WIND DIRECTIONS IN ALL MONTHS:MINIMA

month= month of the year where January=1
December=12

wind=wind direction where 0=calm 1=N 2=NE 3=E 4=SE
5=S 6=SW 7=W 8=NW 9=mean for month

alt22=altitudinal coefficient (°C per kilometre)

lat22=latitudinal coefficient (°C per kilometre)

lng22=longitudinal coefficient (°C per kilometre)

r2=coefficient of determination in alt lat lng regression

		a	b	c	
month	**wind**	**alt22**	**lat22**	**lng22**	**r2**
1	9	-6.04	-0.00288	-0.00569	0.770
1	0	-3.64	-0.01065	-0.00806	0.392
1	1	-5.88	0.00012	0.00769	0.642
1	2	-4.63	-0.00070	0.01330	0.288
1	3	-6.87	-0.00039	0.00143	0.727
1	4	-5.35	-0.01042	-0.00965	0.430
1	5	-6.05	-0.00101	-0.01125	0.736
1	6	-6.57	-0.00104	-0.00926	0.807
1	7	-7.16	-0.00668	-0.00563	0.831
1	8	-5.53	-0.00432	0.00344	0.690
2	9	-6.27	-0.00289	-0.00362	0.768
2	0	-3.73	-0.01089	-0.00415	0.270
2	1	-6.24	0.00140	0.00209	0.590
2	2	-7.20	0.00211	0.00289	0.800
2	3	-7.95	0.00112	-0.00026	0.777
2	4	-7.92	0.00040	0.00053	0.793
2	5	-6.43	-0.00521	-0.00569	0.696
2	6	-6.27	-0.00279	-0.00987	0.795
2	7	-6.59	-0.00220	-0.00207	0.787
2	8	-7.02	-0.00281	0.00164	0.815
3	9	-6.96	-0.00580	-0.00245	0.841
3	0	-5.16	-0.01756	-0.00107	0.629
3	1	-6.85	-0.00845	0.00213	0.751
3	2	-4.80	-0.00947	0.00828	0.359
3	3	-7.94	-0.01943	-0.00757	0.831
3	4	-8.73	-0.00533	-0.00340	0.727
3	5	-7.58	-0.00358	-0.00838	0.736

3	6	-6.80	-0.00383	-0.00471	0.819
3	7	-7.78	-0.00567	-0.00067	0.879
3	8	-6.94	-0.00250	-0.00033	0.812
4	9	-6.47	-0.00519	-0.00233	0.811
4	0	-5.20	-0.00683	-0.00361	0.651
4	1	-6.22	-0.00201	0.00225	0.825
4	2	-6.71	-0.00290	-0.00230	0.775
4	3	-7.15	-0.00732	0.00181	0.829
4	4	-8.56	-0.02837	-0.00949	0.784
4	5	-5.17	-0.00633	-0.00879	0.529
4	6	-6.89	-0.00602	-0.00464	0.736
4	7	-5.86	-0.00159	0.00073	0.776
4	8	-7.09	-0.00539	-0.00245	0.843
5	9	-5.90	-0.01036	-0.00336	0.726
5	0	-3.90	-0.01747	-0.00516	0.394
5	1	-6.05	-0.00815	-0.00017	0.686
5	2	-5.38	-0.01449	-0.00557	0.722
5	3	-6.95	-0.01481	-0.01221	0.695
5	4	-4.01	-0.01868	-0.00544	0.432
5	5	-4.19	-0.01073	-0.00846	0.373
5	6	-6.81	-0.00680	-0.00120	0.818
5	7	-7.37	-0.00303	0.00513	0.861
5	8	-6.46	-0.00953	0.00060	0.713
6	9	-6.20	-0.00762	-0.00256	0.738
6	0	-5.26	-0.01303	0.00305	0.581
6	1	-6.16	-0.00532	-0.00390	0.777
6	2	-6.84	-0.00934	-0.00049	0.761
6	3	-7.49	-0.01068	-0.01490	0.685
6	4	-4.07	-0.00454	-0.01025	0.330
6	5	-5.61	-0.00904	-0.00683	0.531
6	6	-6.82	-0.00545	-0.00010	0.804
6	7	-6.36	-0.00989	-0.00058	0.755
6	8	-5.87	-0.00264	0.00449	0.794
7	9	-5.67	-0.00866	-0.00147	0.707
7	0	-3.57	-0.01238	-0.00274	0.407
7	1	-6.49	-0.00942	-0.00049	0.856
7	2	-4.63	-0.00964	0.00302	0.524
7	3	-4.90	-0.01966	-0.00793	0.450
7	4	-2.33	-0.00953	-0.00411	0.094
7	5	-4.68	-0.00988	-0.00973	0.449
7	6	-6.47	-0.00233	0.00047	0.787
7	7	-6.04	-0.00519	0.00165	0.724
7	8	-6.81	-0.00877	0.00283	0.825
8	9	-6.18	-0.00662	0.00035	0.771
8	0	-4.12	-0.00890	-0.00361	0.313
8	1	-5.32	-0.00568	0.00847	0.639
8	2	-7.70	-0.00455	0.01824	0.842
8	3	-5.78	-0.00876	-0.00401	0.581

8	4	-3.50	-0.00905	-0.01037	0.083
8	5	-5.63	-0.00837	-0.00274	0.663
8	6	-7.29	-0.00680	0.00146	0.853
8	7	-7.07	-0.00424	-0.00116	0.853
8	8	-6.59	-0.00554	0.00195	0.815
9	9	-5.83	-0.00817	0.00076	0.639
9	0	-4.67	-0.01419	0.00263	0.405
9	1	-5.03	-0.01016	0.00534	0.474
9	2	-4.44	-0.01831	0.01205	0.324
9	3	-7.32	-0.02274	-0.00196	0.482
9	4	-4.60	-0.01631	-0.00990	0.314
9	5	-5.93	-0.01038	-0.00354	0.585
9	6	-5.83	-0.00438	-0.00304	0.676
9	7	-7.06	-0.00681	-0.00140	0.701
9	8	-6.23	-0.00610	0.00674	0.669
10	9	-5.51	-0.00789	-0.00087	0.601
10	0	-3.51	-0.01187	0.00018	0.247
10	1	-4.79	-0.00577	0.01450	0.558
10	2	-5.29	-0.01054	0.00232	0.343
10	3	-6.22	-0.00502	0.00288	0.700
10	4	-6.60	-0.00185	0.00108	0.608
10	5	-5.90	-0.00103	-0.00399	0.664
10	6	-5.90	-0.01083	-0.00159	0.587
10	7	-5.98	-0.00548	-0.00231	0.676
10	8	-7.86	-0.01138	0.00236	0.748
11	9	-5.08	-0.00466	0.00068	0.595
11	0	-4.36	-0.00843	-0.00208	0.360
11	1	-5.35	-0.00766	0.01137	0.576
11	2	-6.61	-0.00280	0.00807	0.721
11	3	-6.07	0.00003	0.00187	0.671
11	4	-6.01	0.00674	0.02381	0.590
11	5	-5.79	-0.00597	-0.00474	0.616
11	6	-5.85	-0.00424	-0.00658	0.703
11	7	-5.64	-0.00544	-0.00090	0.606
11	8	-3.83	-0.00509	0.01047	0.463
12	9	-5.76	-0.00571	-0.00164	0.718
12	0	-3.98	-0.00410	0.00518	0.425
12	1	-7.01	0.00153	0.01092	0.799
12	2	-5.83	-0.00313	0.00496	0.629
12	3	-7.13	-0.00267	0.00527	0.655
12	4	-7.07	-0.01708	-0.00432	0.723
12	5	-6.80	-0.00582	-0.00662	0.794
12	6	-5.80	-0.00697	-0.00691	0.688
12	7	-7.04	-0.00499	-0.00268	0.851
12	8	-4.02	-0.00744	0.00227	0.305

APPENDIX 7
COMPUTER ROUTINE FOR CALCULATING T_{ex} AND T_{acc}

*Starred lines are comments. The model is written in Stata language.

```
*File to calculate expected degree day accumulation T_acc for airflow scenarios
*Input is the mean and standard deviation of mean daily temperatures
*The mean (avtp) and standard deviation (stdev) of daily temperatures for each airflow
*are contained in a file. The example given below is for sea-level
*Calculate the z-score for the growth threshold of 6°C
gen zg=(6-avtp0)/stdev0
*Convert this to probability of a single daily temperature being greater than 6°C
gen cmnorprg=normprob(zg)
gen norprg=1-cmnorprg
*Calculate the average temperature above zg, assuming a standard normal distribution
gen aveexczg=(1/sqrt(2*_pi))*(exp(-(zg^2)/2))/norprg
*Convert this to a temperature relevant to actual distribution
gen aveexcg=(aveexczg*stdev0)+avtp0
*Mean excess over 6°C is:
gen excessg=aveexcg-6
*Expected number of growing days in month
gen days=norprg*31
*Corrections for months with less than 31 days
replace days=norprg*30 if month==4 | month==6 | month==9 | month==11
replace days=norprg*28 if month==2
*Calculate accumulated temperatures for scenario
gen cugrowth=days*excessg
```